INSTITUTO SUPERIOR TÉCNICO

UNIVERSIDADE TÉCNICA DE LISBOA

INSTITUTO SUPERIOR TÉCNICO

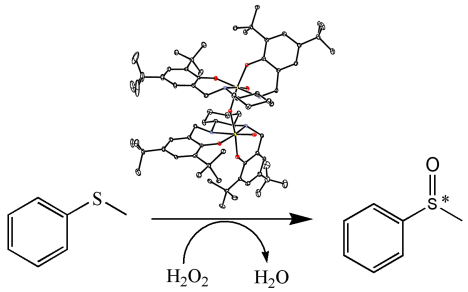

Chiral Transition Metal Complexes as Catalysts for Sustainable Oxygen Transfer Reactions

Pedro Miguel Santos Ferreira Adão

Supervisor: Doctor João Emídio da Silva da Costa Pessoa

Co-Supervisor: Doctor Carlos Alberto Mateus Afonso

Thesis approved in public session to obtain the PhD Degree in Chemistry

Jury final classification: Pass with distinction

Jury

Chair person: Chairman of the IST Scientific Board

Members of the Committee:

Doctor Carlos Alberto Mateus Afonso

Doctor Ana Cristina Moreira Freire

Doctor João Emídio da Silva da Costa Pessoa

Doctor Ana Margarida Sousa Dias Martins

Doctor Maria Isabel Rodrigues Correia

2011

INSTITUTO SUPERIOR TÉCNICO

UNIVERSIDADE TÉCNICA DE LISBOA

INSTITUTO SUPERIOR TÉCNICO

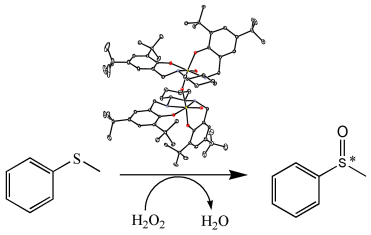

Chiral Transition Metal Complexes as Catalysts for Sustainable Oxygen Transfer Reactions

Pedro Miguel Santos Ferreira Adão

Supervisor: Doctor João Emídio da Silva da Costa Pessoa

Co-Supervisor: Doctor Carlos Alberto Mateus Afonso

Thesis approved in public session to obtain the PhD Degree in Chemistry

Jury final classification: Pass with distinction

Jury

Chair person: Chairman of the IST Scientific Board

Members of the Committee:

Doctor Carlos Alberto Mateus Afonso, Full Professor, Faculdade de Farmácia da Universidade de Lisboa

Doctor Ana Cristina Moreira Freire, Associate Professor (with Habilitation), Faculdade de Ciências da Universidade do Porto

Doctor João Emídio da Silva da Costa Pessoa, Associate Professor (with Habilitation), Instituto Superior Técnico, Universidade Técnica de Lisboa

Doctor Ana Margarida Sousa Dias Martins, Associate Professor (with Habilitation), Instituto Superior Técnico, Universidade Técnica de Lisboa

Doctor Maria Isabel Rodrigues Correia, Assistant Researcher, Instituto Superior Técnico, Universidade Técnica de Lisboa

Funding institution: Fundação para a Ciência e a Tecnologia

2011

To my family

To Sónia

Abstract

The work described in this thesis concerns the synthesis, characterisation and reactivity of homogeneous and heterogeneous complexes of titanium, vanadium and copper with Schiff base/reduced Schiff base ligands. A general introduction to the thesis subject and context is first presented, followed by the description of the synthesis of chiral aminophenolate-class Schiff base and reduced Schiff base ligand precursor compounds. The synthesis of tetradentate complexes of Ti^{IV} of the reduced Schiff base type and the reactivity of these complexes in enantioselective sulfoxidations is also addressed as well as the synthesis of the corresponding tetradentate complexes of $V^{IV}O$ of the Schiff base and reduced Schiff base type. The performance of these complexes for enantioselective sulfoxidations and alkene oxidations is also described. The synthesis of aminoalcohol-derived tridentate complexes of $V^{IV}O$ of reduced Schiff base type and of aminoacid-derived tridentate reduced Schiff base complexes of $V^{IV}O$ and the reactivity of these complexes as catalysts for enantioselective sulfoxidations is also addressed. Heterogeneous versions of the catalysts are also prepared and characterized and their reactivity and recycle ability for enantioselective sulfoxidations described. Finally, the synthesis of tetradentate reduced Schiff base complexes of Cu^{II} is also addressed as is their reactivity as catalysts for enantioselective sulfoxidations.

Resumo

O trabalho apresentado nesta tese trata da síntese, caracterização e reactividade de complexos homogéneos e heterogéneos de titânio, vanádio e cobre da classe das bases de Schiff/bases de Schiff reduzidas. Apresenta-se primeiro uma introdução geral ao contexto e tema da tese seguida da descrição da síntese de compostos quirais precursores de ligandos da classe dos aminofenolatos. A síntese de complexos tetradentados de Ti^{IV} do tipo base de Schiff reduzida e a respectiva reactividade em sulfoxidações enantiosselectivas é também descrita assim como a síntese de complexos tetradentados de $V^{IV}O$ do tipo base de Schiff e base de Schiff reduzida. A reactividade dos mesmos em sulfoxidações enantiosselectivas e oxidações de alcenos é também descrita. A síntese de complexos tridentados de $V^{IV}O$ do tipo base de Schiff e base de Schiff reduzida derivados de aminoalcoóis e de aminoácidos assim como a reactividade dos mesmos em sulfoxidações enantiosselectivas é também relatada. Apresenta-se também a síntese e caracterização de versões heterogéneas dos catalisadores preparados assim como a reactividade dos mesmos em sulfoxidações enantiosselectivas. Finalmente, é descrita a síntese de complexos tetradentados de Cu^{II} do tipo base de Schiff reduzida assim como a reactividade dos mesmos em sulfoxidações enantiosselectivas.

Keywords

Aminophenolate ligands

Schiff base ligands

Reduced Schiff base ligands

Homogeneous catalysis

Heterogeneous catalysis

Vanadium complexes

Titanium complexes

Copper complexes

Sulfoxidations

Enantioselective synthesis

Palavras-chave

Ligandos aminofenolato

Bases de Schiff

Bases de Schiff reduzidas

Catálise homogénea

Catálise heterogénea

Complexos de vanádio

Complexos de titânio

Complexos de cobre

Sulfoxidações

Síntese enantiosselectiva

Acknowledgements

The work presented in this thesis was mainly performed at *Centro de Química Estrutural (CQE)*, *Instituto Superior Técnico (IST)*, under the supervision of Doctor João Costa Pessoa, with co-supervision of Doctor Carlos Afonso. The work presented in Chapters 3 and 4 was performed under the supervision of Doctor Isabel Correia. I am grateful to this institution for the use of its facilities.

I am grateful to *Fundação para a Ciência e a Tecnologia (FCT)* for a PhD grant (SFRH/BD/40279/2007) and other financial support to this work.

I must thank my PhD supervisor João Costa Pessoa for his guidance, support and patience during my PhD. His valuable suggestions during this voyage through the rich, but complex, chemistry of vanadium have made this work possible. I have learned enormously from his teachings and advices. I am very grateful for his dedication throughout my PhD and, in particular, during the last stage for the preparation of this dissertation.

I thank my PhD co-supervisor Doctor Carlos Afonso for his valuable guidance and suggestions during my PhD. His vast knowledge of Organic Chemistry and valuable teachings served as an inspiration for the creation of many compounds described in this work. I am grateful for his availability and valuable support whenever doubts arose regarding synthetic procedures.

I thank Doctor Isabel Correia (*IST*) for her guidance and patience during my first couple of years here at CQE. During the period prior to my PhD, her valuable teachings have prepared me for the path that lied ahead. In particular, Chapters 3 and 4 were possible thanks to her constant support.

I am grateful to Doctor Fernando Avecilla (*University of Coruña*) for solving and refining all crystal structures described in this work. His contribution as crystallographer was crucial for the better understanding of the chemistry of the Ti^{IV} and $V^{IV}O$ complexes described in Chapters 3 and 4.

I would like to thank Doctor Mannar Maurya (*Indian Institute of Technology of Roorkee*) for his valuable collaboration in the oxidation of alkenes and valuable discussions.

I would like to thank Doctor Maxim Kuznetsov (*IST*) for the theoretical calculations presented in Chapter 4. His valuable collaboration enabled the better understanding of the elusive mechanisms behind vanadium-promoted alkene oxidations.

I thank Doctor Rui Teives Henriques (*IST*) for the magnetic studies presented in Chapter 4. I also would like to thank him for his valuable guidance and support during my study of electron paramagnetic resonance spectroscopy.

I would like to thank Doctor Ana Isabel Tomaz (*IST*) for her valuable teachings regarding electron paramagnetic resonance spectroscopy.

I am very grateful to Doctor Ana Margarida Martins and Doctor Sónia Barroso for the opportunity to test their own titanium and vanadium compounds in catalytic sulfoxidation. While the results of this collaborative effort are not presented in this work, they were of great importance for the better understanding of the catalytic systems described herein.

I would like to thank Doctor Maria Conceição Oliveira and Ana Dias for their assistance regarding mass spectrometry.

A big thanks to all my colleagues and friends: Sérgio Marques, Ivan Sabino, Andreia Mota, Marta Figueiras, Gisela Gonçalves, Amit Kumar, Ana Sofia Ferreira, Clara Gomes, Rui Munhá, Vânia André, Konstantin Luzyanin, Cláudia Figueira, Luís Alves, Sofia Gama, Kamila Koci, Jarek Sebestik, Enoch Cobbina, Raquel Teixeira, Raquel Correia and to all those that, by involuntary omission, are not mentioned herein.

Finally, and most importantly, I must thank my family for their constant support, for the opportunity to get where I stand today for believing in me. Last, but definitely not least, I thank my beloved Sónia for her love, support, friendship and patience.

Pedro Miguel Santos Ferreira Adão

Table of Contents

Index of Figures

Index of Schemes

Index of Tables

Symbols and Abbreviations

δ	Delta-conformation of a chelating ring
δ	Chemical shift
ε	Molar absorptivity
λ	Lambda-conformation of a chelating ring
λ	Wavelength
μ	Bridging ligand
$\Delta\varepsilon$	Molar circular dichroism
μ_B	Bohr magneton
^{13}C NMR	Carbon-13 nuclear magnetic resonance spectroscopy
^{1}H NMR	Proton nuclear magnetic resonance spectroscopy
4-PPNO	4-phenylpyridine-N-oxide
^{51}V NMR	Vanadium-51 nuclear magnetic resonance spectroscopy
5-MeOsal	*5*-methoxysalicylato
A	Absorbance
A	Hyperfine coupling constant
A_0	Isotropic hyperfine coupling constant
AARSB	**A**mino**a**cid-derived **r**educed **S**chiff **b**ase
AB	Two-spin system involving nucleus A and nucleus B
ABX	Three-spin system involving nucleus A , nucleus B and nucleus X
AC	Activated carbon
Acac	Acetylacetonate
AMX	Three-spin system involving nucleus A , nucleus M and nucleus X
AORSB	**A**minoalcoh**o**l-derived **r**educed **S**chiff **b**ase
APT	Attached Proton Test
BINOL	1,1'-binaphthyl-2,2'-diol
bmim	1-butyl-3-methylimidazolium
bmpyr	1-butyl-1-methylpyrrolidinium
Bn	Benzyl
BZA	Benzaldehyde
BZAC	Benzoic acid
CD	Circular Dichroism
Chan	From (sal-chan) = 2,2'-(1*R*,2*R*)-**c**yclo**h**exane-1,2-diylbis(az**an**ediyl)bis(methylene)diphenolate)

CHP	Cumene hydroperoxide
CHP	Cumyl hydroperoxide
CT	Charge-transfer
CW	Continuous wave
DCE	1,2-dichloroethane
DFT	Density Functional Theory
DMF	*N,N*-dimethylformamide
DMSO	Dimethyl Sulfoxide
DPEHP	1,1-diphenylethyl hydroperoxide
EA	Elemental Analysis
E_a^{ap}	Apparent activation energy
ee	Enantiomeric excess
emim	1-ethyl-3-methylimidazolium
EPR	Electron Paramagnetic Ressonance
ESI-MS	Electrospray Ionization Mass Spectroscopy
fac	*facial*
FT-IR	Fourier Transform Infrared Spectroscopy
g	Landé g-factor
GC	Gas Chromatography
HMBC	Heteronuclear Multiple Bond Correlation
HOMO	Highest Occupied Molecular Orbital
HPLC	High Performance Liquid Chromatography
HSQC	Heteronuclear Single Quantum Coherence
LMCT	Ligand-to-metal charge-transfer
LUMO	Lowest Unoccupied Molecular Orbital
MAO	methyl aluminoxane
mCPBA	*m*-chloro-peroxybenzoic acid
mer	*meridional*
m_I	Nuclear spin state
$^nJ_{AB}$	Coupling constant between atoms A and B, separated by n bonds
NMO	*N*-methylmorpholine-*N*-oxide
NMR	Nuclear Magnetic Ressonance
omim	3-methyl-1-octylimidazolium
PEG	Polyethyleneglycol
PHAA	Phenylacetaldehyde
PHED	1-phenylethane-1,2-diol
PIP	piperazine

PS	Polystyrene
R	Absolute configuration *R* at a chiral atom
RSB	Reduced Schiff base
RTIL	Room temperature ionic liquid
S	Absolute configuration *S* at a chiral atom
S	Species
SAL	Salicylaldehyde
Salan	2,2'-(ethane-1,2-diylbis(azanediyl))bis(methylene)diphenol
Salen	2,2'-(1*E*,1′*E*)-(ethane-1,2-diylbis(azan-1-yl-1-ylidene))bis(methan-1-yl-1-ylidene)diphenol (**sal**icylidene-1,2-ethyl**en**ediamine)
SO	Styrene oxide
SWNT	Single-walled carbon nanotube
TBHP	*Tert*-butyl hydroperoxide
Tf	Triflato
THF	Tetrahydrofuran
THP	Triphenyl hydroperoxide
TMSCl	Ttrimethylsilyl chloride
TMSCN	Trimethylsilyl cyanide
TS	Transition state
UHP	Urea:H_2O_2 adduct
UV–Vis	Ultraviolet–visible
σ_{dia}	Shielding diamagnetic term
σ_{para}	Shielding paramagnetic term
Δm_S	Change in spin state

Chapter 1

Introduction

1. Introduction

1.1. General background

Nowadays, the concern for the environmental impact of a chemical process has become nearly as important as the efficiency and selectivity of the process itself. Other than being efficient and selective, a catalyst should have sufficient chemical stability so that it can be recovered from the reaction mixture and recycled. This is normally possible with heterogeneous catalysts and often not easily possible with homogeneous catalysts. The importance of catalysts based on metal complexes has been growing, partly due to their scope of applications and versatility. Many of the properties of a given transition metal catalyst are dictated by the ligand. Therefore, the development of a ligand conferring versatility, activity, selectivity and recyclability is a core aspect of catalysis. In addition to describing the state-of-the-art in which the present work is inserted, this introductory chapter will present an overview of the ligand precursor classes and of the respective transition metal complexes that served as an inspiration for those used in the present work.

1.2. Ligand precursors and their $V^{IV}O$ and Ti^{IV} complexes

From the vast number of ligands developed for transition metal coordination catalysts, the extensive aminophenol ligand class stands out for the versatility, ease of preparation, structural diversity and high complexation ability of the ligand precursor compounds. Noteworthy are the well-known Schiff Base "salen" type ligands, such as those used in the Mn^{III}-catalyzed asymmetric epoxidation of olefins.[1] Also well-known are Schiff Base ligands derived from aminoalcohols and salicylaldehydes employed in the $V^{IV}O$-catalyzed asymmetric oxidation of prochiral thioethers.[2]

Other well-known variants of the aminophenol class are the aminebisphenol ligands used in Ti^{IV}- and Zr^{IV}-catalyzed olefin polymerizations.[3] Due to the extensiveness of the aminophenol ligand class and of the scope of application of the respective metal

complexes, the following sections will be dedicated only to the ligand "subclasses" and transition metals relevant to the present work.

1.2.1. Tetradentate N_2O_2 ligand precursors

1.2.1.1. Salen-type ligand precursors

The salen-type ligands are known for their versatility. The relative ease of preparation of such ligands allows facile structural modifications by simply changing either the starting amine or 2-hydroxybenzaldehyde. When ethylenediamine is combined with two equivalents of salicylaldehyde, the result is the chelating Schiff base known as salicylidene-1,2-ethylenediamine, or "salen". Compounds containing the unit **L1.1** represented in Figure 1.1 are frequently called salen-type compounds (or derivatives). The reduced variant, known as "tetrahydrosalen" or "salan", is represented by **L1.2**.

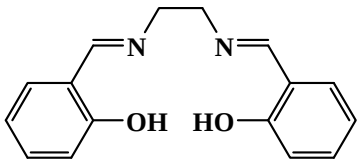

L1.1

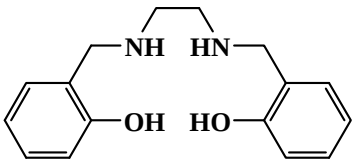

L1.2

Figure 1.1. Structures of salen, **L1.1**, and its reduced version, tetrahydrosalen or salan, **L1.2**.

The salen are dianionic tetradentate ligand precursor compounds, bearing a "hard" N_2O_2 donor set. These ligands have similarities to porphyrins, but are more easily prepared. One feature of these compounds is the ability to coordinate through the imine nitrogens and stabilize different metal centers in lower oxidation states.[4,5] Another important feature is the ease by which chirality is introduced to a metal complex by use of a chiral diamine. The sp^3 carbons C8 and C8' (see Figure 1.2) become stereogenic when R is a group other than a hydrogen atom. Since these stereogenic carbons are close to the metal ion, induction of chirality to the metal centre can be expected. The groups at C3 and C3' may also exert an important influence over the overall activity and enantioselectivity of the M(salen) catalyst. It has been reported that a bulky alkyl or aryl group at these positions can improve enantiomeric excesses in processes such as

asymmetric epoxidations and sulfide oxidations by forcing the complex to spatially arrange itself and introducing restrictions on the approach of the substrate to the metal centre.[6,7,8]

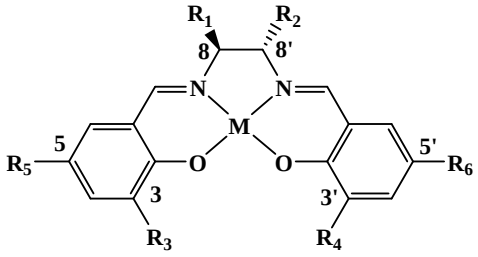

L1.3

Figure 1.2. Generic structural formula of a salen-type metal complex.

Recent work using M(salen) catalysts further attests the efficiency and versatility of the salen-based systems. Indeed, the elaborate M(salen) catalysts used by Katsuki and co-workers in a wide variety of asymmetric catalytic processes, ranging from epoxidation to addition reactions, show the advantages the salen-based systems have over other systems, namely the M(porphyrin) systems.[9,10,11,12,13]

1.2.1.2. Ti^{IV}(salen) complexes

After the success of the Sharpless-Katsuki Ti^{IV} isopropoxide/diethyltartrate[14] and Jacobsen's chiral Mn^{III}(salen) systems in asymmetric epoxidations,[1] the time came to combine the best of both catalytic systems in one: the inexpensive, non-toxic and readily available Ti^{IV} halides or alkoxides with the highly versatile and easily prepared salen ligand. In 1991, Fujita and co-workers developed chiral Ti^{IV}(salen) catalysts **L1.4** and **L1.5** (see Figure 1.3), that promoted the asymmetric oxidation of sulfides into sulfoxides with organic hydroperoxides (Scheme 1.1).[15] The authors reported sulfoxide yields as high as 95% along with enantiomeric excesses reaching 61% when using **L1.4** as catalyst, triphenyl hydroperoxide (THP) as oxidant and methanol as solvent, at 0 ºC.

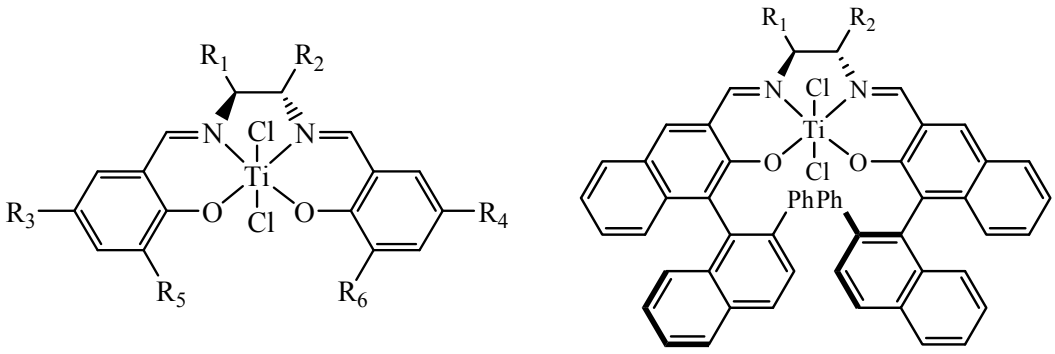

L1.4 R_1,R_2 = -$(CH_2)_4$- ; R_3,R_4,R_5,R_6=H-

L1.5 R_1= CH_3-; R_2 =H-; R_3,R_4,R_5,R_6=H-

L1.6..R_1,R_2 = -$(CH_2)_4$-; R_3,R_4,R_5,R_6=*t*-Bu-

L1.7 $R1,R_2$ = -$(CH_2)_4$-

Figure 1.3. Structural formulas of the Ti^{IV}(salen) complexes used by the group of Fujita in asymmetric sulfoxidation.

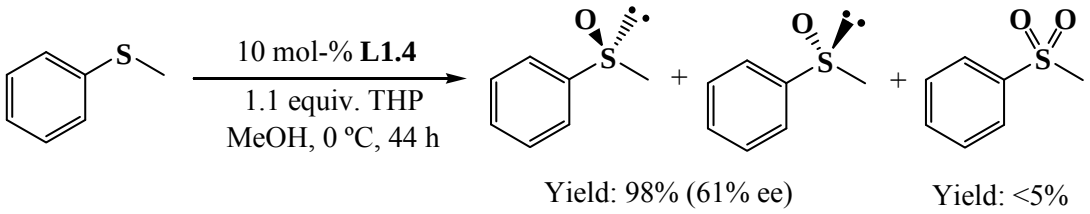

Scheme 1.1. Ti^{IV}(salen)-promoted asymmetric sulfoxidation.

The group of Katsuki also studied the performance of the chiral Ti^{IV}(salen) complexes in a variety of catalytic processes, epoxidation and sulfoxidation being the most emphasized. Katsuki's chiral Ti^{IV}(salen) catalyst **L1.7** (see Figure 1.3) used the same ligand as the previous Mn^{III} system, and proved adequate at oxidizing unfunctionalized alkenes, allylic alcohols, and alkyl aryl sulfides with the added advantage of using H_2O_2 or urea:H_2O_2 adduct (UHP) instead of organic hydroperoxides or iodosylarenes (Scheme 1.2).[16] The authors emphasized the notable efficiency and enantioselectivity of the Ti^{IV}(salen) system in epoxidation and sulfoxidation in solvents other than organochlorides.

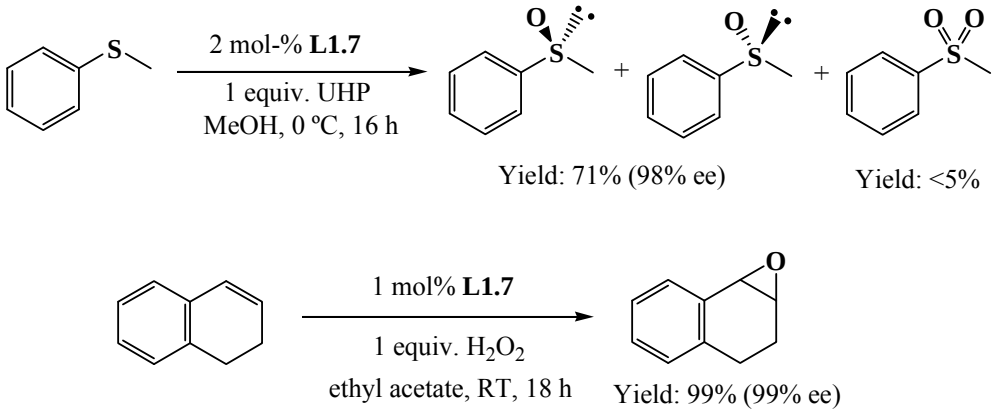

Scheme 1.2. Ti^{IV}(salen)-promoted asymmetric sulfoxidation and epoxidation.

The Ti^{IV}(salen) catalysts also proved effective in other synthetic processes, such as cyanohydrin synthesis. Notable examples include the chiral Ti^{IV}(salen) catalyst **L1.6** (see Figure 1.3) reported by North and co-workers for the asymmetric cyanation of aldehydes and ketones using trimethylsilyl cyanide (TMSCN) (Scheme 1.3).[17]

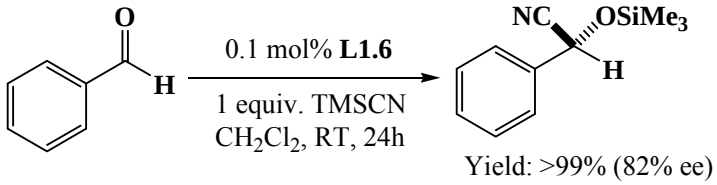

Scheme 1.3. Ti^{IV}(salen)-promoted asymmetric aldehyde cyanation.

Zhao and co-workers employed **L1.6** for asymmetric ring-opening of epoxides, using dithiophosporic acid as the nucleophile (Scheme 1.4).[18] The authors reported 2-hydroxythiol yields as high as 90% coupled with enantiomeric excesses of 73%.

Kozlowski and co-workers reported a Ti^{IV}(salen) catalyst **L1.8** (see Figure 1.4) bearing aminomethyl substituents in the phenolate 3-position which proved efficient at mediating the addition of diethylzinc to α-ketoesters (Scheme 1.5).[19] The authors reported α-hydroxyester yields of 93% and enantiomeric excesses of 83% with **L1.8**.

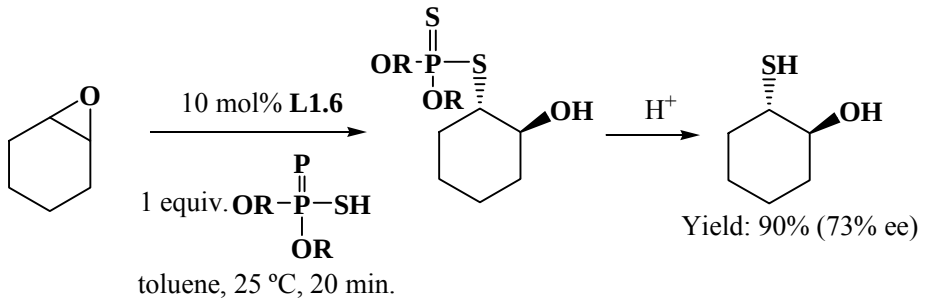

Scheme 1.4. Ti^{IV}(salen)-promoted asymmetric epoxide ring opening.

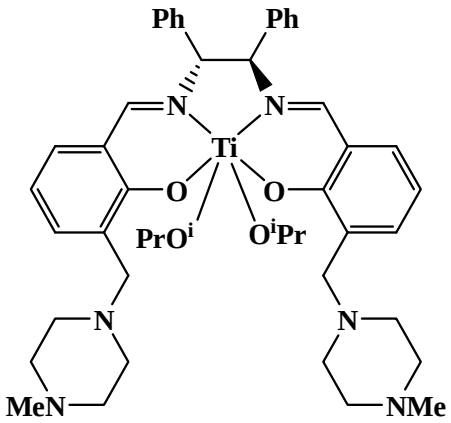

L1.8

Figure 1.4. Structural formula of the Ti^{IV}(salen) complex used by Kozlowski and co-workers.

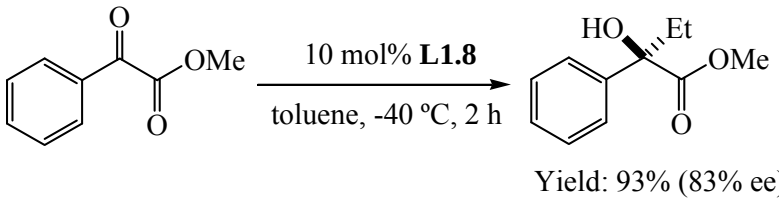

Scheme 1.5. Ti^{IV}(salen)-promoted asymmetric diethylzinc addition to ketones.

The wide scope of application of Ti^{IV}(salen) compounds is demonstrated with the use of these compounds as polymerization catalysts. Long and co-workers[20] reported a unique Ti^{IV}(salen) catalyst bearing ferrocenyl groups in the ligand structure (**L1.9**, see Figure 1.5) that proved effective for the ring opening polymerization of racemic lactide (Scheme 1.6). The authors reported the redox-controlling behavior of the ferrocenyl groups and their respective role in improving the activity of the Ti^{IV}(salen) catalyst.

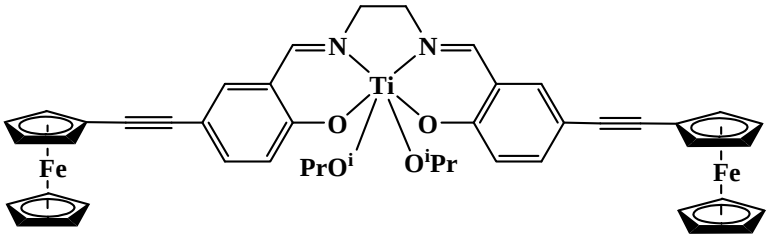

L1.9

Figure 1.5. Structural formula of the Ti^{IV}(salen) complex used by Long and co-workers.

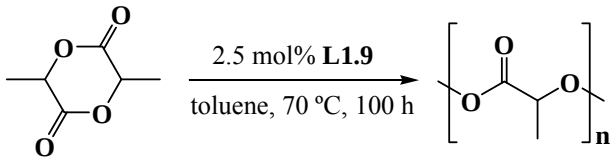

Scheme 1.6. Ti^{IV}(salen)-promoted *rac*-lactide ring-opening polymerization.

Olefin polymerization was also demonstrated to be possible with this class of compounds. For instance, Bialek and co-workers[21] employed the Ti^{IV}(salen) compound **L1.10** (see Figure 1.6) in the polymerization of ethylene, using methyl aluminoxane (MAO) as initiator (Scheme 1.7).

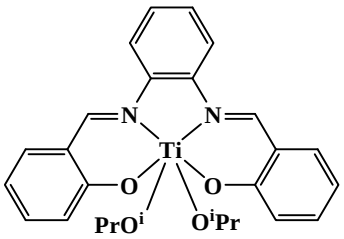

L1.10

Figure 1.6.- Structural formula of the Ti^{IV}(salen) complex used by Bialek and co-workers.

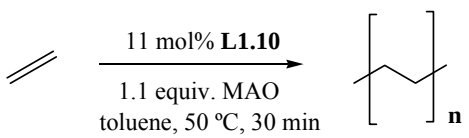

M_w: 431000 g mol^{-1}

Scheme 1.7. Ti^{IV}(salen)-promoted ethylene polymerization.

High valent titanium compounds are known to mediate other carbon-carbon bond formation reactions such as the pinacol coupling of aromatic aldehydes.[22] One of the first instances where Ti^{IV}(salen) compounds are used in pinacol coupling comes from the 1999 report of Cozzi and co-workers, where **L1.6** (see Figure 1.3) effectively promotes the pinacol coupling of benzaldehyde, in the presence of metallic Mn (Scheme 1.8).[23] While the author did not test the catalyst for enantioselectivity, the very low formation of the achiral *meso* product was emphasized.

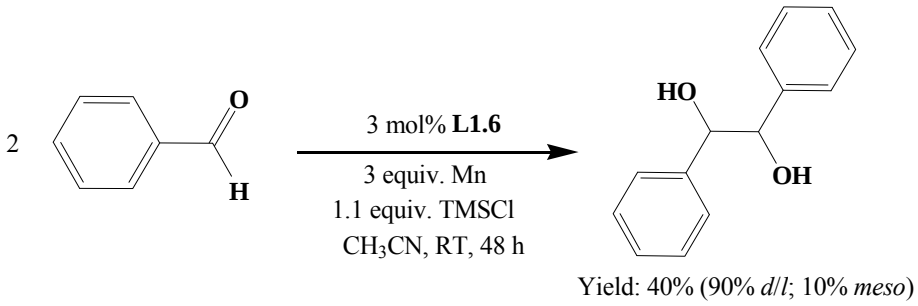

Scheme 1.8. Ti^{IV}(salen)-promoted asymmetric pinacol coupling.

The aforementioned instances where Ti^{IV}(salen) compounds were successfully employed as mediators in a variety of chemical processes show the potential of this compound class as catalysts in an industrial context.

1.2.1.3. $V^{IV}O$(salen) complexes

In 1977, Sharpless and co-workers introduced a $V^{IV}O$ catalyst that used a chiral hydroxamic acid **L1.11** as ligand (Scheme 1.9). This vanadium-based system promoted the epoxidation of allylic alcohols with enantiomeric excess up to 50%, using *tert*-butyl hydroperoxide as terminal oxidant. The same authors would later improve this system and increase the enantiomeric excess to 80% with a proline derived ligand.[24,25]

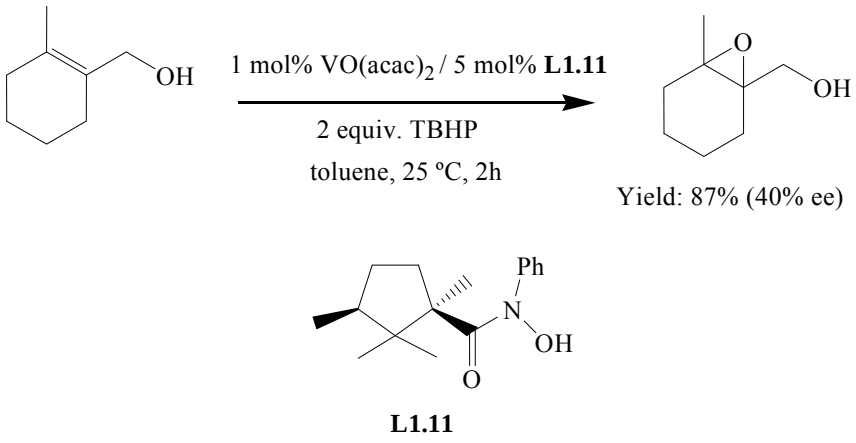

L1.11

Scheme 1.9. $V^{IV}O$(hydroxamic acid)-promoted asymmetric epoxidation.

It was only after the discovery of the presence of vanadium in nitrogenases and haloperoxidades that vanadium received considerable attention and became a stronger candidate for catalytic processes, namely, sulfoxidation.[26] Fujita et al. reported the oxidation of thioanisole with optically active salen-type $V^{IV}O$ (**L1.12** to **L1.15,** see Figure 1.7) and $V^{V}O$ complexes, using cumene hydroperoxide as terminal oxidant. Despite obtaining moderate to high yields (56-96% sulfoxide), enantioselectivities were as high as 42%.[7] The authors emphasized that *o*-vanillin-derived salen catalyst **L1.14** gave the best results in terms of enantioselectivity. The conclusion was that the existence of alkoxy groups at the C3 and C3' carbons can improve enantioselectivity, and such improvement was assigned to steric effects. Curiously, when these alkoxy groups at the C3 and C3' were replaced by *tert*-butyl groups the enantiomeric excess dropped to 10%. A similar detrimental steric bulk effect was possibly also behind the poor performance of Jacobsen's catalyst in asymmetric sulfoxidations.[27]

Similarly to the Ti^{IV}(salen) analogues, the applicability range of the $V^{IV}O$(salen) compound class was explored. The work carried out by the group of North illustrates the remarkable effectiveness of the $V^{IV}O$(salen) catalysts in carbon-carbon bond formation, namely in cyanohydrin synthesis.

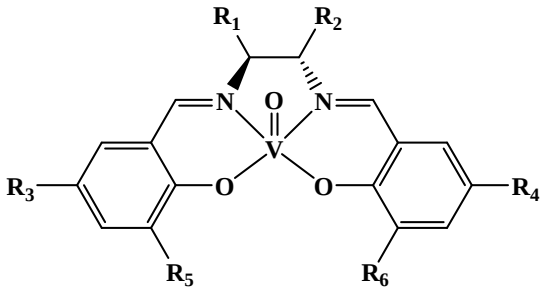

L1.12 R_1,R_2 = -$(CH_2)_4$- ; R_3, R_4, R_5, R_6=H- **L1.14** R_1, R_2 = -$(CH_2)_4$-; R_3, R_4=H-; R_5, R_6=MeO-

L1.13 R_1= CH_3-; R_2 =H-; R_3, R_4,R_5,R_6=H- **L1.15** R_1, R_2 = -$(CH_2)_4$-; R_3, R_4, R_5, R_6=*t*-Bu-

Figure 1.7. Structural formulas of various $V^{IV}O$(salen) complexes.

In 2000, North and co-workers employed **L1.15** (see Figure 1.7) in the asymmetric cyanation of aromatic aldehydes, obtaining cyanohydrin yields over 90% along with moderate to very high enantiomeric excesses, ranging from 50 to 90%. Noteworthy is the high activity of this $V^{IV}O$(salen) catalyst despite the low catalyst loading of 0.1 mol%. Later iterations of this system allowed the use of KCN as cyanide source instead of TMSCN and increased enantiomeric excesses.[28] Compound **L1.15** was also used by the same authors in the asymmetric Strecker reaction, obtaining very high yields of α-aminonitriles and moderate to high enantioselectivities (Scheme 1.10).[29]

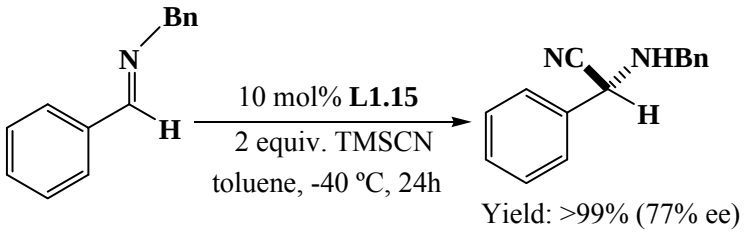

Scheme 1.10. $V^{IV}O$(salen)-promoted asymmetric imine cyanation.

In 2004, Katsuki and co-workers reported a $V^{V}O$(salen) catalyst based on their elaborate ligand precursors (**L1.16**, see Figure 1.8) to carry out Meerwein-Ponndorf-Verley aldehyde cyanations with high yields and enantioselectivities (Scheme 1.11).[30]

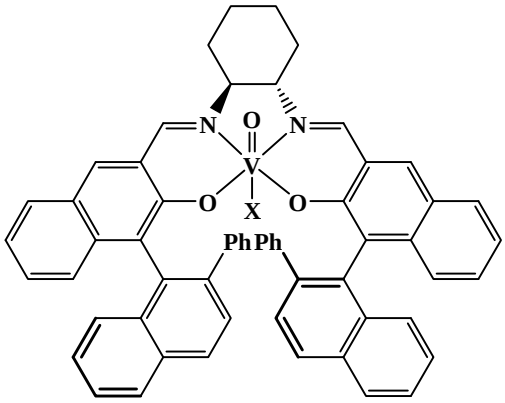

L1.16 X = ClO_4^-

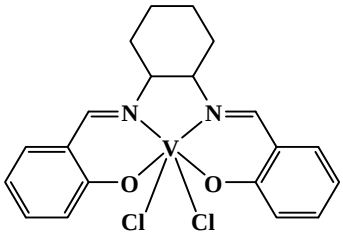

L1.17

Figure 1.8. Structural formulas of $V^{V}O$(salen) complexes.[30]

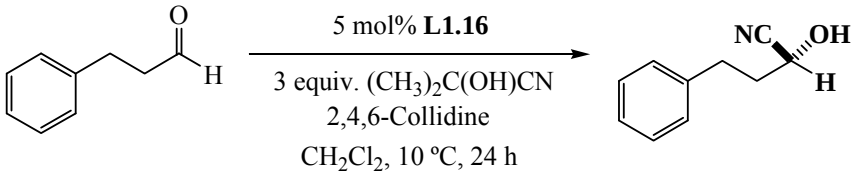

Scheme 1.11. $V^{IV}O$(salen)-promoted asymmetric aldehyde cyanation.

Vanadium-based salen-type compounds also proved active as ethylene polymerization catalysts, as reported in 2008 by Bialek and co-workers.[31] The catalyst employed by the authors was in fact a non-oxo [V^{IV}{salen}Cl_2] compound (**L1.17**, see Figure 1.8), very similar to the Ti^{IV}(salen) compound **L1.10** (see Figure 1.6) used previously by the same authors in ethylene polymerization. While the reaction conditions required stoichiometric amounts of Et_2AlCl as initiator, the authors emphasized the relatively short duration of the reaction (30 minutes).

The latter instance demonstrates how a vanadium-salen catalyst can serve as a potential alternative to metallocene catalysts, with the added advantages of the salen class of compounds in terms of handling, preparation, characterization and stability.

1.2.1.4. The tetrahydrosalen or salan-type compounds

One of the disadvantages of the "salen" compounds is their tendency to undergo hydrolysis in presence of water.[32] This is an important aspect to take into account when water is used as a solvent, or when water-containing reagents are used. This problem may be solved by reducing the Schiff base to the corresponding amine, thus obtaining a ligand precursor compound which is more resistant to decomposition, the so-called "salan" or tetrahydrosalen compounds. This class of compounds and the respective metal complexes are part of the diaminobis(phenolate) subclass, widely known for their use by Kol and co-workers in olefin polymerization.[33] To obtain the "salan", the salen precursor is reduced with a reducing agent such as sodium borohydride, or the required diamine is reacted with a 2,4-disubstituted phenol and formaldehyde in a modified Mannich reaction.[34] There are important differences between the salen- and the salan-type compound classes, as a result of the carbon-nitrogen double bond reduction. Unlike the "salen", the "salan" ligands are unable to stabilize the lower oxidation states of the metal centre, mostly due to the lack of π-back-donation from the metal.[5,35] As such, "salan" complexes of low valence metals may spontaneously oxidize to higher oxidation states when exposed to air. The hydrogenation of the imine bond also confers greater flexibility to the ligand and allows it to coordinate more easily in a folded, *cis*-geometry, whereas salen complexes are more stable in a planar *trans*-geometry.[6,36] This added flexibility may not always be beneficial. Walsh and co-workers noted that the *cis*-geometry preferred by Ti^{IV}(salan) induced chirality at the metal centre, regardless of the chirality elements present in the salan-type ligand structure. Moreover, a mixture of *cis* diastereoisomers (*cis*-α and *cis*-β) is always obtained, though the diastereoisomer proportion can be controlled to some extent.[37] Kol and co-workers further explored this particular characteristic of M(salan) compounds.[38] The authors reiterated the initial observations made by the group of Walsh, but also noted that Ti^{IV}(salan) complexes tend to adopt C_2-symmetric *cis*-β geometries. Additionally, the diastereoisomeric ratio can be effectively controlled with adequate ligand design. The possible *cis*-β isomers of a Ti^{IV}(salan) compound are shown in Figure 1.9.

This inevitable formation of diastereoisomeric mixtures poses an obstacle to stereochemistry regulation, which could account for the very limited work made with this ligand class. Despite this, recent work has shown the potential of Ti^{IV}(salan) and $VO^{IV,V}$(salan) complexes in asymmetric oxo-transfer reactions with oxidants such as hydrogen peroxide.[39,40]

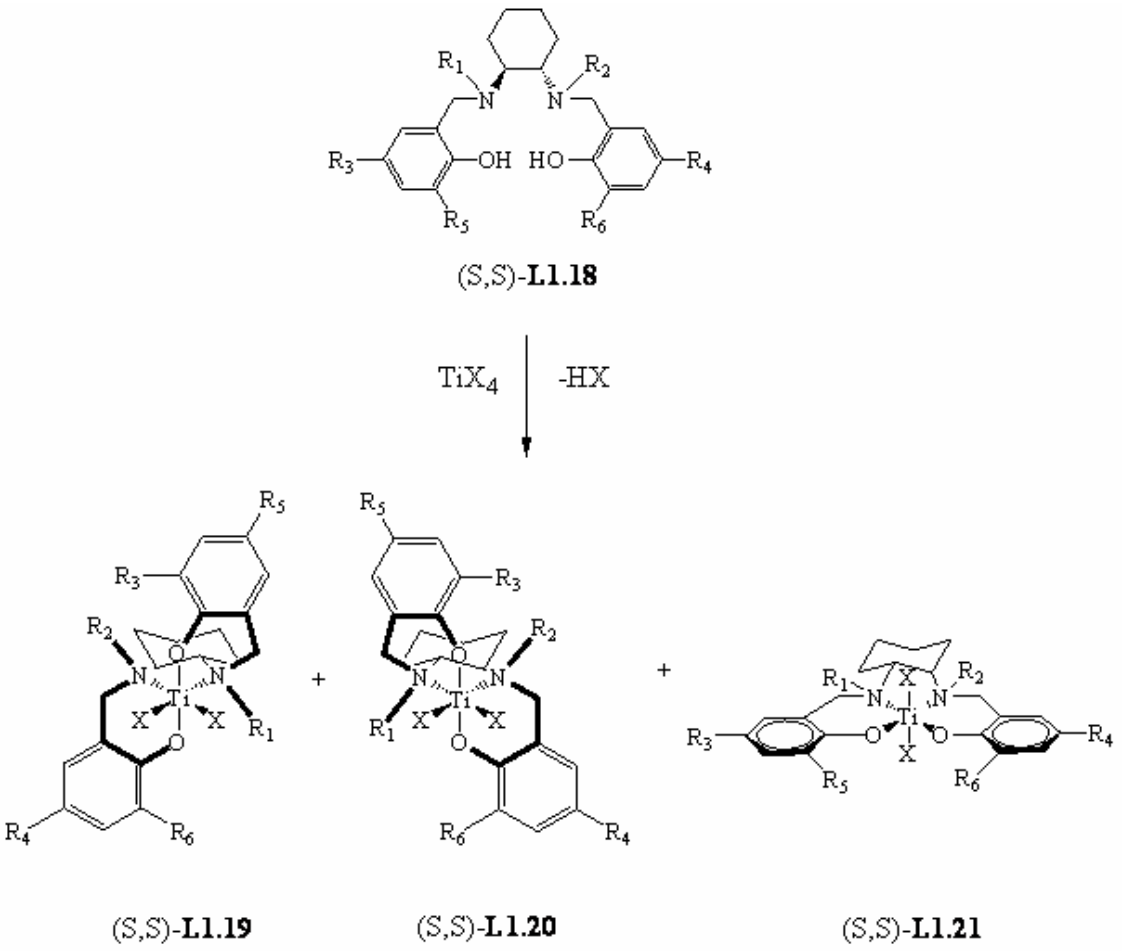

Figure 1.9. The possible diastereoisomers of a Ti^{IV}(salan) complex. Three are possible, but only the *cis*-forms (S,S)-Δ-**L1.19** and (S,S)-Λ-**L1.20** have chirality at the metal centre.

1.2.1.5. Ti^{IV}(salan) complexes

Most of the work with chiral Ti^{IV}(salan) in epoxidations and sulfoxidations has been done by Katsuki and co-workers.[41] A simplified variant (**L22**, see Figure 1.10) of their

highly effective salen ligand, **L1.7** (see Figure 1.3) developed for the older manganese systems was used for this Ti^{IV}(salan) system, which proved to have an equal, if not superior, efficacy to the older salen systems. The authors reported high epoxide yields and enantiomeric excesses over 90% for several alkene substrates when using H_2O_2 as terminal oxidant. However, such systems also require a higher catalyst loading of 5 mol%.

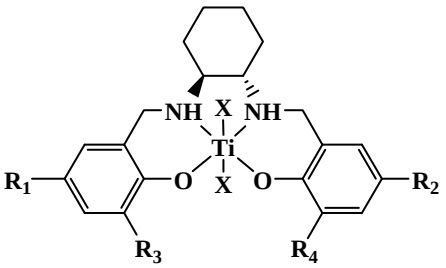

L1.22 R_1,R_2 = H-; R_3,R_4= Ph-; X = μ-O-

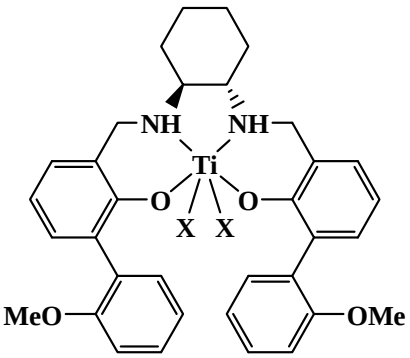

L1.23 X = μ-O-

L1.24 R_1,R_2,R_3,R_4= H-; X = μ-O-

Figure 1.10. Structural formula of the Ti^{IV}(salan) complexes used by Katsuki and co-workers.[41]

A year after the 2006 report on **L1.22**, the same authors improved this design by using a slightly different version of this catalyst (**L1.23**, see Figure 1.10) and adding a phosphate buffer to the reaction mixture.[42] These modifications translated into epoxide yields and enantiomeric excesses above 95% for a variety of alkene substrates.

In 2008, Bryliakov and co-workers[43] used Ti^{IV}(salan) **L1.22** and a structurally simpler version **L1.24** (see Figure 1.10) for the asymmetric sulfoxidation of benzyl phenyl sulfide, but with sulfoxide yields between 60-70 % and enantioselectivities not exceeding 88%. Both compounds exhibited slightly lower activities and enantioselectivities compared to those obtained with the Ti^{IV}(salen) compound **L1.7** (see Figure 1.3).

The aforementioned instances attest the growing potential of the titanium-based salan-type catalysts, but given their late inception as catalysts, the amount of reports dealing with this class of compounds is still limited.

1.2.1.6. $VO^{IV/V}$(salan) complexes

Identically to the Ti^{IV}(salan), the chemistry of $VO^{IV,V}$(salan) systems remains largely unexplored since their implementation as catalysts is relatively recent. In 2004, Zhu and co-workers showed the potential of *in situ* generated $VO^{IV,V}$(salan) catalysts **L1.25** to **L1.30** (see Figure 1.11) in asymmetric sulfoxidation of thioanisole.[44] The authors reported high yields and very high enantioselectivities with compounds **L1.25** and **L1.26**, but these results required the use of $CHCl_3$ as solvent.

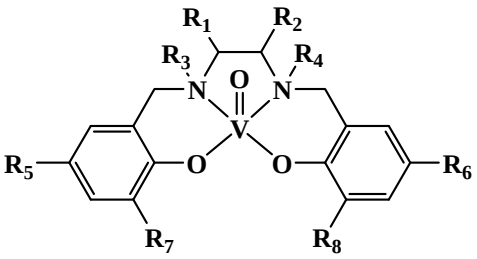

L1.25 R_1, R_2 = -$(CH_2)_4$-; R_3, R_4, R_5, R_6, R_7, R_8= H-

L1.26 R_1, R_2 = -$(CH_2)_4$-; R_3, R_4= H-; R_5, R_6, R_7, R_8= ^{t}Bu-

L1.27 R_1, R_2 = Ph-; R_3, R_4, R_5, R_6, R_7, R_8= H-

L1.28 R_1, R_2 = Ph-; R_3, R_4= H-; R_5, R_6, R_7, R_8= ^{t}Bu-

L1.29 R_1, R_2 = -$(CH_2)_4$-; R_3, R_4= Me-; R_5, R_6, R_7, R_8= H-;

L1.30 R_1, R_2 = -$(CH_2)_4$-; R_3, R_4, R_5, R_6 = H-; R_7, R_8= Ph-

Figure 1.11. Structural formulas of various $V^{IV}O$(salan) complexes.

Later in 2008, Bryliakov and Talsi[43] tested *in situ* generated compounds **L1.25** and **L1.30** also in asymmetric sulfoxidations, but reported results contrasting the ones published earlier by the group of Zhu, with compounds **L1.25** and **L1.30** giving significantly lower enantioselectivies (lower than 10%).

1.2.2. Tridentate NO_2 compounds

1.2.2.1. Aminoalcohol and aminoacid-derived Schiff base ligand precursors

The first well-known examples of catalysts derived from aminoalcohols are from Bolm and Bienewald[2] in 1995, with the application of *in situ* $V^{IV}O$ catalysts for the asymmetric oxidation of thioethers with hydrogen peroxide. The ligand precursor compounds reported by the authors can be considered a "half-salen", as it shares many features with the salen-type ligands and can also be conveniently prepared by condensation of the appropriate aminoalcohol and salicylaldehyde. Another characteristic of this system is that it relies on chiral aminoalcohols, with most, such as L-*tert*-leucinol, L-phenylalaninol or L-valinol, being derivatives of naturally occurring aminoacids. The use of naturally occurring aminoacids in place of aminoalcohols would be a logical step after the development of the aminoalcohol-based systems. Indeed, (i) aminoalcohols are more expensive than the respective parent aminoacids and (ii) the aminoalcohol chiral pool is more limited. Despite being structurally simpler than the salen or salan counterparts, these tridentate ligand precursor compounds have, in principle, an expanded range of possibilities for structural and electronic fine-tuning, considering the wider aminoacid and aminoalcohol chiral pool.

1.2.2.2. Aminoalcohol-derived Ti^{IV} Schiff base complexes

Given the notoriety of the aminoalcohol-derived $V^{IV}O$(Schiff base) system developed by the group of Bolm[2] and its subsequent iterations,[45,46] several authors attempted to develop a titanium variant of this system as a mean to supersede the Ti^{IV}(salen) systems while expanding the scope of application. In fact, the use of aminoalcohol-derived Ti^{IV}(Schiff base) catalysts predates the inception of the notorious $V^{IV}O$(Schiff base) system by two years. In 1993, Oguni and co-workers reported several L-*tert*-leucinol-, L-valinol- and L-phenylalaninol-based Ti^{IV}(Schiff base) catalysts (**L1.31** to **L1.39**, see Figure 1.12) for aldehyde cyanation with TMSCN.[47] The authors reported moderate cyanohydrin yields of ca. 60% with **L1.35** but very high enantiomeric excesses over 90%.

In 2000, Walsh and co-workers[48] reported several indanol-derived *in situ* Ti^{IV}(Schiff base) catalysts (**L1.39** to **L1.44**, see Figure 1.12) for aldehyde cyanation with TMSCN. The authors reported cyanohydrin yields similar to those reported earlier by Oguni and co-workers, but slightly higher enantiomeric excesses when the same substrate was used.

In 2004, Vilaivan and co-workers[49] reported several aminoalcohol-derived Ti^{IV}(reduced Schiff base) catalysts (**L1.45** to **L1.53**, see Figure 1.13) for imine cyanation (Strecker reaction), obtaining quantitative yields (over 99% yield of α-aminonitrile) and 98% enantioselectivities with compound **L1.45**.

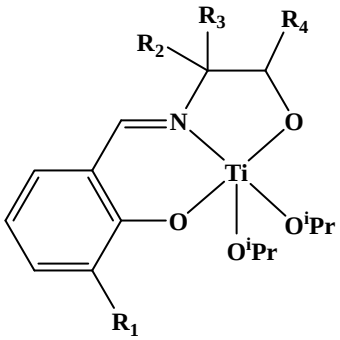

L31-38

L1.31 R_1= H-; R_2 = ^{i}Pr-; R_3 = H-; R_4 = H-

L1.32 R_1= H-; R_2 = ^{t}Bu-; R_3 = H-; R_4 = H-

L1.33 R_1= H-; R_2 = ^{i}Pr-; R_3 = H-; R_4 = Ph-

L1.34 R_1= ^{t}Bu-; R_2 = Me-; R_3 = H-; R_4 = H-

L1.35 R_1= ^{t}Bu-; R_2 = ^{i}Pr-; R_3 = H-; R_4 = H-

L1.36 R_1= ^{t}Bu-; R_2 = ^{t}Bu-; R_3 = H-; R_4 = H-

L1.37 R_1= ^{t}Bu-; R_2 = H-; R_3 = Ph-; R_4 = H-

L1.38 R_1= ^{t}Bu-; R_2 = ^{i}Pr -; R_3 = H-; R_4 = Ph-

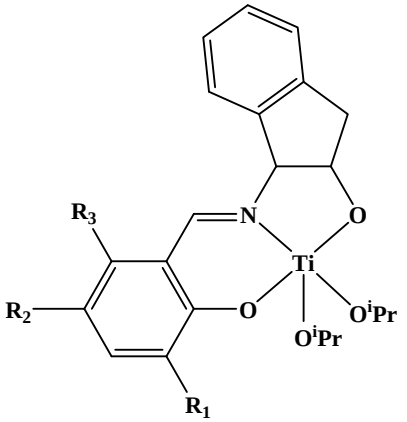

L47-53

L1.39 R_1= H-; R_2 = H-; R_3 = H-

L1.40 R_1= ^{t}Bu-; R_2 = ^{t}Bu-; R_3 = H-

L1.41 R_1= ^{t}Bu -; R_2 = H-; R_3 = H-

L1.42 R_1= MeO-; R_2 = H-; R_3 = H-

L1.43 R_1= Br-; R_2 = Br-; R_3 = H-

L1.44 R_1= ^{t}Bu-; R_2, R_3 = Ph-

Figure 1.12. Structural formulas of aminoalcohol-derived Ti^{IV}(Schiff base) complexes.

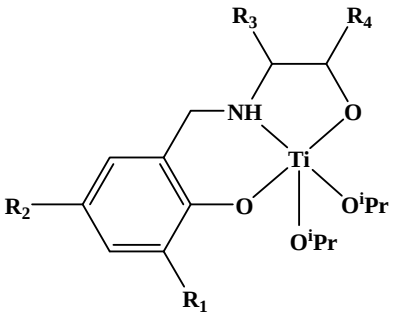

L1.45 R_1, R_2, R_4 = H-; R_3 = $PhCH_2$-
L1.46 R_1, R_2, R_4 = H-; R_3 = Me-
L1.47 R_1, R_2, R_4 = H-; R_3 = ^{i}Pr-
L1.48 R_1, R_2, R_4 = H-; R_3 = ^{t}Bu-
L1.49 R_1, R_2, R_4 = H-; R_3 = Ph-
L1.50 R_1, R_2, R_4 = H-; R_3 = ^{i}Bu-
L1.51 R_1, R_2, R_4 = H-; R_3 = ^{sec}Bu-
L1.52 R_1, R_2, R_3 = H-; R_4 = Me-
L1.53 R_1, R_2= ^{t}Bu-; R_4 = H-; R_3 = $PhCH_2$-

Figure 1.13. Structural formulas of the Ti^{IV}(reduced Schiff base) complexes reported by Vilaivan and co-workers.[49]

In 2006, Bryliakov and Talsi[50] used an *in situ* Ti^{IV} version of Bolm's system for the enantioselective sulfoxidation. The authors screened a variety of Schiff base ligands by employing different combinations of substituted salicylaldehydes and chiral aminoalcohols (**L1.54** to **L1.59**, including **L1.40**, see Figure 1.14), obtaining sulfoxide yields over 90%, but moderate enantioselectivities not exceeding 60%.

A relatively recent report by Chai and co-workers[51] shows the potential of a polymeric μ-oxo Ti^{IV}(Shiff base) compound (**L1.58**, see Figure 1.14) in asymmetric Strecker reactions. The authors emphasized the higher activity and enantioselectivity of the oligomeric μ-oxo Ti^{IV}(Schiff base) catalyst compared to the monomeric alkoxy derivatives reported earlier, which reflected in quantitative yields (over 99%) of α-aminonitrile and high enantiomeric excesses of ca. 90% after 15 minutes of reaction time.

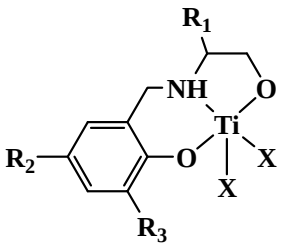

L1.54 R_1, R_2, R_3 = ^{t}Bu-; X= ^{i}PrO-

L1.55 R_1 = ^{t}Bu-; R_2, R_3= I-; X= ^{i}PrO-

L1.56 R_1 = ^{i}Pr-; R_2, R_3= ^{t}Bu-; X= ^{i}PrO-

L1.57 R_1 = Ph-; R_2=H-; R_3= ^{t}Bu-; X= ^{i}PrO-

L1.58 R_1 = ^{t}Bu-; R_2, R_3= H-; X= μ-O-

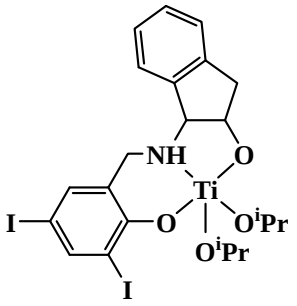

L1.59

Figure 1.14. Structural formulas of aminoalcohol-derived Ti^{IV}(Schiff base) complexes.

Another recent report by Jaworska and co-workers[52] includes a α-pinene-derived Ti^{IV}(Schiff base) catalyst **L1.60** (see Figure 1.15) for aldehyde cyanation with TMSCN. The authors reported very high enantiomeric excesses (99%) and high yields with *E*-cinnamaldehyde.

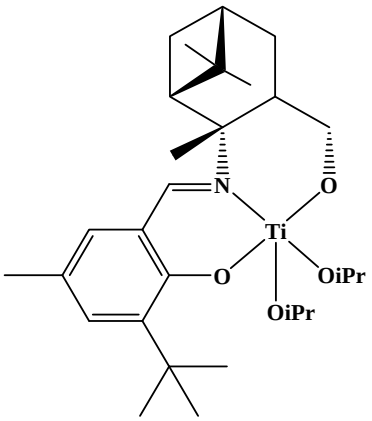

L1.60

Figure 1.15. Structural formula of the α-pinene Ti^{IV}(Schiff base) complex reported Jaworska and co-workers.[52]

In 2006, Bekolon and co-workers[53] reported a L-valinol-derived Ti^{IV}(Schiff base) catalysts **L1.61** and **L1.62** (see Figure 1.16) for several enantioselective processes. These compounds were described by the authors as a possible dinuclear Ti^{IV}(Schiff base) compound which effectively catalyzed the asymmetric cyanation of aldehydes.

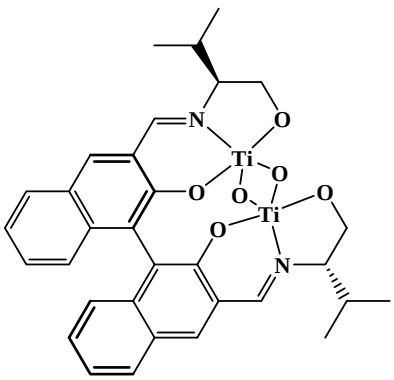

L1.61

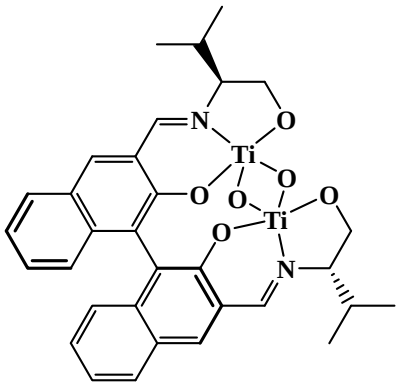

L1.62

Figure 1.16. Structural formulas of the aminoacid-derived Schiff base ligand precursor compounds reported by Bekolon and co-workers.[53]

1.2.2.3. Aminoalcohol-derived $V^{IV}O$ Schiff base complexes

The *tert*-leucinol based "half-salen" $V^{IV}O$ catalysts **L1.63** and **L1.64** (see Figure 1.17) developed by Bolm and Bienewald was remarkable in that it was able to carry out the asymmetric sulfoxidation of thioanisole, giving yields of 94% and enantiomeric excesses reaching 70%, using aqueous hydrogen peroxide as oxidant, with a catalyst loading of as little as 1 mol%.[2] The immediate advantages of this catalytic system were the use of readily available starting materials, the simple reaction conditions, the high activities and good enantioselectivities for this catalytic process. Moreover, it offered a departure from the earlier Kagan-Modena $Ti^{IV}(iPrO)_4$/diethyltartrate/TBHP system (TBHP = *tert*-butyl hydroperoxide) and higher enantioselectivities than the $V^{IV}O$(salen) system devised by the group of Fujita. [7,54]

Other authors tried to improve the initial ligand design by fine-tuning the steric and electronic properties of the ligand precursors. This was achieved either by modifying the aminoalcohol side chain or by modifying the aryl group substituents. Berkessel and co-

workers[45] used the tridentate "half-salen" compound **L1.65** (see Figure 1.17) also for asymmetric sulfoxidations, obtaining sulfoxide yields of 92% and enantiomeric excesses of 78%.

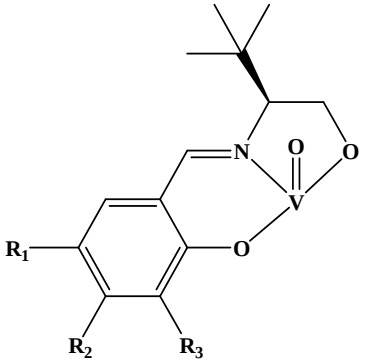

L1.63 R_1 =NO_2-; R_2 = H; R_3= ^{t}Bu-

L1.64 R_1, R_3 = ^{t}Bu-; R_2 = H-

L1.65 R_1, R_2 = -C_4H_4-; R_3= naphthyl-

L1.66 R_1, R_3 = I-; R_2 = H-

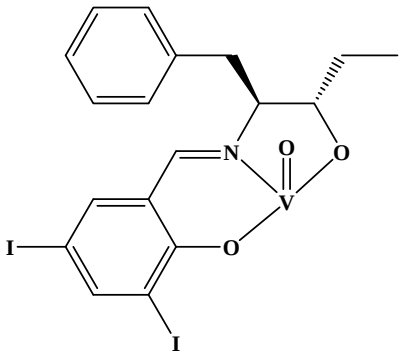

L1.67

Figure 1.17. Structural formulas of the aminoalcohol-derived $V^{IV}O$(Schiff base) complexes used in asymmetric sulfoxidations.

Noteworthy is the significant improvement over the original system that was achieved by Jackson and co-workers[46] with the use of 3,5-diiodosalicylaldehyde, while maintaining *tert*-leucinol as the chiral aminoalcohol precursor (**L1.66**, Figure 1.17). This variant proved highly active and enantioselective, giving sulfoxide yields above 85% and enantiomeric excesses surpassing 95% for a variety of thioether substrates.

In 2009, Li and co-workers[55] confirmed the effectiveness of this compound class in the asymmetric thioether oxidation. The author reported nearly enantiopure sulfoxides and yields as high as 80%, by using **L1.67** (see Figure 1.17) as catalyst.

Despite the relatively large amount of reports regarding aminoalcohol-derived $V^{IV}O$(Schiff base) compounds, the scope is mostly focused on asymmetric sulfoxidation, whereas the respective titanium analogues demonstrated a wider applicability.

1.2.2.4. Aminoacid-derived Ti^{IV} Schiff base complexes

In 1992, Inoue and co-workers[56] reported aminoacid-derived *in situ* Ti^{IV}(Schiff base) catalysts for alkene epoxidation, which used compounds **L1.68** to **L1.70** as ligands (see Figure 1.18). These *in situ* catalysts were employed in the epoxidation of various terpenoid-class substrates with 1,1-diphenylethyl hydroperoxide (DPEHP), giving moderate to high yields and enantioselectivities.

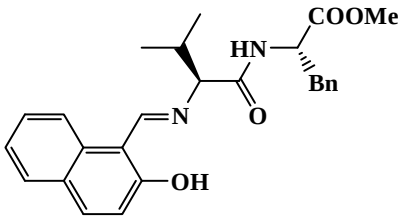

L1.68

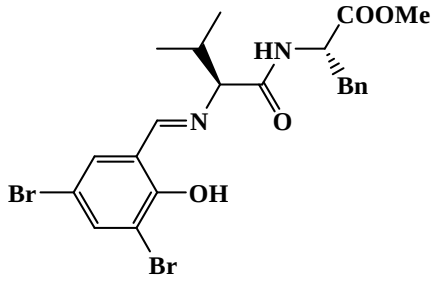

L1.69

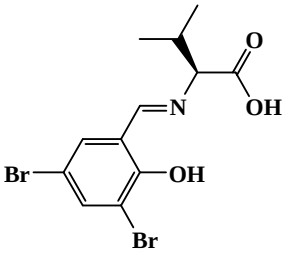

L1.70

Figure 1.18. Structural formulas of the aminoacid-derived Schiff base ligand precursor compounds reported by Inoue and co-workers.[56]

Later, in 2006, You and co-workers[57] reported dipeptide-based *in situ* Ti^{IV}(Schiff base) catalysts for the asymmetric pinacol coupling of aldehydes, using compounds **L1.71** and **L1.72** as ligands (see Figure 1.19). This system was noteworthy due to its ability to give 1,2-diol yields of ca. 90% and enantiomeric excesses of ca. 70%, while giving negligible amounts of the achiral *meso* 1,2-diol.

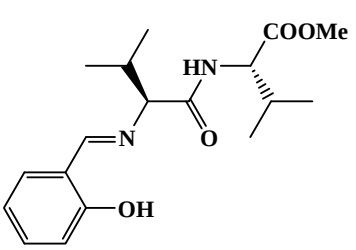

L1.71

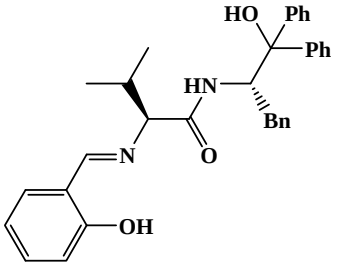

L1.72

Figure 1.19. Structural formulas of the aminoacid-derived Schiff base ligand precursor compounds reported by You and co-workers.[57]

1.2.2.5. Aminoacid-derived $V^{IV/V}O$ Schiff base complexes

In 1989, Fujita and co-workers[58] reported several aminoacid-derived $V^{V}O$(Schiff base) catalysts (**L1.73** to **L1.75**, see Figure 1.20) for the asymmetric sulfoxidation of thioanisole, using TBHP as the terminal oxidant. The authors reported moderate to high sulfoxide yields but low enantioselectivities not exceeding 14% with compound **L1.73**.

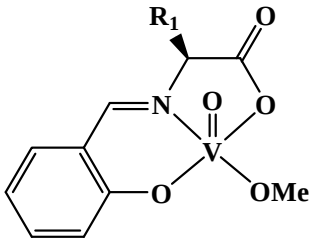

L1.73 R_1 = Me-
L1.74 R_1 = Bn-
L1.75 R_1 = ^{i}Pr-

Figure 1.20. Structural formulas of the aminoacid-derived $V^{V}O$(Schiff base) compounds reported by Fujita and co-workers.[58]

In 2004, Maeda and co-workers[59] further explored the aminoacid-derived $V^{IV}O$ and $V^{V}O$(Schiff base) systems and reported compounds **L1.76** to **L1.84** (see Figure 1.21), describing their application in asymmetric thioanisole oxidation. However, despite obtaining sulfoxide yields greater than 90% in the majority of cases, enantiomeric excesses would not exceed 20% with the L-lysine derived catalyst **L1.82** which gave the best results in terms of enantioselectivity.

There are important differences between this system and the aminoalcohol-derived $V^{IV}O$(Schiff base) systems previously mentioned. Maeda uses a $V^{IV}O$(Schiff base)

precatalyst, whereas the aminoalcohol versions systems rely mostly on *in situ* generation of the catalysts, often using an excess of ligand. The main structural difference between the aminoacid and the aminoalcohol-based systems resides in the donor atom group set: the metal centre is coordinated to a carboxylate oxygen donor atom instead of an alcohol oxygen donor atom. This factor is responsible for the significant difference in enantioselectivities for asymmetric thioether oxidation.

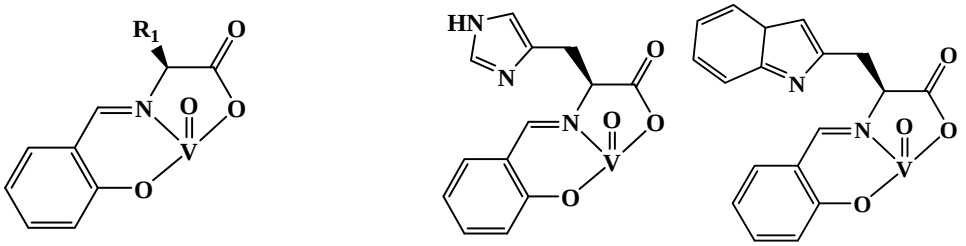

L1.76 R_1=H- **L1.77** R_1= ^{i}Pr- **L1.83** **L1.84**
L1.78 R_1=Me **L1.79** R_1= ^{i}Bu-
L1.80 R_1=^{sec}Bu- **L1.81** R_1=$CH_3SCH_2CH_2$
L1.82 R_1=$H_2NCH_2(CH2)_3$-

Figure 1.21. Structural formulas of the aminoacid-derived $V^{V}O$(Schiff base) compounds reported by Maeda and co-workers.

Unlike the aminoalcohol counterparts, the aminoacid-derived $V^{IV}O$(Schiff base) compounds saw notable application beyond asymmetric sulfoxidation. In 2002, Gong and co-workers[60a] reported a L-valine-based $V^{IV}O$ version of compound **L1.61** for the oxidative coupling of naphthol, using O_2 as the oxidant (Scheme 1.12). This system was further refined by Sasai and co-workers by replacing L-valine by L-*tert*-leucine as the aminoacid precursor (**L1.85**, see Figure 1.22).[60b,60c]

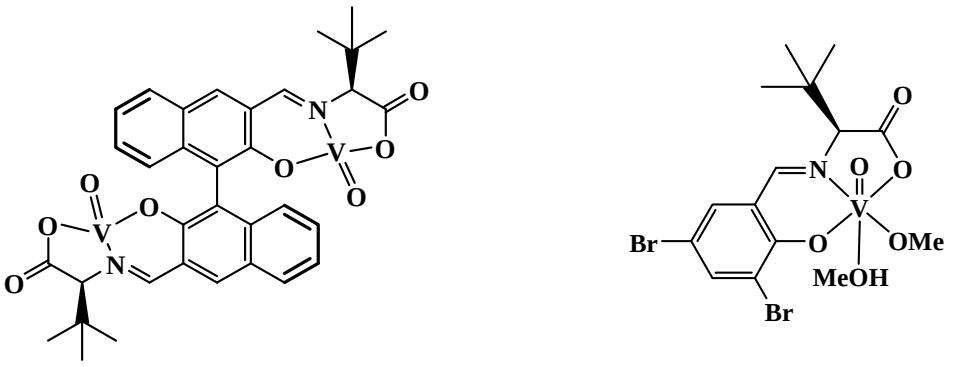

L1.85 **L1.86**

Figure 1.22. Structural formulas of L-*tert*-leucine-derived $V^{IV}O$(Schiff base) compounds.

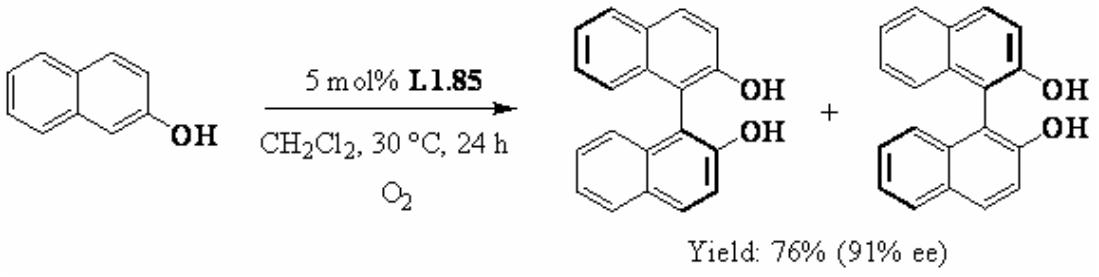

Scheme 1.12. $V^{IV}O$(Schiff base)-promoted asymmetric oxidative coupling of naphthol.

Recently, Chen and co-workers[61] reported the L-*tert*-leucine $V^{V}O$(Schiff base) compound **L1.86** (see Figure 1.22) for asymmetric aerobic oxidation of α-hydroxy-ketones to 1,2-diketones. The authors reported nearly enantiopure α-hydroxy-ketones after resolution reactions with **L1.86**.

1.3. Heterogeneous catalysts

Despite the great potential of the homogeneous aminophenol class of complexes, they still fail to make a significant impact in the industry of fine chemical synthesis. One reason lies in the difficulty of recovery and regeneration of an often expensive chiral catalyst. Another reason is that most of the catalysts still require hazardous organic solvents to function as required. In the case of asymmetric oxidations, some catalysts have the added disadvantage of requiring expensive oxidants such as iodosylarenes or organic hydroperoxides, but most recent systems already use cheaper, environmentally benign oxidants such as H_2O_2. The recovery problem can be solved by immobilizing the catalyst on an insoluble solid, thus creating a heterogeneous catalyst that can be easily recovered from the reaction mixture. Such catalysts, however, tend to exhibit lower performances compared to the respective homogeneous versions, as immobilization implies some degree of interference with the catalyst structure. The following sections will briefly describe the most commonly applied immobilization methods, some relevant to the present work, and how those methods are applied to various transition metal catalysts.

1.3.1. Immobilization on solid supports

The most convenient way to improve the recyclability of a homogeneous catalyst is through immobilization on an insoluble solid matrix. This can be achieved primarily by four different methodologies: adsorption, encapsulation, covalent tethering and electrostatic interaction. The immobilization by adsorption relies on the van der Waals interactions between the support matrix and the catalyst. Encapsulation is the encasing of a catalyst inside a rigid superstructure such as the zeolite-Y aluminosilicate supercages. Like the adsorption method, encapsulation normally does not require structural modification of the catalyst structure and only imposes constraints on molecular movement. In contrast, covalent tethering imposes structural modification to the catalyst structure. This usually is done by introducing adequate functional groups to the catalyst structure that act as covalent anchoring points to the support matrix. The degree of structural alteration compounded with the movement and spatial arrangement constrains often imposed may result in lowered catalyst performance compared to the homogeneous variant. Electrostatic immobilization is similar to adsorption, but electrostatic ion-ion interactions are involved instead of weak van der Waals interactions. The following sections will describe some of the most notable examples where these techniques were successfully applied.

1.3.1.1. Polymer supported catalysts

Of the available solid polymer supports, polystyrene is the most widely used due to its versatility and durability. Functionalized polystyrene can be prepared by copolymerizing styrene with a wide range of adequately 4-substituted vinylbenzenes. For instance, chloromethylated polystyrene, also known as Merrifield resin,[62] serves as a very versatile platform for the development of polymer-supported catalysts. Because the chloromethyl group easily undergoes S_n2 substitution reactions with a wide range of nucleophiles, the polymer can be easily modified to tailor-made specifications. A cross-linker is usually added (divinylbenzene) to ensure polymer insolubility, particularly in

solvents known to dissolve polystyrene. Well-known derivatives of this resin include the Wang resin (*p*-benzyloxybenzyl alcohol substituted polystyrene).[63]

Indeed, the advantageous properties of cross-linked polystyrene were soon used in the development of heterogeneous aminophenolate-class catalysts. Notable instances where polystyrene was successfully used as a solid support include the 1996 report by Salvadori and co-workers, [64] describing a polystyrene supported version of Jabosen's Mn^{III}(salen) catalyst for asymmetric epoxidation. The authors attempted to address the serious shortcoming of this well-known catalyst: its tendency to form inert di-μ-oxo-Mn^{IV}. The authors emphasized that the low local concentration of Mn^{III}(salen) in the rigid polymer matrix can minimize the formation of the undesired di-μ-oxo-Mn^{IV} species, as the monomeric Mn^{III}(salen) units have a restricted movement and are kept apart. The Mn^{III}(salen) compound **L1.87** (see Figure 1.23) contained vinyl groups at the C5 and C5' carbons, making it polymerizable with styrene and divinylbenzene. In the presence of *m*-chloro-peroxybenzoic acid (mCPBA) / *N*-methylmorpholine-*N*-oxide (NMO), this immobilized catalyst promoted styrene epoxidation, giving 99% epoxide yield and 15% enantiomeric excess. With *cis*-β-methylstyrene, yields reached 94% with a maximum enantiomeric excess of 41%. The authors successfully recycled the catalyst up to five times without loss of performance. Nevertheless, in terms of enantioselectivity, the immobilized catalyst was still very inferior to its homogeneous version.

In an attempt to make the immobilized catalyst mimic its homogeneous counterpart, spacer groups were introduced between the active site and the support (**L1.88** and **L1.89,** see Figure 1.24). This had a positive effect in overall enantioselectivities of styrene epoxidation and *cis*-methylstyrene, increasing enantiomeric excesses to 26% and 62%, respectively.[65]

Sherrington and co-workers[66] further improved this design on the basis that proximity of the metal centre to the rigid support possibly inhibited a non-planar asymmetric transition state crucial to the enantioselective process. While their initial hypothesis was correct, their catalyst would greatly degrade after reuse. Seebach and co-workers[67] reported Mn^{III}(salen) catalysts immobilized in a dendritic fashion (**L1.90** see Figure 1.23) which was capable of epoxidizing 1-phenylcyclohexene in 75% yield and 84% enantiomeric excess, also under the same conditions reported by Salvatori and co-

workers. The authors successfully recycled **L1.90** up to ten times without loss of performance.

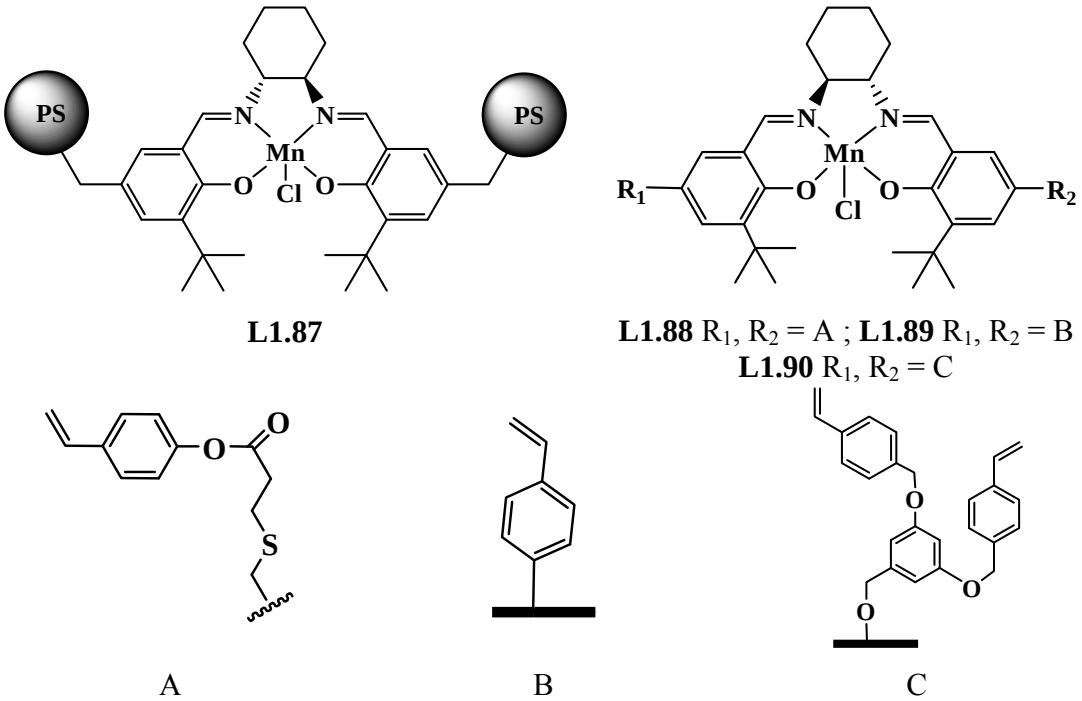

L1.87

L1.88 R_1, R_2 = A ; **L1.89** R_1, R_2 = B
L1.90 R_1, R_2 = C

Figure 1.23. Structural formula of polystyrene supported Mn^{III}(salen) catalysts.

More recently, Hiti and co-workers[68] reported a polystyrene-supported Mn^{III}(salen) Katsuki-type catalyst **L1.91** (see Figure 1.24) capable of epoxidizing 1,2-dihydronaphthalene, giving epoxide yields of 70% and enantiomeric excesses reaching 94% in the presence of 4-phenylpyridine-N-oxide (4-PPNO), using NaOCl as the terminal oxidant. The authors hypothesized that the bulky ligand may have prevented the formation of inactive μ-oxomanganese(IV) species and the single covalent bond to the support ensured that the active site would have a behavior similar to its homogeneous counterpart. While the reactions were slow, this catalyst could be reused up to six times.

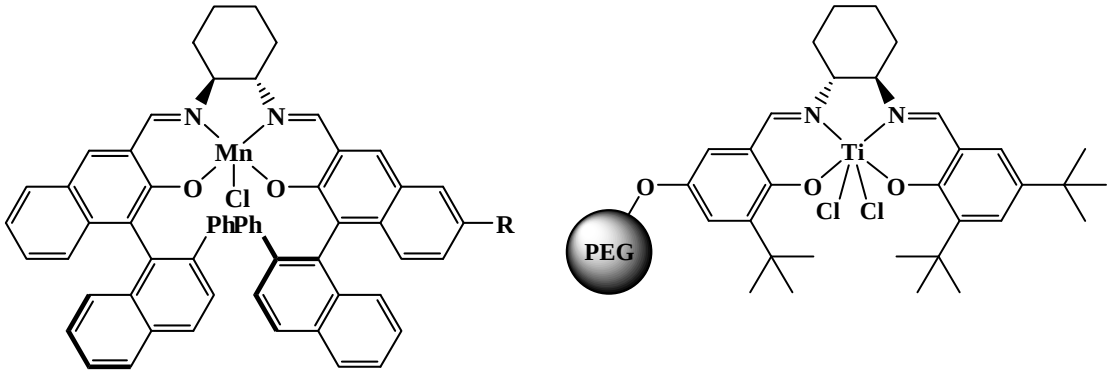

L1.91 R= PS-PhCOO$(CH_2)_3$- **L1.92**

Figure 1.24. Polystyrene-supported Mn^{III}(salen) and Ti^{IV}(salen) catalysts.

The examples above show how an important catalyst, but with recovery problems, can be modified to be reused multiple times while maintaining the effectiveness of the original homogeneous system. The implementation of polymer supports was also attempted in other catalytic systems.

In respect to polymer supported Ti^{IV}(salen) and Ti^{IV}(salan) catalysts, the amount of work carried out regarding these compound classes is scarce.

In 2005, Venkatamaran and co-workers[69] reported the polyethyleneglycol (PEG) supported Ti^{IV}(salen) catalyst **L1.92** (see Figure 1.25) for the asymmetric cyanation of aldehydes. The authors reported quantitative cyanohydrins yields (>99%) and enantiomeric excesses reaching 86%.

Likewise, the amount of reports regarding polymer supported, aminoalcohol and aminoacid derived Ti^{IV}(Schiff base) catalysts is limited. In 2001, Jackson and co-workers[70] reported a polystyrene supported, L-threonine-derived Ti^{IV}(Schiff base) catalyst **L1.93** (see Figure 1.25) for asymmetric sulfoxidation of thioanisole. The authors reported a quantitative sulfoxide yield (>99%) and enantiomeric excess of 64% for **L1.93**. Moreover, the authors successfully recycled the catalyst four times without apparent loss of performance.

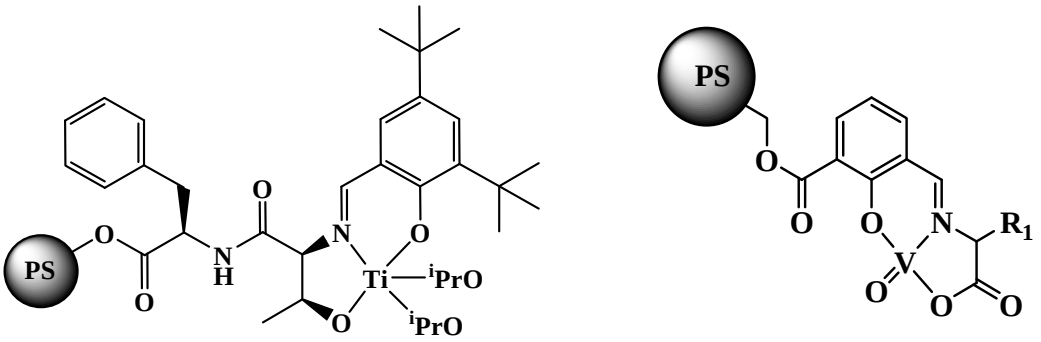

L1.93

L1.94 R_1 = Me-
L1.95 R_1 = ^{sec}Bu-

Figure 1.25. Polystyrene-supported aminoalcohol-derived Ti^{IV}(Schiff base) and aminoacid-derived $V^{IV}O$(Schiff base) catalysts.

The effort to develop aminophenolate class $V^{IV}O$ catalysts has been greater, however, with most of the published reports focusing on the development of heterogeneous $V^{IV}O$(salen) catalysts, which have found application in several processes, enantioselective or otherwise.

Notable examples include the extensive work carried out by the groups of Maurya and Costa Pessoa. The authors reported various polystyrene supported aminoalcohol and aminoacid derived $V^{IV}O$(Schiff base) catalysts for a wide range of oxidation processes.[71] Aminoacid-derived compounds **L1.94** and **L1.95** (see Figure 1.25) were used in the oxidation of cyclohexene using hydrogen peroxide as terminal oxidant (Scheme 1.13) and were successfully reused three times without loss of activity.[72]

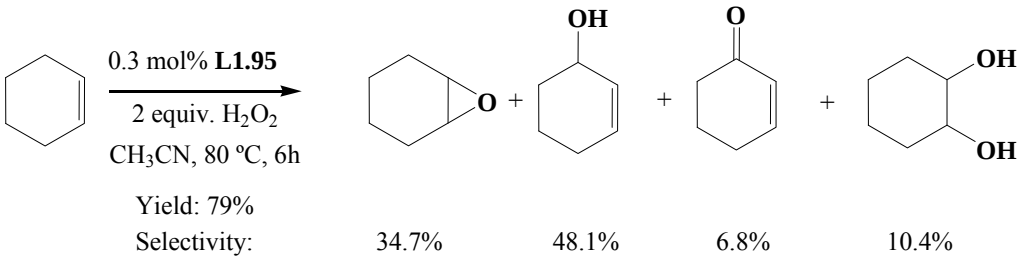

Scheme 1.13. Polymer-supported $V^{IV}O$(Schiff base)-promoted oxidation of cyclohexene.

The authors also reported several aminoalcohol derived $V^{IV}O$(Schiff base) catalysts (**L1.96** to **L1.99**, see Figure 1.26) for the oxidation of styrene with hydrogen peroxide.[72]

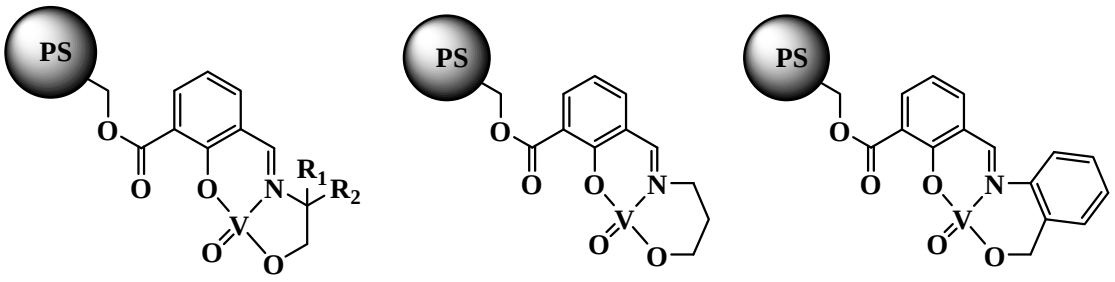

L1.96 R_1 = Me-; R_2 = H- **L1.98** **L1.99**
L1.97 R_1, R_2 = Me-

Figure 1.26. Polystyrene-supported $V^{IV}O$(Schiff base) catalysts reported by Maurya and co-workers.

Though compounds **L1.96** to **L1.99** lack chirality, these are remarkable for their ability to promote oxidative cleaving and dihydroxylation of alkenes. Common reagents used in these processes are either stoichiometric $NaIO_4$ and/or catalytic OsO_4, being the latter used for the Upjohn and Sharpless alkene dihydroxylations.[73] These processes are of great importance in fine chemical synthesis, particularly in pharmaceutical industry, where the production of most active ingredients often involves oxidative cleaving and/or dihydroxylation of carbon-carbon double bonds.[74] While Maurya and co-workers employed harsher conditions than those typically used for the osmium-catalyzed processes to achieve oxidative cleaving and dihydroxylation of alkenes, the major advantages are the replacement of the notoriously toxic osmium tetroxide catalyst by a recyclable heterogenenized catalyst and the use of hydrogen peroxide as oxidant instead of $NaIO_4$ or O_3.

The same group also reported a recyclable L-cysteine derived $V^{IV}O$(Schiff base) catalyst **L1.100** (see Figure 1.28) for oxidative amination of styrene using diethylamine and imidazole (Scheme 1.14). This system is also remarkable due to its ability to promote carbon-nitrogen bond formation using non-activated alkenes, which are known to be generally resistant to nucleophilic attack.[75] Moreover, this type of process is commonly associated with expensive heavier late metal catalysts (*eg*. Pd, Rh and Ru).[76] The authors emphasized the preferable formation of anti-Markovnikov products by **L1.100**.

Development of heterogeneous versions of well-known $V^{IV}O$-based catalysts has also received attention. In 2004, Sartori and co-workers[77] reported polystyrene-supported versions of chiral aminoalcohol-derived $V^{IV}O$(Schif base) catalysts for asymmetric sulfoxidation of thioanisole. In fact, compound **L1.101** (see figure 1.27) was a

polystyrene supported version of the $V^{IV}O$(Schiff base) catalyst reported in 1995 by Bolm and Bienewald.[2] Sulfoxide yields of 75% and enantiomeric excesses of 56% were obtained, which are comparable to the result obtained initially by the group of Bolm. In addition, **L1.101** could be used up to four times with minimal loss of activity or selectivity.

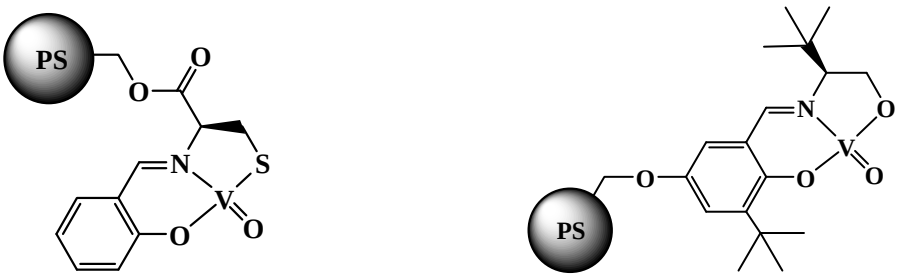

L1.100 **L1.101**

Figure 1.27. Polystyrene-supported L-aminoacid-derived $V^{IV}O$(Schiff base) catalysts.

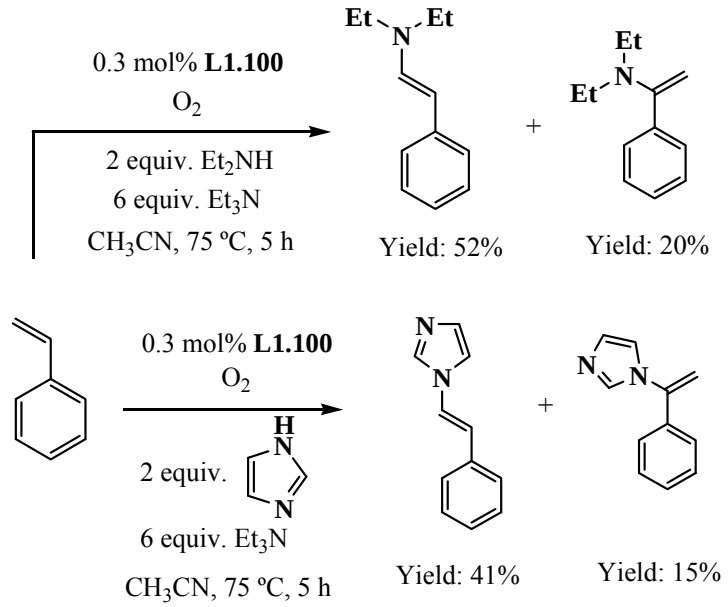

Scheme 1.14. Polymer-supported $V^{IV}O$(Schiff base)-promoted oxidative amination.

Other authors focused in the immobilization of late transition metal aminophenolate catalysts. Heterogeneous copper catalysts, being based on a biologically relevant, relatively cheap and readily available late transition metal, have naturally received increased attention. A notable example is the polystyrene-supported Cu^{II}(salen) catalyst

L1.102 (see Figure 1.28) for the asymmetric addition of TMSCN to aromatic ketones, reported by Rajagopal and co-workers in 2010.[78] This system was capable of giving cyanohydrin yields above 80% and enantiomeric excesses ranging between 52% and 84%. The authors successfully recycled **L1.102** five times, but experienced a 15% loss of enantioselectivity (from 80% to 65%) after the fifth run.

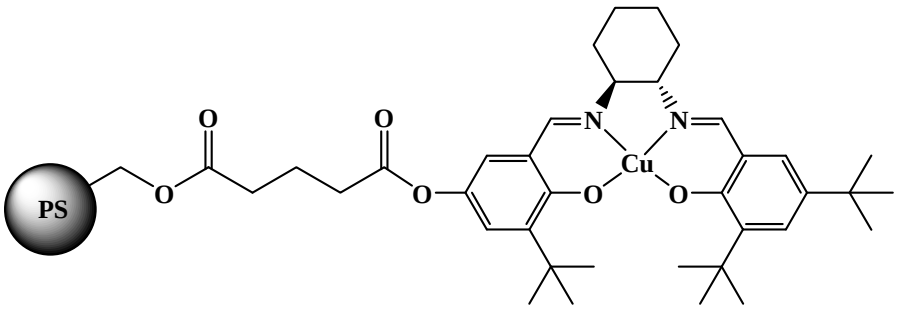

L1.102

Figure 1.28. Polystyrene-supported Cu^{II}(salen) catalyst used by Rajagopal and co-workers.

Polystyrene remains one of the most popular solid supports used for catalyst immobilization due to several reasons: it is a cheap and readily available material; it is chemically inert but easily modifiable. Polystyrene resins have disadvantages: they are not biodegradable; polystyrene is a brittle material and highly cross-linked rigid resins tend to break down after a few uses. Nevertheless, the chemical inertness and versatility of polystyrene far outweigh its disadvantages.

1.3.1.2. Encapsulated catalysts

Most of the work done with encapsulated catalysts regards Mn^{III}(salen) catalysts for asymmetric epoxidation, which reflects the importance of this system. In this technique, the catalyst is confined within the supercages of a zeolite or other mesoporous solid. The concept behind this immobilization technique is to obtain a heterogeneous catalyst possessing all the characteristics of the homogeneous counterpart by minimizing structural alteration to the complex itself. One well-known example is the immobilization of the Mn^{III}(salen) catalyst **L1.103** (see Figure 1.29) within zeolite Y supercages reported by Corma and co-workers in 1997.[79] The zeolite is first partially ion-exchanged with Mn^{II} ions, followed by sequential additions of the ligand building blocks. This technique is

known as the "ship-in-a-bottle" immobilization. This catalyst was tested in the epoxidation of *cis*-β-methylstyrene and indene with NaOCl as oxidant. The reaction was slower as a result of the increased difficulty of reagent diffusion within the zeolite superstructure. The moderate enantiomeric excesses obtained could also be a result of the rigidity imposed on the catalyst structure by the close-fit zeolite superstructure, which may interfere with the crucial asymmetric transition state.[80]

In a more recent report, Li and co-workers used a mesoporous silica encapsulated version of Jacobsen's Mn^{III}(salen) catalyst (**L1.104**, see Figure 1.30) in the asymmetric epoxidation of 6-cyano-2,2-dimethylchromene with NaOCl.[81] The authors obtained epoxide yields greater than 99% and enantiomeric excesses of 90%, surpassing the activity and enantioselectivity displayed by the homogeneous version for the same substrate (97% epoxide yield and 80% enantiomeric excess). The authors also reported gradual loss of activity and enantioselectivity with successive recycling.

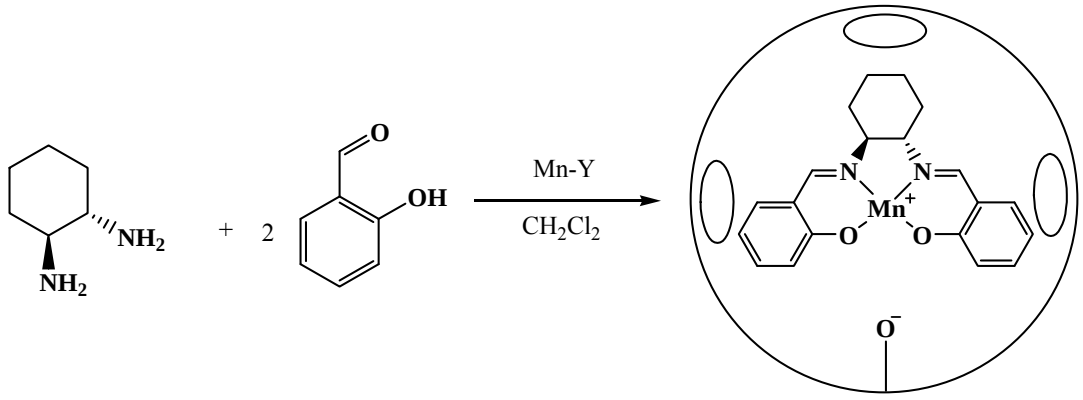

L1.103

Figure 1.29. Zeolite Y encapsulated Mn^{III}(salen) catalyst reported by Corma and co-workers.

Regarding encapsulated $V^{IV}O$ and Cu^{II} aminophenolate-class catalysts, extensive work has been carried out by the group of Maurya. In 2003, Maurya and co-workers[82] reported zeolite Y encapsulated $V^{IV}O$(salen) catalysts **L1.105** to **L1.106** (see figure 1.31) for the oxidation of phenol with hydrogen peroxide (Scheme 1.15).

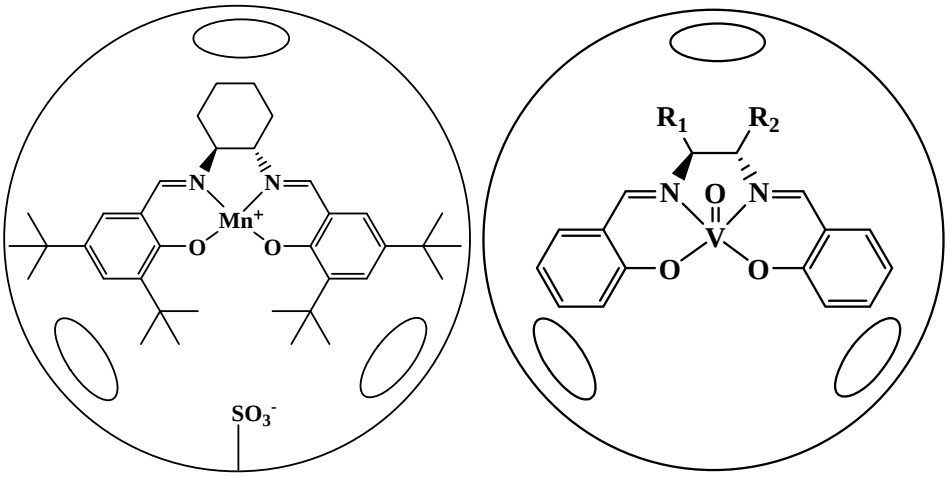

L1.104

L1.105 R_1 = -$(CH_2)_4$-

L1.106 R_1 = H-; R_2 = Me-

Figure 1.30. Structural formulas of encapsulated Mn^{III}(salen) and $V^{IV}O$(salen) catalysts.

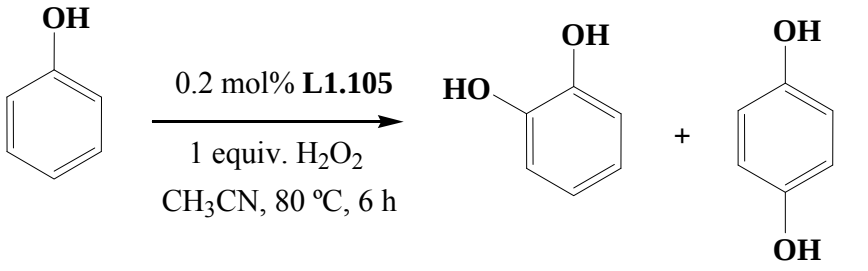

Scheme 1.15. Encapsulated $V^{IV}O$(salen)-promoted phenol oxidation.

Later, in 2007, the same group used compound **L1.105** in the oxidation of styrene and cyclohexene.[83] The authors noted the tendency of **L1.105** to promote oxidative cleaving of carbon-carbon double bonds and dihydroxylation in the case of styrene. For cyclohexene, **L1.105** favored allylic oxidation products. In addition, **L1.105** was also tested in the oxidation of cyclohexane with hydrogen peroxide (Scheme 1.16).

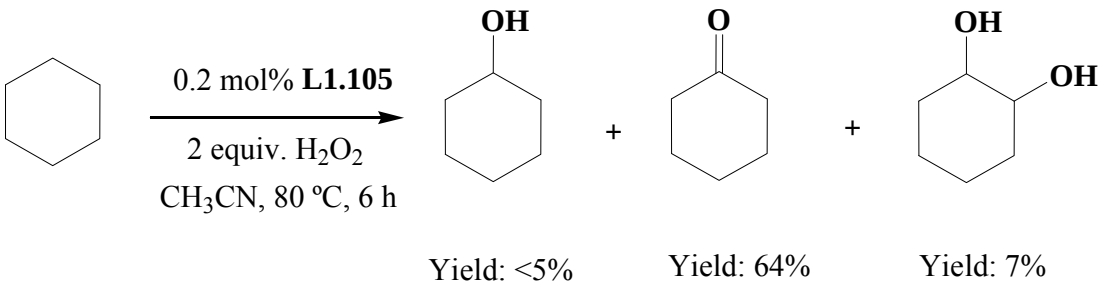

Scheme 1.16. Encapsulated $V^{IV}O$(salen)-promoted cyclohexane oxidation.

In the same year, Maurya and co-workers[84] reported encapsulated Cu^{II}(salen) compounds **L1.107** and **L1.108** (see Figure 1.31) for the oxidation of styrene, cyclohexene and thioanisole with hydrogen peroxide. The authors observed, in the case of styrene, the tendency of compounds **L1.107** and **L1.108** to exclusively favor the formation of oxidative cleaving products, despite the lower activity of both catalysts under similar conditions used for **L1.105**. In the case of cyclohexene, compounds **L1.107** and **L1.108** exhibited high activities, giving cyclohexene conversions greater than 80% after 6 hours. Like compound **L1.105**, both favored allylic oxidation, although the authors observed a greater amount of the respective epoxide.

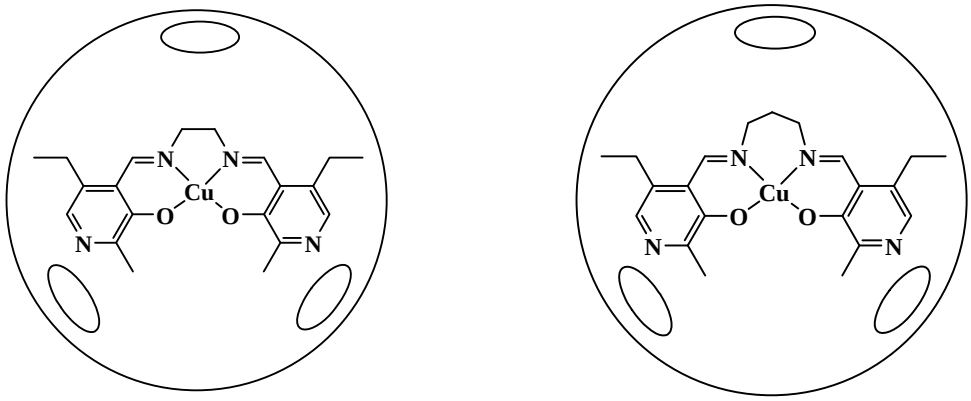

L1.107 **L1.108**

Figure 1.31. Zeolite Y encapsulated Cu^{II}(salen) catalyst reported by Maurya and co-workers.[84]

The authors also observed that replacing H_2O_2 with TBHP resulted in a significantly lowered activity. Compounds **L1.107** and **L1.108** proved particularly active in the

sulfoxidation of thioanisole, since the authors employed as little as 0.04 mol% of catalyst to achieve *ca*. 80% thioether conversion in 3 hours.

Encapsulation remains an effective alternative to covalent tethering given that structural modification of the catalyst is rarely required and the support often exhibits greater chemical and mechanical resistance than polymer supports. In addition, aluminosilicates are ubiquitous naturally occurring materials, making these a cost effective alternative to polymer supports. One disadvantage of zeolites is the rigid and relatively small supercage pore size and volume. As a result, encapsulation of catalysts bearing bulky ligand structures is often impaired. Manipulation of the zeolite supercage structure can result in loss of crystallinity and degradation of the material.

1.3.1.3. Silica supported catalysts

Silica supports, namely ordered mesoporous silicas, present an alternative to zeolites in many aspects: well-ordered, uniform, but tunable pore arrays; large surface areas; the material allows chemical modification without pore and superstructure degradation. Mesoporous silicas MCM-41 and SBA-15 are two of the most widely used types of siliceous materials for the development of heterogeneous catalysts. Moreover, since silica can be chemically modified, these materials bridge the gap between polymer and zeolite supports.

The terminal silanol groups allow catalyst immobilization through covalent bonding or ionic interaction and this technique is recognized as one of the best options for catalyst immobilization. Choudary and co-workers[85] reported various chiral Mn^{III}(salen) catalysts anchored on silica gel through covalent bonding with a propyl spacer. Of these, catalyst **L1.109** (see Figure 1.32) epoxidized styrene in high yields (95% epoxide) but low enantioselectivities (15% ee), when using mCPBA as terminal oxidant and *N*-methyl morpholine-*N*-oxide (NMO) as co-oxidant. Better results were obtained in the epoxidation of *cis*-β-methylstyrene under the same conditions (76% epoxide, 36% ee). The authors recycled the catalyst three times without decrease in enantioselectivity. Improvements were observed when using mesoporous materials such as MCM-41. The pore diameters of these siliceous materials allow encapsulation without the steric

constraints of the zeolites and the surface of this type of support allows immobilization through covalent bonding.

Another successful example is the MCM-41 immobilized chiral Mn^{III}(salen) complex **L1.110** (see Figure 1.32) and its application in alkene epoxidation with m-CPBA/NMO, reported by Kim and co-workers.[86] Here, the authors immobilized the catalyst onto a silica or siliceous support in a stepwise manner, by using a diformylphenol as a building block for the ligand and bridge to the support. The surface of the mesoporous support was modified with (3-aminopropyl)trimethoxysilane, thus yielding an aminated MCM-41 support. These free amine groups were then condensed with the free formyl groups of the complex, effectively binding the complex to the support. The authors obtained styrene epoxide in 92% yield and 89% ee at -78ºC, after 4h of reaction. The results obtained with the homogeneous version, under the same conditions, were 97% yield and 84% ee.

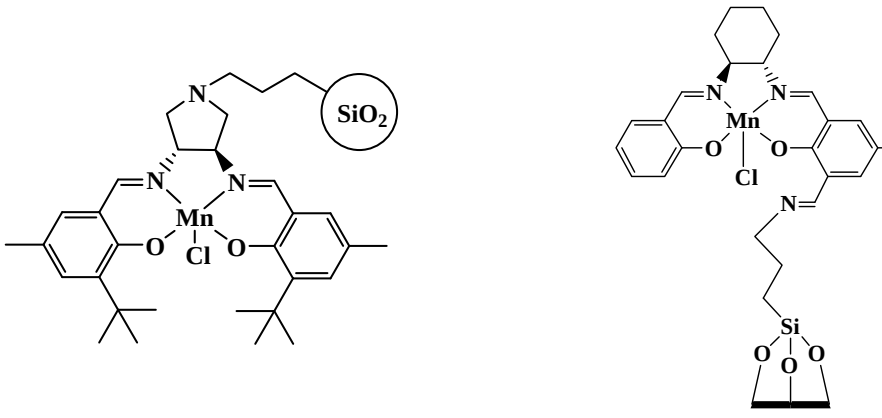

L1.109 **L1.110**

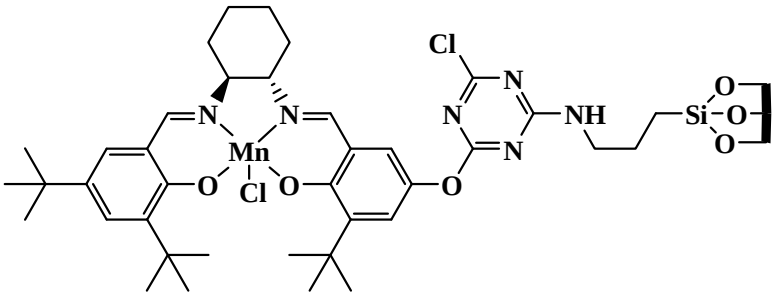

L1.111

Figure 1.32. Silica supported Mn^{III}(salen) and catalysts.

In 2006, Freire and co-workers[87] reported a Mn^{III}(salen) catalyst supported onto a hexagonal mesoporous silica support, using cyanuric chloride as a mediator between the amine functionalized silica and the catalyst (**L1.111**, see Figure 1.32). The authors obtained α-methylstyrene epoxide in 24% yield and 18% ee at 0ºC, after 24h of reaction using NaOCl as oxidant. The catalyst was employed in a second catalytic run, giving slightly higher enantioselectivities. The results obtained with the homogeneous version under the same conditions were 83% epoxide yield with 60% enantiomeric excess.

Apart from the extensive effort done to turn Mn^{III}(salen) systems recyclable, Corma and co-workers[88] used a silica-supported chiral $V^{IV}O$(salen) catalyst **L1.112** (see Figure 1.33) in the asymmetric aldehyde cyanation. Similarly as described before, the siliceous material was modified with an alkoxysilane. In this case, (3-mercaptopropyl)trimethoxysilane was used to impregnate the surfaces of amorphous silica, ITQ-2 and MCM-41 with nucleophilic thiol groups. The salen ligands contained chloromethyl groups in the C5 phenolate moiety carbons which reacted with an ω-unsaturated long-chain alcohol, which in turn reacted with the free thiol groups present on the support surface.

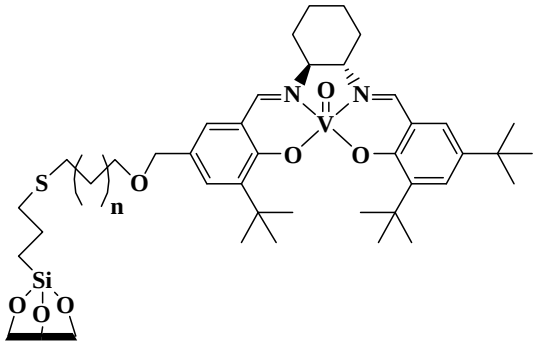

L1.112

Figure 1.33. Silica supported $V^{IV}O$(salen) catalyst used by Corma and co-workers.[88]

The authors reported a maximum cyanohydrin yield of 70% and 63% enantiomeric excess for the asymmetric addition of TMSCN to benzaldehyde in dichloromethane, at room temperature. When chloroform was used instead of dichloromethane, at 0ºC, the yields and enantiomeric excesses improved (78% conversion, 85% ee).[88]

1.3.2. Ionic liquids as supports

The ionic liquids are regarded as potential replacements for conventional, volatile organic solvents used in chemical processes. They have a near-zero vapor pressure and are non-flammable. The level of interaction with other solvents can be fine-tuned with adequate cations or anions. For example, an ionic liquid that is immiscible with an organic solvent could prove useful in the process of extracting the desired products and recycling the catalyst. One of the most used class of ionic liquids is the 1,3-dialkylimidazolium class, being the 1-butyl-3-methylimidazolium salts a well-known example (see Figure 1.34).

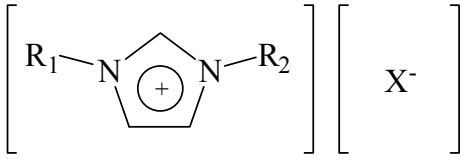

Figure 1.34. The general structure of a 1,3-dialkylimidazolium salt. R_1 and R_2 represent alkyl groups. X represents the counter ion.

Overall, the ionic liquid behaves much like a solid support but without imposing mobility constraints or chemical modifications to the catalyst. As such, catalyst reusability may be increased while preserving the performance. Song and co-workers[89] reported the asymmetric epoxidation of alkenes in a mixture of 1-butyl-3-methylimidazolium hexafluorophosphate ([bmim][PF_6])/dichloromethane, using Jacobsen's catalyst and NaOCl as terminal oxidant. Indeed, Song obtained yields ranging from 72 to 86% and enantiomeric excesses from 84 to 96% in epoxidation of various alkenes, together with shorter reaction times. The epoxidation of 2,2'-dimethylchromene took 2 hours to complete in the presence of the ionic liquid, whereas the same reaction had a duration of 6 hours using a conventional solvent. As the authors expected, the catalyst could be easily recovered and used again up to five times with minimal loss of enantioselectivity.

In 2010, Freire and co-workers[90] also employed Jacobsen's catalyst for epoxidation of 6-cyano-2,2-dimethylchromene, using a range of 1,3-dialkylimidazolium and tetra-

alkyl- dimethylguanidinium class RTILs. Of the various oxygen sources tested, NaOCl proved to be more suitable in this case, as the authors reported moderate to high epoxide yields and top enantiomeric excesses of *ca*. 70% for both RTIL classes, after 6 hours at room temperature. While the catalyst could be reused up to five times, significantly lower epoxide yields and slightly lower enantioselectivities were observed after each cycle.

Corma and co-workers[91] used a chiral $V^{IV}O$(salen) catalyst in asymmetric cyanation, having 1,3-dialkylimidazolium salts as solvents, and observed that yields and selectivity are dependent of the counter-anion type. In the cyanation of benzaldehyde, the $V^{IV}O$(salen) catalyst **L1.15** afforded 90% ee in dichloromethane, a slightly lower 89% ee in [emim][PF_6], 85% ee in [bmim][PF_6] and 40% enantiomeric excess in [bmim][Cl] (emim = 1-ethyl-3-methylimidazolium). The use of hydrophilic salts with anions such as Cl^- or BF_4^- resulted in lowered yields and enantioselectivities. This system retained its performance after five catalytic cycles.

1.4. Overview and objectives of the present work

The present work began with the exploration of $V^{IV}O$(salen) and $V^{IV}O$(salan) chemistry and the application of the developed complexes in asymmetric sulfoxidation. Despite the sole 2004 report from Zhu and co-workers[44] regarding the *in situ* $V^{IV}O$(salan), the chemistry of $V^{IV}O$(salan) precatalyts was, and still is, largely unexplored. Thus it became one of the aims of this work to develop and properly characterize of $V^{IV}O$(salan) precatalysts, along with the determination and optimization of their catalytic activities towards the asymmetric oxidation of thioanisole and also towards the oxidation of styrene, cumene and cyclohexene. It was also an objective of this work to develop and characterize a range of Ti^{IV}(salan) catalysts. While Katsuki and co-workers have carried out many studies with their elaborate Ti^{IV}(salan) type catalysts, this work focused in understanding and optimizing the chemistry of structurally simpler Ti^{IV}(salan) precatalysts. The development of aminoalcohol and aminoacid-derived tridentate $V^{IV}O$ precatalysts was another objective. The reduced Schiff base aminoalcohol-derived $V^{IV}O$ precatalysts were intended to be a departure from Bolm's Schiff base *in situ* $V^{IV}O$ catalyst system. The reduced Schiff base, aminoacid-derived

$V^{IV}O$ precatalysts were intended to be employed in the final stages of this work. The functionalized side-chains of aminoacids such as L-tyrosine and L-cysteine make them good candidates for immobilization on polymer supports, thus providing adequate starting materials for stepwise development of polymer-supported $V^{IV}O$ precatalysts. Therefore, the main objectives of the present work are (i) the development and study of homogeneous and heterogeneous versions of the Ti^{IV} and $V^{IV}O$(salan) precatalysts, and (ii) of the aminoalcohol and aminoacid-derived tridentate $V^{IV}O$ precatalysts.

1.5. References

1 Jacobsen, E. N.; Loebach, J. L.; Wilson, S. R.; Zhang, W. *J. Am. Chem. Soc.* **1990**, *112*, 2801-2803.

2 Bolm, C.; Bienewald, F. *Angew. Chem. Int. Ed. Engl*. **1995**, *34*, 2640-2642.

3 Gendler, S.; Groysman, S.; Goldschmidt, Z.; Shuster, M.; Kol, M. *J. of Polym. Sci. Part A: Polym. Chem*. **2006**, *44*, 1136-1146.

4 Cozzi, P. G. *Chem. Soc. Rev.* **2004**, *33*, 410-421.

5 Nitschke, J. R. *Angew. Chem. Int. Ed.* **2004**, *43*, 3073-3075.

6 Katsuki, T.; Bunnai, S.; Matsumoto, K. *Chem. Commun.* **2007**, 3619-3627.

7 Nakajima, K.; Kojima, M.; Kojima, K.; Fujita, J. *Bull. Chem. Soc. Jpn.* **1990**, 2620-2630.

8 Jacobsen, E. N.; Brandes, B. D. *J. Org. Chem.* **1994**, *59*, 4378-4380.

9 Tanaka, H.; Nishikawa, H.; Uchida, T.; Katsuki, T. *J. Am. Chem. Soc*. **2010**, *132*, 12034-12041.

10 Suematsu, H.; Katsuki, T. *J. Am. Chem. Soc*. **2009**, *131*, 14218-14219.

11 Suematsu, H.; Katsuki, T. *J. Am. Chem. Soc*. **2010**, *132*, 4510-4511.

12 Mizoguchi, M.; Uchida, T.; Ishida, K.; Katsuki, T. *Tetrahedron Lett.* **2009**, *50*, 3432-3435.

13 Ichinose, M.; Suematsu, H.; Katsuki. T. *Angew. Chem*. **2009**, *121*, 3167-3169.

14 Sharpless, B.; Katsuki, T. *J. Am. Chem. Soc.* **1980,** *102*, 5974-5976.

15 Nakajima, K.; Sasaki, C.; Kojima, M.; Fujita, J. *Bull. Chem. Soc. Jpn*. **1991**, 1318-1324.

16 (a) Katsuki, T.; Bunnai, S. *Tetrahedron. Lett.* **2001**, *42*, 8333-8336; (b) Katsuki, T.; Sato, B. *Tetrahedron Lett.* **2001**, *42*, 3873-3876; (c) Matsumoto, K.; Sawada, Y.;Saito, B.; Sakai, K.; Katsuki, T. *Angew. Chem.* **2005**, *117*, 5015-5019; (d) Katsuki, T.; Sato, B.; Tomoaki, T. *Tetrahedron Lett.* **2002**, *43*, 3259-3262.

17 (a) Belokon, Y.; Ikonnikov, N.; Moscalenko, M.; North, M.; Orlova, S,; Tararov, V.; Yashkina, L. *Tetrahedron: Asymm.* **1996***, 7*, 851-855; (b) Belokon, Y. N.; Green, B.; Ikonnikov, N. S.; North, M.; Tararov, V. *Tetrahedron Lett.* **1999**, *40*, 8147-8150; (c) Belokon, Y. N.; Green, B.; Ikonnikov, N. S.; North, M.; Tararov, V.; Parsons, T. *Tetrahedron Lett.* **2001**, *57*, 771-779; (d) Belokon, Y. N.; Clegg, W.; Harrington, R. W.; Young, C.; North, M. *Tetrahedron* **2007**, *63*, 5287-5299.

18 Zhou, Z.; Li, Z.; Quanyong, W.; Liu, B.; Li, K.; Zhao, G.; Zhou, Q.; Tang, C., *J. Organomet. Chem.* **2006**, *691*, 5790-5797.

19 Fennie, M. W.; DiMauro, E. F.; O'Brien, E. M.; Annamalai, V.; Kozlowski, M. C. *Tetrahedron* **2005**, *61*, 6249-6265.

20 Gregson, C. K. A.; Gibson, V. C.; Long, N. J.; Marshall, E. L.; Oxford, P. J.; White, A. J. P. *J. Am. Chem. Soc.* **2006**, *128*, 7410-7411.

21 Bialek, M.; Czaja, K.; Szydlo, E., *J. Polym. Sci.: A: Polym. Chem*. **2009**, *47*, 565-575.

22 Ramón, D. J.; Yus, M. *Chem. Rev*. **2006**, *106*, 2126-2208.

23 Bandini, M.; Cozzi, P. G.; Morganti, S.; Umani-Ronchi, A. *Tetrahedron Lett.* **1999**, *40,* 1997-2000.

24 Bolm, C. *Coord. Chem. Rev.* **2003**, *237*, 245-256.

25 Michaelson, R.C.; Palermo, R.E.; Sharpless, K.B. *J. Am. Chem. Soc*. **1977**, *99*, 1990-1992.

26 (a) Robinson, R.L.; Eady, R.R.; Richardson, T.H.; Miller, R.W.; Hawkins, M.; Postgate, J.R. *Nature* **1986**, *322*, 388-390; (b) Vilter, H. *Phytochemistry* **1984,** *23*, 1387-1390; (c) Arbor, J.M.; de Boer, M.; Garner, C.D.; Hasnain, S.S.; Wever, R. *Biochemistry* **1989**, *28*, 7968-7973.

27 Palucki, M; Hanson, P.; Jacobsen*,* E. N. *Tetrahedron Lett.* **1992**, *33*, 7111-7114.

28 (a) Belokon, Y. N.; North, M.; Parsons, T. *Org. Lett*. **2000**, *2*, 1617-1619; **(b)** Belokon, Y. N.; Clegg, W.; Harrington, R. W.; Young, C.; North, M. *Tetrahed*ron **2007**, *63*, 5287-5299; (c) Belokon, Y. N.; Clegg, W.; Harrington, R. W.; Maleev, V. I.; North, M.; Pujol, M. O.; Usanov, D. L.; Young, C. *Chem. Eur. J.* **2009**, *15*, 2148-2165.

29 Blacker, J.; Clutterbuck, L. A.; Crampton, M. R.; Grosjean, C.; North, M. *Tetrahedron: Asymm.* **2006**, *17,* 1449-1456.

30 Watanabe, A.; Matsumoto, K.; Shimada, Y.; Katsuki, T. *Tetrahedron Lett.* **2004**, *45*, 6229-6233.

31 Bialek, M.; Czaja, K. *J. Polym. Sci. A: Polym. Chem*. **2008**, *46*, 6940-6949.

32 Baleizão, C.; Garcia, H. *Chem. Rev.* **2006**, *106*, 3987-4043.

33 (a) Groysman, S.; Goldberg, I.; Goldschmidt, Z.; Kol, M. *Inorg. Chem.* **2005**, *44*, 5073-5080; (b) Segal, S.; Goldberg, I.; Kol, M. *Organometallics* **2005,** *24,* 200-202; (c) Tshuva, E. Y.; Goldberg, I.; Kol, M. *Inorg. Chem.* **2001**, *40,* 4263-4270.

34 (a) Atwood, D. A. *Coord. Chem. Rev.* **1997**, *165*, 267-296; (b) Lubben, M; Feringa, B. L. *J. Org. Chem.* **1994**, *59*, 2227-2233; (c) Tshuva, E. Y.; Natalie Gendeziuk, N.; Kol, M. *Tetrahedron Lett.*, **2001**, *42*, 6405–6407.

35 Kizirian, J. *Chem. Rev.* **2008**, *108*, 140-205.

36 Valko. M,; Rudolph, M.; Pelikan, P.; Paulus, H.; Müller, L.; Mazur, M.; Langfelderova, H.; Jäger, E.; Elias, H.; Böttcher, A. *Inorg. Chem.* **1993**, *32,* 4131-4138.

37 Balsells, J.; Carroll, P. J.; Walsh, P. J. *Inorg. Chem.* **2001**, *40*, 5568-5574.

38 Yeori, A.; Groysman, S.; Goldberg, I.; Kol, M. *Inorg. Chem.* **2005**, *44*, 4466-4468.

39 (a) Adão, P.; Costa Pessoa, J.; Henriques, R. T.; Kuznetsov, M. L.; Avecilla, F.; Maurya, M. R.; Kumar, U.; Correia, I. *Inorg. Chem.* **2009**, *48*, 3542-3561; (b) Adão, P.; Avecilla, F.; Bonchio, M.; Carraro, M.; Costa Pessoa, J.; Correia, I. *Eur. J. Inorg. Chem.* **2010**, 5568-5578; (c) Adão, P.; Maurya, M. R.; Kumar, U.; Avecilla, F.; Henriques, R. T.; Kusnetsov, M. L.; Costa Pessoa, J.; Correia, I. *Pure Appl. Chem*. **2009**, *81*, 1279-1296.

40 Okamatsu, T.; Irie, R.; Katsuki, T. *J. Organomet. Chem.* **2007**, *692*, 645-653.

41 Sawada, Y.; Matsumoto, K.; Kondo, S.; Watanabe, H.; Ozawa, T.; Suzuki, K.; Saito, B.; Katsuki, T. *Angew. Chem.* **2006**, *118*, 3558-3560.

42 Katsuki, T.; Matsumoto, K.; Ohara, Y.; Kondo, S.; Shimada, Y. *Synlett* **2007**, *15*, 2445-2447.

43 Bryliakov, K. P.; Talsi, E. P. *Eur. J. Org. Chem.* **2008***,* 3369-3376.

44 Sun, J.; Zhu, C.; Dai, Z.; Yang, M; Pan, Y.; Hu, H. *J. Org. Chem.* **2004**, *69*, 8500-8503.

45 Vetter, A. H.; Berkessel, A. *Tetrahedron Lett*. **1998**, *39*, 1741-1744.

46 Drago, C.; Caggiano, L.; Jackson, R. F. W. *Angew. Chem.* **2005**, *117*, 7387-7389.

47 Hayashi, M.; Miyamoto, Y.; Inoue, T.; Oguni, N. *J. Org. Chem.* **1993**, *58*, 1515-1522.

48 Flores-Lopéz, L. Z.; Parra-Hake, M.; Somanathan, R.; Walsh, P. J. *Organomet.* **2000**, *19*, 2153-2160.

49 Banphavichit, V.; Mansawat, W.; Bhanthumnavin, W.; Vilaivan, T. *Tetrahedron* **2004**, *60*, 10559-10568.

50 Bryliakov, K. P.; Talsi, E. P. *J. Mol. Cat. A: Chem.* **2007**, *264*, 280-287.

51 Seayad, A. M.; Ramalingam, B.; Yoshinaga, K.; Nagata, T.; Chai, C. L. L. *Org. Lett.* **2010**, *12*, 264-267.

52 Jaworska, M.; Błocka, E.; Kozakiewicz, A.; Wełniak, M. *Tetrahedron: Asymm.* **2011**, *22*, 648-657.

53 (a) Belokon, Y. N.; Chusov, D.; Borkin, D. A.; Yashkina, L. V.; Dmitriev, A. V.; Katayeva, D.; North, M. *Tetrahedron: Asymm*. **2006**, *17*, 2328-2333. (b) Belokon, Y. N.; Chusov, D.; Borkin, D. A.; Yashkina, L. V.; Bolotov, P.; Skrupskaya, T.; North, M. *Tetrahedron: Asymm*. **2008**, *19*, 459-466. (c) Belokon, Y. N.; Chusov, D.; Peregudov, A. S., Yashkina, L. V.; Timofeeva, G. I.; Maleev, V. I.; North, M.; Kagan, H. B. *Adv. Synth. Catal*. **2009**, *351*, 3157-3167.

54 (a) Pitchen, P.; Kagan, H. B. *Tetrahedron Lett*. **1984**, *25,* 1049-1052**;** (b) Di Furia, F.; Modena, G.; Seraglia, R. *Synthesis* **1984**, *4*, 325-326.

55 Wu, Y.; Liu, J.; Li, X.; Chan, A. S. C. *Eur. J. Org. Chem.* **2009**, 2607-2610.

56 Iseki, Y.; Kudo, M.; Mori, A.; Inoue, S. *J. Org. Chem*. **1992**, *57*, 6329-6331.

57 Wen, J.; Zhao, J.; Wang, X.; Dong, J.; You, T. *J. Mol. Cat. A: Chem*. **2006**, *245* 242-247.

58 Nakajima, K.; Kojima, M.; Toriumi, K.; Saito, K.; Fujita*,* J. *J. Bull. Chem. Soc. Jpn*. **1989**, *62*, 760-767.

59 Ando, R.; Inden, H.; Sugino, M.; Ono, H.; Sakaeda, D.; Yagyu, T.; Maeda, M. *Inorg. Chim. Act*. **2004**, *357*, 1337-1344.

60 (a) Luo, Z.; Liu, Q.; Gong, L.; Cui, X.; Mi, A.; Jiang, Y. *Chem. Commun*. **2002**, 914-915. (b) Somei, H.; Asano, Y.; Yoshida, T.; Takizawa, S.; Yamataka, H.; Sasai, H. *Tetrahedron Lett.* **2004**, *45*, 1841-1844. (c) Takizawa, S.; Katayama, T.; Somei, H.; Asano, Y.; Yoshida, T.; Kameyama, C.; Rajesh, D.; Onitsuka, K.; Suzuki, T.; Mikami, M.; Yamataka, H.; Jayaprakash, D.; Sasai, H. *Tetrahedron* **2008**, *64*, 3361-3371.

61 Chen, C.; Kao, J.; Salunke, S. B.; Lin, Y. *Org. Lett*. **2011**, *13*, 26-29.

62 Merrifield, R. B. *J. Am. Chem. Soc.* **1963**, 85, 2149-2154.

63 Wang, S. *J. Am. Chem. Soc.* **1973**, *95*, 1328-1333.

64 Minutolo, F.; Pinit, D.; Salvadori, P. *Tetrahedron Lett,* **1996**, *37*, 3375-3378.

65 Minutolo, F.; Pinit, D.; Petri, A.; Salvadori, P. *Tetrahedron Asymm.* **1996**, *7*, 2293-2302.

66 (a) Canali, L.; Sherrington, D.C.; Deleuze, H. *React. Funct. Polym.* **1999**, *40*, 155-168; (b) Canali, L.; Cowan, E.; Deleuze, H.; Gibson, C. L.; Sherrington, D. C. *J. Chem. Soc*., *Perkin Trans.* **2000**, 2055-2066.

67 Sellner, H.; Karjalainen,J. K.; Seebach, D. *Chem. Eur. J.* **2001**, *7*, 2874-2887.

68 Smith, K.; Liu, C.; El-Hiti, G. A. *Org. Biomol. Chem.* **2006**, *4*, 917-927.

69 Anyanwu, U. K.; Venkataraman, D. *Green Chem.* **2005**, *7*, 424-425.

70 Green, S. D.; Monti, C.; Jackson, R. F. W.; Anson, M. S.; Macdonald, S. J. F. *Chem. Commun.* **2001**, 2594-2595.

71 Maurya, M. R.; Kumar, A.; Costa Pessoa, J. *Coord. Chem. Rev*. **2011**, doi:10.1016/j.ccr.2011.01.050.

72 Maurya, M. R.; Kumar, M.; Kumar, A.; Costa Pessoa, J. *Dalton Trans*. **2008** 4220-4232.

73 Berrisford, D. J.; Bolm, C.; Sharpless; K. B. *Angew. Chem. Intl. Ed.* **1995**, *34*, 1059-1070.

74 Caron, S.; Dugger, R. W.; Ruggeri, S. G.; Ragan, J. A.; Brown, D. H. *Chem. Rev.* **2006**, *106*, 2943-2989.

75 Müller, T. E.; Beller, M. *Chem. Rev.* **1998**, *98*, 675-703.

76 (a) Kondo, T.; Okada, T.; Mitsudo, T. *J. Am. Chem. Soc.* **2002**, *124*, 186-187; (b) Brice, J. L.; Harang, J. E.; Timokhin, V. I.; Anastasi, N. R.; Stahl, S. S. *J. Am. Chem. Soc.* **2005**, *127*, 2868-2869; (c) Srinivasarao, V. N.; Talluri, S. K.; Shyla, G.; Rumugam, S. A. *Tetrahedron Lett.* **2007**, *48*, 65-68.

77 Barbarini, A.; Maggi, R.; Muratori, M.; Sartori, G.; Sartorio, R. *Tetrahedron: Asymm.* **2004**, *15*, 2467-2473.

78 Rajagopal, G.; Selvaraj, S.; Dhahagani, K. *Tetrahedron: Asymm.* **2010**, *21*, 2265-2270.

79 Sabater, M. J.; Corma, A.; Domenech, A.; Fornés, V.; García, H. *Chem. Commun.* **1997**, 1285-1286.

80 McMorn, P.; Hutchings, G. H. *Chem. Soc. Rev.* **2004**, *33*, 108-122.

81 Zhang, H.; Li, C. *Tetrahedron* **2006**, *62*, 6640-6649.

82 Maurya, M. R.; Kumar, M.; Titinchi, S. S. J.; Abbo, H. S.; Chand, C. *Catal. Lett*. **2003**, *86*, 97-105.

83 Maurya, M. R.; Chandrakar, A. K.; Chand, S. *J. Mol. Cat. A: Chem*. **2007**, *270* 225-235.

84 Maurya, M. R.; Singh, B.; Adão, P.; Avecilla, F.; Costa Pessoa, J. *Eur. J. Inorg. Chem.* **2007**, 5720-5734.

85 Choudary, B. M.; Chowdari, N. S.; Kantam M. L.; Santhi, P. L. *Catal. Lett.* **2001**, *76*, 213-218.

86 (a) Xia, Q. H.; Ge, H. Q.; Ye, C. P.; Liu, Z. M.; Su, K. X. *Chem. Rev.* **2005**, 105, 1603-1662; (b) Fan, Q.; Li, Y.; Chan, A. S. C. *Chem. Rev.* **2002**, 102*,* 3385-3466.

87 Silva, A. R.; Wilson, K.; Clark, J. H.; Freire, C. *Micro. Meso. Mat*., **2006**, *91*, 128-138.

88 Baleizão, B.; Gigante, B.; Garcia, H.; Corma, A. *J. Cat.* **2003**, 215, 199-207.

89 Song, C. E. *Chem. Commun.* **2004**, 1033-1043.

90 Teixeira, J.; Rosa Silva, A.; C. Branco, L.; A. M. Afonso, C.; Freire, C. *Inorg. Chim. Acta* **2010**, 3321-3329.

91 Baleizão, C.; Gigante, B.; Garcia, H.; Corma, A. *Green Chem.* **2002**, *4*, 272-274.

Chapter 2

Ligand Precursors

2. Ligand Precursors

2.1. Introduction

As mentioned early in the previous chapter, the aminophenol class of compounds is known for the relatively straightforward methods of preparation. Schiff base compounds such as the salen can be prepared readily by direct condensation of the appropriate diamine with salicylaldehyde derivatives in a 1 to 2 stoichiometric ratio. The reduced derivatives or salan-type compounds can be obtained by reducing the carbon-nitrogen double bond with a mild reducing agent such as sodium borohydride (Scheme 2.1).[1]

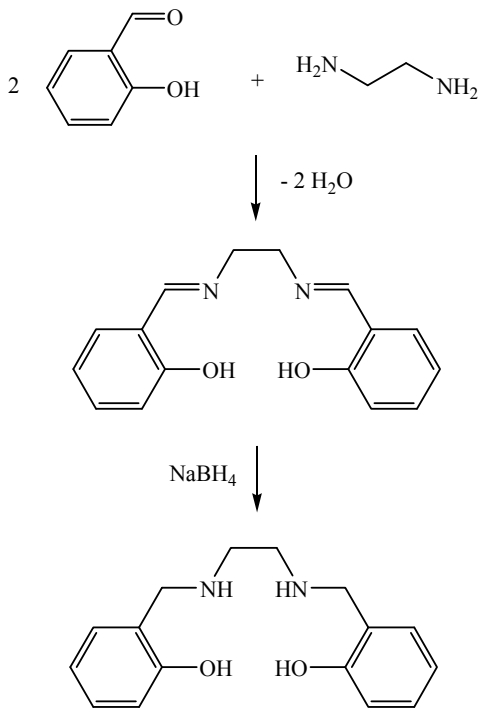

Scheme 2.1. General preparation procedure of a salan-type compound.

When the salicylaldehyde derivative necessary for the synthesis of a reduced salen derivative is not available, it is possible to use structurally similar phenols in a modified single-step Mannich reaction to achieve the same goal. Typically this process employs

the required primary or secondary amine, a non-enolizable aldehyde such as formaldehyde and a substituted phenol in a 1:2:2 stoichiometric ratio (Scheme 2.2).[2] While this reaction skips the Schiff base reduction step mentioned earlier, it is prone to side-reactions when primary amines are used. A common side product of Mannich reactions of this kind is the 1,3-benzoxazine, which tends to form when a primary amine is used. Fortunately, the 1,3-benzoxazine by-product can be converted into the desired salan compound by heating it in an acidic medium.

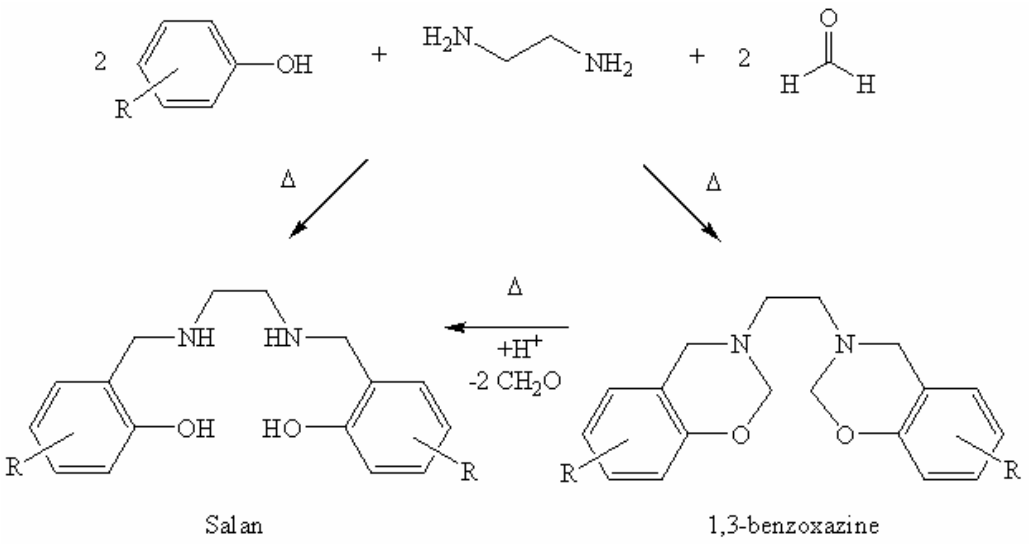

Scheme 2.2. Preparation of a salan-type compound by a Mannich reaction.

Beside to the relative straightforward preparation methods, the wide variety and availability of the starting materials makes this compound class a privileged one. Indeed, it is possible to make an aminophenol-type compound from just about any primary or secondary amine and substituted salicylaldehyde or phenol in a single condensation step. This opens many possibilities for the design and fine-tuning of transition metal catalysts, as each can be easily fine-tuned for a given chemical process by simply changing one of the starting building blocks.

The following sections will present the preparation and characterization of a variety of aminophenol-type compounds that were used as ligands in the preparation of the transition metal catalysts described in the following chapters.

2.2. Ligand precursor preparation: Results and discussion

2.2.1. Salen-type ligand precursors

Compounds *R,R*-**1a**, *S,S*-**2a**, *R,R*-**3a,** *S,S*-**4a,** *S,S*-**5a,** and *R,R* **-6a** were prepared according to reported procedures[3,4,5,6] in which the required chiral diamine, being 1R,2R-cyclohexane-1,2-diamine, 1S,2S-cyclohexane-1,2-diamine or 1S,2S-diphenylethylene-1,2-diamine, is reacted with two equivalents of salicylaldehyde, *o*-vanillin or pyridoxal in methanol. The preparation and employment of the salen compounds was mostly for comparative purposes. With the exception of *R,R*-**3a**, most of the compounds *R,R*-**1a**, *S,S*-**2a**, *S,S*-**4a** and *S,S*-**5a** have been already reported, the characterization of the featured salen compounds will not have the same depth as for the reduced Schiff base compounds described in the following sections. Figure 2.1 depicts the structural formulas of the compounds prepared.

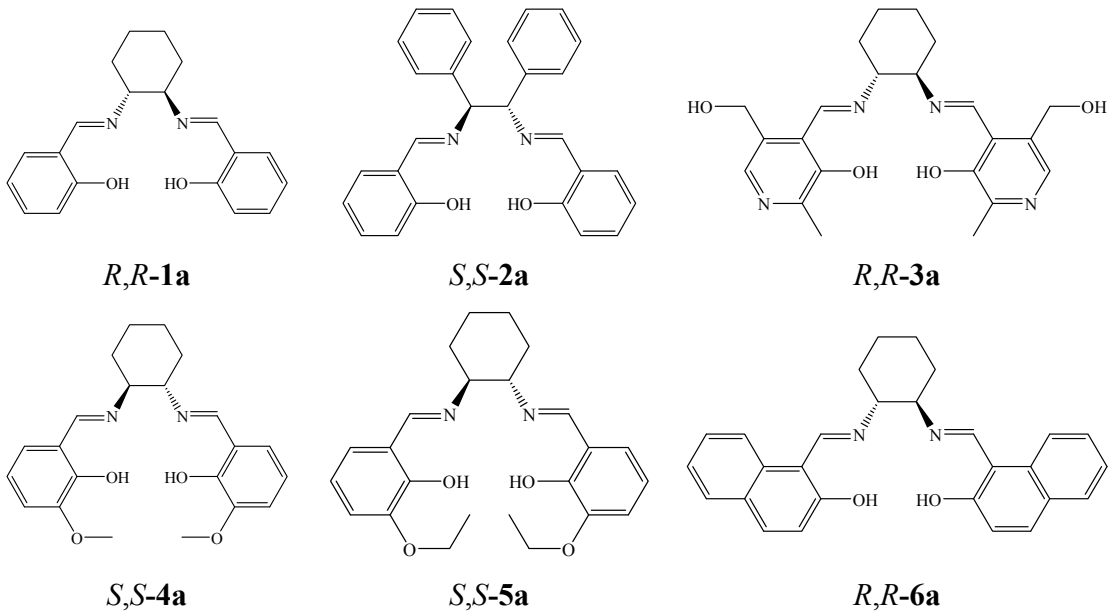

Figure 2.1- Structural formulas of the prepared salen compounds depicting their respective configuration at the stereogenic centers.

The ^{1}H-NMR spectra of the salen compounds present a singlet at *ca*. 8.35 ppm, arising from the single proton of the imine moiety, thus confirming the isolation of the desired salen compound. In some cases, namely in *R,R*-**1a** (see Figure 2.2), appears to

exist a duplication or broadening of signals, observable in ^{1}H NMR, which may be a consequence of restricted bond rotation. The broadening is more prevalent in the signals corresponding to the cyclohexane ring protons.

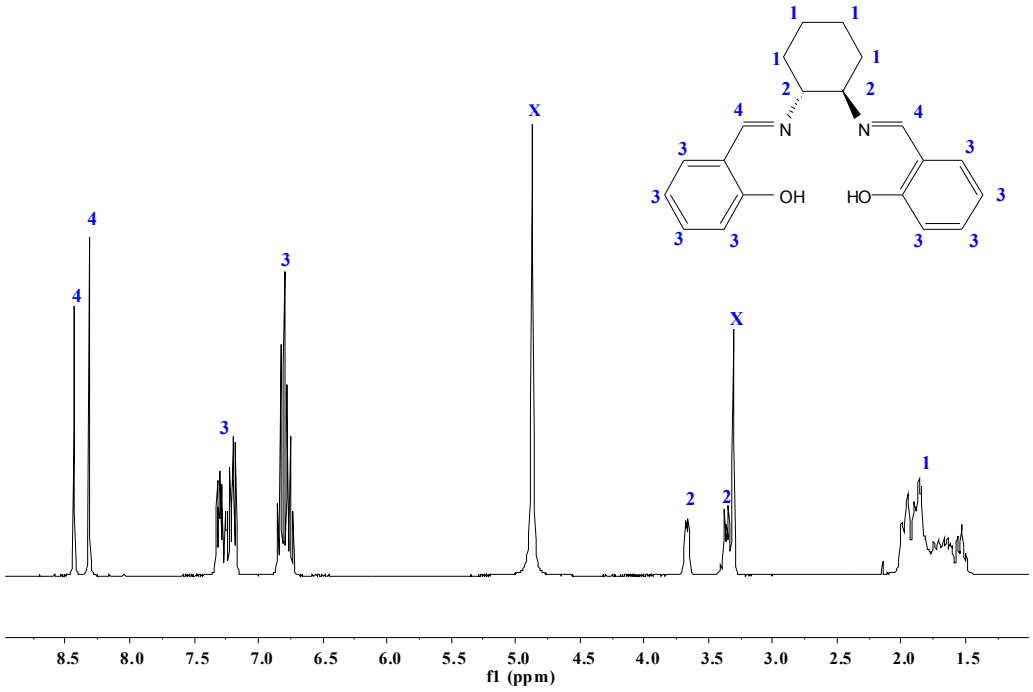

Figure 2.2- ^{1}H-NMR spectra of the salen compound *R,R*-**1a** indicating C_1-symmetry tending to C_2-symmetry in CD_3OD. The spectra from the other salen variants are very similar to this spectrum. The letter (X) represents deuterated solvent signals.

Additional information was obtained from FT-IR spectroscopy. Other than the expected stretching bands for aliphatic and aromatic C-H bonds, all IR spectra display an intense absorption at 1627 cm^{-1}, consistent with the existence of a N=C bond.

Crystals of *S,S*-**5a** and *R,R*-**6a** suitable for single crystal X-ray diffraction were obtained from slow evaporation of acetonitrile and methanolic solutions, respectively. The ORTEP diagrams are presented below in Figures 2.3 and 2.4. The selected parameters are listed in Table 2.1.

The asymmetric unit of the crystal structures of both *S,S*-**5a** and *R,R*-**6a** contains only one neutral molecule. *S,S*-**5a** crystallizes in the triclinic system, space group *P*-1. *R,R*-**6a** crystallizes in the orthorhombic system, $P2_12_12_1$ space group. The N=CH lengths in both cases are consistent with the double bond nature of N=C. The torsion angles C5-

C6-C7-N1 and N2-C14-C15-C16 observed in *S,S*-**5a** are very close to 180º (+174.37(11)º and +173.30(11)º, respectively). Although not depicted, intramolecular hydrogen bond interactions O_{phenol}-H•••N_{imine} are present in *S,S*-**5a** . The existence of hydrogen bonding and the conjugation of the N=C double bonds with the aromatic rings contribute to the rigidity of the molecular structure. The planes defined by N1-C7-C6-C1-O1 and N2-C14-C15-C20-O2 present mean deviations of 0.0258 Å and 0.0272 Å, respectively. The cyclohexane ring is in chair conformation and both chiral carbons have *S* configuration.

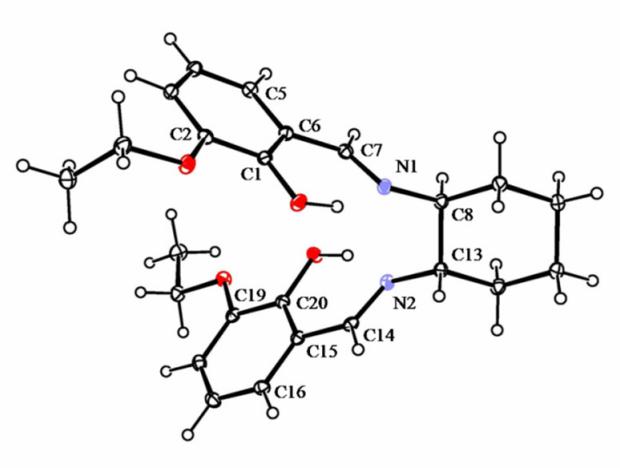

Figure 2.3- ORTEP-3 diagram of *S,S*-**5a**, using 30 % probability level ellipsoids.

The structure of *R,R*-**6a** also exhibits torsion angles very close to 180º, with -179.18(22)º for C5-C6-C7-N1 and +176.67(20)º for N2-C14-C15-C16. Intramolecular hydrogen bond interactions O_{phenol}-H.•••N_{imine} are also present. Similarly to *S,S*-**5a** , *R,R*-**6a** exhibits a rigid structure, with the mean deviations from the planes defined by N1-C7-C6-C1-O1 and N2-C14-C15-C20-O2 being 0.0133 Å and 0.0102 Å, respectively. Similarly to *S,S*-**5a**, the cyclohexane ring is in chair conformation but both chiral carbons have *R* configuration.

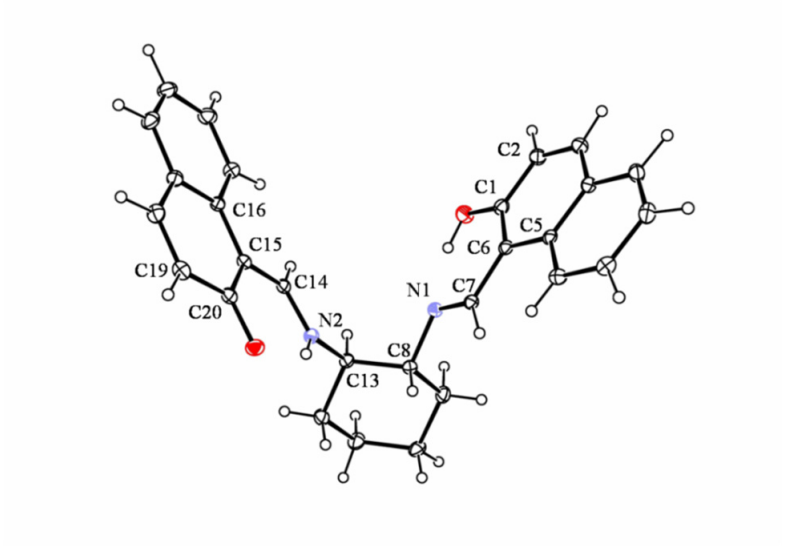

Figure 2.4- ORTEP-3 diagram of *R,R*-**6a**, using 30 % probability level ellipsoids.

Table 2.1. Selected bond lengths for *S,S*-**5a** and *R,R*-**6a**.

	S,S-**5a**	*R,R*-**6a**
	Bond lengths (Å)	
O(1)-C(1)	1.353(14)	1.337(3)
O(2)-C(20)	1.353(14)	1.276(3)
N(1)-C(7)	1.279(16)	1.288(3)
N(1)-C(8)	1.462(15)	1.466(3)
N(2)-C(14)	1.275(15)	1.309(3)
N(2)-C(13)	1.462(15)	1.465(3)
C(8)-C(13)	1.535(16)	1.533(3)
C(14)-C(15)	1.460(16)	1.407(3)
C(6)-C(7)	1.459(16)	1.454(3)
	Bond angles (º)	
N(1)-C(8)-C(13)	108.55(9)	109.71(19)
N(1)-C(8)-C(9)	110.37(9)	107.93(18)
N(1)-C(7)-C(6)	121.97(11)	121.3(2)
N(2)-C(14)-C(15)	123.07(11)	124.3(2)
C(13)-C(8)-C(9)	110.50(10)	110.17(19)
C(8)-C(13)-C(12)	110.56(10)	111.5(2)
N(2)-C(13)-C(8)	108.45(9)	110.72(18)
N(2)-C(13)-C(12)	110.79(9)	110.23(19)
C(14)-N(2)-C(13)	118.01(10)	123.6(2)
C(7)-N(1)-C(8)	118.23(10)	119.4(2)

2.2.2. Tetrahydrosalen or salan-type compounds

Compounds *R*,*R*-**1**, *S*,*S*-**2**, *R*,*R*-**3,** *S*,*S*-**4,** *S*,*S*-**5,** *S*,*S*-**6,** *R*,*R*-**7** and *S*,*S*-**10** (see Figure 2.5.) were prepared by reduction of the respective salen precursors with $NaBH_4$ in methanol. All of the salan compounds were isolated as their hydrochloride salts to facilitate the removal of organic and inorganic contaminants. Compounds *R*,*R*-**8** and *R*,*R*-**9** were prepared by reacting the tartrate salt of (1*R*,2*R*)-cyclohexane-1,2-diamine or (1*S*,2*S*)-cyclohexane-1,2-diamine with formaldehyde and the appropriate substituted phenol in a modified Mannich reaction in methanol. All compounds were characterized by ^{1}H NMR, $^{13}C\{^{1}H\}$ NMR, HSQC, HMBC, FT-IR and elemental analysis. Characterization by single crystal X-ray diffraction was possible for *R*,*R*-**1**, *R*,*R*-**3**, *S*,*S*-**4** and *R*,*R*-**8**. Figure 2.5 depicts the structural formulas of the compounds prepared.

The ^{1}H NMR spectra of the featured salan compounds are very similar with each other. All are consistent with C_2-symmetry in solution (see Figure 2.6). As a consequence, the phenolate and amine backbone protons of each half of the molecule are magnetically equivalent. The result is a simplified ^{1}H NMR spectrum, where only half of the proton resonances are observable.

^{1}H NMR spectra of (1*S*,2*S*)-diphenylethylene-1,2-diamine derived compounds *S*,*S*-**2** and *S*,*S*-**10** are further simplified. In all cases the protons of the methylene group bridging the phenolate and the diamine moieties appear clearly as an AB system, characteristic of diastereotopic protons. In (1*R*,2*R*)-cyclohexane-1,2-diamine or (1*S*,2*S*)-cyclohexane-1,2-diamine derived compounds, the cyclohexane ring proton signals are visibly broadened to the point that no multiplets are discernible. This broadening may result from a slower cyclohexane conformation exchange on the NMR time scale.

The first observable characteristic of the obtained IR spectra is the non-observation of the strong N=C stretching band at 1627 cm^{-1}. Conversely, an N-H stretching band is visible around at 3400-3200 cm^{-1} in most cases.

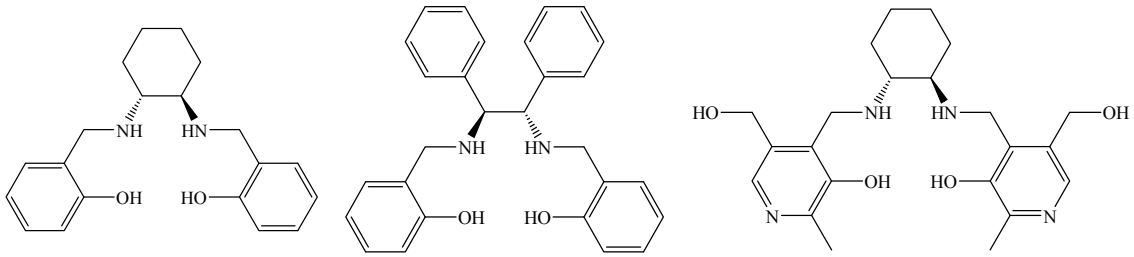

R,*R*-**1**

S,*S*-**2**

R,*R*-**3**

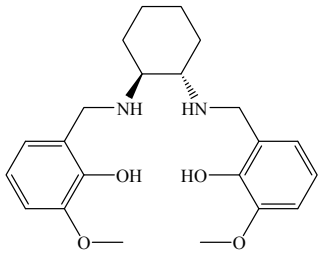

S,*S*-**4**

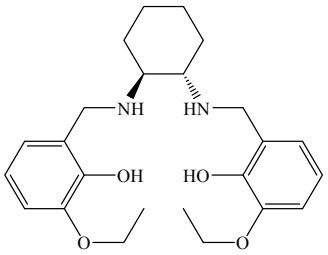

S,*S*-**5**

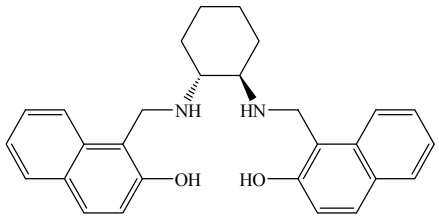

S,*S*-**6**

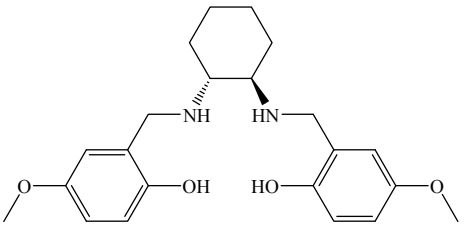

R,*R*-**7**

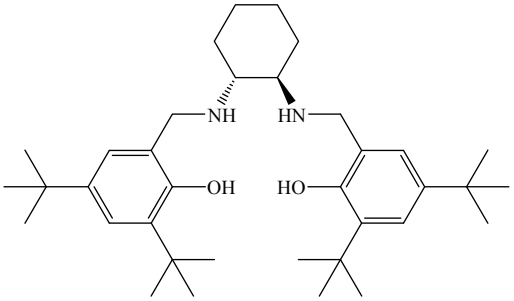

R,*R*-**8**

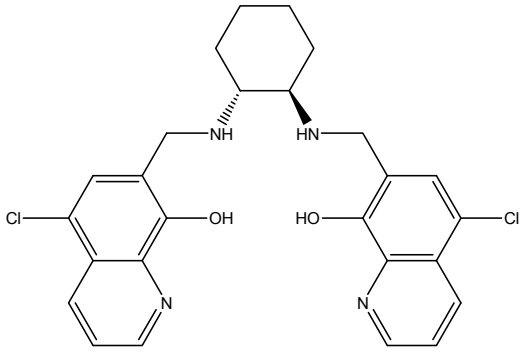

R,*R*-**9**

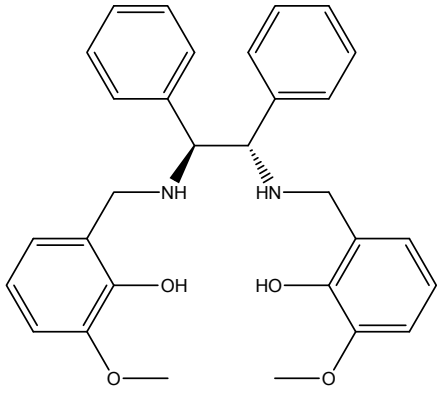

S,*S*-**10**

Figure 2.5- Structural formulas of the prepared salan compounds depicting the respective configuration at their stereogenic centers.

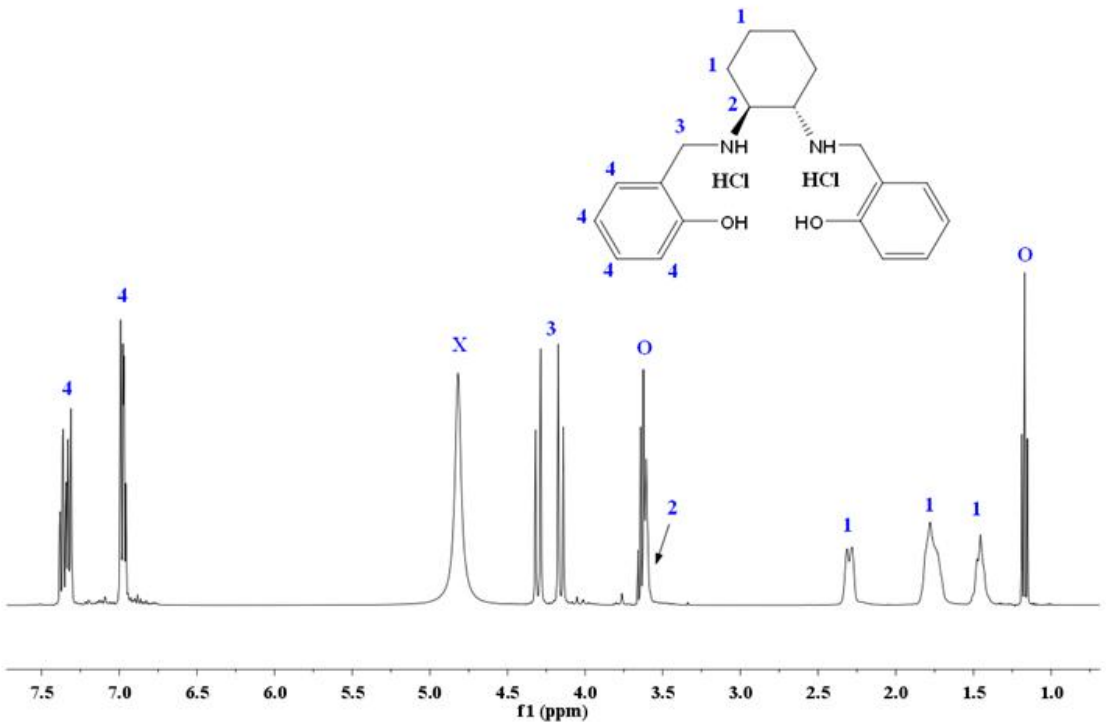

Figure 2.6- ^{1}H-NMR spectrum of *R,R*-**1** indicating C_2-symmetry in D_2O solution. The spectra of the other salan variants are very similar to this spectrum. The AB multiplet pattern is identified by **3**. The letters **X** and **O** represent the deuterated solvent and ethanol signals respectively.

Single crystals of *R,R*-**1**, *S,S*-**4** and *R,R*-**8** suitable for X-ray diffraction crystallography were obtained by slow evaporation of the respective solutions in 2-propanol. Crystals of *R,R*-**3** were obtained by slow evaporation of an aqueous solution. The respective ORTEP diagrams are presented below in Figures 2.7, 2.8, 2.9 and 2.10. The selected parameters are listed in Tables 2.2 and 2.3.

Figure 2.7 depicts *R,R*-**1** as a dicationic molecule with two protons in each amine groups. The compound crystallizes in the monoclinic system, space group $P2_1$. The asymmetric unit also contains two chloride anions, one molecule of water and one molecule of 2-propanol. The NH_2-CH_2 bond lengths are in agreement with the expected length of a N-C single bond.

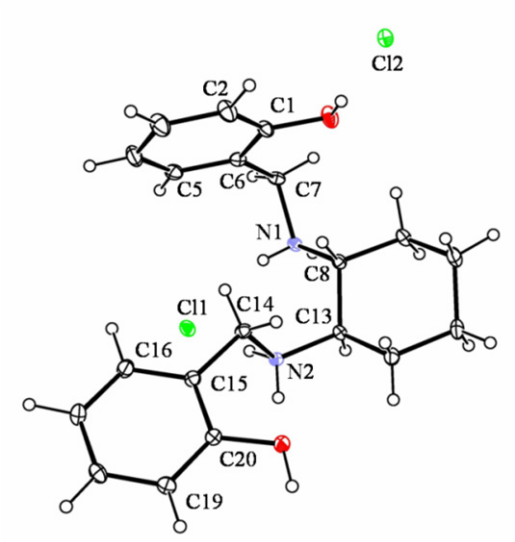

Figure 2.7- ORTEP-3 diagram of *R*,*R*-**1**, using 30 % probability level ellipsoids.

The torsion angles C(5)-C(6)-C(7)-N(1) and N(2)-C(14)-C(15)-C(16) observed in *R*,*R*-**1** are -82.49(25)º and -106.85(25)º, respectively, indicating a much more flexible molecular structure. The observed torsion angles are in contrast with the near 180º torsion angles observed in the more rigid structure of the salen counterpart *R*,*R*-**1a**. Both chiral carbons have *R* configuration. The intermolecular hydrogen bonding also contributes to the distorted structure of *R*,*R*-**1**, namely O_{phenol}-H•••Cl and N_{amine}-H•••Cl interactions. The protonation of the amine groups prevents the existence of intramolecular O_{phenol}-H•••N_{amine} hydrogen bonds. The intermolecular hydrogen bond interactions H.•••Cl may be classified depending on the interaction length.[7] Lengths shorter than 2.52 Å are considered short, whereas lengths ranging between 2.52-2.95 Å and 2.95-3.15 Å are considered intermediate and long, respectively. All O_{phenol}-H•••Cl and N_{amine}-H•••Cl interactions present have lengths shorter than 2.52 Å.

Figure 2.8 depicts *R*,*R*-**3** as a tetracationic molecule, where both amine and both pyridine groups are protonated. This compound crystallizes in the monoclinic system, space group *C*2. The asymmetric unit contains half a molecule of *R*,*R*-**3**, one molecule of water and two chloride anions. The other half of the structure is generated by symmetry operations.

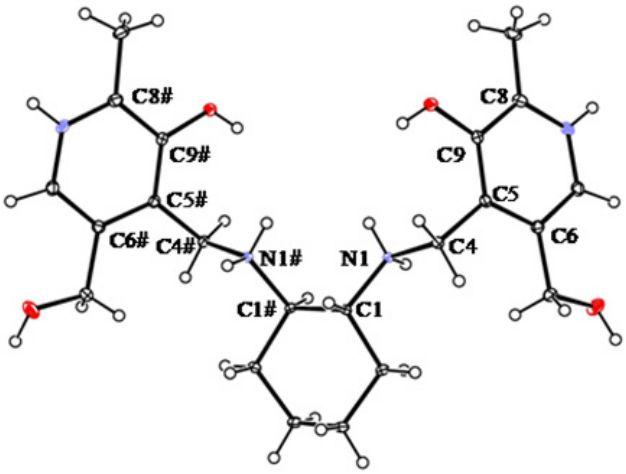

Figure 2.8- ORTEP-3 diagram of *R*,*R*-**3**, using 30 % probability level ellipsoids. The chloride anions and the solvent molecules were omitted for clarity. The atoms labeled with # were generated using symmetry transformation 2-x, y, 1-z.

As in *R*,*R*-**1**, the NH_2-CH_2 bond lengths are in agreement with the expected length for a N-C single bond. The torsion angle C(4)-C(5)-C(6)-N(1) observed in *R*,*R*-**3** is +93.46(18)º, comparable to the ones observed in *R*,*R*-**1**. Intramolecular O_{phenol}-H•••N_{amine} hydrogen bonds are prevented due to the protonation of the amine groups but intermolecular $O_{alcohol}$-H•••O_{water} hydrogen bonds are present, as well as N_{amine}-H••• O_{water} bonds. Short and intermediate N_{amine}-H•••Cl and $O_{alcohol}$-H•••Cl hydrogen bonds are also present.

Table 2.2. Selected bond lengths and angles for *R*,*R*-**1**, and *R*,*R*-**3**.

R,*R*-**1**		*R*,*R*-**3**	
Bond lengths (Å)			
O(1)-C(1)	1.366(3)	N(1)-C(4)	1.506(2)
O(2)-C(20)	1.373(3)	N(1)-C(1)	1.510(2)
N(1)-C(7)	1.508(3)	O(1)-C(9)	1.346(2)
N(1)-C(8)	1.513(3)		
N(2)-C(14)	1.508(3)		
N(2)-C(13)	1.520(3)		
Bond angles (º)			
C(14)-N(2)-C(13)	117.32(19)	C(4)-N(1)-C(1)	113.99(12)
C(7)-N(1)-C(8)	115.21(19)	O(1)-C(9)-C(5)	125.80(17)
N(1)-C(7)-C(6)	111.24(17)	O(1)-C(9)-C(8)	114.07(17)
N(2)-C(14)-C(15)	109.89(19)	N(1)-C(4)-C(5)	109.70(13)
O(1)-C(1)-C(2)	122.71(2)		
O(1)-C(1)-C(6)	117.03(2)		
O(2)-C(20)-C(15)	115.88(19)		
O(2)-C(20)-C(19)	123.32(19)		

The structure of *S*,*S*-**4**, depicted in Figure 2.9, differs from the other structures as the asymmetric unit contains a single neutral molecule. This compound crystallizes in the orthorhombic system, space group $P2_12_12_1$. Curiously, there is a migration of a phenol proton to the neighboring amine group. As a result of this protonation, the two NH_2-CH_2 and C-O bond lengths differ. For instance, C(2)-O(3) is shorter than C(21)-O(4) by 0.047 Å, and N(1)-C(8) is longer than N(2)-C(15) by 0.035 Å. The torsion angles C(6)-C(7)-C(8)-N(1) and N(2)-C(15)-C(16)-C(17) observed in *S*,*S*-**4** are +127.05(2)º and +111.64(3)º, respectively. Strong intramolecular O_{phenol}-H•••N_{amine} hydrogen bonds are present, contrary to what was observed previously in *R*,*R*-**1** and *R*,*R*-**3**.

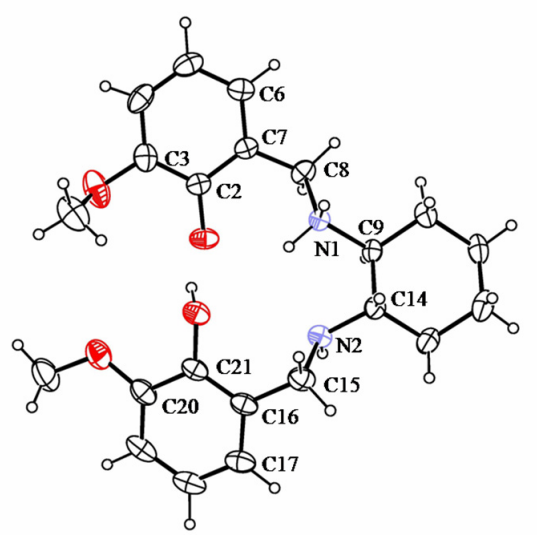

Figure 2.9- ORTEP-3 diagram of *S*,*S*-**4**, using 30 % probability level ellipsoids.

Figure 2.10 depicts *R*,*R*-**8** as a distorted structure which crystallizes in the orthorhombic system, space group $P2_12_12_1$. The asymmetric unit contains one neutral molecule. The torsion angles C(5)-C(6)-C(15)-N(1) and N(2)-C(22)-C(23)-C(28) observed in *R*,*R*-**8** are +136(2)º and +50(3)º, respectively. Similarly to what was observed in *S*,*S*-**4**, intramolecular O_{phenol}-H•••N_{amine} hydrogen bonds are present. A common feature of all described crystal structures is the chair conformation adopted by the cyclohexane ring.

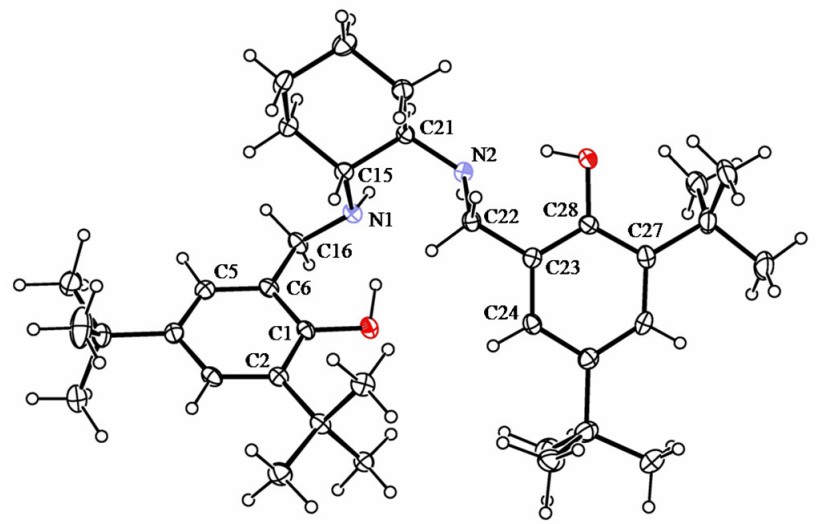

Figure 2.10- ORTEP-3 diagram of *R*,*R*-**8**, using 30 % probability level ellipsoids.

Table 2.3. Selected bond lengths and angles for *S*,*S*-**4** and *R*,*R*-**8**.

S,*S*-**4**		*R*,*R*-**8**	
Bond lengths (Å)			
N(1)-C(8)	1.493(3)	N(1)-C(15)	1.474(3)
N(1)-C(9)	1.500(3)	N(1)-C(16)	1.473(3)
N(2)-C(15)	1.458(3)	N(2)-C(21)	1.471(3)
N(2)-C(14)	1.459(3)	N(2)-C(22)	1.480(3)
C(2)-O(3)	1.321(2)	C(1)-O(1)	1.369(3)
C(21)-O(4)	1.368(3)	C(28)-O(2)	1.381(3)
Bond angles (º)			
C(8)-N(1)-C(9)	114.08(16)	C(15)-N(1)-C(16)	117.33(19)
C(15)-N(2)-C(14)	115.76(17)	C(21)-N(2)-C(22)	116.65(18)
O(3)-C(2)-C(3)	123.3(2)	O(1)-C(1)-C(6)	119.14(19)
O(3)-C(2)-C(7)	120.81(18)	O(1)-C(1)-C(2)	119.64(19)
O(4)-C(21)-C(16)	119.60(2)	O(2)-C(28)-C(27)	119.51(2)
O(4)-C(21)-C(20)	120.11(2)	O(2)-C(28)-C(23)	119.34(19)
N(1)-C(8)-C(7)	112.01(19)	N(1)-C(15)-C(6)	111.85(18)
N(2)-C(15)-C(16)	110.03(19)	N(2)-C(22)-C(23)	109.92(18)

The information provided by elemental analysis agrees satisfactorily with the expected molecular formulas for the prepared salan compounds. Solvent molecules, namely water, must be taken into account given the hygroscopic nature of the hydrochloride salts.

2.2.3. Aminoalcohol-derived compounds

Compounds *R*-**11**, *S*-**12**, *S*-**13**, and *S*-**14** were prepared by procedures similar to those described in previous section. First, the Schiff base was generated in methanol by condensing the chiral aminoalcohol with one equivalent of salicylaldehyde or any other substituted derivative. Since the objective was to obtain the reduced Schiff base compound, the generated Schiff base was reduced on site with $NaBH_4$. Except for *S*-**13**, all compounds were obtained as their hydrochloride salts to facilitate isolation and purification. Compound *S*-**13** could be easily obtained as the free base. The Schiff base compounds *S*-**15** and *S*-**16** were prepared similarly to the featured salen compounds solely for comparative purposes. All compounds were characterized by ^{1}H-NMR, ^{13}C-NMR, HSQC, HMBC, FT-IR and elemental analysis. Figure 2.11 depicts the structural formulas of the compounds prepared.

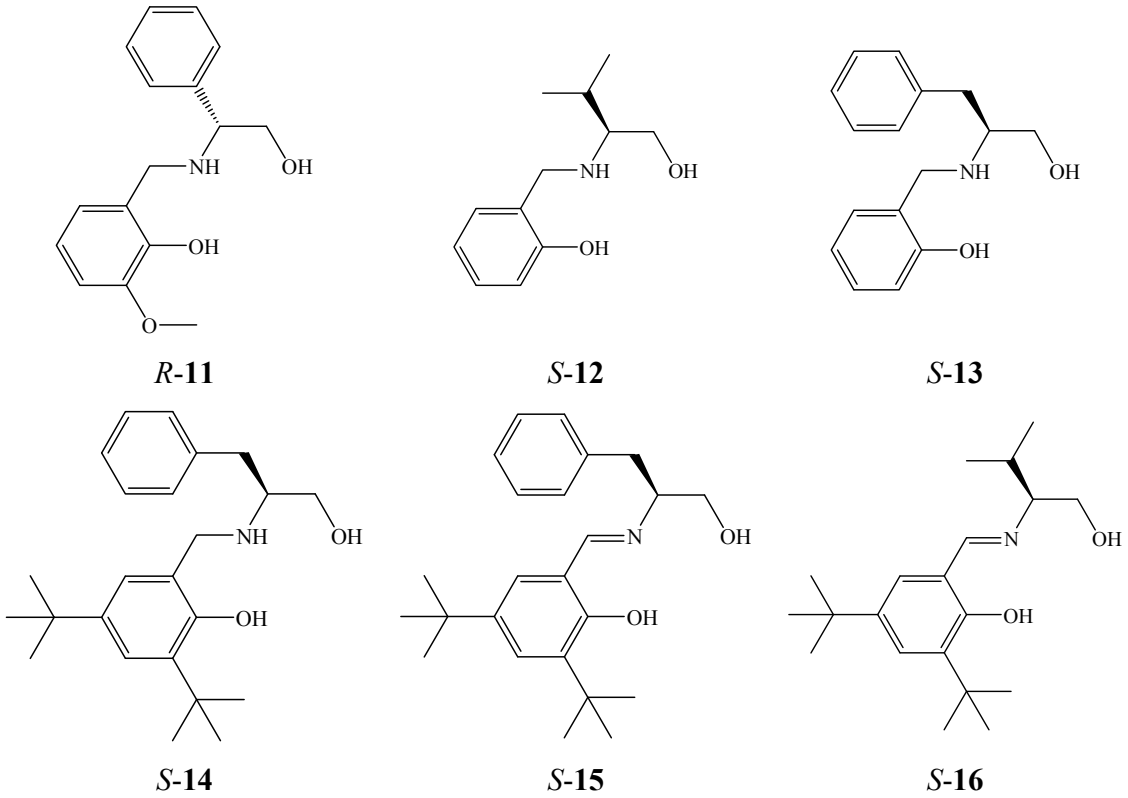

R-**11** *S*-**12** *S*-**13**

S-**14** *S*-**15** *S*-**16**

Figure 2.11- Structural formulas of the prepared aminoalcohol-derived compounds depicting their respective configuration.

The ^{1}H-NMR spectra of the featured aminoalcohol-derived compounds differ significantly from each other, as a result of the distinct aminoalcohol side-chains. Also, in contrast with what was observed with the tetradentate salan compounds, the ^{1}H-NMR spectra indicate C_1-symmetry in solution, which is consistent with the highly asymmetric structure of the compounds and with the prevalence of magnetically non-equivalent protons. Figures 2.12 to 2.15 show the ^{1}H-NMR spectra of compounds *R*-**11** to *S*-**14**.

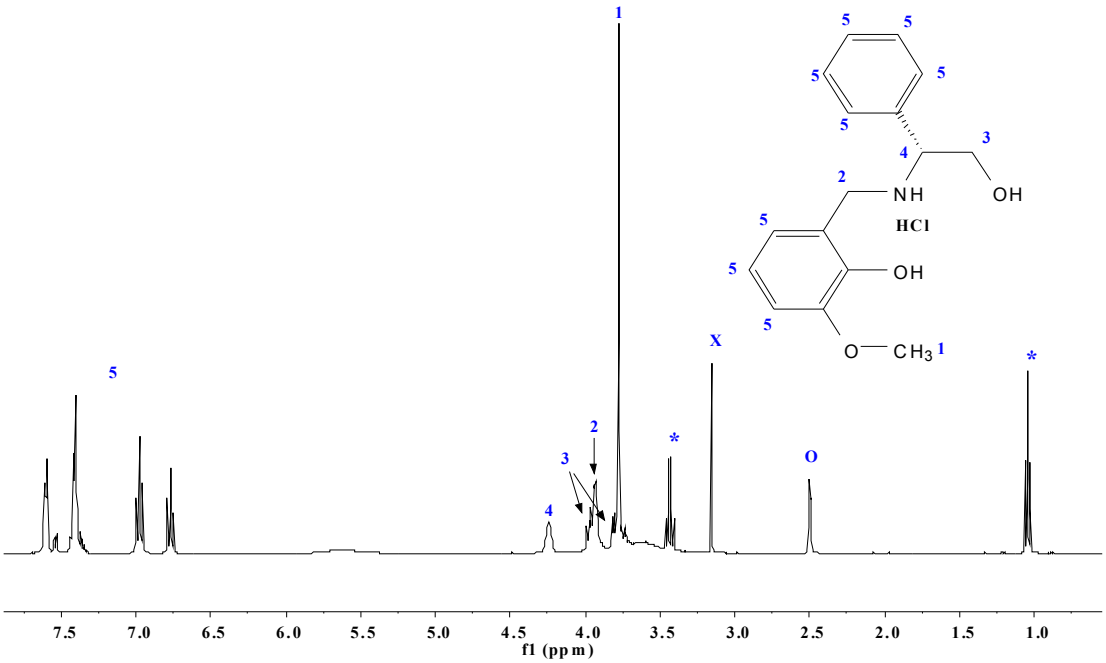

Figure 2.12- ^{1}H-NMR spectrum of *R*-**11** indicating C_1-symmetry in DMSO-d_6 solution. The asterisk and letters X and O represent residual ethanol, methanol and the deuterated solvent, respectively.

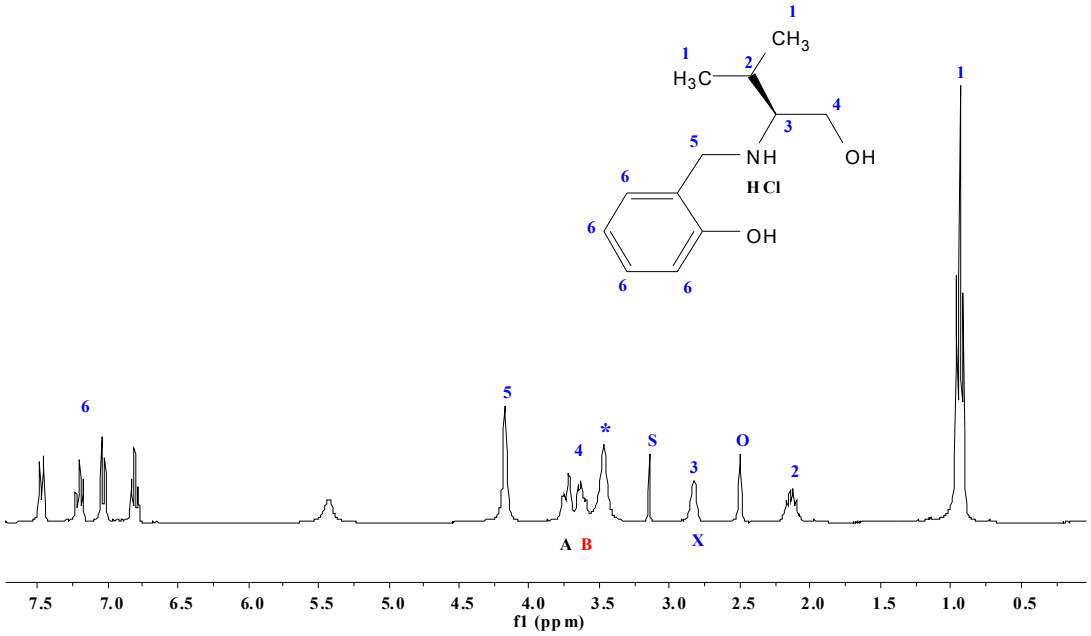

Figure 2.13- ^{1}H-NMR spectrum of *S*-**12** indicating C_1-symmetry in DMSO-d_6 solution. Due to the use of deuterated DMSO, the ABX multiplet pattern can be identified but the X multiplet is not resolved. The asterisk and letters S and O represent water, methanol and the deuterated solvent, respectively.

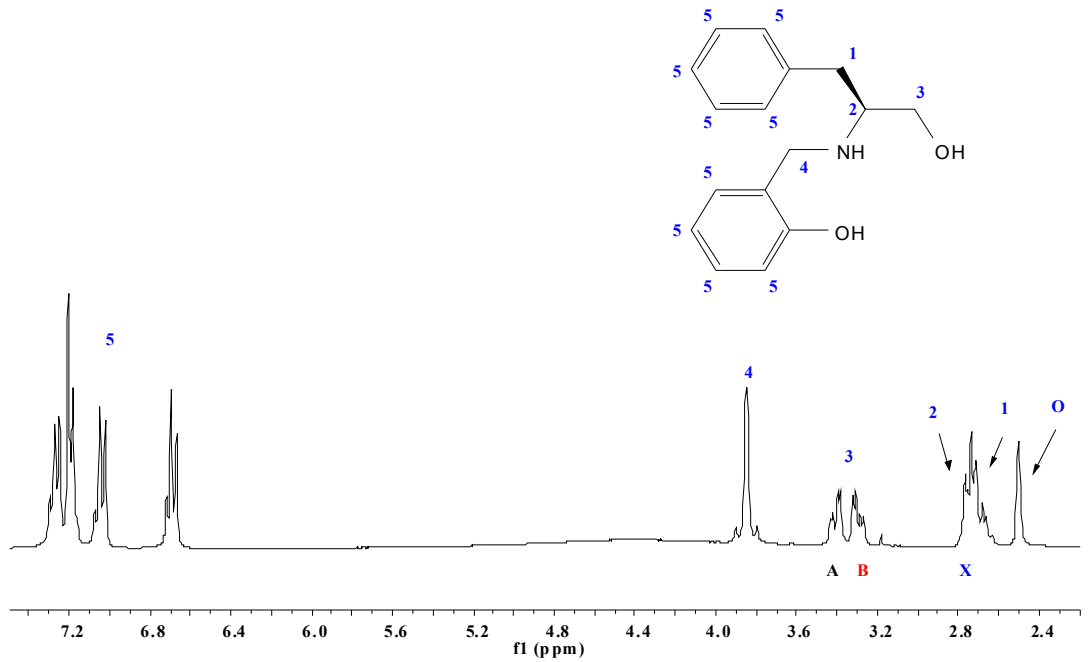

Figure 2.14- ^{1}H-NMR spectrum of *S*-**13** indicating C_1-symmetry in DMSO-d_6 solution. The ABX multiplet pattern is resolved but the X multiplet is overlapped with the resonances from the side-chain protons. The letter O represents the deuterated solvent.

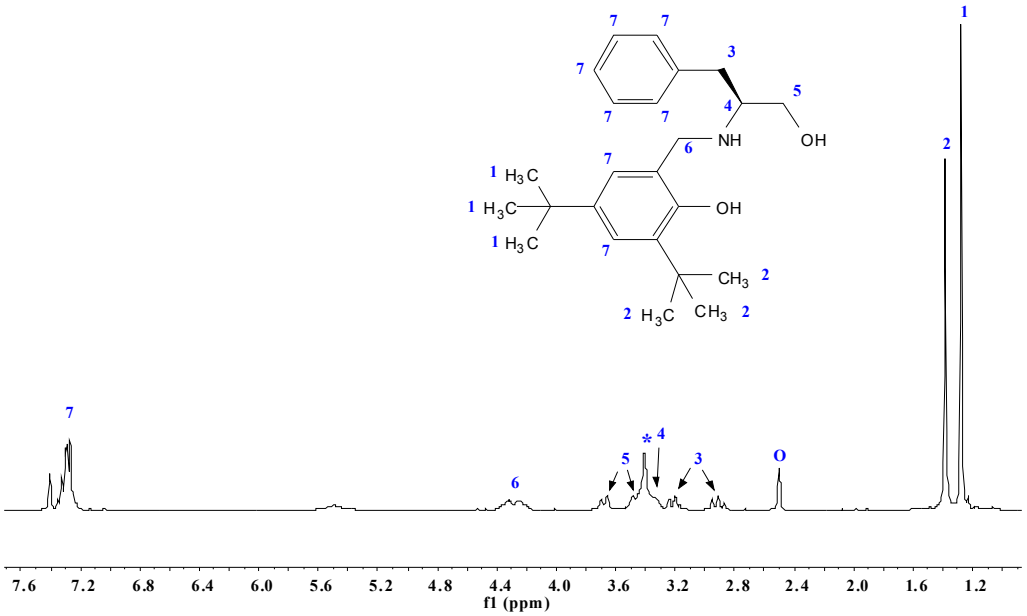

Figure 2.15- ^{1}H-NMR spectrum of *S*-**14** indicating C_1-symmetry in DMSO-d_6 solution. The resonances from the protons of the aminoalcohol moiety are all distinct. The asterisk and letter O represent the water residue and the deuterated solvent, respectively.

Common features are the three-spin system arising from the aminoalcohol backbone and side-chain methylene groups, which indicate diastereotopy. In some cases, namely compounds *S*-**13** and *S*-**15** (see Figures 2.14 and 2.16, respectively), resolved ABX verging on AMX multiplet patterns are visible. As such, the corresponding coupling constants cannot be obtained correctly by direct measurement in the case of ABX spin systems due to deceptive simplicity. Usually such analysis requires spectrum simulation which goes beyond the scope of the strictly necessary compound characterization. The methylene group bridging the phenolate and the diamine moieties does not appear as an AB system, contrasting with what was observed in the salan compounds.

Additional information was obtained by FT-IR spectroscopy and, as expected, all reduced Schiff base compounds yield a N-H stretching band is visible around 3400-3200 cm^{-1} while the Schiff base compounds yield the intense N=C stretching band at 1627 cm^{1}.

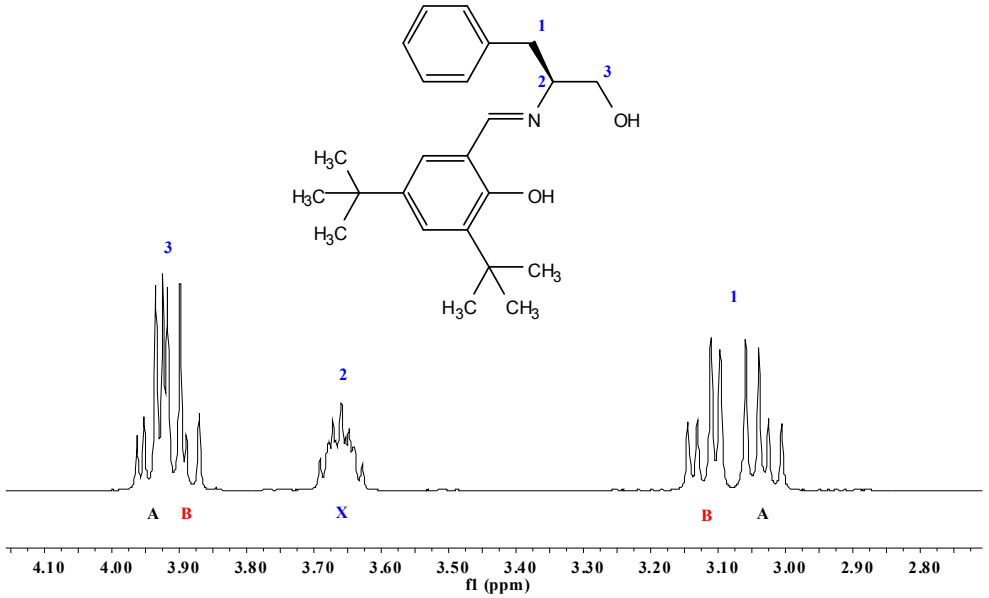

Figure 2.16- Expansion of the ^{1}H-NMR spectrum of *S*-**15** in $CDCl_3$ solution. The spectrum clearly exhibits two ABX multiplet patterns with the upfield pattern 1 verging on AMX. Methyne group proton 2 is the H_x proton in both three-spin systems.

Single crystals of *S*-**14** suitable for X-ray diffraction were obtained from slow evaporation of the respective solution in isopropanol. The ORTEP diagram is presented below in Figure 2.17 and the selected parameters are listed in Table 2.4.

Figure 2.17 depicts *S*-**14** as a distorted structure which crystallizes in the orthorhombic system, space group $P2_12_12_1$. The asymmetric unit contains one cationic molecule and one chloride anion. The torsion angle C(16)-C(11)-C(10)-N(1) observed in *S*-**14** is -90.04(2)º. Intramolecular O_{phenol}-H.•••N_{amine} hydrogen bonds do not exist possibly due to protonation of the amine nitrogen, but long N_{amine}-H•••Cl, $O_{alcohol}$-H.•••Cl and O_{phenol}-H.•••Cl hydrogen bonds are present. The structure exhibits disorder in the aromatic ring due to the existence of two energetically similar conformations. This disorder is reflected in the phenol oxygen, which is present in the positions O(2A) and O(2B) with 28% and 72% occupancy, respectively.

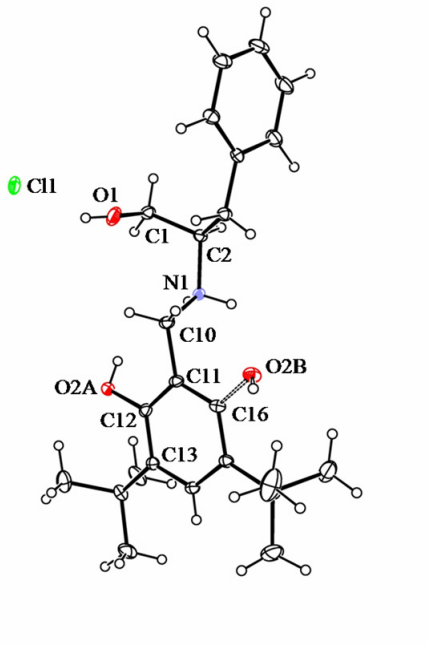

Figure 2.17- ORTEP-3 diagram of *S*-**14**, using 30 % probability level ellipsoids.

Table 2.4. Selected bond lengths and angles for *S*-**14**.

S-**14**	
Bond lengths (Å)	
N(1)-C(2)	1.515(3)
N(1)-C(10)	1.504(3)
O(1)-C(1)	1.405(3)
O(2)-C(12)	1.412(3)
Bond angles (º)	
C(2)-N(1)-C(10)	118.71(17)
N(1)-C(10)-C(11)	109.81(18)
O(1)-C(1)-C(2)	109.51(2)
O(2)-C(12)-C(13)	119.20(2)
O(2)-C(12)-C(11)	119.90(2)

The information provided by elemental analysis agrees satisfactorily with the expected molecular formulas for the prepared aminoalcohol compounds. As stated in the previous section, solvent molecules were taken into account given the hygroscopic nature of the hydrochloride salts.

2.2.4. Aminoacid-derived compound precursors

Compounds *S*-**17**, *S*-**18**, *R*-**19**, *R*-**20**, *S*-**21**, *S*-**22**, *R*-**23** and *R*-**24** were prepared using a similar synthetic procedure described in previous sections. Prior to the generation of the Schiff base and its reduction with $NaBH_4$, the required aminoacid was converted to its basic form with methanolic KOH. Special care was taken when using L-cysteine. To minimize cystine formation, all operations involving L-cysteine were carried out under a N_2 atmosphere. All compounds were obtained as their hydrochloride salts to facilitate isolation and purification. However, the conversion of the compounds into their acid forms in alcoholic medium also promoted the formation of the respective esters. Tripodal *S*-**26** was prepared using an adaptation of a reported procedure[8] by condensing basic L-alanine with formaldehyde and the appropriate disubstituted phenol in a single step Mannich reaction. The compound was obtained as the oxalate salt to allow separation from the monosubstituted by-product *S*-25. Tripodal *S*-**27** was prepared by condensing basic L-alanine with two equivalents of salicylaldehyde in a double reductive amination process using the milder reducing agent $NaBH(CH_3COO)_3$.[1] All compounds were characterized by ^{1}H NMR, ^{13}C NMR, HSQC, HMBC, FT-IR and elemental analysis. Figure 2.18 depicts the structural formulas of the compounds prepared.

Similarly to what was described in the previous section, the ^{1}H-NMR spectra of the featured aminoacid-derived compounds are fairly complex and differ according the aminoacid side-chains. Their highly asymmetric structure and the predominance of magnetically non-equivalent protons both indicate C_1-symmetry in solution in all cases. All ^{1}H NMR spectra exhibit intricate three-spin multiplet patterns resultant from spin coupling of aminoacid side-chain protons. Figures 2.19 and 2.21 show the ^{1}H-NMR spectra of *S*-**17** and *R*-**19**, respectively.

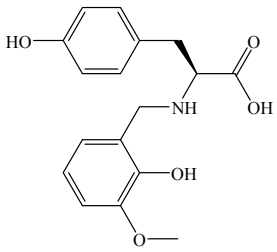

***S*-17**

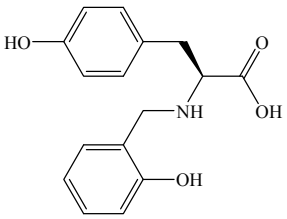

***S*-18**

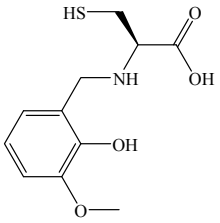

***R*-19**

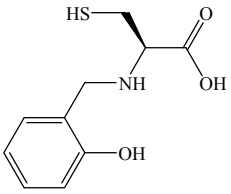

***R*-20**

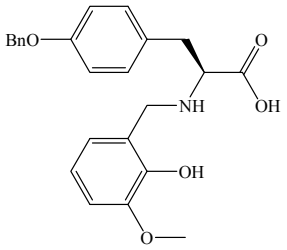

***S*-21**

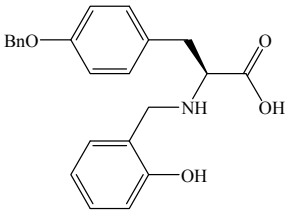

***S*-22**

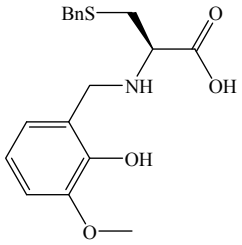

***R*-23**

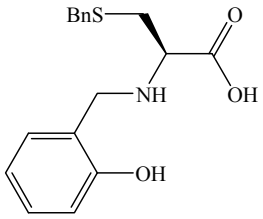

***R*-24**

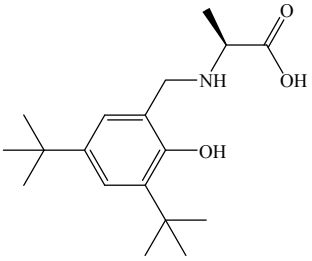

***S*-25**

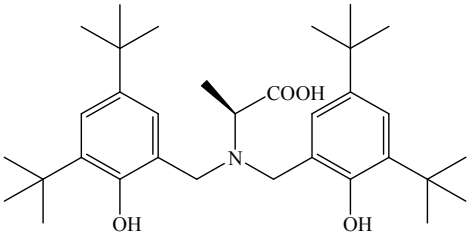

***S*-26**

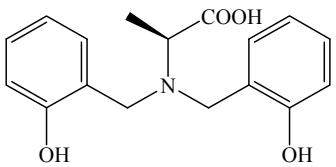

***S*-27**

Figure 2.18- Structural formulas of the prepared aminoacid-derived compounds depicting their respective configuration.

A three-spin AMX system is particularly evident in the ^{1}H-NMR spectra of *S*-**17** (see Figures 2.19 and 2.20). In this particular case the resonances at 3.05 and 3.28 ppm are part of a doublet of doublets resulting from geminal H_A-H_M coupling with $^{2}J_{AM}$ of 13.9 Hz. Each signal is then split again into a doublet of doublets by coupling with H_X, but the AB system at 3.05 ppm has $^{3}J_{AX}$ of 8.4 Hz while the AB system at 3.28 ppm has $^{3}J_{MX}$ of 4.4 Hz. As a result of the marked magnetic non-equivalence exhibited by these diastereotopic benzylic protons, the resonance at 3.92 ppm corresponding to the lone proton attached to chiral carbon is also an AB system with coupling constants $^{3}J_{AX}$ of 7.9 Hz and $^{3}J_{MX}$ of 4.8 Hz. These AMX multiplet patterns occur in all ^{1}H-NMR spectra of the L-tyrosine derived compounds while the L-cysteine derived ones yield three-spin ABX multiplet systems verging on AMX.

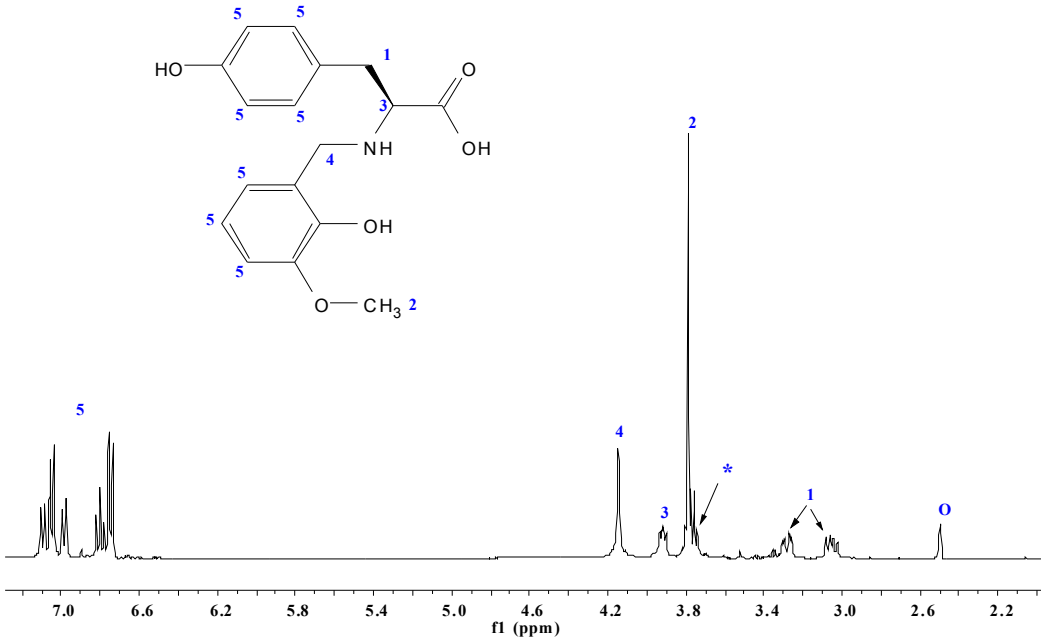

Figure 2.19- ^{1}H-NMR spectrum of *S*-**17** in DMSO-d_6 solution. The presented spectrum clearly exhibits a three-spin AMX multiplet pattern. The asterisk and letter O represent ethanol residue and the deuterated solvent, respectively.

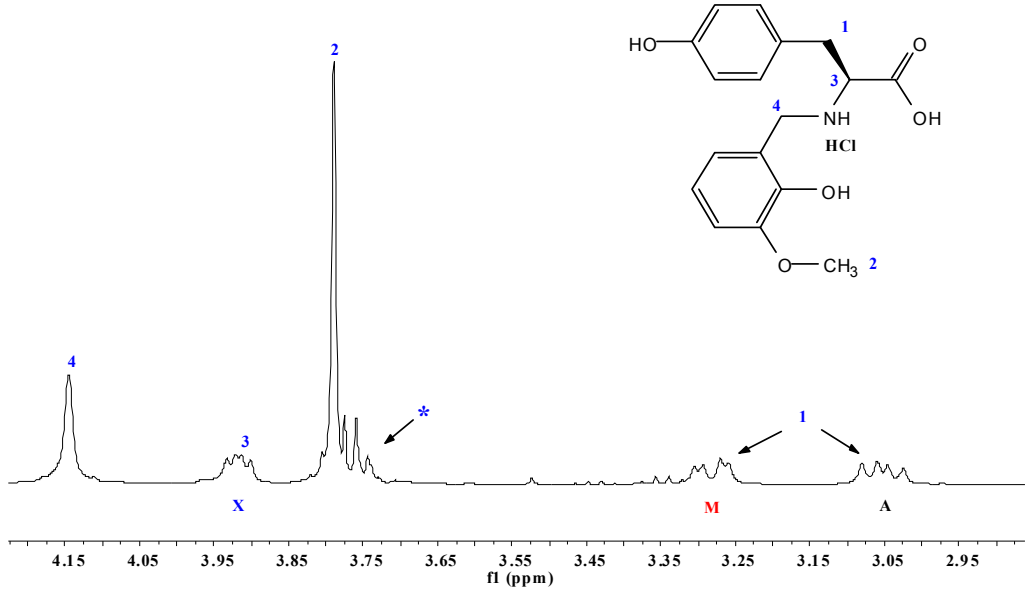

Figure 2.20- ^{1}H-NMR spectrum of *S*-**17** in DMSO-d_6 solution with the AMX multiplet pattern in more detail. The asterisk represents an ethanol residue.

Spectra of L-cysteine derived compounds such as *R*-**19** (see Figure 2.11) have additional complexity due to the almost inevitable presence of the corresponding disulfide by-products which yield signals often overlapping those originated from the main product. Alkyl ester derivatives of the prepared compounds are also present, though in varying extents, due to the formation of the respective hydrochloride salts in alcoholic solutions.

The tripodal L-alanine derived compounds gave simpler spectra, reflecting the simple structure of L-alanine. In addition, the monophenolate and bisphenolate products could be rapidly identified in ^{13}C NMR by the characteristic chemical shifts of the methylene groups bridging the phenol and aminoacid moieties, as depicted in Figure 2.22. Separation of the bisphenolate products is often difficult, especially when the 1,3-benzoxazine by-product is present. While the monophenolate product can be recovered as either a hydrochloride or oxalate salt, the respective salts of the 1,3-benzoxazine impurities exhibit solubility similar with the salts of bisphenolate products. Additionally, the degradation of the 1,3-benzoxazine impurities cannot be accomplished by heating in acid ethanol as the bisphenolate products tend to decompose in these conditions.

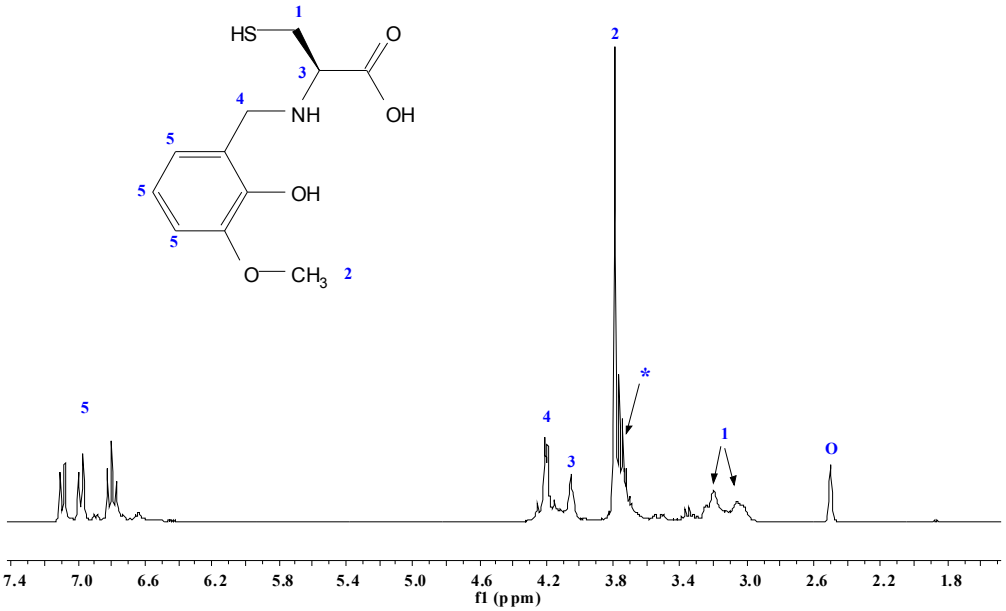

Figure 2.21- ^{1}H-NMR spectrum of *R*-**19** in DMSO-d_6 solution. The presented spectrum clearly exhibits a three-spin ABX multiplet pattern verging on AMX. The asterisk and letter O represent isopropanol residue and deuterated solvent, respectively.

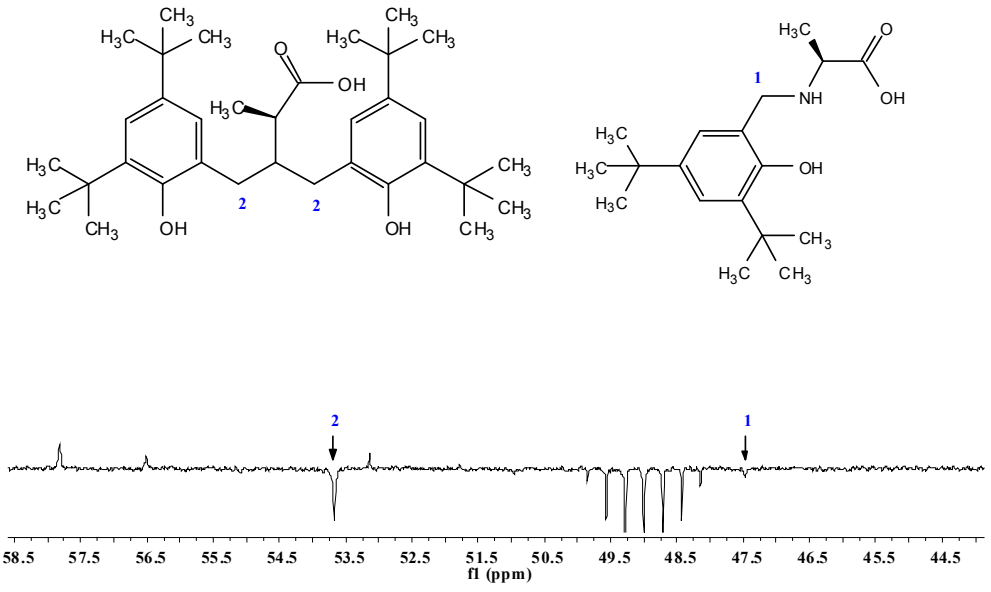

Figure 2.22- Section of the ^{13}C{^{1}H} NMR APT spectra of *S*-**26** in CD_3OD solution where the two possible Mannich reaction products can be identified: the monophenolate (1) and the tripodal bisphenolate (2).

Additional information was obtained by FT-IR spectroscopy. All reduced aminoacid derived compounds yield a N-H stretching band around 3400-3200 cm^{-1} and a carboxyl C=O stretching band at 1738 cm^{-1}. No single crystals suitable for X-ray diffraction were obtained. The information provided by elemental analysis agrees satisfactorily with the expected molecular formulas for the prepared aminoacid compounds. As stated in the previous section, solvent molecules were taken into account given the hygroscopic nature of the hydrochloride salts.

2.3. Conclusions

A wide array of chiral compounds was successfully prepared and characterized. In the case of the tetradentate salen and salan compounds, chirality was introduced by employing chiral diamines such as (1*R*,2*R*)-cyclohexane-1,2-diamine, (1*S*,2*S*)-cyclohexane-1,2-diamine or (1*S*,2*S*)-1,2-diphenylethylene-1,2-diamine. The tridentate compounds tapped into the wider and more readily available chiral pool of the aminoalcohols and aminoacids. Chiral aminoalcohols such as L-valinol, L-phenylalaninol and D-phenylglycinol were successfully employed in the preparation of tridentate compounds. Aminoacid-derived compounds based on L-tyrosine and L-cysteine were also prepared with success, although tripodal compounds based on L-alanine proved difficult to synthesize and isolate. Compound preparation was made mainly by reductive amination of salicylaldehyde derivatives, while some cases required a modified Mannich reaction for successful preparation. The conversion of the compounds as their hydrochloride or oxalate salts simplified the general purification and isolation processes and subsequent handling, though the Schiff bases and some of the reduced Schiff base compounds could be isolated without resorting to this methodology.

2.4. Experimental section

2.4.1. General Considerations

Unless stated otherwise, all preparations and subsequent manipulations were made without resorting to inert atmosphere techniques. All solvents and reagents were purchased from commercial suppliers and used as received.

2.4.2. Characterization Techniques

2.4.2.1. Nuclear Magnetic Resonance Spectroscopy (NMR)

1D NMR (^{1}H, ^{13}C-{1H}, ^{13}C-{1H} APT) and 2D NMR (HSQC and HMBC) spectra were recorded on Bruker Advance II+ 300 and 400 MHz (UltraShield Magnet) instruments at ambient temperature, unless stated otherwise. ^{1}H and ^{13}C chemical shifts (δ) are expressed in ppm relative to Me_4Si. Whenever calculation is possible, coupling constants *J* are given in Hz and multiplicities are presented as: br (broad), s (singlet), d (doublet), dd (double doublet), t (triplet), q (quartet), sept (septet) and m (multiplet).

2.4.2.2. Infrared Spectroscopy (FT-IR)

FT-IR spectra were recorded in KBr using a *JASCO FT/IR-430* spectrometer.

2.4.2.3. Elemental Analysis (EA)

Elemental analyses were carried out at *Laboratório de Análises* of *Instituto Superior Técnico,* using a EA110 CE automatic analyzer Instrument. The results presented are the average values obtained from two independent determinations.

2.4.2.4. X-Ray crystallography

Single crystals suitable for X-ray diffraction crystallography were obtained as described in the compound preparation methods sections. The data collection, structure solution and refinement for all the featured crystal structures in this Chapter were done by Dr. Fernando Avecilla at the Departamento de Química Fundamental of Universidade da Coruña. X-ray data for *R*,*R*-**1**, *R*,*R*-**3**, *S*,*S*-**4**, *R*,*R*-**6a**, *S*,*S*-**5a**, *R*,*R*-**8** and *S*-**13** were

collected on a Bruker Smart 1000 CCD diffractometer and on a Bruker Kappa X8 Apex CCD diffractometer. Data were collected at room temperature. Reflections were measured from a hemisphere of data collected of frames, each covering 0.3º in ω. The reflections measured were corrected for Lorentz and polarization effects, and for absorption by semiempirical methods based on symmetry-equivalent and repeated reflections. Complex scattering factors were taken from the program package SHELXTL.[9] For *R*,*R*-**1**, *R*,*R*-**3**, *S*,*S*-**4**, *R*,*R*-**8** and *S*-**13** the absolute configuration was established by refinement of the enantiomorph polarity parameter.[10] The structures were solved by direct methods and refined by full-matrix least-squares methods on F^2. The non-hydrogen atoms were refined with anisotropic thermal parameters in all cases. The hydrogen atoms were left to refine freely in all cases.

Table 2.5. Crystal data and refinement data for *S*,*S*-**5a** and *R*,*R*-**6a**.

Compound	*S*,*S*-**5a**	*R*,*R*-**6a**
Empirical formula	$C_{24}H_{30}N_2O_4$	$C_{28}H_{26}N_2O_2$
Formula weight	410.50	422.51
Temperature / K	100(2)	100(2)
Wavelength / Å	0.71073	0.71073
Crystal system	Triclinic	Orthorhombic
Space group	*P*-1	$P2_12_12_1$
Unit cell dimensions	a = 10.0324(4) α = 116.1610(10) b =11.5043(5) β = 109.6540(10) c =11.7327(5) γ = 97.3130(10)	a =9.3699(7) α= 90° b =9.4651(8) β= 90° c =25.339(2) γ = 90°
Volume / Å^3	1082.07(8)	2247.2(3)
Z	2	4
Density (calculated) / mg/m^3	1.245	1.260
Absorption coefficient /mm^{-1}	0.086	0.079
Crystal size / mm^3	0.27 × 0.22 × 0.17	0.40 × 0.43 × 0.28
Reflections collected	14827	21766
Independent reflections	4118 [R(int) = 0.0297]	2679 R(int) = 0.0448]
Goodness-of-fit on F_2	1.043	1.116
Final R indices [I>2σ (I)]	R1 = 0.0397, wR2 = 0.1020	R1 = 0.0362, wR2 = 0.1108
Absolute structure parameter		0(10)

Table 2.6. Crystal data, data collection and refinement data for *R*,*R*-**1** and *R*,*R*-**3**.

Compound	*R*,*R*-**1**	*R*,*R*-**3**
Empirical formula	$C_{23}H_{38}Cl_2N_2O_4$	$C_{22}H_{36}Cl_4N_4O_4$
Formula weight	477.45	580.36
Temperature / K	100(2)	100(2)
Wavelength / Å	0.71073	0.71073
Crystal system	Monoclinic	Monoclinic
Space group	$P2_1$	$C2$
Unit cell dimensions	a = 9.0813(4) α= 90°	a = 12.7428(5) α= 90°
	b = 16.0307(7) β = 117º	b = 9.7347(3) β= 104º
	c = 9.8496(4) γ = 90°	c = 11.4164(4) γ = 90°
Volume / Å^3	1273.27(9)	1374.18(8)
Z	2	2
Density (calculated) / mg/m^3	1.245	1.403
Absorption coefficient /mm^{-1}	0.285	0.470
Crystal size / mm^3	0.40 × 0.43 × 0.28	0.42 × 0.37 × 0.30
Reflections collected	9352	6363
Independent reflections	4232 [R(int) = 0.0149]	2437 [R(int) = 0.0145]
Goodness-of-fit on F2	1.033	1.154
Final R indices [I>2σ(I)]	R1 = 0.0222, wR2 = 0.0614	R1 = 0.0222, wR2 = 0.0614
Absolute structure parameter	0.01(5)	0.04(4)

Table 2.7. Crystal data, data collection and refinement data for *S*,*S*-**4** and *R*,*R*-**8**.

Compound	*S*,*S*-**4**	*R*,*R*-**8**
Empirical formula	$C_{22}H_{30}N_2O_4$	$C_{36}H_{58}N_2O_2$
Formula weight	386.48	550.84
Temperature / K	293(2) K	293(2) K
Wavelength / Å	0.71073	0.71073 Å
Crystal system	Orthorhombic	Orthorhombic
Space group	$P2_12_12_1$	$P2_12_12_1$
Unit cell dimensions	a = 12.7428(5) Å α= 90°	a= 12.1902(4) Å α= 90°
	b = 9.7347(3) Å β= 90°	b= 13.9090(4) Å β= 90°
	c = 11.4164(4) Å γ = 90°	c= 20.4266(6) Å γ = 90°
Volume / Å^3	2019.12(17)	3463.40(18)
Z	4	4
Density (calculated) / mg/m^3	1.271	1.056
Absorption coefficient /mm^{-1}	0.087	0.064
Crystal size / mm^3	0.50 × 0.23 × 0.23	0.42 × 0.23 × 0.10
Reflections collected	24365	28969
Independent reflections	4932 [R(int) = 0.0473]	8434 [R(int) = 0.0610]
Goodness-of-fit on F2	1.088	1.029
Final R indices [I>2sigma(I)]	R1 = 0.0443, wR2 = 0.0971	R1 = 0.0521, wR2 = 0.1094
Absolute structure parameter	0.4(13)	0.5(14)

Table 2.8. Crystal data, data collection and refinement data for *S*-**14**.

Compound	*S*-**14**	
Empirical formula	$C_{24}H_{35}ClNO_2$	
Formula weight	404.98	
Temperature / K	293(2) K	
Wavelength / Å	0.71073	
Crystal system	Orthorhombic	
Space group	$P2_12_12_1$	
Unit cell dimensions	a = 8.6795(2)	α= 90°
	b = 15.8201(3)	β= 90°
	c = 16.7277(3)	γ = 90°
Volume / Å^3	2296.89(8)	
Z	4	
Density (calculated) / mg/m^3	1.171	
Absorption coefficient /mm^{-1}	0.185	
Crystal size / mm^3	0.36 × 0.10 × 0.09	
Reflections collected	30067	
Independent reflections	5751 [R(int) = 0.0531]	
Goodness-of-fit on F2	1.050	
Final R indices [I>2sigma(I)]	R1 = 0.0475, wR2 = 0.1229	
R indices (all data)	R1 = 0.0598, wR2 = 0.1353	
Absolute structure parameter	0.92(7)	

2.4.3. Compound Preparation Methods

2.4.3.1. Salen-type compounds

Synthesis of 2,2'-(1*E*,1'*E*)-(cyclohexane-1,2-diylbis(azan-1-yl-1-ylidene))bis(methan-1-yl-1-ylidene)diphenol (*R*,*R*-1a)

The tartrate salt of (1*R*,2*R*)-cyclohexane-1,2-diamine or (1*S*,2*S*)-cyclohexane-1,2-diamine (1.00 g, 3.78 mmol) was suspended in 25 mL of methanol. KOH (0.43g, 7.26 mmol) was added and dissolved. Salicylaldehyde (0.95 g, 7.79 mmol) was then added to the reaction mixture. After 30 minutes, the solvent was evaporated and the bright yellow residue was washed with copious amounts of water and small portions of a 1:1 ethanol:water mixture. Yield: 1.09 g, 90 %. ^{1}H NMR (300 MHz, CD_3OD, ppm): δ 1.53, 1.86, 1.95, 2.00 [8H, m, -CH_2-], 3.36 [1H, m, CH_2C*H*-N], 3.67 [1H, m, CH_2C*H*-N], 6.79 [4H, m, aromatic], 7.19, 7.30 [4H, m, aromatic], 8.31 [1H, s, Ar-C*H*=N], 8.43 [1H, s, Ar-C*H*=N]. IR (cm^{-1}): 1627

(νC=N), 1280 (νC-O). Elemental analysis for $C_{20}H_{22}N_2O_2 \cdot 0.1C_2H_5OH$: calcd. C 74.2, H 7.0, N 8.6; found C 74.4, H 7.4, N 8.7.

Synthesis of 2,2'-(1*E*,1'E)-(1,2-diphenylethane-1,2-diyl)bis(azan-1-yl-1-ylidene)bis(methan-1-yl-1-ylidene)diphenol (*S*,*S*-2a)

The procedure was similar to that used for the synthesis of *R,R*-**1a**. Reagents: (1*S*,2*S*)-1,2-diphenylethane-1,2-diamine (0.3 g, 1.41 mmol), salicylaldehyde (0.35 g, 2.83 mmol). The compound was obtained as a bright yellow solid. Yield: 0.58 g, 98 %. ^{1}H NMR (300 MHz, DMSO-d_6, ppm): δ 5.08 [2H, s, Ar-C*H*-], 6.85 [4H, m, aromatic], 7.25 [14H, m, aromatic], 8.52 [2H, s, Ar-C*H*=N]; IR (cm^{-1}): 1627 (νC=N), 1269 (νC-O); Elemental analysis for $C_{28}H_{24}N_2O_2 \cdot 0.4C_2H_5OH$: calcd. C 78.6, H 5.8, N 6.6; found C 78.6, H 6.0, N 7.0.

Synthesis of 4,4'-(1*E*,1'*E*)-(1*R*,2*R*)-cyclohexane-1,2-diylbis(azan-1-yl-1-ylidene)bis(methan-1-yl-1-ylidene)bis(5-(hydroxymethyl)-2-methylpyridin-3-ol) (*R*,*R*-3a)

The procedure was similar to that used for the synthesis of *R,R*-**1a**. Reagents: (1*R*,2*R*)-cyclohexane-1,2-diamine (5.28 g, 20 mmol), pyridoxal hydrochloride (8.12 g, 40 mmol) were used as starting building blocks. The compound was obtained as a bright yellow solid. Yield: 8.13 g, 98 %. (300 MHz, DMSO-d_6, ppm): δ 1.68, 1.84, 1.98, 2.09 [8H, m, -CH_2-], 2.67 [6H, s, CH_3-Ar], 3.75 [2H, m, CH_2C*H*-N], 4.72 [4H, s, HOCH_2-Ar], 8.09 [2H, s, aromatic], 9.01 [2H, s, Ar-C*H*=N], IR (cm^{-1}): 1627 (νC=N), 1290 (νC-O). Elemental analysis for $C_{22}H_{28}N_4O_4 \cdot 0.7H_2O$: calcd. C 62.2, H 7.0, N 13.2; found C 62.2, H 7.2, N 13.5.

Synthesis of 6,6'-(1*E*,1'*E*)-(1*R*,2*R*)-cyclohexane-1,2-diylbis(azan-1-yl-1-ylidene)bis(methan-1-yl-1-ylidene)bis(2-methoxyphenol) (*R*,*R*-4a)

The procedure was similar to that used for the synthesis of *R,R*-**1a**. Reagents: (1*R*,2*R*)-cyclohexane-1,2-diamine (2.32 g, 8.78 mmol), 3-methoxysalicylaldehyde (2.67 g, 17.57 mmol). The compound was obtained as a bright yellow solid. Yield: 2.76 g, 82 %. ^{1}H NMR (300 MHz, DMSO-d_6, ppm): δ 1.45, 1.63, 1.79, 1.87 [8H, m, -CH_2-], 3.33 [2H, m,

CH_2CH-N], 3.72 (6H, s, CH_3O-Ar], 6.79, 6.94 [6H, m, aromatic], 8.47 [2H, s, Ar-C*H*=N]; IR (cm^{-1}) 1627 (νC=N), 1290 (νC-O). Elemental analysis for $C_{22}H_{26}N_2O_4 \cdot 0.35C_4H_{10}O$: calcd. C 68.9, H 7.3, N 6.9; found C 68.9, H 7.7, N 7.3.

Synthesis of 6,6'-(1*E*,1'*E*)-(1*S*,2*S*)-cyclohexane-1,2-diylbis(azan-1-yl-1-ylidene)bis(methan-1-yl-1-ylidene)bis(2-ethoxyphenol) (*S*,*S*-5a)

The procedure was similar to that used for the synthesis of *R,R*-**1a**. After filtration, the bright yellow solid obtained was washed with small amounts of dichloromethane. Reagents: (1*S*,2*S*)-cyclohexane-1,2-diamine (2.32 g, 8.78 mmol), 3-ethoxysalicylaldehyde (2.91 g, 17.53 mmol). The compound was obtained as a bright yellow solid. Yield: 3.6 g, 98 %. ^{1}H NMR (300 MHz, DMSO-d_6, ppm): δ 1.29, 1.36 [6H, t, $^3J_{HH}$ = 7.0 Hz, CH_3CH_2O-Ar], 1.44, 1.80, 1.91, 1.97 [8H, m, -CH_2-], 3.67 [2H, m, CH_2CH-N], 4.0, 4.09 [4H, q, $^3J_{HH}$ = 7.0 Hz, CH_3CH_2O-Ar], 6.63, 6.73, 6.94, 7.11 [2H, m, aromatic], 8.50 [2H, s, Ar-C*H*=N]. IR (cm^{-1}): 1653 (νC=N), 1252 (νC-O). Elemental analysis for $C_{24}H_{30}N_2O_4 \cdot 3.5H_2O \cdot 2.5CH_2Cl_2$: calcd. C 62.4, H 7.6, N 5.0; found C 62.2, H 7.7, N 5.1. Crystals suitable for single crystal X-ray diffraction were grown from acetonitrile solutions. 0.1 g of **5a** was dissolved in *ca*. 10 mL of acetonitrile and the resulting solution was filtered and transferred to a clean lint-free 20 mL glass flask. Yellow crystals were obtained by slow evaporation of the solvent upon *ca*. four weeks.

Synthesis of 1,1'-(1*E*,1'*E*)-(1*R*,2*R*)-cyclohexane-1,2-diylbis(azan-1-yl-1-ylidene)bis(methan-1-yl-1-ylidene)dinaphthalen-2-ol (*R*,*R*-6a)

The procedure was similar to that used for the synthesis of *R,R*-**1a**. Reagents: 1*R*,2*R*-cyclohexane-1,2-diamine (2.32 g, 8.78 mmol), 2-hydroxy-1-naphthaldehyde (3.02 g, 17.57 mmol). The compound was obtained as a bright yellow solid. Yield: 3.70 g, 75 %. ^{1}H NMR (400 MHz, DMSO-d_6, ppm): δ 1.43, 1.73, 2.25, 2.29 [8H, m, -CH_2-], 3.57 [2H, m, CH_2CH-N], 6.73, 7.16, 7.36, 7.58, 7.66, 8.00 [12H, m, aromatic], 9.13 [2H, s, Ar-C*H*=N]. IR (cm^{-1}): 1627 (νC=N), 1290 (νC-O). Elemental analysis for $C_{28}H_{26}N_2O_2 \cdot 0.2CH_3OH$: calcd. C 79.0, H 6.3, N 6.5; found C 79.1, H 6.6, N 6.3. Crystals suitable for single crystal X-ray diffraction were grown from methanolic solutions. 0.1 g of **6a** was dissolved in *ca*. 10 mL of methanol and the resulting solution was filtered and

transferred to a clean lint-free 20 mL glass flask. Yellow crystals were obtained by slow evaporation of the solvent upon *ca*. two weeks.

2.4.3.2. Salan-type compounds

Synthesis of (1*R*,2*R*)-N^1,N^2-bis(2-hydroxybenzyl)cyclohexane-1,2-diaminium chloride (*R*,*R*-1)

The tartrate salt of (1*R*,2*R*)-cyclohexane-1,2-diamine or (1*S*,2*S*)-cyclohexane-1,2-diamine (1.00g, 3.78 mmol) was suspended in 25 mL of methanol. KOH (0.43g, 7.26 mmol) was added and dissolved. Salicylaldehyde (0.95 g, 7.8 mmol) was added to the suspension and $NaBH_4$ was slowly added till the reaction mixture became colorless. The pH was then adjusted to 1-1.5 with an aqueous 4 M HCl solution. The solvent was evaporated and the white residue extracted with an ethanol:diethyl ether (70:30) liquid phase, the inorganic solids being separated by filtration. By evaporation of the solvent, a white solid was obtained which was then washed with diethyl ether. Yield: 0.95 g, 78 %. ^{1}H NMR (400 MHz, D_2O, ppm): δ 1.43, 1.73, 2.25, 2.29 [8H, m, -CH_2-], 3.57 [2H, m, CH_2CH-N^+H_2], 4.13, 4.27 [4H, d, $^2J_{HH}$ = 13 Hz, Ar-CH_2-N^+H_2], 6.95 [4H, m, aromatic], 7.33 [4H, m, aromatic]. ^{13}C-{^{1}H} NMR (100 MHz, D_2O, ppm): δ 20.27, 24.39 [4C, -CH_2-], 43.76 [2C, Ar-CH_2-N^+H_2], 56.33 [2C, -(CH_2)$_2$-CH-N^+H_2], 114.48, 115.37, 119.63, 130.56, 130.71, 153.85 [12C, aromatic]. IR (cm^{-1}): 3212 (νN–H), 1269 (νC-O). Elemental analysis for $C_{20}H_{28}N_2O_2 \cdot 2H_2O$: calcd. C 55.2, H 7.4, N 6.4; found C 55.2, H 7.4, N 6.4. Crystals suitable for single crystal X-ray diffraction were grown from isopropanol solutions. 0.1 g of *R,R*-**1** was dissolved in *ca*. 10 mL of isopropanol and the resulting solution was filtered and transferred to a clean lint-free 20 mL glass flask. Colorless crystals were obtained by slow evaporation of the solvent after four weeks.

Synthesis of (1*S*,2*S*)-N^1,N^2-bis(2-hydroxybenzyl)-1,2-diphenylethane-1,2-diaminium chloride (*S*,*S*-2)

The procedure was similar to that used for the synthesis of *R*,*R*-**1**. Reagents: (1*S*,2*S*)-1,2-diphenylethane-1,2-diamine (0.3 g, 1.4 mmol), salicylaldehyde (0.35 g, 2.8 mmol). The compound was obtained as a white solid. Yield: 0.54 g, 78 %. ^{1}H NMR (400 MHz,

DMSO-d_6, ppm): δ 3.59 [2H, t, $^3J_{HH}$ = 6.6 Hz, Ar-C*H*-N^+H], 3.70, 3.89 [4H, d, $^2J_{HH}$ = 12.6 Hz, Ar-CH_2-N^+H_2], 6.80 [4H, m, aromatic], 6.89 [4H, m, aromatic], 7.21 [6H, m, aromatic], 7.33 [4H, m, aromatic]. ^{13}C-{^{1}H} NMR (100 MHz, DMSO-d_6, ppm): δ 45.07 [2C, Ar-*C*H2-N^+H2], 56.33 [2C, Ar-*C*HN^+H2], 114.48, 115.37, 119.63, 130.56, 130.71, 153.85 [24C, aromatic]. IR (cm^{-1}): 3222 (νN–H), 1266 (νC-O). Elemental analysis for $C_{28}H_{32}N_2O_2{\cdot}2H_2O{\cdot}C_3H_7OH$: calcd. C 62.7, H 7.1, N 5.0; found C 62.5, H 6.7, N 4.6.

Synthesis of 4,4'-(1*R*,2*R*)-cyclohexane-1,2-diylbis(ammoniodiyl)bis(methylene)bis(3-hydroxy-5-(hydroxymethyl)-2-methylpyridinium) chloride (*R*,*R*-3)

The procedure was similar to that used for the synthesis of *R*,*R*-**1**. Reagents: (1*R*,2*R*)-cyclohexane-1,2-diamine (2.64 g, 10 mmol), pyridoxal hydrochloride (4.06 g, 20 mmol). The compound was obtained as a pale yellow solid. Hygroscopic. Yield: 3.66 g, 89 %. ^{1}H NMR (400 MHz, CD_3OD, ppm): δ 1.52, 1.74, 1.93, 2.53 [8H, m, -CH_2-], 2.72 [6H, s, CH_3-Ar], 3.67 [2H, m, -CH_2C*H*N^+H_2], 4.49, 4.65 [4H, d, $^2J_{HH}$= 13.1 Hz, Ar-CH_2-N^+H_2], 4.93 [4H, s, $^2J_{HH}$, HOCH_2-Ar], 8.27 [2H, s, aromatic]. ^{13}C-{^{1}H} NMR (100 MHz, CD_3OD, ppm): δ 14.01 [2C, *C*H_3Ar], 21.27, 25.39 [4C, -*C*H_2-], 41.31 [2C, *C*H_2-Ar], 60.26 [2C, HO*C*H_2-Ar], 60.31 [2C, -CH_2*C*HN^+H_2], 131.85, 136.90, 141.23, 143.73, 155.61 [10C, aromatic]. IR (cm^{-1}): 3250 (νN–H), 1254 (νC-O). Elemental analysis for $C_{22}H_{34}N_4O_4Cl_2{\cdot}7.5H2O$: calcd. C 42.31, H 7.91, N 8.97; found: C 42.5, H 7.5, N 8.6. Brown crystals suitable for single crystal X-ray diffraction were obtained from the moist, viscous compound which crystallized after several months.

Synthesis of (1*S*,2*S*)-N1,N2-bis(2-hydroxy-3-methoxybenzyl)cyclohexane-1,2-diaminium chloride (*S*,*S*-4)

Procedure was similar to that used for the synthesis of *R*,*R*-**1**. Reagents: 1*S*,2*S*-cyclohexane-1,2-diamine (1.19 g, 4.5 mmol), 3-methoxysalicylaldehyde (1.36 g, 9.1 mmol). The compound was obtained as a light-brown solid. Yield: 1.38 g, 67 %. ^{1}H NMR (300 MHz, CD_3OD, ppm): δ 1.43, 1.73, 2.25, [8H, m, -CH_2-], 3.55 [2H, m, -CH_2C*H*-N^+], 3.81 [6H, s, CH_3O-], 4.20, 4.34 [4H, d, $^2J_{HH}$ = 13.2 Hz, Ar-CH_2-N^+H_2], 6.91 [4H, m, aromatic], 7.1 [2H, m, aromatic]. ^{13}C-{^{1}H} NMR (400 MHz, D_2O, ppm): δ 20.33, 24.90 [4C, -*C*H_2-], 43.60 [2C, Ar-*C*H_2-N^+H_2], 54.40 [2C, -$(CH_2)_2$-*C*H-N^+H_2],

55.40 [2C, *C*H_3O-], 112.67, 115.37, 119.59, 121.85, 143.28, 146.29 [12C, aromatic]. IR (cm^{-1}): 3250 (νN–H), 1259 (νC-O). Elemental analysis for $C_{22}H_{32}N_2O_4Cl_2 \cdot 2H_2O$: calcd. C 53.3., H 7.3, N 5.7; found: C 53.1, H 7.4, N 5.4. Crystals suitable for single crystal X-ray diffraction were grown from isopropanol solutions. 0.1g of *S*,*S*-**4** was dissolved in *ca*. 10 mL of isopropanol and the resulting solution was filtered and transferred to a clean lint-free 20 mL glass flask. Colorless crystals were obtained by slow evaporation of the solvent after four weeks.

Synthesis of (1*R*,2*R*)-N1,N2-bis(3-ethoxy-2-hydroxybenzyl)cyclohexane-1,2-diaminium chloride (*R*,*R*-5)

Procedure was similar to that used for the synthesis of *R*,*R*-**1**. Reagents: 1*R*,2*R*-cyclohexane-1,2-diamine (1.14g, 4.33 mmol), 3-ethoxysalicylaldehyde (1.44 g, 8.7 mmol). The compound was obtained as a light-brown solid. Yield: 1.35 g, 64 %. ^{1}H NMR (400 MHz, DMSO-d_6, ppm): 1.28 [6H, m, -C*H*$_3$], 1.32, 1.53, 1.74, 2.27 [8H, m, -C*H*$_2$-], 3.52 [2H, s, -CH$_2$C*H*-N$^+$], 4.02 [4H, m, -C*H*$_2$-O], 4.06, 4.21 [4H, d, $^2J_{HH}$ = 12.7 Hz, Ar-C*H*$_2$-N$^+$H$_2$], 6.85, 6.99 [6H, m, aromatic]. ^{13}C-{^{1}H} NMR (400 MHz, DMSO-d_6, ppm): δ 15.36 [2C, *C*H$_3$CH$_2$O-], 23.33, 27.05 [4C, -*C*H$_2$-], 44.69 [2C, Ar-*C*H$_2$-N$^+$H$_2$], 58.08 [2C, -(CH$_2$)$_2$-*C*H-N$^+$H$_2$], 65.63 [2C, CH$_3$*C*H$_2$O-], 115.46, 118.73, 121.49, 123.96, 145.85, 147.82 [12C, Ar]. IR (cm^{-1}): 3242 (νN–H), 1238 (νC-O). Elemental analysis for $C_{24}H_{36}N_2O_4Cl_2 \cdot 0.5H_2O \cdot 1.5C_2H_5OH$: calcd. C 57.3, H 8.2, N 5.0; found: C 57.4, H 7.6, N 4.2.

Synthesis of (1*S*,2*S*)-*N*^{1},*N*^{2}-bis((2-hydroxynaphthalen-1-yl)methyl)cyclohexane-1,2-diaminium chloride (*S*,*S*-6)

The procedure was similar to that used for the synthesis of *R*,*R*-**1**. Reagents: (1*S*,2*S*)-cyclohexane-1,2-diamine (2.12 g, 8.03 mmol), 2-hydroxy-1-naphthaldehyde (2.80 g, 16.3 mmol). The compound was obtained as a hygroscopic pale-yellow solid. Yield: 3.27 g, 82 %. ^{1}H NMR (300 MHz, CD$_3$OD, ppm): δ 1.41, 1.57, 1.84, 2.17 (8H, m, -C*H*$_2$-), 3.35 (2H, m, -CH$_2$C*H*NH), 4.79 (4H, s, ArC*H*$_2$NH), 7.14, 7.33, 7.58, 7.70, 7.86, 8.23 (12H, m, aromatic). ^{13}C-{^{1}H} NMR (75 MHz, CD$_3$OD, ppm): δ 23.96, 30.42 [4C, -*C*H$_2$-], 42.16 [2C, Ar-*C*H$_2$-N$^+$H$_2$], 53.23 [2C, -(CH$_2$)$_2$-*C*H-N$^+$H$_2$], 118.72, 120.97, 123.35, 125.27,

126.50, 128.77, 129.13, 130.61, 135.47, 152.93 [20C, aromatic]. IR (cm^{-1}): 3252 (νN–H), 1272 (νC-O). Elemental analysis for $C_{28}H_{32}N_2O_2Cl_2 \cdot 2.5H_2O$: calcd. C 61.8, H 6.9, N 5.1; found C 61.4, H 6.8, N 4.7.

Synthesis of (1*R*,2*R*)-*N*^{1},*N*^{2}-bis(2-hydroxy-5-methoxybenzyl)cyclohexane-1,2-diaminium chloride (*R*,*R*-7)

The procedure was similar to that used for the synthesis of *R*,*R*-**1**. Reagents: (1*R*,2*R*)-cyclohexane-1,2-diamine (1.02 g, 3.7 mmol), 5-methoxysalicylaldehyde (1.2 g, 7.7 mmol). The compound was obtained as a pale-yellow solid. Yield: 1.57 g, 89 %. ^{1}H NMR (400 MHz, CD_3OD, ppm): δ 1.45, 1.74, 1.87, 2.44 (8H, m, -C*H*$_2$-), 3.63 (2H, m, -CH_2C*H*NH), 3.75 (6H, s, ArOC*H*$_3$), 4.25 (4H, s, ArC*H*$_2$NH), 6.87 (4H, m, aromatic), 7.13 (2H, m, aromatic). ^{13}C-{^{1}H} NMR (400 MHz, D_2O, ppm): δ 22.89, 27.88 [4C, -*C*H$_2$-], 45.52 [2C, Ar-*C*H$_2$-N$^+$H$_2$], 56.47 [2C, *C*H$_3$O-], 58.06 [2C, -(CH$_2$)$_2$-*C*H-N$^+$H$_2$], 117.23, 117.95, 118.25, 118.50, 151.17, 154.44 [12C, aromatic]. IR (cm^{-1}): 3450 (νN–H), 1209 (νC-O). Elemental analysis for $C_{22}H_{32}N_2O_4Cl_2 \cdot CH_3OH$: calcd. C 56.2, H 7.4, N 5.7; found C 56.1, H 7.5, N 5.3.

Synthesis of 6,6'-(1*R*,2*R*)-cyclohexane-1,2-diylbis(azanediyl)bis(methylene)bis(2,4-di-tert-butylphenol) (*R*,*R*-8)

The tartrate of (1*R*,2*R*)-cyclohexane-1,2-diamine (0.37 g, 1.4 mmol) was suspended in 25 mL of MeOH, and 2 equivalents of aqueous $NaHCO_3$ were added. In a separate flask, 2 equiv. of 2,4-di-*tert*-butylphenol (0.58 g, 2.8 mmol) were dissolved in 20 mL of MeOH, and 4 equiv. of formaldehyde (0.17 g, 5.6 mmol, 37 % aqueous solution) were added. The two solutions were mixed and refluxed for 3 h. A viscous mixture formed, which was washed with water and small amounts of MeOH and diethyl ether. To decompose any 1,3-benzoxazine impurities, the solid was dissolved in ethanol and the pH was lowered to *ca*. 1-15. The mixture was heated to boiling point for *ca*.1 h. The mixture was cooled down, and after the addition of diethyl ether, the white hydrochloride precipitate was obtained. The hydrochloride salt was then neutralized in a saturated aqueous $NaHCO_3$ solution, from which the neutral compound readily precipitated. The obtained white solid was filtered and washed with water. Yield (neutral compound): 0.7 g, 91 %. ^{1}H-NMR

(300 MHz, CD_3OD, ppm): 1.31, 1.43 [36H, s, Ar-C(CH_3)$_3$], 1.73, 1.89, 2.45 [8H, m, -CH_2-], 3.65 [2H, m, $CH_2CHN^+H_2$], 4.18 [4H, q, $^2J_{HH}$=12.7 Hz, Ar-CH_2-N^+H_2], 7.41, 7.47 [4H, d, $^4J_{HH}$=2.4 Hz, aromatic]. ^{13}C-{^{1}H} NMR (75 MHz, CD_3OD, ppm): δ 23.03, 28.45 [4C, -CH_2-], 29.88, 31.33 [12C, Ar-C(CH_3)$_3$], 34.07, 34.75 [4C, Ar-C(CH_3)$_3$], 46.51, [2C, Ar-CH_2-N^+H_2], 57.78 [2C, -(CH_2)$_2$-CH-N^+H_2], 121.56, 124.10, 127.11, 139.22, 142.33, 151.60 [12C, aromatic]. IR (cm^{-1}): 1606 (δN–H), 1260 (νC-O). Elemental analysis for $C_{36}H_{58}N_2O_2 \cdot 4H_2O$: C 69.9, H 10.7, N 4.5; found: C 69.9, H 10.8, N 4.5. Crystals suitable for single crystal X-ray diffraction were grown from acetonitrile solutions. 0.1 g of *R*,*R*-**8** was dissolved in *ca*. 10 mL of isopropanol and the resulting solution was filtered and transferred to a clean lint-free 20 mL glass flask. Colorless crystals were obtained by slow evaporation of the solvent after four weeks.

Synthesis of 7,7'-(1R,2R)-cyclohexane-1,2-diylbis(ammoniodiyl)bis(methylene)bis(5-chloro-8-hydroxyquinolinium) chloride (*R*,*R*-9)

The tartrate of (1*R*,2*R*)-cyclohexane-1,2-diamine (2.78 g, 10.5 mmol) was suspended in 25 mL of MeOH, and 2 equivalents of aqueous $NaHCO_3$ were added. In a separate flask, 2 equiv. of 5-chloro-8-hydroxyquinoline (3.76 g, 21.0 mmol) were dissolved in 20 mL of MeOH, and 2.5 equiv. of formaldehyde (0.79 g, 26.3 mmol, 37 % aqueous solution) were added. The two solutions were mixed and refluxed for 3 h. A pale green solid formed, which was washed with water and small amounts of MeOH and diethyl ether. To decompose any 1,3-benzoxazine impurities, the solid was dissolved in ethanol and the pH was lowered to *ca*. 1-15. The mixture was heated to boiling point for *ca*.1 h. The mixture was cooled down, and after the addition of diethyl ether, a bright yellow hydrochloride precipitate was obtained. The hydrochloride salt was then neutralized in a saturated aqueous $NaHCO_3$ solution, from which the neutral compound readily precipitated. The obtained yellow solid was filtered and washed with water. Yield (hydrochloride salt): 1.86 g, 27 %. ^{1}H-NMR (300 MHz, DMSO-d_6, ppm): 1.19, 1.29, 1.78, 2.42 [8H, m, -CH_2-], 3.72 [2H, m, $CH_2CHN^+H_2$], 4.46 [2H, d, $^2J_{HH}$=13.2 Hz, Ar-CH_2-N^+H_2], 4.54 [2H, d, $^2J_{HH}$=13.2 Hz, Ar-CH_2-N^+H_2], 7.86, 8.17, 8.62, 9.03 [8H, m, aromatic]. ^{13}C-{^{1}H} NMR (75 MHz, DMSO-d_6, ppm): δ 22.40, 25.36 [4C, -CH_2-], 42.42, [2C, Ar-CH_2-N^+H_2], 56.01 [2C, -(CH_2)$_2$-CH-N^+H_2], 116.16, 118.84, 123.99, 126.48, 130.35, 134.92, 137.01, 148.65,

151.02 [18C, aromatic]. IR (cm^{-1}): 3450 (νN–H), 1260 (νC-O). Elemental analysis for $C_{26}H_{30}N_4O_2Cl_6 \cdot 3H_2O$: C 45.1, H 5.2, N 7.7; found: C 44.8, H 5.2, N 8.0.

Synthesis of (1*S*,2*S*)-N^1,N^2-bis(2-hydroxybenzyl)-1,2-diphenylethane-1,2-diaminium chloride (*S*,*S*-10)

The procedure was similar to that used for the synthesis of *R*,*R*-**1**. Reagents: (1*S*,2*S*)-1,2-diphenylethane-1,2-diamine (0.3 g , 1.4 mmol), 3-methoxysalicylaldehyde (0.43 g, 2.8 mmol). The compound was obtained as a white solid. Yield: 0.61 g, 78 %. ^{1}H NMR (400 MHz, DMSO-d_6, ppm): δ 3.59 [2H, t, $^3J_{HH}$ = 6.6 Hz, Ar-C*H*-N$^+$H], 3.81 [6H, s, CH_3O-], 3.70, 3.89 [4H, d, $^2J_{HH}$ = 12.6 Hz, Ar-CH_2-N$^+$H$_2$], 6.80 [4H, m, aromatic], 6.89 [2H, m, aromatic], 7.21 [6H, m, aromatic], 7.33 [4H, m, aromatic]. ^{13}C-{^{1}H} NMR (100 MHz, DMSO-d_6, ppm): δ 45.07 [2C, Ar-*C*H2-N$^+$H2], 55.40 [2C, *C*H$_3$O-], 56.33 [2C, Ar-*C*HN$^+$H2], 114.48, 115.37, 119.63, 130.56, 130.71, 153.85 [24C, aromatic]. IR (cm^{-1}): 3222 (νN–H), 1266 (νC-O). Elemental analysis for $C_{30}H_{34}N_2O_4 \cdot 2H_2O$: calcd. C 60.7, H 6.5, N 4.7; found C 60.5, H 6.7, N 4.7.

2.4.3.3. Aminoalcohol-derived compounds

Synthesis of (*R*)-2-hydroxy-*N*-(2-hydroxy-3-methoxybenzyl)-1-phenylethanaminium chloride (*R*-11)

The procedure was similar to that used for the synthesis of *R*,*R*-**1**. D-phenylglycinol (1.5 g, 10.9 mmol) was condensed with 3-methoxysalicylaldehyde (1.67 g, 11.0mmol) in 25 mL of methanol. $NaBH_4$ was added to the solution until it became colorless. The pH was then adjusted to 1-1.5 with an aqueous 4 M HCl solution. The solvent was evaporated and the white residue extracted with an ethanol:diethyl ether (70:30) liquid phase, the inorganic solids being separated by filtration. By evaporation of the solvent, a white solid was obtained which was then washed with diethyl ether. Yield: 2.9 g, 85 %. ^{1}H NMR (400 MHz, DMSO-d_6, ppm): δ 3.78 [3H, s, CH_3O-Ar], 4.24 [1H, s, Ar-C*H*(CH_2OH)], 3.93 [2H, m, -CH_2OH], 3.93 [2H, s, Ar-CH_2N$^+$H$_2$], 6.77, 6.98, 7.41 [8H, m, aromatic], ^{13}C-{^{1}H} NMR (300 MHz, DMSO-d_6, ppm): δ 43 [1C, Ar-*C*H$_2$N$^+$H$_2$], 56 [1C,*C*H$_3$O-Ar], 62 [1C, -*C*H$_2$OH], 63 [1C, Ar-*C*H(CH$_2$OH)], 112, 118, 119, 123, 127.7, 128.4, 128.6, 128.8, 128.9, 133.6, 145, 147 [12C, aromatic]. IR (cm^{-1}): 3369 (νN–H), 1493 (νC=C), 1223

(νC-O). Elemental analysis for $C_{16}H_{20}NO_3Cl \cdot 2\ H_2O$: calcd. C 55.6, H 7.0, N 4.1; found C 55.3, H 6.8, N 4.1.

Synthesis of (*S*)-1-hydroxy-*N*-(2-hydroxybenzyl)-3-methylbutan-2-aminium chloride (*S*-12)

The procedure was similar to that used for the synthesis of *R*-**11**. Reagents: L-valinol (1.00 g, 9.7 mmol), salicylaldehyde (1.19 g, 9.7 mmol). Dichloromethane was used for washing instead of diethyl ether. The compound was obtained as a white solid. Hygroscopic.Yield: 1.89 g, 80 %. ^{1}H NMR (300 MHz, DMSO-d_6, ppm): δ 0.95 [6H, t, $^3J_{HH}$= 7 Hz , $(CH_3)_2CH$-], 2.15 [1H, m, $(CH_3)_2CH$-], 2.84 [1H, m, ^{i}Pr-C*H*-], 3.65, 3.73 [2H, m, $^-CH_2OH$)], 4.18 [2H, s, Ar-$CH_2N^+H_2$], 6.81, 7.01, 7.21, 7.49 [4H, m, aromatic], ^{13}C-{^{1}H} NMR (75MHz, DMSO-d_6, ppm): δ 17.59, 19.31 [2C, $(CH3)_2CH$-], 26.15 [1C, $(CH3)_2CH$-], 43.95 [1C, Ar-CH_2-N^+H_2], 57.29 [1C, -CH_2OH], 63.45 [1C, ^{i}Pr-C*H*-], 115.55, 118.04, 119.04, 130.27, 131.82, 156.36 [6C, aromatic]. IR (cm^{-1}): 3143 (νN–H), 1506 (νC=C), 1266 (νC-O). Elemental analysis for $C_{12}H_{20}NO_2Cl \cdot 0.7CH_2Cl_2$: calcd. C 50.0, H 7.1, N 4.6; found C 50.0, H 7.5, N 4.7.

Synthesis of (S)-2-((1-hydroxy-3-phenylpropan-2-ylamino)methyl)phenol (*S*-13)

The procedure was similar to that used for the synthesis of *R*-**11**. Reagents: L-phenylalaninol (1.00 g, 6.6 mmol), salicylaldehyde (0.81 g, 6.6 mmol). The addition of water after the reduction induced the precipitation of a flaky while solid. The compound was obtained as the free base. The compound was obtained as a white solid. Yield: 1.10g, 65%. ^{1}H NMR (300 MHz, DMSO-d_6, ppm): δ 2.73 [2H, m, Ar-CH_2CH-], 2.73 [1H, m, Ar-CH_2C*H*-], 3.30, 3.41 [2H, m, -CH_2OH], 3.85 [2H, s, Ar-$CH_2N^+H_2$], 6.69, 7.05, 7.19, 7.27 [9H, m, aromatic], ^{13}C-{^{1}H} NMR (75MHz, DMSO-d_6, ppm): δ 37.613 [1C, Ar-CH_2CH-], 48.06 [1C, Ar-CH_2-N^+H_2], 60.21 [1C, Ar-CH_2CH-], 61.89 [1C, -CH_2OH], 155.18, 118.79, 125.17, 126.27, 128.19, 128.57, 128.92, 129.60, 139.83, 157.63 [12C, aromatic]. IR (cm^{-1}): 3318 (νN–H), 1458 (νC=C), 1241 (νC-O). Elemental analysis for $C_{16}H_{19}NO_2 \cdot 0.1H_2O$: calcd. C 74.2, H 7.5, N 5.4; found C 74.2, H 7.9, N 5.4.

Synthesis of (*S*)-*N*-(3,5-di-tert-butyl-2-hydroxybenzyl)-1-hydroxy-3-phenylpropan-2-aminium chloride (*S*-14)

The procedure was similar to that used for the synthesis of *R*-**11**. Reagents: L-phenylalaninol (1.00 g, 6.6 mmol), 3,5-di-*tert*-butylsalicylaldehyde (1.55 g, 6.6 mmol). The free compound is a viscous liquid and conversion to the respective hydrochloride salt was required. The compound was obtained as an off-white solid. Yield: 2.15 g, 80 %. ^{1}H NMR (300 MHz, DMSO-d_6, ppm): δ 1.27, 1.43 [18H, s, Ar-C(CH_3)$_3$], 2.91, 3.20 [2H, t, $^{3}J_{HH}$= 12.0 Hz, Ar-CH_2CH-], 3.37 [1H, m, Ar-CH$_2$CH-], 3.47, 3.68 [2H, d, $^{2}J_{HH}$= 11.8 Hz, -CH_2OH], 4.29 [2H, m, Ar-CH_2-N^{+}H$_2$], 7.29 [7H, m, aromatic], ^{13}C-{^{1}H} NMR (75 MHz, DMSO-d_6, ppm): δ 30.07, 32.12 [6C, Ar-C(*C*H$_3$)$_3$], 34.04 [1C, Ar-*C*H$_2$CH-], 34.68, 35.75 [2C, Ar-*C*(CH$_3$)$_3$], 45.00 [1C, Ar-*C*H$_2$N^{+}H$_2$], 58.42 [1C, -*C*H$_2$OH], 61.15[1C, Ar-CH$_2$*C*H-], 122.52, 124.96, 127.61, 129.40, 130.10, 137.79, 140.02, 143.16, 152.61 [12C, aromatic]. IR (cm^{-1}): 3300 (νN–H), 1466 (νC=C), 1250 (νC-O). Elemental analysis for $C_{24}H_{36}NO_2$·0.2C_6H_{14}: calcd. C 71.5, H 9.2, N 3.3; found C 71.3, H 9.5, N 3.5. Crystals suitable for single crystal X-ray diffraction were grown from isopropanol solutions. 0.1g of *S*-**12** was dissolved in *ca*. 10 mL of isopropanol and the resulting solution was filtered and transferred to a clean lint-free 20 mL glass flask. Colorless crystals were obtained by slow evaporation of the solvent after four weeks.

Synthesis of (*S*,*E*)-2,4-di-tert-butyl-6-((1-hydroxy-3-phenylpropan-2-ylimino)methyl)phenol (*S*-15)

The procedure was similar to that used for the synthesis of *R,R*-**1a**. Reagents: L-phenylalaninol (0.53 g, 3.5 mmol), 3,5-di-*tert*-butylsalicylaldehyde (0.82 g, 3.5 mmol. The compound was obtained as a bright yellow solid. Yield: 1.09 g, 85 %. ^{1}H NMR (400 MHz, $CDCl_3$, ppm): δ 1.43, 1.60 [18H, s, Ar-C(CH_3)$_3$], 3.08 [2H, m, Ar-CH_2CH-], 3.67 [1H, m, Ar-CH$_2$CH-], 3.92 [2H, m, -CH_2OH], 7.15 [1H, d, $^{4}J_{HH}$= 2.4 Hz, aromatic], 7.33, 7.41 [5H, m, aromatic], 7.53 [1H, d, $^{4}J_{HH}$= 2.4 Hz, aromatic], 8.33 [2H, m, Ar-CH=N], ^{13}C-{^{1}H} NMR (75 MHz, DMSO-d_6, ppm): δ 29.74, 31.45 [6C, Ar-C(*C*H$_3$)$_3$], 34.18, 35.25 [2C, Ar-*C*(CH$_3$)$_3$], 39.48, [1C, Ar-*C*H$_2$CH-], 66.30 [1C, -*C*H$_2$OH], 73.69 [1C, Ar-CH$_2$*C*H-], 117.52, 126.32, 126.56, 127.34, 128.31, 129.58, 136.79, 138.16, 140.32, 158.16 [12C, aromatic], 167.36 [1C, Ar-*C*H=N]. IR (cm^{-1}): 1626 (νC=N), 1250 (νC-O).

Elemental analysis for $C_{24}H_{33}NO_2 \cdot 0.2H_2O$: calcd. C 77.7, H 9.1, N 3.8; found C 77.7, H 9.4, N 3.9.

Synthesis of (*S,E*)-2,4-di-tert-butyl-6-((1-hydroxy-3-methylbutan-2-ylimino)methyl)phenol (*S*-16)

The procedure was similar to that used for the synthesis of *R,R*-**1a**. Reagents: L-valinol (0.52 g, 5.1 mmol), 3,5-di-*tert*-butylsalicylaldehyde (1.19 g, 5.1 mmol). A bright yellow solid was obtained. Yield: 1.05 g, 65 %. ^{1}H NMR (400 MHz, $CDCl_3$, ppm): δ 1.00 [6H, m, $(CH_3)_2$CH-], 1.31, 1.46 [18H, s, Ar-C(CH_3)$_3$], 1.95 [1H, m, $(CH_3)_2$C*H*-], 3.03 [1H, m, ^{i}Pr-C*H*-], 3.81 [2H, m, -CH_2OH)], 7.14, 7.41 [2H, d, $^4J_{HH}$= 2.2Hz, aromatic], ^{13}C-{^{1}H} NMR (100MHz, $CDCl_3$, ppm): δ 19.41, 19.95 [2C, ($CH3)_2$CH-], 30.94 [1C, $(CH3)_2$CH-], 29.21, 32.10 [6C, Ar-C(CH_3)$_3$], 34.18, 35.55 [2C, Ar-C(CH_3)$_3$], 64.62 [1C, -CH_2OH], 78.65 [1C, ^{i}Pr-C*H*-], 117.84, 126.26, 127.27, 136.96, 140.36, 158,26 [6C, aromatic], 167.36 [1C, Ar-CH=N]. IR (cm^{-1}): 1626 (νC=N), 1276 (νC-O). Elemental analysis for $C_{20}H_{33}NO_2 \cdot 0.3C_4H_{10}O$: calcd. C 74.5, H 10.6, N 4.1; found C 74.5, H 11.0, N 4.3.

2.4.3.4. Aminoacid-derived compounds

Synthesis of (*S*)-1-carboxy-*N*-(2-hydroxy-3-methoxybenzyl)-2-(4-hydroxyphenyl)ethanaminium chloride (*S*-17)

The procedure was an adaptation of the procedure used for the synthesis of *R,R*-**1**. L-Tyrosine (5.01 g, 27.6 mmol) was neutralized with one equivalent of KOH (1.55 g, 27.6 mmol) in 200 mL of methanol. One equivalent of 3-methoxysalicylaldehyde (4.19 g, 27.6 mmol) was then added to the resulting clear solution. After 30 minutes of vigorous stirring the resulting Schiff base was filtered and washed with small amounts of methanol. The Schiff base was suspended in methanol and reduced with $NaBH_4$. The reduction was considered to be complete when the reaction mixture became colorless. The pH was then adjusted to 1-1.5 with an aqueous 4 M HCl solution. The solvent was evaporated and the white residue extracted with ethanol, the inorganic solids being separated by filtration. By evaporation of the solvent, a colorless oil was obtained which was then dissolved in minimum amount possible of isopropanol. The resulting solution

was filtered again and diethyl ether was added to the filtrate until the precipitation of the hydrochloride salt was complete. The resulting white solid was filtered and washed with diethyl ether. In some cases the resulting solid became a viscous paste. When such happened, the liquid phase was discarded by careful decantation. The residue was washed with a small amount of diethyl ether and the liquid phase discarded by decantation. The residue was extracted with methanol and the resulting solution was evaporated to dryness. Yield: 7.8g, 81%. ^{1}H NMR (400 MHz, DMSO-d_6, ppm): δ 3.05 [1H, dd, $^{2}J_{HH}$= 13.8 Hz, $^{3}J_{HH}$ = 8.4 Hz, Ar-CH_2CH-], 3.28 [1H, dd, $^{2}J_{HH}$= 13.8 Hz, $^{3}J_{HH}$ = 4.4 Hz, Ar-CH_2CH-], 3.79 [3H, s, CH_3O-Ar], 3.98 [1H, dd, $^{3}J_{HH}$= 8.4 Hz, $^{3}J_{HH}$ = 4.4 Hz, Ar-CH$_2$CH-], 4.15 [2H, s, Ar-CH_2-N^{+}H$_2$], 6.78, 7.03 [7H, m, aromatic], ^{13}C-{^{1}H} NMR (100 MHz, DMSO-d_6, ppm): δ 34.52 [1C, Ar-CH$_2$CH-], 44.52 [1C, Ar-CH$_2$N^{+}H$_2$], 56.03 [1C, CH$_3$O-Ar], 60.19 [1C, Ar-CH$_2$$C$H-], 112.57, 115.53, 118.20, 119.26, 123.55, 124.81, 130.50, 145.54, 147.82, 156.86 [12C, aromatic], 169.51 [1C, COOH]. IR (cm^{-1}): 3214 (νN–H), 1738 (νC=O)$_{carboxyl}$, 1274 (νC-O), Elemental analysis for $C_{17}H_{20}NO_5Cl{\cdot}2CH_3OH$: calcd. C 54.6, H 6.8, N 3.4; found C 54.6, H 6.6, N 3.1.

Synthesis of (*S*)-1-carboxy-*N*-(2-hydroxybenzyl)-2-(4-hydroxyphenyl)ethanaminium chloride (*S*-18)

The procedure was similar to the one that was used for the synthesis of *S*-**17**. Reagents: L-tyrosine (4.68 g, 25.9 mmol), KOH (1.45 g, 25.9 mmol), salicylaldehyde (3.16 g, 25.9 mmol). The compound was obtained as a hygroscopic white solid. Yield: 7.1 g, 85 %. ^{1}H NMR (400 MHz, DMSO-d_6, ppm): δ 3.03 [1H, dd, $^{2}J_{HH}$= 14.0 Hz, $^{3}J_{HH}$ = 8.1 Hz, Ar-CH_2CH-], 3.28 [1H, dd, $^{2}J_{HH}$= 14.0 Hz, $^{3}J_{HH}$ = 4.8 Hz, Ar-CH_2CH-], 3.93 [1H, dd, $^{3}J_{HH}$= 8.1 Hz, $^{3}J_{HH}$ = 4.8 Hz, Ar-CH$_2$CH-], 4.12 [2H, s, Ar-CH_2-N^{+}H$_2$], 6.72, 6.82, 7.01, 7.22, 7.41 [8H, m, aromatic], ^{13}C-{^{1}H} NMR (100 MHz, DMSO-d_6, ppm): δ 34.31 [1C, Ar-CH$_2$CH-], 44.46 [1C, Ar-CH$_2$N^{+}H$_2$], 60.08 [1C, Ar-CH$_2$$C$H-], 115.39, 117.53, 119.06, 124.74, 130.39, 132.05, 156.86 [12C, aromatic], 169.51 [1C, COOH]. IR (cm^{-1}): 3222 (νN–H), 1738 (νC=O)$_{carboxyl}$, 1233 (νC-O). Elemental analysis for $C_{16}H_{18}NO_4Cl{\cdot}1.2CH_3OH$: calcd. C 57.0, H 6.4, N 3.9; found C 57.1, H 6.2, N 3.7.

Synthesis of (*R*)-1-carboxy-*N*-(2-hydroxy-3-methoxybenzyl)-2-mercaptoethanaminium chloride (*R*-19)

The procedure was similar to the one that was used for the synthesis of *S*-**17**. Reagents: L-cysteine (4.12 g, 34.0 mmol), KOH (1.91 g, 34.0 mmol), 3-methoxysalicylaldehyde (5.17 g, 34.0 mmol). The entire process, up to the reduction of the pH to *ca*. 1.5, was carried out under nitrogen atmosphere. The compound was obtained as a hygroscopic white solid. Yield: 7.5 g, 75 %. ^{1}H NMR (300 MHz, DMSO-d_6, ppm): δ 3.04, 3.22 [2H, m, HS-CH_2CH-], 3.79 [3H, s, CH_3O-Ar], 4.05 [1H, m, HS-CH$_2$CH-], 4.20 [2H, s, Ar-CH_2-N$^+$H$_2$], 6.80, 6.99, 7.09 [3H, m, aromatic], ^{13}C-{^{1}H} NMR (75 MHz, DMSO-d_6, ppm): δ 23.49 [1C, HS-*C*H$_2$CH-], 44.74 [1C, Ar-*C*H$_2$N$^+$H$_2$], 56.58 [1C, *C*H$_3$O-Ar], 60.27 [1C, HS-CH$_2$*C*H-], 112.85, 117.96, 119.25, 123.60, 145.54, 147.74 [6C, aromatic], 168.32 [1C, *C*OOH]. IR (cm^{-1}): 3263 (νN–H), 1734 (νC=O)$_{carboxyl}$, 1240 (νC-O), Elemental analysis for $C_{11}H_{16}NO_4SCl{\cdot}1.3C_3H_7OH$: calcd. C 48.1, H 7.2, N 3.8, S 8.5; found C 47.9, H 7.0, N 3.6, S 8.6.

Synthesis of (*R*)-1-carboxy-*N*-(2-hydroxybenzyl)-2-mercaptoethanaminium chloride (*R*-20)

The procedure was similar to the one that was used for the synthesis of *R*-**19**. Reagents: L-cysteine (5.08 g, 42.0 mmol), KOH (2.3g, 42.0 mmol), salicylaldehyde (5.11g, 42.0 mmol). The compound was obtained as a hygroscopic white solid. Yield: 9.05 g, 82 %. ^{1}H NMR (400 MHz, DMSO-d_6, ppm): δ 3.05, 3.20 [2H, m, HS-CH_2CH-], 4.08 [1H, m, HS-CH$_2$CH-], 4.18 [2H, s, Ar-CH_2-N$^+$H$_2$], 6.81, 7.00, 7.21, 7.44 [4H, m, aromatic], ^{13}C-{^{1}H} NMR (100 MHz, DMSO-d_6, ppm): δ 23.88 [1C, HS-*C*H$_2$CH-], 45.07 [1C, Ar-*C*H$_2$N$^+$H$_2$], 60.25 [1C, HS-CH$_2$*C*H-], 115.53, 117.54, 119.06, 130.85, 132.22, 156.14 [6C, aromatic], 168.36 [1C, *C*OOH]. IR (cm^{-1}): 3373 (νN–H), (1742 (νC=O)$_{carboxyl}$, 1260 (νC-O). Elemental analysis for $C_{10}H_{14}NO_3SCl{\cdot}0.75H_2O{\cdot}0.25CH_3OH$: calcd. C 42.9, H 5.7, N 5.0, S 11.5; found C 43.1, H 6.1, N 5.0, S 11.4.

Synthesis of sodium (S)-3-(4-(benzyloxy)phenyl)-2-(2-hydroxy-3-methoxybenzylamino)propanoate (*S*-21)

The procedure was similar to the one that was used for the synthesis of *S*-**17**. Reagents: O-benzyl-L-tyrosine (1.06 g, 3.9 mmol), KOH (0.22 g, 3.9 mmol), 3-methoxysalicylaldehyde (0.59 g, 3.9 mmol). Reduction of pH was not necessary. The sodium salt of the prepared compound precipitated from water. The compound was obtained as a white solid. Yield: 1.03 g, 62 %. ^{1}H NMR (400 MHz, CD_3OD, ppm): δ 2.86 [1H, dd, $^{2}J_{HH}$= 14.2 Hz, $^{3}J_{HH}$ = 8.3 Hz, Ar-CH_2CH-], 3.13 [1H, dd, $^{2}J_{HH}$= 14.2 Hz, $^{3}J_{HH}$ = 4.9 Hz, Ar-CH_2CH-], 3.48 [1H, dd, $^{3}J_{HH}$= 8.3 Hz, $^{3}J_{HH}$ = 4.9 Hz, Ar-CH$_2$C*H*-], 3.77 [1H, d, $^{2}J_{HH}$= 13.4 Hz Ar-CH_2-NH], 3.81 [3H, s, CH_3O-Ar], 4.03 [1H, d, $^{2}J_{HH}$= 13.4 Hz Ar-CH_2-NH], 5.06 [2H, s, Ar-CH_2-OAr], 6.63, 6.72, 6.90, 7.17, 7.35 [12H, m, aromatic], ^{13}C-{^{1}H} NMR (100 MHz, CD_3OD, ppm): δ 38.58 [1C, Ar-*C*H$_2$CH-], 49.37 [1C, Ar-*C*H$_2$NH], 56.78 [1C, *C*H$_3$O-Ar], 65.40 [1C, Ar-CH$_2$*C*H-], 70.92 [1C, Ar-*C*H$_2$-OAr], 113.08, 116.13, 120.26, 122.97, 128.54, 128.82, 129.48, 130.79, 131.35, 138.81, 147.35, 149.11, 159.17 [18C, aromatic], 177.08 [1C, *C*OO$^-$]. IR (cm^{-1}): 3176 (νN–H), 1594 (νC=O)$_{carboxylate}$, 1249 (νC-O), Elemental analysis for $C_{24}H_{24}NO_5Na{\cdot}1H_2O$: calcd. C 64.4, H 5.9, N 3.1; found C 64.4, H 6.1, N 3.0.

Synthesis of (*S*)-3-(4-(benzyloxy)phenyl)-2-(2-hydroxybenzylamino)propanoic acid (*S*-22)

The procedure was similar to the one that was used for the synthesis of *S*-**17**. Reagents: O-benzyl-L-tyrosine (0.76 g, 2.8 mmol), KOH (0.16 g, 2.8 mmol), salicylaldehyde (0.34 g, 2.8 mmol). The neutral compound precipitated from water during the acidification step as a white solid. Yield: 1.01 g, 96 %. ^{1}H NMR (400 MHz, DMSO-d_6, ppm): δ 2.81 [1H, dd, $^{2}J_{HH}$= 13.9 Hz, $^{3}J_{HH}$ = 7.9 Hz, Ar-CH_2CH-], 3.03 [1H, dd, $^{2}J_{HH}$= 13.9 Hz, $^{3}J_{HH}$ = 5.3 Hz, Ar-CH_2CH-], 3.48 [1H, dd, $^{3}J_{HH}$= 7.9 Hz, $^{3}J_{HH}$ = 5.3 Hz, Ar-CH$_2$C*H*-], 3.62 [1H, d, $^{2}J_{HH}$= 13.6 Hz Ar-CH_2-NH], 3.81 [1H, d, $^{2}J_{HH}$= 13.6 Hz Ar-CH_2-NH], 6.75, 6.97, 7.15, 7.40 [4H, m, aromatic], ^{13}C-{^{1}H} NMR (100 MHz, DMSO-d_6, ppm): δ 35.92 [1C, Ar-*C*H$_2$CH-], 47.99 [1C, Ar-*C*H$_2$NH], 62.28 [1C, Ar-CH$_2$*C*H-], 69.28 [1C, Ar-*C*H$_2$-OAr], 109.95, 114.75, 115.36, 118.91, 127.69, 127.82, 128.48, 130.33, 133.11, 137.37, 153.55, 157.06 [18C, aromatic], 171.08 [1C, *C*OOH]. IR (cm^{-1}): 3170 (νN–H), 1738

(νC=O)$_{carboxyl}$, 1248 (νC-O), Elemental analysis for $C_{23}H_{23}NO_4 \cdot 0.2H_2O$: calcd. C 72.5, H 6.2, N 3.7; found C 72.7, H 6.2, N 3.6.

Synthesis of (*R*)-3-(benzylthio)-2-(2-hydroxy-3-methoxybenzylamino)propanoic acid (*R*-23)

The procedure was similar to the one that was used for the synthesis of *S*-**16**. Reagents: S-benzyl-L-cysteine (1.01 g, 4.8 mmol), KOH (0.27 g, 4.8 mmol), 3-methoxysalicylaldehyde (0.72 g, 4.8 mmol). The neutral compound precipitated from water during the acidification step as a white solid. Yield: 1.45 g, 87 %. ^{1}H NMR (300 MHz, DMSO-d_6, ppm): δ 2.88, 3.10 [2H, m, BnS-C*H*$_2$CH-], 3.64 [1H, m, BnS-CH$_2$C*H*-], 3.69 [2H, s, Ar-C*H*$_2$-S], 3.88 [3H, s, C*H*$_3$O-Ar], 4.20 [1H, d, $^2J_{HH}$= 13.0 Hz Ar-C*H*$_2$-NH], 4.32 [1H, d, $^2J_{HH}$= 13.0 Hz Ar-C*H*$_2$-NH], 6.87, 7.04, 7.27 [8H, m, aromatic], ^{13}C-{^{1}H} NMR (75 MHz, DMSO-d_6, ppm): δ 32.52 [1C, BnS-*C*H$_2$CH-], 36.54 [1C, Ar-*C*H$_2$-S-], 47.87 [1C, Ar-*C*H$_2$NH], 56.76 [1C, *C*H$_3$O-Ar], 60.99 [1C, BnS-CH$_2$*C*H-], 114.02, 118.69, 121.02, 123.91, 128.32, 129.65, 130.19, 138.93, 145.54, 147.74 [12C, aromatic], 168.32 [1C, *C*OOH]. IR (cm^{-1}): 3253 (νN–H), 1734 (νC=O)$_{carboxyl}$, 1240 (νC-O). Elemental analysis for $C_{18}H_{21}NO_4S \cdot 1.7H_2O$: calcd. C 57.2, H 6.5, N 3.7, S 8.5; found C 57.1, H 6.4, N 3.7, S 8.3.

Synthesis of (*R*)-2-(benzylthio)-1-carboxy-N-(2-hydroxybenzyl)ethanaminium chloride (*R*-24)

The procedure was similar to the one that was used for the synthesis of *R*-**19**. Reagents: S-benzyl-L-cysteine (2.5 g, 11.8 mmol), KOH (0.66 g, 11.8 mmol), salicylaldehyde (1.40 g, 11.8 mmol). The compound was obtained as a white solid. Yield: 2.8 g, 69 %. ^{1}H NMR (400 MHz, CD$_3$OD, ppm): δ 2.97, 3.09 [2H, m, BnS-C*H*$_2$CH-], 3.73 [2H, q, $^2J_{HH}$= 13.2 Hz, Ar-C*H*$_2$-S-], 4.03 [1H, m, BnS-CH$_2$C*H*-], 4.26 [2H, s, Ar-C*H*$_2$-N$^+$H$_2$], 6.92, 7.26 [9H, m, aromatic], ^{13}C-{^{1}H} NMR (100 MHz, CD$_3$OD, ppm): δ 37.78 [1C, BnS-*C*H$_2$CH-], 36.62 [1C, Ar-*C*H$_2$-S-], 47.85 [1C, Ar-*C*H$_2$NH], 59.12 [1C, BnS-CH$_2$*C*H-], 116.37, 118.08, 121.20, 128.49, 129.65, 129.71, 130.19, 132.62, 132.87, 138.93, 157.54[12C, aromatic], 169.71 [1C, *C*OOH]. IR (cm^{-1}): 3134 (νN–H), 1740 (νC=O)$_{carboxyl}$, 1261 (νC-

O). Elemental analysis for $C_{17}H_{20}NO_3SCl{\cdot}0.5H_2O{\cdot}0.5C_3H_7OH$: calcd. C 56.9, H 6.5, N 3.5, S 7.9; found C 56.7, H 6.4, N 3.6, S 8.2.

Synthesis of (*S*)-1-carboxy-*N*-(3,5-di-tert-butyl-2-hydroxybenzyl)ethanaminium chloride (*S*-25)

The procedure was an adaptation of the one used for the synthesis of *R,R*-**8**. L-alanine (3.34 g, 37.5 mmol) was suspended in 100 mL of methanol. One equivalent of KOH (2.13 g, 37.5 mmol) was added to solubilize the aminoacid. Once the dissolution was completed, one equivalent of formaldehyde (1.12 g, 37.5 mmol, 37 % aqueous solution) was added. Finally, one equivalent of 2,4-di-*tert*-butylphenol (7.73 g, 37.5 mmol) was added to the mixture. After a 24h reflux and subsequent cooling down of the reaction mixture, the solvent was removed by evaporation. The residue was extracted with a minimal amount of methanol and the solution was acidified with aqueous 4M HCl until pH 1.5-2. Water was added till precipitation of the hydrochloride was complete. The resulting solid was filtered, washed with water and diethyl ether. An off-white solid was obtained. Yield: 4.47g 34%. ^{1}H NMR (400 MHz, CD_3OD, ppm): δ 1.32, 1.43 [18H, s, $(CH_3)_3$C-Ar], 1.64 [3H, d, $^3J_{HH}$=7.3 Hz, CH_3CH-], 4.0[1H, q, $^3J_{HH}$=7.3 Hz, CH_3CH-], 4.32 [2H, s, Ar-CH_2-N^+H_2], 7.29, 7.41 [2H, d, $^4J_{HH}$=2.2 Hz aromatic], ^{13}C-{^{1}H} NMR (100 MHz, CD_3OD, ppm): δ 15.31 [1C, CH_3CH-], 29.99, 31.96 [6C, $(CH_3)_3$C-Ar], 35.15, 36.14 [2C, $(CH_3)_3C$-Ar], 47.27 [1C, Ar-$CH_2N^+H_2$], 56.23 [1C, CH_3CH-], 121.96, 126.68, 127.25, 140.81, 145.15, 153.00 [6C, aromatic], 172.01 [1C, COOH]. IR (cm^{-1}): 3274 (νN–H), 1743 $(\nu C{=}O)_{carboxyl}$, 1225 (νC-O). Elemental analysis for $C_{18}H_{30}NO_3Cl{\cdot}0.5H_2O$: calcd. C 61.3, H 8.9, N 4.0; found C 61.0, H 9.0, N 4.3.

Synthesis of (*S*)-1-carboxy-*N*,*N*-bis(3,5-di-tert-butyl-2-hydroxybenzyl)ethanaminium carboxyformate (*S*-26)

The procedure was adapted from the one used for the synthesis of *S*-**25**. L-alanine (1.60 g, 18.0 mmol) was suspended in 50mL of methanol. One equivalent of KOH (1.00 g, 18.0 mmol) was added to solubilize the aminoacid. Once the dissolution was completed, two equivalents of formaldehyde (1. 08g, 36.0 mmol, 37 % aqueous solution) were added. Finally, two equivalents of 2,4-di-*tert*-butylphenol (7.40 g, 36.0 mmol) were added to the

mixture. After a 24 h reflux and subsequent cooling down of the reaction mixture, the solvent was removed by evaporation. The residue was extracted with a minimal amount of methanol and the solution was acidified with two equivalents of oxalic acid dihydrate (4.53 g, 36.0 mmol). Water was added until precipitation of the oxalate salts was complete. The resulting solid was filtered out and the aqueous filtrate was discarded. The obtained precipitate was extracted with diethyl ether and the remaining solid filtered out and discarded. The ether solution was evaporated and the residue was extracted with *n*-hexane. The remaining solid was filtered, washed with *n*-hexane and water. The compound was obtained as an off-white solid. Yield: 1.12 g, 10 %. ^{1}H NMR (300 MHz, CD_3OD, ppm): δ 1.23, 1.39 [36H, s, $(CH_3)_3$C-Ar], 1.47 [3H, d, $^{3}J_{HH}$=7.3 Hz, CH_3CH-], 3.65 [1H, q, $^{3}J_{HH}$=7.3 Hz, CH_3CH-], 3.73, 4.19 [4H, d, $^{2}J_{HH}$=13.4 Hz Ar-CH_2-N^+H_2], 7.06, 7.28 [2H, d, $^{4}J_{HH}$=2.3 Hz aromatic], ^{13}C-{^{1}H} NMR (75 MHz, CD_3OD, ppm): δ 9.17 [1C, CH_3CH-], 30.79, 31.83 [12C, $(CH_3)_3$C-Ar], 35.24, 35.92 [4C, $(CH_3)_3C$-Ar], 53.58 [2C, Ar-$CH_2N^+H_2$], 57.52 [1C, CH_3CH-], 122.14, 125.28, 126.65, 138.39, 143.18, 153.81 [12C, aromatic], 163.08, [2C, COO^-] 176.01 [1C, COOH]. IR (cm^{-1}): 3234 (νN–H), 1740 $(\nu C{=}O)_{carboxyl}$, 1261 (νC-O). Elemental analysis for $C_{35}H_{53}NO_8 \cdot 2.5H_2O$: calcd. C 63.6, H 8.9, N 2.1; found C 63.6, H 8.7, N 2.4.

Synthesis of (S)-2-(bis(2-hydroxybenzyl)amino)propanoic acid (*S*-27)

L-alanine (2.01g, 22.6 mmol) was suspended in ethanol. One equivalent of KOH (1.26 g, 22.6 mmol) was added to solubilize the aminoacid. Once the dissolution was completed, two equivalents of salicylaldehyde (5.51 g, 45.2 mmol) were added. Finally, a slight excess of of $NaBH(AcO)_3$ (10.00 g, 47.4 mmol) was added to the mixture. After stirring for 24 h, the solvent was removed by evaporation. The residue was triturated with saturated aqueous solution of $NaHCO_3$ and then with water. The resulting white solid was filtered and washed with water. The compound was obtained as a white solid. Yield: 1.66g, 24%. ^{1}H NMR (300 MHz, acetone-d_6, ppm): δ 1.48 [3H, d, $^{3}J_{HH}$=7.2 Hz, CH_3CH-], 3.59 [1H, q, $^{3}J_{HH}$=7.3 Hz, CH_3CH-], 3.92, 4.08 [4H, d, $^{2}J_{HH}$=13.2 Hz Ar-CH_2-NH], 6.82, 7.18 [8H, m, aromatic], ^{13}C-{^{1}H} NMR (75 MHz, acetone-d_6, ppm): δ 9.75 [1C, CH_3CH-], 50.60 [2C, Ar-CH_2NH], 57.58 [1C, CH_3CH-], 115.62, 119.10, 120.61, 129.39, 130.71, 156.63 [12C, aromatic], 174.01 [1C, COOH]. IR (cm^{-1}): 3234 (νN–H), 1740

($\nu C{=}O)_{carboxyl}$, 1261 (νC-O). Elemental analysis for $C_{16}H_{17}NO_4 \cdot 0.75C_2H_5OH$: calcd. C 65.3, H 6.7, N 4.4; found C 65.3, H 6.4, N 3.9.

2.5. References

1 Abdel-Magid, A. F.; Carson, K. G.; Harris, B. D.; Maryanoff, C. A.; Shah, R. D. *J. Org. Chem.* **1996,** *61,* 3849-3862.

2 Tshuva, E. Y.; Gendeziuk, N.; Kol, M. *Tetrahedron Letters* **2001**, *42*, 6405-6407.

3 Nakajima, K.; Kojima, K.; Kojima, M.; Fujita, J. *Bull. Chem. Soc. Jpn*. **1990**, *63*, 2620-2630.

4 Sasaki, C.; Nakajima, K.; Kojima, M.; Fujita, J. *Bull. Chem. Soc. Jpn*. **1991**, *64*, 1318-1324.

5 Correia, I.; Costa Pessoa, J.; Teresa Duarte, M.; Henriques, R. T.; Piedade, M. F. M.; Veiros, L. F.; Jakusch, T.; Kiss, T.; Dörnyei, A.; Castro, M. M. C. A.; Geraldes, C. F. G. C.; Avecilla, F. *Chem. Eur. J*. **2004**, *10*, 2301-2317.

6 Gulloti, M.; Pasini, A.; Fantucci, P.; Ugo, R.; Gillard, R. D. *Gaz. Chim. Ital*. **1972**, *102*, 855-892.

7 Aullo´n, G.; Bellamy, D.; Brammer, L.; Bruton, E. A.; Orpen, G. *J. Chem. Soc., Chem. Commun.* **1998**, 653-654.

8 Barroso, S.; Adão, P.; Madeira, F.; Teresa Duarte, M.; Costa Pessoa, J.; Martins, A. M. *Inorg. Chem.* **2010**, *49*, 7452-7463.

9 Sheldrick, G. M. *SHELXS-97*, revision 5.1; University of Göttingen: Göttingen, Germany, 1997.

10 (a) Flack, H. D.; Bernardinelli, G. *Acta Crystallogr., A,* **1999**, *A55*, 908-915. (b) Flack, H. D.; Bernardinelli, G. *J. Appl. Crystallogr.* **2000**, *33*, 1143-1148.

Chapter 3

Titanium(IV) Salan Complexes

3. Titanium(IV) Salan Complexes

3.1. Introduction

Since Sharpless and Katsuki developed the titanium diethyltartrate system for asymmetric olefin epoxidation in 1980,[1] the use of high valent titanium compounds in asymmetric catalysis has been steadily growing ever since. In addition to its abundance, to being of relatively low toxicity[2] and of low cost, high valent titanium is well-known for its reactivity. Indeed, Ti^{IV} compounds have been used to mediate a wide range of reactions (see Figure 3.1). High valent titanium compounds are even capable of mediating carbon-carbon coupling reactions processes, such as allylic alkylations and cross-couplings,[3,4] that are typically promoted by late metal compounds.

Some of the most useful methods for carbon-carbon bond construction are promoted by high valent titanium compounds. Such are the pinacol and McMurry cross-coupling reactions. The pinacol coupling reaction is particularly noteworthy as it yields chiral 1,2-diols.[5]

In previous years, titanocenes were widely used as mediators in titanium catalyzed processes, but issues regarding catalyst preparation and modification prompted a departure from metallocene based catalysts. Taking into consideration the affinity of titanium towards “hard” N- and O-donors, the development of ligand supports containing such donor atoms gained interest. High valent titanium aminophenolate catalysts stand out due to their successful application in a wide variety of asymmetric processes. Part of this success is a consequence of the inherent characteristics of the aminophenol class of ligands: N- and O-donors stabilize the electropositive metal centre while the robust and modifiable ligand structure allows for tailor-made reactivity, without sacrificing stability, towards a variety of catalytic processes.

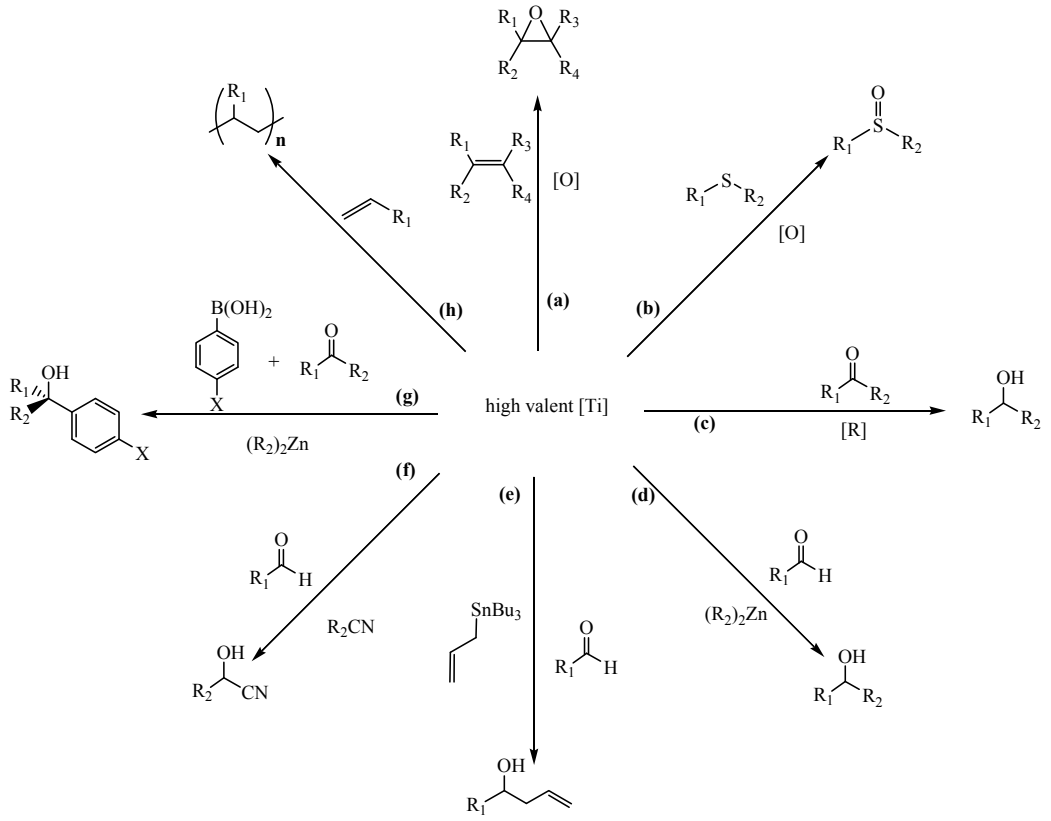

Figure 3.1. Catalytic processes that are mediated by high valent titanium complexes: olefin (a) and thioether oxidations[6] (b), aldehyde and ketone reductions (c), aldehyde alkylations (d), allylic alkylations (e), aldehyde cyanations (f), aldehyde and ketone arylations (g), olefin polymerizations (h).[11,12,13]

Notable examples combining the potential of high valent titanium with the versatility of aminophenol ligands, particularly the salen- and salan-type, include chiral *in situ* Ti^{VI}(salan) complexes reported by Katsuki and co-workers[7] which promote the highly enantioselective epoxidation of olefins, using hydrogen peroxide as the terminal oxidant (Scheme 3.1).

In 2008, Bryliakov and co-workers[8] used chiral Ti^{IV}(salan) complexes in the asymmetric oxidation of thioethers and resolution of sulfoxides, also using hydrogen peroxide as a terminal oxidant. Despite the moderate to high chemoselectivities and high yields, enantioselectivity was highly dependent of substrate structure (Scheme 3.2).

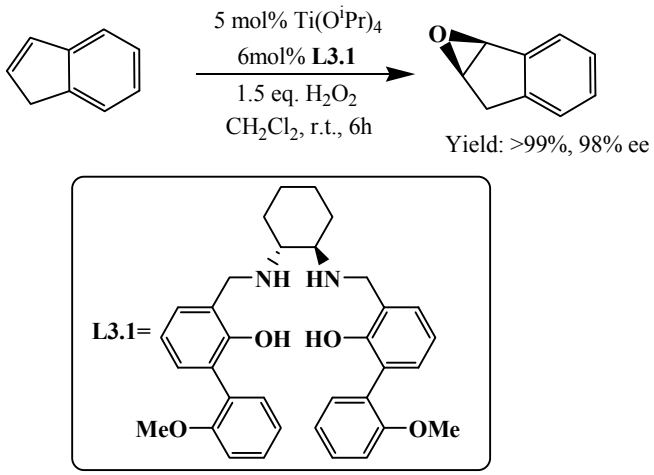

Scheme 3.1. Ti^{IV}(salan)-promoted asymmetric alkene epoxidation.

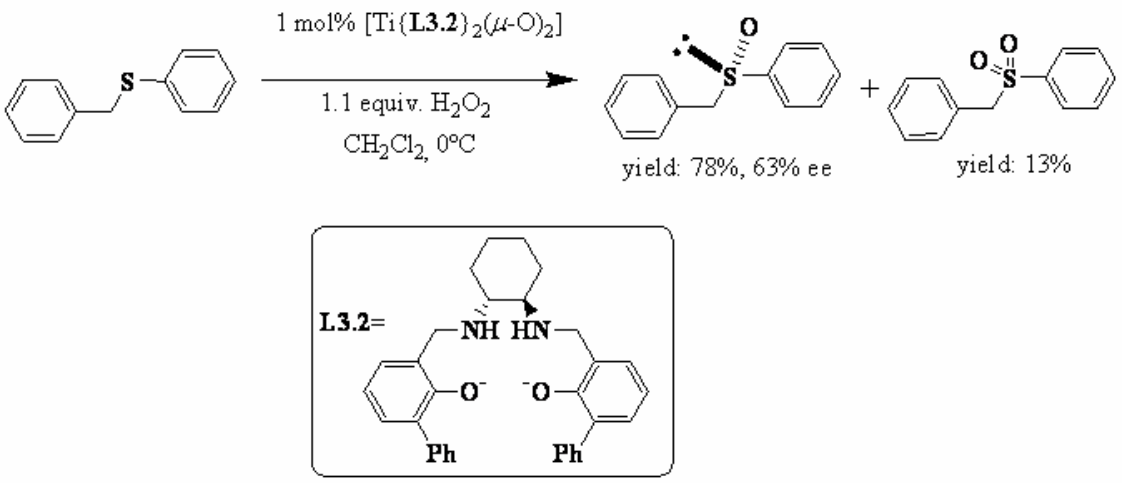

Scheme 3.2. Ti^{IV}(salan)-promoted asymmetric sulfoxidation.

Kozlowski and co-workers[9] used Ti^{IV}(salen) complexes in the asymmetric alkylation of aromatic aldehydes and α-ketoesters, using diethylzinc as the alkylating agent (Scheme 3.3).

Bekolon and co-workers[10] successfully employed Ti^{IV}(salen) complexes in asymmetric cyanation of aromatic aldehydes, using KCN as the cyanide source instead of trimethylsilylcyanide, with yields and enantiomeric excesses surpassing 90% in most cases (Scheme 3.4).

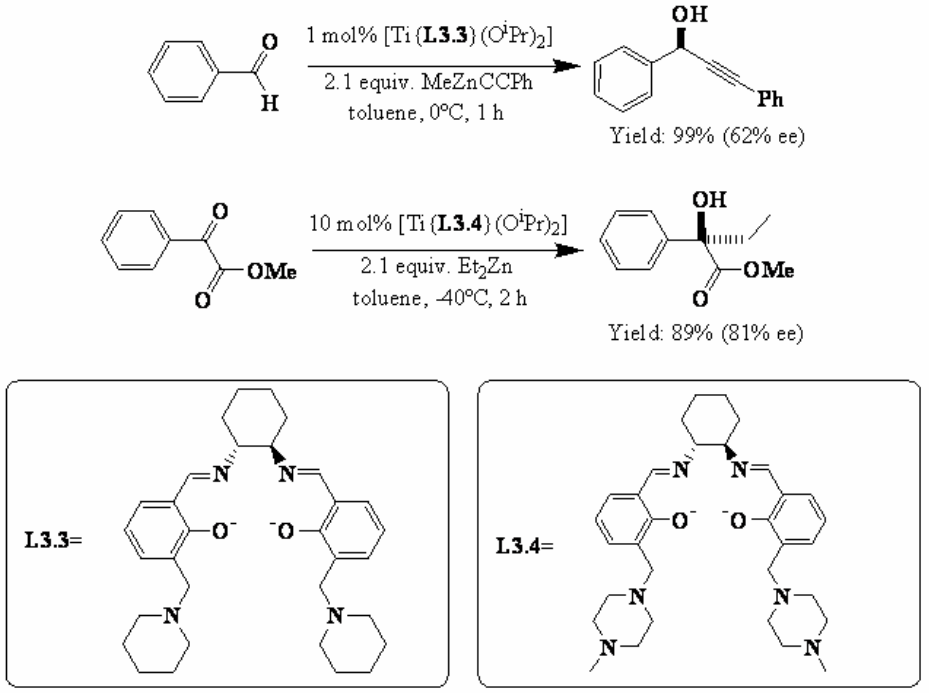

Scheme 3.3. Ti^{IV}(salen)-promoted asymmetric addition of diethylzinc to aldehydes and ketones.

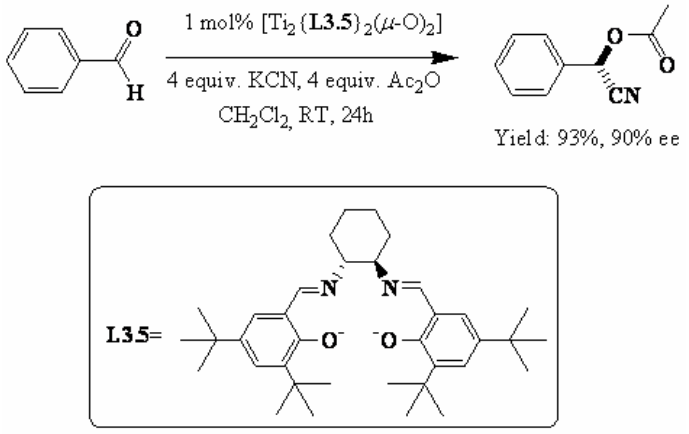

Scheme 3.4. Ti^{IV}(salen)-promoted asymmetric cyanation of aldehydes.

Kol and co-workers[11,12,13] used Ti^{IV}(salan) complexes in the polymerization of olefins, namely 1-hexene and propylene, obtaining polymers with high molecular weight. It should be noted that although the ligands employed in this system were achiral, the *fac-fac* wrapping around the metal centre produced chiral C_2-symmetric complexes. This chirality at the metal centre may have favored the formation of isotactic polymers (Scheme 3.5).

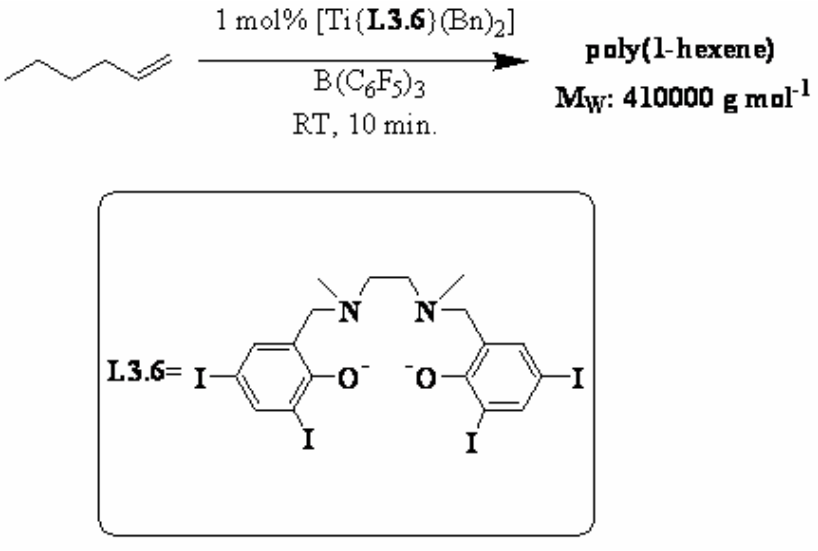

Scheme 3.5. Ti^{IV}(salan)-promoted polymerization of 1-hexene.

The same authors used the structurally related tripodal diaminobisphenolate Ti^{VI}complexes in the ring-opening polymerization of cyclic lactones (Scheme 3.6) [14]

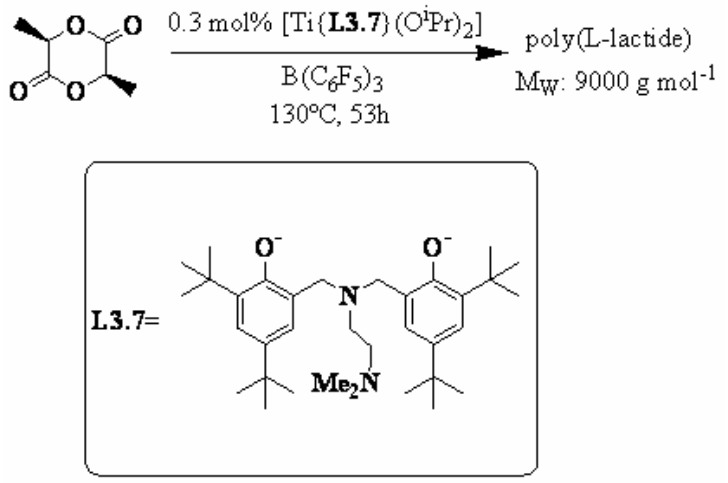

Scheme 3.6. Ti^{IV}(diaminebisphenolate)-promoted polymerization of L-lactide.

Despite the wide scope of applicability, aminophenolate Ti^{IV} complexes are better suited for oxygen transfer reactions, given their affinity for reactive oxygen species. Group 4 transition metals are known for their oxophilicity. Indeed, aminophenolate complexes based on group 4 transition metals readily hydrolyze when in presence of water, often forming μ-oxo polymeric species. Titanium compounds are interesting due

to the fact that the resulting μ-oxo compounds can often possess increased activity and selectivity when compared to their precursor alkoxy or halo complexes (see Figure 3.2).[8]

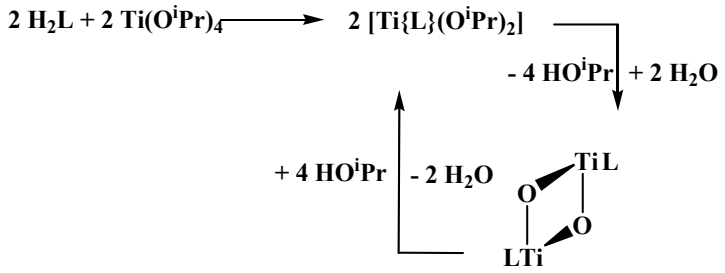

Figure 3.2. Conversion of an alkoxy Ti^{IV} complex into its μ-oxo bridged variant by reaction with water.

This tolerance towards water is of particular importance for the development of environmentally benign processes. Nowadays, most oxygen transfer processes employing this class of compounds take advantage of this combination of stability towards water with oxophilicity and use aqueous hydrogen peroxide as a terminal oxidant in place of organic oxidants. As such, aminophenolate Ti^{IV} complexes show great potential as candidates for the development of cheaper and environmentally friendly oxidation processes.

One of the widely known oxidation processes is the oxidation of thioethers to the corresponding sulfoxides or sulfones. Sulfoxides are noteworthy because the sulfur atom becomes chiral if the alkyl substituents are different. Chiral sulfoxides are important due to their use as chiral auxiliaries in catalytic processes and as active pharmaceutical ingredients, such as the proton pump inhibitor esomeprazole, used in the treatment of acid-induced stomach disorders, and the analeptic armodafinil. [15,16,17,18]

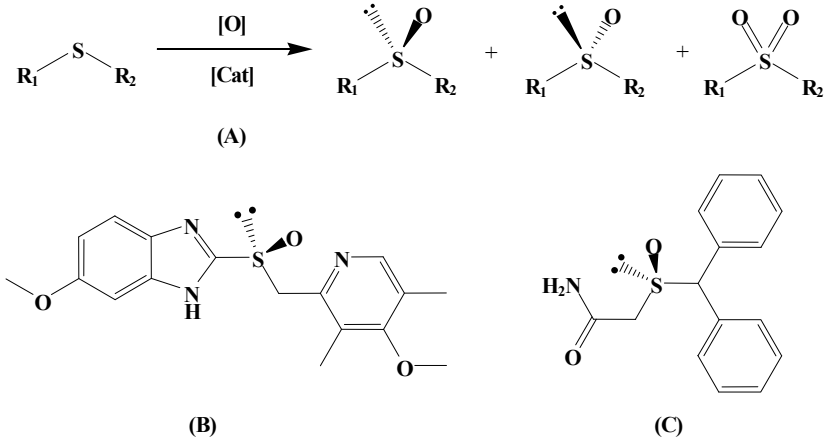

Figure 3.3. Catalytic oxidation of a thioether (A). This process constitutes the most direct route to important sulfoxides such as esomeprazole (B) and armodafinil (C).

Being esomeprazole one of the most biggest-selling pharmaceutical drugs in the world, there is a strong drive to improve the efficiency of current methods employed to produce these compounds. Separation of the desired products can be made by optical resolution, resolution by chemical transformation and catalytic enantioselective synthesis. Catalytic oxidation of prochiral thioethers provides the most direct route to the desired chiral sulfoxide. The first successful catalytic method for the production of enantiopure sulfoxides was that developed independently by Kagan and Modena in 1984, which is based on the Sharpless $Ti(O^iPr)_4$/diethyltartrate system. Despite the very high yields and enantiomeric excesses typical of the $Ti(O^iPr)_4$/diethyltartrate systems, the process also employs toxic chlorinated solvents, hazardous organic peroxides as terminal oxidants and is not very efficient. Most of the newly-developed Ti^{IV}-based systems still require either toxic solvents or organic peroxides to achieve optimal results,[19] but the Ti^{IV}(salen) and Ti^{IV}(salan) stand out for their aforementioned qualities, namely their stability, activity, and selectivity in a broad range of applications.

Aiming to improve activity and enantioselectivity, yet using less toxic solvents and using aqueous hydrogen peroxide as oxidant, Ti^{IV}(salan) compounds were prepared and tested.

With these characteristics in mind, this Chapter will describe the development of relatively simple, environmentally friendly, yet robust Ti^{IV}(salan) catalytic systems for asymmetric oxidation of thioethers.

3.2. Chiral Ti^{IV}(salan) compound preparation: results and discussion

Current methodologies for the preparation of Ti^{IV}(salan) complexes almost exclusively employ commercially available and relatively cheap titanium alkoxide precursors such as $Ti^{IV}(O^iPr)_4$. Titanium chlorides often prove too reactive and require oxygen and moisture-free environments during handling. Complexes $[Ti^{IV}(salan)(O^iPr)_2]$ can be readily obtained by reacting the titanium precursor directly with the appropriate salan ligand precursor in isopropanol. Partial hydrolysis to the μ-oxo species may be prevented if the preparation is conducted in moisture-free conditions, but in this particular case it is actually desirable to obtain the μ-oxo species. All the prepared Ti^{IV}(salan) compounds were obtained in their μ-oxo forms as yellow solids after treatment with water (see Figure 3.4).

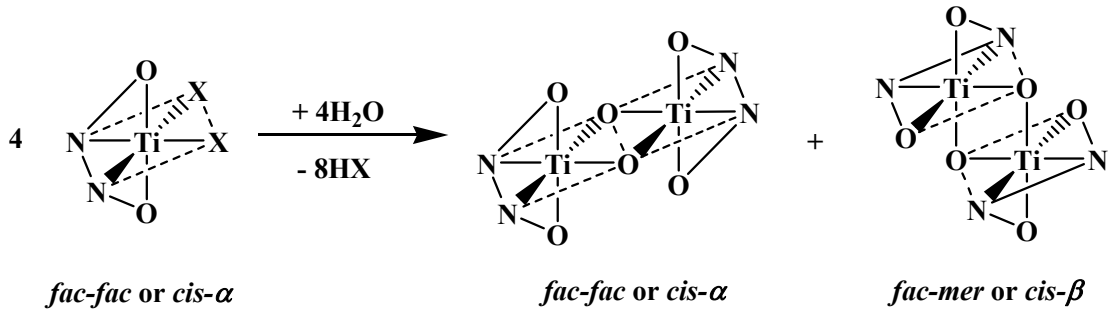

Figure 3.4. After treatment with water, a halo or alkoxy Ti^{IV}(salan) is converted into its polymeric μ-oxo variants, which often exhibit multiple geometries and helicities.

The isolation of the Ti^{IV}(salan) compounds as μ-oxo species introduced some limitations to their characterization. Because of the polymeric nature of these compounds, solubility issues were often encountered. In addition, characterization by NMR was also limited due to the possible existence of oligomeric μ-oxo species in solution which yield very complex spectra. Characterization relied mainly in elemental analysis, circular dichroism (CD), UV-Vis and IR spectroscopy, and mass spectrometry when possible.

Characterization of the prepared Ti^{IV}(salan) complexes *R*,*R*-**28**, *S*,*S*-**29**, *R*,*R* -**30**, *R*,*R* -**31** and *S*,*S*-**32** (See Figure 3.5) by NMR proved difficult as the ^1H and $^{13}C\{^1H\}$ NMR spectra of the isolated μ-oxo species could not always be adequately interpreted. Viable spectra could be obtained when the sample was prepared in the presence of a solvent that

promotes the cleavage of the μ-oxo bonds. Indeed, ^{1}H and $^{13}C\{^{1}H\}$ NMR spectra of *R*,*R*-**28** were obtained with a DMSO-d_6 sample containing a slight excess of ethanol relative to the amount of complex used in the sample, though the other remaining complexes failed to yield adequate spectra by the same method. It should be noted that the objective was to characterize the isolated μ-oxo species and not the alkoxy species generated in alcoholic solutions, given that the catalytic applications described in this Chapter employ aprotic solvents and μ-oxo Ti^{IV}(salan) compounds as pre-catalysts.

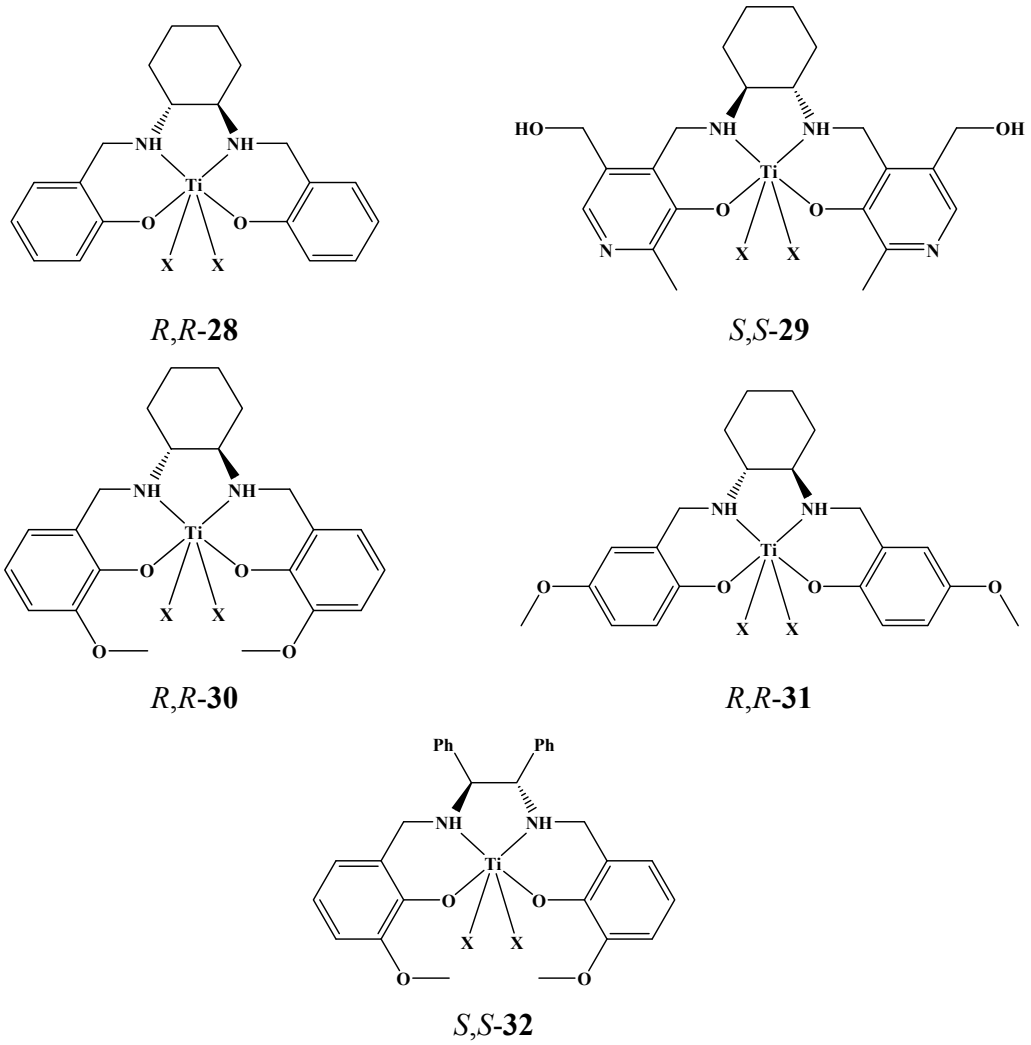

R,*R*-**28** *S*,*S*-**29**

R,*R*-**30** *R*,*R*-**31**

S,*S*-**32**

Figure 3.5. Structural formulas of the prepared Ti^{IV}(salan) compounds. The letter X denotes the μ-oxo ligand.

The ^{1}H NMR spectrum obtained for *R,R*-**28** in the presence of ethanol (see Figure 3.6) is indicative of C_2-symmetry in solution, which in turn indicates that a monomeric alkoxy species with *fac-fac* (*cis*-α) geometry may be present. A given *μ*-oxo Ti^{IV}(salan) complex can generate species possessing *mer-mer* (*trans*), *fac-fac* (*cis*-α) and *fac-mer* (*cis*-β) geometries (see Figure 3.4) which may yield significantly different ^{1}H and ^{13}C{^{1}H} NMR spectra, depending on whether their symmetry in solution is C_{2v}, C_2 or closer to C_1.[20,21,22]

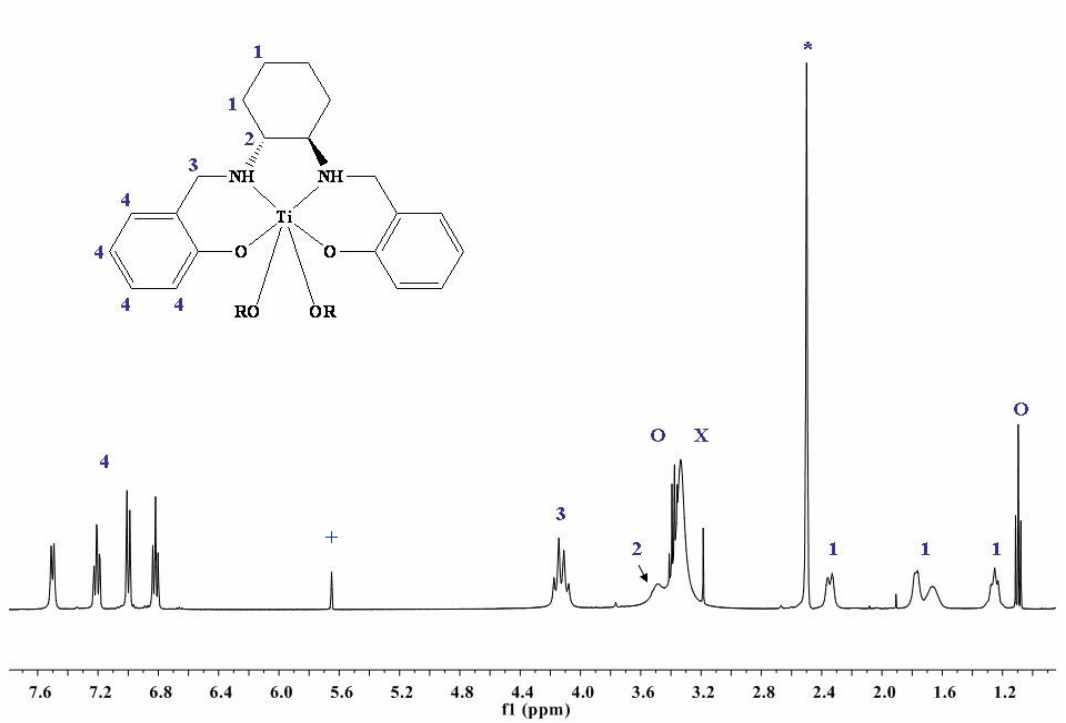

Figure 3.6. ^{1}H NMR spectrum of *R,R*-**28** in DMSO-d_6 (*) in the presence of CD_2Cl_2 (+)and ethanol (**O**). The spectrum is strikingly similar to the one obtained for *R,R*-**1**. The letter X denotes the water signals-

Figure 3.7 depicts the ^{1}H NMR spectrum of *μ*-oxo *R,R*-**30** where the presence of these multiple conformations introduce significant complexity to the obtained ^{1}H and ^{13}C{^{1}H} NMR spectra. The *cis* geometries are remarkable as each exhibit distinct helicities, *Λ* and *Δ*, which render the Ti^{VI}(salan) complex chiral both at the metal and nitrogen atoms (see

Figure 3.8). Salan-type ligands bind to early transition metals preferably in the *cis*-α geometry leading to C_2-symmetric complexes, though the less common C_1-symmetric *cis*-β geometry is also observed.[23] Salen-type ligands prefer the C_{2v}-symmetric *trans* or, to a lesser extent, *cis*-β wrappings around the metal centre as a result of their structural rigidity. C_{2v}-symmetric octahedral complexes are not chiral at the Ti^{IV} centre. The *Λ*- and *Δ*-*cis* diastereoisomer ratio can be controlled by using the adequate ligand system. Balsells and co-workers[13] reported the controlled formation of chiral-at-the-metal Ti^{IV}(salan) complexes bearing achiral salan-type ligands. This brings into attention an important factor: if the *Λ*- and *Δ*-*cis* diastereoisomer ratio is *ca*. 1:1, the overall chirality at the metal centre corresponds to that of a racemic mixture. This may have implications in the performance of the Ti^{IV}(salan) catalyst for enantioselective synthesis.[15]

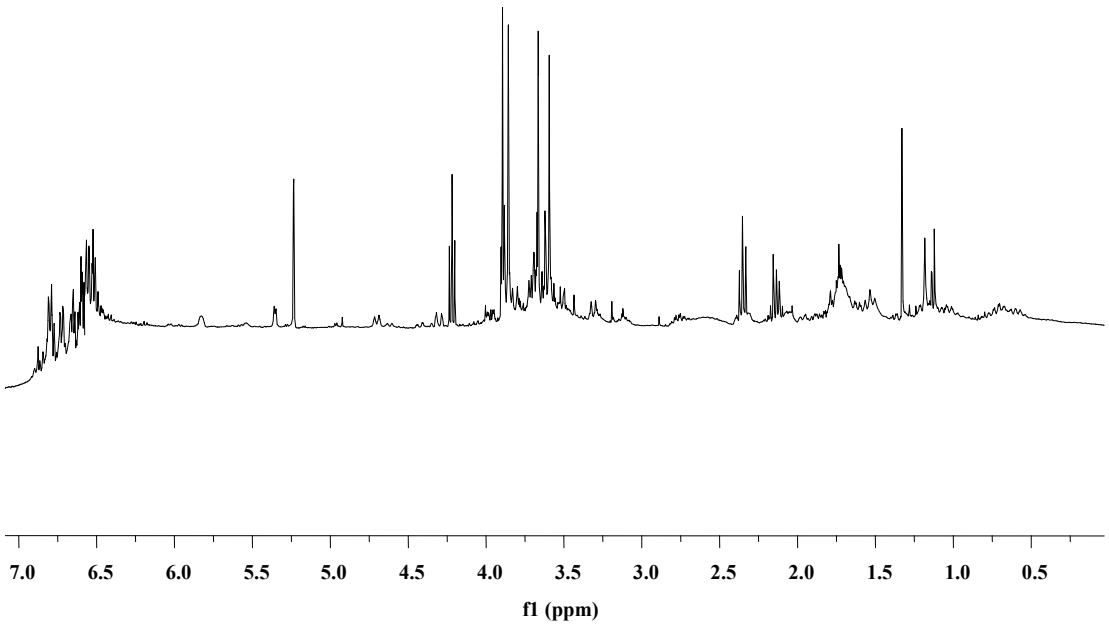

Figure 3.7. ^{1}H NMR spectrum of *R,R*-**30** in CD_2Cl_2. The existence of multiple magnetically non-equivalent conformations in solution is responsible for the complexity of NMR spectra of *μ*-oxo Ti^{IV}(salan) species.

Additional chirality can be introduced to the salan ligand by the use of a chiral diamine precursor. A Ti^{IV}(salan) complex bearing a chiral salan-type ligand will have five chiral centers if a *cis* geometry is adopted: the Ti^{IV} atom, the nitrogen donor atoms and the diamine backbone chiral carbons. Of these, only the carbon atoms retain their

configuration, whereas the chirality at the Ti^{IV} and the nitrogen atoms may depend on the adopted *cis* geometry. A consequence of this is the possibility of Ti^{IV}(salan) complexes with opposed chirality at the ligand sharing the same chirality at the metal centre and nitrogen donor atoms and vice-versa.[24] Despite this complex compounding of chirality factors and the possible impact on Ti^{IV}(salan) catalyst perfomance, the best form to confer permanent chirality on a Ti^{IV}(salan) complex is to use a chiral salan-type ligand.

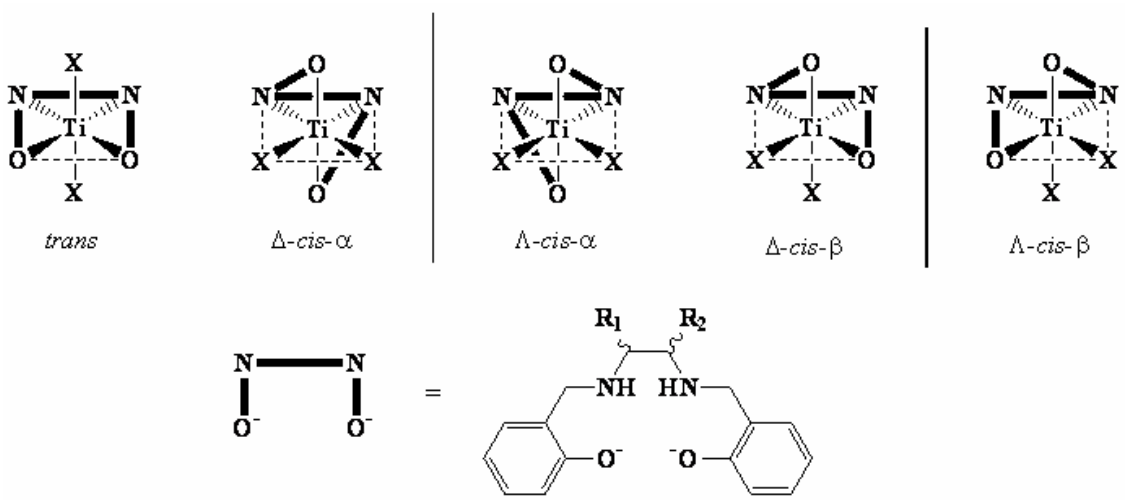

Figure 3.8. The potential configurational isomers of a Ti^{VI}(salan) complex. The *cis* isomers are chiral at the metal centre. If no other chiral centre exists they will present as racemic mixtures. If the ligand contains stereogenic centers for the *cis*-α and *cis*-β isomers one of the enantiomers may be more stable.

It was possible to obtain viable NMR spectra of μ-oxo *S,S*-**32** where, despite the complexity, it was possible to identify the major species. Figure 3.9 depicts a ^{1}H NMR spectrum of μ-oxo *S,S*-**32**, with a major species exhibiting C_2-symmetry in solution, indicative of *cis*-α geometry. The remaining minor resonances may result from species with different conformations, though the overlapping main signals do not allow identification. Compound *S,S*-**29** could not be analyzed by NMR due to insolubility in aprotic solvents. Compound *R,R*-**31** gave very complex NMR spectra not allowing the characterization of the complex by NMR.

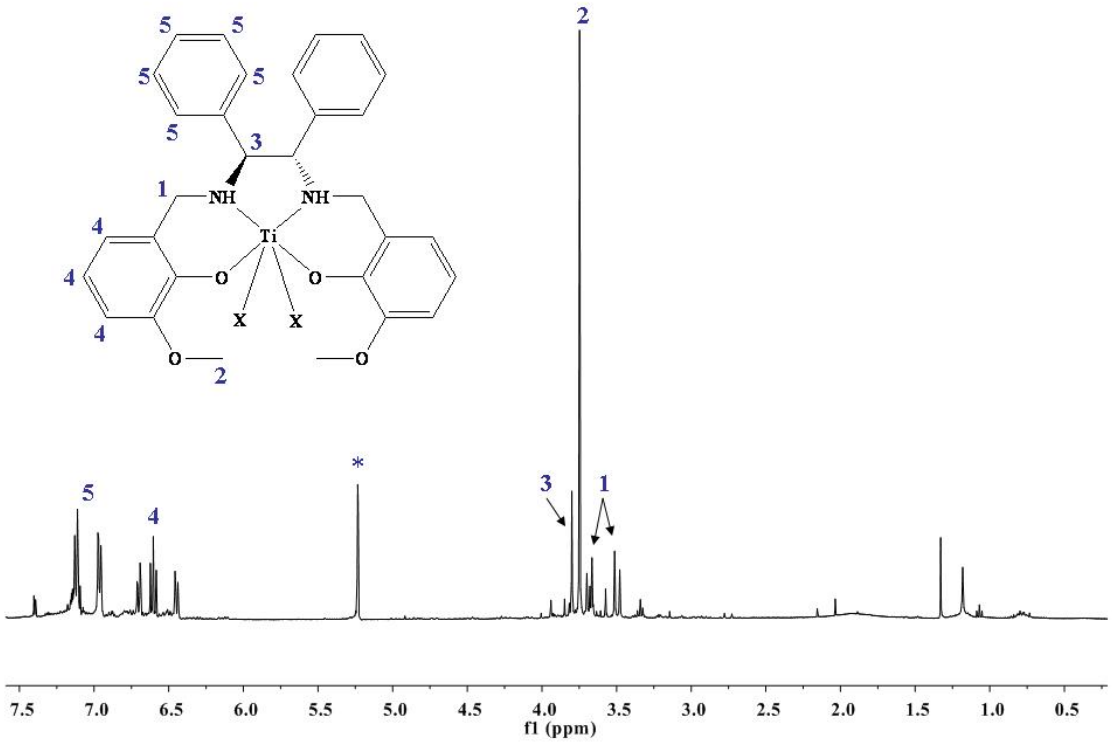

Figure 3.9. ^{1}H NMR spectrum of *S,S*-**32** in CD_2Cl_2 (*). The existence of multiple magnetically non-equivalent conformations in solution is visible, but the C_2-symmetric species are predominant.

Controlling the stereochemistry exhibited by chiral Ti^{IV}(salan) complexes may be possible with proper ligand design. This can either be done by manipulating the diamine backbone or the phenol moiety substituents.[25] Given the wider variety of substituted salicylaldehydes or phenols relative to chiral diamines, most Ti^{IV}(salan) systems are optimized by changing the phenol moiety substituents.

Unfortunately, the effect of diastereoisomeric ratio on overall chirality cannot be measured by NMR techniques alone. One technique that can confirm the chirality of the prepared Ti^{IV}(salan) in solution is Circular Dichroism (CD) spectroscopy. Figures 3.10 and 3.11 show the CD and UV-Vis spectra of the representative μ-oxo *R,R*-**28**, *R,R*-**30**, *S,S*-**32** and Table 3.1 lists the relevant λ_{max}, molar absorptivity (ε) and molar circular dichroism ($\Delta\varepsilon$) values.

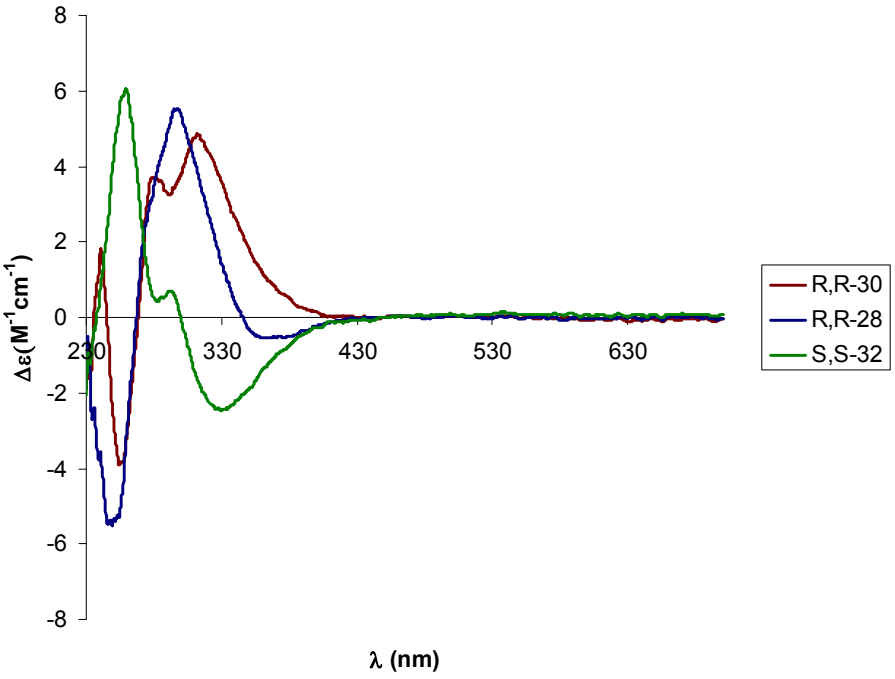

Figure 3.10. Circular dichroism spectra of *R,R*-**28**, *R,R*-**30**, *R,R*-**32** in CD_2Cl_2. The spectra were recorded with 4.39 mM (*R,R*-**28**), 4.61 mM (*R,R*-**30**), 4.41 mM (*S,S*-**32**) solutions, with a 0.2 mm optical path cell.

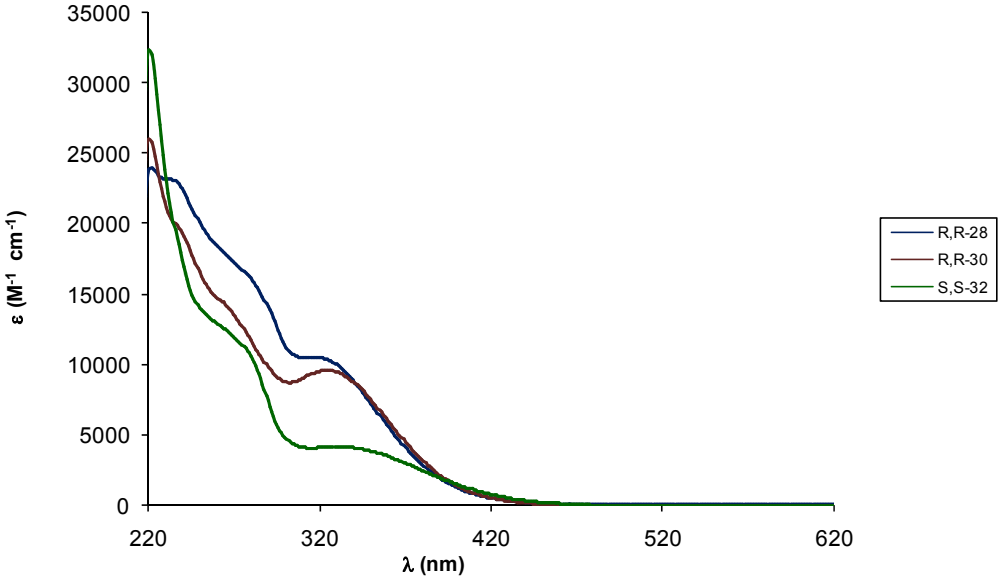

Figure 3.11. Isotropic absorption spectra (Uv-Vis) of *R,R*-**28**, *R,R*-**30**, *R,R*-**32** in CD_2Cl_2. The spectra were recorded with 0.52 mM (*R,R*-**28**), 0.47 mM (*R,R*-**30**), 0.42 mM (*S,S*-**32**) solutions, with a 1 mm optical path cell.

Table 3.1. λ_{max} , ε and Δε values for *R,R*-**28**, *R,R*-**30** and *S,S*-**32**.

CD					
R,R-**28**		*R,R*-**30**		*S,S*-**32**	
λ (nm)	Δε ($M^{-1}cm^{-1}$)	λ (nm)	Δε ($M^{-1}cm^{-1}$)	λ (nm)	Δε ($M^{-1}cm^{-1}$)
354	-0.48	312	4.85	330	-2.46
295	5.52	280	3.72	292	0.69
246	-5.49	256	-3.81	260	6.03
		241	1.83		
UV-Vis					
λ (nm)	ε ($M^{-1}cm^{-1}$)	λ (nm)	ε ($M^{-1}cm^{-1}$)	λ (nm)	ε ($M^{-1}cm^{-1}$)
316	10543	325	9598	333	4180
231	23203	221	26046	221	32351
222	23961				

The CD spectra of μ-oxo *R,R*-**28**, *R,R*-**30** and *S,S*-**32** are clearly indicative of chirality in solution. Noteworthy is the mirror-image resemblance of the spectra given by *R,R*-**30** and *S,S*-**32**, which possess opposite configurations at the ligand chiral centers. Since Ti^{IV} is a d^0 species, only signals corresponding to ligand-based and CT transitions are observed mostly in the UV region. The fact that the ligand-based and CT transitions yield CD bands is an indicator of efficient transmission of chirality, considering that the chiral centers are no less than two bonds away from the aromatic rings. The obtained CD spectra are usually complemented with UV-Vis spectra to facilitate the identification of the relevant absorption bands.

It should be noticed that all of the prepared Ti^{IV}(salan) complexes exhibit a bright yellow color, whereas the ligands are colorless. This yellow coloration may be due to a redshift of the aromatic CT transitions caused by the coordination of the phenolate oxygen atoms to the Ti^{IV} center. Indeed, the UV-Vis spectra of μ-oxo *R,R*-**28**, *R,R*-**30** and *S,S*-**32** show the first CT transition band encompassing a small part of the violet region. Unfortunately the μ-oxo Ti^{VI}(salan) compounds *S,S*-**29** proved insoluble in aprotic solvents and the measurement of the respective CD and UV-Vis spectra was not possible. No CD and UV-Vis spectra were measured for the compound *R,R*-**31**, as it was solely prepared for ascertaining the influence of ligand structure on catalytic behavior.

Crucial structural information was obtained by the X-ray diffraction of single crystals of *R,R*-**28**. While most of Ti^{IV}(salan) compounds characterized by X-ray diffraction are alkoxy monomers,[21] μ-oxo species can be dimeric,[26] trimeric[27] or tetrameric as is the case of *R,R*-**28**. The ORTEP diagram of *R,R*-**28** is presented below and the selected parameters are listed in Table 3.2.

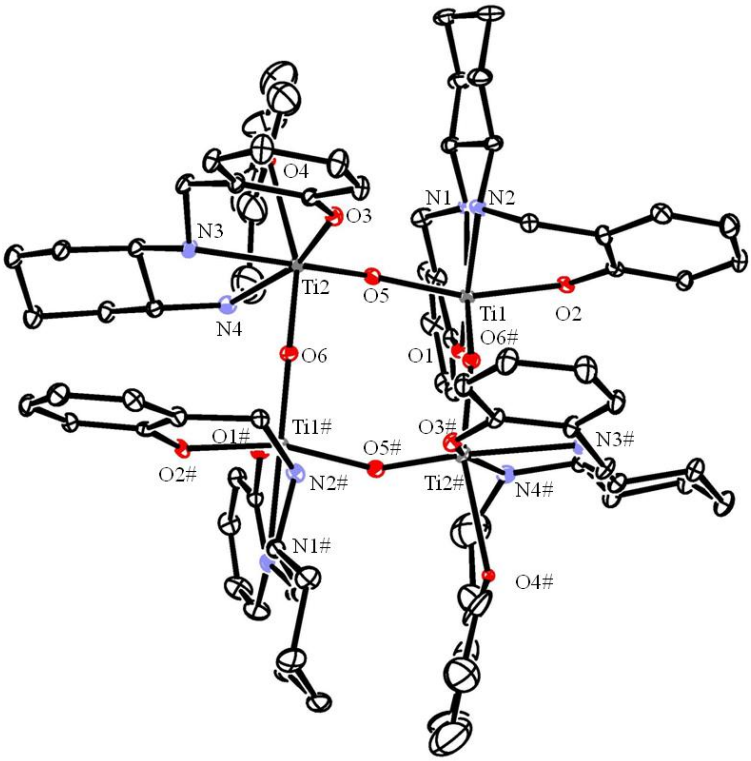

Figure 3.12. ORTEP-3 diagram of *R,R*-**28**, using 30 % probability level ellipsoids. The hydrogen atoms were omitted for clarity. The atoms labeled with # were generated using the symmetry transformation -x, 1-y, z.

Figure 3.12 depicts *R,R*-**28** as a tetrameric structure with each monomeric unit presenting *cis*-β geometry. The asymmetric unit contains only half of the molecule, and the other half was generated using symmetry transformations. The μ-oxo and the phenolate ligands occupy mutually *cis* positions. Remarkably, both Λ and Δ diastereoisomers are present: two monomers are Λ and the other two are Δ (see Figure 3.13).

Table 3.2. Selected bond lengths and angles for *R,R*-**28**.

R,R-**28**					
Bond lengths (Å)		Bond angles (°)[a]			
Ti(1)-O(6)	1.777(3)	O(6)-Ti(1)-O(1)	102.52(13)	O(5)-Ti(2)-N(3)	172.77(14)
Ti(1)-O(1)	1.890(3)	O(6)-Ti(1)-O(5)#	99.63(11)	O(6)-Ti(2)-N(3)	82.58(12)
Ti(1)-O(5)*	1.907(3)	O(1)-Ti(1)-O(5)#	95.03(13)	O(3)-Ti(2)-N(3)	86.54(13)
Ti(1)-O(2)	1.962(3)	O(6)-Ti(1)-O(2)	94.79(12)	N(4)-Ti(2)-N(3)	76.64(13)
Ti(1)-N(2)	2.204(4)	O(1)-Ti(1)-O(2)	94.02(12)	O(5)-Ti(2)-O(4)	94.16(10)
Ti(1)-N(1)	2.286(3)	O(5)#-Ti(1)-O(2)	160.88(11)	O(6)-Ti(2)-O(4)	161.61(10)
O(1)-C(1)	1.327(5)	O(6)-Ti(1)-N(2)	94.96(13)	O(3)-Ti(2)-O(4)	91.03(10)
N(1)-C(7)	1.480(5)	O(1)-Ti(1)-N(2)	162.22(13)	N(4)-Ti(2)-O(4)	81.89(10)
N(1)-C(8)	1.488(5)	O(5)#-Ti(1)-N(2)	85.14(13)	N(3)-Ti(2)-O(4)	81.86(10)
Ti(2)-O(5)	1.755(3)	O(2)-Ti(1)-N(2)	81.14(11)	C(20)-O(2)-Ti(1)	133.2(2)
Ti(2)-O(6)	1.884(3)	O(6)-Ti(1)-N(1)	171.57(14)	C(13)-N(2)-Ti(1)	113.2(2)
Ti(2)-O(3)	1.894(3)	O(1)-Ti(1)-N(1)	85.64(13)	C(14)-N(2)-Ti(1)	110.9(2)
Ti(2)-N(4)	2.205(4)	O(5)#-Ti(1)-N(1)	81.54(12)	C(21)-O(3)-Ti(2)	135.7(2)
Ti(2)-N(3)	2.289(3)	O(2)-Ti(1)-N(1)	82.239(11)	C(27)-N(3)-Ti(2)	112.3(2)
Ti(2)-O(4)	2.375(3)	N(2)-Ti(1)-N(1)	76.78(13)	C(28)-N(3)-Ti(2)	109.5(3)
O(2)-C(20)	1.320(4)	C(1)-O(1)-Ti(1)	137.9(3)	C(34)-N(4)-Ti(2)	112.3(5)
N(2)-C(13)	1.480(5)	C(7)-N(1)-Ti(1)	112.7(2)	C(33)-N(4)-Ti(2)	113.5(2)
N(2)-C(14)	1.488(5)	C(8)-N(1)-Ti(1)	108.0(2)	Ti(2)-O(5)-Ti(1)#	147.27(18)
O(3)-C(21)	1.344(5)	O(5)-Ti(2)-O(6)	100.20(11)	Ti(1)-O(6)-Ti(2)	149.87(17)
N(3)-C(27)	1.488(5)	O(5)-Ti(2)-O(3)	99.62(13)		
N(3)-C(28)	1.500(5)	O(6)-Ti(2)-O(3)	97.77(12)		
N(4)-C(34)	1.499(13)	O(5)-Ti(2)-N(4)	96.87(13)		
N(4)-C(33)	1.500(5)	O(6)-Ti(2)-N(4)	85.03(12)		
O(4)-C(40)	1.027(14)	O(3)-Ti(2)-N(4)	162.48(13)		

[a] The atoms labeled with # were generated using symmetry transformation -x, 1-y, z.

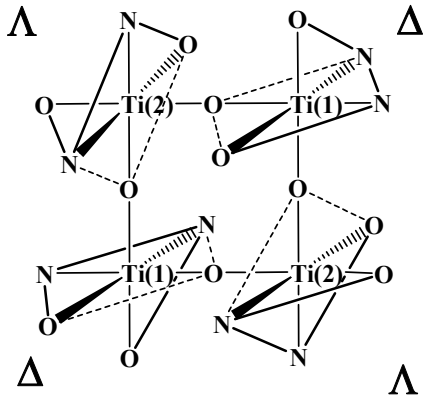

Figure 3.13. Representation of the octahedral Ti^{IV} centres in *R,R*-**28** bearing *Δ* and *Λ* configurations.

The Ti^{IV} centers adopt a distorted octahedral geometry with each tetradentate salan ligand coordinating through both O_{phenol} and both N_{amine} donor atoms. The bridging μ-oxo oxygen atoms complete the octahedral coordination sphere. The cyclohexane ring adopts the chair conformation with the chiral carbons in *R* configuration. The Ti(1)-O(5)-Ti(2#)

angle is 147.30(18)º, slightly narrower than the Ti(1)-O(6)-Ti(2) angle of 149.87(17)º. The Ti-μ-oxo bonds also differ in terms of length. The titanium-oxygen bonds Ti(1)-O(6) and Ti(2)-O(5), *trans* to the secondary amine nitrogens, have lengths of 1.777(3)Å and 1.755(3)Å, respectively. These short lengths are indicative of pronounced π-donation from the μ-oxo ligand to the metal. The titanium-oxygen bonds Ti(1)-O(5) and Ti(2)-O(6), *trans* to the phenolate oxygens, are longer and weaker with lengths of 1.907(3)Å and 1.884(3)Å respectively. There is also a small difference in the titanium-nitrogen bonds, as the Ti-N_{amine} bonds *trans* to the Ti-μ-oxo bonds are slightly longer. The same elongation effect is observed on the Ti-$O_{phenolate}$ bonds. Each metal centre is part of a 5-membered chelate ring and two 6-membered chelate rings. The best planes containing the 5-membered chelate ring Ti(1)-N(1)-C(8)-C(13)-N(2) and the 6-membered chelate ring Ti(1)-O(1)-C(1)-C(6)-C(7)-N(1) deviate from the equatorial plane by 6.45º and 11.33º, respectively. The plane containing the remaining 6-membered chelate ring Ti(1)-O(2)-C(20)-C(15)-C(14)-N(2) defines a dihedral angle of 83.63º with the equatorial plane. The dihedral angles defined by the planes containing the Ti(2) chelate rings Ti(2)-N(3)-C(28)-C(33)-N(4), Ti(2)-O(3)-C(21)-C(26)-C(27)-N(3) and Ti(2)-O(4)-C(40)-C(35)-C(34)-N(4) and the equatorial plane are 7.78º, 9.30º and 83.70º, respectively, which are very close to the angles obtained for the Ti(1) chelate ring planes. The 5-membered chelate ring Ti(1)-N(1)-C(8)-C(13)-N(2) displays δ-conformation, while the other 5-membered chelate ring Ti(1)-N(1)-C(8)-C(13)-N(2) displays the λ-conformation.

ESI-MS studies were also conducted with the prepared Ti^{VI}(salan) compounds that exhibited sufficient solubility in organic solvents. It should be noted that the mass assignments are for the most probable species having no more than ±1 divergence in m/z from the observed peak. The assigned species also take into account the behavior of Ti^{IV}(salan) compounds in aprotic and protic solvents. Compounds *R,R*-**30**, *R,R*-**31** and *S,S*-**32** could be analyzed in acetonitrile which facilitated the preservation of the μ-oxo species. Compounds *R,R*-**28** and *S,S*-**29** required the use of methanol as solvent instead of acetonitrile.

Figure 3.14 shows the ESI-MS spectrum of *R,R*-**30**. It is possible to observe a monomeric $[TiL_2H]^+$ species (m/z= 817.8), a dimeric μ-oxo $[Ti_2L_2OH]^+$ species (m/z= 879.1), a dimeric di-μ-oxo $[Ti_2L_2O_2H]^+$ species (m/z= 897.6), a possibly dimeric

$[Ti_2L_3O]^+$ species (m/z= 1265.5) with a μ-oxo bridge and an extra ligand molecule, (m/z= 897.6), a trimeric tri-μ-oxo $[Ti_3L_3O_3]^+$ species (m/z= 1344.4), the sodium adduct of the trimeric $[Ti_3L_3O_3Na]^+$ species (m/z= 1367.3) and the tetrameric tetra-μ-oxo $[Ti_4L_4O_4]^+$ species (m/z= 1792.8), which appears as the major peak.

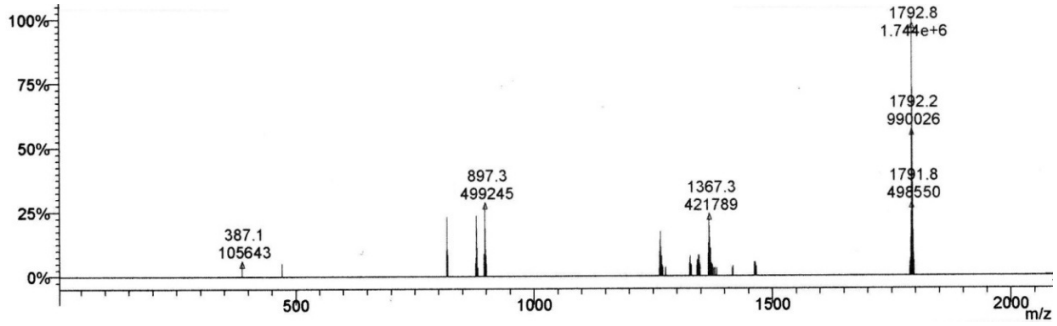

Figure 3.14. ESI-MS spectrum of *R,R*-**30** in acetonitrile. Polymeric μ-oxo species are prevalent.

The ESI-MS spectrum of *R,R*-**31** shown in Figure 3.15 is far simpler but indicative of demetallation under the ESI-MS conditions. The major peak is assigned to the monomeric $[TiL_2H]^+$ species (m/z= 817.2), although the potassium adducts of a tri-μ-oxo trimeric species $[Ti_3L_3O_3K]^+$ (m/z= 1383.1) and the tetrameric tetra-μ-oxo $[Ti_4L_4O_4K]^+$ species (m/z= 1831.8) are also visible.

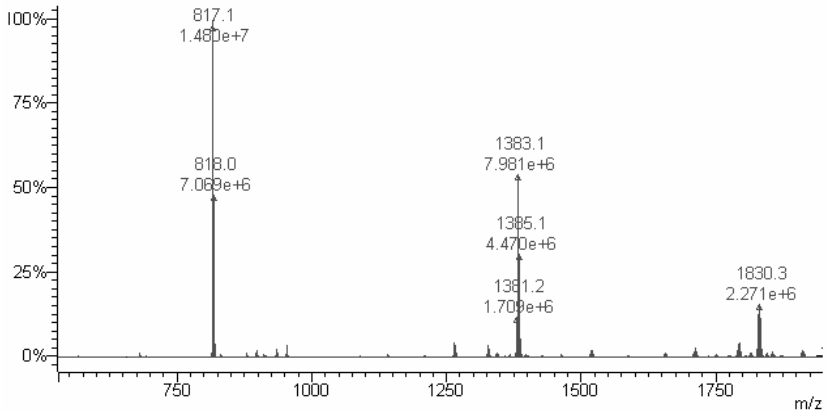

Figure 3.15. ESI-MS spectrum of *R,R*-**31** in acetonitrile. Polymeric μ-oxo species are prevalent.

Similarly to what was observed for *R,R*-**31**, the ESI-MS spectrum of *S,S*-**32** shown in Figure 3.16 is also simple and indicative of demetallation under the ESI-MS conditions.

The major peaks are that of the protonated ligand *S,S*-**10** (m/z= 485.1) and its fragmentation products (m/z= 137.0, 196.0, 332.0). The monomeric $[TiL_2H]^+$ species (m/z= 1013.3) is present along with a dimeric μ-oxo $[Ti_2L_2OH]^+$ species (m/z= 1075.2).

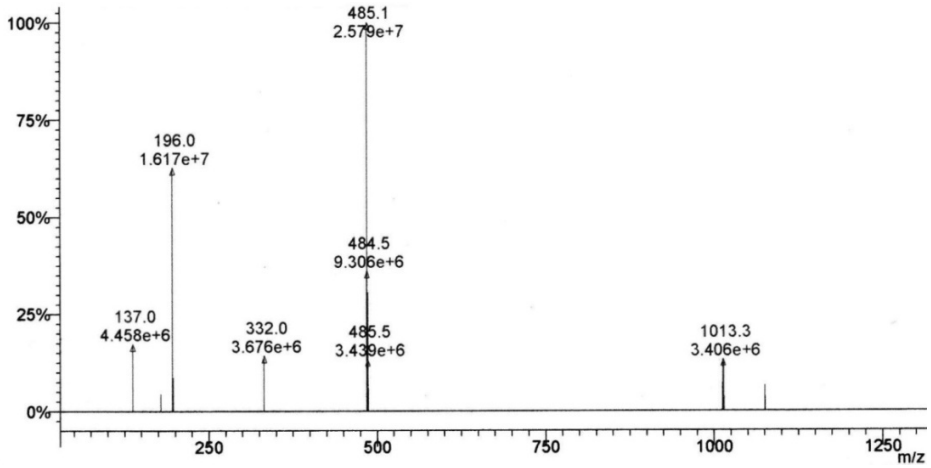

Figure 3.16. ESI-MS spectrum of *S,S*-**32** in acetonitrile. Low mass peaks are indicative of fragmentation. The intense peak given by the ligand also indicates demetallation under the conditions used for the analysis.

Figure 3.17 shows the ESI-MS spectra of *R,R*-**28** in methanol. The use of methanol as solvent was necessary due to very low solubility in acetonitrile. As expected, one of the major peaks can either be assigned to a monomeric methoxy species $[TiL(OCH_3)]^+$ or a trimeric di-μ-oxo $[Ti_3L_3O_2(OCH_3)_2]^{3+}$ species (m/z= 403.0) containing two methoxy groups. A trimeric di-μ-oxo $[Ti_3L_3O_2(OCH_3)(O^iPr)]^{3+}$ species (m/z= 413.1) may be present, considering that the metal precursor used in the preparation was $Ti^{IV}(O^iPr)_4$ and that the hydrolysis may not have been complete. As was observed with the previous compounds, a monomeric $[TiL_2H]^+$ species (m/z= 697.1) is also present, indicative of the tendency of these compounds to suffer demetallation under the conditions employed in the ESI-MS analysis. A tetrameric tetra-μ-oxo $[Ti_4L_4O_4(H_2O)(HOCH_3)]^{2+}$ (m/z= 801.2) species may also be present.

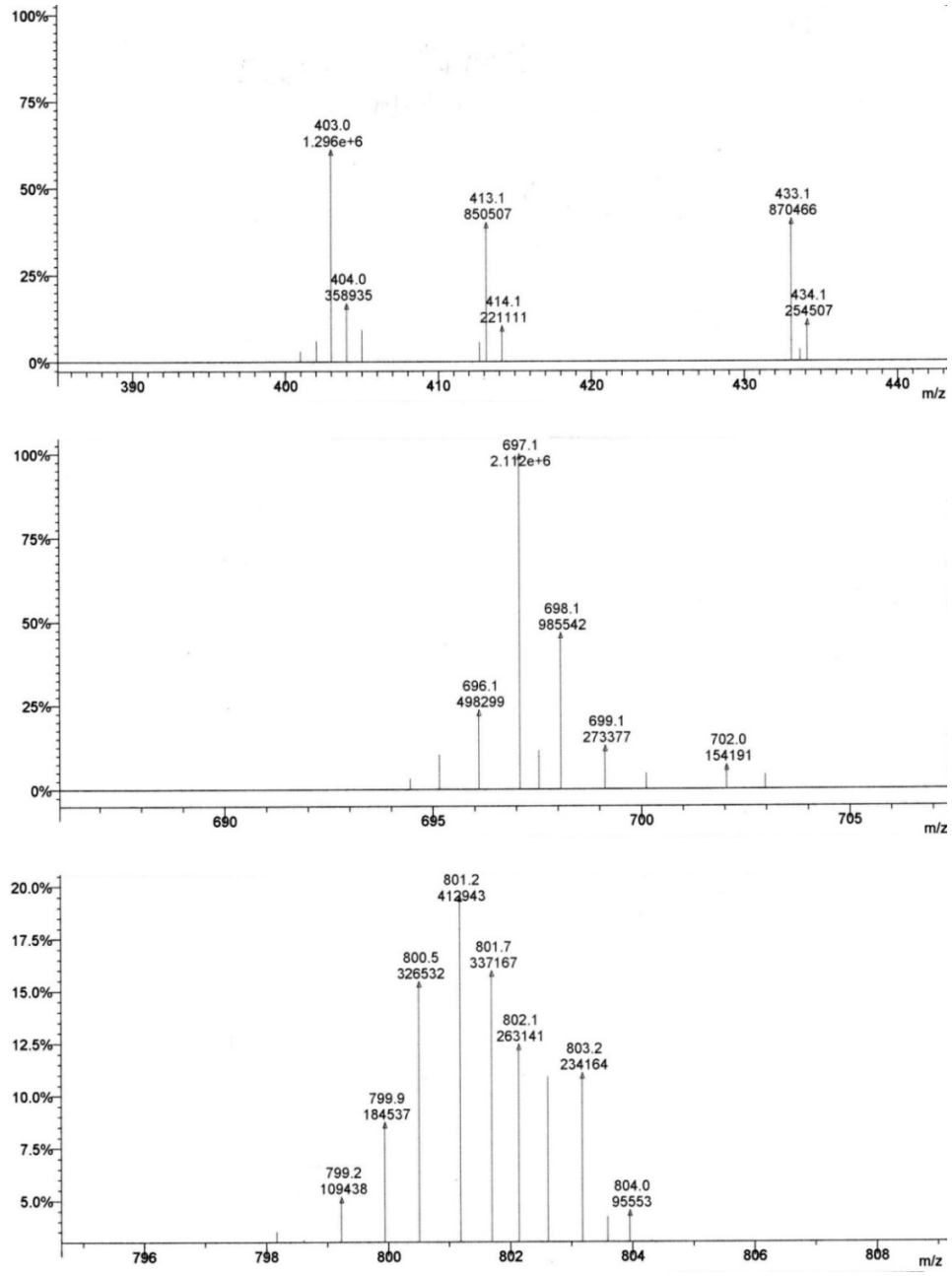

Figure 3.17. ESI-MS spectrum of *R,R*-**28** in methanol. Methoxy species are present as major species.

Figure 3.18 shows the ESI-MS spectrum of *S,S*-**29** in methanol. The major peak is assigned to the monomeric methoxy species $[TiL(OCH_3)]^+$ (m/z= 493.0). The remaining relevant peaks also are assigned to a dimeric μ-oxo $[Ti_2L_2O]^+$ species (m/z= 939.4), a dimeric μ-oxo $[Ti_2L_2O(OCH_3)]^+$ species (m/z= 971.4) and a dimeric μ-oxo $[Ti_2L_2O(OCH_3)_2]^+$ species (m/z= 1003.1).

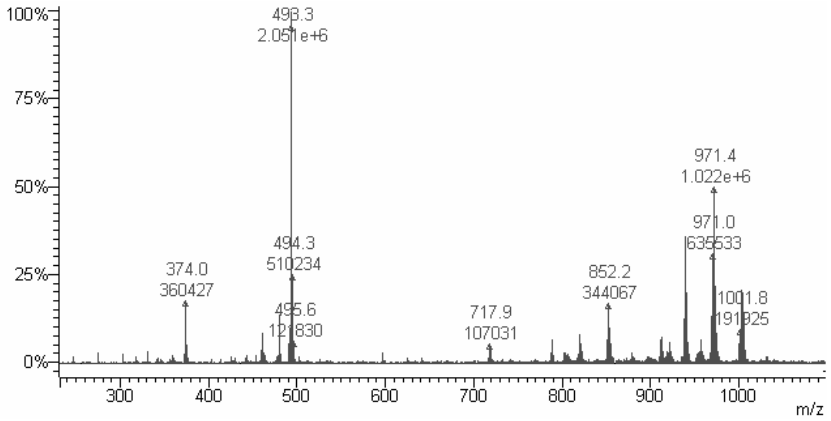

Figure 3.18. ESI-MS spectrum of *S,S*-**29** in methanol. Methoxy species are present as major species.

The ESI-MS experiments carried out with these compounds indicate aggregation of the Ti^{IV} (salan) compounds into structures containing at least two Ti-O units as a result of the hydrolysis of the parent isopropoxy complexes. The prevalence of alkoxy species in the spectra of *R,R*-**28** and *S,S*-**29** also indicates that the Ti-O-Ti bridge may be effectively cleaved using an alcohol, converting the μ-oxo complex back into an alkoxy complex.

Characterization of the prepared Ti^{IV}(salan) compounds by FT-IR spectroscopy was also made. The main IR stretching frequencies are listed in Table 3.3. In addition to the expected C-H and C-O stretching bands, all compounds exhibit a ν(N-H) band at around 3250 cm^{-1}. The identification of the ν(Ti-O-Ti) band was also attempted. Non-linear μ-oxo bridges often yield ν(Ti-O-Ti) bands at *ca*. 827 cm^{-1}, whereas linear μ-oxo bridges yield ν(Ti-O-Ti) bands around 865-885 cm^{-1}.[28] All compounds exhibited intense ν(Ti-O-Ti) bands around 813-887 cm^{-1}.

Finally, all the prepared Ti^{VI}(salan) compounds gave elemental analysis results consistent with polymeric μ-oxo species having either water or alcohols as vestigial contaminants.

Table 3.3. IR stretching frequencies for the prepared Ti^{IV}(salan) catalysts.

Stretching mode	*R,R*-**28**	*S,S*-**29**	*R,R*-**30**	*R,R*-**31**	*S,S*-**32**
			Wavenumber (cm^{-1})		
ν(N-H)	3246	3216	3227	3216	3227
ν(C-O)	1270	1248	1246	1248	1248
ν(Ti-O)	865	887	865	887	866

3.3. Catalytic applications : Asymmetric sulfoxidation of thioanisole

The prepared Ti^{IV}(salan) compounds were screened for their catalytic potential in the asymmetric sulfoxidation of thioanisole, a thioether frequently used as a model substrate. In all cases the final products were *R* and/or *S* methyl phenyl sulfoxide and/or the sulfone. The conversion percentage represents the sum of sulfoxide and sulfone amounts relative to the initial substrate quantity. Several parameters were optimized including catalyst loading, temperature and solvent. Control reactions made to test the oxidation of thioanisole in the absence of catalyst gave very low conversions to sulfoxide even after a 24 hour period at room temperature: 9 % in DCE, 3 % in acetone, 2 % in ethyl acetate, 2 % in acetinitrile, 0% of sulfone in all control reactions. All the obtained results are presented in Table 3.4.

Table 3.4. Sulfoxidation of thioanisole with the Ti^{IV}(salan) catalysts **28**, **29**, **30**, **31** and **32**.[a]

Entry	Catalyst	Solvent	mol% catalyst	T(ºC)	Conv (%)	ee (%)	sulfone (%)
1	*R,R*-**28**	DCE	0.015	0	16	8 (R)	0
2	*R,R*-**28**	DCE	0.24	0	95	50 (R)	13
3	*R,R*-**28**	DCE	1.0	0	94	51 (R)	16
4	*R,R*-**28**	DCE	5.0	0	97	51 (R)	13
5[d]	*R,R*-**28**	DCE	1.0	0	99	56 (R)	15
7[d]	*R,R*-**28**	$(CH_3)_2CO$	1.0	0	64	35 (R)	8
8	*R,R*-**28**	$CH_3)_2CO$	1.0	0	83	33 (R)	17
9[d]	*R,R*-**28**	AcOEt	1.0	0	45	28 (R)	9
10	*R,R*-**28**	AcOEt	1.0	0	76	21 (R)	26
11[d]	*R,R*-**28**	EtOH	1.0	0	96	9 (R)	7
12[c]	*R,R*-**28**	$(CH_3)_2CO$	1.0	0	84	38 (R)	14
13[c]	*R,R*-**28**	AcOEt	1.0	0	88	46 (R)	27
14[b,f]	*S,S*-**29**	DCE/MeOH	1.0	0	20	21 (R)	0
15	*S,S*-**29**	$(CH_3)_2CO$	1.0	0	0	0	0
16	*S,S*-**30**	DCE	1.0	10	87	21 (S)	20
17	*R,R*-**30**	DCE	1.0	0	85	22 (R)	23
18	*R,R*-**30**	$(CH_3)_2CO$	1.0	0	53	19 (R)	8
19	*R,R*-**31**	DCE	1.0	0	81	41 (R)	14
20[d]	*R,R*-**31**	$(CH_3)_2CO$	1.0	0	61	44 (R)	8
21	*R,R*-**31**	$CH_3)_2CO$	1.0	0	82	41 (R)	14
22[d]	*R,R*-**31**	AcOEt	1.0	0	60	38 (R)	15
23	*R,R*-**31**	AcOEt	1.0	0	79	30 (R)	23
24[d]	*R,R*-**31**	EtOH	1.0	0	67	13 (R)	5
25[c,d,e]	*R,R*-**31**	$(CH_3)_2CO$	1.0	25	37	25(R)	0
26[c]	*R,R*-**31**	$(CH_3)_2CO$	1.0	0	63	38(R)	7
27[c]	*R,R*-**31**	AcOEt	1.0	0	88	47(R)	23
28	*S,S*-**32**	DCE	1.0	10	86	8 (S)	20

[a]Conditions: nS=1 mmol, nH_2O_2:nS=1.2 and t=24 h.[b] nH_2O_2:nS = 1.5. [c] Slow addition of oxidant. [d] Reaction time was 3h. [e] 5% aqueous H_2O_2 was used as oxidant. [f] Solvent used was a 1:1 mixture of DCE and MeOH.

The best results were obtained with *R,R*-**28** (entries 1 to 13), which bears no substituents in the phenolate rings, in 1,2-dichloroethane (DCE). Catalyst loadings as low as 0.25 mol% are sufficient to obtain conversions higher than 90% with 50% of enantiomeric excess (entry 2). Catalysts with *R,R* configuration favored the formation of the *R*-sulfoxide, while the catalysts with *S,S* configuration gave the *S*-sulfoxide. Sulfone percentages were generally low, but kinetic profiling demonstrated that catalytic assay duration may be partly responsible for increased sulfone formation. Kinetic profiling of both the thioether sulfoxidation and sulfoxide resolution revealed interesting information about the processes behind the overall enantiomeric excesses (see Figure 3.19). The profile of the thioether sulfoxidation using *R,R*-**28**, 1 mmol of substrate and 1.2 mmol of H_2O_2 in DCE at 0 ºC shows that the reaction neared its completion after 2 hours, with a conversion of 97%, an enantiomeric excess of 54% and a sulfone percentage of 11%. After 3 hours, it is possible to observe a slight decrease in the amount of *S* sulfoxide and an increase in sulfone, from 11 to 15%, with an increase in enantiomeric excess from 54 to 56%. This indicates that the reaction proceeds till all of the oxidant is consumed and that extended reaction period results in increased sulfone formation.

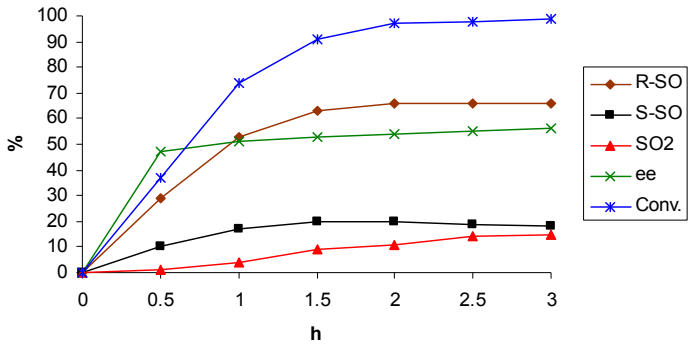

Figure 3.19. Profile of the sulfoxidation of thioanisole in DCE. Conditions: 1 mol-% of *R,R*-**28**, 1 mmol of sulfoxide, 1.2 mmol of H_2O_2 at 0 ºC; SO: sulfoxide; SO2: sulfone.

The kinetic resolution of the racemic sulfoxide using *R,R*-**28**, 1 mmol of sulfoxide, 0.5 mmol of H_2O_2 in DCE at 0ºC was also carried out (see Figure 3.20) and its profile confirmed a tandem process involving the oxidation of the thioether and sulfoxide. The profile clearly shows that the *S*-sulfoxide is preferably consumed over the *R*-sulfoxide.

After one hour, 47% of sulfoxide is converted to sulfone and the final enantiomeric excess is 34%.

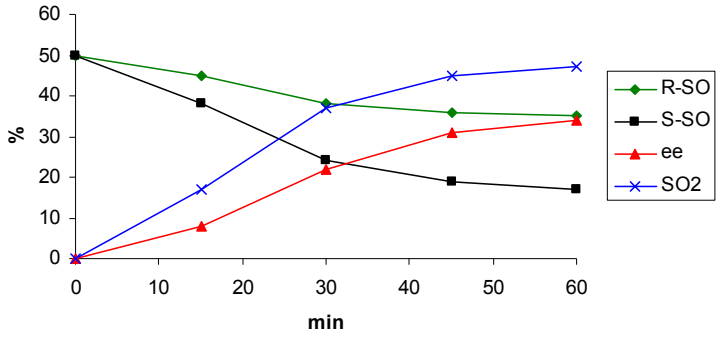

Figure 3.20. Kinetic resolution of racemic methyl phenyl sulfoxide in DCE. Conditions: 1 mol-% of *R,R*-**28**, 1 mmol of sulfoxide, 0.5 mmol of H_2O_2 at 0 ºC; SO: sulfoxide; SO2: sulfone.

The low solubility of *S,S*-**29** in aprotic solvents may be behind the poor results obtained using this catalyst. Indeed, the reaction in DCE only proceeded after the addition of methanol and even then the conversion after 24h did not exceed 20% (entries 14 and 15). No reaction was observed when acetone was used as solvent. The reactions using *R,R*-**30**, which bears methoxy groups at the 3-position of the aromatic rings, gave significantly lower enantiomeric excesses when compared to the catalytic runs conducted with *R,R*-**28** (entries 16 to 18). The lower conversions after 24 hours also indicate that the reaction is comparatively slower, whereas the reactions carried out with *R,R*-**28** reached near completeness after 3 hours under the same conditions. $V^{IV}O$(salen) and $V^{IV}O$(salan) catalysts bearing methoxy groups in the 3-position of the phenolate moieties demonstrated superior performance over the respective variants that had no substituents at that position.[29,33] The same rationale was applied for the present Ti^{IV}(salan) catalytic systems but a detrimental influence in the reactivity and enantioselectivity was observed, contrary to the initial expectations. Taking into account the relative proximity of the methoxy groups to the O_{phenol} donor atoms and the oxophilicity of the Ti^{IV} atom, one explanation for this behavior could be the increased likelihood of the Ti^{IV} metal center bearing a (O_{phenol}, O_{phenol}, O_{ether}, O_{ether}) donor set, where chiral transmission is less efficient, instead of (O_{phenol}, O_{phenol}, N_{amine}, N_{amine}). When the methoxy group substituents were placed in the 5-position of the phenolate moieties, as it is the case of *R,R*-**31**, the

obtained sulfoxide conversions and enantiomeric excesses were similar to those obtained with *R,R*-**28** (entries 19, 20, 21, 22, 26 and 27).

The influence of the phenolate moiety substituents on Ti^{IV}(salan) catalyst performance in sulfoxidations has been documented[8, 30,31] but a clear trend in behavior is difficult to establish, as it depends of both electronic and steric hindrance factors. For asymmetric sulfoxidations employing Ti^{IV}(salan) catalysts, generally the best results are obtained with catalysts that bear aryl substituents or no substituents at the 3-position of the phenolate moieties. Bulky alkyl groups such as *tert*-butyl and adamantyl tend to interfere negatively with catalyst reactivity and enantioselectivity.

The diamine backbone also exerts significant influence over catalyst enantioselectivity. For instance, *S,S*-**32** with a (1*R*,2*R*)-1,2-diphenylethane-1,2-diamine backbone, exhibited much lower enantioselectivity when compared to the cyclohexane-1,2-diamine variant *R,R*-**30** under the same conditions (entry 28).

The solvent also played an important role in the overall sulfoxidation results. Of the solvents tested, DCE provided the best results. Ethanol would be a desirable replacement for chlorinated solvents if high conversions, low by-product quantities and short reaction times are desired (entries 11 and 24). However, enantiomeric excesses did not exceed 9% for *R,R*-**28** and 13% for *R,R*-**31** indicating that alkoxy Ti^{IV}(salan) compounds, either employed as pre-catalysts or generated *in situ*, indeed may not exhibit the same enantioselectivity as the μ-oxo variants in asymmetric sulfoxidation. Ethyl acetate can be used in place of DCE without much negative impact in the catalyst performance if the oxidant is added slowly to the reaction mixture over a period of 24 hours. Such are the cases of the reactions where *R,R*-**28** was used as catalyst. A conversion of 88% and an enantiomeric excess of 46%, values comparable to the reactions carried out in DCE, were obtained when ethyl acetate was used as solvent (entry 13). A significant decrease in enantioselectivity was observed when acetone was used instead (entries 8 and 12). When *R,R*-**31** was used as catalyst under these conditions, a slight gain in enantioselectivity from 44 to 47% was observed compared to the reaction run in DCE (entries 20 and 27). While lower conversions and enantiomeric excesses were obtained when acetone was used as solvent, *R,R*-**31** gave results comparable to those obtained with ethyl acetate when the oxidant was added quickly in a single portion.

3.4. Conclusions

Several Ti^{IV}(salan) compounds were synthesized and characterized. All compounds were isolated directly as polymeric μ-oxo species, which reportedly exhibit superior performance over the alkoxy or halo derivatives in asymmetric oxidations. Characterization by NMR of the μ-oxo species had constraints due to either solubility issues or remarkably complex ^{1}H and $^{13}C\{^{1}H\}$ spectra. NMR spectra complexity was due to multiple magnetically non-equivalent conformations present in solution, although viable spectra were obtained from the alkoxy species generated *in situ*. Crystal structure of *R,R*-**28** was obtained and it revealed that *R,R*-**28** is a $[Ti_4\{R,R\text{-}\mathbf{1}\}_4(\mu\text{-}O)_4]$ tetrameric μ-oxo species where all Ti units exhibit *cis*-β geometry, though two Ti units have Λ-configuration and the other two bear Δ-configuration. The chirality of the prepared compounds was confirmed by CD spectroscopy. ESI-MS experiments confirmed the polymeric nature of the μ-oxo Ti^{IV}(salan) compounds and also indicated the tendency of the Ti-O-Ti bridge to react with alcohols.

The prepared Ti^{IV}(salan) compounds were employed as asymmetric sulfoxidation catalysts, using hydrogen peroxide as terminal oxidant. In general, high conversions and moderate enantioselectivities were obtained. Compound *R,R*-**28**, bearing the simplest ligand, gave the best conversions and enantioselectivities at 0ºC in DCE. Reaction times under these conditions are relatively short, with a catalytic run reaching near completion after 3 hours. Reactions can be conducted with as little as 0.25 mol% of *R,R*-**28** without any apparent negative effect. Solvent effect was tested by replacing DCE with less toxic solvents such as ethyl acetate, acetone and ethanol. Ethyl acetate proved to be a potential replacement for DCE, whereas the use of acetone or ethanol caused a significant decrease in enantioselectivity and, in some cases, conversion. Catalytic runs conducted with *R,R*-**30** and *R,R*-**31** confirmed the importance of the substituents at the 3-position of the phenolate moieties. Methoxy group substituents proved detrimental to the catalyst performance. Diamine backbone played an important part in catalyst performance, where the cyclohexane-1,2-diamine derived *R,R*-**30** outperformed the 1,2-diphenylethane-1,2-diamine derived *S,S*-**32** under the same conditions. Kinetic profiling demonstrated that the overall enantiomeric excesses are the result of two distinct catalytic processes

occurring in tandem. In addition to the more selective formation of the *R* sulfoxide, the *S* sulfoxide is preferably converted to sulfone, thus increasing the apparent enantiomeric excess.

3.5. Experimental section

3.5.1. General considerations

Unless stated otherwise, all preparations and subsequent manipulations were made without resorting to inert atmosphere techniques. All solvents and reagents were purchased from commercial suppliers and used as received.

3.5.2. Characterization techniques

3.5.2.1. Nuclear Magnetic Resonance Spectroscopy (NMR)

1D NMR (^{1}H, ^{13}C-{1H}, ^{13}C-{1H} APT) and 2D NMR (HSQC and HMBC) spectra were recorded on Bruker Advance II+ 300 and 400 MHz (UltraShield Magnet) instruments at ambient temperature, unless stated otherwise. ^{1}H and ^{13}C chemical shifts (δ) are expressed in ppm relative to Me_4Si. Whenever calculation is possible, coupling constants *J* are given in Hz and multiplicities are presented as: br (broad), s (singlet), d (doublet), dd (double doublet), t (triplet), q (quartet), sept (septet) and m (multiplet).

3.5.2.2. Infrared (FT-IR), UV and Vis (UV-Vis) and Circular Dichroism (CD) Spectroscopy

FT-IR spectra were recorded in KBr using a *JASCO FT/IR-430* spectrometer. UV-Vis spectra were recorded in CH_2Cl_2 using a Shimadzu U-2000 spectrophotometer. CD spectra were recorded in CH_2Cl_2 using a Jasco J-720 Spectropolarimeter.

3.5.2.3. Elemental Analysis (EA)

Elemental analyses were carried out at *Laboratório de Análises* of *Instituto Superior Técnico,* using EA110 CE automatic analyzer Instruments. The results presented are the average values obtained from two independent determinations.

3.5.2.4. High performance liquid chromatography (HPLC)

The analysis of the products obtained in catalytic sulfoxidations was done by HPLC using a Jasco system equipped with a Daicel Chiralpak IA column, a 870-UV Intelligent UV-Vis detector, two 880-PU Intelligent HPLC Pumps, a 2-line degasser 880-51 and a Rheodyne 725i injector (5 L). The system uses a Borwin software for data acquisition and analysis.

3.5.2.5. ESI-MS

The ESI mass experiments were made by Prof. Maria da Conceição Oliveira and Msc. Ana Dias at *Centro de Química Estrutural* of *Instituto Superior Técnico*. The ESI mass spectra were obtained on a Varian 500-MS LC Ion trap mass spectrometer equipped with an electrospray ion source, operated in the positive mode. The operated parameters were optimized for maximum abundance of the ions of interest, and were as follows: ion spray voltage, +5 kV; capillary voltage, 80 V; RF loading, 90%. Nitrogen was used as nebulising and drying gas, at pressure of 35 and 15 psi, respectively; drying gas temperature, 350 ◦C.

3.5.2.6. X-Ray crystallography

Single crystals suitable for X-ray diffraction studies were obtained as described in the ligand preparation methods. The data collection, structure solution and refinement for all the featured crystal structures in this Chapter were done by Dr. Fernando Avecilla at the *Departamento de Química Fundamental* of *Universidade da Coruña*. X-ray data for *R,R*-**28** were collected on a Bruker Kappa X8 Apex CCD diffractometer at room temperature. Reflections were measured from a hemisphere of data collected of frames,

each covering 0.3º in ω. The reflections measured were corrected for Lorentz and polarization effects, and for absorption by semiempirical methods based on symmetry-equivalent and repeated reflections. Complex scattering factors were taken from the program package SHELXTL.[32] The absolute configuration was established by refinement of the enantiomorph polarity parameter.[33] The structures were solved by direct methods and refined by full-matrix least-squares methods on F^2. The non-hydrogen atoms were refined with anisotropic thermal parameters in all cases. The hydrogen atoms were left to refine freely.

Table 3.5. Crystal data, data collection and refinement data for compound *R,R*-**28**.

Compound	*R,R*-**28**.	
Empirical formula	$C_{80}H_{96}N_8O_{12}Ti_4$	
Formula weight	1553.25	
Temperature / K	100(2)	
Wavelength / Å	0.71073 Å	
Crystal system	Tetragonal	
Space group	$I4_1$	
Unit cell dimensions	a = 24.0490(4) Å	α= 90°
	b = 24.0490(4) Å	β= 90°
	c = 12.4115(5) Å	γ = 90°
Volume / Å^3	7178.2(3)	
Z	4	
Density (calculated) / mg/m^3	1.437	
Absorption coefficient /mm^{-1}	0.500	
Crystal size / mm^3	0.49 × 0.32 × 0.18	
Reflections collected	35129	
Independent reflections	8897 [R(int) = 0.0292]	
Goodness-of-fit on F2	1.073	
Final R indices [I>2sigma(I)]	R1 = 0.0571, wR2 = 0.1559	
R indices (all data)	R1 = 0.0606, wR2 = 0.1592	
Absolute structure parameter	0.05(3)	

3.5.3. General procedure for sulfoxidation of thioanisole

The catalytic experiments were carried out at atmospheric pressure, at a constant temperature, in a glass batch reactor, equipped with magnetic stirrer, thermometer and condenser. In a typical run, the solid catalyst (0.25 to 10 mol%) and thioanisole (1 mmol) were dissolved in the appropriate solvent (4 mL). Then the oxidant (1.2 to 1.5 mmol), hydrogen peroxide 30 wt% aqueous solution, was added to the stirring mixture. Control

experiments were carried out in the absence of catalyst. Samples of the reaction mixture were withdrawn periodically and analyzed on a Jasco HPLC system equipped with a Daicel Chiralpak IA column. The eluent used was hexane/ethyl acetate (60:40) with a flow of 1 mL/min. The calibration curves for each reagent and product, namely sulfide, sulfoxide and sulfone, were determined using standards and similar HPLC procedures and these calibrations used for the quantitative analyses. Diphenylsulfone was used as an internal standard.

3.5.4. Ti^{IV}(salan) compound preparation methods

Synthesis of [Ti(*R*,*R*-1)], *R*,*R*-28

$Ti^{IV}(O^iPr)_4$ (1.1 g, 3.9 mmol) was added to a methanolic solution (25 mL) of *R*,*R*-**1** (1.7 g, 3.9 mmol) and the solution turned to orange. A 2M aqueous solution of KOH was added dropwise till pH 7–8. A yellow solid precipitated after 15 min. Water (100 mL) was added and the solid was filtered and washed with water and *n*-hexane. The resulting yellow solid was then dissolved in CH_2Cl_2, filtered to remove any traces of TiO_2, and the solvent was evaporated. A yellow solid was obtained. Yield: 0.36 g, 19 %. NMR analysis of μ-oxo species was not possible due to very complex spectra. ^{1}H NMR of alkoxy species were generated *in situ* by addition of a drop of ethanol to the sample. (400 MHz, DMSO-d_6, ppm): δ 1.25, 1.69, 1.78, 2.35 [8H, m, -C*H*$_2$-], 3.48 [2H, m, CH_2C*H*-NH], 4.09, 4.16 [4H, d, $^2J_{HH}$ = 13 Hz, Ar-C*H*$_2$-NH], 6.82 [2H, m, aromatic], 7.00 [2H, m, aromatic], 7.21 [2H, m, aromatic], 7.50 [2H, m, aromatic]. ^{13}C-{^{1}H} NMR of alkoxy species generated *in situ* (100 MHz, DMSO-d_6, ppm): δ 22.11, 26.00 [4C, -*C*H_2-], 42.85 [2C, Ar-*C*H_2-NH], 56.61 [2C, -(*C*H_2)$_2$-CH-NH], 115.31, 118.84, 130.31, 131.86, 156.10 [12C, aromatic]. IR (cm^{-1}): 3246 ν(N–H), 1270 ν(C-O), 865 ν(Ti–O). Elemental analysis for $C_{20}H_{24}N_2O_3Ti{\cdot}CH_2Cl_2$ (monomer): calcd. C 53.30, H 5.54, N 5.92; found C 53.7, H 5.9, N 6.0. Crystals suitable for single crystal X-ray diffraction were grown from acetonitrile solutions. 0.1g of *R*,*R*-**28** was dissolved in *ca*. 10 mL of acetonitrile and the resulting solution was filtered and transferred to a clean lint-free 20 mL glass flask. Colorless crystals were obtained by slow evaporation of the solvent after four weeks.

Synthesis of [Ti(*S*,*S*-3)], *S*,*S*-29

The procedure was similar to that used for the synthesis of *R*,*R*-**28**. Reagents: $Ti^{IV}(O^iPr)_4$ (0.25 g, 0.90 mmol), *S*,*S*-**3** (0.50 g, 0.90 mmol). The compound was obtained as a light-yellow solid. Yield: 0.29 g, 57 %. The NMR characterization of μ-oxo species was not possible due to solubility issues. IR (cm^{-1}): 3216 ν(N–H), 1248 ν(C-O), 887 ν(Ti–O). Elemental analysis for $C_{24}H_{36}N_4O_6Ti{\cdot}2H_2O$ (monomer): calcd. C 51.44, H 7.19, N 10.00; found C 51.6, H 7.2, N 9.6.

Synthesis of [Ti(*R*,*R*-4)], *R*,*R*-30

The procedure was similar to that used for the synthesis of *R*,*R*-**28**. Reagents: $Ti^{IV}(O^iPr)_4$ (0.63 g, 2.22 mmol), *R*,*R*-**4** (1.02 g, 2.22 mmol). The compound was obtained as a yellow solid. Yield: 0.22 g, 21%. The NMR characterization of μ-oxo species was not possible due to very complex spectra. IR (cm^{-1}): 3227 ν(N–H), 1246 ν(C-O), 865 ν(Ti–O). Elemental analysis for $C_{22}H_{28}N_2O_5Ti{\cdot}1.5H_2O$ (monomer): calcd. C 55.59, H 6.57, N 5.89; found C 55.8, H 6.7, N 5.7.

Synthesis of [Ti(*R*,*R*-7)], *R*,*R*-31

The procedure was similar to that used for the synthesis of *R*,*R*-**28**. Reagents: $Ti^{IV}(O^iPr)_4$ (0.29 g, 1.00 mmol), *R*,*R*-**7** (0.47 g, 1.00 mmol). The compound was obtained as a yellow solid. Yield: 0.33 g, 68 %. The NMR characterization of μ-oxo species was not possible due to very complex spectra. IR (cm^{-1}): 3216 ν(N–H), 1248 ν(C-O), 887 ν(Ti–O). Elemental analysis for $C_{44}H_{56}N_4O_{10}Ti_2{\cdot}3.5H_2O$ (di-μ-oxo bridged dimer): calcd. C 55.07, H 6.62, N 5.84; found C 55.0, H 6.2, N 5.5.

Synthesis of [Ti(*S*,*S*-10)], *S*,*S*-32

The procedure was similar to that used for the synthesis of *R*,*R*-**28**. The extraction step was made using THF. Reagents: $Ti^{IV}(O^iPr)_4$ (0.11 g, 0.36 mmol), *S*,*S*-**10** (0.20 g, 0.36 mmol). The compound was obtained as an orange-yellow solid. Yield: 0.22g, 13%. The NMR characterization of μ-oxo species was possible despite spectra complexity. ^1H NMR of μ-oxo species (400 MHz, CD_2Cl_2, ppm): δ 3.58, 3.77 [4H, d, $^2J_{HH}$ = 13.5 Hz, Ar-CH_2-NH], 3.83 [6H, s, CH_3O-], 3.89 [2H, s, Ar-C*H*-NH], 6.53 [2H, m, aromatic], 6.69

[2H, m, aromatic], 6.79 [2H, m, aromatic], 7.05 [4H, m, aromatic], 7.21 [6H, m, aromatic]. ^{13}C-{^{1}H} NMR of μ-oxo species (100 MHz, CD_2Cl_2, ppm): δ 49.49 [2C, Ar-*C*H_2-NH], 56.45 [2C, C*H*$_3$O-], 68.25 [2C, Ar-*C*H-NH], 119.38, 121.52, 124.56, 128.02, 128.68, 128.81, 139.77, 146.94, 148.26 [24C, aromatic]. IR (cm^{-1}): 3227 ν(N–H), 1248 ν(C-O), 866 ν(Ti–O). Elemental analysis for $C_{30}H_{30}N_2O_5Ti$·THF (monomer): calcd. C 66.02, H 6.19, N 4.53; found C 66.0, H 6.4, N 4.8.

3.6. References

1 Sharpless, B.; Katsuki, T. *J. Am. Chem. Soc.* **1980,** *102*, 5974-5976.

2 Bermudez, E.; Mangum, J. B.; Asghariam, B.; Wong, B. A.; Reverdy,E. E.; Janszen, D. B.; Hext, P. M.; Warheit, D. B.; Everitt, J. I. *Toxicol. Sci.* **2002**, *70*, 86-97.

3 Lysenko, I. L.; Kim, K.; Lee, H. G.; Cha, J. K. *J. Am. Chem. Soc*. **2008**, *130*, 15997-16002.

4 Ramón, D. J.; Yus, M. *Chem. Rev*. **2006**, *106*, 2126-2208.

5 Bensari, A.; Renaud, J.-L.; Riant, O. *Org. Lett.* **2001**, *3*, 3863-3865.

6 Tanaka, T.; Saito, B.; Katsuki, T. *Tetrahedron Lett*. **2002**, *43*, 3259-3262.

7 Shimada, Y.; Kondo, S.; Ohara, Y.; Matsumoto, K.; Katsuki, T. *Synlett* **2007**, *15*, 2445-2447.

8 Bryliakov, K. P.; Talsi, E. P. *Eur. J. Org. Chem.* **2008**, 3369-3376.

9 Fennie, M. W.; DiMauro, E. F.; O'Brien, E. M.; Annamalai, V.; Kozlowski, M. C. *Tetrahedron* **2005**, *61*, 6249-6265.

10 Belokon, Y. N.; Caveda-Cepas, S.; Green, B.; Ikonnikov, N. S.; Khrustalev, V. N.; Larichev, V. S.; Moscalenko, M. A.; North, M.; Orizu, C.; Tararov, V. I.; Tasinazzo, M.; Timofeeva, G. I.; Yashkina, L. V. *J. Am. Chem. Soc.* **1999**, *121,* 3968-3973.

11 Cohen, A.; Kopilov, J.; Lamberti, M.; Venditto, V.; Kol, M. *Macromolecules* **2010**, *43*, 1689-1691.

12 Segal, S.; Goldberg, I.; Kol, M. *Organometallics* **2005,** *24,* 200-202.

13 Balsells, J.; Carroll, P. J.; Walsh, P. J. *Inorg. Chem.* **2001**, *40*, 5568-5574.

14 Gendler, S.; Segal, S.; Goldberg, I.; Goldschmidt, Z.; Kol, M. *Inorg. Chem*. **2006**, *45*, 4783-4790.

15 Maezaki, N.; Sakamoto, A.; Nagahashi, N.; Soejima, M.; Li, Y.; Imamura, T.; Kojima, N.; Ohishi, H.; Sakaguchi, K.; Iwata, C.; Tanaka, T. *J. Org. Chem.* **2000,** *65,* 3284-3291.

16 Wagner, G.; Haukka, M. *Chem. Soc*., *Dalton Trans*. **2001**, 2690-2697.

17 Chen, J.; Chen, J.; Lang, F.; Zhang, X.; Cun, L.; Zhu, J.; Deng, J.; Liao, J. *J. Am. Chem. Soc***. 2010**, *132*, 4552-4553.

18 Fernández, I.; Valdivia, V.; Leal, M. P.; Khiar, N. *Org. Lett*. **2007**, *9*, 2215-2218.

19 Wojaczynska, E.; Wojaczynski, J. *Chem. Rev.* **2010,** *110,* 4303-4356.

20 Yeori, A.; Gendler, S.; Groysman, S.; Goldberg, I.; Kol, M. *Inorg. Chem. Comm*. **2004**, *7*, 280-282.

21 Matsumoto, K.; Saito, B.; Katsuki, T. *Chem. Commun*. **2007**, 3619-3627.

22 Kim , S. H.; Lee, J.; Kim, D. J.; Moona, J. H.; Yoon, S.; Oh, H. J.; Do, Y.; Ko, Y. S.; Yim, J.; Kim, Y. *J. Organomet. Chem*. **2009**, *694*, 3409-3417.

23 Adão, P.; Avecilla, F.; Bonchio, M.; Carraro, M., Costa Pessoa, J.; Correia, I. *Eur. J. Inorg. Chem.* **2010**, 5568-5578.

24 Yeori, A.; Groysman, S.; Goldberg, I.; Kol, M. *Inorg. Chem*. **2005**, *44*, 4466-4468.

25 Sergeeva, E.; Kopilov, J.; Goldberg, I.; Kol, M. *Chem. Commun*. **2009**, 3053-3055.

26 Groysman, S.; Sergeeva, E.; Goldberg, I.; Kol, M. *Eur. J. Inorg.Chem.* **2005**, 2480-2485.

27 Peri, D.; Meker, S.; Manna, C. M.; Tshuva, E. Y. *Inorg. Chem*. **2011**, *50*, 1030-1038.

28 Piszczek, P.; Richert, M.; Grodzicki, A.; Głowiak, T.; Wojtczak, A. *Polyhedron* **2005**, *24*, 663-670.

29 Nakajima, K.; Kojima, K.; Kojima, M.; Fujita, *J. Bull. Chem. Soc. Jpn*. **1990**, *63*, 2620-2630.

30 Sasaki, C.; Nakajima, K.; Kojima, M.; Fujita, J. *Bull. Chem. Jpn*. **1991**, *64*, 1318-1324.

31 Adão, P.; Costa Pessoa, J.; Henriques, R. T.; Kuznetsov, M. L.; Avecilla, F.; Maurya, M. R.; Kumar, U.; Correia, I. *Inorg. Chem*. **2009,** *48***,** 3542-3561.

32 Sheldrick, G. M. *SHELXS-97*, revision 5.1; University of Göttingen: Göttingen, Germany, 1997.

33 (a) Flack, H. D.; Bernardinelli, G. *Acta Crystallogr., A,* **1999**, *A55*, 908-915. (b) Flack, H. D.; Bernardinelli, G. *J. Appl. Crystallogr.* **2000**,*33*, 1143-1148.

Chapter 4

Vanadium(IV) Salan Complexes

4. Vanadium(IV) Salan Complexes

4.1. Introduction

The interest in enantioselective catalytic processes mediated by vanadium had its inception with the chiral hydroxamic acid/$V^{IV}O(acac)_2$ system for the enantioselective epoxidation of allylic alcohols devised by Sharpless and co-workers in 1977.[1,2] This interest is partly due to the number of properties vanadium shares with its Group 4 neighbor, titanium: it is a relatively abundant, oxophilic element with a rich chemistry, dominated by the higher oxidations states. High valent vanadium is present in biological systems, and notable vanadium-based catalysts of biological origin are the vanadium-dependent bromoperoxidases, found in brown seaweeds such as *Ascophyllum nodosum*.[3] These enzymes, bearing a V^V cofactor, are capable of promoting asymmetric sulfoxidation of thioethers in aqueous medium with moderate yields, but with enantiomeric excesses surpassing 80%.

A number of properties of vanadium make its compounds particularly interesting over titanium, namely its +4 oxidation state chemistry being dominated by the remarkably stable, paramagnetic d^1 diatomic oxocation VO^{2+}. Additionally, ^{51}V is the major isotope (>99% in abundance) with a nuclear spin of 7/2. This opens many possibilities for the characterization and uses of either paramagnetic V^{IV} compounds or diamagnetic V^V compounds. Beside their effectiveness in oxidation reactions, high valent vanadium compounds are also capable of mediating a wide scope of enantioselective catalytic processes (see Figure 4.1).[1,4,5,9]

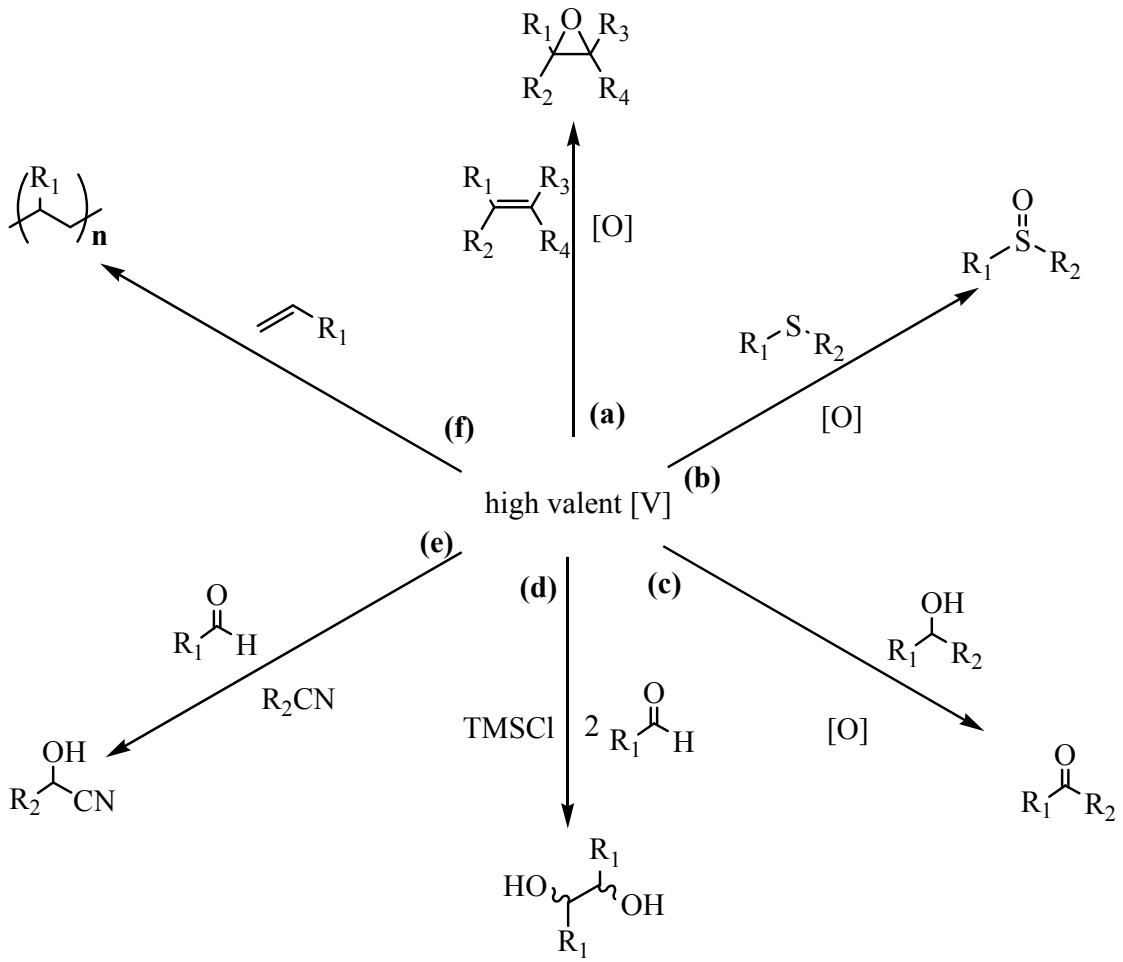

Figure 4.1. Catalytic processes that are mediated by high valent vanadium complexes: olefin (a) and thioether oxidations (b), alcohol oxidations (c), pinacol couplings (d), aldehyde cyanations (e) and olefin polymerizations (f).

Vanadium, being an early transition metal, has an affinity for "hard" N- and O-donor atoms, though it is not as oxophilic as titanium. As a consequence, ligand support development has been focused mainly on ligands containing N- and O-donor atoms. High valent vanadium aminophenol compounds, namely the salen- and salan-type, have been employed successfully as catalysts in an array of asymmetric reactions.

Notable examples include the chiral $V^{IV}O$(salen) complexes reported by Fujita and co-workers and their successful use as catalysts in asymmetric sulfoxidation, using cumene hydroperoxide (CHP) as terminal oxidant (Scheme 4.1).[6]

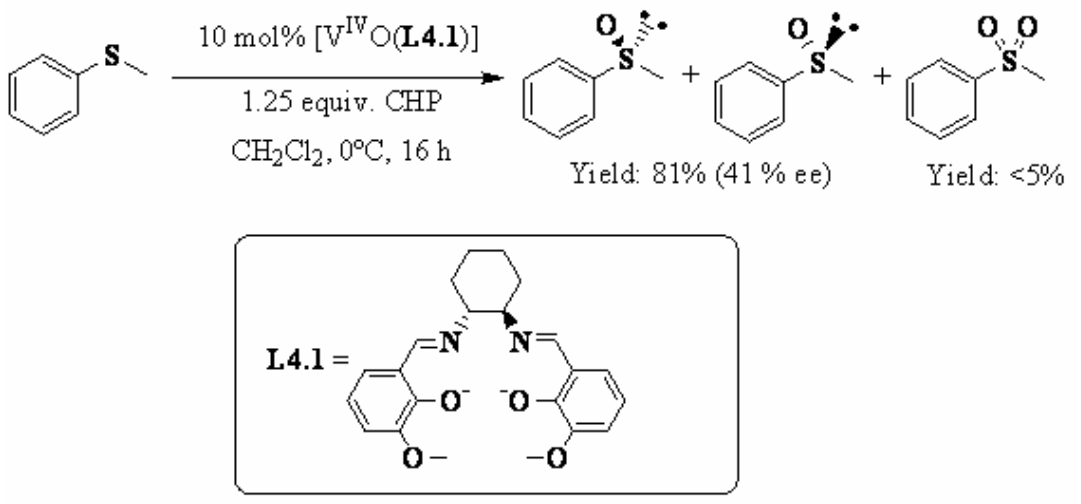

Scheme 4.1. $V^{IV}O$(salen)-promoted asymmetric sulfoxidation.

Already in 2000, Bekolon and co-workers[7] reported an efficient $V^{IV}O$(salen) system for asymmetric cyanation of aldehydes, surpassing the titanium analogs in terms of enantioselectivity. Catalyst loadings as low as 0.1 mol-% could effectively produce complete conversions of the employed aromatic aldehyde with enantiomeric excesses as high as 94% (Scheme 4.2).

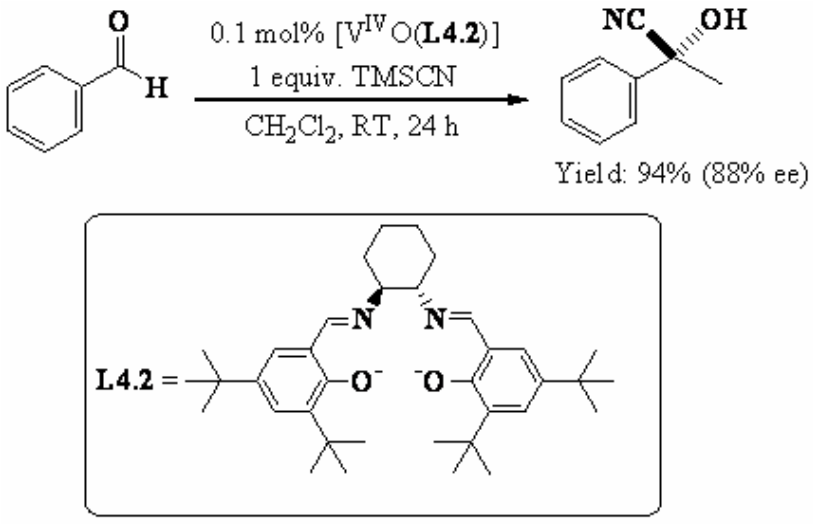

Scheme 4.2. $V^{IV}O$(salen)-promoted asymmetric cyanation of aldehydes.

In 2004, Katsuki and co-workers[8] used a $V^{V}O$(salen) catalyst based on their signature ligand for Meerwein–Ponndorf–Verley cyanation of aldehydes also obtaining high yields and enantiomeric excesses (Scheme 4.3).

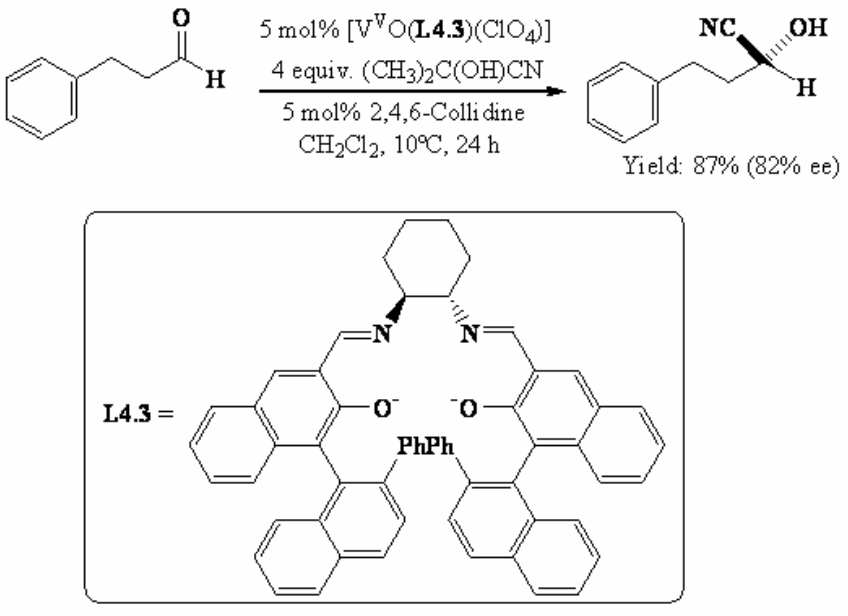

Scheme 4.3. $V^{IV}O$(salen)-promoted asymmetric cyanation of aldehydes.

Zhu and co-workers[9] reported an *in situ* $V^{IV}O$(salan) system for the asymmetric sulfoxidation, using hydrogen peroxide as terminal oxidant. High yields coupled with enantiomeric excesses over 90% were obtained with this system (Scheme 4.4).

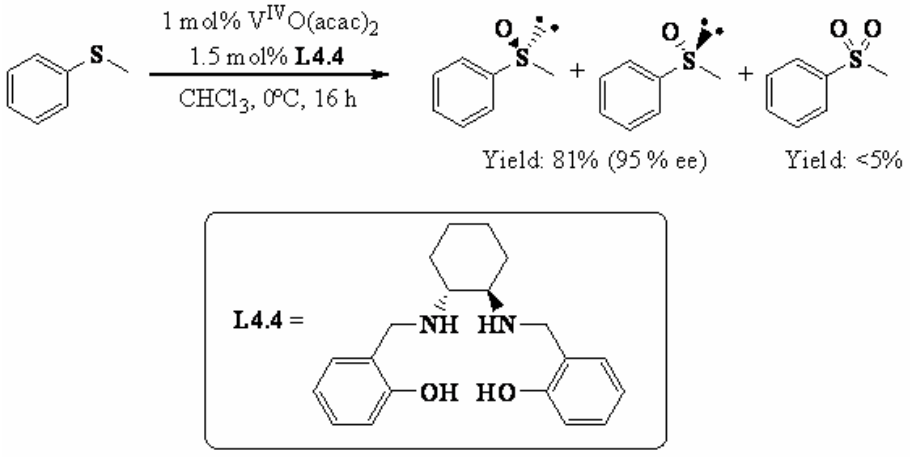

Scheme 4.4. $V^{IV}O$(salan)-promoted asymmetric sulfoxidation.

More recently, Sun and co-workers[10] used *in situ* $V^{IV}O$(salen) and $V^{IV}O$(salan) catalysts for asymmetric pinacol coupling of aromatic aldehydes. In addition to the high yields and enantioselectivities, the authors reported low formation of the achiral *meso* product (Scheme 4.5).

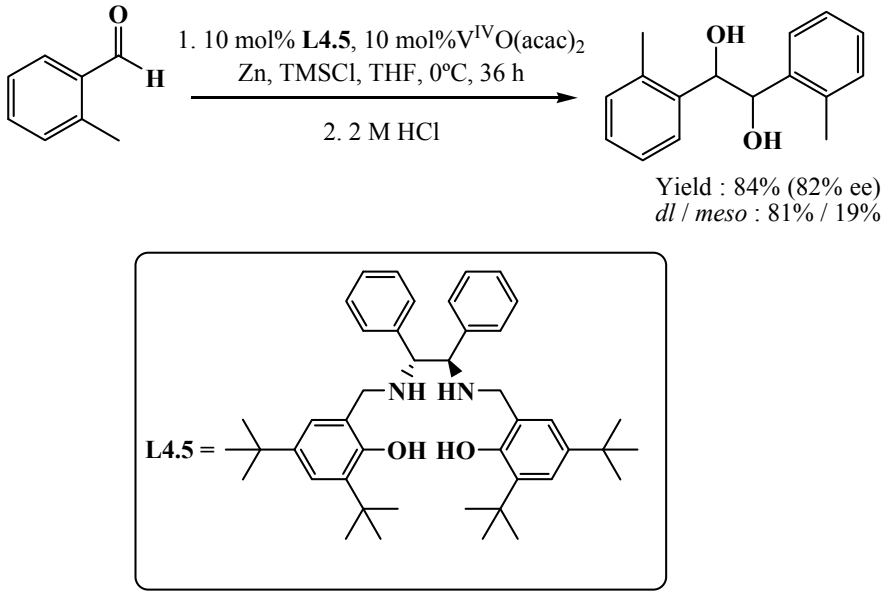

Scheme 4.5. $V^{IV}O$(salan)-promoted asymmetric pinacol coupling.

The scope of work involving V-(salen) compounds is more limited compared to work involving the titanium analogues. In-depth reports involving V-(salan) compounds are very scarce.[7,11,12,13] This is surprising considering that the salen- and salan-type compounds are specially suited as ligands in early transition metal complexes and are, for instance, responsible for the success of the titanium-based systems. This scarceness involving vanadium salen and salan compounds may possibly be due to vanadium's rich and often complicated chemistry of its higher oxidation states.

This Chapter describes a in-depth study of $V^{IV}O$ and $V^{V}O$(salan) compounds, their behavior in asymmetric sulfoxidation of thioethers and in the oxidation of cyclohexene, styrene and cumene.

4.2. Chiral $V^{IV}O$(salan) compound preparation: results and discussion

Vanadium presents a series of advantages over titanium concerning the preparation of the respective salen and salan compounds. Readily available and stable $V^{IV}O$ sources such as $V^{IV}OCl_2$, $V^{IV}OSO_4$ and $V^{IV}O(acac)_2$ can be used and stored almost indefinitely without degradation. The preparation methods described in this Chapter relied exclusively on commercial aqueous $V^{IV}OCl_2$ solutions (50% by weight) which are air-stable. $V^{IV}O$(salen) and $V^{IV}O$(salan) compounds can be prepared by reacting the vanadium precursor with the appropriate ligand precursor in aqueous or alcoholic medium, under an inert atmosphere. The desired complex precipitates from the reaction mixture after the medium pH is adjusted to *ca*. 7-8 with *e.g*. aqueous potassium hydroxide. The solid compounds are reasonably air-stable and can be handled similarly to the μ-oxo Ti^{IV} analogues. The structural formulas of the prepared $V^{IV}O$(salen) and $V^{IV}O$(salan) compounds *R*,*R*-**33**, *S*,*S*-**34**, *S*,*S*-**35**, *S*,*S*-**36**, *R*,*R*-**37**, *R*,*R*-**38**, *S*,*S*-**39**, *S*,*S*-**40**, *S*,*S*-**41**, *S*,*S*-**42**, *S*,*S*-**43**, *R*,*R*-**44**, *R*,*R*-**45** and *R*,*R*-**46** are presented in Figures 4.2a to 4.2d.

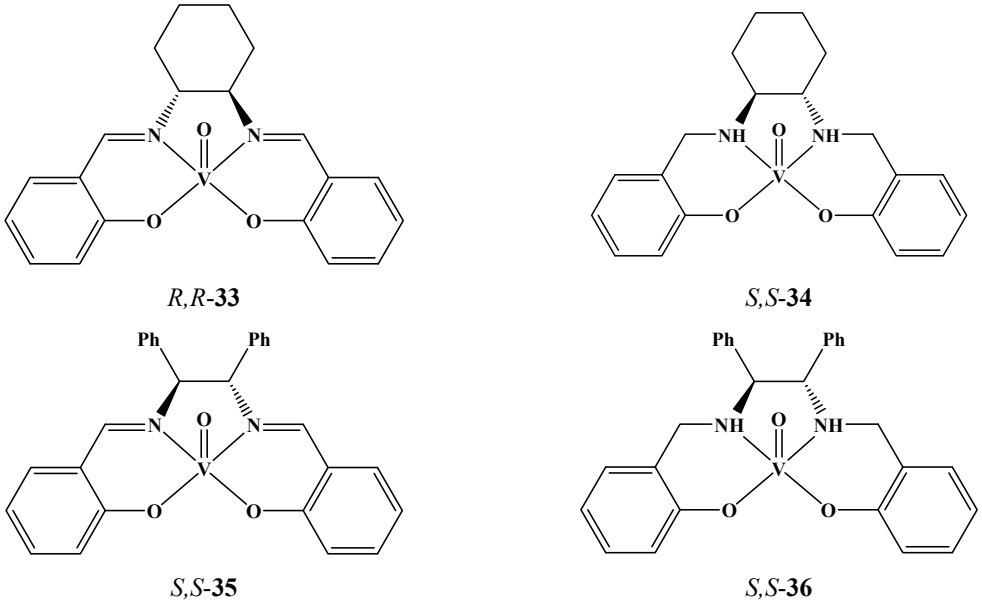

R,*R*-**33** *S*,*S*-**34**

S,*S*-**35** *S*,*S*-**36**

Figure 4.2a. Structural formulas of the prepared $V^{IV}O$(salen) and $V^{IV}O$(salan) compounds depicting the respective configuration at their stereogenic centers. The N_{amine} atoms of the $V^{IV}O$(salan) compounds also become stereogenic centers upon coordination to the metal ion.

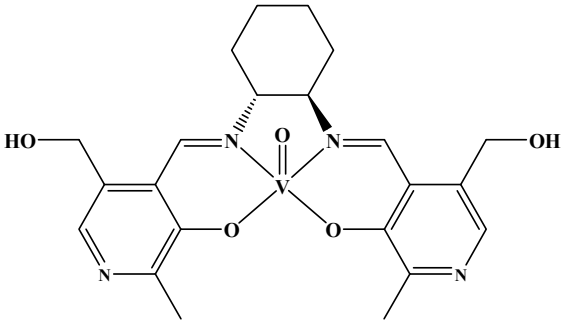

R,R-**37**

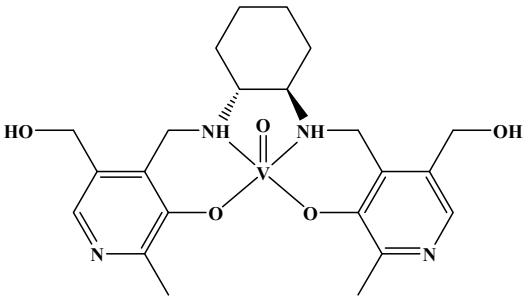

R,R-**38**

Figure 4.2b. Structural formulas of the prepared $V^{IV}O$(salen) and $V^{IV}O$(salan) compounds depicting the respective configuration at their stereogenic centers. The N_{amine} atoms of the $V^{IV}O$(salan) compounds also become stereogenic centers upon coordination to the metal ion.

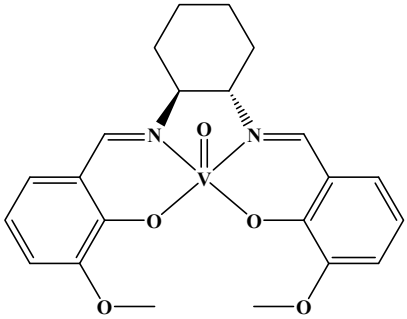

S,S-**39**

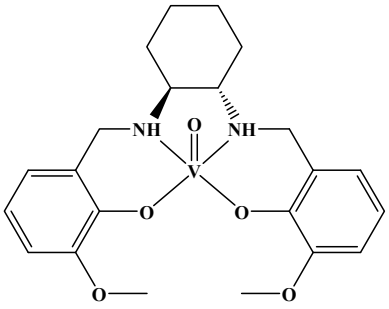

S,S-**40**

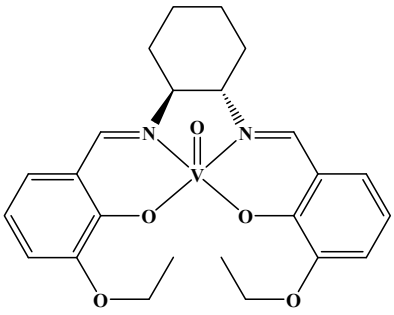

S,S-**41**

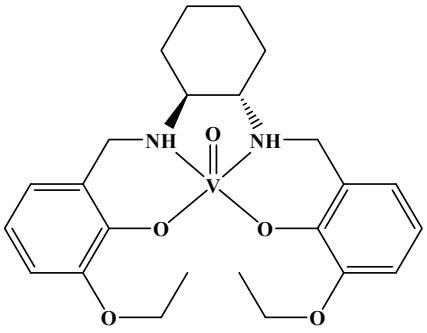

S,S-**42**

Figure 4.2c. Structural formulas of the prepared $V^{IV}O$(salen) and $V^{IV}O$(salan) compounds depicting the respective configuration at their stereogenic centers. The N_{amine} atoms of the $V^{IV}O$(salan) compounds also become stereogenic centers upon coordination to the metal ion.

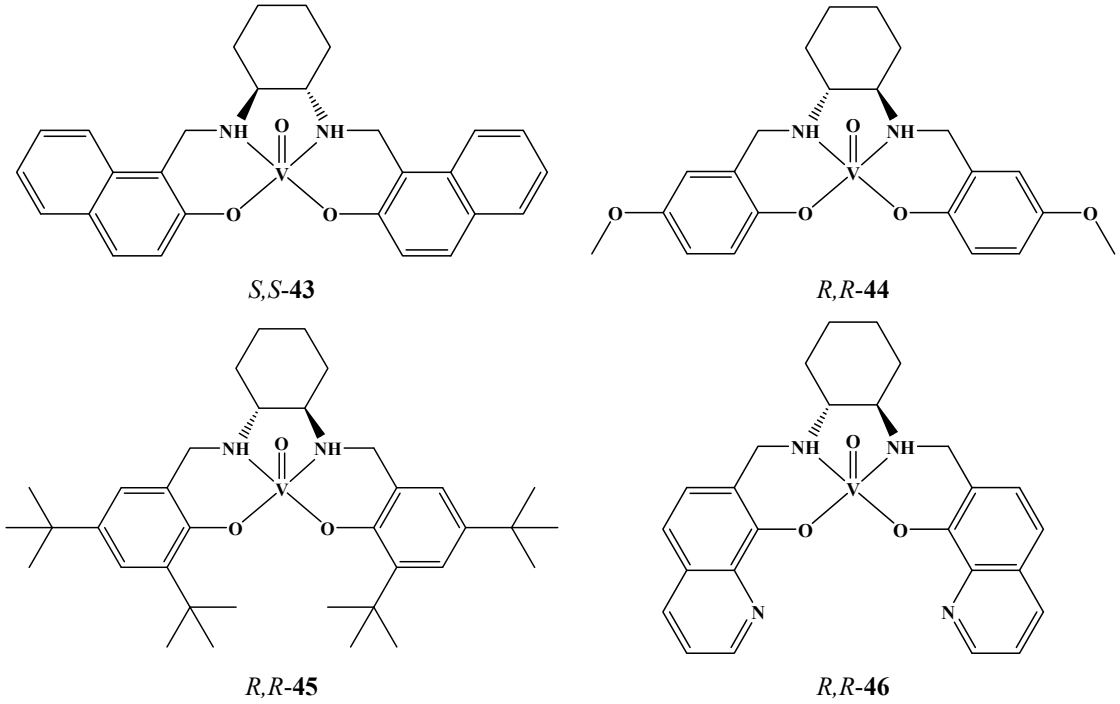

Figure 4.2d. Structural formulas of the prepared $V^{IV}O$(salen) and $V^{IV}O$(salan) compounds depicting the respective configuration at their stereogenic centers. The N_{amine} atoms of the $V^{IV}O$(salan) compounds also become stereogenic centers upon coordination to the metal ion.

All $V^{IV}O$(salen) and $V^{IV}O$(salan) compounds were obtained as either monomeric green solids or polymeric brown solids. The V^{V} compounds (*S,S*-**34a**, *S,S*-**36a**, *S,S*-**40a**, *S,S*-**42a**, *S,S*-**43a** and *R,R*-**45a**) were obtained by slow oxidation of solutions prepared from the respective $V^{IV}O$ compounds. The $V^{IV}O$(salen) compounds are included for comparative purposes. Crystal structures obtained for four V^{V} compounds (*R,R*-**33b**, *S,S*-**39b**, *S,S*-**36b** and *R,R*-**45b**) obtained in this way confirmed the formation of dimeric μ-oxo $[(V^{V}O\{L\})_2(\mu\text{-}O)]$ species (L =salen, salan; see Figure 4.3).

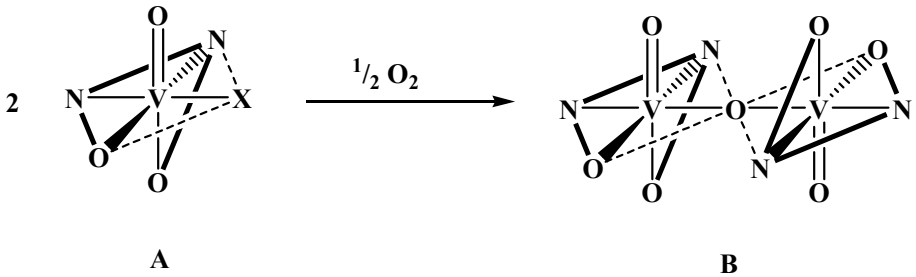

Figure 4.3. Oxidation of a $V^{IV}O$(salan) compound to a $[V^{V}O(salan)]_2O$ dimer in solution. The letter X denotes a solvent molecule.

^{1}H and ^{51}V NMR characterization of the prepared $V^{IV}O$ compounds is not viable due to the paramagnetic nature of the d^{1} $V^{IV}O$ species. ^{51}V NMR characterization was carried out with previously oxidized $V^{IV}O$(salan) compounds. Electron Paramagnetic Resonance (EPR) was used extensively and effectively to probe the coordination sphere of the paramagnetic metal centre. Results obtained using EPR will be discussed in a separate section. Characterization was complemented with elemental analysis, circular dichroism spectroscopy (CD), UV-Vis and IR spectroscopy and mass spectrometry when possible. Discussion of the characterization results will be separated in sections, given that the spectroscopic properties of $V^{IV}O$ and V^{V} compounds allow a more in-depth analysis.

4.2.1. Characterization by ^{51}V NMR spectroscopy

^{51}V NMR spectra of the V^{V}-(salan) compounds were measured from the respective methanol, acetonitrile, dichloromethane and 1,2-dichloroethane solutions, and the relevant parameters are listed in Table 4.1.

A strong solvent effect is observed in all cases. For instance, compound *S,S*-**34a** yields a major signal at -488 ppm and a minor peak at -546 ppm when dissolved in methanol while in aprotic solvents all major signals are shifted upfield at around -540 ppm. The same is observed for the previously isolated V^{V} compounds *S,S*-**34a**, *S,S*-**36a** and *R,R*-**45a**. The signals at -488, -501 and -499 ppm observed for these cases are assigned to a alkoxy species [$V^{V}O${salan}(CH_3O)], containing a $V^{V}O^{3+}$ core. These chemical shift values are comparable to those reported for structurally related vanadium alkoxy species.[14,15] The alkoxy species may also present isomers, depending on the binding site of the alkoxy group. The presence of such alkoxy species is admitted in light of what was observed for the Ti^{IV} analogues: formation of μ-oxo species with μ-oxo bridges labile towards protic organic solvents such as alcohols. Figures 4.4, 4.5 and 4.6 show the ^{51}V NMR spectra of oxidized *S,S*-**34**, *S,S*-**36** and *R,R*-**45** in methanol. It should be noted that spectra shown in Figures 4.6 and 4.7 were obtained from the dissolution of the crystalline μ-oxo [$V^{V}O${salan}$_2$(μ-O)] dimeric compounds in methanol.

Table 4.1. ^{51}V NMR parameters for the oxidized solutions of the $V^{IV/V}O$(salan) compounds.

^{51}V NMR			
Compound	**Solvent**	**Time[a] (h)**	**δ (ppm)**
S,S-**34a**	CH_3OH	24	-488 (>95 %), -543
	CH_2Cl_2	4	-540
	DCE	24	-548
	DMSO	4	-551
	CH_3CN	3	-536 (5 %), -551 (90 %), -565 (5 %)
S,S-**36a**	CH_2Cl_2	4	-549
	DMSO	4	-537
S,S-**40a**	DCE	120	-442, -450, -479, -484, -527, -549
S,S-**42a**	DCE	120	-493, -530, -550, -625, -642
S,S-**43a**	DCE	120	-473, -538, -639
R,R-**45a**	DCE	1	-472, -506, -528, -546, -669
	DCE	120	-549
S,S-**34a**[b]	CH_3OH		-487
	CH_2Cl_2		-546
	CH_3CN		-537 (5 %), -551 (90 %), -565 (5 %)
S,S-**36a**[c]	CD_3OD		-501, -549
	CD_2Cl_2		-557
R,R-**45a**[c]	CD_3OD		-499, -555
	CD_2Cl_2		-550

[a]Time necessary for complete oxidation to V^V in solution. [b]Compound previously oxidized in solution. [c]Samples prepared from crystalline μ-oxo species.

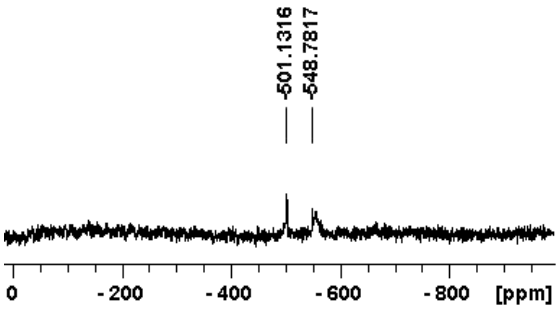

Figure 4.4. ^{51}V NMR of *S,S*-**36a** in methanol. The major peak at -501 ppm is assigned to a methoxy species [V^VO{salan}(CH_3O)]. The upfield peak at -548 ppm may be due to an isomeric V^VO{salan}(CH_3O)] species.

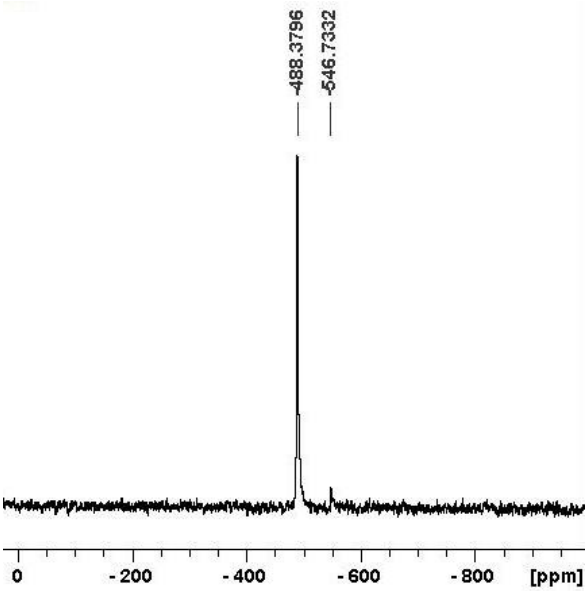

Figure 4.5. ^{51}V NMR of *S,S*-**34a** in methanol. The major peak at -488 ppm is assigned to a methoxy species [$V^{V}O${salan}(CH_3O)]. The minor peak may be due to an isomeric [$V^{V}O${salan}(CH_3O)] species.

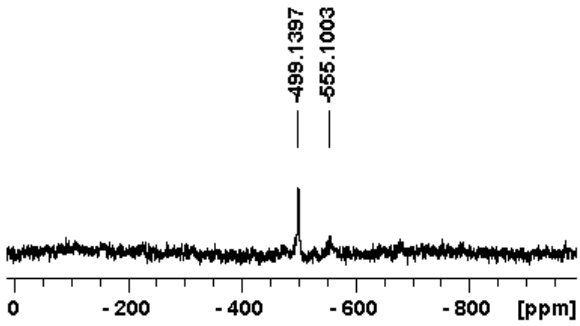

Figure 4.6. ^{51}V NMR of *R,R*-**45a** in methanol. The major peak at -499 ppm is assigned to a methoxy species [$V^{V}O${salan}(CH_3O)]. The upfield minor peak at -555 ppm may be due to an isomeric [$V^{V}O${salan}(CH_3O)] species.

The isomeric forms of the [$V^{V}O${salan}(CH_3O)] species can be distinguished in the case of oxidized *S,S*-**36a** and *R,R*-**45a**, with a $\Delta\delta$ of *ca*. 50 ppm. Considering that salan-type complexes favour *fac-fac* (*cis*-α) and *fac-mer* (*cis*-β) geometries, the possible isomeric forms for *S,S*-**36a** and *R,R*-**45a** are presented in Figure 4.7.

When *S,S*-**34**, *S,S*-**36** and *R,R*-**45** are dissolved and oxidized in aprotic solvents, single upfield signals at *ca.* -540 ppm are observed. These can either be attributed to dimeric μ-oxo [($V^{V}O${salan}$)_2(\mu$-O)] species[16,17] with a μ-oxo bridged $V^{V}_2O_3^{4+}$ core or a

monomeric [$V^{V}O_2${Hsalan}] species containing a $V^{V}O_2^{+}$ core, as ^{51}V NMR does not provide unambiguous information in this respect.[18]

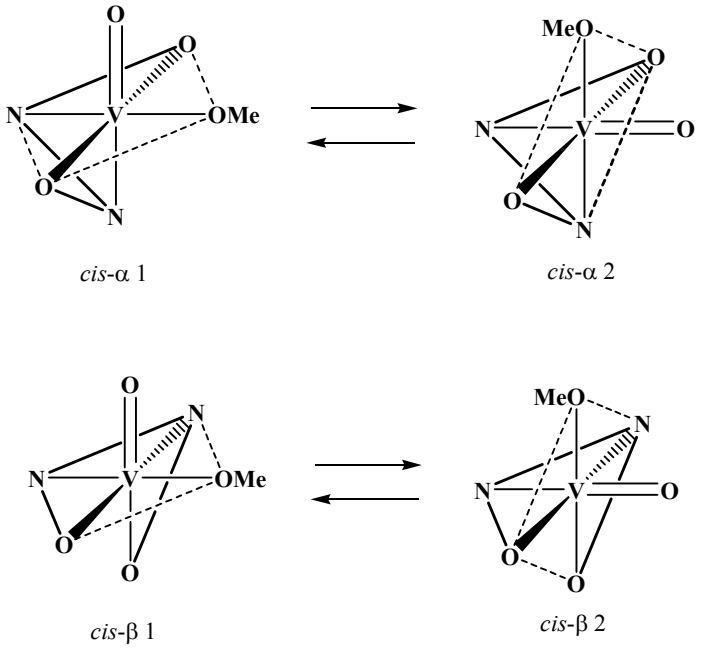

Figure 4.7. Possible geometric isomers of monomeric methoxy species of *S,S*-**34a**, *S,S*-**36a** and *R,R*-**45a** in methanolic solution.

The monomeric [$V^{V}O_2${Hsalan}] species are hydrolytic products obtained when the ligand support is incapable of stabilizing the $V^{V}O^{3+}$ core.[16] Differentiation of both species is only possible after complementary analysis of electronic absorption spectra. Figure 4.8 shows the possible pathways for the formation of the aforementioned V^{V} species in the presence of methanol and water.

The ^{51}V-NMR spectra obtained for *S,S*-**34a** in acetonitrile (see Figure 4.9) are noteworthy due to the exhibited "triplet-like" patterns. Precautions were taken to confirm that the minor peaks were not rotation bands. The major peak at -551 ppm, similarly to what is observed in dichloromethane solution, may correspond to a dimeric μ-oxo [($V^{V}O${salan}$)_2(\mu$-O)] species. The two smaller signals may correspond to geometric isomers of the dimeric μ-oxo species.

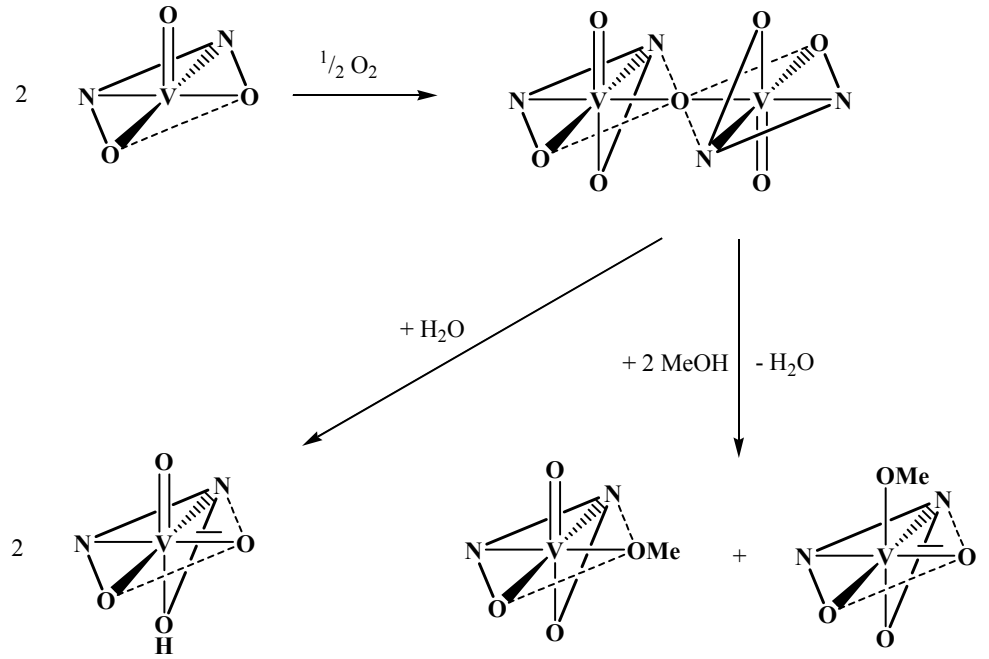

Figure 4.8. Conversion of a $V^{IV}O$(salan) compound into its dimeric μ-oxo form. The dimeric form can be subsequently converted into a monomeric alkoxy form in the presence of an alcohol or a monomeric $V^{V}O_2^{+}$ in the presence of water if hydrolytic stability is low.

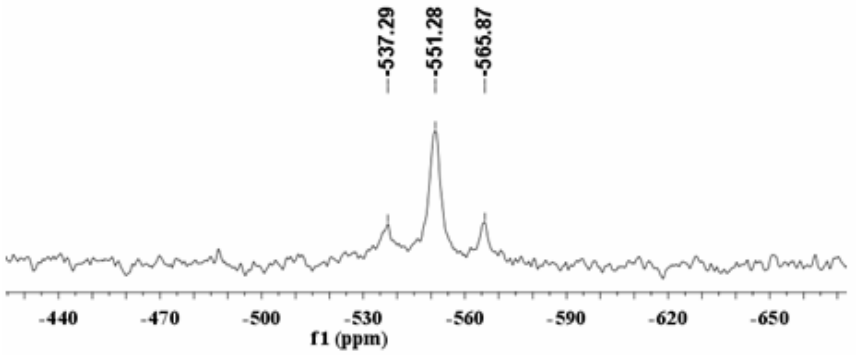

Figure 4.9. ^{51}V NMR spectrum of *S,S*-**34a** in acetonitrile. The major peak at -551 ppm is assigned to a dimeric μ-oxo [($V^{V}O${salan}$)_2(\mu$-O)] species. The minor peaks may be due to geometric isomers.

The difference in chemical shift observed for the alkoxy species and the μ-oxo species can be explained in terms of the shielding experienced by the V^{V} centre. Thus it follows that highly electronegative "hard" donors (O, N, F) shift ^{51}V chemical shifts upfield, to more negative values, as a result of increased shielding at the V^{V} centre. The greater the polarizability of the donor atoms, the greater is the shift downfield towards positive chemical shift values. Reported instances of this trend include the chemical shifts

of $V^{V}OF_3$ (-700 ppm), $V^{V}O(OCH_3)_3$ (-598 ppm), $V^{V}OCl_3$ (0 ppm) and $V^{V}OBr_3$ (+ 432 ppm).[19,20] For monomeric $V^{V}O$ compounds with a (N_{amine}, N_{amine}, $O_{phenolate}$, $O_{phenolate}$) donor set a similar shift is observed when a Cl ligand is replaced with an alkoxy ligand, causing an upfield shift from -257 to -418 and -504 ppm, with a $\Delta\delta$ of 161 and 247 ppm, respectively.[13] The chemical shifts of ^{51}V are primarily governed by the paramagnetic deshielding parameter σ_{para} which correlates inversely to the HOMO-LUMO ΔE gap. Non-polarizable electronegative ligands cause a stabilization of the HOMO, increasing ΔE. The result is a decrease of σ_{para} and an increase of the global shielding parameter σ.

$$\sigma = \sigma_{dia} + \sigma_{para} \qquad (4.1)$$

Ligand bulk also has a similar but much less pronounced effect in the observed chemical shifts. Bulkier ligands may cause upfield shifts. This may explain the approximate 50 ppm difference between the monomeric [$V^{V}O${salan}(CH_3O)] and dimeric [$(V^{V}O\{salan\})_2(\mu$-O)] species observed in methanol and dichloromethane solutions.

The remaining compounds *S,S*-**40**, *S,S*-**42** and *S,S*-**43** required lengthy periods for oxidation in solution. Even after 5 days of exposure to air, the obtained ^{51}V NMR spectra for these compounds revealed multiple species. The distorted signals and baseline may be a consequence of vestigial amounts of paramagnetic species. Pyridoxal-based compounds proved far too insoluble to be properly characterized by ^{51}V NMR. Figures 4.10, 4.11 and 4.12 show the ^{51}V NMR spectra of compounds *S,S*-**40a**, *S,S*-**42a** and *S,S*-**43a** in 1,2-dichloroethane.

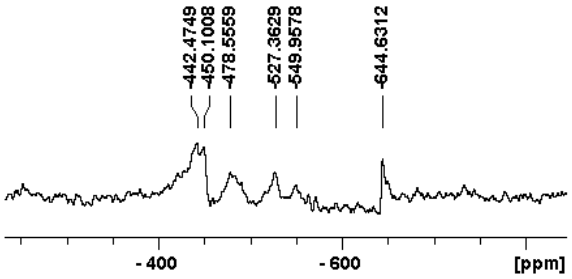

Figure 4.10. ^{51}V NMR spectrum of *S,S*-**40a** in 1,2-dichloroethane after 5 days. The multiple peaks and baseline distortion are indicative of compound stability towards oxidation of the $V^{IV}O$ center.

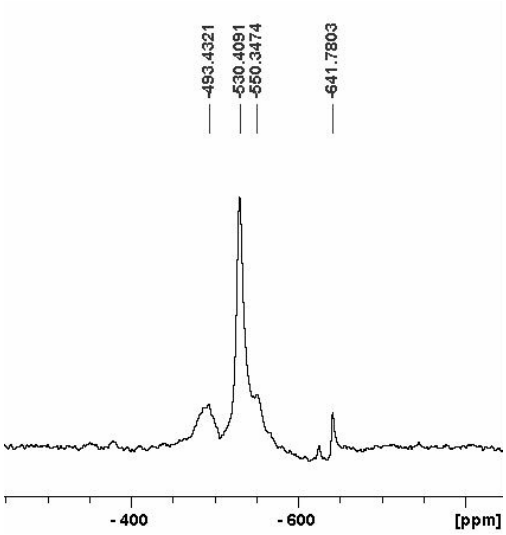

Figure 4.11. ^{51}V NMR spectrum of *S,S*-**42a** in 1,2-dichloroethane after 5 days.

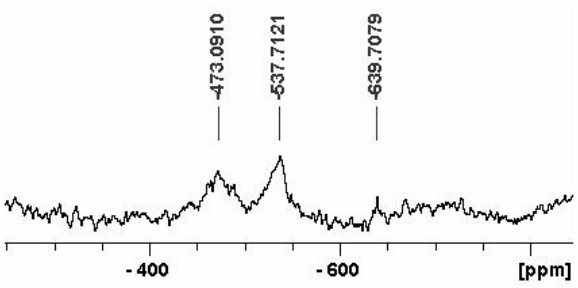

Figure 4.12. ^{51}V NMR spectrum of *S,S*-**43a** in 1,2-dichloroethane after 5 days.

The signals at around -450 ppm may correspond to monomeric [$V^{V}O${salan}(OH)] species, considering that the oxidations were not made in moisture-free conditions. The signals around -530 ppm may be due to dimeric [($V^{V}O${salan})$_2$(μ-O)] species or monomeric [$V^{V}O_2${Hsalan}] species. The minor signals observed at *ca*. -640 may be indicative of peroxy species generated from reaction with molecular oxygen.

Experimental data concerning peroxy species will be accessed along with the reactivity studies of the prepared $V^{IV}O$(salan) compound in thioether sulfoxidation and alkene oxidation reactions.

4.2.2. Characterization by CD and UV-Vis spectroscopy

Circular dichroism spectroscopy was used to confirm if the prepared $V^{IV}O$ and V^{V} compounds exhibited chirality in solution. Detection of chirality associated with the electronic *d-d* transitions proved difficult. The $V^{IV}O$ core typically adopts square-pyramidal geometries and, less commonly, octahedral geometries. Square-pyramidal $V^{IV}O$ may exhibit three *d-d* transitions (see Figure 4.13). For simplicity the model proposed by Ballhausen and Gray may be assumed:[53] two transitions at ca. 800-600 nm (band **I**, d_{xy}-d_{yz}) and 600-520 nm (band **II**, d_{xy}-d_{x2-y2}). The third transition (band **III**, d_{xy}-d_{z2}) falls in the UV region and is often masked by intense charge transfer bands.

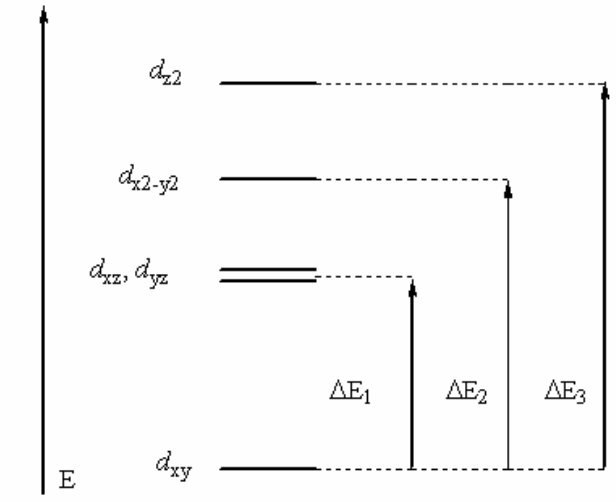

Figure 4.13. Energy levels and possible electronic transitions for square-pyramidal $V^{IV}O$ species.

The detection of chirality associated with the *d-d* transitions would effectively confirm chiral transmission to the metal centre of $V^{IV}O$(salan) compounds, but band **I** and band **II** are usually weak. Also, most of the analyzed $V^{IV}O$(salan) compounds showed a tendency to rapidly oxidize in solution. The resulting V^{V} species often yielded charge transfer bands so intense and broad that the signals from the parent $V^{IV}O$ species were completely masked. Nevertheless, the CD and UV-Vis spectra of the representative $V^{IV}O$(salan) complexes *S,S*-**34** and *S,S*-**36** were recorded and compared with the spectra of the parent $V^{IV}O$(salen) compounds *R,R*-**33** and *S,S*-**35** (see Figures 4.14 and 4.15). The

relevant absorption maximum wavelengths (λ_{max}), molar absorptivity (ε) and molar circular dichroism ($\Delta\varepsilon$) values are listed in Table 4.2.

There are considerable differences between the CD spectra given by the salen and salan compounds. Both $V^{IV}O$(salen) compounds *R,R*-**33** and *S,S*-**35** exhibit intense CD signals in the swept wavelength range. The CD signals visible at *ca*. 580 nm and 470 nm may be associated with the C=N double bond n-π^* band and the $O_{phenolate}$-V_d transitions. The remaining signals are due to aromatic π-π* and charge transfer transitions. Despite having opposite configurations, both compounds yield similar spectra. The spectra of the $V^{IV}O$(salan) compounds *S,S*-**34** and *S,S*-**36** are comparatively much less intense. In fact, *S,S*-**36** failed to yield a spectrum with intensity comparable to the salen compounds even with a ten-fold concentration and the presence of minute amounts of ascorbic acid. The observed CD signals for *S,S*-**34** and *S,S*-**36** fall in the UV region, though it is possible to discern a *d-d* band **II** at *ca*. 550 nm. The UV-Vis spectra of *R,R*-**33** and *S,S*-**35** share similarities, namely in the energy of the *d-d* band **II** at 584 nm, with ε = 152 M^{-1} cm^{-1} for both cases, and the C=N double bond n-π^* transition at *ca*. 410-420 nm. The *d-d* band **I** signals are not easily distinguishable in both cases**.** The spectrum of *S,S*-**34** shows indication of partial oxidation with a comparatively intense band at 524 nm (ε = 512 M^{-1} cm^{-1}). The *d-d* band **I** is also not easily discernible. Conversely, the *d-d* band **I** is visible at 780 nm (ε = 45 M^{-1} cm^{-1}) in the spectrum of *S,S*-**36** along with the *d-d* band **II** at 552 nm (ε = 120 M^{-1} cm^{-1}). Both *S,S*-**34** and *S,S*-**36** lack the C=N double bond n-π^* transition dominant in salen compounds.

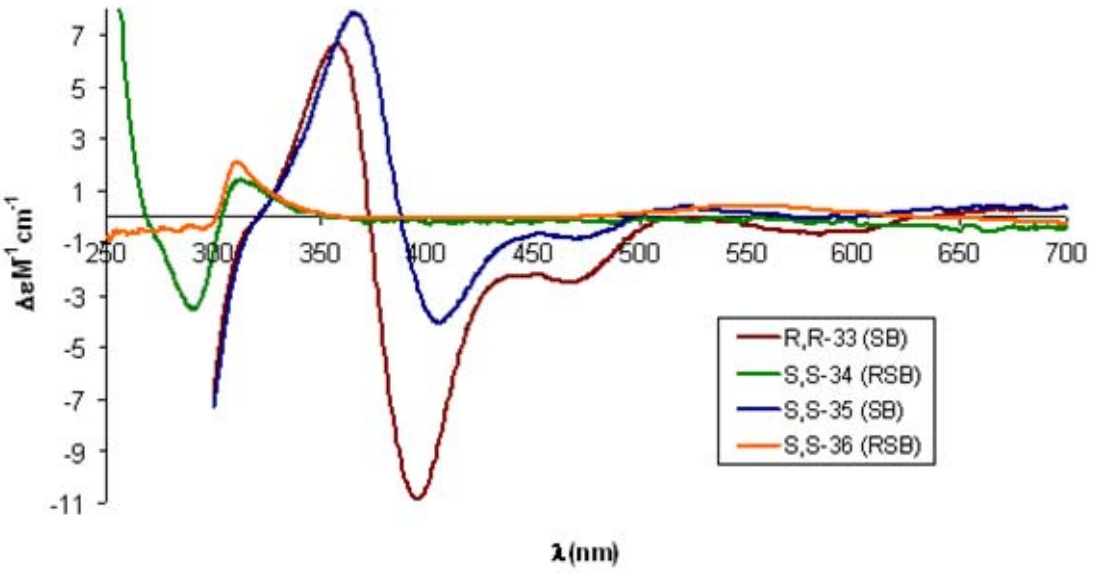

Figure 4.14. CD spectra of *R,R*-**33** (CH_2Cl_2), *S,S*-**35** (CH_2Cl_2), *S,S*-**34** (DMSO) and *S,S*-**36** (DMSO). The spectra were recorded with 0.46 mM (*R,R*-**33**), 0.45 mM (*S,S*-**34**), 0.5 mM (*S,S*-**35**) and 4.2 mM (*S,S*-**36**) solutions and a 1 mm optical path cell. The solution of *S,S*-**36** required the presence of ascorbic acid to delay compound oxidation.

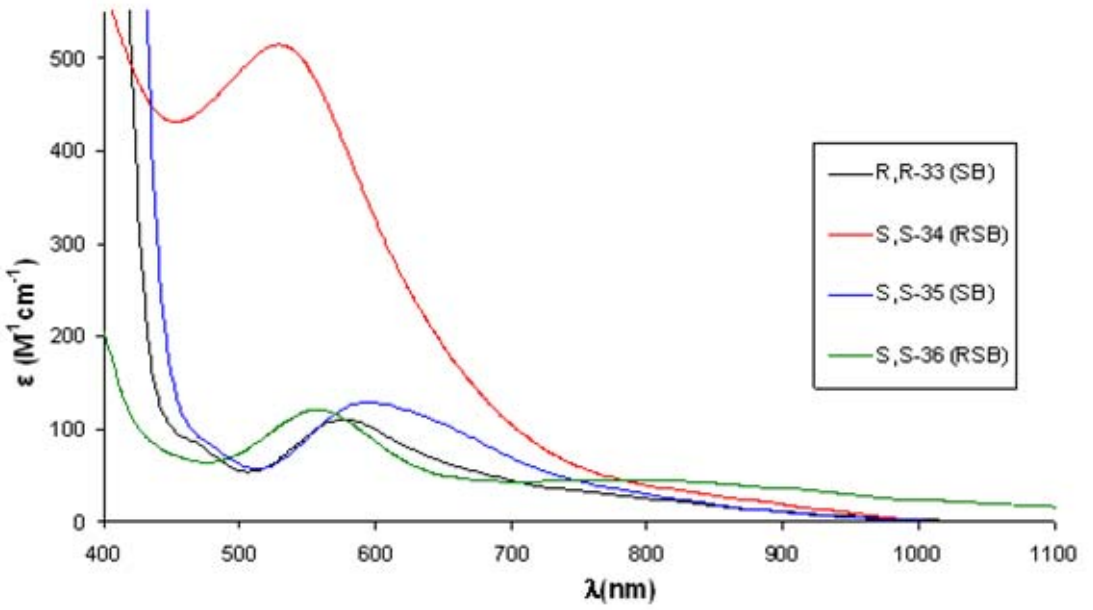

Figure 4.15. Isotropic absorption spectra (UV-Vis) of *R,R*-**33** (CH_2Cl_2), *S,S*-**35** (CH_2Cl_2), *S,S*-**34** (DMSO), *S,S*-**36** (DMSO). The spectra were recorded with 4.6 mM (*R,R*-**33**), 4.6 mM (*S,S*-**34**), 5.0 mM (*S,S*-**35**), 3.9 mM (*S,S*-**36**) solutions, with a 10 mm optical path cell.

Table 4.2. λ_{max}, ε and Δε values for *R,R*-**33**, *S,S*-**34**, *S,S*-**35** and *S,S*-**36**.

CD							
R,R-**33**		*S,S*-**34**		*S,S*-**35**		*S,S*-**36**	
λ (nm)	Δε ($M^{-1}cm^{-1}$)	λ (nm)	Δε ($M^{-1}cm^{-1}$)	λ (nm)	Δε ($M^{-1}cm^{-1}$)	λ (nm)	Δε ($M^{-1}cm^{-1}$)
667	0.36	313	1.46	680	0.42	554	0.46
584	-0.66			520	0.42	311	2.11
466	-2.51			470	-0.78		
395	-10.85			405	-4.03		
358	6.66			366	7.86		
UV-Vis							
λ (nm)	ε ($M^{-1}cm^{-1}$)	λ (nm)	ε ($M^{-1}cm^{-1}$)	λ (nm)	ε ($M^{-1}cm^{-1}$)	λ (nm)	ε ($M^{-1}cm^{-1}$)
584	152	524	512	584	152	780	45
414	762			424	640	552	120

The CD and UV-Vis spectra of the $V^{IV}O$(salan) complexes *S,S*-**40**, *S,S*-**42**, *S,S*-**43** and *R,R*-**45** were also recorded (see Figures 4.16 and 4.17). The relevant λ_{max}, ε and Δε values are listed in Table 4.3. The UV-Vis spectra and respective parameters of *S,S*-**41** and *S,S*-**42** are also included.

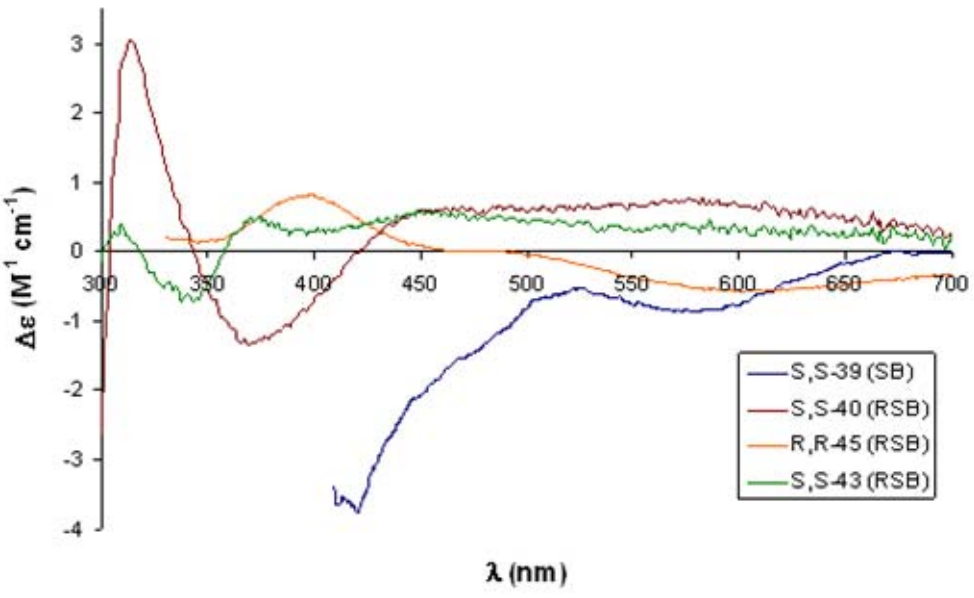

Figure 4.16. CD spectra of *S,S*-**39** (DMSO), *S,S*-**40** (CH_3CN), *S,S*-**43** (DMSO), and *R,R*-**45** (CH_3CN). The spectra were recorded with 5.3 mM (*S,S*-**39**), 1.3 mM (*S,S*-**40**), 1.2 mM (*S,S*-**43**) and 10.4 mM (*R,R*-**45**) solutions with a 1 mm optical path cell.

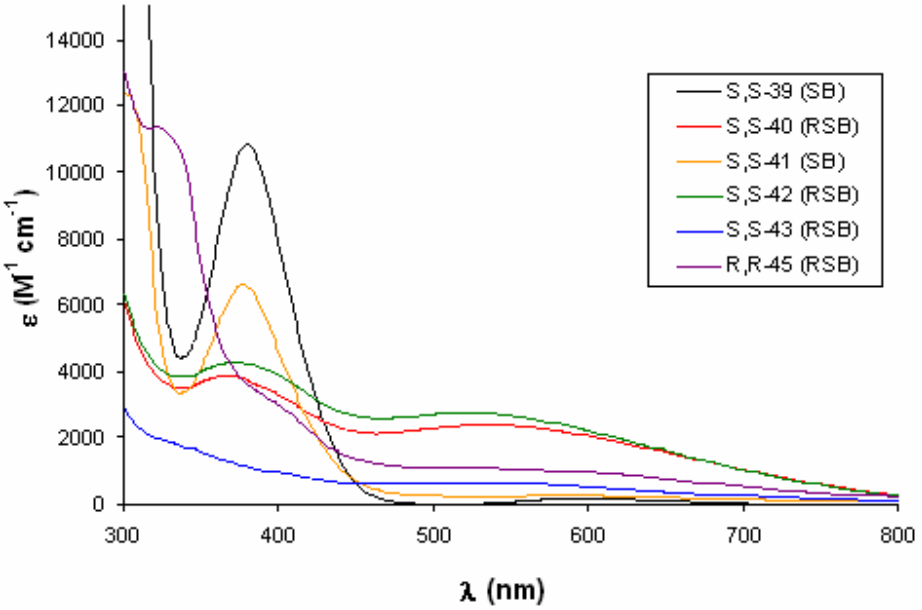

Figure 4.17. Isotropic absorption spectra (Uv-Vis) of *S,S*-**39**, *S,S*-**40**, *S,S*-**41**, *S,S*-**42**, *S,S*-**43** and *R,R*-**45** in DMSO. The spectra were recorded with 0.12mM (*S,S*-**39**), 0.27mM (*S,S*-**40**), 0.21mM (*S,S*-**43**), and 0.24mM (*R,R*-**45**) solutions, with a 5mm optical path cell.

Table 4.3. λ_{max}, ε and ε values for *S,S*-**39**, *S,S*-**40**, *S,S*-**43** and *R,R*-**45**.

CD							
S,S-**39**		*S,S*-**40**		*S,S*-**43**		*R,R*-**45**	
λ (nm)	Δε ($M^{-1}cm^{-1}$)	λ (nm)	Δε ($M^{-1}cm^{-1}$)	λ (nm)	Δε ($M^{-1}cm^{-1}$)	λ (nm)	Δε ($M^{-1}cm^{-1}$)
578	-0.87	576	0.76	566	0.38	643	-0.51
551	-0.77	369	-1.34	449	0.59	394	0.80
411	-3.66			374	0.52		
				333	-0.56		
				305	0.39		
UV-Vis							
λ (nm)	ε ($M^{-1}cm^{-1}$)	λ (nm)	ε ($M^{-1}cm^{-1}$)	λ (nm)	ε ($M^{-1}cm^{-1}$)	λ (nm)	ε ($M^{-1}cm^{-1}$)
597	155	533	2375	516	1099	523	654
380	10840	367	3862	323	11347		
S,S-**41**		*S,S*-**42**					
λ (nm)	ε ($M^{-1}cm^{-1}$)	λ (nm)	ε ($M^{-1}cm^{-1}$)				
585	238	520	2733				
377	6600	371	4283				

All recorded spectra exhibit CD signals, thus confirming that the prepared compounds exhibit chirality in solution. The CD spectra were complemented with the electronic absorption spectra to facilitate identification of the relevant electronic transitions associated with the observed CD signals. In *S,S*-**39** and *S,S*-**41** the n-π^* band is clearly visible at ca. 370-380 nm. In *S,S*-**40**, *S,S*-**43** and *R,R*-**45** a quite high intensity band is observed in the 450-750 nm range, due to $O_{phenolate}$-V_d transitions. The *d*-*d* transitions cannot be distinguished below these quite intense transitions.

The high molar absorptivity values for *S,S*-**39**, *S,S*-**40**, *S,S*-**41**, *S,S*-**42**, *S,S*-**43** and *R,R*-**45**, much greater than those of *R,R*-**33**, *S,S*-**34**, *S,S*-**35** and *S,S*-**36** could be due to partial oxidation to the corresponding V^V forms. In fact, it is known that V^VO-phenolate compounds can present very intense colors either in solution or solid state. This coloration is due to charge transfer transitions involving the phenolate oxygen donor $p\pi$ orbital and the empty $d\pi$* orbitals, where *p* and *d* represent the oxygen lone pair and the metal d orbitals, respectively. These charge transfer absorptions appear in the 500-600 nm range, red-shifted in comparison with the corresponding $V^{IV}O$ compounds. The presence of such intense transitions not only is typical in V^VO-phenolate compounds but also very characteristic of complexes containing phenolates bound to a V^VO^{3+} core.[4,12,13,14,21] This spectroscopic data may indeed serve as a reiteration of the possibility that the V^V species responsible for the ^{51}V NMR chemical shifts at *ca*. -540 ppm in aprotic solvents are V^VO^{3+} and not VO_2^+ species.

The evolution of such charge transfer bands in the oxidation of *S,S*-**34** in DMSO solution was followed by UV-Vis and CD spectroscopy. The CD spectra recorded over a period of 75 minutes is shown in Figure 4.18. The relevant λ_{max} and $\Delta\varepsilon$ values are listed in Table 4.4.

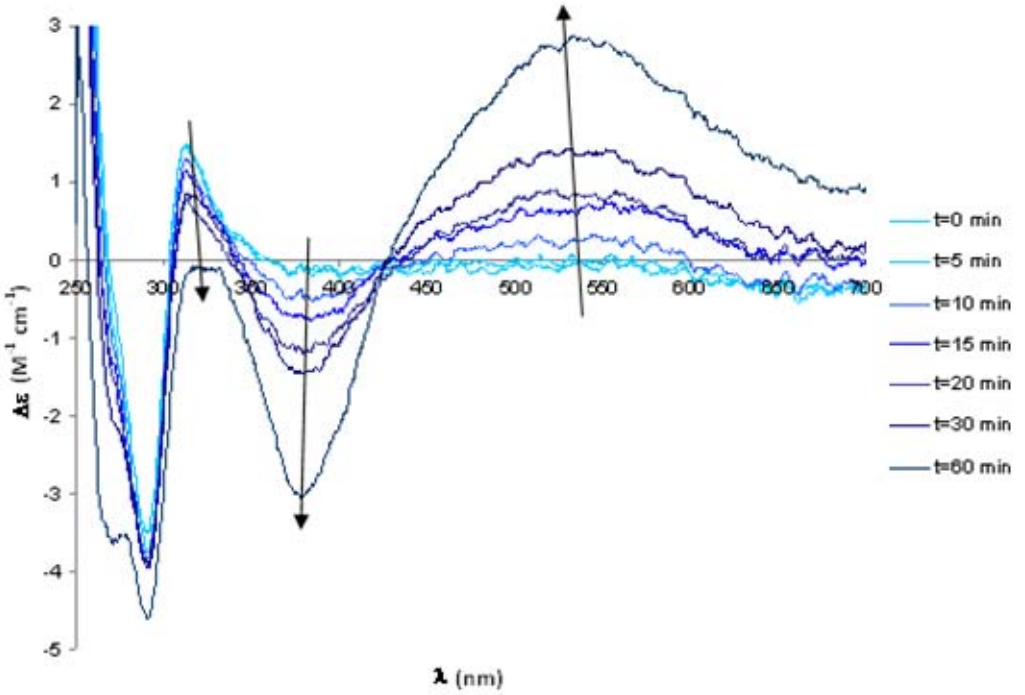

Figure 4.18. CD spectra of *S,S*-**34** in DMSO during oxidation. The spectra were recorded with a 0.46 mM solution with a 1 mm optical path cell.

Table 4.4. λ_{max} and $\Delta\varepsilon$ values for *S,S*-**34** during oxidation in DMSO solution.

S,S-**34**.					
λ (nm)	t (min)	Δε ($M^{-1}cm^{-1}$)	λ (nm)	t (min)	Δε ($M^{-1}cm^{-1}$)
	0			0	-0.17
	5			5	-0.17
	10	0.26		10	-0.46
530	15	0.6	375	15	-0.69
	20	0.81		20	-1.16
	30	1.41		30	-1.46
	60	2.84		60	-3.0

The same evolution was monitored by UV-Vis spectroscopy. The recorded UV-Vis spectra over a period of 75 minutes are shown in Figure 4.19. The relevant λ_{max} and $\Delta\varepsilon$ values are listed in Table 4.5.

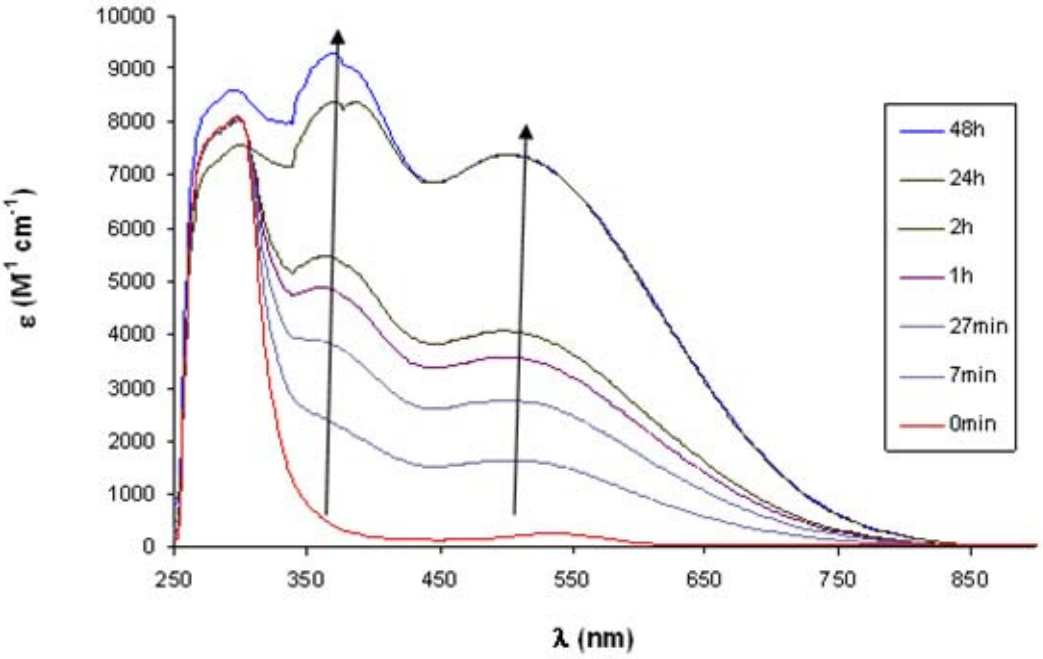

Figure 4.19. Isotropic absorption spectra (Uv-Vis) of *S,S*-**34** in DMSO during oxidation. The spectra were recorded with a 0.3 mM solution and a 1 cm optical path cell.

Table 4.5. λ_{max} and ε values for *S,S*-**34** during oxidation in DMSO solution.

S,S-**34**.					
λ (nm)	t (min)	ε ($M^{-1}cm^{-1}$)	λ (nm)	t (min)	ε ($M^{-1}cm^{-1}$)
	0	193		0	
	7	1637		7	
	27	2770		27	3866
500	60	3580	362	60	4880
	120	4067		120	5470
	1440	7387		1440	8273
	2880	7383		2880	9197

Figure 4.19 depicts only a faint *d-d* band **II** signal at *ca*. 550 nm at t=0. As the oxidation from V^{IV} to V^{V} progresses, broad signals appear at *ca*. 530 nm. The UV region also registers some changes, but not so remarkable. A similar evolution is observed in the UV-Vis spectrum of *S,S*-**34**. At t=0 the spectrum corresponds to a $V^{IV}O$ species with the

weak band **I** and band **II** visible at *ca*. 800 and 530 nm, respectively. After 24h, the spectrum stabilizes and the lower energy band initially visible at 530 nm is transformed into a band at λ_{max} = 500 nm with ε = 7387 M^{-1} cm^{-1}. Another new band appears at 362 nm with ε = 9197 M^{-1} cm^{-1}. During the oxidation process, the color of the DMSO solution evolves from a light magenta to a very dark red. The intense signal within the 500-600 nm range, associated to the red-shifted charge transfer transition typical of $V^{V}O$-phenolate compounds containing a $V^{V}O^{3+}$ core, is clearly visible in both CD and UV-Vis spectra. The same change in coloration is observed during the air-induced oxidation of the remaining $V^{IV}O$(salan) compounds.

Solubility issues prevented the CD and UV-Vis study of the $V^{IV}O$(salan) compounds *S,S*-**37** and *S,S*-**38**.

4.2.3. Characterization by EPR spectroscopy

Electron Paramagnetic Resonance (EPR) spectroscopy will have a special focus in this Chapter given the importance of this technique in the characterization of $V^{IV}O$ compounds.

The +4 oxidation state of vanadium is represented by the uniquely stable VO^{2+} cation. This species has a number of properties that makes it especially suited for EPR analysis: it is a ground state S=1/2 system where the unpaired 3*d* electron resides in a mostly non-bonding, non-degenerate d_{xy} orbital with no other excited energy levels nearby, allowing for room-temperature EPR experiments with high resolution; the mostly non-bonding character of the d_{xy} orbital ensures a limited interaction between the unpaired electron and the donor atoms in the coordination sphere. ^{51}V has a nuclear spin of 7/2. Therefore, isotropic continuous wave (CW) EPR spectra of $V^{IV}O$ compounds will show 8 lines, each separated by the isotropic hyperfine coupling constant $\mathbf{A_0}$, apart from second-order effects. The $\mathbf{g_0}$ factor determines the placement of these lines along the swept magnetic field. Figure 4.20 depicts a typical isotropic X-Band EPR spectrum of a $V^{IV}O$ species.

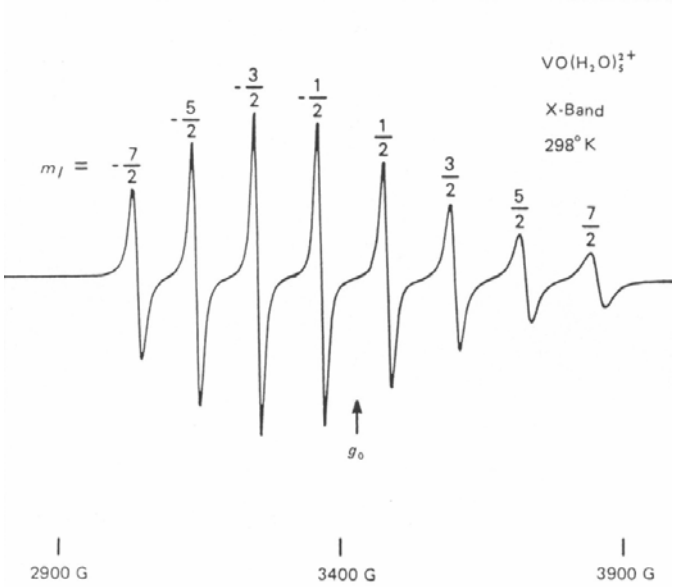

Figure 4.20. Isotropic first-derivative X-band EPR spectrum of aqueous $V^{IV}O(H_2O)_5^{2+}$ measured at room temperature.[22]

The observed microwave absorption phenomenon in isotropic conditions can be explained with equation 4.2, where **h** is Planck's constant, **ν** is microwave frequency, $\mathbf{g_0}$ is the adimentional isotropic "**g-factor**", also known as the Landé factor, $\mathbf{B_0}$ is the external magnetic field, $\boldsymbol{\mu_B}$ is the Bohr magneton, $\mathbf{\Delta m_S}$ is the change in spin state, $\mathbf{A_0}$ is the isotropic hyperfine coupling constant and $\mathbf{m_I}$ is the nuclear spin state.[22,54]

$$\mathbf{h\,\nu = g_0\,\mu_B\,B_0\,\Delta m_S + A_0\,\Delta m_S\,m_I} \qquad (4.2)$$

When molecule movement is restricted by solvent viscosity or by lower temperatures, the electronic interaction with $\mathbf{B_0}$ ceases to be orientation-independent and the molecule symmetry becomes relevant. In such conditions, equation 4.2 can be expanded into the following equations: [22,54]

$$\mathbf{h\,\nu = g_x\mu_B\,B_0\,\Delta m_S + A_x\,\Delta m_S\,m_I} \qquad (4.3)$$
$$\mathbf{h\,\nu = g_y\mu_B\,B_0\,\Delta m_S + A_y\,\Delta m_S\,m_I} \qquad (4.4)$$
$$\mathbf{h\,\nu = g_z\,\mu_B\,B_0\,\Delta m_S + A_z\,\Delta m_S\,m_I} \qquad (4.5)$$

where both **g** and **A** are split into *x*, *y* and *z*-components. The equations 4.3 to 4.5 explain the additional signals observed in anisotropic $V^{IV}O$ EPR spectra. Despite being more

complex, anisotropic EPR spectra often yield more information. Anisotropy will depend on the sample temperature, on the solvent used and on the ligand to which the $V^{IV}O$ unit is coordinated.

When vanadium is concerned, there are degrees of anisotropy that need to be taken into account. These degrees of anisotropy often lead to quite different EPR spectra and, consequently, to different parameters. When $\mathbf{g_z} > \mathbf{g_x} = \mathbf{g_y}$, the EPR spectrum is said to have "axial" symmetry. An "axial" EPR spectrum of a $V^{IV}O$ sample should display 16 signals, but most overlap near the central region of the field. A "rhombic" EPR spectrum has three sets of **g** and **A** values**,** one per symmetry axis. Therefore, 24 signals should be expected, but in a X-band EPR spectrum most of these signals are not sufficiently resolved or simply overlap. Complexes with symmetry lower than C_{4v} are more likely to yield "rhombic" spectra recorded at low temperatures. The designation of the obtained anisotropic parameters for each symmetry, as the relation between the anisotropic parameters to the isotropic parameters is shown below:[22]

"Axial" symmetry**:**

$$\mathbf{g_x} = \mathbf{g_y} = \mathbf{g_\perp} \; ; \; \mathbf{g_z} = \mathbf{g_\parallel} \quad (4.6)$$

$$\mathbf{A_x} = \mathbf{A_y} = \mathbf{A_\perp} \; ; \; \mathbf{A_z} = \mathbf{A_\parallel} \quad (4.7)$$

$$\mathbf{g_o} = (2\mathbf{g_\perp} + \mathbf{g_\parallel})/\,3 \quad (4.8)$$

$$\mathbf{A_o} = (2\mathbf{A_\perp} + \mathbf{A_\parallel})/\,3 \quad (4.9)$$

"Rhombic" symmetry**:**

$$\mathbf{g_x} \neq \mathbf{g_y} \neq \mathbf{g_z} \quad (4.10)$$

$$\mathbf{A_{xx}} \neq \mathbf{A_{yy}} \neq \mathbf{A_z} \quad (4.11)$$

$$\mathbf{g_o} = (\mathbf{g_x} + \mathbf{g_y} + \mathbf{g_z})/\,3 \quad (4.12)$$

$$\mathbf{A_o} = (\mathbf{A_x} + \mathbf{A_y} + \mathbf{A_z})/\,3 \quad (4.13)$$

Unfortunately, one cannot deduce symmetry from an EPR spectrum. X-band spectra with slight rhombicity will appear axial due to signal overlapping or lack of signal resolution. The following figure (Figure 4.21) shows an example of anisotropy in a $V^{IV}O$ EPR spectrum.

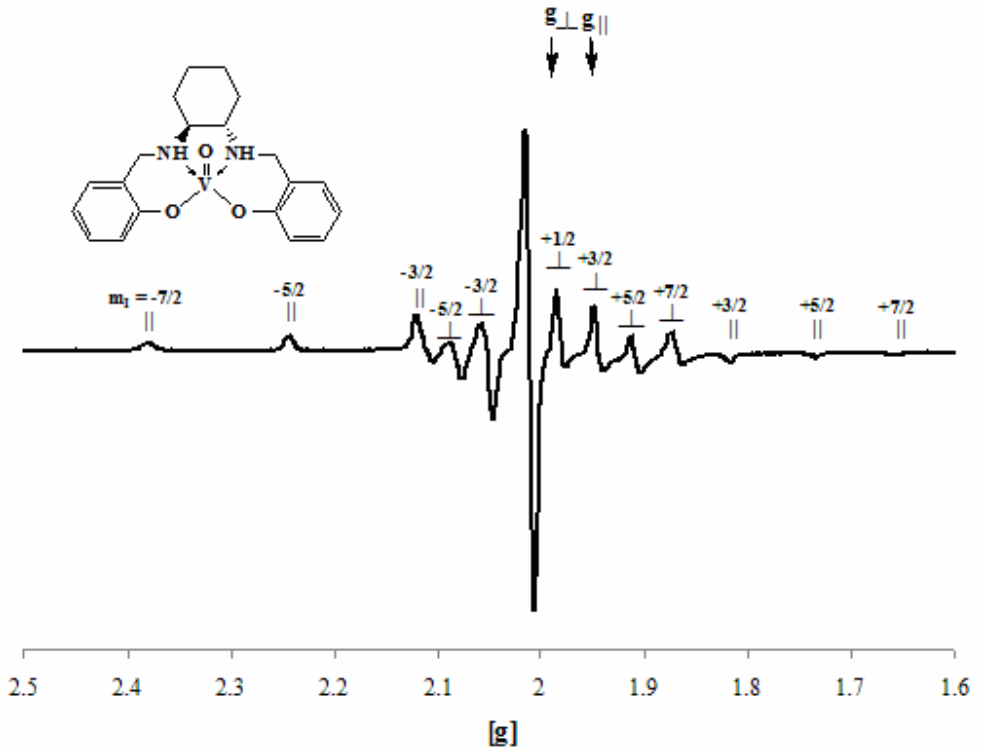

Figure 4.21. First derivative "axial" X-band EPR spectrum taken from a 2.0 mM solution *S,S*-**34** in DMSO, at 77K. Additional splittings are present in the central field region. The overlap of signals in this region does not allow their identification, but does not impede calculation of the spin Hamiltonian parameters **g** and **A**.

All of the EPR spectra obtained for the featured $V^{IV}O$(salen) and $V^{IV}O$(salan) compounds are anisotropic due to the need of recording the spectra from frozen samples. The freezing of EPR samples is a procedure used for $V^{IV}O$ compounds that show a tendency to oxidize once in solution. Such is the case of the prepared $V^{IV}O$(salan) compounds. These low temperature solid solutions will not only preserve $V^{IV}O$ species long enough for a proper EPR analysis, but will also mitigate non-resonant microwave absorption from the solvent, a phenomenon which may render samples EPR silent.

After the measurement of the EPR spectra, these are subject to simulation with the appropriate software.[23] Software simulation may yield accurate prediction of spin Hamiltonian parameters **g** and **A**. Of these two, the hyperfine coupling constant **A** is more important to characterize the environment surrounding the metal centre. In the case of anisotropic $V^{IV}O$ EPR spectra, the hyperfine coupling constant $\mathbf{A_z}$ is the most important parameter. It serves as a measure of the overall influence that donor groups in equatorial

plane exert on the electron density around the V=O centre. It is from this parameter that equatorial donor groups and binding modes are predicted. The $\mathbf{g_z}$ is also important as it relates directly to the electronic structure of the V=O bond and its value correlates inversely with $\mathbf{A_z}$.[22] The parameter values for the components perpendicular to the *z* axis are comparatively much smaller. These are estimated from signals that are either poorly resolved or overlapped, making it difficult to establish any relation with the ligand field. As such, the parameter values for the perpendicular components are rarely used for this kind of structural elucidation.

To help with the interpretation of $V^{IV}O$ EPR spectra, an empirical relation known as "the additivity rule" is used. This "additivity rule", developed by Holyk[24] and Chasteen,[22] states that the value of the anisotropic $\mathbf{A_z}$ for $V^{IV}O$ complexes may be estimated by the sum of the individual contributions of each equatorial ligand, as expressed by equation 4.14. Table 4.6 shows the contributions to $\mathbf{A_z}$ for common donor groups.

$$A_z^{est} = A_z^{L1} + A_z^{L2} + A_z^{L3} + A_z^{L4} \qquad (4.14)$$

Table 4.6. Contribution to $\mathbf{A_z}$ of various donor groups.[22,25,24]

Donor group	$\mathbf{A_z}$ contribution ($\times \mathbf{10^{-4}\ cm^{-1}}$)
H_2O	45.7
Imidazole	40.1 - 45.5[a]
Aliphatic imine	37 - 44.4
Pyridine	40.4 - 44.1[a]
Cl^-	44.1
Amide O RC(O)NR'R''	43.7
$RCOO^-$, $ArCOO^-$	42.1
PO_4^{3-}	42.5
RNH_2, R_2NH, R_3N	40.1
OH^-	38.7
ArO^-	38.6
acetylacetonate	83/2[b]
Amide N (deprotonated)	30 - 43
RO^-	35.3
ArS^-	35.3
RS^-	31.9

[a] Values are dependent on the dihedral angle between the V=O and N=C units.
[b] Mean value for when both acetylacetonate oxygen donors are equatorial.

Taking into account the $\mathbf{A_z}$ values of Table 4.6, equatorial donor groups bound to the $V^{IV}O$ moiety can be deduced by using the additivity rule. Despite being extremely useful, equation 4.14 should be used with caution. The accepted error limit is $\pm 3 \times 10^{-4}$ cm^{-1}, but multiple combinations of donor groups can give identical $\mathbf{A_z^{est}}$ within the error limit. Another important point is that this rule does not predict ligand coordination *trans* to the V=O bond. It can only be safely applied to square-pyramidal $V^{IV}O$ compounds. In contradiction to the initial understanding, several studies have shown that the presence of a solvent molecule coordinated *trans* to the V=O bond may alter experimental $\mathbf{A_z}$ significantly.[26,27] Curiously, solvent molecules coordinated *cis* to the V=O bond appear to exert a much smaller influence on the experimental $\mathbf{A_z}$, even though the *trans* position is occupied by a donor function belonging to the main ligand. Despite its shortcomings, the additivity rule remains the main tool used to predict which donor group bind equatorially to $V^{IV}O$ units.

With this brief description of the technique and the information it yields, the results obtained from the prepared $V^{IV}O$(salen) and $V^{IV}O$(salan) compounds will now be presented and discussed.

The X-band EPR spectra of the frozen DMSO solutions (77K) of the featured salen and salan compounds were measured and simulated with the ROKI program, developed by Rockenbauer and Korecz.[23] The spectra either exhibit “axial” symmetry or “axial” with slight rhombicity. Figure 4.23 shows the obtained X-band EPR spectra for the prepared $V^{IV}O$ compounds. Table 4.7 lists the corresponding spin Hamiltonian parameters and predicted equatorial donor groups.

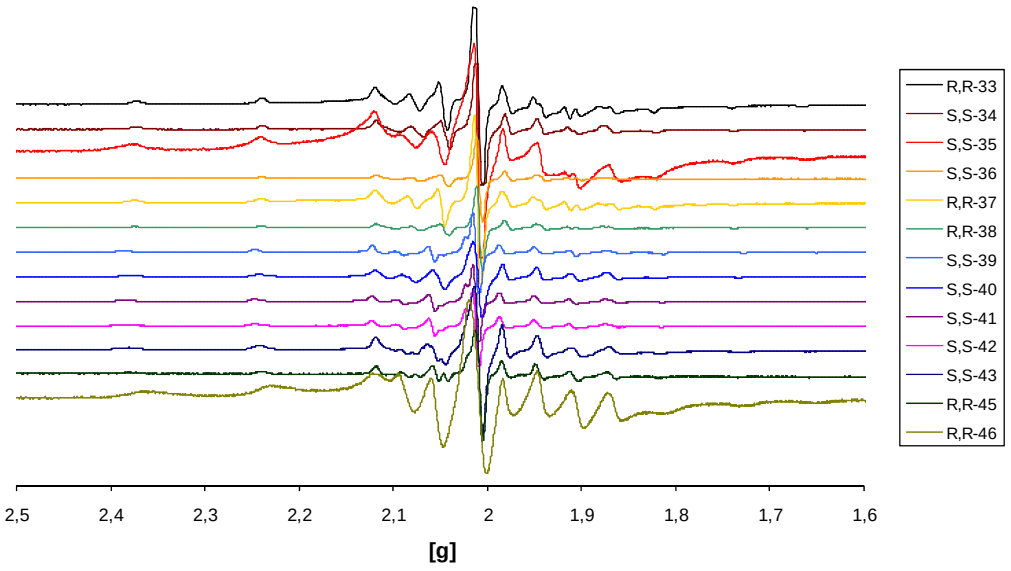

Figure 4.22. First derivative X-band EPR spectrum taken from DMSO and DMF sample of the presented $V^{IV}O$(salen) and $V^{IV}O$(salan) compounds, at 77K.

For all $V^{IV}O$ compounds analyzed, the patterns of the EPR spectra are consistent with the existence of a single species in solution. $V^{IV}O$(salen) and $V^{IV}O$(salan) compounds, much like the Ti^{IV}(salan) compounds discussed in Chapter 3, can adopt three distinct octahedral geometries, if the coordination of a solvent molecule is admitted. Again, the *mer-mer* (*trans*), *fac-mer* (*cis*-β) and *fac-fac* (*cis*-α) geometries become important since they dictate which donor groups reside in the equatorial plane of the $V^{IV}O$ center. A consequence of this is that a $V^{IV}O$ compound capable of adopting these geometries can generate multiple geometric isomers simultaneously, each with different $\mathbf{g}_z$ and $\mathbf{A}_z$ parameters. Figure 4.23 depicts all relevant geometries for the analyzed $V^{IV}O$(salen) and $V^{IV}O$(salan) compounds, with the expected $\mathbf{A_z}$ values for each one considering the following contributions: $\mathbf{A}_{i,N,amine}= 40.1 \times 10^{-4}$ cm^{-1}; $\mathbf{A}_{i,N,imine}= 40.7 \times 10^{-4}$ cm^{-1}; $\mathbf{A}_{i,O.phenolate}= 38.8 \times 10^{-4}$ cm^{-1}; $\mathbf{A}_{i,O.DMF}= 43.7 \times 10^{-4}$ cm^{-1}; $\mathbf{A}_{i,O.DMSO}= 41.1 \times 10^{-4}$ cm^{-1}.

Table 4.7. Experimental spin Hamiltonian parameters for the featured tetradentate $V^{IV}O$ complexes.

Compound	g_x, g_y (or $g_\perp$)	A_x, A_y (or $A_\perp$) $\times 10^{-4}$ cm^{-1}	g_z (or $g_{//}$)	A_z (or $A_{//}$) $\times 10^{-4}$ cm^{-1}	Predicted equatorial donor set	Possible geometry
R,R-**33**[a]	1.983	50.5	1.959	157.4	N_{imine}, N_{imine}, O_{ArO-}, O_{ArO-}	*trans*
S,S-**34**[a]	1.976	50.9	1.957	158.3	N_{amine}, N_{amine}, O_{ArO-}, O_{ArO-}	*trans*
S,S-**35**[a]	1.978	53.7	1.955	160.0	N_{imine}, O_{ArO}^-, O_{ArO}^-, O_{DMSO}	*cis*-α
S,S-**36**[a]	1.978	54.1	1.954	161.8	N_{amine}, N_{amine}, O_{ArO}^-, O_{DMSO}	*cis*-β
R,R-**37**[a]			1.957	158.8	N_{imine}, N_{imine}, O_{ArO-}, O_{ArO-}	*trans*
R,R-**38**[a]			1.957	159.6	N_{imine}, O_{ArO}^-, O_{ArO}^-, O_{DMSO}	*cis*-α
S,S-**39**[b]	1.982	55.1	1.955	164.4	N_{imine}, N_{imine}, O_{ArO}^-, O_{DMF}	*cis*-β
S,S-**40**[b]	1.983, 1.976	55.6, 52.6	1.954	160.1	N_{amine}, O_{ArO}^-, O_{ArO}^-, O_{DMF}	*cis*-α
S,S-**41**[b]	1.981, 1.983	50.7 58.7	1.956	164.1	N_{imine}, N_{imine}, O_{ArO}^-, O_{DMF}	*cis*-β
S,S-**42**[b]	1.979	53.3	1.9551	161.7	N_{amine}, O_{ArO}^-, O_{ArO}^-, O_{DMF}	*cis*-α
S,S-**43**[a]	1.982, 1.976	59.8, 50.9	1.955	161.1	N_{amine}, N_{amine}, O_{ArO}^-, O_{DMSO}	*cis*-β
R,R-**45**[b]	1.976, 1.982	49.1, 55.9	1.9545	160.8	N_{amine}, O_{ArO}^-, O_{ArO}^-, O_{DMF}	*cis*-α
R,R-**46**[b]			1.962	162.0	N_{amine}, N_{amine}, O_{ArO-}, O_{DMF} N_{py}, N_{py}, O_{ArO-}, O_{ArO-}	*cis*-β

[a] EPR spectrum measured with DMSO solution. [b] EPR spectrum measured with DMF solution.

Compounds *R,R*-**33**, *S,S*-**34** and *R,R*-**37** exhibit comparatively low $\mathbf{A_z}$ values, consistent with the *trans* geometry **a**. Compounds *S,S*-**35**, *S,S*-**40**, *S,S*-**42**, *R,R*-**38** and *R,R*-**45** exhibit $\mathbf{A_z}$ values which may raise some doubt as to whether a *trans* or *cis* species is present. For *S,S*-**35** and *R,R*-**38**, the closest $\mathbf{A_z^{est}}$ to the experimental value is the one given by the *cis*-α binding mode **g** which predicts an equatorial donor group consisting of (N_{imine}, O_{ArO}^-, O_{ArO}^-, O_{DMSO}). Compounds *S,S*-**40**, *S,S*-**42** and *R,R*-**45** may adopt the binding mode **f**, with $\mathbf{A_z^{est}}$=161.4 $\times 10^{-4}$ cm^{-1} and an equatorial donor group consisting of (N_{amine}, O_{ArO}^-, O_{ArO}^-, O_{DMF}). The remaining compounds have $\mathbf{A_z^{exp}}$ greater than 161.0 $\times 10^{-4}$ cm^{-1} and considering the solvent used in each case it is more likely that these adopt *cis*-β geometries: binding mode **c** is assigned to compounds *S,S*-**39**, *S,S*-**41** and *R,R*-**46**; **d** for compounds *S,S*-**36** and *S,S*-**43**. The *cis* *Δ* and *Λ* diastereoisomers cannot be

distinguished in EPR, although the fact that a *cis* species is detected is good indicator of chirality at the metal centre.

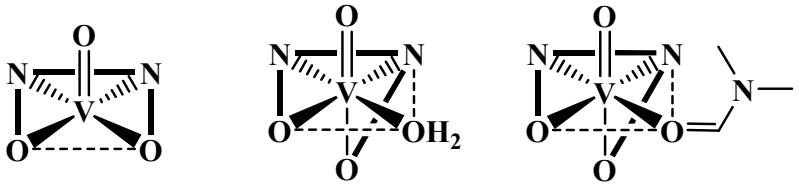

a

(N_{amine}):
$\mathbf{A_z^{est}} = 157.8 \times 10^{-4}$ cm^{-1}
(N_{imine}):
$\mathbf{A_z^{est}} = 159.0 \times 10^{-4}$ cm^{-1}

b

(N_{amine}):
$\mathbf{A_z^{est}} = 164.7 \times 10^{-4}$ cm^{-1}
(N_{imine}):
$\mathbf{A_z^{est}} = 165.9 \times 10^{-4}$ cm^{-1}

c

(N_{amine}):
$\mathbf{A_z^{est}} = 162.7 \times 10^{-4}$ cm^{-1}
(N_{imine}):
$\mathbf{A_z^{est}} = 163.9 \times 10^{-4}$ cm^{-1}

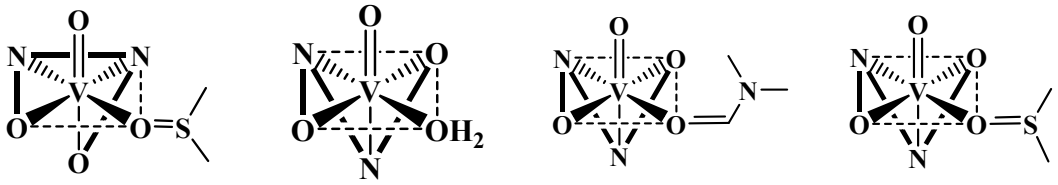

d

(N_{amine}):
$\mathbf{A_z^{est}} = 160.5 \times 10^{-4}$ cm^{-1}
(N_{imine}):
$\mathbf{A_z^{est}} = 161.7 \times 10^{-4}$ cm^{-1}

e

(N_{amine}):
$\mathbf{A_z^{est}} = 163.4 \times 10^{-4}$ cm^{-1}
(N_{imine}):
$\mathbf{A_z^{est}} = 164.0 \times 10^{-4}$ cm^{-1}

f

(N_{amine}):
$\mathbf{A_z^{est}} = 161.4 \times 10^{-4}$ cm^{-1}
(N_{imine}):
$\mathbf{A_z^{est}} = 162.0 \times 10^{-4}$ cm^{-1}

g

(N_{amine}):
$\mathbf{A_z^{est}} = 159.2 \times 10^{-4}$ cm^{-1}
(N_{imine}):
$\mathbf{A_z^{est}} = 159.9 \times 10^{-4}$ cm^{-1}

Figure 4.23. Possible geometries adopted by the analyzed $V^{IV}O$(salen) and $V^{IV}O$(salan) in solution.

Compound *R,R*-**46** bears a hexadentate ligand and the possibility that the $V^{IV}O$ centre may be coordinated to the $N_{pyridine}$ donor atoms instead of the N_{amine} donor atoms must be considered. It is known that the V=O/N−C dihedral angle influences the overall $\mathbf{A_z}$ contributions of sp^2 nitrogen donors such as pyridines, imidazoles and even imines (see Figure 4.24).[28] Pyridine and imidazole donor nitrogens have a contribution of 44.1×10^{-4} cm^{-1} for a dihedral angle of 90º, while 40.3×10^{-4} cm^{-1} is the value expected for a 0º dihedral angle. The $\mathbf{A_z}$ contribution for the imine donors is considered to be 40.7×10^{-4} cm^{-1}, though it has been reported that the contribution can go as high as 44.4×10^{-4} cm^{-1}, while values as low as 36.7×10^{-4} cm^{-1} have been also reported.[22,25]

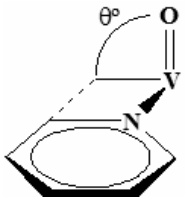

Figure 4.24. The dihedral angle between a perpendicular pyridine donor and the V=O bond.

Taking into account the flexibility of the ligand, the equatorial N_{py} dihedral angles in mode **c** can be such that the respective $\mathbf{A_z^{est}}$ values can match the obtained $\mathbf{A_z^{exp}}$ for *R,R*-**46**, making it impossible to distinguish between a (N_{amine}, N_{amine}, $O_{phenolate}$, O_{DMF}) and a ($N_{pyridine}$, $N_{pyridine}$, $O_{phenolate}$, O_{DMF}) donor set.

Despite the uncertainty in assigning geometries to the analyzed compounds, all exhibit $\mathbf{A_Z^{exp}}$ values between 157 and 164 $\times 10^{-4}$ cm^{-1}, well within the expected range for $V^{IV}O$ aminophenolate compounds such as the $V^{IV}O$(salen) and $V^{IV}O$(salan). This in itself strongly indicates a successful preparation of the compounds and their stability in solution.

4.2.4. Characterization by X−Ray Diffraction

Three crystal and molecular structures of dimeric μ-oxo $V^{V}O$ compounds were obtained by single crystal X-ray diffraction methods and revealed important information about the nature of $V^{V}O$(salen) and $V^{V}O$(salan) compounds in the solid state. The ORTEP diagrams of the $V^{V}O$(salen) compounds *R,R*-**33b** and *S,S*-**39b** are presented below and the selected parameters are listed in Table 4.8.

Figures 4.25 and 4.26 depict the structural formulas of *R,R*-**33b** and *S,S*-**39b** as dimeric structures with each monomeric unit bridged by two μ-oxo ligands. Both structures share many similarities. In both cases, the asymmetric unit contains each one a dimeric molecule. *R,R*-**33** crystallizes in the monoclinic system, space group $P2_1$ and *S,S*-**39** crystallizes in the triclinic system, space group $P1$. Both molecules are the result of the slow oxidation compounded with partial hydrolysis of the respective salen ligand. One of the imine bonds hydrolyzes and the ligands behave as tridentate donors, binding the V^{V} center through the O_{phenol}, N_{imine} and N_{imine}. Similar behavior was found for *S,S*-**39b** where a dimeric di-μ-oxo V^{V} complex was also obtained. The structures of *R,R*-**33b** and

S,S-**39b** are examples of the instability of the salen compounds towards hydrolysis and stand in contrast with the crystal structures obtained for the $V^{V}O$(salan) compounds *S,S*-**36b** and *R,R*-**45b**, which contain intact ligand structures. The V^{V} centers adopt a distorted octahedral geometry with the tridentate ligand donor atoms in the plane perpendicular to the V=O bond and the μ-oxo ligands completing the coordination sphere.

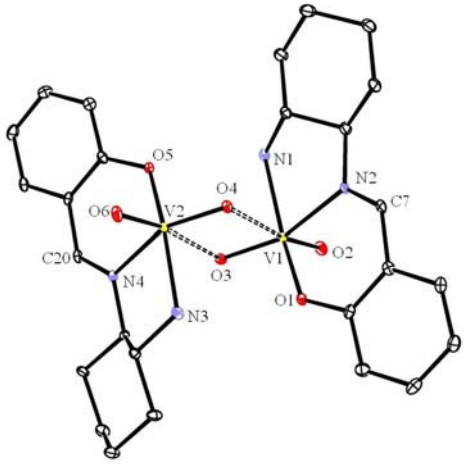

Figure 4.25. ORTEP-3 diagram of the molecular structure of *R,R*-**33b**, using 30 % probability level ellipsoids. The hydrogen atoms were omitted for clarity.

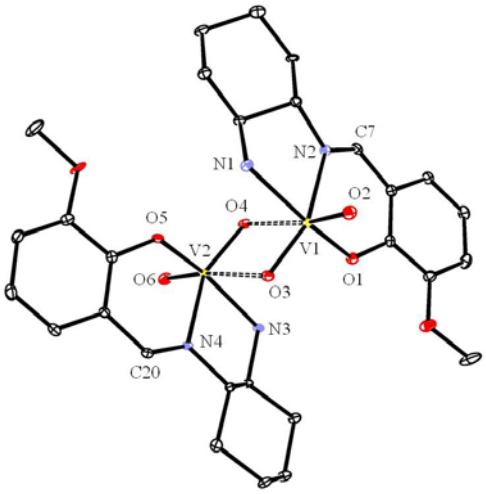

Figure 4.26. ORTEP-3 diagram of the molecular structure of *S,S*-**39b**, using 30 % probability level ellipsoids. The hydrogen atoms were omitted for clarity.

Table 4.8. Selected bond lengths and angles for *R,R*-**33b** and *S,S*-**39b**.

R,R-**33b**				*S,S*-**39b**			
Bond lengths (Å)		Bond angles (º)		Bond lengths (Å)		Bond angles (º)	
V(1)-O(1)	1.926(3)	O(1)-V(1)-O(2)	102.7(1)	V(1)-O(1)	1.915(1)	O(1)-V(1)-O(2)	102.1(1)
V(1)-O(2)	1.614(3)	O(2)-V(1)-O(3)	105.9(1)	V(1)-O(2)	1.622(2)	O(2)-V(1)-O(3)	107.0(1)
V(1)-O(3)	1.679(3)	O(2)-V(1)-O(4)	171.4(1)	V(1)-O(3)	1.667(2)	O(2)-V(1)-O(4)	171.8(1)
V(1)-O(4)	2.335(3)	O(2)-V(1)-N(1)	95.1(1)	V(1)-O(4)	2.409(2)	O(2)-V(1)-N(1)	95.0(1)
V(1)-N(1)	2.144(3)	O(2)-V(1)-N(2)	95.7(1)	V(1)-N(1)	2.130(2)	O(2)-V(1)-N(2)	98.4(1)
V(1)-N(2)	2.186(4)	O(3)-V(2)-O(6)	171.1(1)	V(1)-N(2)	2.183(3)	O(3)-V(2)-O(6)	173.1(1)
N(2)-C(7)	1.273(5)	O(4)-V(2)-O(6)	106.4(1)	N(2)-C(7)	1.295(5)	O(4)-V(2)-O(6)	107.9(1)
N(4)-C(20)	1.298(5)	O(5)-V(2)-O(6)	100.8(1)	N(4)-C(20)	1.279(5)	O(5)-V(2)-O(6)	100.9(1)
V(2)-O(3)	2.302(3)	O(6)-V(2)-N(3)	93.1(1)	V(2)-O(3)	2.437(2)	O(6)-V(2)-N(3)	93.9(1)
V(2)-O(4)	1.669(3)	O(6)-V(2)-N(4)	99.0(1)	V(2)-O(4)	1.663(2)	O(6)-V(2)-N(4)	102.8(1)
V(2)-O(5)	1.927(3)	V(1)-O(3)-V(2)	101.7(1)	V(2)-O(5)	1.914(3)	V(1)-O(3)-V(2)	102.2(1)
V(2)-O(6)	1.610(3)	V(1)-O(4)-V(2)	100.7(1)	V(2)-O(6)	1.623(3)	V(1)-O(4)-V(2)	103.5(1)
V(2)-N(3)	2.126(2)			V(2)-N(3)	2.127(3)		
V(2)-N(4)	2.154(4)			V(2)-N(4)	2.171(3)		

The cyclohexane ring adopts the chair conformation with the chiral carbons in *R* configuration in *R,R*-**33b** and *S* configuration in *S,S*-**39b**. The average length of the C=N double bonds (1.286 Å) is similar to the average bond length observed for C=N double bonds (1.289 Å) in the salen compounds *S,S*-**5a** and *R,R*-**6a** (see Chapter 2). There is a difference between the C=N bond length in each monomeric unit. For instance, in *R,R*-**33b**, the N(2)-C(7) bond, with 1.273(5) Å, is slightly shorter than N(4)-C(20) with 1.298(5) Å, though both nitrogen atoms are *trans* to a μ-oxo ligand. There are considerable differences between the μ-oxo bonds: in *R,R*-**33b**, the μ-oxo bonds V(1)-O(4) and V(2)-O(3) trans to the terminal V=O oxo bonds V(1)-O(2) and V(2)-O(6) are almost twice as long as the μ-oxo bonds V(1)-O(3) and V(2)-O(4) trans to the imine nitrogen donor, with 2.335(3) Å for V(1)-O(4), 2.302(3) Å for V(2)-O(3), 1.679(3) Å for V(1)-O(3) and 1.669(3) Å for V(2)-O(4). These bond length differences are the result of a pronounced *trans* influence exerted by the terminal oxo ligands O(2) and O(6).

A different analysis of this length difference is possible: in *R,R*-**33b**, the terminal oxo bonds exhibit lengths typical of V^{V}=O bonds,[55] with 1.614(3) Å for V(1)-O(2) and 1.610(3) Å for V(2)-O(6). The lengths are also very close to those of V(1)-O(3) and V(2)-O(4), possibly themselves terminal oxo bonds. This raises the question of whether the structures are indeed two $V^{V}O^{3+}$ units linked by two μ-oxo ligands, forming a $V_2O_4^{2+}$ core or two $V^{V}O_2^{+}$ units linked by V=O•••V intermolecular interactions, represented by V(1)-O(4) and V(2)-O(3). Another indication of the double bond character of the V(1)-

O(3) and V(2)-O(4) bonds is the angle formed with the terminal oxo bonds V(1)-O(2) and for V(2)-O(6). The O(2)-V(1)-O(3) angle is 105.9(1)º and the The O(4)-V(2)-O(6) angle is 106.4(1)º, being both values very close to what is observed for $V^{V}O_2^+$ cores with two *cis* V=O double bonds (107-110º).[16,29,30,31] A similar but slightly more pronounced phenomenon can be observed with the same bonds in *S,S*-**39b**.

The μ-oxo bond angles in *R,R*-**33b** are 101.7(1)º for V(1)-O(3)-V(2) and 100.7(1)º for V(1)-O(4)-V(2). For *S,S*-**39b** the observed μ-oxo bond angles are 102.2(1)º for V(1)-O(3)-V(2) and 103.5(1)º for V(1)-O(4)-V(2). In both cases, these bond angles are consistent with those reported for similar $V^{V}O$ compounds.[18]

The 5-membered chelate rings V(1)-N(1)-C(1)-C(6)-N(2) and V(2)-N(3)-C(14)-C(19)-N(4) of *R,R*-**33b** exhibit λ-conformation. The same chelate rings in *S,S*-**39b** exhibit the opposite δ-conformation. Intramolecular N_{imine}-H•••$O_{phenolate}$ hydrogen bonding is present in both structures.

The possible configurations of a $[V^{V}O(\mu\text{-}O)_2V^{V}O]$ core in complexes consisting of two edge-sharing octahedral $V^{V}O$ centers are shown in Figure 4.27. The configuration is defined by the orientation of the V=O bonds relative to the plane defined by the two V atoms and the μ-oxo ligands (*syn*, *anti*), and with the facial or meridional disposition of the tridentate ligands (*orthogonal, coplanar, twist*).[56] Both *R,R*-**33b** and *S,S*-**39b** adopt *anti-coplanar* configuration (see Figure 4.28).

Table 4.9 lists the dihedral angles defined by the 5- and 6-membered chelate rings with the planes perpendicular to the V=O bond for both *R,R*-**33b** and *S,S*-**39b**. Near coplanarity of the 5- and 6-membered chelate rings with the equatorial planes is observed in both structures.

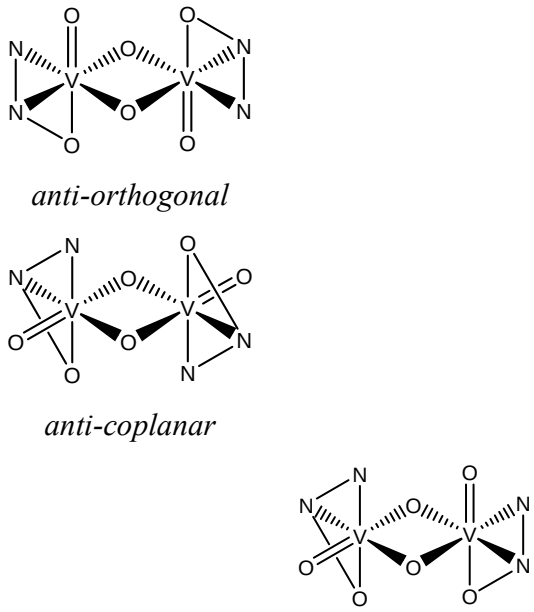

Figure 4.27. The possible configurations of a $[V^{V}O(\mu\text{-}O)_2V^{V}O]$ core in complexes consisting of two edge-sharing octahedral $V^{V}O$ centers.

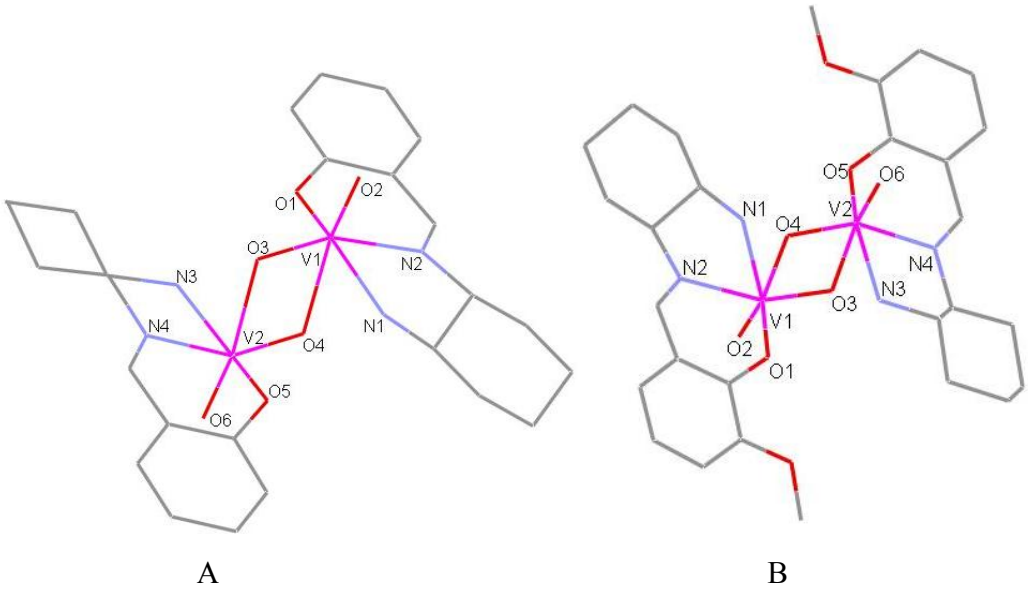

Figure 4.28. Wireframe diagrams of *R*,*R*-**33b** (A) and *S*,*S*-**39b** (B) exhibiting *anti-coplanar* configurations.

Table 4.9. Dihedral angles formed by the chelate rings and the equatorial planes in *S,S*-**33b**.

5-membered			6-membered		
Chelate ring	Equatorial plane	θ (º)	Chelate ring	Equatorial plane	θ (º)
		R,R-**33b**			
V(1)-N(1)-C(1)-C(6)-N(2)	O(1)-O(3)-N(1)-N(2)	15.4	V(1)-O(1)-C(13)-C(8)-C(7)-N(2)	O(1)-O(3)-N(1)-N(2)	5.6
V(2)-N(3)-C(14)-C(19)-N(4)	O(4)-O(5)-N(3)-N(4)	14.7	V(2)-O(5)-C(26)-C(21)-C(20)-N(4)	O(4)-O(5)-N(3)-N(4)	7.3
		S,S-**39b**			
V(1)-N(1)-C(1)-C(6)-N(2)	O(1)-O(3)-N(1)-N(2)	15.6	V(1)-O(1)-C(13)-C(8)-C(7)-N(2)	O(1)-O(3)-N(1)-N(2)	9.5
V(2)-N(3)-C(14)-C(19)-N(4)	O(4)-O(5)-N(3)-N(4)	17.2	V(2)-O(5)-C(26)-C(21)-C(20)-N(4)	O(4)-O(5)-N(3)-N(4)	9.0

The ORTEP diagram of *S,S*-**36b** is presented below (see Figure 4.29) and the selected parameters are listed in Table 4.10. The asymmetric unit of *S,S*-**36b** contains two dimeric molecules, two water and 3.5 isopropanol molecules. *S,S*-**36b** crystallizes in the monoclinic system, space group *C*2. The chiral carbons have *S* configuration. Figure 4.30 depicts *S,S*-**36b** as a dimeric molecular structure with each monomeric unit bridged by a single μ-oxo ligand. The V^V centers adopt distorted octahedral geometries with the ligand coordinated through two $O_{phenolate}$ and two N_{amine} donors in a *cis*-β fashion, the oxo and μ-oxo ligands completing the coordination sphere. The four V=O bonds, V(1)-O(3), V(2)-O(6), V(3)-O(10) and V(4)-O(13) share very similar lengths (1.622(3), 1.623(3), 1.617(3) and 1.620(3) Å, respectively), typical of V^V=O double bonds. The μ-oxo bonds V(1)-O(7), V(2)-O(7), V(3)-O(14) and V(4)-O(14) are comparatively longer (1.840(3), 1.792(3), 1.850(3) and 1.799(3) Å, respectively) as a result of a lower π character. The μ-oxo bond angles in *S,S*-**36b** are wider than those observed for either *R,R*-**33b** and *S,S*-**39b**, with V(1)-O(7)-V(2) and V(3)-O(14)-V(4) having 146.4(2)º and 152.0(2)º, respectively.

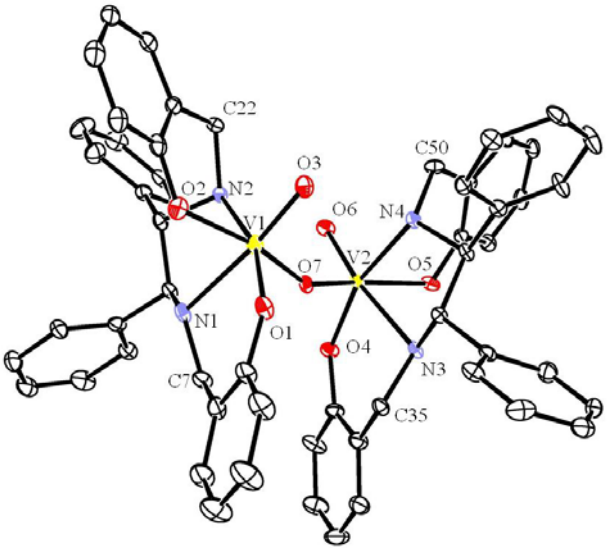

Figure 4.29. ORTEP-3 diagram of one of the dimer molecules of *S,S*-**36b**, using 30 % probability level ellipsoids. The hydrogen atoms and isopropanol and water solvent molecules were omitted for clarity.

Table 4.10. Selected bond lengths and angles for the presented dimer molecule of *S,S*-**36b**.

S,S-**36b**			
Bond lengths (Å)		Bond angles (º)	
V(1)-O(1)	1.832(3)	O(1)-V(1)-O(3)	105.2(1)
V(1)-O(2)	1.906(3)	O(2)-V(1)-O(3)	96.7(1)
V(1)-O(3)	1.622(3)	O(3)-V(1)-N(1)	169(2)
V(1)-O(7)	1.840(3)	O(3)-V(1)-N(2)	92.7(2)
V(1)-N(1)	2.275(4)	O(3)-V(1)-O(7)	98.0(1)
V(1)-N(2)	2.153(4)	O(6)-V(2)-O(4)	103.0(1)
V(2)-O(4)	1.849(3)	O(6)-V(2)-O(5)	96.0(1)
V(2)-O(5)	1.936(3)	O(6)-V(2)-O(7)	98.7(1)
V(2)-O(6)	1.623(3)	O(6)-V(2)-N(3)	171.1(2)
V(2)-O(7)	1.792(3)	O(6)-V(2)-N(4)	93.8(1)
V(2)-N(3)	2.289(4)	V(1)-O(7)-V(2)	152.0(2)
V(2)-N(4)	2.141(4)		
N(1)-C(7)	1.474(6)		
N(2)-C(22)	1.506(6)		
N(3)-C(35)	1.458(6)		
N(4)-C(50)	1.460(5)		

The possible configurations of a [$V^{V}O(\mu$-O)$V^{V}O$] core in complexes consisting of single ligand-sharing octahedral $V^{V}O$ centers are shown in Figure 4.30.[56] The configuration is defined by the orientation of the V=O bonds relative to the plane defined by the two V atoms and the μ-oxo ligands (*syn*, *anti, twist*), and with the angularity of the μ-oxo bonds (*linear, angular*). Both dimeric structures in *S,S*-**36b** adopt a *twist-angular* configuration with the planes containing V(1)-O(3) and V(2)-O(6) forming a dihedral

angle of 79.7º. For the second dimeric structure the planes containing V(3)-O(10) and V(4)-O(13) form a dihedral angle of 73.6º.

The V-N_{amine} bonds *trans* to the terminal oxo bonds display a slight elongation relative to the V-N_{amine} bonds *trans* to the V-$O_{phenolate}$ bonds. In turn, the V-$O_{phenolate}$ bonds also suffer an elongation when *trans* to the μ-oxo bonds.

Table 4.11 lists the dihedral angles formed by the best planes containing the 5- and 6-membered chelate rings and the V=O equatorial planes. The dihedral angle values for each monomer unit are very similar to each other. In all monomeric units, the planes from two chelate rings (5-membered and 6-membered) are nearly coplanar but form dihedral angles ranging from 75.7 to 86.1º with the equatorial plane. The plane from the remaining 6-membered chelate ring is almost coplanar with the equatorial plane. This is in accordance with the *cis*-β geometry adopted by each monomer unit, which coincides with the geometry predicted for the parent $V^{IV}O$(salan) compound *S,S*-**36** in solution by EPR analysis. All 5-membered chelate rings in *S,S*-**36b** adopt the δ-conformation.

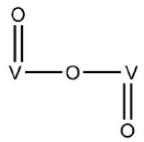

anti-linear

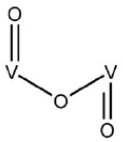

anti-angular

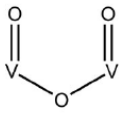

syn-angular

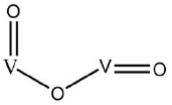

twist-angular

Figure 4.30. The possible configurations of a [$V^{V}O(\mu$-O)$V^{V}O$] core in complexes consisting of single ligand-sharing octahedral $V^{V}O$ centers.

Intramolecular N_{amine}-H•••O=V hydrogen bonding is present along with intermolecular N_{amine}-H•••$O_{alcohol}$ and $O_{alcohol}$-H•••$O_{phenolate}$ hydrogen bonding with the isopropanol solvent molecules.

Table 4.11. Dihedral angles formed by the chelate ring and the equatorial planes in *S,S*-**36b**.

S,S-**36b**					
5-membered			6-membered		
Chelate ring	Equatorial plane	θ (º)	Chelate ring	Equatorial plane	θ (º)
V(1)-N(1)-C(8)-C(15)-N(2)	O(1)-O(2)-N(2)-O(7)	85.2	V(1)-O(2)-C(28)-C(23)-C(22)-N(2)	O(1)-O(2)-N(2)-O(7)	17.8
			V(1)-O(1)-C(1)-C(6)-C(7)-N(1)	O(1)-O(2)-N(2)-O(7)	75.7
V(2)-N(3)-C(43)-C(36)-N(4)	O(4)-O(7)-N(4)-O(5)	84.7	V(2)-O(5)-C(56)-C(51)-C(50)-N(4)	O(4)-O(7)-N(4)-O(5)	16.7
			V(2)-O(4)-C(29)-C(34)-C(35)-N(3)	O(4)-O(7)-N(4)-O(5)	78.5
V(3)-N(5)-C(64)-C(71)-N(6)	O(8)-O(9)-N(6)-O(14)	83.1	V(3)-O(9)-C(84)-C(79)-C(78)-N(6)	O(8)-O(9)-N(6)-O(14)	16.7
			V(3)-O(8)-C(57)-C(62)-C(63)-N(5)	O(8)-O(9)-N(6)-O(14)	82.7
V(4)-N(7)-C(92)-C(99)-N(8)	O(11)-O(12)-N(8)-O(14)	85.42	V(4)-O(12)-C(112)-C(107)-C(106)-N(8)	O(11)-O(12)-N(8)-O(14)	14.0
			V(4)-O(11)-C(85)-C(90)-C(91)-N(7)	O(11)-O(12)-N(8)-O(14)	86.1

The ORTEP diagram for *R,R*-**45b** (see Figure 4.31) shows a structure with many similarities with the one obtained for *S,S*-**36b**. *R,R*-**45b** also consists in a dimeric molecular structure with each monomer unit bridged by a single μ-oxo ligand. The asymmetric unit of *R,R*-**45b** contains a single dimeric molecule and two DMF solvent molecules. *R,R*-**45b** crystallizes in the monoclinic system, space group $P2_1/c$, a centrosymmetric space group. This indicates that both *R,R* and *S,S* enantiomers of **45b** are co-crystallized, as a result of an incomplete diamine resolution. Here the V^V centers also adopt distorted octahedral geometries with the ligand coordinated through two $O_{phenolate}$ and two N_{amine} donors in a *cis*-β fashion and the oxo and μ-oxo ligands completing the coordination sphere. The selected parameters for the structure of *R,R*-**45b** are listed in Table 4.12.

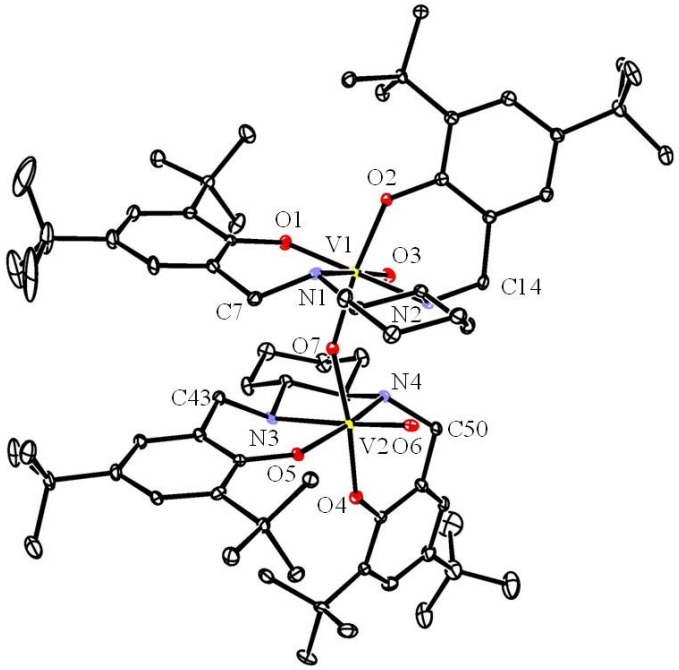

Figure 4.31. ORTEP-3 diagram of *R*,*R*-**45b**, using 30 % probability level ellipsoids. The hydrogen atoms and DMF solvent molecules were omitted for clarity.

Table 4.12. Selected bond lengths and angles for *R*,*R*-**45b**.

R,*R*-**45b**			
Bond lengths (Å)		Bond angles (º)[a]	
V(1)-O(1)	1.836(3)	O(1)-V(1)-O(3)	103.5(1)
V(1)-O(2)	1.904(3)	O(2)-V(1)-O(3)	95.5(1)
V(1)-O(3)	1.627(3)	O(3)-V(1)-N(1)	172.8(1)
V(1)-O(7)	1.842(3)	O(3)-V(1)-N(2)	95.1(1)
V(1)-N(1)	2.278(4)	O(3)-V(1)-O(7)	97.4(1)
V(1)-N(2)	2.146(3)	O(6)-V(2)-O(4)	97.5(1)
V(2)-O(4)	1.932(3)	O(6)-V(2)-O(5)	103.4(1)
V(2)-O(5)	1.827(3)	O(6)-V(2)-O(7)	98.0(1)
V(2)-O(6)	1.627(3)	O(6)-V(2)-N(3)	173.0(1)
V(2)-O(7)	1.805(3)	O(6)-V(2)-N(4)	94.8(2)
V(2)-N(3)	2.302(4)	V(1)-O(7)-V(2)	150.5(2)
V(2)-N(4)	2.132(4)		
N(1)-C(7)	1.483(5)		
N(2)-C(14)	1.489(6)		
N(3)-C(43)	1.494(6)		
N(4)-C(50)	1.508(6)		

The two V=O bonds, V(1)-O(3) and V(2)-O(6) have 1.627(3) Å in length, typical in V^{V}=O double bonds. The μ-oxo bonds V(1)-O(7) and V(2)-O(7) are comparatively longer with 1.842(3) and 1.805(3) Å, respectively, resultant of a lower π character. The

μ-oxo bond angles in *R,R*-**45b** are comparable to those observed for *S,S*-**36b**, with V(1)-O(7)-V(2) 150.05(2)º.

Similarly to *S,S*-**36b**, *R,R*-**45b** adopts a *twist-angular* configuration with the planes containing V(1)-O(3) and V(2)-O(6) forming a dihedral angle of 86.7º.

Table 4.13 lists the dihedral angles formed by the best planes containing the 5- and 6-membered chelate rings and the V=O equatorial planes. The dihedral angle values for each monomer unit are very similar to each other and comparable to the angles observed in *S,S*-**36b**. Near coplanarity of the planes from two chelate rings (5-membered and 6-membered) is also observed, with each forming dihedral angles ranging from 72.8 to 85.0º with the equatorial plane. The plane from the remaining 6-membered chelate ring is almost coplanar with the equatorial plane. These dihedral angles are in accordance with the *cis*-β geometry adopted by each monomer unit. However, EPR analysis of the reduced version of *R,R*-**45b** in solution predicted a *cis*-α geometry. Because the structure crystallized in a centrosymmetric space group, both δ and λ chelate ring conformations are present in *R,R*-**45b**.

Table 4.13. Dihedral angles formed by the chelate ring and the equatorial planes in *R,R*−**45b**.

R,R-**45b**					
5-membered			6-membered		
Chelate ring	Equatorial plane	θ (º)	Chelate ring	Equatorial plane	θ (º)
V(1)-N(1)-C(8)-C(13)-N(2)	O(1)-O(2)-N(2)-O(7)	85.0	V(1)-O(2)-C(20)-C(15)-C(14)-N(2)	O(1)-O(2)-N(2)-O(7)	17.4
			V(1)-O(1)-C(1)-C(6)-C(7)-N(1)	O(1)-O(2)-N(2)-O(7)	72.8
V(2)-N(3)-C(44)-C(49)-N(4)	O(4)-O(7)-N(4)-O(5)	83.8	V(2)-O(4)-C(56)-C(51)-C(50)-N(4)	O(4)-O(7)-N(4)-O(5)	10.7
			V(2)-O(5)-C(37)-C(42)-C(43)-N(3)	O(4)-O(7)-N(4)-O(5)	76.5

Intramolecular N_{amine}-H•••O=V hydrogen bonding is present along with intermolecular N_{amine}-H•••O_{DMF} hydrogen bonding with the DMF solvent molecules.

4.2.5. Characterization by Mass spectrometry

ESI-MS studies were conducted with $V^{IV}O$(salan) compounds *S,S*-**34** and *S,S*-**36** in acetonitrile. Both compounds were left to oxidize in solution prior to analysis to avoid the appearance of polymeric $V^{IV}O$ species and facilitate the preservation of any resultant μ-oxo species.

In the case of *S,S*-**34** (see Figure 4.32), it is possible to observe the ligand as a L^+ species (L=salan, m/z= 326.9), a $[VOL]^+$ species (m/z= 390.8) and its sodium adduct $[VOLNa]^+$ (m/z= 412.6). Minor peaks include a sodium adduct of a dinuclear $[V_2O_2L_2Na]^+$ species (m/z= 801.8) indicating that $V^{IV}O$ species are still present.

The ESI-MS spectrum of *S,S*-**36** is comparatively simple (see Figure 4.33). It is possible to observe a $[VOL]^+$ species (m/z= 489.0) and its sodium adduct $[VOLNa]^+$ (m/z= 512.0). The VOL aggregates observed in solutions of *S,S*-**34** are not seen in this case. No μ-oxo species were detected in both cases.

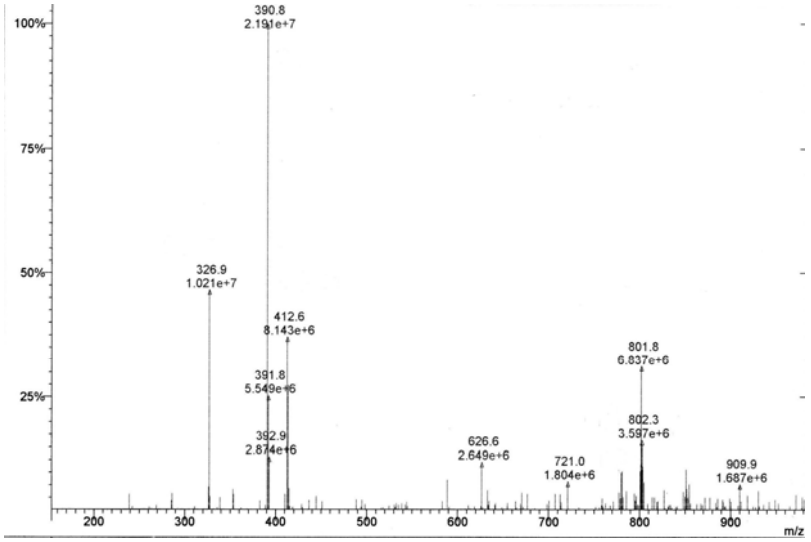

Figure 4.32. ESI-MS spectrum of *S,S*-**34** in acetonitrile.

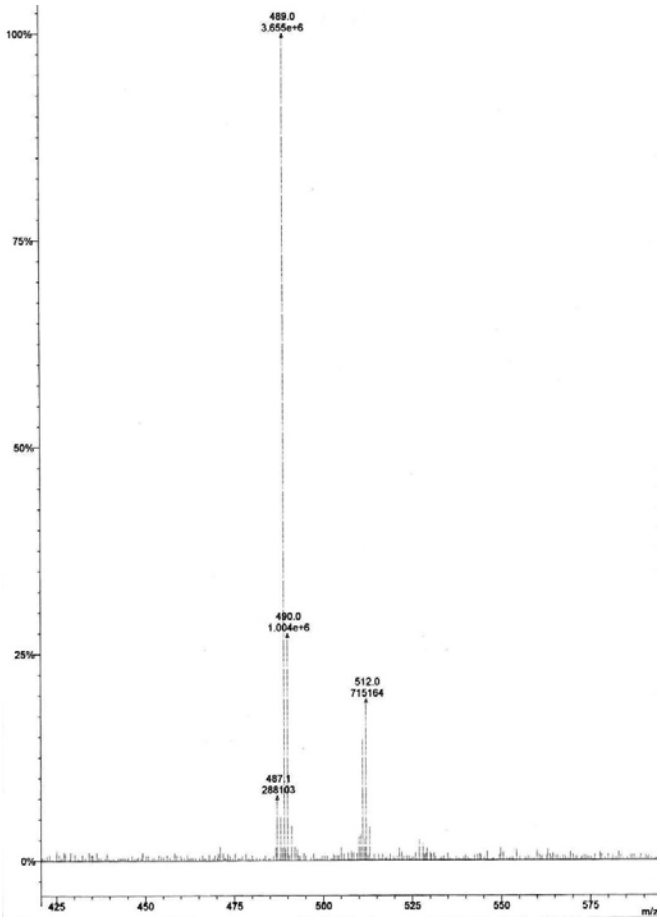

Figure 4.33. ESI-MS spectrum of *S,S*-**36** in acetonitrile.

4.2.6. Characterization by Infrared spectroscopy

One of the most relevant information given by Infrared spectroscopy (FT-IR) for $V^{IV}O$(salen) and $V^{IV}O$(salan) compounds is the V=O bond stretching frequency. Most of the prepared $V^{IV}O$(salen) compounds were found to be monomeric in the solid state and all exhibited a ν(V=O) band at *ca*. 980 cm^{-1}. In contrast, the $V^{IV}O$(salan) compounds, all exhibited a ν(V=O) band at *ca*. 840-890 cm^{-1}, which is indicative of polymeric V=O•••V=O species. The binding of a O_{oxo} *trans* to a V=O bond causes a lengthening and subsequent weakening of that bond. The result is a shift of the corresponding stretching frequency to a lower wavenumber. The main IR stretching frequencies are listed in Table 4.14.

Table 4.14. IR stretching frequencies for the prepared $V^{IV}O$(salen) and $V^{IV}O$(salan) complexes.

Stretching mode	*R,R*-**33**	*S,S*-**34**	*S,S*-**35**	*S,S*-**36**	*R,R*-**37**
			Wavenumber (cm^{-1})		
ν(N-H)		3241		3427	
ν(C=N)	1620		1606		1626
ν(C-O)	1200	1266	1201	1267	1266
ν(V=O)	990	879	983	882	888
	R,R-**38**	*S,S*-**39**	*S,S*-**40**	*S,S*-**43**	*S,S*-**45**
			Wavenumber (cm^{-1})		
ν(N-H)	3228		3242	3252	
ν(C=N)		1618			
ν(C-O)	1248	1249	1238	1241	1237
ν(V=O)	885	977	845	962	879

4.2.7. Magnetic properties

The magnetic properties of $V^{IV}O$(salan) compounds *S,S*-**34** and *S,S*-**36** were studied in the 4-300 K temperature range at 5*T* using the Faraday method. The paramagnetic susceptibility curves for *S,S*-**34** and *S,S*-**36** are shown in the figures below.

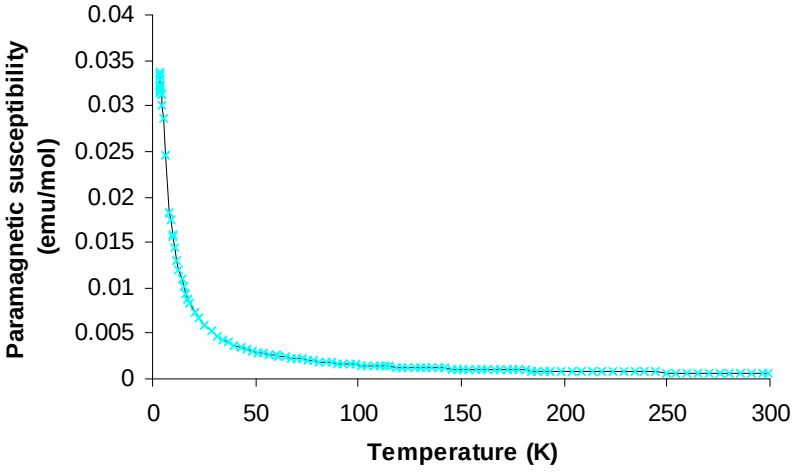

Figure 4.35. Paramagnetic susceptibility as a function of T for compound *S,S*-**34**.

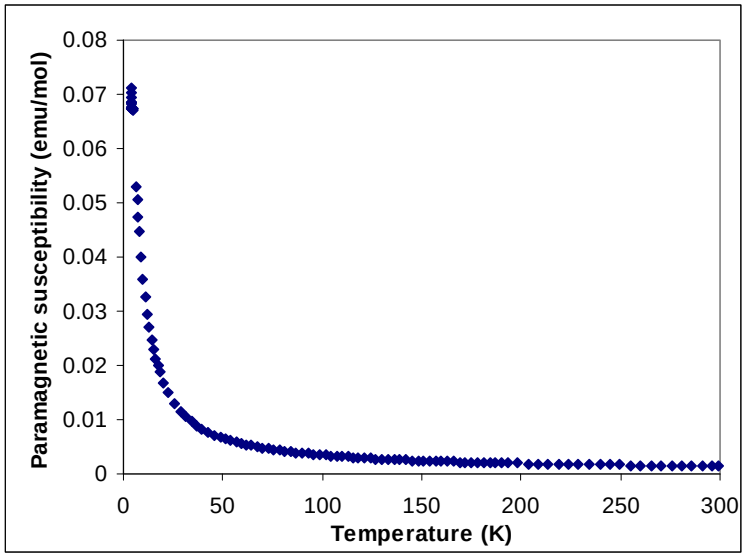

Figure 4.35. Paramagnetic susceptibility as a function of T for compound *S,S*-**36**.

For *S,S*-**34** the μ_{eff} values in the range 90-300 K are 1.1-1.2 μ_B (see Figure 4.34). The μ_{eff} values for *S,S*-**36** in the range 90-300 K are 1.7-1.9 μ_B (see Figure 4.35). Therefore, either strong antiferromagnetic interactions are operating in *S,S*-**34** (and not so strong in *S,S*-**36** possibly due to steric factors), or in the solid sample used for the magnetic measurements part of the V^{IV} oxidized to V^{V}. The Curie-Weiss plot does not give satisfactory results assuming all V atoms are V^{IV}. From the value of the Curie constant C = 0.115 emu K mol^{-1}, we would conclude that around ca. 55% of the V atoms have spin ½ (the rest should be V^{V}-centres).

4.2.8. Elemental Analysis

All the prepared $V^{VI}O$(salen) and $V^{VI}O$(salan) compounds gave elemental analysis results consistent with monomeric species having either water or alcohols as contaminants. The elemental analysis from $V^{V}O$(salan) compounds obtained from the slow oxidation of the parent $V^{IV}O$(salan) compounds also were consistent with dimeric species containing either water or alcohols as vestigial contaminants.

4.3. Catalytic applications

4.3.1. Asymmetric sulfoxidation of thioanisole

Similarly to what was done in Chapter 3, the prepared $V^{IV}O$(salan) compounds were screened for their catalytic potential in the asymmetric sulfoxidation of thioanisole under a variety of conditions. In all cases, the final products were either *R*- or *S*-methyl phenyl sulfoxide and/or the sulfone. The obtained results are summarized in Table 4.15.

Compound *S,S*-**40** gave the best results in terms of enantioselectivity and conversion (entries 19 to 25). *S,S*-**40** exhibited similar enantioselectivities to its simpler titanium analog *R,R*-**28** and performed better than its direct titanium analog *R,R*-**30**. The observed sulfone percentages are higher than those obtained with the titanium analogues, however. The use of acetonitrile (entry 27) or acetone (entries 28 and 29) as solvents had a substantially negative impact on the enantiomeric excess. This reduction in enantioselectivity is greater in acetonitrile, where a difference of 29% in enantiomeric excess is observed compared to the reaction in DCE (entry 24). Ethyl acetate can be used as a replacement for DCE, as the enantiomeric excess and sulfone percentages obtained using the former as solvent are comparable to those obtained in the latter, although the conversion is lower in ethyl acetate (entry 30). In addition, catalyst loadings can be reduced down to 0.5 mol% without any apparent detrimental effect to conversion and enantioselectivity, although reaction time is longer (entry 25). Conversely, compound *S,S*-**34**, bearing the simplest ligand, had a noticeable lower performance compared to the 3-methoxy substituted *S,S*-**40** (entries 2 to 12). In fact, lowering the temperature had little beneficial effect to enantioselectivity but a major negative effect on activity (entry 8). When *S,S*-**34** was used at ambient temperature in dichloromethane, conversion was 87% and enantiomeric excess was 21% after 6 hours, whereas in DCE at 0ºC the conversion did not go beyond 44% after 48 hours, with a slightly superior 26% in enantiomeric excess (entries 5 and 8). Significant reduction in enantioselectivity was observed when acetonitrile or acetone was used as solvent, regardless of the temperature at which the reaction was run (entries 9 to 11). Significant reduction in both conversion and enantiomeric excess values was observed with the reduction of catalyst loading (entries 2 to 4).

Table 4.15. Sulfoxidation of thioanisole with the VO^{IV}(salan) catalysts.[a]

Entry	Catalyst	Solvent	mol% catalyst	T(ºC)	t (h)	Conv (%)	ee (%)	sulfone (%)
1	*R,R*-**33**	DCE	1.0	0	19	99	10 (S)	8
2[d]	*S,S*-**34**	CH_2Cl_2	0.25	20	24	10	0	0
3[d]	*S,S*-**34**	CH_2Cl_2	0.5	20	24	7	3 (R)	0
4[d]	*S,S*-**34**	CH_2Cl_2	0.75	20	24	20	7(R)	0
5[e]	*S,S*-**34**	CH_2Cl_2	1.0	20	6	87	21(R)	22
6[e]	*S,S*-**34**	CH_2Cl_2	1.5	20	6	88	20(R)	12
7[e]	*S,S*-**34**	CH_2Cl_2	2.0	20	6	90	17(R)	11
8	*S,S*-**34**	DCE	1.0	0	48	44	26(R)	3
9	*S,S*-**34**	CH_3CN	1.0	20	4	81	0	9
10	*S,S*-**34**	$(CH_3)_2CO$	1.0	0	24	91	7(R)	9
11	*S,S*-**34**	$(CH_3)_2CO$	1.0	20	2	86	2(R)	7
12	*S,S*-**34**	CH_3CN	2.5	0	18	93	15(R)	18
13	*S,S*-**35**	DCE	1.0	0	19	99	26(S)	45
14[c]	*S,S*-**36**	CH_2Cl_2	2.5	20	5	99	8(S)	9
15	*S,S*-**36**	DCE	1.0	0	72	81	0	19
16	*R,R*-**37**	DCE	1.0	0	24	0	0	0
17	*R,R*-**38**	DCE	1.0	0	24	0	0	0
18[b]	*R,R*-**38**	$(CH_3)_2CO$	1.0	20	2	98	0	4
19	*S,S*-**39**	DCE	1.0	0	24	99	14(R)	32
20	*S,S*-**40**	DCE	1.0	0	18	96	50(R)	35
21	*S,S*-**40**	DCE	10.0	0	18	90	38(R)	22
22	*S,S*-**40**	DCE	5.0	0	18	92	39(R)	24
23	*S,S*-**40**	DCE	2.5	0	18	95	43(R)	29
24	*S,S*-**40**	DCE	1.0	0	18	99	41(R)	27
25	*S,S*-**40**	DCE	0.5	0	48	91	50(R)	28
26	*S,S*-**40**	DCE	0.25	0	48	0	0	0
27	*S,S*-**40**	CH_3CN	1.0	0	18	97	12(R)	20
28[b]	*S,S*-**40**	$(CH_3)_2CO$	1.0	0	24	78	25(R)	17
29[b]	*S,S*-**40**	$(CH_3)_2CO$	1.0	20	2	83	9(R)	9
30[b]	*S,S*-**40**	AcOEt	1.0	0	24	72	36(R)	28
31	*R,R*-**41**	DCE	1.0	0	24	84	0	16
32	*R,R*-**42**	DCE	1.0	0	24	96	19(S)	47
33	*R,R*-**42**	$(CH_3)_2CO$	1.0	0	24	80	17(S)	17
34[b]	*S,S* -**43**	DCE	1.0	0	24	55	2(S)	0
35[b]	*R,R*-**44**	DCE	1.0	0	24	42	13(R)	3
36[b]	*R,R*-**44**	$(CH_3)_2CO$	1.0	0	24	88	7(S)	9
37[b]	*R,R*-**44**	$(CH_3)_2CO$	1.0	20	2	83	3(S)	6
38	*R,R*-**45**	DCE	1.0	0	48	91	14(S)	30
39[b]	*R,R*-**45**	$(CH_3)_2CO$	1.0	0	24	24	18(S)	2
40[b]	*R,R*-**46**	$(CH_3)_2CO$	1.0	0	24	0	0	0

[a]Conditions: nS=1 mmol, nH_2O_2:nS=1.5. [b] nH_2O_2:nS = 1.2. [c] Slow addition of oxidant. [d] 15% aqueous H_2O_2 was used as oxidant. [e] 20% aqueous H_2O_2 was used as oxidant.

Again, the phenol moiety substituents appear to play an important role in the catalyst performance. The results obtained with $V^{IV}O$(salan) compounds *S,S*-**34** and *S,S*-**40** indicate that a methoxy group in the 3-position of the ligand phenolate moieties promotes the enantioselective process, as opposed to what was observed with their direct Ti^{IV}(salan) analogues *R,R*-**28** and *R,R*-**30**. Interestingly, the $V^{IV}O$(salan) compound *S,S*-

44 bearing a methoxy group in the 5-position performed similarly to *S,S*-**34** in terms of enantioselectivity, giving very similar results under the same conditions but with much shorter reaction times in DCE (entries 35 to 37). This clearly indicates the importance of a methoxy group in the 3-position when $V^{IV}O$(salan) compounds are concerned. When the methoxy group was replaced with a bulkier ethoxy group, a significant reduction in enantioselectivity was observed (entries 32 and 33). When bulkier *tert*-butyl groups were present in the phenolate 3-position, enantioselectivity dropped even further, along with reactivity (entries 36 and 37). The trends in enantioselectivity and reactivity are in line with the results reported by Fujita and co-workers.[4] The likelihood of a $V^{IV}O$ center coordinating to a ($O_{phenol,}$ $O_{phenol,}$ O_{ether}, O_{ether}) donor group in compound *S,S*-**40** is reduced considering that high valent vanadium is not as oxophilic as a high valent titanium. Also, the results obtained from EPR analysis of the $V^{IV}O$(salan) precatalysts provide reliable information to discard that possibility. The methoxy group in the phenolate 3-position, in addition to being polar and relatively small, may contribute to a greater stability of *S,S*-**40** in face of hundred-fold concentrations of oxidant by increasing the electron density of the aromatic rings, thus making the phenolate donor a stronger Lewis base capable of establishing a stronger bond to a electron-poor $V^{V}O$ center. It is known that V^{IV} and V^{V} compounds tend to undergo ligand exchange in the presence of high peroxide concentrations.[46] A salan-type compound with electron-rich phenol moieties may indeed bind more strongly to an electron-poor $V^{V}O$ center, slowing down the aforementioned ligand exchange. The difference in enantioselectivities between *S,S*-**40**, *S,S*-**42**, *R,R*-**44** and *R,R*-**45** is also an indication that the steric hindrance and polarity at the phenolate 3-position are as important as the electronic activation of the phenolate moieties.

The pyridoxal derivatives proved far too insoluble in DCE to yield any results (entries 16 and 17). Additionally, complete catalyst decomposition was apparent after the 24h reaction period. Nevertheless, high conversion was obtained when acetone was used as solvent, though there was no enantiomeric excess (entry 18). Similarly, compound *R,R*-**46** proved too insoluble to allow any catalytic experiment.

Diamine backbone influence was also tested. Compounds based on 1,2-diphenylethane-1,2-diamine exhibited significantly lower enantioselectivities and activities compared to those derived from cyclohexane-1,2-diamine (entries 13 to 15).

Kinetic resolution of racemic methyl phenyl sulfoxide was also carried out to ascertain the role of the sulfoxide oxidation in the observed overall enantiomeric excesses. Table 4.16 lists the results obtained for *S,S*-**34**, *S,S*-**35** and *S,S*-**40**.

Table 4.16. Kinetic resolution of methyl phenyl sulfoxide with *S,S*-**34**, *S,S*-**35** and *S,S*-**40**.[a]

Entry	Catalyst	t (h)	Conv (%)	ee (%)	sulfone (%)
1	*S,S*-**34**	24	44	9(R)	44
		48	61	25(R)	61
2	*S,S*-**35**	24	45	18(R)	45
		48	65	29(R)	65
3	*S,S*-**40**	24	44	6(S)	44
		48	58	11(S)	58

[a]Conditions: 1 mol% catalyst, 1 mmol thioanisole , nH_2O_2:nS=1.5, T=0ºC, 4 mL DCE, single addition of aqueous H_2O_2 20% (w/v).

Generally, the enantiomeric excesses are very low after 24 hours. The *ca*. 44% conversions to sulfone observed after 24 hours in the three cases indicate that the oxidation of sulfoxide to sulfone is a slower process than the oxidation of thioether to sulfoxide. Even after a 48 hour period the reactions did not reach completion. This stands in contrast with what was observed in the Ti^{IV}(salan) catalyzed sulfoxide resolution, where 47% conversion of the sulfoxide to sulfone was reached after 1 hour at 0ºC in DCE with only 0.5 equivalents of oxidant, but with a 34% enantiomeric excess.

The tandem thioether and sulfoxide oxidation processes observed in the Ti^{IV}(salan) catalyzed sulfoxidations, discussed in Chapter 3, are also present in these systems, although the low 24 hour period enantiomeric excesses obtained in the sulfoxide resolution show that the sulfoxide oxidation process may have a much lesser impact. This is particularly true for *S,S*-**40**, where only 11% enatiomeric excess was obtained even after a 48 hour period (entry 3).

As expected, the V^{IV}O(salan) compounds *S,S*-**34**, *S,S*-**40** and *S,S*-**42** proved superior to their parent V^{IV}O(salen) compounds *R,R*-**33**, *S,S*-**39** and *S,S*-**41** in terms of enantioselectivity. The increase in enantioselectivity may be due to the increased likelihood of the salan catalysts to adopt the highly asymmetric, chiral-at-metal *cis*-α and

cis-β geometries whereas the salen catalysts favor the *trans* geometries lacking chirality at the metal centre and are less stable compound.

4.3.2. Oxidation of styrene

The $V^{IV}O$(salen) compounds *R,R*-**33**, *S,S*-**35** and the $V^{IV}O$(salan) compounds *S,S*-**34** and *S,S*-**36** were screened for their catalytic potential in the oxidation of styrene with hydrogen peroxide. The stereoselectivity of the catalysts employed in this reaction was not an objective. In fact, the reaction does not yield the corresponding styrene oxide but double bond cleavage and hydroxylation products such as benzaldehyde (bza), benzoic acid (bzac), phenylacetaldehyde (phaa) and 1-phenylethane-1,2-diol (phed) were obtainrd (Scheme 4.6). Of these, only 1-phenylethane-1,2-diol possesses stereogenic centers. All the obtained results are summarized in Table 4.17.

Compounds *R,R*-**33,** *S,S*-**34** and *R,R*-**38** exhibit the highest catalytic activity with *ca*. 70% conversion of styrene after 5h, while *S,S*-**35**, *S,S*-**36** and *R,R*-**37** gave 52, 58 and 65% conversion respectively. Noteworthy is the better performance of the $V^{IV}O$(salan) compounds compared to their parent $V^{IV}O$(salen) compounds.

The cyclohexane-1,2-diamine derived catalysts exhibit higher activity but lower selectivity than the 1,2-diphenylethane-1,2-diamine derived catalysts, with the exception of the pyridoxal derived catalysts which displayed high activities and selectivities towards the formation of benzaldehyde (entries 3 and 6).

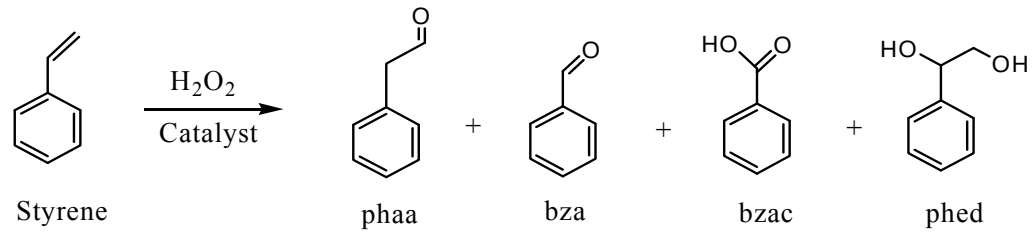

Scheme 4.6. V^{V}-(salan)-promoted styrene oxidation.

Table 4.17. Oxidation of styrene with *R,R*-**33**, *S,S*-**34**, *S,S*-**35**, *S,S*-**36**, *R,R*-**37** and *R,R*-**38**.[a]

Entry	Catalyst	Conv (%)	TOF (h^{-1})	Selectivity (mol%)[b]			
				phaa	bza	bzac	phed
1	*R,R*-**33**	69	6.9	13	59	21	7
2	*S,S*-**35**	52	5.2	2	91	5	2
3	*R,R*-**37**	65	6.5	5	85	8	2
4	*S,S*-**34**	71	7.1	16	41	34	4
5	*S,S*-**36**	58	5.8	10	66	13	11
6	*R,R*-**38**	76	5.6	6	92	1	1

[a]Conditions: 2 mol% catalyst, 5 mmol styrene , nH_2O_2:nS=2.0, T=80ºC, t=5h, 10 mL CH_3CN, single addition of aqueous H_2O_2 30% (w/v). [b] phaa = phenylacetaldehyde; bza = benzaldehyde; bzac = benzoic acid; phed = 1-phenylethane-1,2-diol.

The absence of epoxide may be due not only to the high reactivity of monosubstituted epoxides but also to the presence of water and relatively high temperatures. Under these conditions, the monosubstituted epoxide may be formed as a short-lived species prone to a ring-opening nucleophilic attack by water. This nucleophilic attack by water may indeed be behind the presence of 1-phenylethane-1,2-diol. Phenylacetaldehyde may be formed by cleavage of a hydroperoxystyrene intermediate. The presence of benzaldehyde and benzoic acid as major products may be due to either the direct oxidative cleavage of the alkene or epoxide[32] or to the glycol cleavage of 1-phenylethane-1,2-diol.[33] The preferred reaction pathways clearly involve C=C bond cleavage.

4.3.3. Oxidation of cyclohexene

Under similar conditions as those used for the oxidation of styrene, compounds *R,R*-**33,** *S,S*-**34**, *S,S*-**35**, *S,S*-**36**, *R,R*-**37** and *R,R*-**38** were tested for their catalytic activity in the oxidation of cyclohexene. Again, the reaction gave multiple products resultant from double bond cleavage and hydroxylation. In addition to ciclohex-2-enol (chol), ciclohex-2-enone (chone) and cyclohexane-1,2-diol (chdol), the epoxide (cho) is also present (Scheme 4.7). Of these, only cyclohexane-1,2-diol possesses enantiomers. The obtained results are summarized in Table 4.18.

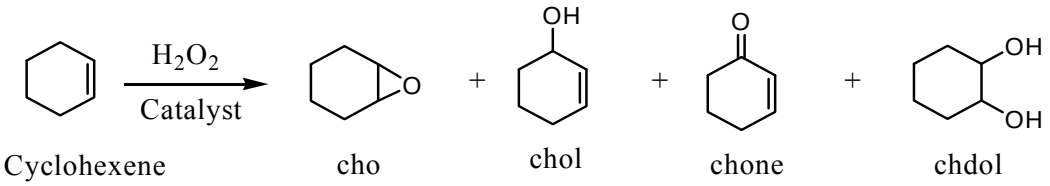

Scheme 4.7. V^{V}-(salan)-promoted cyclohexene oxidation.

Table 4.18. Oxidation of cyclohexene with *R,R*-**33**, *S,S*-**34**, *S,S*-**35**, *S,S*-**36**, *R,R*-**37** and *R,R*-**38**.[a]

Entry	Catalyst	Conv (%)	TOF (h^{-1})	Selectivity (mol-%)[b]			
				cho	chdol	chol	chone
1	*R,R*-**33**	62	6.2	9	65	20	6
2	*S,S*-**35**	55	5.5	5	65	22	8
3	*R,R*-**37**	71	7.1	7	77	14	9
4	*S,S*-**34**	66	6.6	6	76	15	3
5	*S,S*-**36**	59	5.9	8	66	19	7
6	*R,R*-**38**	79	7.9	5	79	5	10

[a]Conditions: 2 mol-% catalyst, 5 mmol cyclohexene , nH_2O_2:nS=2.0, T=80ºC, t=5h, 10 mL CH_3CN, single addition of aqueous H_2O_2 30% (w/v). [b] cho = 1,2-epoxycyclohexane; chol = cyclohex-2-enol; chone = cyclohex-2-enone; chdol = cyclohexane-1,2-diol.

Similarly to what was observed in the oxidation of styrene, the best results in terms of activity were obtained with the cyclohexane-1,2-diamine derived compounds (entries 1, 3, 4 and 6). The pyridoxal derived compounds *R,R*-**37** and *R,R*-**38** exhibited the highest activities and selectivity towards the formation of the dihydroxylated product, cyclohexane-1,2-diol (entries 3 and 6). Again, the $V^{IV}O$(salan) compounds *S,S*-**34**, *S,S*-**36** and *R,R*-**38** exhibited superior activities and selectivities towards the formation of cyclohexane-1,2-diol over their $V^{IV}O$(salen) versions. Contrary to what was observed with styrene, C=C bond cleavage does not occur with cyclohexene. Terminal alkenes are typically more reactive than internal alkenes and the corresponding epoxides follow the same trend. Ring-opening hydroxylation resultant from nucleophilic attack of water to the epoxide ring appears to be the preferred reaction pathway. This explains why cyclohexane-1,2-diol is the major product in all cases. Despite the tendency for hydroxylation, the disubstituted 1,2-epoxycyclohexane predictably exhibits some resistance to nucleophilic attack due to steric hindrance. The significant percentages of

allylic oxidation products cyclohex-2-enol and cyclohex-2-enone indicate C-H bond activation in addition to the epoxide hydroxylation pathways.

4.3.4. Oxidation of cumene

In light of the results obtained in the oxidation of cyclohexene, the C-H bond activation ability of compounds *R,R*-**33,** *S,S*-**34**, *S,S*-**35**, *S,S*-**36**, *R,R*-**37** and *R,R*-**38** was screened. The oxidation of cumene with hydrogen peroxide gave as final products acetophenone (acp), 2-phenylpropanal (ppa), 2-phenylpropan-2-ol (ppo) and the epoxide 1,2-epoxy-2-phenylpropane (mso) (Scheme 4.8). The obtained results are summarized in Table 4.19.

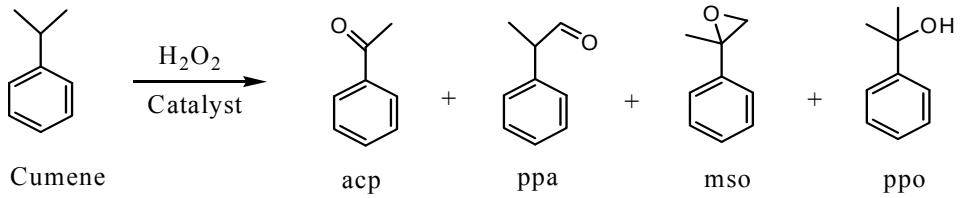

Scheme 4.8. V^{V}-(salan)-promoted cumene oxidation.

Table 4.19. Oxidation of cumene with *R,R*-**33**, *S,S*-**34**, *S,S*-**35**, *S,S*-**36**, *R,R*-**37** and *R,R*-**38**.[a]

Entry	Catalyst	Conv (%)	TOF (h^{-1})	Selectivity (mol%)[b]			
				acp	ppa	mso	ppo
1	*R,R*-**33**	35	2.1	71	19	12	8
2	*S,S*-**35**	38	2.3	56	23	15	6
3	*R,R*-**37**	42	2.5	63	18	9	3
4	*S,S*-**34**	33	2.0	68	25	5	12
5	*S,S*-**36**	32	1.9	59	17	10	14
6	*R,R*-**38**	39	2.3	65	21	8	19

[a]Conditions: 2 mol% catalyst, 3 mmol cumene , nH_2O_2:nS=3.0, T=80ºC, t=5h, 10 mL CH_3CN, single addition of aqueous H_2O_2 30% (w/v). [b] acp = acetophenone; ppa = 2-phenyl-2-propanal; mso = 1,2-epoxy-2-phenylpropane; ppo = 2-phenylpropan-2-ol.

All compounds exhibited moderate activities between 32 to 42% towards the oxidation of cumene. The major reaction product, acetophenone, indicates C-C bond

cleavage as the preferred reaction pathway. This C-C bond cleavage may occur by intermediate of the oxidative cleavage of 1,2-epoxy-2-phenylpropane (mso) or by oxidative C-C cleavage of 2-phenyl-2-propanal (ppa).[34] The epoxide itself may be resultant from the epoxidation of α-methylstyrene, which in turn is a hydrolysis product of the generated cumene hydroperoxide. The superior percentages of 2-phenyl-2-propanal (ppa) relative to 2-phenylpropan-2-ol also indicates a preference of the tested catalysts to promote C-H activation of the CH_3 groups over the benzylic CH group. In contrast to the previous reactions, the $V^{IV}O$(salen) compounds exhibit identical activities and selectivities to the $V^{IV}O$(salan) compounds. The tested compounds are therefore capable of C-H activation and functionalization although with moderate conversions.

4.3.5. Reactivity and mechanistic considerations

Reactivity studies with the prepared $V^{IV}O$(salan) compounds were made with the purpose of gaining insight into the mechanism of thioether and alkene oxidation and understand the factors that might affect the activity and enantioselectivity.

The spectroscopic data presented in the previous sections show that the $V^{IV}O$(salan) compounds readily undergo oxidation when in solution. The electronic absorption spectroscopy data, the data obtained from ^{51}V NMR and the data published in the literature indicate that the resulting oxidized species may be a VO^{3+} instead of a VO_2^+ species, though no definitive conclusions can be made.[4,12,13,14,19]

It was also necessary to assess the nature of the interaction of the prepared $V^{IV}O$(salan) compounds with the oxidant, hydrogen peroxide, used in all the catalytic experiments. ^{51}V NMR remains the best means to monitor the V^V species resultant from H_2O_2 oxidation.

One hour after the dissolution of *S,S*-**34** in methanol the UV-Vis spectrum displayed the two intense ligand-to-metal charge transfer (LMCT) bands at *ca*. 500 and 330 nm, previously observed also in DMSO solution, typical of phenolate-bound V^V species. Upon the successive addition of H_2O_2 equivalents, these LMCT bands gradually disappear accompanied with the loss of the intense dark-red coloration. Figure 4.36 shows the variation of the ^{51}V NMR chemical shifts given by *S,S*-**34** in methanol during

the addition of H_2O_2, which indicate a significant change in chemical shifts during the addition of H_2O_2.

Two peaks are observed after 24 hours after dissolution of *S,S*-**34** in methanol; a major peak at 488 ppm assigned to a methoxy species [V^VO{salan}(CH_3O)] and a minor one at -547 ppm assigned to a [V^VO{salan}$]_2O$ or a [V^VO_2{Hsalan}] species. After addition of a single equivalent of oxidant, a new peak at *ca*. -580 ppm arises. The new peak is assigned to a monoperoxovanadate species, probably [$V^VO(O_2)${salan}]$^-$ or [$V^VO(O_2)${Hsalan}].[35] As the oxidant is added a new and gradually more intense signal at -648 ppm appears. This signal remains after the addition of a large excess of H_2O_2 and it is assigned to the inorganic diperoxovanadates, probably [$V^VO(O_2)_2(H_2O)$]$^-$ resultant from ligand exchange.[36,46]

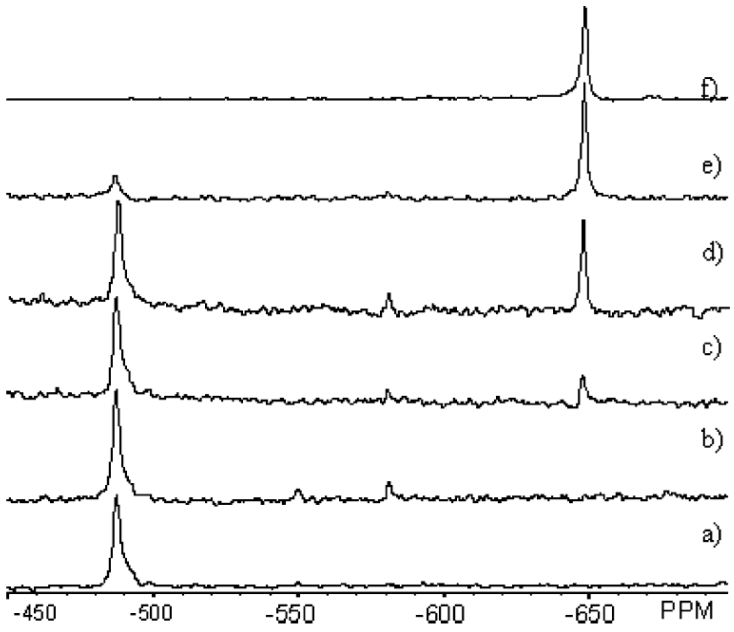

Figure 4.36. ^{51}V NMR spectrum of oxidized *S;S*-**34** in methanol. (a) 24h upon dissolution; (b) after addition of 1 equiv. of H_2O_2; (c) addition of 2 equiv. of H_2O_2; (d) addition of 4 equiv. of H_2O_2; (e) addition of 10 equiv. of H_2O_2; (f) addition of a large excess of H_2O_2.

The peak at -488 ppm becomes noticeably smaller after the addition of 10 equivalents of oxidant and disappears after the addition of a large excess. The sample color evolves from the typical dark red to orange and finally to yellow.

This dissociation phenomenon in the presence of high peroxide concentration may explain the moderate enantioselectivities observed in the asymmetric sulfoxidations. The

electron-poor $V^{V}O$ center prefers the coordination to peroxo ligands over the salan ligand, generating the achiral inorganic diperoxovanadate. The significant difference in activities and enantioselectivities between *S,S*-**34** and *S,S*-**40** indicates that the electron-rich phenolates of *S,S*-**40** may stabilize the complex against dissociation.

The $V^{IV}O$(salen) compounds are more resistant to oxidation when in solution. However, upon the addition of 0.5 equivalents of H_2O_2 to a methanolic solution of *R,R*-**33**, a peak of very low intensity appears at -570 ppm. This signal is assigned to the monoperoxocomplex $[V^{V}O(O_2)\{salen\}]^-$ or $[V^{V}O(O_2)\{Hsalen\}]$. With higher concentrations of oxidant, only the inorganic peroxovanadates at *ca*. -670 ppm are observed (see Figure 4.37). After a 24 hour period since the addition of oxidant, a ^1H NMR spectrum of the *R,R*-**33**/H_2O_2 solution was recorded and it revealed a sharp aldehyde proton signal at 10 ppm, which is indicative of decomposition by ligand hydrolysis (see Figure 4.38). However, no such signal was observed in the ^1H NMR spectrum of the previous *S,S*-**34**/H_2O_2 solution after 24 hours.

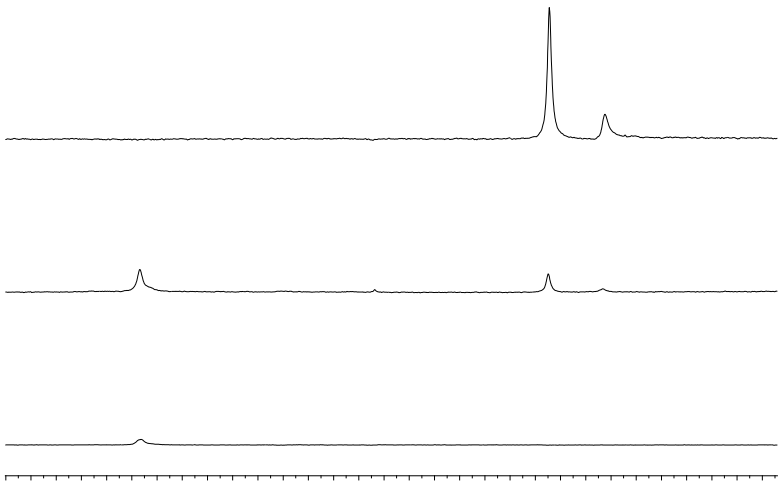

Figure 4.37. ^{51}V NMR spectrum of oxidized *R,R*-**33** in methanol. (a) after addition of 0.5 equiv. of H_2O_2; (b) addition of 1.5 equiv. of H_2O_2; (c) addition of 25 equiv. of H_2O_2.

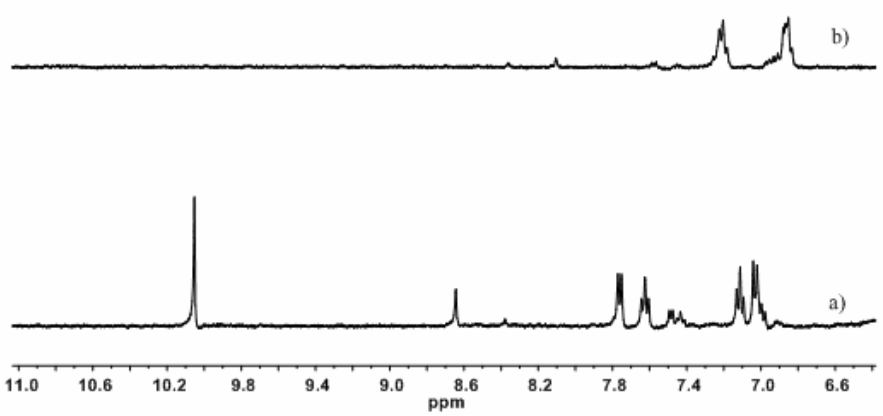

Figure 4.38. Aromatic zone of the ^{1}H NMR spectra of oxidized *R,R*-**33** (a) and *S,S*-**34** (b) in methanol after 24h after addition of H_2O_2.

Reactivity of *S,S*-**34** towards thioanisole and methyl phenyl sulfoxide was also assessed. ^{51}V NMR spectra of separate DCE solutions of oxidized *S,S*-**34** before and after addition of the thioether or the sulfoxide are shown in Figures 4.39 to 4.41.

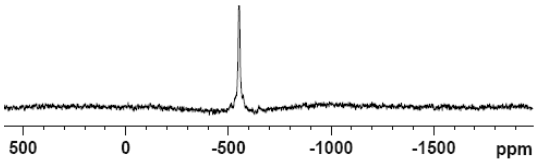

Figure 4.39. ^{1}H NMR spectrum of oxidized *S,S*-**34** in DCE after 24h.

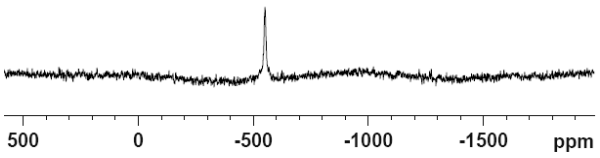

Figure 4.40. ^{1}H NMR spectrum of oxidized *S,S*-**34** in DCE after addition of 20 equivalents of thioanisole.

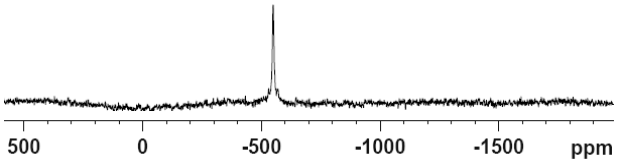

Figure 4.41. ^{1}H NMR spectrum of oxidized *S,S*-**34** in DCE after addition of 1 equivalent of methyl phenyl sulfoxide.

There is no apparent change of the main peak at -550 ppm after the addition of 20 equivalents of thioanisole. Coordination of the "soft" thioether sulfur to a "hard" $V^{V}O$ center should cause a significant downfield shift which in this case is not observed.[37] Either there is no interaction between the thioether and the $V^{V}O$ complex or if there is any interaction, it is tenuous and not observable in the NMR time scale.

The same is observed when the sulfoxide is present. Though the sulfoxide preferably coordinates through the oxygen atom, such coordination should cause some change in the chemical shifts.

The information obtained from these indicates that there is no direct coordination of the thioether sulfur donor atom or the sulfoxide oxygen atom to the metal center.

Instead, the mechanism can be primarily based on the interation of a monoperoxocomplex with the thioether substrate. A possible mechanism may be suggested based on the proposals of Pecoraro and co-workers for tetradentate V-nitrilotriacetate systems (see Figure 4.42).[38]

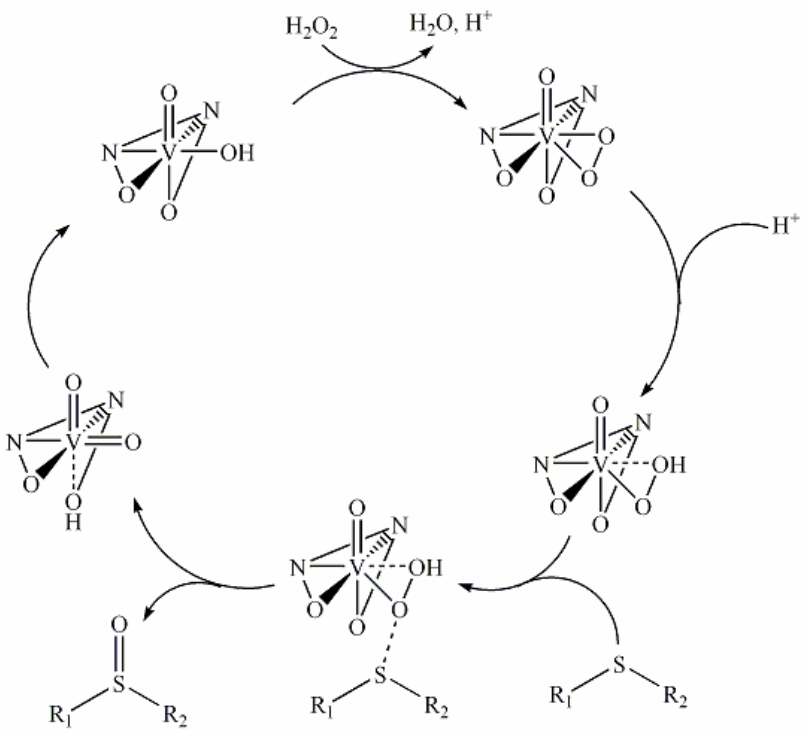

Figure 4.42. Possible mechanism for the $V^{V}O$(salan) catalyzed thioether sulfoxidation.

The mechanism considers the formation of a transient hydroperoxo $V^{V}O$ species. The protonation of one of the peroxo ligand oxygen donors enhances the electrophilicity of the other metal-bound peroxo oxygen atom. This may translate into a lowered activation barrier for the S_n2-type reaction between the peroxo species and the sulfur nucleophile.

No Density Functional Theory (DFT) calculations were made so far to verify the plausibility of the mechanism proposed above in light of the obtained spectroscopic data. In the present system the structure of the hydroperoxo complex $V^{V}O(OOH)(salan)^{+}$ was never refined in the calculations described below. Indeed, when trying to refine the structure of such complex, a monodentate species was obtained (see below). However, DFT calculations were carried out for the $V^{V}O(salan)$ catalyzed oxidation of alkenes and the three possible pathways are shown in Figure 4.43.[58]

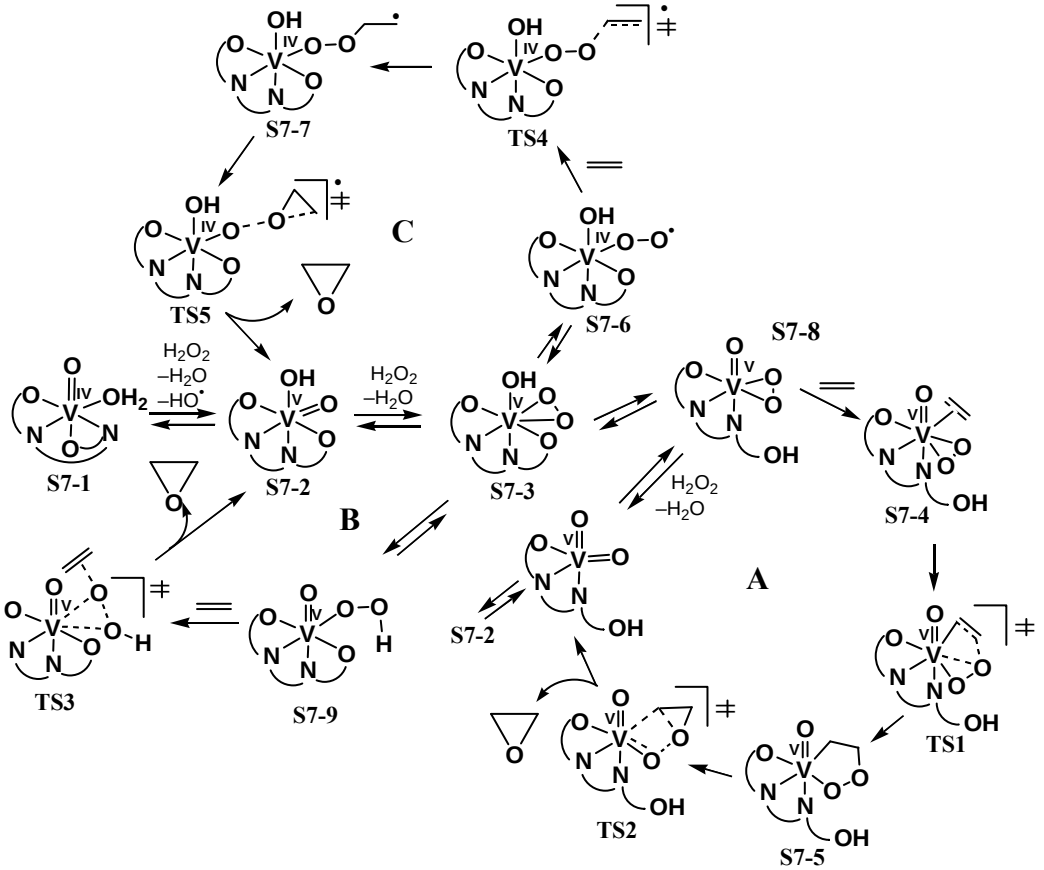

Figure 4.43. Outline of plausible mechanisms of alkene oxidation catalyzed by the $V^{V}O(salan)$ complexes. A separate numbering of the structures is used in this scheme for the model complexes starting with **S7-**, and for the calculated transition states starting with **TS-**.

To elucidate which of the proposed pathways (A), (B) and (C) is the most likely, quantum-chemical calculations for the model complexes with the ligand L being $\{CH_2\text{-}NH\text{-}CH_2\text{-}CH{=}CH\text{-}O^-\}_2$ were made to determine the most favorable geometric isomer of the transition species **TS**.[39] To simplify the calculations, the alkene substrate was considered to be ethylene (see Figure 4.44).

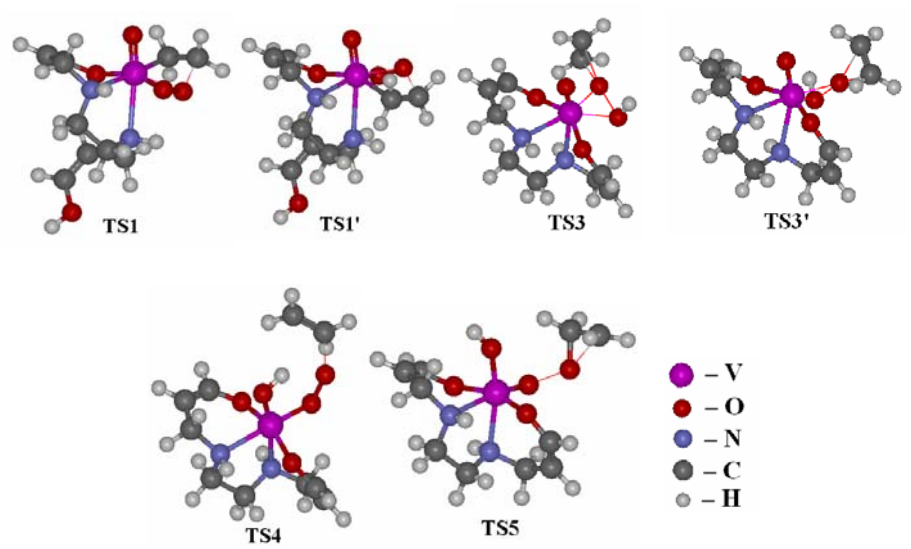

Figure 4.44. Equilibrium geometries of the calculated transition states included in Figure 4.43.

In the first step of the reaction, the starting $V^{IV}O$ complex **S7-1** is oxidized by H_2O_2 to a $V^{V}O$ complex **S7-2** which further reacts with the oxidant to generate the peroxo intermediate **S7-3**.[40,41] The next stage involves the epoxidation of the C=C double bond by the peroxo intermediate **S7-3**, a process that can follow any of the proposed pathways (A), (B) and (C).

Pathway (A) is a Mimoun-type mechanism which involves the coordination of an alkene molecule to the metal center, followed by the formation of a peroxometallocyclic intermediate **S7-5**. This intermediate decomposes into the epoxide and the $V^{V}O$ complex **S7-2**. The generation of intermediates **S7-4** and **S7-5** and transition state **TS1** requires the liberation of a coordination site by means of protonation and decoordination of an oxygen donor atom of the ligand.[39] It may be assumed that a proton migration from the OH

ligand to one of the ligand oxygen donors occurs, prompting the aforementioned decoordination and the formation of an additional V=O double bond. The calculations also revealed that **TS1** with the oxygen donor atoms of both the L and alkylperoxo ligands being in *trans* position is more stable by 1.9 kcal mol^{-1} than **TS1'** with the said oxygen donor atoms in *cis* position (see Figure 4.44). The apparent activation energy (E_a^{ap}) for **TS1** relative to complex **S7-3** is 32.7 kcal mol^{-1}.

The second pathway (B) is a Sharpless-type mechanism that predicts a concerted one-step epoxidation process where a direct attack of the alkene on the peroxo ligand occurs. Intermediates **S7-3** and **S7-9** may start the reaction.[42] The calculations indicate that this pathway is energetically more favorable than pathway (A) by 2.9 kcal mol^{-1}. The two transition states **TS3** and **TS3'** corresponding to *anti* and *syn* attack by the alkene to the hydroperoxo ligand in **S7-9** have very similar energies, differing only by 0.3 kcal mol^{-1}. The E_a^{ap} for **TS3** relative to complex **S7-3** is 24.5 kcal mol^{-1}, making this pathway significantly more likely than pathway (A).

The third pathway (C) is a mechanism based on the generation of diradical vanadium-peroxo complex **S7-6** followed by an attack of the alkene and formation of the diradical alkylperoxo intermediate **S7-7**.[43] The second step of this mechanism is found to be rate limiting as **TS5** is 3.0 kcal mol^{-1} higher in energy than **TS4**. The E_a^{ap} for **TS5** relative to complex **S7-3** is 26.4 kcal mol^{-1}, slightly higher than the E_a^{ap} for pathway (B).

The above calculations suggest that the most probable route for alkene epoxidation is a Sharpless-type mechanism involving the hydroperoxo species **S7-9**.

The impact of the simplification introduced with the model ligand L $\{CH_2\text{-}NH\text{-}CH_2\text{-}CH{=}CH\text{-}O^-\}_2$ on the calculation results was also studied. The energy of the key species present on the most plausible pathways, (B) and (C), using a model ligand L $\{CH_2\text{-}NH\text{-}CH_2\text{-}(o\text{-}C_6H_4O^-)\}_2$ structurally closer to the salan ligands was calculated (see Figure 4.45).

For the Sharpless-type mechanism (B), the activation barrier of **TS3ph** relative to **S7-3ph** increases only by 0.6 kcal mol^{-1} compared to the activation barrier of **TS3** relative to **S7-3**. The diradical mechanism (C) sees no difference between the activation barriers of **TS5ph** relative to **S7-3ph** and **TS5** relative to **S7-3**. Also, the Sharpless-type mechanism remains the most favorable.

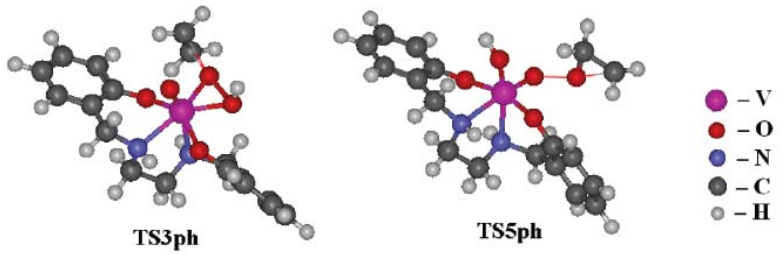

Figure 4.45. Equilibrium geometries of the calculated transition states bearing a model salan-type ligand.

DFT calculations were also made for a $V^{IV}O$ species **S8-1** containing an alkene molecule directly coordinated to the metal center (see Figure 4.46). Long V-C bond distances were obtained (2.649 and 2.677 Å) and a significant higher energy difference from the $V^{IV}O$ species **S7-1** was obtained. **S8-1** was 11 kcal mol^{-1} higher in energy than the water adduct **S7-1**. This corroborates why the *S,S*-**34**/styrene adduct was never detected in both EPR and ^{51}V NMR studies upon adding a hundred fold excess of styrene, regardless of the presence of hydrogen peroxide.

S8-1: $V^{IV}O(C_2H_4)(L)$

Figure 4.46. Equilibrium geometry of the calculated transition state containing an alkene molecule directly coordinated to the metal centre.

DFT calculations with the initial model system also indicate that a monodentate hydroperoxo species **S7-9** is clearly preferred over bidentate peroxo or hydroperoxo species **S8-2**.

4.4. Conclusions

Several $V^{IV}O$(salen) and $V^{IV}O$(salan) compounds were synthesized and characterized. All compounds were isolated as either green monomeric species in the case of the salen compounds or brown polymeric species in the case of the salan compounds. Characterization by ^{51}V-NMR of the $V^{V}O$(salan) compounds was possible after slow oxidation in solution of the corresponding $V^{IV}O$(salan) precursors. ^{51}V-NMR spectra showed a strong solvent influence on observed chemical shifts. Coordinating protic solvents such as methanol generate methoxy species such as $[V^{V}OL(CH_3O)]$ which yield signals with a downfield shift. Aprotic solvents appear to preserve the μ-oxo bond of a probable $[V^{V}OL]O_2$ species or the integrity of a $[V^{V}O_2HL]$ species, which yield signals with an upfield shift. Characterization by CD and UV-Vis spectroscopy of the prepared compounds was also made. Chirality in solution was confirmed by CD spectroscopy. The oxidized salan species obtained in solution were also characterized by CD and UV-Vis spectroscopy. Complementary analysis with the obtained ^{51}V-NMR data and comparison with literature results indicates that the resultant oxidized species may likely contain a VO^{3+} core instead of a VO_2^{+}. EPR analysis proved very useful in the characterization of the $V^{IV}O$(salen) and $V^{IV}O$(salan) compounds. With this technique, it was possible to confirm the successful preparation of these compounds and predict the respective geometries adopted in solution.

Important information was obtained from crystal structures of two V^{V}-salen compounds and two V^{V}-salan compounds. The obtained structures show dimeric μ-oxo species with VO^{3+} cores. Noteworthy is the fact that the salen compounds were obtained as their "half-salen" versions due to hydrolysis, whereas the salan compounds remained structurally intact.

Two $V^{IV}O$(salan) compounds were oxidized in solution prior to ESI-MS analysis. Very simple spectra were obtained. In one case, polymeric $V^{IV}O$ species were detected. The observed monomeric species yield little information about the nature of $V^{V}O$ species in solution.

The magnetic properties of two of the $V^{IV}O$(salan) compounds were studied but their tendency towards oxidation led to inconclusive results.

The prepared $V^{IV}O$(salen) and $V^{IV}O$(salan) compounds were employed as asymmetric sulfoxidation catalyst precursors, with hydrogen peroxide as the terminal oxidant. In general, high conversions and moderate enantioselectivities were obtained. Compound *S,S*-**40**, bearing methoxy groups in the phenolate 3-positions gave the best results in terms of activity and enantioselectivity at 0ºC in DCE. Reaction times using these catalysts under these conditions are much longer compared to the reaction times obtained with the Ti^{IV}(salan) analogues, taking between 24 to 48 hour to reach completion. In contrast, reaction times at ambient temperature are much faster, taking between 2 to 6 hours to reach completion, but enantioselectivities drop drastically. Catalyst loading of *S,S*-**40** as small as 0.5 mol-% can be used without negative impact to enantiomeric excess but reaction time is increased. Several solvents were tested to replace DCE and CH_2Cl_2. Reactions in acetone and acetonitrile gave high conversions and relatively low sulfone percentages, but enantiomeric excesses were low. Only ethyl acetate proved to be a suitable replacement for the chlorinated solvents. The reaction run in ethyl acetate, with *S,S*-**40** as catalyst, under the same conditions used for the reactions in DCE gave conversion and enantiomeric excess comparable to the best results obtained in DCE.

The results obtained for *S,S*-**34**, *S,S*-**40**, *R,R*-**44** and *R,R*-**45** demonstrated again the importance of the phenolate moiety substituents at the 3-position. As opposed to what was observed with the Ti^{IV}(salan) analogues, a methoxy group in this position proved beneficial and increased enantioselectivity, while increased steric bulk in this position was detrimental to catalyst performance. Kinetic resolution of racemic sulfoxide demonstrated also the existence of two oxidation processes occurring in tandem, but low enantioselectivities and moderate conversions were obtained after 24 and 48 hour periods in the presence of an excess of oxidant. This indicates that the process of sulfoxide oxidation to sulfone is slow and has minimal impact on overall enantiomeric excesses. Several $V^{IV}O$(salen) and $V^{IV}O$(salan) compounds were tested in the oxidation of styrene, cyclohexene and cumene with H_2O_2. In all cases, the epoxide was either absent or was a minor product. The reactions pathways preferred the formation of multiple products by C=C double bond oxidative cleavage in the case of styrene and cumene while the cyclohexene C=C double bond undergoes dihydroxylation.

Reactivity studies were made in an attempt to disclose aspects of the $V^{IV}O$(salan) catalyzed thioether oxidation. UV-Vis and ^{51}V NMR experiments showed that in the presence of high oxidant concentrations, the catalyst undergoes dissociation and form achiral inorganic diperoxovanadates. In addition, no interaction with the thioether substrate or the sulfoxide product was detected, which may imply that the oxidation mechanisms do not involve V-$S_{thioether}$ and V-$O_{sulfoxide}$ interactions. A possible mechanism was proposed but computational calculations need to be made to verify its plausibility in light of the obtained spectroscopic data.

DFT calculations were made to disclose the possible mechanism of $V^{IV}O$(salan) catalyzed alkene oxidation. These calculations indicate that a Sharpless-type mechanism is more likely, with no coordination of the olefin to the metal center. Instead, the peroxide coordinates and this is followed by protonation and attack by the alkene. EPR and ^{51}V NMR experiments showed that indeed no detectable coordination of styrene to the metal centre of either $V^{IV}O$(salan) and $V^{V}O$(salan) complexes occurs, regardless of presence or absence of oxidant. This reiterates the possibility of a Sharpless-type mechanism.

4.5. Experimental section

4.5.1. General considerations

Unless stated otherwise, all preparations were made under inert atmosphere. Subsequent manipulations after compound preparation did not require inert atmosphere techniques. All solvents and reagents were purchased from commercial suppliers and used as received.

4.5.2. Characterization techniques

4.5.2.1. Nuclear Magnetic Resonance Spectroscopy (NMR)

1D NMR (^{1}H, ^{51}V) spectra were recorded on Bruker Advance II+ 300 and 400 MHz (UltraShield Magnet) instruments at ambient temperature, unless stated otherwise. ^{1}H chemical shifts (δ) are expressed in ppm relative to Me_4Si. ^{51}V chemical shifts (δ) are

expressed in ppm relative to neat $VOCl_3$. Whenever calculation is possible, coupling constants *J* are given in Hz and multiplicities are presented as: br (broad), s (singlet), d (doublet), dd (double doublet), t (triplet), q (quartet), sept (septet) and m (multiplet).

4.5.2.2. Infrared (FT-IR), UV and Vis (UV-Vis) and Circular Dichroism (CD) Spectroscopy

FT-IR spectra were recorded in KBr using a *JASCO FT/IR-430* spectrometer. UV-Vis spectra were recorded using a Shimadzu U-2000 spectrophotometer. CD spectra were recorded using a Jasco J-720 Spectropolarimeter.

4.5.2.3. Elemental Analysis (EA)

Elemental analyses were carried out at *Laboratório de Análises* of *Instituto Superior Técnico,* using EA110 CE automatic analyzer Instruments. The results presented are the average values obtained from two independent determinations.

4.5.2.4. High performance liquid chromatography (HPLC)

The analysis of the products obtained in catalytic sulfoxidation reactions was done by HPLC using a Jasco system equipped with a Daicel Chiralpak IA column, a 870-UV Intelligent UV-Vis detector, two 880-PU Intelligent HPLC Pumps, a 2-line degasser 880-51 and a Rheodyne 725i injector (5 μL). The system uses Borwin software for data acquisition and analysis.

4.5.2.5. ESI-MS

The ESI mass experiments were made by Prof. Maria da Conceição Oliveira and Msc. Ana Dias at *Centro de Química Estrutural* of *Instituto Superior Técnico*. The ESI mass spectra were obtained on a Varian 500-MS LC Ion trap mass spectrometer equipped with an electrospray ion source, operated in the positive mode. The operated parameters

were optimized for maximum abundance of the ions of interest, and were as follows: ion spray voltage, +5 kV; capillary voltage, 80 V; RF loading, 90%. Nitrogen was used as nebulising and drying gas, at pressure of 35 and 15 psi, respectively; drying gas temperature, 350 ºC.

4.5.2.6. Electron paramagnetic resonance spectroscopy (EPR)

The electron paramagnetic resonance (EPR) spectra were recorded at 77 K (on glasses made by freezing solutions in liquid nitrogen) with a Bruker ESP 300E X-band spectrometer. The measured spectra were then simulated with the appropriate simulation software developed by Rockenbauer and Korecz.[21]

4.5.2.7. X-Ray crystallography

Single crystals suitable for X-ray diffraction crystallography were obtained as described in the ligand preparation methods. The data collection, structure solution and refinement for all the featured crystal structures in this Chapter were performed by Dr. Fernando Avecilla at the *Departamento de Química Fundamental* of *Universidade da Coruña*. X-ray data for *R,R*-**33,** *S,S*-**39**, *R,R*-**45** were collected on a Bruker Kappa X8 Apex CCD diffractometer and data for *S,S*-**36** were collected on a Bruker Smart 1000 CCD at room temperature. Reflections were measured from a hemisphere of data collected of frames, each covering 0.3º in ω. The reflections measured were corrected for Lorentz and polarization effects, and for absorption by semiempirical methods based on symmetry-equivalent and repeated reflections. Complex scattering factors were taken from the program package SHELXTL.[44] The absolute configuration was established by refinement of the enantiomorph polarity parameter.[45] The structures were solved by direct methods and refined by full-matrix least-squares methods on F^2. The non-hydrogen atoms were refined with anisotropic thermal parameters in all cases. The hydrogen atoms were left to refine freely.

Table 4.20. Crystal data, data collection and refinement data for compound *R,R*-**33b**.

Compound	*R,R*-**33b**	
Empirical formula	$C_{26}H_{34}N_4O_6V_2$	
Formula weight	600.45	
Temperature / K	100(2)	
Wavelength / Å	0.71073 Å	
Crystal system	Monoclinic	
Space group	$P2_1$	
Unit cell dimensions	a = 8.9787(9) Å	α= 90°
	b = 12.3991(12) Å	β= 103.657(2)°
	c = 11.9723(12) Å	γ = 90°
Volume / Å^3	1259.2(2)	
Z	2	
Density (calculated) / mg/m^3	1.540	
Absorption coefficient /mm^{-1}	0.711	
Crystal size / mm^3	0.29×0.13×0.07	
Reflections collected	12371	
Independent reflections	4787 [R(int) = 0.0382]	
Goodness-of-fit on F2	1.039	
Final R indices [I>2sigma(I)]	R1 = 0.0524, wR2 = 0.0948	
R indices (all data)	R1 = 0.0399, wR2 = 0.1087	
Absolute structure parameter	0.01(3)	

Table 4.21. Crystal data, data collection and refinement data for compound *S,S*-**36b**.

Compound	*S,S*-**36b**	
Empirical formula	$C_{61.25}H_{66}N_4O_{9.75}V_2$	
Formula weight	1116.06	
Temperature / K	100(2)	
Wavelength / Å	0.71073 Å	
Crystal system	Monoclinic	
Space group	*C*2	
Unit cell dimensions	a = 24.8548(19) Å	α= 90°
	b = 13.8673(11) Å	β= 98.3800(10)°
	c = 33.590(3) Å	γ = 90°
Volume / Å^3	11452.9(15)	
Z	2	
Density (calculated) / mg/m^3	1.294	
Absorption coefficient /mm^{-1}	0.387	
Crystal size / mm^3	0.40×0.20×0.15	
Reflections collected	64390	
Independent reflections	19287 [R(int) = 0.0651]	
Goodness-of-fit on F2	1.035	
Final R indices [I>2sigma(I)]	R1 = 0.1125, wR2 = 0.1629	
R indices (all data)	R1 = 0.0670, wR2 = 0.1852	
Absolute structure parameter	0.031(17)	

Table 4.22. Crystal data, data collection and refinement data for compound *S,S*-**39b**.

Compound	*S,S*-**39b**	
Empirical formula	$C_{28}H_{38}N_4O_8V_2$	
Formula weight	660.50	
Temperature / K	100(2)	
Wavelength / Å	0.71073 Å	
Crystal system	Triclinic	
Space group	*P*1\	
Unit cell dimensions	a = 7.3583(10) Å	α= 72.932(2)°
	b = 7.8797(10) Å	β= 82.466(2)°
	c = 12.8270(17) Å	γ = 83.366(2)°
Volume / Å^3	702.50(16)	
Z	1	
Density (calculated) / mg/m^3	1.561	
Absorption coefficient /mm^{-1}	0.724	
Crystal size / mm^3	0.38×0.12×0.08	
Reflections collected	6764	
Independent reflections	4490 [R(int) = 0.0168]	
Goodness-of-fit on F2	1.161	
Final R indices [I>2sigma(I)]	R1 = 0.0327, wR2 = 0.0809	
R indices (all data)	R1 = 0.0282, wR2 = 0.0931	
Absolute structure parameter	0.98(3)	

Table 4.23. Crystal data, data collection and refinement data for compound *R,R*-**45b**.

Compound	*R,R*-**45b**	
Empirical formula	$C_{78}H_{126}N_6O_9V_2$	
Formula weight	1393.73	
Temperature / K	100(2)	
Wavelength / Å	0.71073 Å	
Crystal system	Monoclinic	
Space group	$P2_1/c$	
Unit cell dimensions	a = 19.503(5) Å	α= 90°
	b = 16.308(5) Å	β= 103.283(5)°
	c = 25.577(5) Å	γ = 90°
Volume / Å^3	7917(4)	
Z	4	
Density (calculated) / mg/m^3	1.169	
Absorption coefficient /mm^{-1}	0.292	
Crystal size / mm^3	0.46×0.11×0.07	
Reflections collected	57358	
Independent reflections	9999 [R(int) = 0.0739]	
Goodness-of-fit on F2	1.160	
Final R indices [I>2sigma(I)]	R1 = 0.1058, wR2 = 0.1884	
R indices (all data)	R1 = 0.0703, wR2 = 0.2174	
Absolute structure parameter		

4.5.2.8. Magnetic susceptibility

The magnetic susceptibility experiments were carried out by Prof. Rui Teives Henriques at the *Departamento de Engenharia Química e Biológica* of *Instituto Superior Técnico*, Lisbon. The magnetic susceptibilities χ were measured by the Faraday method in the temperature range of 3–300 K, at 5T. Data were corrected for the diamagnetic contribution using the Pascal constants.[57] The magnetic susceptibility of both complexes fit well the Curie-Weiss law with a temperature independent paramagnetism (TIP) term [$\chi = C/(T-\theta) + TIP$]. The experiments were carried out using a superconducting longitudinal Faraday system (Oxford Instruments), with possible static magnetic field in the range 0-7 T (usually for thermal sweeps, a magnetic field of 5 T is used) and field gradient up to 10 T/m. Temperature range: 4.2-300K, possible to go down to He lambda point by pumping over liquid helium accumulated in the VTI (Variable Temperature Insert). Polycrystalline samples (typically 10 to 30 mg) are placed inside a previous calibrated thin-wall Teflon bucket. The force is measured with a microbalance (Sartorius S3D-V), applying forward and reverse field gradients (maximum balance readout 110 mg).

4.5.3. General procedure for sulfoxidation of thioanisole

The catalytic experiments were carried out at atmospheric pressure, at a constant temperature, in a glass batch reactor, equipped with magnetic stirrer, thermometer and condenser. In a typical run, the solid catalyst (0.25 to 10 mol%) and thioanisole (1 mmol) were dissolved in the appropriate solvent (4 mL). Then the oxidant (1.2 to 1.5 mmol), hydrogen peroxide (30 wt% aqueous solution) was added to the stirring mixture. Control experiments were carried out in the absence of catalyst. Samples of the reaction mixture were withdrawn periodically and analyzed on a Jasco HPLC system equipped with a Daicel Chiralpak IA column. The eluent used was hexane/ethyl acetate (60:40) with a flow of 1 mL/min. The calibration curves for each reagent and product, namely sulfide, sulfoxide and sulfone, were determined using similar HPLC procedures and these

calibrations used for the quantitative analyses. Diphenylsulfone was used as an internal standard.

4.5.4. General procedure for alkene oxidation

The alkene oxidations were carried out in the group of Prof. Mannar R. Maurya at the *Indian Institute of Technology of Roorkee*, India. All catalytic reactions for the oxidation of styrene, cyclohexene, and cumene were carried out using 50 mL double-neck reaction flasks fitted with a septum and a water condenser. In a typical styrene oxidation experiment, styrene (0.52 g, 5 mmol), aqueous 30% H_2O_2 (1.13 g, 10 mmol), and the catalyst (0.10 mmol, 2 mol%) were mixed in CH_3CN (10 mL), and the reaction was carried out at 80 °C with stirring. For cyclohexene oxidation, cyclohexene (0.41 g, 5 mmol), aqueous 30% H_2O_2 (1.13 g, 10 mmol), and the catalyst (0.10 mmol, 2 mol%) were mixed in CH_3CN (10 mL) and the reaction was carried out at 80 °C with stirring. For cumene oxidation, cumene (0.36 g, 3 mmol), aqueous 30% H_2O_2 (1.02 g, 9 mmol), and the catalyst (0.06 mmol, 2 mol%) were mixed in CH_3CN (10 mL) and the reaction was carried out at 80 °C with stirring. During the course of the reaction, 0.5 mL of the reaction mixture were withdrawn every half hour, extracted with petroleum ether (5 × 2 mL), and analyzed quantitatively by gas chromatography, using a Thermax Nicolet gas chromatograph with an HP-1 capillary column (30 m × 0.25 mm × 0.25 μm). The identity of the products in alkene oxidation was determined by GC-MS using a Perkin-Elmer Clarus 500 and comparing the detected product fragments with the libraries available.

4.5.5. DFT calculations

The DFT calculations presented in this Chapter were carried out by Dr. Maxim Kuznetsov at the *Centro de Química Estrutural* of *Instituto Superior Técnico*, TU Lisbon. The full geometry optimization of V-salan model complexes and transition states was carried out at the DFT level of theory using Becke's three-parameter hybrid exchange functional[47] in combination with the gradient-corrected correlation functional of Lee, Yang, and Parr[48] (B3LYP) with the help of the Gaussian 98[49] program package.

Symmetry operations were not applied for all structures. The geometry optimization was carried out using a relativistic Stuttgart pseudopotential describing 10 core electrons and the appropriate contracted basis set (8s7p6d1f)/ [6s5p3d1f][50] for the vanadium atom and the 6-31G(d) basis set for other atoms. Then, single-point calculations were done with the 6-311+G(d,p) basis set on the nonmetal atoms, and solvent effects were taken into account by using the polarizable continuum model[51] in the CPCM version[52] with CH_3CN as a solvent. The Hessian matrix was calculated analytically for all optimized structures to prove the location of the correct minimum (no "imaginary" frequencies) or saddle points (only one negative eigenvalue).

4.5.6. $V^{IV}O$(salen) and $V^{IV}O$(salan) compound preparation methods

General preparation procedure

$V^{IV}OCl_2$ was added to a methanolic (25 mL) solution of the appropriate ligand under a nitrogen atmosphere. The pH was adjusted to *ca*. 7-8 with a 1 M aqueous solution of NaOH. The addition of water (25 mL) induced the complete precipitation of $V^{IV}O$ compound. The precipitate was filtered and washed with water, minimal amounts of methanol and lastly diethyl ether. The recovered solid was then dried under vacuum. This method was used for all the described $V^{IV}O$ compounds.

Synthesis of [$V^{IV}O$(*R*,*R*-1a)], *R*,*R*-33

Reagents: $V^{IV}OCl_2$ (1.5 g, 8.8 mmol), *S*,*S*-**1a** (2.8 g, 8.8 mmol). The compound was obtained as a blue–green solid. Yield: 2.2 g, 64 %. EPR (DMSO): $\mathbf{A_z}$=157.4 × 10^{-4} cm^{-1}; $\mathbf{g_z}$=1.959. IR (cm^{-1}): 990 ν(V=O); Elemental analysis for $C_{20}H_{20}N_2O_3V{\cdot}0.5H_2O$: calcd. C 60.61, H 5.34, N 7.07; found C 60.5, H 5.7, N 6.9. Crystals of *R*,*R*-**33b** suitable for single crystal X-ray diffraction were grown from DMF solution. 0.1g of *R*,*R*-**33** was dissolved in *ca*. 10 mL of DMF and the resulting solution was filtered and transferred to a clean lint–free 20 mL glass flask. Light green crystals of *R*,*R*-**33b** were obtained by partial evaporation of the solvent after five weeks.

Synthesis of [$V^{IV}O$(*S*,*S*-1)], *S*,*S*-34

Reagents: $V^{IV}OCl_2$ (0.8 g, 4.6 mmol), *S*,*S*-**1** (1.8 g, 4.6 mmol). The compound was obtained as a brown solid. Yield: 1.4 g, 79 %. EPR (DMSO): $\mathbf{A_z}$=158.3 × 10^{-4} cm^{-1}; $\mathbf{g_z}$=1.957. IR (cm^{-1}): 879 ν(V=O). Elemental analysis for $C_{20}H_{24}N_2O_3V{\cdot}CH_3OH$: calcd. C 59.57, H 6.67, N 6.76; found C 59.3, H 6.6, N 6.9.

Synthesis of [$V^{IV}O$(*S*,*S*-2a)], *S*,*S*-35

Reagents: $V^{IV}OCl_2$ (0.4 g, 2.3 mmol), *S*,*S*-**2a** (0.97 g, 0.90 mmol). The compound was obtained as a brown solid. Yield: 0.56 g, 50 %. EPR (DMSO): $\mathbf{A_z}$=160.0 ×10^{-4} cm^{-1}; $\mathbf{g_z}$=1.955. IR (cm^{-1}): 983 ν(V=O). Elemental analysis for $C_{28}H_{22}N_2O_3V{\cdot}0.2H_2O$: calcd. C 68.84, H 4.61, N 5.73; found C 68.9, H 5.1, N 5.9.

Synthesis of [$V^{IV}O$(*S*,*S*-2)], *S*,*S*-36

Dichloromethane was used instead of diethyl ether in the washing procedure. Reagents: $V^{IV}OCl_2$ (0.44 g, 2.5 mmol), *S*,*S*-**2a** (1.524 g, 2.5 mmol). The compound was obtained as a brown solid. Yield: 1.0 g, 80 %. EPR (DMSO): $\mathbf{A_z}$=161.8 ×10^{-4} cm^{-1}; $\mathbf{g_z}$=1.954. IR (cm^{-1}): 882 ν(V=O). Elemental analysis for $C_{28}H_{26}N_2O_3V{\cdot}1.5CH_2Cl_2$: calcd. C 57.44, H 4.74, N 4.55; found C 57.3, H 5.0, N 4.9. Crystals of *S*,*S*-**36b** suitable for single crystal X–ray diffraction were grown from of isopropanol and dichloromethane solution. 0.1g of *S*,*S*-**36** was dissolved in *ca*. 10 mL of a 1:1 mixture of isopropanol and dichloromethane and the resulting solution was filtered and transferred to a clean lint–free 20 mL glass flask. Dark red crystals of *S*,*S*-**36b** were obtained by evaporation of the solvent after four weeks.

Synthesis of [$V^{IV}O$(*R*,*R*-3a)], *R*,*R*-37

Reagents: $V^{IV}OCl_2$ (1.7 g, 9.9 mmol), *S*,*S*-**3a** (4.1 g, 9.9 mmol). The compound was obtained as a brick–red solid. Yield: 2.9 g, 61 %. EPR (DMSO): $\mathbf{A_z}$=158.8 × 10^{-4} cm^{-1}; $\mathbf{g_z}$=1.957. IR (cm^{-1}): 888 ν(V=O). Elemental analysis for $C_{22}H_{26}N_4O_5V{\cdot}3H_2O$: calcd. C 49.72, H 6.07, N 10.54; found C 49.7, H 6.1, N 10.7.

Synthesis of [$V^{IV}O$(*R*,*R*-3)], *R*,*R*-38

Reagents: $V^{IV}OCl_2$ (1.3 g, 7.7 mmol), *S*,*S*-**3** (4.3 g, 7.7 mmol). The compound was obtained as a pink solid. Yield: 2.0 g, 54 %. EPR (DMSO): $\mathbf{A_z}$=158.3 × 10^{-4} cm^{-1}; $\mathbf{g_z}$=1.957. IR (cm^{-1}): 885 ν(V=O). Elemental analysis for $C_{22}H_{30}N_4O_5V{\cdot}2.5H_2O$: calcd. C 50.19, H 6.70, N 10.64; found C 50.4, H 6.6, N 10.6.

Synthesis of [$V^{IV}O$(*S*,*S*-4a)], *S*,*S*-39

Reagents: $V^{IV}OCl_2$ (0.4 g, 2.1 mmol), *S*,*S*-**4a** (0.8 g, 2.1 mmol). The compound was obtained as a green solid. Yield: 0.9 g, 95 %. EPR (DMSO): $\mathbf{A_z}$=164.4 × 10^{-4} cm^{-1}; $\mathbf{g_z}$=1.955. IR (cm^{-1}): 977 ν(V=O). Elemental analysis for $C_{22}H_{24}N_2O_5V{\cdot}0.5H_2O{\cdot}2MeOH$: calcd. C 55.39, H 6.39, N 5.38; found C 55.6, H 6.4, N 5.8. Crystals of *S*,*S*-**39b** suitable for single crystal X–ray diffraction were grown from DMF solution. 0.1g of *S*,*S*-**39** was dissolved in *ca*. 10 mL of DMF and the resulting solution was filtered and transferred to a clean lint-free 20 mL glass flask. Yellow crystals of *S*,*S*-**39b** were obtained by partial evaporation of the solvent after five weeks.

Synthesis of [$V^{IV}O$(*S*,*S*-4)], *S*,*S*-40

Reagents: $V^{IV}OCl_2$ (0.05 g, 0.3 mmol), *S*,*S*-**4** (0.14 g, 0.30 mmol). The compound was obtained as a brown solid. Yield: 0.13 g, 90 %. EPR (DMF): $\mathbf{A_z}$=160.1 × 10^{-4} cm^{-1}; $\mathbf{g_z}$=1.954. IR (cm^{-1}): 845 ν(V=O). Elemental analysis for $C_{22}H_{28}N_2O_5V{\cdot}0.5H_2O{\cdot}MeOH$: calcd. C 56.02, H 6.79, N 5.66; found C 56.1, H 6.8, N 5.7

Synthesis of [$V^{IV}O$(*S*,*S*-5a)], *S*,*S*-41

Reagents: $V^{IV}OCl_2$ (0.17 g, 1.0 mmol), *S*,*S*-**5a** (0.4 g, 1.0 mmol). The compound was obtained as a green solid. Yield: 0.3 g, 64 %. EPR (DMF): $\mathbf{A_z}$=164.1 × 10^{-4} cm^{-1}; $\mathbf{g_z}$=1.956. IR (cm^{-1}): 990 ν(V=O). Elemental analysis for $C_{24}H_{28}N_2O_5V{\cdot}H_2O{\cdot}0.5CH_2Cl_2$: calcd. C 55.00, H 5.84, N 5.24; found C 54.9, H 5.8, N 5.4

Synthesis of [$V^{IV}O$(*S*,*S*-5)], *S*,*S*-42

Reagents: $V^{IV}OCl_2$ (0.1 g, 0.6 mmol), *S*,*S*-**5** (0.3 g, 0.6 mmol). The compound was obtained as a brown solid. Yield: 0.2 g, 70 %. EPR (DMF): $\mathbf{A_z}$=161.7 × 10^{-4} cm^{-1};

$\mathbf{g_z}$=1.955. IR (cm^{-1}): 842 ν(V=O). Elemental analysis for $C_{24}H_{32}N_2O_5V{\cdot}H_2O$: calcd. C 58.08, H 6.89, N 5.64; found C 58.1, H 6.9, N 5.4

Synthesis of [V^{IV}O(*S*,*S*-6)], *S*,*S*-43

Reagents: $V^{IV}OCl_2$ (0.26 g, 1.5 mmol), *S*,*S*-**6** (0.75 g, 1.5 mmol). The compound was obtained as a grey solid. Yield: 0.6 g, 80 %. EPR (DMF): $\mathbf{A_z}$=161.1 × 10^{-4} cm^{-1}; $\mathbf{g_z}$=1.955. IR (cm^{-1}): 962 ν(V=O). Elemental analysis for $C_{28}H_{28}N_2O_3V{\cdot}MeOH$: calcd. C 66.53, H 6.16, N 5.35; found C 66.7, H 6.1, N 5.0

Synthesis of [V^{IV}O(*R*,*R*-7)], *R*,*R*-44

Reagents: $V^{IV}OCl_2$ (0.12 g, 0.71 mmol), *R*,*R*-**7** (0.32 g, 0.71 mmol). The compound was obtained as a dark–brown solid. Yield: 0.23 g, 72 %. Elemental analysis for $C_{22}H_{28}N_2O_5V{\cdot}H_2O$: calcd. C 56.29, H 6.44, N 5.97; found C 56.6, H 6.3, N 5.8

Synthesis of [V^{IV}O(*R*,*R*-8)], *R*,*R*-45

Reagents: $V^{IV}OCl_2$ (0.23 g, 1.3 mmol), *R*,*R*-**5** (0.81 g, 1.3 mmol). Instead of diethyl ether, *n*–pentane was used during the washing procedure. The compound was obtained as a grey solid. Yield: 0.55 g, 70 %. EPR (DMF): $\mathbf{A_z}$=160.8 × 10^{-4} cm^{-1}; $\mathbf{g_z}$=1.955. IR (cm^{-1}): 879 ν(V=O). Elemental analysis for $C_{36}H_{56}N_2O_3V{\cdot}C_5H_{12}$: calcd. C 71.66, H 10.01, N 4.05; found C 71.5, H 10.3, N 3.9 Crystals of *R*,*R*-**45b** suitable for single crystal X-ray diffraction were grown from an isopropanol and dichloromethane solution. 0.1g of *R*,*R*-**45** was dissolved in *ca*. 10 mL of a 1:1 mixture of isopropanol and dichloromethane and the resulting solution was filtered and transferred to a clean lint-free 20 mL glass flask. Dark red crystals of *R*,*R*-**45b** were obtained by evaporation of the solvent after four weeks.

Synthesis of [V^{IV}O(*R*,*R*-9)], *R*,*R*-46

Reagents: $V^{IV}OCl_2$ (0.2 g, 1.1 mmol), *R*,*R*-**9** (0.71 g, 1.1 mmol). The compound was obtained as a brown solid. Yield: 0.4 g, 65 %. EPR (DMF): $\mathbf{A_z}$=162.0 × 10^{-4} cm^{-1}; $\mathbf{g_z}$=1.962. Elemental analysis for $C_{26}H_{25}N_4O_3ClV{\cdot}3H_2O$: calcd. C 47.83, H 4.79, N 8.58; found C 47.6, H 4.5, N 8.7

4.6. References

1 Bolm, C. *Coord. Chem. Rev.* **2003**, *237*, 245-256.

2 Michaelson, R. C.; Palermo, R. E.; Sharpless, K. B. *J. Am. Chem. Soc*. **1977**, *99*, 1990-1992.

3 Brink, H. B.; Tuynman, A.; Dekker, H. L.; Hemrika, W.; Izumi, Y.; Oshiro, T.; Schoemaker, H. E.; Wever, R. *Inorg. Chem.* 1998, *37,* 6780-6784.

4 Radosevich, A. T.; Musich, C.; Toste, F. D. *J. Am. Chem. Soc*. **2005**, *127*, 1090-1091.

5 Meppelder, G. M.; Halbach, T. S.; Spaniol, T. P.; Mülhaupt, R.; Okuda, J. *J. Organomet. Chem*. **2009**, *694*, 1235–1237.

6 Nakajima, K.; Kojima, K.; Kojima, M.; Fujita, *J. Bull. Chem. Soc. Jpn*. **1990**, *63*, 2620-2630.

7 Belokon, Y. N.; North, M.; Parsons, T. *Org. Lett.* **2000***, 2*,1617-1619.

8 Watanabe, A.; Matsumoto, K; Shimada, Y.; Katsuki, T. *Tetrahedron Lett.* **2004**, *45*, 6229–6233.

9 Sun, J.; Zhu,C.; Dai, Z.; Yang, M.; Pan, Y.; Hu, H. *J. Org. Chem.* **2004**, *69*, 8500-8503.

10 Sun, J.; Dai, Z.; Li, C.; Pan, X.; Zhu, C. *J. Organomet. Chem*. **2009**, *694*, 3219–3221.

11 Sun, J.; Dai, Z.; Yang, M.; Pan, X.; Zhu, C. *Synthesis* **2008**, *13*, 2100-2104.

12 Adão, P.; Costa Pessoa, J.; Henriques, R. T.; Kuznetsov, M. L.; Avecilla, F.; Maurya, M. R.; Kumar, U.; Correia, I. *Inorg. Chem.* **2009**, *48*, 3542-3561.

13 Adão, P.; Costa Pessoa, J.; Henriques, R. T.; Kuznetsov, M. L.; Avecilla, F.; Maurya, M. R.; Kumar, U.; Correia, I. *Pure. Appl. Chem.* **2009**, *81*, 1279-1296.

14 Lorber, C. *Pure Appl. Chem*. **2009**, *81*, 1205–1215.

15 Barroso, S.; Adão, P.; Madeira, F.; Teresa Duarte, M.; Costa Pessoa, J.; M. Martins, A. *Inorg. Chem*. **2010**, *49*, 7452–7463.

16 Schmidt, H.; Bashirpoor, M.; Rehder, D. *J. Chem. Soc., Dalton Trans*. ***1996,*** 3865-3870.

17 Chatterjee, P. B.; Bhattacharya, S.; Audhya,A.; Choi, K.; Endo, A.; Chaudhury, M. *Inorg. Chem.* **2008**, *47*, 4891-4902.

18 Colpas, G. J.; Hamstra, B. J.; Kampf, J. W.; Pecoraro, V. J. *Inorg. Chem.* **1994**, *33,* 4669-4675.

19 Rehder, D.; Weidemann, C.; Duch, A.; Priebsch, W. *Inorg. Chem*. **1988,** *27***,** 584-587.

20 Priebsch, W.; Rehder, D. *Inorg. Chem.* **1990**, *29*, 3013-3019.

21 (a) Sharma, N.; Sood, A. K.; Bhatt, S. S.; Chaudhry, S. C. *Polyhedron* **1997**, *16*, 4055-4060. (b) Liu, S.; Gao, S. *Polyhedron* **1998**, *17*, 81-84. (c) Neves, A.; Ceccatto, A. S.; Erasmus-Buhr, C.; Gehring, S.; Haase, W.; Paulus, H.; Nascimento, O. R.; Batistae, A. A. *J . Chem. Soc., Chem. Commun*. **1993**, 1782-1784. (d) Cornman, C. R.; Kampf, J.; Pecoraro, V. L. *Inorg. Chem.* **1992**, *31*, 1981–1983.

22 Chasteen, N. D. in: Berliner, L. J.; Reuben, J. (Eds.), *Biological Magnetic Resonance*, Plenum Press, New York, **1981**, *3*, 53-119.

23 (a) WinEPR Simfonia v1.25 Bruker Analytische Messtechnik GmbH, 1996. (b) Rockenbauer, A.; Korecz, L. *Appl. Magn. Reson.* **1996**, *10*, 29-43.

24 Holyk, N. H., *An electron paramagnetic resonance study of model oxovanadium(IV) complexes in aqueous solution; Correlation of magnetic properties with ligand type and metal structure*, M. S. Thesis, University of New Hampshire, Durham, New Hampshire, **1979**.

25 (a) Costa Pessoa, J.; Calhorda, M. J.; Cavaco, I.; Correia, I.; Duarte, M. T.; Félix, V.; Henriques, R.T.; Piedade, M. F. M.; Tomaz, I. *J. Chem. Soc*., *Dalton Trans*. **2002**, 4407-4415 (b) Smith II, T. S.; Root, C. A.; Kampf, J. W.; Rasmussen, P. G.; Pecoraro, V. L. *J. Am. Chem. Soc.* **2000,** *122,* 767-775 (c) Cornman, C. R.; Zovinka, E. P.; Boyajian, Y. D.; Geiser-Bush, K. M.; Boyle, P. D.; Singh, P. *Inorg. Chem.* **1995**, *34* , 4213-4219 (d) Hamstra, B. J.; Houseman, A. L. P.; Colpas, G. J.; Kampf, J. W.; LoBrutto, R.; Frasch, W. D.; Pecoraro, V. L. *Inorg. Chem.* **1997,** *36,* 4866-4874 (e) Tasiopoulos, A. J.; Troganis, A. N.; Evangelou, A.; Raptopoulou, C. P.; Terzis, A.; Deligiannakis, Y.; Kabanos, T. A. *Chem. Eur. J.*, **1999**, 910-921. (f) Houseman, A. L. P.; LoBrutto, R.; Frasch, W. D. *Biochemistry* **1995**, *34*, 3277-3285. (g) Jakusch, T.; Buglyo, P.; Tomaz, A. I.; Costa Pessoa. J.; Kiss, T. *Inorg. Chim. Acta* **2002**, *339*, 119-128.

26 Gorelsky, S.; Micera, G.; Garribba, E. *Chem. Eur. J.* **2010**, *16*, 8167-8180.

27 Garribba, E.; Micera, G.; Sanna, D. *Inorg. Chim. Acta* **2006**, *359*, 4470-4476.

28 Micera, G.; Pecoraro, V. L.; Garribba, E. *Inorg. Chem*. **2009**, *48*, 5790-5796.

29 Gonzalez-Baro, A.C.; Castellano, E. E.; Piro, O. E.; Parajo-Costa, B. S. *Polyhedron* **2005**, *24*, 49–55.

30 Root, C. A.; Hoeschele, J. D.; Cornman, C. R.; Kampf, J. W.; Pecoraro, V. L. *Inorg. Chem.* **1993**, *32*, 3855-3861.

31 Romanowski, G.; Kwiatkowski, E.; Nowicki, W.; Kwiatkowski, M.; Lis, T. *Polyhedron* **2008**, *27*, 1601–1609.

32 (a) Binder, C. M.; Dixon, D. D.; Almaraz, E.; Tius, M. A.; Singaram, B. *Tetrahedron Lett.* **2008**, *49*, 2764–2767. (b) Liu, S.; Reddy, K. V.; Lai, R. Y. *Tetrahedron* **2007**, *63*, 1821–1825.

33 Kirihara, M.; Yoshida, K.; Noguchi, T.; Naito, S.; Matsumoto, N.; Ema, Y.; Torii, M.; Ishizuka, Y.; Souta, I. *Tetrahedron Lett.* **2010**, *51*, 3619–3622.

34 Tokunaga, M.; Aoyama, H.; Shirogane, Y.; Obora, Y.; Tsuji, Y. *Catalysis Today* **2006**, *117*, 138–140.

35 Conte, V.; Furia, F. D.; More, S. *Inorg. Chim. Act*a **1998**, *172*, 62-47.

36 Slebodnick, C.; Pecoraro, V. L. *Inorg. Chim. Acta* **1998**, *283*, 37-43.

37 Hector, A. L.; Levason, W.; Middleton, A. J.; Reid, G.; Webster, M. *Eur. J. Inorg. Chem.* **2007**, 3655–3662.

38 (a) Schneider, C. S.; Penner-Hahn,J. E.; Pecoraro, V. L. *J. Am. Chem. Soc*. **2008**, *130*, 2712-2713. (b) Smith , T. S.; Pecoraro, V. L. *Inorg. Chem.* **2002**, *41*, 6754-6760. (c) Kravitz, J. Y.; Pecoraro, V. L.; Carlson, H. A. *J. Chem. Theory Comput.* **2005,** *1,* 1265-1274. (d) Balcells, D.; Maseras, F.; Ujaque, G. *J. Am. Chem. Soc*. **2005**, *127*, 3624-3634. (e) Balcells, D.; Maseras, F.; Lledós, A. *J. Org. Chem.* **2003**, *68*, 4265–4274.

39 (a) Correia, I.; Costa Pessoa, J.; Duarte, M. T.; Henriques, R. T.; Piedade, M. F. M.; Veiros, L. F.; Jakusch, T.; Kiss, T.; Dornyei, A.; Castro, M. M. C. A.; Geraldes, C. F. G. C.; Avecilla, F. *Chem. Eur. J.* **2004**, *10*, 2301–2317. (b) Correia, I.; Costa Pessoa, J.; Duarte, M. T.; Piedade, M. F. M.; Jackush,T.; Kiss, T.; Castro, M. M. C. A.; Geraldes, C. F. G. C.; Avecilla, F. *Eur. J. Inorg. Chem.* **2005**, 732–744.

40 Shul'pin, G. B.; Kozlov, Y. N.; Nizova, G. V.; Süss-Fink, G.; Stanislas, S.; Kitaygorodskiy, A.; Kulikova, V. S. *J. Chem. Soc., Perkin Trans.2* **2001**, 1351–1371.

41 Khaliullin, R. Z.; Bell, A. T.; Head-Gordon, M. *J. Phys. Chem. B* **2005**, *109*, 17984–17992.

42 Sharpless, K. B.; Townsend, J. M.; Williams, D. R. *J. Am. Chem. Soc.* **1972**, *94*, 295–296.

43 Kala Raj, N. K.; Ramaswamy, A. V.; Manikandan, P. *J. Mol. Catal.A: Chem.* **2005**, *227*, 37–45.

44 Sheldrick, G. M. *SHELXS-97*, revision 5.1; University of Göttingen: Göttingen, Germany, 1997.

45 (a) Flack, H. D.; Bernardinelli, G. *Acta Crystallogr., A* **1999**, *A55*, 908-915. (b) Flack, H. D.; Bernardinelli, G. *J. Appl. Crystallogr.* **2000**, *33*, 1143-1148.

46 Butler, A.; Clague, M. J.; Meister, G. E. *Chem. Rev.* **1994,** *94,* 625-638.

47 Becke, A. D. *J. Chem. Phys.* **1993**, *98*, 5648–5652.

48 Lee, C.; Yang, W.; Parr, R. G. *Phys. Rev. B: Condens. Matter Mater. Phys.* **1988**, *37*, 785–789.

49 Frisch, M. J.; Trucks, G. W.; Schlegel, H. B.; Scuseria, G. E.; Robb, M. A.; Cheeseman, J. R.; Zakrzewski, V. G.; Montgomery, J. A., Jr.; Stratmann, R. E.; Burant, J. C.; Dapprich, S.; Millam, J. M.; Daniels, A. D.; Kudin, K. N.; Strain, M. C.; Farkas, O.; Tomasi, J.; Barone, V.; Cossi, M.; Cammi, R.; Mennucci, B.;

Pomelli, C.; Adamo, C.; Clifford, S.; Ochterski, J.; Peterson, G. A.; Ayala, P. Y.; Cui, Q.; Morokuma, K.; Malick, D. K.; Rabuck, A. D.; Raghavachari, K.; Foresman, J. B.; Cioslowski, J.; Ortiz, J. V.; Baboul, A. G.; Stefanov, B. B.; Liu, G.; Liashenko, A.; Piskorz, P.; Komaromi, I.; Gomperts, R.; Martin, R. L.; Fox, D. J.; Keith, T.; Al-Laham, M. A.; Peng, C. Y.; Nanayakkara, A.; Challacombe, M.; Gill, P. M. W.; Johnson, B.; Chen, W.; Wong, M. W.; Andres, J. L.; Gonzalez, C.; Head-Gordon, M.; Replogle, E. S.; Pople, J. A. *Gaussian 98*, revision A.9; Gaussian Inc.:Pittsburgh, PA, **1998**.

50 Dolg, M.; Wedig, U.; Stoll, H.; Preuss, H. *J. Chem. Phys.* **1987**, *86*, 866–872.

51 Tomasi, J.; Persico, M. *Chem. Rev.* **1994**, *94*, 2027–2094.

52 Barone, V.; Cossi, M. *J. Phys. Chem. A* **1998**, *102*, 1995–2001.

53 Ballhausen, C. J.; Gray, H. B. *Inorg. Chem*. **1962**, *1*, 111-122.

54 Eaton, G. R.; Eaton, S. S.; Barr, D. P.; Weber, R. T. *Quantitative EPR*, SpringerWien, NewYork, **2010**.

55 (a) Gonzalez-Baro, A. C.; Castellano, E. E.; Piro, O. E.; Parajón-Costa, B. S. Polyhedron **2005**, *24*, 49–55. (b) Rayati, S.; Sadeghzadeh, N.; Khavasi, H. R. *Inorg. Chem. Comm*. **2007**, *10,* 1545–1548. (c) Plass, W. *Inorg. Chim. Act*. **1996**, *244*, 221-229. (d) Schmidt, H.; Bashirpoor, M.; Rehder, D. *J. Chem. Soc, Dalton Trans*. **1996***,* 3865-3870.

56 Plass, W. *Angew. Chem., Int. Ed. Engl*. **1996**, *35*, 627-631.

57 Selwood, P. W. *Magnetochemistry*, Interscience, New York **1956**, 78.

58 Kuznetsov, M. L.; Costa Pessoa, J. *Dalton Trans.* **2009**, 5460–5468.

Chapter 5

Aminoalcohol-derived Vanadium(IV) Complexes

5. Aminoalcohol-derived Vanadium(IV) Complexes

5.1. Introduction

Despite the popularity of the salen catalysts, those used in asymmetric synthesis relied heavily on cyclohexane-1,2-diamine as the chiral structural precursor. It is one of the more readily available and cheapest chiral diamines and is also one of the most efficient carriers of chirality in this compound class. The results described in the previous chapter showed that 1,2-diphenylethane-1,2-diamine-based catalysts were amply inferior in every aspect to the cyclohexane-1,2-diamine-based catalysts. While the salen and the related salan compounds remain structurally versatile, the diamine chiral pool is limited when compared to the chiral pool of naturally occurring molecules such as the aminoacids, aminoalcohols and aminosugars. Structural simplicity is also desirable when developing a catalytic system with potential industrial applications, where cost reduction is important. The change from a tetradentate salen- or salan-type catalyst to a tridentate aminophenolate-class catalyst derived from aminoacids or aminoalcohols is a reasonable alternative: lower amounts of substituted salicylaldehyde precursors are necessary and no additional amine resolution procedures are necessary as most chiral aminoacids and aminoalcohols are available commercially.

The use of chiral aminoalcohols in the development of simpler catalysts for asymmetric synthesis had its inception with the *tert*-leucinol-based $V^{IV}O$(Schiff base) catalytic system used in asymmetric sulfoxidation reported by Carsten Bolm and Frank Bienewald in 1995 (Scheme 5.1).[1] While the aminoalcohol-based $V^{IV}O$(Schiff base) compounds were structurally simpler than the related $V^{IV}O$(salen), this system represented a step forward from the chiral diamine-based $V^{IV}O$(salen) catalytic system reported by Fujita and co-workers in respect to enantioselectivity and activity: the aforementioned $V^{IV}O$(Schiff base) system did not require low temperatures to exhibit high enantioselectivity and used cheap and environmentally benign aqueous hydrogen peroxide as terminal oxidant instead of organic hydroperoxides; catalyst loadings as low as 0.01 mol% could be used; the $V^{IV}O$ precatalyst could be generated *in situ* further simplifying the application of this catalytic system.

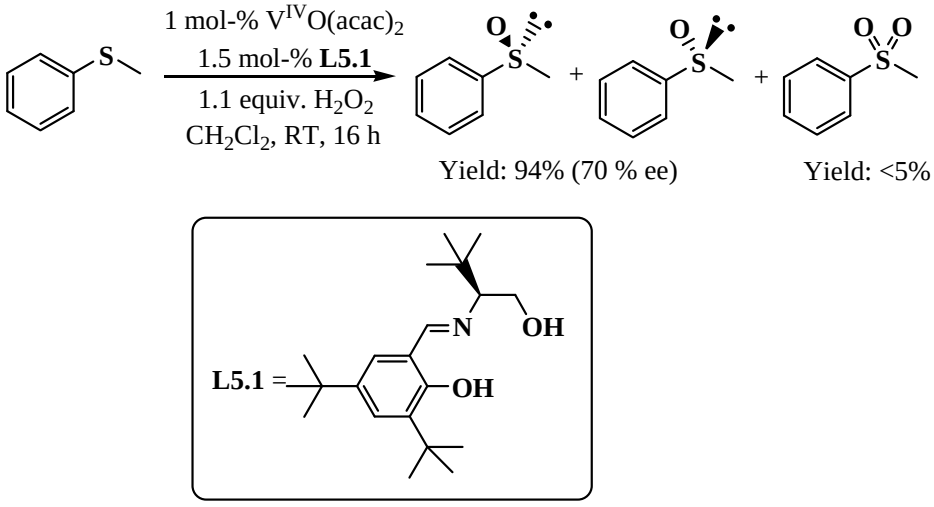

Scheme 5.1. Aminoalcohol-derived $V^{IV}O$(Schiff base)-promoted asymmetric sulfoxidation.

The major advantage of the system devised by Bolm and Bienewald was that it tapped into a much wider chiral pool, given that most commercially available chiral aminoalcohols derive directly from naturally occurring chiral aminoacids. The wider possibility of choice conferred a greater versatility to the aminoalcohol-derived $V^{IV}O$(Schiff base) catalytic systems, given that the possibilities for fine-tuning the catalyst properties were expanded despite the structural simplicity.

Indeed, many authors made use of this versatility and developed important improvements on the original design brought by Bolm and Bienewald.

In 1998, Vetter and Berkessel[2] reported various *tert*-leucinol-derived $V^{IV}O$(Schiff base) catalysts for the asymmetric sulfoxidation of thioethers, which were based on the binaphthyl structural motif. The axial chirality exhibited by the binaphthyl moiety constituted an additional chirality element that reinforced enantioselectivity (Scheme 5.2). The intention behind this structural variation was to induce chiral amplification by introducing another element of chirality in addition to the single chiral carbon present in the aminoalcohol backbone. The authors did observe a significant improvement over the original design in terms of activity and enantioselectivity as a result of chiral amplification, in particular when axial chirality was present.

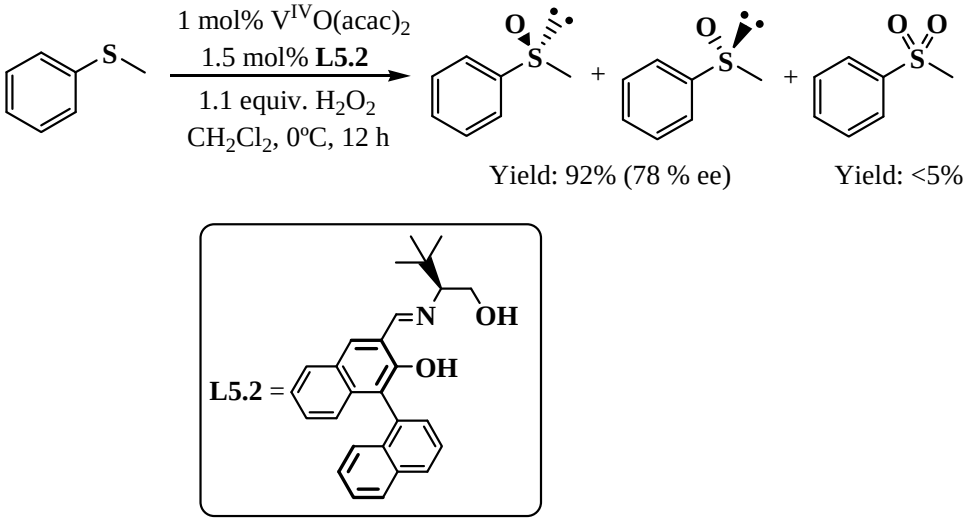

Scheme 5.2. Aminoalcohol-derived $V^{IV}O$(Schiff base)-promoted asymmetric sulfoxidation.

Six years later, in 2004, Ahn and co-workers[3] reported *tert*-leucinol-derived $V^{IV}O$(Schiff base) catalysts based on the well known BINOL phenols as a means to improve activity and enantioselectivity (Scheme 5.3).

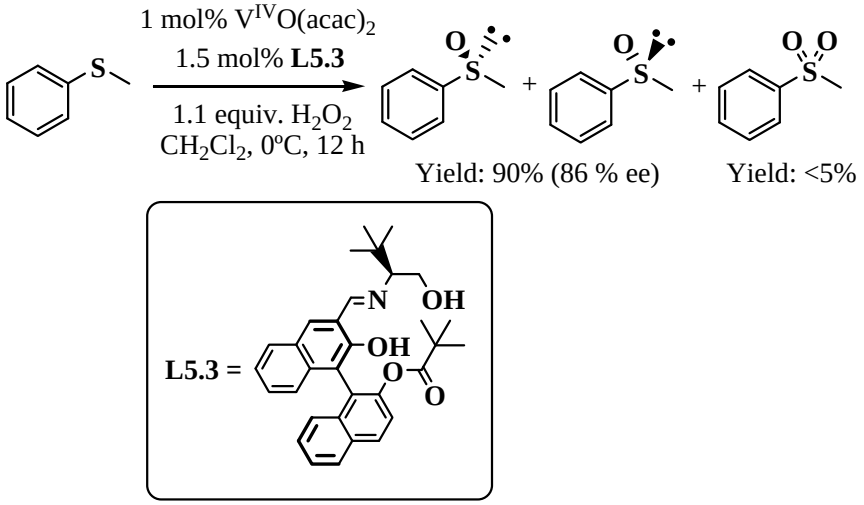

Scheme 5.3. Aminoalcohol-derived $V^{IV}O$(Schiff base)-promoted asymmetric sulfoxidation.

The authors also observed that the chirality element in the phenolate moiety by itself is not responsible for asymmetric induction, as catalysts derived from achiral 2-aminoethanol gave no enantiomeric excess. This illustrated how important it is for a

given aminoalcohol-derived $V^{IV}O$(Schiff base) that the stereogenic centers to be as close as possible to the donor atoms and the metal centre.

In 2005, Zhao and co-workers attempted to improve the aminoalcohol-derived $V^{IV}O$(Schiff base) system using a different approach.[4] The authors departed from the *tert*-leucinol structural motif and employed simpler and cheaper aminoalcohols such as L-phenylalaninol, L-valinol and L-isoleucinol. Cheap and commercially available salicylaldehyde was used as the aromatic aldehyde instead of the more complex substituted salicylaldehydes used by previous authors. The tandem thioether-to-sulfoxide and sulfoxide-to-sulfone oxidation processes were used to achieve enantiomeric excesses up to 99% at a cost of sulfoxide yields. Finally, the authors also noted that the use of $V^{IV}O$(Schiff base) precatalysts isolated in anticipation proved beneficial to enantioselectivity. This also minimized the ligand waste associated with the previous *in situ* methods (Scheme 5.4).

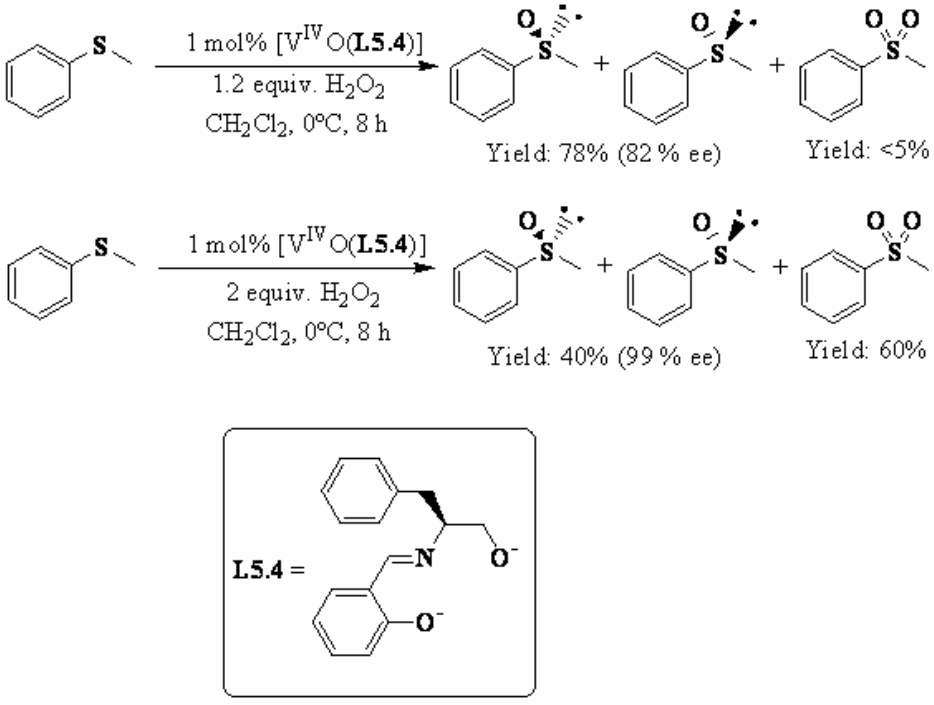

Scheme 5.4. Aminoalcohol-derived $V^{IV}O$(Schiff base)-promoted asymmetric sulfoxidation.

In the same year, Jackson and co-workers[5] reported a highly selective *tert*-leucinol -derived $V^{IV}O$(Schiff base) system that used 3,5-diiodosalicylaldehyde as a structural precursor. High sulfoxide yields were obtained and enantiomeric excesses were greater

than 95% with a variety of thioether substrates. This system illustrates how minimal alterations to the original design may yield significant gains in catalyst performance (Scheme 5.5).

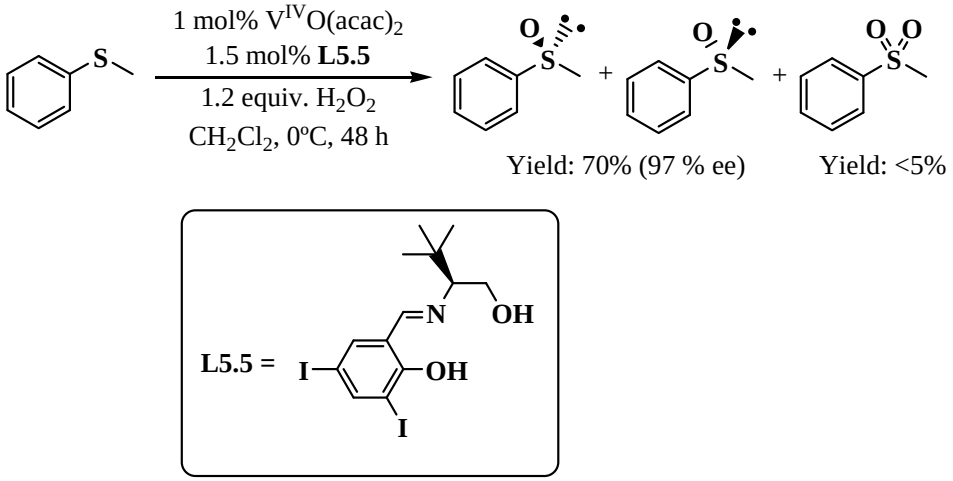

Scheme 5.5. Aminoalcohol-derived $V^{IV}O$(Schiff base)-promoted asymmetric sulfoxidation.

To demonstrate that the aminoalcohol structural precursors do not need to be restricted to those directly derived from L-aminoacids, Ruff and co-workers[6] devised several *in situ* $V^{IV}O$(Schiff base) catalysts derived from D-aminosugars that would give sulfoxide yields up to 97% coupled with 60% in enantiomeric excess (Scheme 5.6).

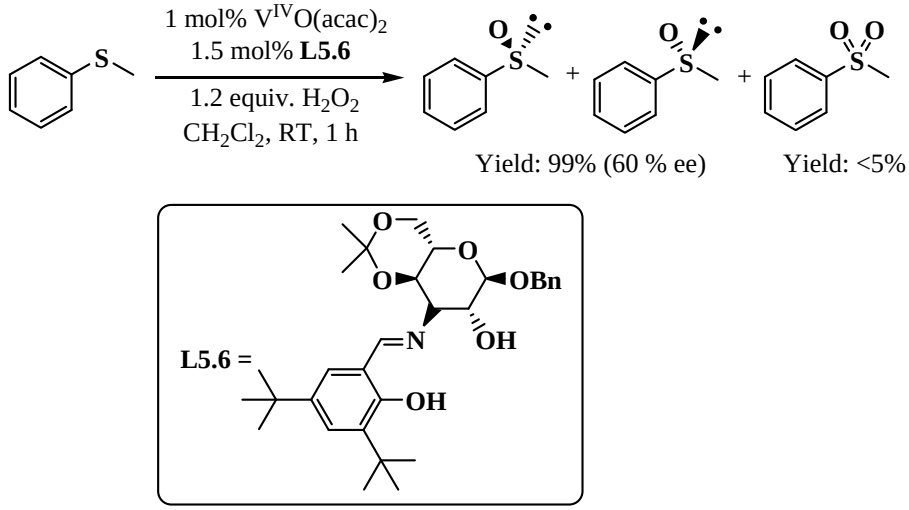

Scheme 5.6. Aminoalcohol-derived $V^{IV}O$(Schiff base)-promoted asymmetric sulfoxidation.

A more recent variant of Bolm's catalytic system was reported by Sun and co-workers in 2009,[7] where the authors developed a closely-related $V^{IV}O$ catalyst based on 4-methyl-5,6,7,8-tetrahydroquinolin-8-ol. While structurally very similar, the ligand used in this system was not a Schiff base. In addition, the catalyst exhibited the best performance in acetone, with sulfoxide yields and enantiomeric excesses similar to those obtained initially by Bolm and Bienewald in chlorinated solvents (Scheme 5.7).

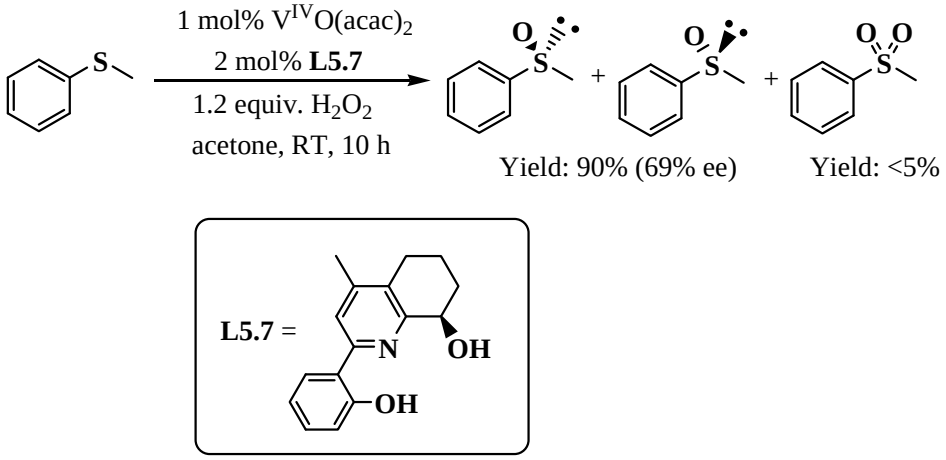

Scheme 5.7. Aminoalcohol-derived $V^{IV}O$(Schiff base)-promoted asymmetric sulfoxidation.

Despite the various iterations of the aminoalcohol-based $V^{IV}O$(Schiff base) catalysts, most share the same flaw inherent from the Schiff base ligand: its tendency to hydrolyze in the presence of water. Also, Bolm's protocol and its variants rely on *in situ* generation of the $V^{IV}O$ precatalyst, and seem to require an excess of ligand precursor relative to the metal precursor to achieve the reported high activities and enantioselectivities. While *in situ* generation of the precatalyst simplifies the entire process, it does not allow adequate characterization of the precatalyst species. As it was shown in the previous Chapter, the characterization of the precatalyst species in solution and in the solid state may yield relevant information about the possible species involved in the catalytic processes studied. The excess of Schiff base ligand precursor used in Bolm's method and replicated by the successive authors that improved the design can be considered wasteful and must be inevitably separated from the final product.

Nevertheless, the superior potential of aminoalcohol-based $V^{IV}O$(Schiff base) catalysts as asymmetric sulfoxidation catalysts relative to the $V^{IV}O$(salen) and $V^{IV}O$(salan) catalysts is evident.

In light of the results obtained in Chapter 4, several related $V^{IV}O$ catalysts bearing aminoalcohol-derived reduced Schiff base ligands were prepared and tested in the asymmetric sulfoxidation of thioanisole. The same rationale behind the development of the $V^{IV}O$(salan) compounds is employed here with the expectation that an increase in enantioselectivity, hydrolytic stability and activity is obtained compared to the original catalysts devised by Bolm and Bienewald, while maintaining a simplified catalyst structure.

5.2. Aminoalcohol-derived $V^{IV}O$ compound preparation: results and discussion

The procedures used for the preparation of the aminoalcohol-derived $V^{IV}O$ compounds were the same as those used for the preparation of $V^{IV}O$(salen) and $V^{IV}O$(salan) compounds described in Chapter 4. The $V^{IV}O$ compounds were readily prepared by reacting aqueous $V^{IV}OCl_2$ with the appropriate aminoalcohol-derived reduced Schiff base (AORSB) ligand under inert atmosphere. The desired complex precipitates from the reaction mixture after the medium pH is adjusted to *ca*. 7-8 with aqueous potassium hydroxide. The solid compounds are relatively air-stable but less so than the related $V^{IV}O$(salan) compounds. All $V^{IV}O$(AORSB) were obtained as brown solids after precipitation. All attempts to obtain suitable crystals for single crystal X-ray diffraction failed. Characterization of the prepared compounds was made mainly by EPR spectroscopy and elemental analysis, as both techniques provided enough information to confirm successful compound preparation. The $V^{IV}O$(AORSB) compounds described in this Chapter were prepared with the purpose of verifying the effect of the reduction of the C=N imine double bond to a C-N single bond on catalyst performance. Additional characterization was not performed as it goes beyond the scope of this Chapter. The structural formulas of the prepared $V^{IV}O$(AORSB) compounds *R*-**47**, *R*-**48**, *R*-**49** and *R*-**50** are shown in Figure 5.1.

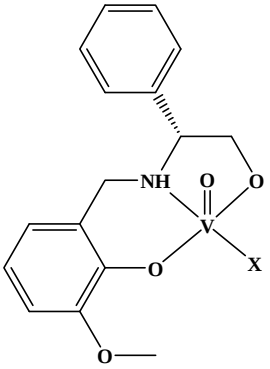

R-**47**

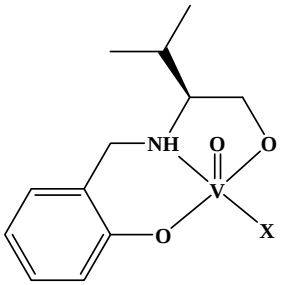

S-**48**

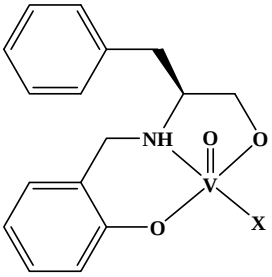

S-**49**

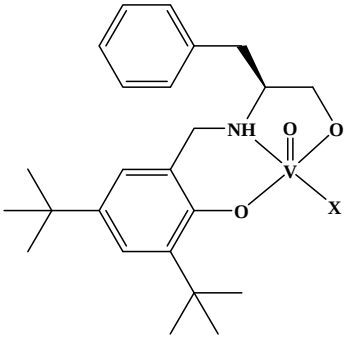

S-**50**

Figure 5.1- Structural formulas of the prepared $V^{IV}O$(AORSB) compounds depicting the respective configuration at their stereogenic centers. The letter X denotes a coordinated solvent molecule.

Figure 5.2 shows the X-band EPR spectra of the $V^{IV}O$(AORSB) compounds in DMF solution, at 77 K. In all cases, a well defined hyperfine structure is present and all spectra have an apparent "axial" symmetry. With the exception of *R*-**47**, all spectra have very similar EPR spectra. All experimental $\mathbf{A_z}$ values were obtained after simulation with the appropriate software.[8] The additivity rule[9] was applied so that the possible donor groups and binding modes in solution could be determined. A secondary species with signal matching those of the remaining $V^{IV}O$(AORSB) compounds was detected in the EPR spectrum of *R*-**47**. The low field signals were of sufficient intensity to allow the calculation of the *z*-component spin Hamiltonian parameters $\mathbf{A_z}$ and $\mathbf{g_z}$. Figure 5.3 shows the low-field region of the EPR spectrum of *R*-**47**, where the respective primary and secondary species are visible and how these compare to the low-field region of EPR spectrum of *S*-**48**.

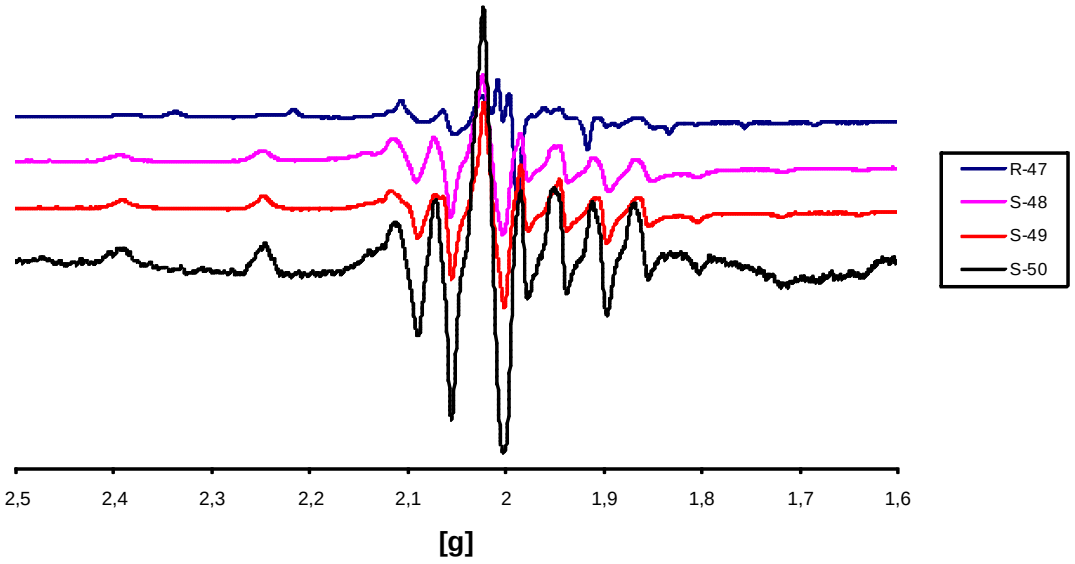

Figure 5.2. First derivative X-band EPR spectra of the prepared $V^{IV}O$(AORSB) complexes. The spectra were recorded from DMF solutions of the compounds, at 77K.

Table 5.1 lists all the calculated spin Hamiltonian parameters and expected donor group sets. Figure 5.4 depicts all possible binding modes, with the expected $\mathbf{A_z}$ values for each. The tridentate $V^{IV}O$(AORSB) complexes are known to form dimeric or even polymeric species in the solid state as well as in solution.[10,11,12] Since dimeric species can often yield very complex EPR spectra or no spectra at all, and the obtained EPR spectra may not give any indication of dinuclear species in solution, the prepared tridentate $V^{IV}O$ complexes will be treated as monomeric. The spectrum of *R*-**47** is remarkably different from the remaining spectra. The spacing between low-field and high-field signals in *R*-**47** is smaller, which indicates a comparatively smaller $\mathbf{A_z}$ value. As mentioned earlier, the low-field region in Figure 5.3 shows the presence of an additional set of faint signals from a secondary species in solution. The low-field signals given by this secondary species appear to match those from *S*-**48**, *S*-**49** and *S*-**50**. The more complex centre-field region of *R*-**47** may be due to the presence of this secondary species. The spectrum of *S*-**50** shows broad distorted lines possibly due to partial spin-spin coupling between $V^{IV}O$ units. This can occur when the compound to be analyzed precipitates from solution as the sample temperature is lowered or when the complex is oligomeric (e.g. dinuclear) in solution.

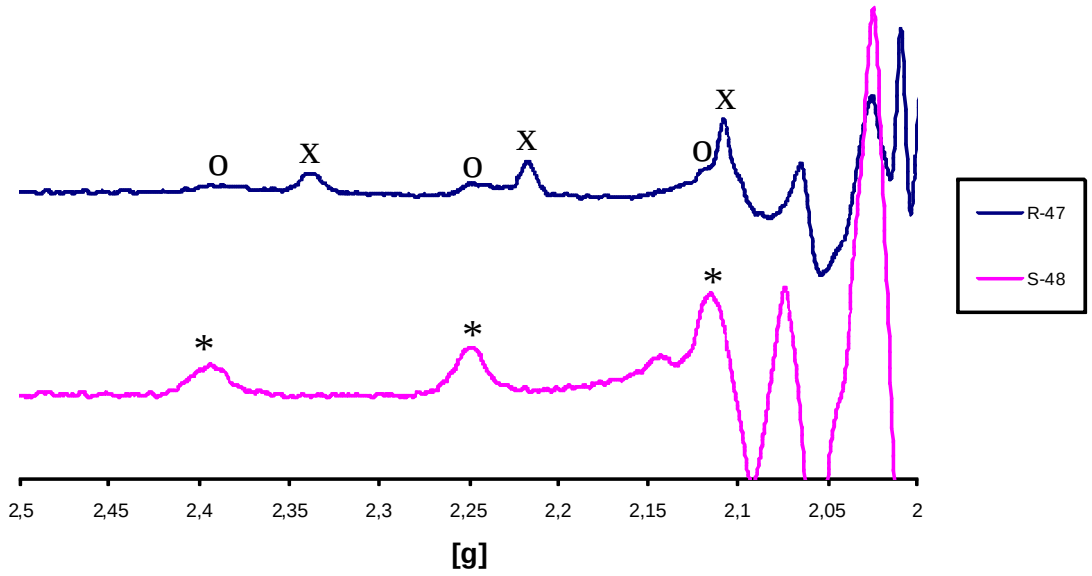

Figure 5.3. First derivative X-band EPR spectra of *R*-**47** and *S*-**48** in the low-field region. The primary species of *R*-**47** is identified as (x) and the secondary species as (o). The primary species of *S*-**48** is identified as (*).

Table 5.1. Experimental spin Hamiltonian parameters for the featured tridentate $V^{IV}O$(AORSB) complexes.[a]

Complex	g_x, g_y (or $g_\perp$)	A_x, A_y (or $A_\perp$) $\times 10^{-4}$ cm^{-1}	g_z (or $g_{//}$)	A_z (or $A_{//}$) $\times 10^{-4}$ cm^{-1}	Predicted equatorial donor set
R-**47**			1.962	149.0	---
R-**47**[b]				165.0[c]	N_{amine}, O_{ArO-}, O_{DMF}, O_{DMF}
S-**48**	1.979,1.987	59.4, 60.6	1.948	168.5	N_{amine}, O_{ArO-}, O_{DMF}, O_{water}
S-**49**	1.979, 1.984	57.6, 60.3	1.948	167.8	N_{amine}, O_{ArO-}, O_{DMF}, O_{water}
S-**50**	1.979, 1.989	58.3, 58.7	1.947	168.5	N_{amine}, O_{ArO-}, O_{DMF}, O_{water}

[a]Spectra of solutions in DMF were measured at 77K. [b] Secondary species. [c] Manually estimated value.

The parameters obtained for *S*-**48**, *S*-**49** and *S*-**50** are very similar. There is anisotropy in the *xy* symmetry plane as is evidenced by the small difference exhibited between *x* and *y* parameter components. As expected, the spin Hamiltonian parameters for the primary species of *R*-**47** are quite different from the rest, having lower values with the exception of $\mathbf{g_z}$. Because the *xy* or perpendicular signals are usually intense, the existence of a secondary species may compromise the estimation of the corresponding parameter values. There is no safe way to distinguish which signals belong to which species and as such, no estimation was made. The possible binding modes in solutions for the $V^{IV}O$(AORSB) compounds and the corresponding estimated $\mathbf{A_z}$ are shown in Figure 5.4.

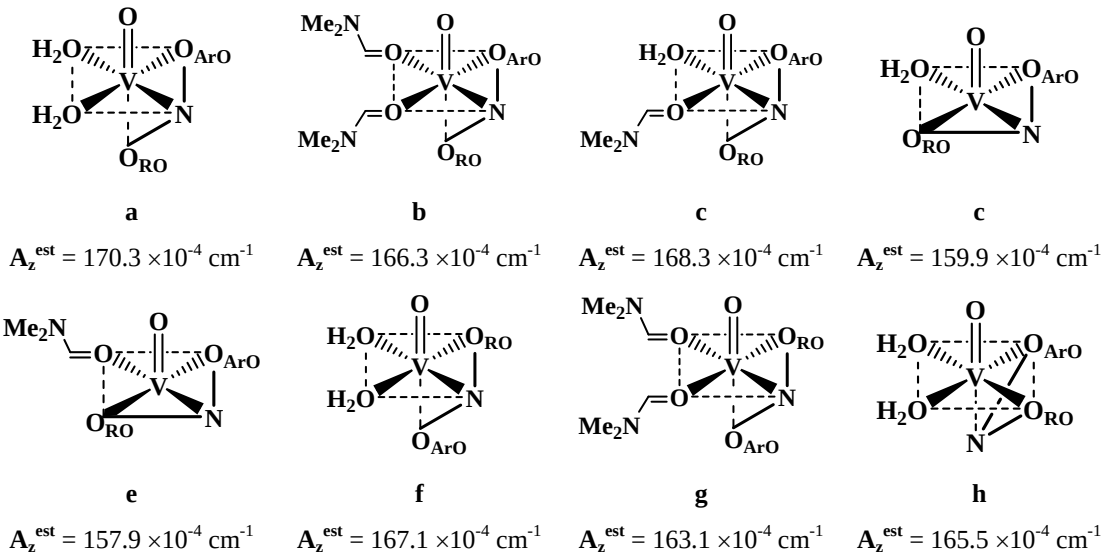

Figure 5.4. Possible binding modes in solution for the featured tridentate $V^{IV}O$(AORSB) complexes.

Considering the accepted estimation error of ± 3 × 10^{-4} cm^{-1},[9] the experimental $\mathbf{A_z}$ values for complexes *S*-**48** to *S*-**50** seem to be in accordance with the proposed binding modes **b**, **c** and **f**. The secondary species of *R*-**47** may adopt conformation **b** or **h** in solution. Nevertheless, the primary species of *R*-**47** appears to be completely different from what is expected. The much lower experimental $\mathbf{A_z}$ obtained for this case could be the result of one of the following possibilities: the $V^{IV}O$ moiety is bound to the amine and alkoxide groups of two ligand units or unreacted aminoalcohol, or the expected complex is under the influence of a solvent molecule *trans* to the V=O bond, as described by Garriba *et al.*[13,14] Without a revised additivity rule that considers this *trans* effect, or adequate theoretical calculations to support the discussion, the true nature of *R*-**47** in DMF solution remains to be well understood.

The prepared $V^{IV}O$(AORSB) compounds gave elemental analysis results consistent with monomeric $V^{IV}O$ compounds having either water or alcohols as vestigial contaminants.

5.3. Catalytic applications: asymmetric sulfoxidation of thioanisole

Similarly to what was done in Chapters 3 and 4, the prepared $V^{IV}O$(AORSB) compounds were screened for their catalytic potential in the asymmetric sulfoxidation of thioanisole under a variety of conditions. In all cases, the final products were either *R*- or *S*-methyl phenyl sulfoxide or the sulfone. All the results obtained are presented in Table 5.2.

Table 5.2. Sulfoxidation of thioanisole with the $V^{IV}O$(AORSB) catalysts.[a]

Entry	Catalyst	Solvent	T(C°)	t (h)	Conv (%)	ee (%)	Sulfone (%)
1	*R*-**47**	DCE	0	24	15	0	0
2	*R*-**47**	CH_2Cl_2	0	24	15	8(S)	0
3[b]	*R*-**47**	CH_2Cl_2	25	4	60	0	7
4	*R*-**47**	CH_3CN	0	24	80	0	12
5[b]	*S*-**48**	DCE	40	4	71	6(S)	8
6[b]	*S*-**48**	CH_2Cl_2	25	4	66	5(S)	6
7	*S*-**48**	CH_2Cl_2	0	24	26	0	1
8	*S*-**48**	$CHCl_3$	0	24	73	3(S)	4
9	*S*-**48**	CH_3CN	0	24	99	0	9
10[b]	*S*-**49**	CH_2Cl_2	0	24	68	4(S)	7
11	*S*-**49**	CH_2Cl_2	25	4	91	1(S)	8
12[b]	*S*-**50**	DCE	40	4	76	11(S)	11
13	*S*-**50**	CH_2Cl_2	0	24	93	6(S)	11
14[b]	*S*-**50**	CH_2Cl_2	25	4	79	9(S)	12
15	*S*-**50**	$CHCl_3$	0	24	93	9(S)	5

[a]Conditions: nS=1 mmol; nH_2O_2:nS=1.5; 1 mol% of catalyst. [b]nH_2O_2:nS = 1.05.

Contrary to what was expected, the $V^{IV}O$(AORSB) catalysts exhibited very low enantioselectivities, despite the high conversions and low sulfone percentages. Reaction temperature seemed to have little effect on the observed enantioselectivities, although there was a slight increase in enantiomeric excess with higher temperature in the case of *S*-**48** (entries 5 to 7) and *S*-**50** (entries 12 to 14). Solvent effect manifested mainly in the conversion percentages. For instance, for *R*-**47**, the reaction run in acetonitrile gave no

enantiomeric excess (entry 4) but gave higher conversions compared to the reaction run on chlorinated solvents at the same temperature. In fact, the reactions in DCE and CH_2Cl_2 at 0 ºC gave low conversions (entries 1 and 2). Of these, some, but low, enantiomeric excess was observed only in CH_2Cl_2 (entry 2). The same trend in terms of conversion was observed for *S*-**48**, although the reaction in CH_2Cl_2 at 0 ºC gave a slightly higher conversion (entry 7). *S*-**49** exhibited a higher activity in CH_2Cl_2 and a slightly higher enantioselectivity than *S*-**48** at the same temperature (entry 10). The increase in reaction temperature was accompanied with a significant increase in conversion without additional sulfone production (entry 11). *S*-**50** gave the best results in terms of activity and enantioselectivity. At 0 ºC in CH_2Cl_2, a conversion of 93% and an enantiomeric excess of 6% was obtained along with 11% of sulfone (entry 13). Replacement of CH_2Cl_2 by $CHCl_3$ caused a slight increase in enantiomeric excess from 6 to 9% and a reduction in sulfone production (entry 15). Increasing the temperature resulted in an additional increase in enantioselectivity when using DCE as solvent (entry 12).

The obtained enantiomeric excesses for the various $V^{IV}O$(AORSB) catalysts are low and do not go beyond 11%. These results may indicate that the C=N double bond present in the ligand structure of Bolm's original catalyst plays an important role in directing the enantioselectivity of the catalytic species. This may result from the rigidity conferred by the C=N double bond. Another factor that may be relevant is the fact that the N_{amine} donor atoms become chiral centers upon coordination, possibly yielding an almost racemic mixture (as far as this stereogenic center is concerned).

The *in situ* versions of the prepared $V^{IV}O$(AORSB) catalysts were also tested in the asymmetric sulfoxidation of thioanisole. The Schiff base ligand precursor compounds *S*-**15** and *S*-**16** were included in this study to observe if the C=N double bond plays indeed such a determinant role in catalyst enantioselectivity. The protocol employed by Bolm and Bienewald was used here. The results obtained for the *in situ* catalysts are presented in Table 5.3. Figure 5.5 shows the structural formulas of the aminoalcohol ligand precursor compounds *R*-**11** to *S*-**16**, first described in Chapter 2.

Table 5.3. Sulfoxidation of thioanisole with the VO^{IV}(AORSB) catalysts.[a]

Entry	Catalyst	Conv (%)	ee (%)	Sulfone (%)
1	$V^{IV}O(acac)_2$ / *R*-**11**	5	15(S)	0
2	$V^{IV}O(acac)_2$ / *S*-**12**	3	0	0
3	$V^{IV}O(acac)_2$ / *S*-**13**	5	5(S)	0
4	$V^{IV}O(acac)_2$ / *S*-**14**	77	6(S)	16
5	$V^{IV}O(acac)_2$ / *S*-**15**	90	42(S)	8
6	$V^{IV}O(acac)_2$ / *S*-**16**	92	50(S)	21

[a]Conditions: 2 mL CH_2Cl_2; nS=1 mmol; nH_2O_2:nS=1.2; 1 mol% of $V^{IV}O(acac)_2$; 1.5 mol% of ligand; T = 0 ºC; t= 24 h.

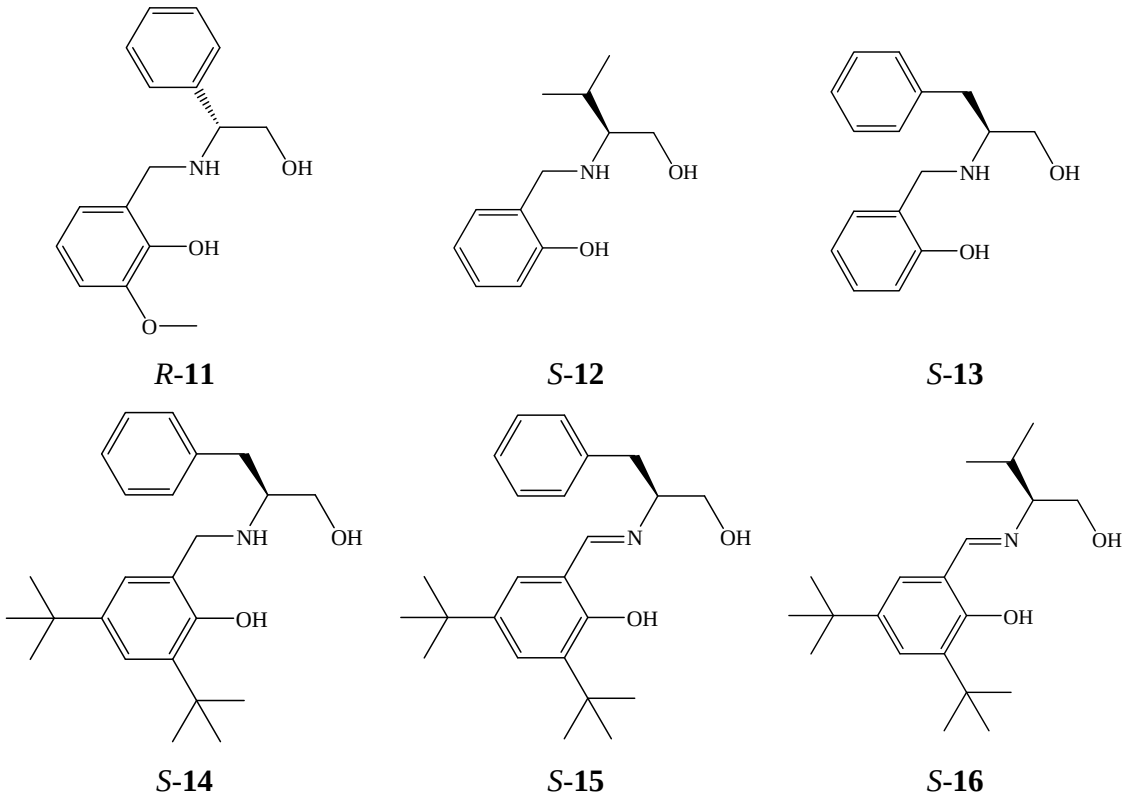

Figure 5.5. Structural formulas of the aminoalcohol-derived ligand precursor compounds depicting their respective configuration.

The *in situ* versions of *R*-**47**, *S*-**48** and *S*-**49** (entries 1, 2 and 3, respectively) gave even lower activities than the precatalyst versions. Only the *in situ* version of *S*-**50** exhibited an activity and enantioselectivity comparable to the precatalyst version at the same temperature and in the same solvent (entry 4). Surprisingly, when the Schiff base

version of *S*-**50** was used, a significant increase in enantioselectivity was obtained from 6 to 42%. This result is also coherent with the results reported by Zhao and co-workers.[4] Structurally, the difference resides only in the type of carbon-nitrogen bond bridging the aminoalcohol and phenolate moieties. In the Schiff base ligand precursor *S*-**15** a C=N double bond is present. This double bond confers rigidity to the ligand structure apparently necessary for asymmetric induction in the sulfoxidation of thioanisole. If this C=N double bond is replaced by a C-N single bond, as is the case of *S*-**14**, the result is a more flexible ligand structure which clearly proves detrimental not only to catalyst enantioselectivity but to overall activity (see Scheme 5.8). When the phenylalaninol motif is replaced by the valinol motif, the result is a Schiff base ligand precursor compound very similar to Bolm's design. Again, when the Schiff base *S*-**16** was used as ligand, a slightly higher conversion and enantiomeric excess was obtained compared to the *in situ* version of *S*-**50** (entry 6). This final result is in agreement with the results obtained by Bolm and Bienewald.

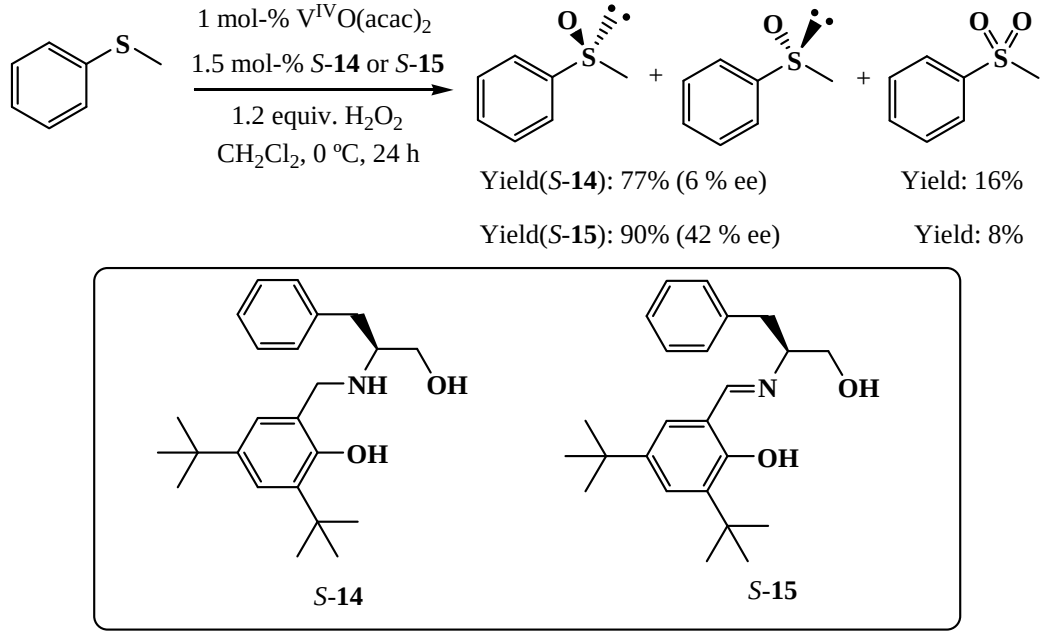

Scheme 5.8. Asymmetric sulfoxidation with *in situ* catalysts based on *S*-**14** and *S*-**15**.

5.4. Conclusions

Several aminoalcohol-derived $V^{IV}O$ compounds bearing structural similarity to the catalysts first reported by Bolm and Bienewald[1] were prepared and characterized by EPR spectroscopy and elemental analysis. Reduction of the Schiff base C=N double bond to a single bond proved beneficial in the case of the $V^{IV}O$(salan) catalysts so the same hypothesis was tested with the $V^{IV}O$(AORSB) compounds. Additionally, reduction of the C=N double bond yields compounds much less susceptible to hydrolysis, thus with higher stability in solution towards decomposition. Contrary to the initial expectations, the $V^{IV}O$(AORSB) compounds bearing reduced Schiff base ligands exhibited both very low activities and enantioselectivities, regardless of temperature and solvent used in the reaction. Replicating Bolm's protocol by using compounds *R*-**11**, *S*-**12**, *S*-**13** and *S*-**14** as the ligand precursors in the *in situ* versions of the described $V^{IV}O$(AORSB) catalysts resulted in lower activities. When the Schiff base compound *S*-**15** was used as ligand in the *in situ* Schiff Base version of *S*-**50**, the obtained enantioselectivities were significantly superior. These results indicate that while a Schiff base catalyst may be more susceptible to hydrolytic degradation, the rigidity conferred to the ligand structure by the imine moiety plays an important role in this catalyst class, particularly as far as enantioselectivity is concerned.

5.5. Experimental section

5.5.1. General considerations

Unless stated otherwise, all preparations were made under inert atmosphere. Subsequent manipulations after compound preparation did not require inert atmosphere techniques. All solvents and reagents were purchased from commercial suppliers and used as received.

5.5.2. Characterization techniques

5.5.2.1. Elemental Analysis (EA)

Elemental analyses were carried out at *Laboratório de Análises* of *Instituto Superior Técnico,* using EA110 CE automatic analyzer Instruments. The results presented are the average values obtained from two independent determinations.

5.5.2.2. High performance liquid chromatography (HPLC)

The analysis of the products obtained in catalytic sulfoxidation reactions was done by HPLC using a Jasco system equipped with a Daicel Chiralpak IA column, a 870-UV Intelligent UV-Vis detector, two 880-PU Intelligent HPLC Pumps, a 2-line degasser 880-51 and a Rheodyne 725i injector (5 L). The system uses Borwin software for data acquisition and analysis.

5.5.2.3. Electron paramagnetic resonance spectroscopy (EPR)

The electron paramagnetic resonance (EPR) spectra were recorded at 77 K (on glasses made by freezing solutions in liquid nitrogen) with a Bruker ESP 300E X-band spectrometer. The measured spectra were then simulated with the ROKI EPR simulation software developed by Rockenbauer and Korecz.[8]

5.5.3. General procedure for sulfoxidation of thioanisole

The catalytic experiments were carried out at atmospheric pressure, at a constant temperature, in a glass batch reactor, equipped with magnetic stirrer, thermometer and condenser. In a typical run, the solid catalyst (0.25 to 10 mol%) and thioanisole (1 mmol) were dissolved in the appropriate solvent (4 mL). Then the oxidant (1.2 to 1.5 mmol), hydrogen peroxide (30 wt% aqueous solution) was added to the stirring mixture. For the catalytic runs using the *in situ* catalysts, the ligand (1.5 mol%), $V^{IV}O(acac)_2$ (1 mol%) and thioanisole (1 mmol) were dissolved in the appropriate solvent (4 mL). Then the oxidant (1.2 to 1.5 mmol) and hydrogen peroxide (30 wt% aqueous solution) were added to the stirring mixture. Control experiments were carried out in absence of catalyst. Samples of the reaction mixture were withdrawn periodically and analyzed on a Jasco

HPLC system equipped with a Daicel Chiralpak IA column. The eluent used was hexane/ethyl acetate (60:40) with a flow of 1 mL/min. The calibration curves for each reagent and product, namely sulfide, sulfoxide and sulfone, were determined using similar HPLC procedures and these calibrations used for the quantitative analyses. Diphenylsulfone was used as an internal standard.

5.5.4. $V^{IV}O$(AORSB) compound preparation methods

General preparation procedure

The procedure was similar to those described in Chapter 4. $V^{IV}OCl_2$ was added to a methanolic (25 mL) solution of the appropriate ligand under a nitrogen atmosphere. The pH was adjusted to *ca*. 7-8 with a 2 M aqueous solution of KOH. The addition of water (25 mL) induced the complete precipitation of $V^{IV}O$ compound. The precipitate was filtered and washed with water, minimal amounts of methanol and lastly *n*-hexane. All compounds are soluble in diethyl ether. The recovered solid was then dried under vacuum. This method was used for all the described $V^{IV}O$ compounds.

Synthesis of [$V^{IV}O$(*R*-11)], *R*-47

Reagents: $V^{IV}OCl_2$ (0.14 g, 0.8 mmol), ***R*-11** (0.25 g, 0.8 mmol). The compound was obtained as a brown solid. Yield: 0.11 g, 40 %. EPR (DMF): $\mathbf{A_z^1}$=149.0 x10^{-4} cm^{-1}; $\mathbf{A_z^2}$=165.0 ×10^{-4} cm^{-1}; $\mathbf{g_z^1}$=1.962. Elemental analysis for $C_{16}H_{17}NO_4V{\cdot}H_2O$: calcd. C 53.94, H 5.38, N 3.93; found C 54.1, H 5.4, N 3.8.

Synthesis of [$V^{IV}O$(*S*-12)], *S*-48

Reagents: $V^{IV}OCl_2$ (0.4 g, 2.0 mmol), ***S*-12** (2.5 g, 2.0 mmol). Dichloromethane was used instead of methanol in the washing procedure. The compound was obtained as a light brown solid. Yield: 0.14 g, 26 %. EPR (DMF): $\mathbf{A_z}$=168.5 ×10^{-4} cm^{-1}; $\mathbf{g_z}$=1.948. Elemental analysis for $C_{12}H_{17}NO_3V{\cdot}1H_2O{\cdot}0.6CH_2Cl_2$: calcd. C 44.10, H 5.93, N 4.08; found C 44.1, H 5.6, N 4.1.

Synthesis of [$V^{IV}O$(*S*-13)], *S*-49

Reagents: $V^{IV}OCl_2$ (0.34 g, 2.0 mmol), ***S*-13** (0.5 g, 2.0 mmol). The compound was obtained as a dark brown solid. Yield: 0.25 g, 39 %. EPR (DMF): $\mathbf{A_z}$=167.8 $\times 10^{-4}$ cm^{-1}; $\mathbf{g_z}$=1.948. Elemental analysis for $C_{16}H_{17}NO_3V \cdot H_2O$: calcd. C 56.48, H 5.63, N 4.12; found C 56.7, H 5.3, N 4.2.

Synthesis of [$V^{IV}O$(*S*-14)], *S*-50

Reagents: $V^{IV}OCl_2$ (0.2 g, 1.2 mmol), ***S*-14** (0.5 g, 1.2 mmol). The compound was obtained as a dark brown solid. Yield: 0.2 g, 38 %. EPR (DMF): $\mathbf{A_z}$=168.5 $\times 10^{-4}$ cm^{-1}; $\mathbf{g_z}$=1.9479. Elemental analysis for $C_{24}H_{33}NO_3V \cdot 0.2H_2O$: calcd. C 65.80, H 7.68, N 3.20; found C 65.8, H 7.9, N 3.2.

5.6. References

1 Bolm. C.; Bienewald, F. *Angew. Chem. Int. Ed. Engl.* **1995**, *34*, 2640-2642.

2 Vetter, A. H.; Berkessel, A. *Tetrahedron Lett.* **1998**, *39*, 1741-1744.

3 Jeong, Y.; Choi, S.; Hwang, Y. D.; Ahn, K. *Tetrahedron Lett.* **2004**, *45*, 9249-9252.

4 Zeng, Q.; Wang, H.; Wang, T.; Cai, Y.; Weng, W.; Zhao, Y. *Adv. Synth. Catal.* **2005**, *347*, 1933-1936.

5 Drago, C.; Caggiano, L.; Jackson, R. F.W. *Angew. Chem.* **2005**, *117*, 7387-7389.

6 Cucciolito, M. E.; Del Litto, R.; Roviello, G.; Ruff, F. *J. Mol. Cat. A: Chem.* **2005**, *236*, 176-181.

7 Liu, H.; Wang, H.; Wang, Y.; Wang, Y.; Sun, H.; Sun, L. *Catal. Commun.* **2009**, *11*, 294-297.

8 Rockenbauer, A.; Korecz, L. *Appl. Magn. Reson.* **1996**, *10*, 29-43.

9 Chasteen, N. D. in: Berliner, L. J.; Reuben, J. (Eds.), *Bio. Magn. Res.*, Plenum Press, New York, **1981**, *3*, 53-119.

10 Rao, S. N.; Mishra, D. D.; Maurya, R. C.; Rao N. N. *Polyhedron* **1997**, *16*, 1825-1829.

11 Li, X.; Lah, M. S.; Pecoraro, V. L. *Inorg. Chem.* **1988**, *27*, 4657-4664.

12 Carrano, C. J.; Nunn, C. M.; Quan, R.; Bonadies, J. A.; Pecoraro, V. L. *Inorg. Chem.*, **1990**, *29*, 944-951.

13 Kiss, E.; Garribba, E.; Micera, G.; Kiss, T.; Sakurai, H. *J. Inorg. Biochem.* **2000**, *78*, 97-108.

14 Gorelsky, S.; Micera, G.; Garribba, E. *Chem. Eur. J.* **2010**, *16*, 8167-8180.

Chapter 6

Aminoacid-derived Vanadium(IV) Complexes

6. Aminoacid-derived Vanadium(IV) Complexes

6.1. Introduction

Shortly after the development by Carsten Bolm and Frank Bienewald of the *tert*-leucinol-based $V^{IV}O$(Schiff base) catalytic system for asymmetric sulfoxidation,[1] the next step would include the use of L-aminoacids as chiral building blocks instead of aminoalcohols. Being naturally occurring compounds, L-aminoacids are cheaper and enjoy greater availability than the aminoalcohol derivatives, making them attractive building blocks in the development of aminophenolate-type catalysts.

Following 1995, various authors reported the preparation of aminoacid-derived $V^{IV}O$(Schiff base) compounds,[2] but application of such compounds in asymmetric synthesis predates Bolm's aminoalcohol-derived $V^{IV}O$(Schiff base) system.

In 1989, Fujita[3] and co-workers reported the characterization of several $V^{V}O$(Schiff base) compounds derived from L-alanine and their application in the asymmetric sulfoxidation of thioanisole, using *tert*-butyl hydroperoxide (TBHP) as oxidant (Scheme 6.1).

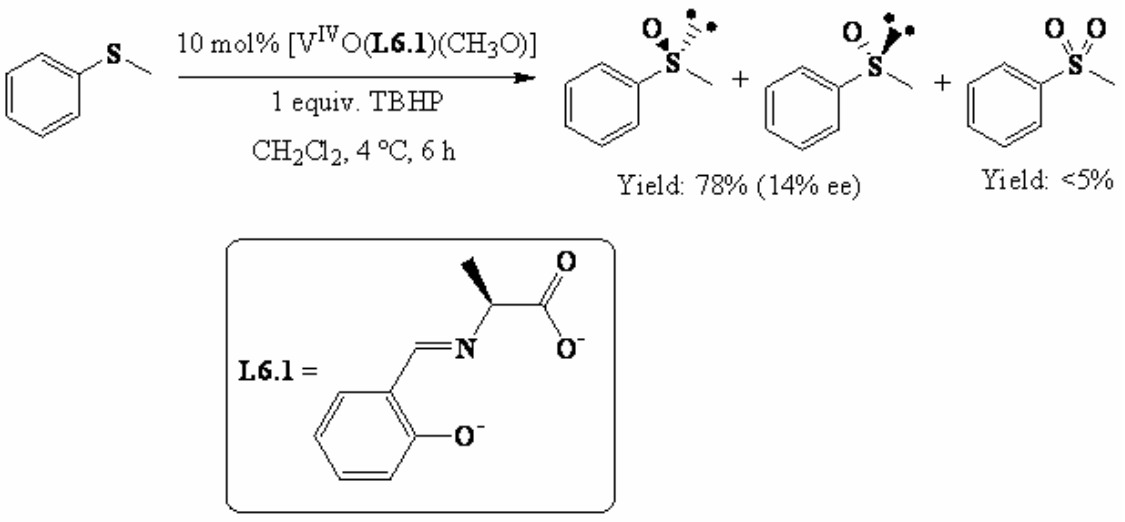

Scheme 6.1. Aminoacid-derived $V^{IV}O$(Schiff base)-promoted asymmetric sulfoxidation.

In 2004, Maeda and co-workers further studied the potential of aminoacid-derived $V^{IV}O$(Schiff base) catalysts by expanding the range of employed L-aminoacids (Scheme 6.2).[4]

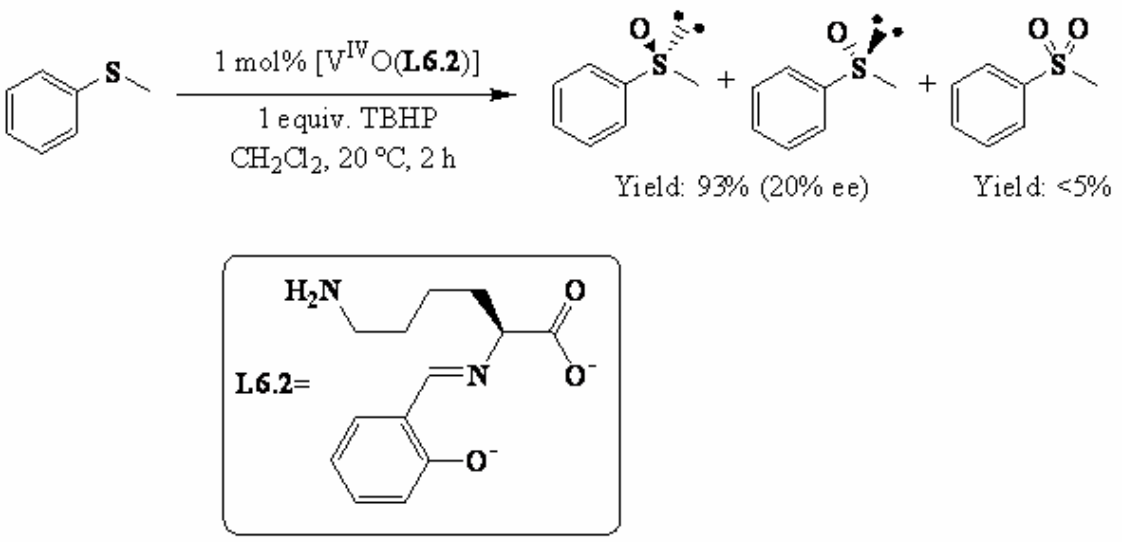

Scheme 6.2. Aminoacid-derived $V^{IV}O$(Schiff base)-promoted asymmetric sulfoxidation.

Comparatively to Bolm's system, aminoacid-derived $V^{IV}O$(Schiff base) catalysts devised by the groups of Fujita and Maeda exhibited a significantly lower enantioselectivity and activity for sulfoxidation as a result of the replacement of the $O_{alcohol}$ donor atom by a $O_{carboxylate}$ donor atom. This can explain the relatively limited amount of reports regarding asymmetric sulfoxidation using these compounds. Aminoacid-derived $V^{IV}O$(Schiff base) catalysts found application in other types of asymmetric reactions. In 2002, Gong and co-workers[5a] reported L-phenylalanine and L-valine dinuclear $V^{IV}O$(Schiff base) compounds (Scheme 6.3) capable of catalyzing the oxidative coupling of naphthols, using O_2 as oxidant. Two years later, Sasai and co-workers[5] expanded the study on this system by using *tert*-leucine and testing different solvents. These catalytic systems are noteworthy due to the use of the BINOL structural motif and the high activities and enantioselectivities observed in the oxidative coupling of 2-naphthol.

Despite the limited work carried out with this class of compounds, there is still much untapped potential, considering that the aminoacid building blocks are not restricted to naturally occurring L-aminoacids.

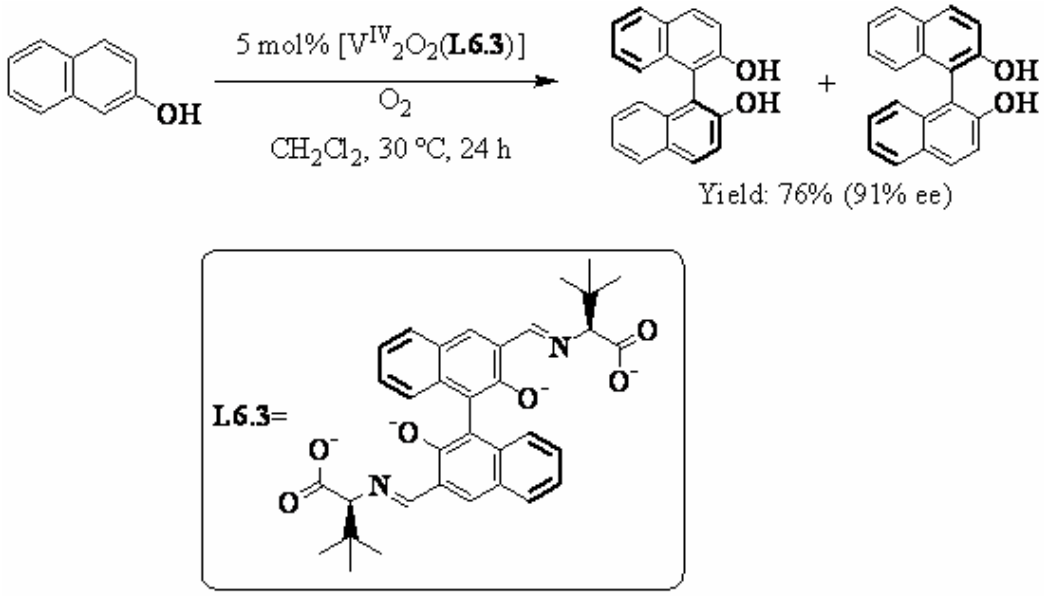

Scheme 6.3. Aminoacid-derived $V^{IV}O$(Schiff base)-promoted asymmetric sulfoxidation.

Additionally, the side-chains of aminoacids may often be functionalized, providing more structural manipulation possibilities. For instance, L-aminoacids such as L-cysteine and L-tyrosine are particularly useful in the design of solid-supported catalysts, where the side-chains provide readily-available anchoring points without additional structural modification to the ligand structure or its building blocks.[8,9] In this respect, the salen-type, salan-type and the aminoalcohol-derived Schiff base compounds present limitations as the respective building blocks often require modification to provide anchoring points for a solid support matrix.

With the objective of providing further insight into the aminoacid-derived $V^{IV}O$ catalytic systems, several related $V^{IV}O$ catalysts bearing aminoacid-derived reduced Schiff base (RSB) ligands were prepared and tested in the asymmetric sulfoxidation of thioanisole. Again, the same hypothesis behind the development of the $V^{IV}O$(salan) and the $V^{IV}O$(RSB) compounds is employed here with the expectation that upon the use of RSB compounds an increase in enantioselectivity, hydrolytic stability and activity is obtained compared to the original catalysts devised by the groups of Fujita and Ando. The prepared compounds were also evaluated for their potential application in the development solid-supported variants.

6.2. Aminoacid-derived $V^{IV}O$ compound preparation: results and discussion

The procedures used for the preparation of the aminoacid-derived $V^{IV}O$ compounds were similar to those used for the complexes described in the previous Chapters. The aminoacid-derived $V^{IV}O$ compounds were readily prepared by reacting aqueous $V^{IV}OCl_2$ with the appropriate aminoacid-derived reduced Schiff base (AARSB) ligand under inert atmosphere. The desired complex precipitates from the reaction mixture after the medium pH is adjusted to *ca*. 7-8 with aqueous potassium hydroxide. The solid compounds are relatively air-stable. All $V^{IV}O$(AARSB) were obtained as grey solids after precipitation. Preparation of the $V^{IV}O$ compounds using ligand precursor compounds *S*-**24**, *S*-**25** and *S*-**26** failed due to the tendency of the resulting complexes to readily undergo oxidation and subsequent degradation. All the attempts to obtain suitable crystals for single-crystal X-ray diffraction were not successful. Characterization of the prepared compounds was made mainly by EPR spectroscopy and elemental analysis. IR, CD and UV-Vis spectroscopic techniques were also used whenever possible. Figure 6.1 depicts the structural formulas of the prepared compounds *S*-**51**, *S*-**52**, *S*-**53**, *S*-**54**, *R*-**55** and *R*-**56**. Preparation of $V^{IV}O$ complexes using L-cysteine derived ligands was not viable due to the interference caused by the side-chain thiol group during the complex synthesis in conjunction with its tendency to oxidize to dissulfide. The same side-chain interference was observed with the L-tyrosine derived ligands, although to a lesser extent.

Circular dichroism spectroscopy (CD) was used to confirm if the prepared $V^{IV}O$ compounds exhibited chirality in solution. There was a special concern regarding the chirality of the obtained L-cysteine derived $V^{IV}O$(AARSB) compounds, as $V^{IV}O$-induced racemization of L-cysteine has been reported.[6]

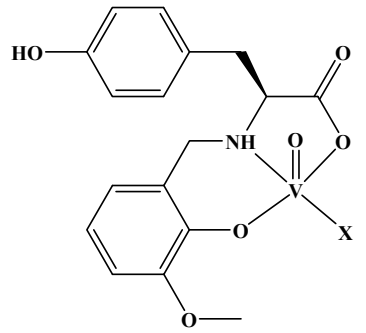

S-**51**

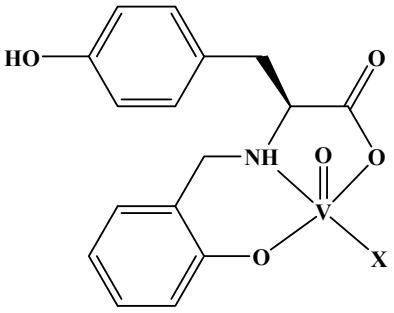

S-**52**

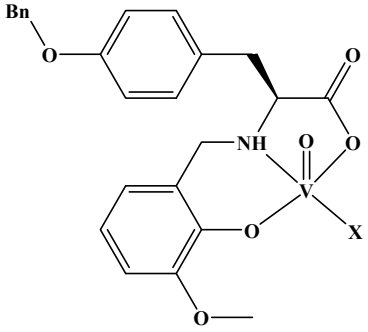

S-**53**

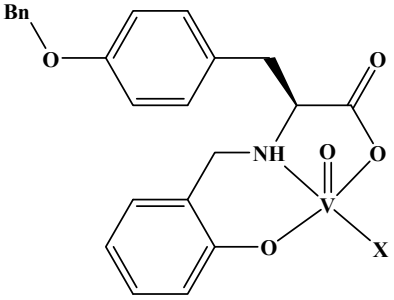

S-**54**

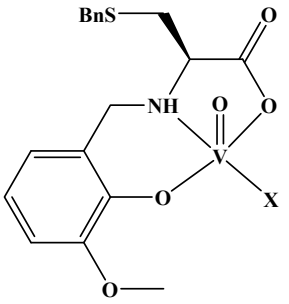

R-**55**

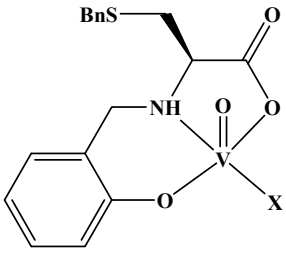

R-**56**

Figure 6.1. Structural formulas of the prepared aminoacid-derived $V^{IV}O$ complexes depicting their respective configuration. The letter X denotes a coordinated solvent molecule.

Also, all compounds exhibited a tendency to oxidize in solution. *S*-**54** did not present the adequate solubility in ethyl acetate, prompting the preparation of more dilute samples containing DMSO. The obtained CD and UV-Vis spectra for compounds *S*-**53**, *S*-**54**, *R*-**55** and *R*-**56** are presented in Figures 6.2 and 6.3, respectively. The relevant λ_{max}, ε and $\Delta\varepsilon$ are listed in Table 6.1.

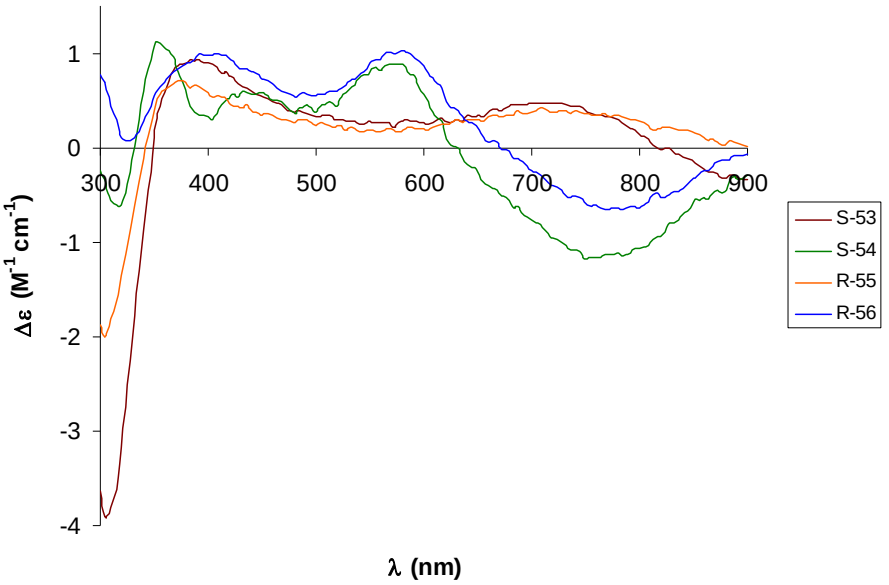

Figure 6.2. CD spectra of *S*-**53**, *R*-**55** and *R*-**56** in ethyl acetate. The CD spectrum of *S*-**54** was recorded from a 1:1 ethyl acetate/DMSO solution. The spectra were recorded with 5.27 mM (*S*-**53**), 2.82 mM (*S*-**54**), 4.83 mM (*R*-**55**) and 5.05 mM (*R*-**56**) solutions with a 1mm optical path cell.

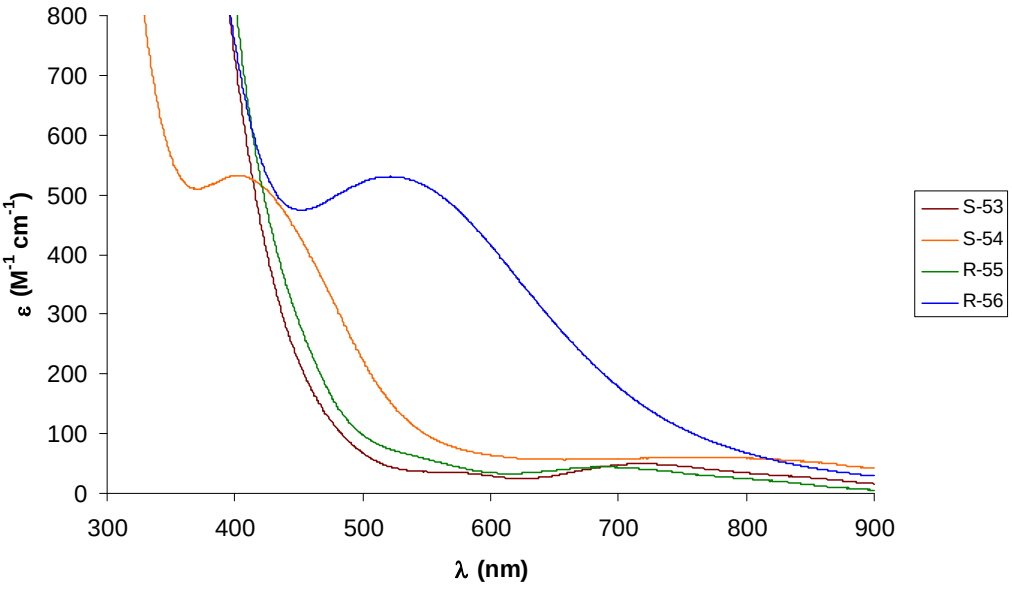

Figure 6.3. Isotropic absorption spectra (UV-Vis) of *S*-**53**, *R*-**55** and *R*-**56** in ethyl acetate. The UV-Vis spectrum of *S*-**54** was recorded from a 1:1 ethyl acetate/DMSO solution. The spectra were recorded with 5.27 mM (*S*-**53**), 2.82 mM (*S*-**54**), 4.83 mM (*R*-**55**) and 5.05 mM (*R*-**56**) solutions with a 1mm optical path cell.

Table 6.1. λ_{max}, ε and Δε values for *S*-**53**, *S*-**54**, *R*-**55** and *R*-**56**.

CD							
S-**53**		*S*-**54**		*R*-**55**		*R*-**56**	
λ (nm)	Δε ($M^{-1}cm^{-1}$)	λ (nm)	Δε ($M^{-1}cm^{-1}$)	λ (nm)	Δε ($M^{-1}cm^{-1}$)	λ (nm)	Δε ($M^{-1}cm^{-1}$)
710	0.47	770	−1.13	710	0.41	770	-0.65
392	0.93	572	0.89	376	0.71	580	1.01
		432	0.59			408	0.99
		352	1.12				
UV-Vis							
λ (nm)	ε ($M^{-1}cm^{-1}$)	λ (nm)	ε ($M^{-1}cm^{-1}$)	λ (nm)	ε ($M^{-1}cm^{-1}$)	λ (nm)	ε ($M^{-1}cm^{-1}$)
720	50	770	41	690	44	520	530
550	37	403	532				

The CD spectra depicted in Figure 6.2 show that the prepared $V^{IV}O$(AARSB) compounds exhibit optical activity in solution. Despite the tendency to quickly oxidize in solution, the *d*-*d* band **I** (see Chapter 4) was detected at *ca*. 710 nm in the cases of *S*-**53** and *R*-**55** and at *ca*. 770 nm in the case of *R*-**56**. The CD spectrum of *S*-**54** exhibits the *d*-*d* **I** band ($d_{xy} \rightarrow d_{xz}, d_{yz}$) at *ca*. 770 nm. Noteworthy is the similarity between the CD spectra of *S*-**53** and *R*-**55**. The structural similarity shared by both complexes is the phenolate moiety, which derives from *o*-vanillin. Apart from the aforementioned *d*-*d* **I** bands for both complexes, an additional signal is visible at *ca*. 400 nm, possibly corresponding to charge-transfer (CT) transitions or to the *d*-*d* **III** bands. Likewise, the CD spectra of *S*-**54** and *R*-**56** show some similarity as well. In addition to the observed *d*-*d* **I** bands at 770 nm, *d*-*d* **II** bands ($d_{xy} \rightarrow d_{x2-y2}$) are observed in both cases at *ca*. 570-550 nm. Signals corresponding to either CT transitions or *d*-*d* **III** bands at *ca*. 400 nm are also observed. The UV-Vis spectra obtained for these compounds are much less detailed, however (see Figure 6.3). Again, the spectra of *S*-**53** and *R*-**55** exhibit marked similarity. In both cases the *d*-*d* **I** bands are present as faint signals at ca. 690-720 nm. The *d*-*d* **II** bands are also visible, but are partially masked by the very intense and broad CT bands. The UV-Vis spectrum of *S*-**54** is comparatively less intense, but the *d*-*d* **I** band is still discernible at *ca*. 770 nm. A broad CT band is observed at 403 nm. The UV-Vis spectrum of *R*-**56** is indicative of oxidation, as the characteristic phenolate-$V^{V}O$ $p\pi$-$d\pi$* charge transfer band

is observable at *ca.* 530 nm. Again, no definitive conclusion can be made regarding whether the V^V center is a V^VO^{3+} or a $V^VO_2^+$ core, but the intensity is not high enough for a V^VO^{3+} compound.

To verify the possibility of compound racemization after oxidation in solution, CD spectra were measured from the samples prepared earlier after a 24 hour period. The obtained CD spectra for compounds *S*-**53**, *S*-**54**, *R*-**55** and *R*-**56** after oxidation are presented in Figures 6.4, 6.5, 6.6, and 6.7. The relevant λ_{max} and $\Delta\varepsilon$ are listed in Table 6.2.

Table 6.2. λ_{max} and $\Delta\varepsilon$ values for *S*-**53**, *S*-**54**, *R*-**55** and *R*-**56** after 24 hour exposure to air.

S-**53**		*S*-**54**		*R*-**55**		*R*-**56**	
λ (nm)	Δε ($M^{-1}cm^{-1}$)	λ (nm)	Δε ($M^{-1}cm^{-1}$)	λ (nm)	Δε ($M^{-1}cm^{-1}$)	λ (nm)	Δε ($M^{-1}cm^{-1}$)
710	0.30	770	0.12	660	-0.10	770	-0.63
392	0.93	556	-0.10	384	1.08	572	0.87
		404	0.35			412	0.82

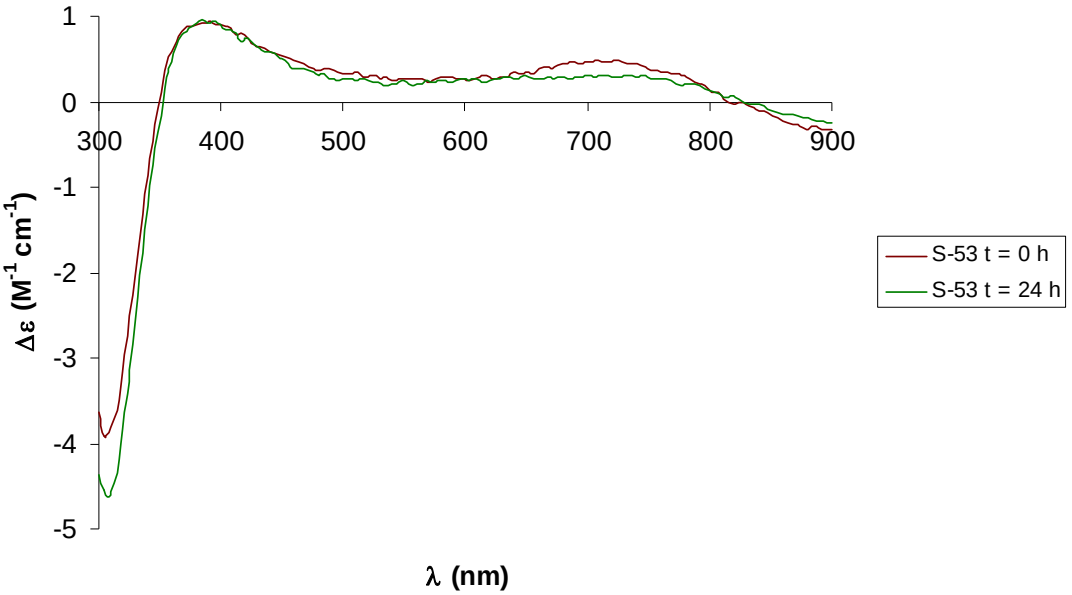

Figure 6.4. CD spectra of *S*-**53** in ethyl acetate before and after a 24 hour period exposure to air. The spectra were recorded with a 5.27 mM (*S*-**53**) solution and a 1 mm optical path cell.

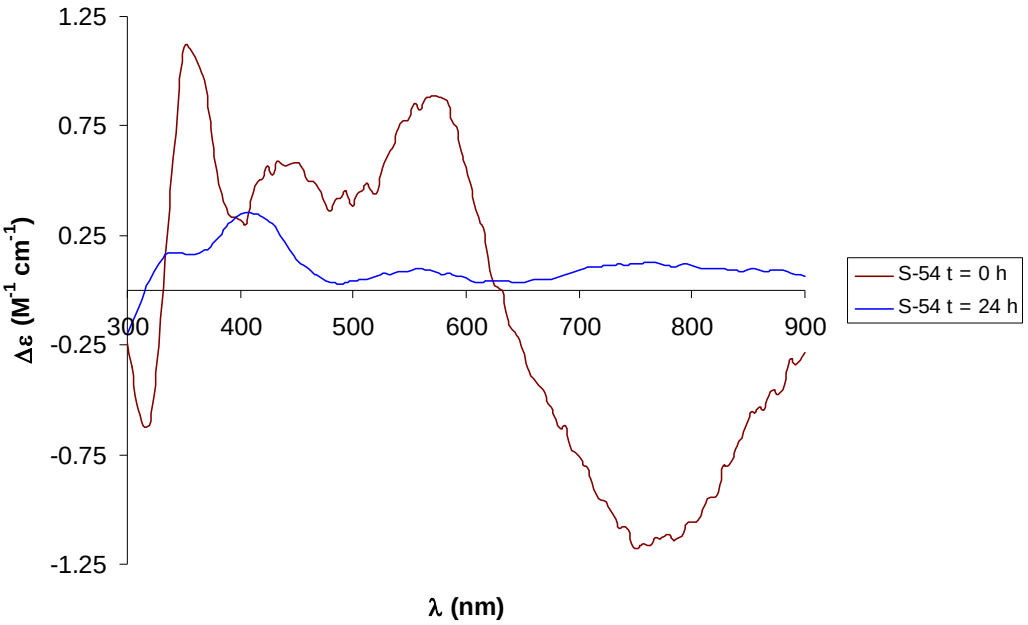

Figure 6.5. CD spectra of *S*-**54** in a 1:1 ethyl acetate/DMSO solution before and after a 24 hour period exposure to air. The spectra were recorded with a 2.82 mM (*S*-**54**) solution and a 1 mm optical path cell.

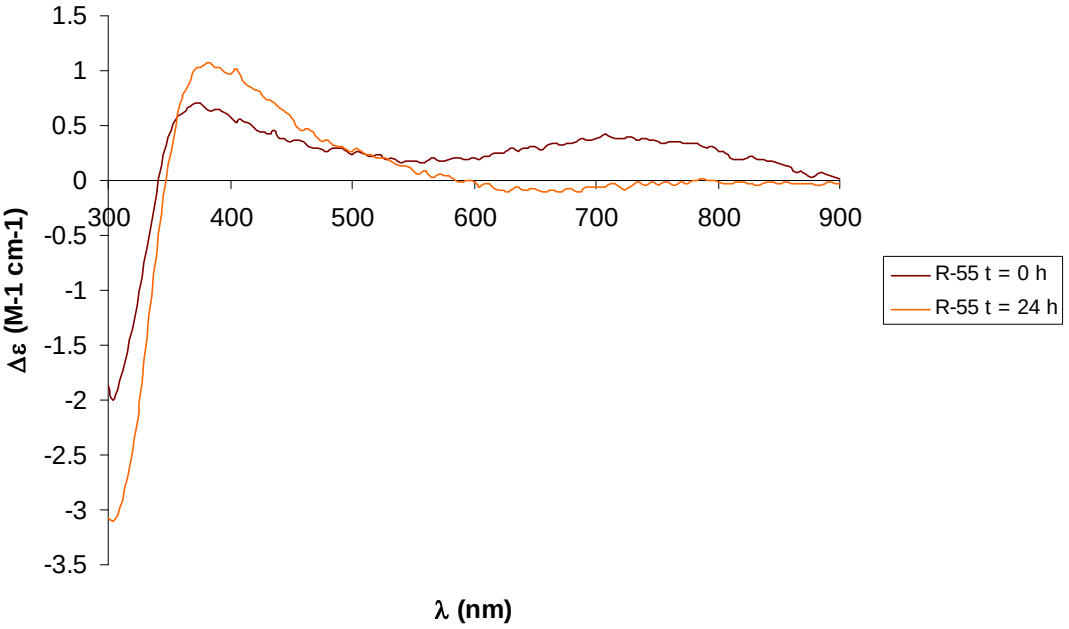

Figure 6.6. CD spectra of *R*-**55** in ethyl acetate before and after a 24 hour period exposure to air. The spectra were recorded with a 4.83 mM (*R*-**55**) solution and a 1 mm optical path cell.

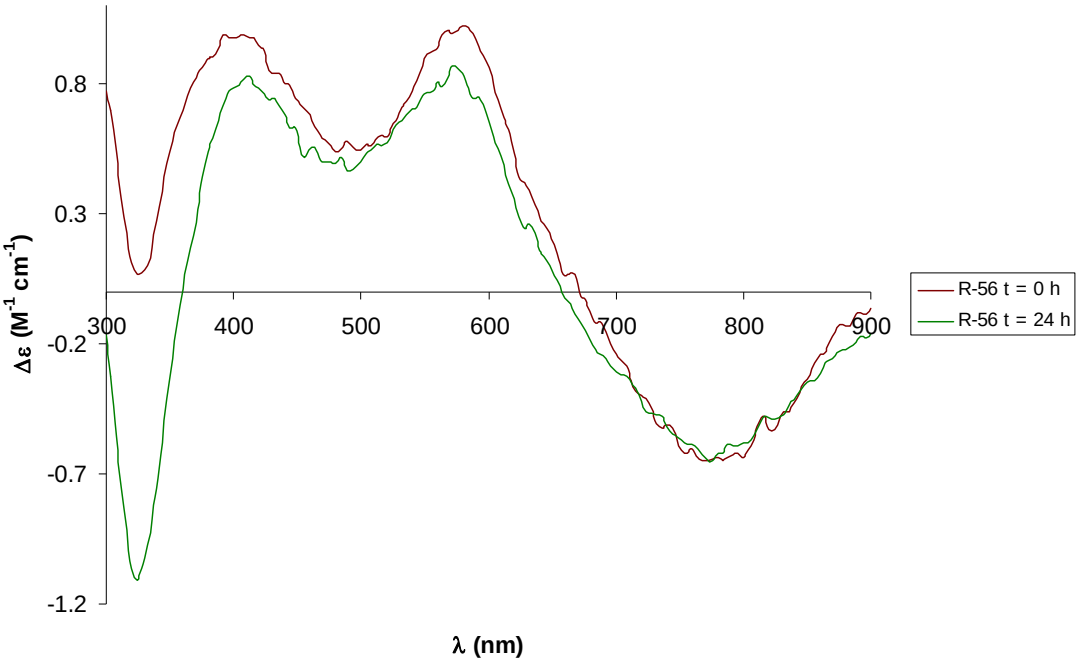

Figure 6.7. CD spectra of *R*-**56** in ethyl acetate before and after a 24 hour period exposure to air. The spectra were recorded with a 5.05 mM (*R*-**56**) solution and a 1 mm optical path cell.

There was minimal change of the CD spectra of *S*-**53** and *R*-**56** after a 24 hour period of exposure to air (see Figures 6.4 and 6.7). Noteworthy is the persistence of the largely unchanged *d-d* **I** bands at 710 nm (from 0.47 to 0.31 $M^{-1}cm^{-1}$) in the case of *S*-**53** and 770 nm (from -0.65 to -0.63 $M^{-1}cm^{-1}$) in the case of *R*-**56**. Remarkable changes were observed in the CD spectrum of *R*-**55** after 24 hours (see Figure 6.6). The *d-d* **I** band initially observed at 710 nm disappeared and a new weaker band with a negative signal at *ca*. 660 nm appeared. The signal at *ca*. 370−400 nm intensified (from 0.71 to 1.08 $M^{-1}cm^{-1}$). The changes seen are probably due to oxidation of the $V^{IV}O$ center. A very drastic change was observed with *S*-**54** (see Figure 6.5). After a 24 hour period of exposure to air, CD spectrum shows a distinct pattern for the *d-d* **I** and **II** bands with greatly reduced intensity, with the **I** band changing signal (from −1.13 to 0.12 $M^{-1}cm^{-1}$). The two bands observed initially at 432 and 352 nm appear to have coalesced into a single band at 404 nm with much lower intensity. These changes in band pattern and intensity indicate that besides oxidation, *S*-**54** is susceptible to a vanadium-induced racemization and/or degradation process during oxidation. The sample of *S*-**54** was the

only one prepared with DMSO which may have further facilitated the oxidation process due to its strongly coordinating nature. The remaining compounds appear to remain largely intact, with *S*-**53** and *R*-**56** resisting oxidation in ethyl acetate solution.

The EPR spectra of compounds *S*-**53**, *S*-**54**, *R*-**55** and *R*-**56** were recorded from DMF solutions at 77 K. Contrasting with what was observed in ethyl acetate, these compounds exhibited a tendency to quickly oxidize after dissolution in DMF. The EPR spectra of *S*-**51** and *S*-**52** were also recorded from methanolic solutions at 77 K. Figure 6.8 shows the EPR spectra obtained for the prepared $V^{IV}O$(AARSB) compounds and Table 6.3 lists the calculated spin Hamiltonian parameters.

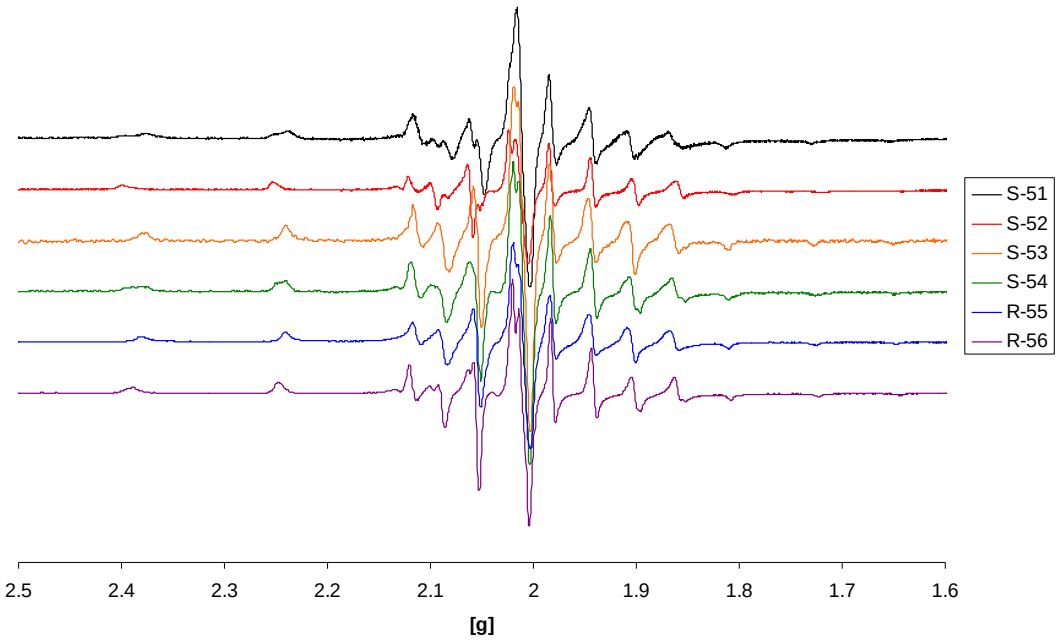

Figure 6.8. First derivative X-band EPR spectrum taken from DMSO, DMF and MeOH samples of the presented $V^{IV}O$(AARSB) compounds, at 77K.

The EPR spectra shown in Figure 6.7 for the described aminoacid-derived $V^{IV}O$ compounds are quite similar. The small differences in the experimental $\mathbf{A_z}$ are mainly due to the solvents used in the preparation of the samples. Secondary species were detected in *S*-**51** and *S*-**54**, although these exhibit $\mathbf{g_z}$ and $\mathbf{A_z}$ parameters very similar to the primary species. Figure 6.9 shows the possible binding modes for the complexes prepared, with the respective estimated $\mathbf{A_z}$ values.

Table 6.3. Experimental spin Hamiltonian parameters for the featured $V^{IV}O$ complexes.

Compound	g_x, g_y (or $g_\perp$)	A_x, A_y (or $A_\perp$) $\times 10^{-4}$ cm^{-1}	g_z (or $g_{//}$)	A_z (or $A_{//}$) $\times 10^{-4}$ cm^{-1}	Predicted equatorial donor set
S-51[a]	1.978, 1.981	51.2, 60.0	1.951	161.7	O_{COO}-, N_{amine}, O_{ArO}-, O_{ROH}
S-52[a]	1.980, 1.978	61.7, 58.6	1.948	168.5	O_{COO}-, N_{amine}, O_{ArO}-, O_{ROH} N_{amine}, O_{ArO}-, O_{ROH}, O_{ROH}
S-53[b]	1.979, 1.979	53.4, 57.9	1.950	162.8	O_{COO}-, N_{amine}, O_{ArO}-, O_{DMF}
S-54[b]	1.979, 1.978	58.0, 56.2	1.949	164.1	O_{COO}-, N_{amine}, O_{ArO}-, O_{DMF}
R-55[b]	1.980, 1.979	55.6, 56.8	1.949	162.4	O_{COO}-, N_{amine}, O_{ArO}-, O_{DMF}
R-56[b]	1.979, 1.978	58.1, 58.2	1.949	165.8	O_{COO}-, N_{amine}, O_{ArO}-, O_{DMF} N_{amine}, O_{ArO}-, O_{DMF}, O_{DMF}

[a] EPR spectrum measured with methanol solution. [b] EPR spectrum measured with DMF solution.

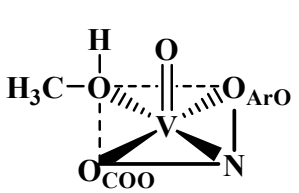

a $A_z^{est} = 166.7 \times 10^{-4}$ cm^{-1}

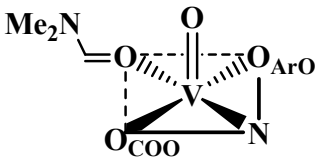

b $A_z^{est} = 164.7 \times 10^{-4}$ cm^{-1}

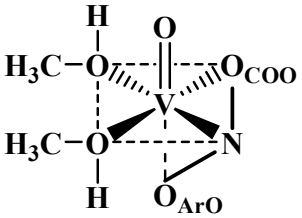

c $A_z^{est} = 173.6 \times 10^{-4}$ cm^{-1}

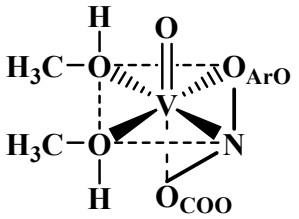

d $A_z^{est} = 170.3 \times 10^{-4}$ cm^{-1}

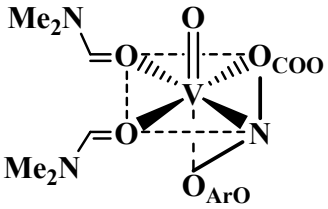

e $A_z^{est} = 169.6 \times 10^{-4}$ cm^{-1}

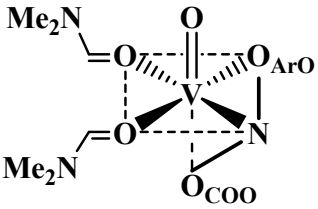

f $A_z^{est} = 166.3 \times 10^{-4}$ cm^{-1}

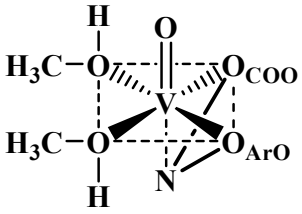

g $A_z^{est} = 173.3 \times 10^{-4}$ cm^{-1}

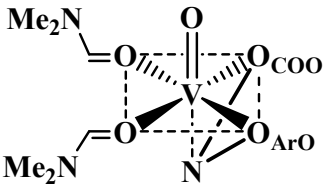

h $A_z^{est} = 168.3 \times 10^{-4}$ cm^{-1}

Figure 6.9. Possible geometries adopted by the analyzed $V^{IV}O$(AARSB) compounds in solution.

In all cases, the experimental $\mathbf{A_z}$ is consistent with the expected equatorial donor group set consisting of [O_{COO}-, N_{amine}, O_{ArO}-, O_{DMF}] or [O_{COO}-, N_{amine}, O_{ArO}-, O_{ROH}] depending on the solvent used in the preparation of the sample (binding modes **a** and **b**).

These results indicate successful compound preparation. Only *S*-**51** exhibits a lower experimental $\mathbf{A_z}$ but it is still within the accepted $\pm 3 \times 10^{-4}$ cm^{-1} error margin for $\mathbf{A_z}$ estimation.[7]

Additional information was obtained from the Infrared (IR) spectra measured from the $V^{IV}O$(AARSB) compounds. Table 6.4 lists the most relevant stretching band frequencies.

Table 6.4. Stretching modes and respective IR frequencies for the featured $V^{IV}O$ complexes.

	S-**51**	*S*-**52**	*S*-**53**	*S*-**54**	*R*-**55**	*R*-**56**
Stretching mode	Frequency (cm^{-1})					
ν(N-H)	3265	3248	3259	3254	3220	3199
$\nu(C=O)_{carboxyl}$	1617	1612	1637	1610	1637	1618
ν(C-O)	1240	1264	1241	1245	1241	1265
ν(V=O)	948	956	945	968	948	968

As expected, carboxyl group C=O stretching bands were observed in all cases in addition to the ν(V=O) bands.

Finally, compounds *S*-**54**, *R*-**55** and *R*-**56** gave acceptable elemental analysis results consistent with monomeric $V^{IV}O$(AARSB) formulations having either water or alcohols as contaminants. The elemental analysis of *S*-**53** can either be assigned to a dimeric μ-oxo $V^{IV}O$ species containing two potassium cations as counter-ions or a monomeric $V^{V}O_2$ species containing a potassium anion as counter-anion (KOH was used as base during compound preparation). Elemental analysis for compounds *S*-**51** and *S*-**52** were made but did not yield results consistent with the expected molecular formulas. The phenol group present in the tyrosine side-chain of both compounds may account for the difficulty in the isolation of these compounds. The base used during the synthesis may deprotonate the tyrosine side-chain phenol group, leaving it susceptible to oxidation and degradation after exposure to air. For this reason, *S*-**51** and *S*-**52** were excluded from the catalytic screening reactions.

6.3. Catalytic applications: asymmetric sulfoxidation of thioanisole

The prepared $V^{IV}O$(AARSB) compounds were screened for their catalytic potential in the asymmetric sulfoxidation of thioanisole under a variety of conditions. In all cases, the final products were either *R*- or *S*-methyl phenyl sulfoxide or the sulfone. The results obtained are presented in Table 6.5.

Table 6.5. Sulfoxidation of thioanisole with the VO^{IV}(AARSB) catalysts.[a]

Entry	Catalyst	Solvent	t (h)	Conv (%)	ee (%)	Sulfone (%)
1	*S*-**53**	DCE	24	0	0	0
2	*S*-**53**	$(CH_3)_2CO$	24	41	26	2
3	*S*-**53**	$(CH_3)_2CO$	48	63	26	4
4	*S*-**53**	EtOH	24	8	0	0
5	*S*-**53**	AcOEt	24	96	3	11
6	*S*-**54**	$(CH_3)_2CO$	24	99	0	5
7	*S*-**54**	AcOEt	24	>99	0	6
8	*R*-**55**	DCE	24	73	0	32
9	*R*-**55**	$(CH_3)_2CO$	24	78	4	4
10	*R*-**55**	AcOEt	24	65	4	3
11	*R*-**56**	DCE	24	72	4	10
12	*R*-**56**	$(CH_3)_2CO$	24	95	6	6
13	*R*-**56**	AcOEt	24	>99	4	5

[a]Conditions: nS=1 mmol; nH_2O_2:nS=1.2; 1 mol% of catalyst; T = 0 ºC.

In general, the obtained enantiomeric excesses were very low. Only *S*-**53** exhibited appreciable enantioselectivity in acetone (entries 2 and 3), but the reaction remained incomplete even after a 48 hour period. This catalyst exhibits no activity in DCE (entry 1), very low activity in ethanol (entry 4) but demonstrated good activity in ethyl acetate (entry 5). Almost complete conversions were obtained with *S*-**54** in acetone and ethyl acetate, although no enantioselectivity was observed (entries 6 and 7). High conversions were obtained with *R*-**55** in DCE, acetone and ethyl acetate but enantioselectivity was non-existent in DCE and was very low in acetone and ethyl acetate (entries 8 to 10). In addition, significant sulfone percentages were obtained when the reaction was run in DCE. High to nearly complete conversions were obtained with *R*-**56** in DCE, acetone and

ethyl acetate but with very low enantioselectivities (entries 11 to 13). These catalysts showed better performance in acetone and/or ethyl acetate relative to DCE in all aspects. Despite the low enantiomeric excesses, complex *S*-**53** exhibits better activity and enantioselectivity in sulfoxidation compared to Fujita's L-alanine-derived and Maeda's L-lysine-derived $V^{IV}O$(Schiff base) complexes (see Schemes 6.1 and 6.2), while requiring less toxic solvents such as acetone and environmentally benign oxidants such as hydrogen peroxide.

6.4. Conclusions

Several $V^{IV}O$ complexes bearing aminoacid-derived reduced Schiff base ligands were synthesized and characterized and their chirality in solution was confirmed by CD spectroscopy. Spectroscopic experiments show that the prepared complexes exhibit resistance to oxidation in ethyl acetate solution but oxidize quickly when dissolved in coordinating solvents such as DMSO or DMF. Complemented with the elemental analysis results, the obtained spectroscopic data confirmed the successful preparation of these compounds.

The prepared $V^{IV}O$ compounds were employed as asymmetric sulfoxidation catalysts, with hydrogen peroxide as the terminal oxidant. In general, high conversions were obtained, though no enantioselectivities were observed with the exception of *S*-**53**. In addition, the tested compounds showed a tendency to perform better in less toxic solvents such as acetone and ethyl acetate.

6.5. Experimental section

6.5.1. General considerations

Unless stated otherwise, all preparations were made under inert atmosphere. Subsequent manipulations after compound preparation did not require inert atmosphere techniques. All solvents and reagents were purchased from commercial suppliers and used as received.

6.5.2. Characterization techniques

6.5.2.1. Infrared (FT-IR), UV and Vis (UV-Vis) and Circular Dichroism (CD) Spectroscopy

FT-IR spectra were recorded in KBr using a *JASCO FT/IR−430* spectrometer. UV-Vis spectra were recorded in CH_2Cl_2 using a Shimadzu U-2000 spectrophotometer. CD spectra were recorded in CH_2Cl_2 using a Jasco J-720 Spectropolarimeter.

6.5.2.2. Elemental analysis (EA)

Elemental analyses were carried out at *Laboratório de Análises* of *Instituto Superior Técnico,* using EA110 CE automatic analyzer Instruments. The results presented are the average values obtained from two independent determinations.

6.5.2.3. High performance liquid chromatography (HPLC)

The analyses of the products obtained in catalytic sulfoxidations was done by HPLC using a Jasco system equipped with a Daicel Chiralpak IA column, a 870-UV Intelligent UV-Vis detector, two 880-PU Intelligent HPLC Pumps, a 2-line degasser 880-51 and a Rheodyne 725i injector (5 μL). The system uses Borwin software for data acquisition and analysis.

6.5.2.4. Electron paramagnetic resonance spectroscopy (EPR)

The electron paramagnetic resonance (EPR) spectra were recorded at 77 K (on glasses made by freezing solutions in liquid nitrogen) with a Bruker ESP 300E X-band spectrometer. The measured spectra were then simulated with the ROKI EPR simulation software developed by Rockenbauer and Korecz.[21]

6.5.3. General procedure for sulfoxidation of thioanisole

The catalytic experiments were carried out at atmospheric pressure, at a constant temperature, in a glass batch reactor, equipped with magnetic stirrer, thermometer and condenser. In a typical run, the solid catalyst (0.25 to 10 mol%) and thioanisole (1 mmol) were dissolved in the appropriate solvent (4 mL). Then the oxidant (1.2 to 1.5 mmol), hydrogen peroxide (30 wt% aqueous solution) was added to the stirring mixture. Control experiments were carried out in the absence of catalyst. Samples of the reaction mixture were withdrawn periodically and analyzed on a Jasco HPLC system equipped with a Daicel Chiralpak IA column. The eluent used was hexane/ethyl acetate (60:40) with a flow of 1 mL/min. The calibration curves for each reagent and product, namely sulfide, sulfoxide and sulfone, were determined using similar HPLC procedures and these calibrations used for the quantitative analyses. Diphenylsulfone was used as an internal standard.

6.5.4. $V^{IV}O$(AARSB) compound preparation methods

General preparation procedure

$V^{IV}OCl_2$ was added to a methanolic (25 mL) solution of the appropriate ligand under a nitrogen atmosphere. The pH was adjusted to *ca*. 7-8 with a 2 M aqueous solution of KOH. The addition of water (25 mL) induced the complete precipitation of the $V^{IV}O$ compound. The precipitate was filtered and washed with water, minimal amounts of methanol and lastly diethyl ether. The recovered solid was then dried under vacuum. This method was used for all the described $V^{IV}O$ compounds.

Synthesis of [$V^{IV}O$(*S*−16)], *S*-51

Reagents: $V^{IV}OCl_2$ (0.28 g, 1.6 mmol), ***S*-16** (0.55 g, 1.6 mmol). The compound was obtained as a dark-grey solid. Yield: 0.4 g, 65 %. EPR (MeOH): $\mathbf{A_z}$=161.7 ×10^{-4} cm^{-1}; $\mathbf{g_z}$=1.951. IR (cm^{-1}): 948 ν(V=O). Elemental analysis for $C_{17}H_{17}NO_6V$·0.5MeOH: calcd. C 52.78, H 4.81, N 3.52; found C 53.1, H 4.8, N 3.1.

Synthesis of [$V^{IV}O$(*S*−17)], *S*-52

Reagents: $V^{IV}OCl_2$ (0.57 g, 3.3 mmol), ***S*-17** (1.06 g, 3.3 mmol). The compound was obtained as a grey solid and is water-soluble. Yield: 0.5 g, 43 %. EPR (MeOH): $\mathbf{A_z}$=168.5 $\times 10^{-4}$ cm^{-1}; $\mathbf{g_z}$=1.948. IR (cm^{-1}): 956 ν(V=O). Elemental analysis for $C_{16}H_{15}NO_5V \cdot 0.7C_4H_{10}O$: calcd. C 55.88, H 5.49, N 3.47; found C 55.9, H 5.1, N 3.1.

Synthesis of [$V^{IV}O$(*S*-20)], *S*-53

Reagents: $V^{IV}OCl_2$ (0.12 g, 0.7 mmol), ***S*-20** (0.30 g, 0.7 mmol). The compound was obtained as a dark grey solid. Yield: 0.3 g, 82 %. EPR (DMF): $\mathbf{A_z}$=162.8 $\times 10^{-4}$ cm^{-1}; $\mathbf{g_z}$=1.950. IR (cm^{-1}): 945 ν(V=O). Elemental analysis for $C_{48}H_{46}NO_7V_2K_2 \cdot 1H_2O$: calcd. C 54.54, H 4.58, N 2.65; found C 54.7, H 4.7, N 2.5.

Synthesis of [$V^{IV}O$(*S*-21)], *S*-54

Reagents: $V^{IV}OCl_2$ (0.13 g, 0.75 mmol), ***S*-21** (0.31 g, 0.75 mmol). The compound was obtained as a grey solid. Yield: 0.1 g, 30 %. EPR (DMF): $\mathbf{A_z}$=164.1 $\times 10^{-4}$ cm^{-1}; $\mathbf{g_z}$=1.949. IR (cm^{-1}): 968 ν(V=O). Elemental analysis for $C_{23}H_{21}NO_5V \cdot 0.3H_2O$: calcd. C 61.69, H 4.86, N 3.13; found C 61.7, H 4.6, N 3.0.

Synthesis of [$V^{IV}O$(*R*-22)], *R*-55

Reagents: $V^{IV}OCl_2$ (0.24 g, 1.4 mmol), ***R*-22** (0.52 g, 1.4 mmol). The compound was obtained as a bluish-grey solid. Yield: 0.4 g, 69 %. EPR (DMF): $\mathbf{A_z}$=162.4 $\times 10^{-4}$ cm^{-1}; $\mathbf{g_z}$=1.949. IR (cm^{-1}): 948 ν(V=O). Elemental analysis for $C_{18}H_{19}NO_5SV \cdot 1.5H_2O$: calcd. C 49.21, H 5.05, N 3.19, S 7.3; found C 49.1, H 4.8, N 3.1, S 7.5.

Synthesis of [$V^{IV}O$(*R*-23)], *R*-56

Reagents: $V^{IV}OCl_2$ (0.26 g, 1.5 mmol), ***R*-23** (0.5 g, 1.5 mmol). The compound was obtained as a grey solid. Yield: 0.3 g, 52 %. EPR (DMF): $\mathbf{A_z}$=162.4 $\times 10^{-4}$ cm^{-1}; $\mathbf{g_z}$=1.949. IR (cm^{-1}): 948 ν(V=O). Elemental analysis for $C_{17}H_{17}NO_4SV \cdot 1H_2O$: calcd. C 51.00, H 4.78, N 3.5, S 8.01; found C 51.2, H 4.7, N 3.4, S 8.1.

6.6. References

1 Bolm. C.; Bienewald, F. *Angew. Chem. Int. Ed. Engl.* **1995**, *34*, 2640-2642.

2 (a) Asgedom, G.; Sreedhara, A.; Kivikoski, J.; Rao, C. P. *Polyhedron* **1997**, *16*, 643-651. (b) Costa Pessoa, J.; Cavaco, I.; Correia, I.; Duarte, M. T.; Gillard, R. D.; Henriques, R. T; Higes, F. G.; Madeira, C.; Tomaz, I. *Inorg. Chim. Acta* **1999**, *293*, 1-11. (c) Costa Pessoa, J.; Cavaco, I.; Correia, I.; Costa, D.; Gillard, R. D.; Henriques, R. T. *Inorg. Chim. Acta* **2000**, *305*, 7-13. (d) Curini, M.; Epifano, F.; Maltese, F.; Marcotullio, M. C. *Tetrahedron Lett.* **2002**, *43*, 3821-3823. (e) Ebel, M.; Rehder, D. *Inorg. Chim. Acta* **2003**, *356*, 210-214.

3 Nakajima, K.; Kojima, M.; Toriumi, K.; Saito, K.; Fujita, J. *Bull. Chem. Soc. Jpn.* **1989**, *62*, 760-767.

4 Ando, R.; Inden, H.; Sugino, M.; Ono, H.; Sakaeda, D.; Yagyu, T.; Maeda, M. *Inorg. Chim. Acta* **2004**, *357*, 1337-1344.

5 (a) Luo, Z.; Liu, Q.; Gong, L.; Cui, X.; Mi, A.; Jiang, Y. *Chem. Commun*. **2002**, 914-915. (b) Somei, H.; Asano, Y.; Yoshida, T.; Takizawa, S.; Yamataka, H.; Sasai, H. *Tetrahedron Lett.* **2004**, *45*, 1841-1844. (c) Takizawa, S.; Katayama, T.; Somei, H.; Asano, Y.; Yoshida, T.; Kameyama, C.; Rajesh, D.; Onitsuka, K.; Suzuki, T.; Mikami, M.; Yamataka, H.; Jayaprakash, D.; Sasai, H. *Tetrahedron* **2008**, *64*, 3361-3371.

6 Costa Pessoa, J.; Calhorda, M. J.; Cavaco, I.; Costa, P. J.; Correia, I.;Costa, D.; Vilas-Boas, L. F.; Félix, V.; Gillard, R. D.; Henriquesa, R. T.; Wiggins, R. *Dalton Trans.* **2004**, 2855-2866.

7 Chasteen, N. D. in: Berliner, L. J.; Reuben, J. (Eds.), *Bio. Magn. Res.* Plenum Press, New York, **1981**, *3*, 53-119.

8 Korbely, B.; Kiss, J. T.; Hernadi, K.; Palinko, I. *J. Mol. Struct*. **2007**, 345-348.

9 Maurya, M. R.; Kumar, U.; Correia, I.; Adão, P.; Costa Pessoa, J. *Eur. J. Inorg. Chem.* **2008**, 577-587.

Chapter 7

Immobilized Titanium(IV) and Vanadium(IV) Complexes

7. Immobilized Titanium(IV) and Vanadium(IV) Complexes

7.1. Introduction

A catalytic system for industrial application must meet certain conditions: it must be economically viable in terms of preparation and application cost; it must exhibit appreciable activity and selectivity under the mildest conditions possible; it must allow easy separation from the reaction products; the catalyst must be recovered and regenerated as many times as possible. Well-known examples of catalysts that meet most of these expectations are the heterogeneous aluminosilicate catalysts used in the fluid catalytic cracking of heavy alkanes into the lighter alkanes that compose most automotive fuels.

The development of simple but cost effective heterogeneous catalysts for the production of fine chemicals is also desirable as the processes involved often require toxic solvents and relatively expensive homogeneous catalysts which cannot be recovered. For instance, Jacobsen's well-known homogeneous Mn^{III}(salen) catalyst for asymmetric epoxidation of alkenes suffers from serious drawbacks that make it unappealing for large-scale industrial application: it is separated from the reaction products with difficulty and it degrades in the presence of the oxidant. Many groups have attempted to develop heterogeneous versions of this Mn^{III}(salen), but the resulting catalysts did not retain the characteristics of the original homogeneous version and required often complex modification to the ligand structure.[1] In addition, the recoverability issue was not resolved, as the Mn^{III}(salen) catalyst still possessed the hydrolytic susceptibility inherent to the salen-type Schiff base ligand.

Development of heterogeneous versions of Ti^{IV}, V^{IV} and V^{V} catalysts is also desirable. Reported heterogeneous versions of the said catalysts are usually prepared by direct covalent anchoring of the catalyst onto the surface of a solid matrix. These methods ensure that the catalyst is locked into place, the solid being easily removed by simple filtration techniques. The drawback of these immobilization techniques is that most have negative impact on overall catalyst performance. Nevertheless, often these present the best solutions to improve catalyst recoverability. Considering the effectiveness of

homogeneous catalytic systems such as Katsuki's Ti^{IV}(salan) epoxidation catalysts,[2] Bekolon's Ti^{IV}(salen) and $V^{IV}O$(salen) cyanation catalysts[3] or Jackson's aminoalcohol-derived $V^{IV}O$(Schiff base) sulfoxidation catalyst,[4] the corresponding heterogeneous versions would grant these proven catalytic systems the recoverability necessary to make them appealing in an industrial context. Notable examples of heterogeneous Ti^{IV}, $V^{IV}O$ and $V^{V}O$ catalysts bearing aminophenolate-class ligands include the polystyrene-supported Ti^{IV} version of Bolm's catalyst for asymmetric sulfoxidation reported by Jackson and co-workers in 2001 (Scheme 7.1).[5] The authors reported activities and enantioselectivities comparable to the original $V^{IV}O$ design reported by Bolm and Bienewald and the heterogeneous catalyst could be recovered four times without loss of performance.

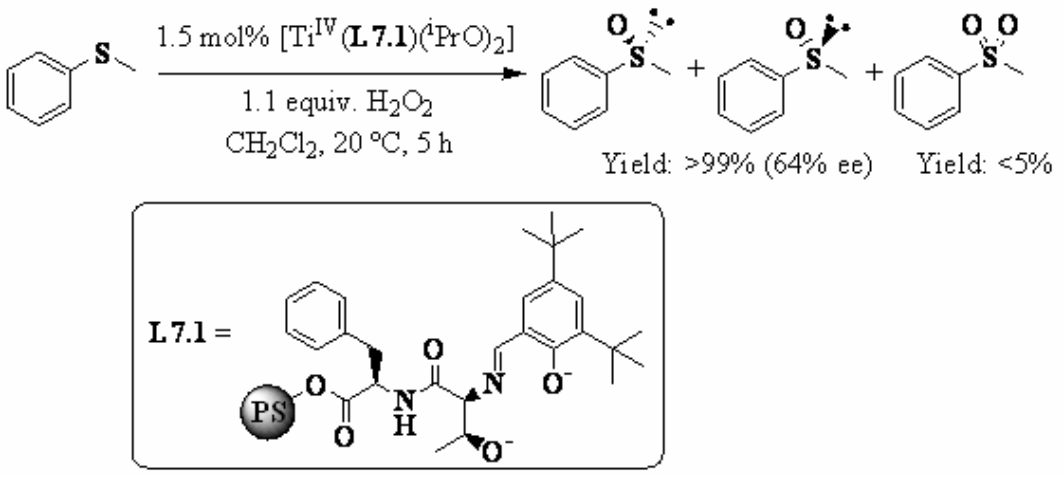

Scheme 7.1. Polystyrene-supported Ti^{IV}(Schiff base)-promoted asymmetric sulfoxidation.

Later in 2004, Sartori and co-workers[6] reported a polystyrene-supported version of Bolm's $V^{IV}O$(Schiff base) catalyst for asymmetric sulfoxidation (Scheme 7.2). Although the reported $V^{IV}O$(Schiff base) catalyst exhibited lower activity and enantioselectivity compared to Bolm's original design, it could be recycled up to four times without any apparent loss of performance whereas the original *in situ* catalyst could not be recovered.

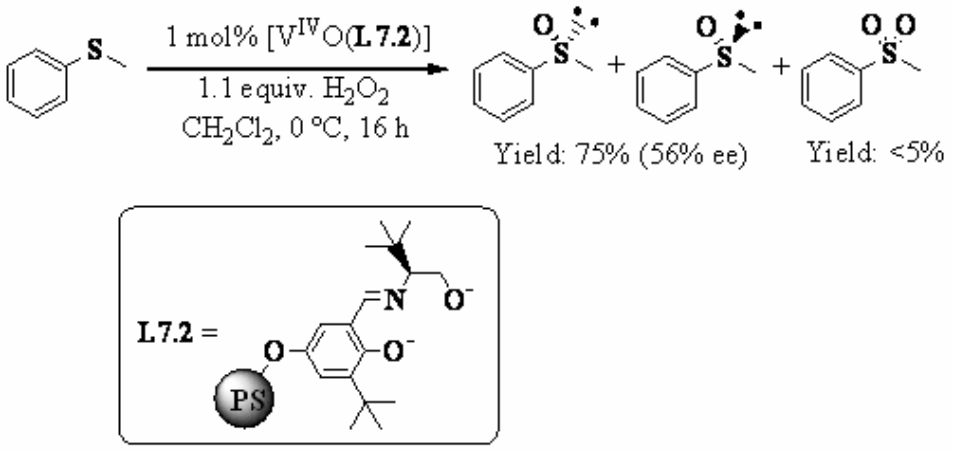

Scheme 7.2. Polystyrene-supported $V^{IV}O$(Schiff base)-promoted asymmetric sulfoxidation.

Also in 2004, Maeda and co-workers[7] reported another polymer-supported variant of Bolm's catalyst for asymmetric sulfoxidation, using commercially-available chloromethylated polystyrene as the solid support matrix and departing from the *tert*-leucinol-derived design. The reported heterogeneous catalysts could be recycled up to three times with only minimal loss of activity (Scheme 7.3).

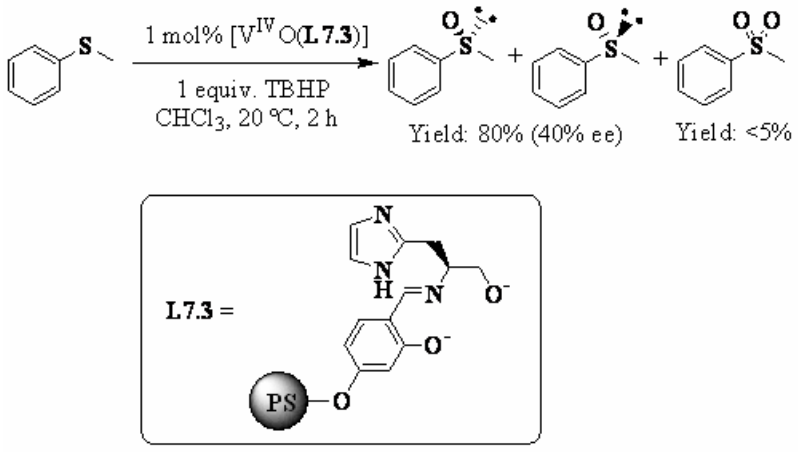

Scheme 7.3. Polystyrene-supported $V^{IV}O$(Schiff base)-promoted asymmetric sulfoxidation.

In 2005, Venkataraman and co-workers[8] reported a poliethyleneglycol-supported Ti^{IV}(salen) system for asymmetric cyanation of aldehydes exhibiting high activity and enantioselectivity (Scheme 7.4). These heterogeneous catalysts could be recycled up to five times without apparent loss of performance.

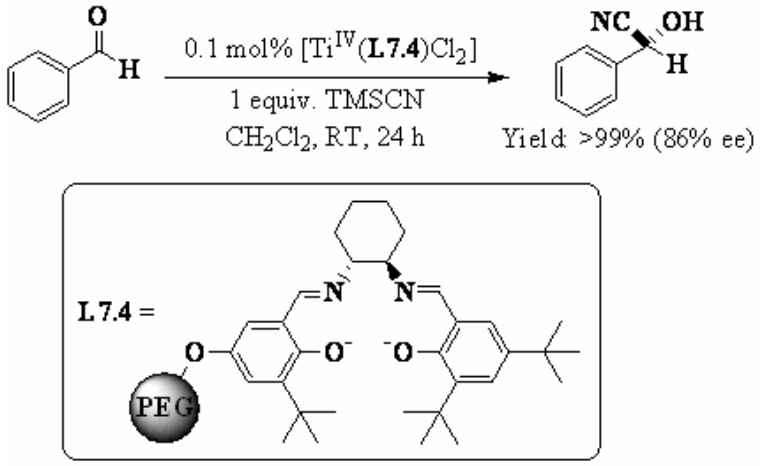

Scheme 7.4. Polyethyleneglycol-supported Ti^{IV}(salen)-promoted asymmetric cyanation of aldehydes.

In 2003, Corma and co-workers[9] reported a silica, activated carbon (AC) and single-walled carbon nanotube (SWNT) supported $V^{IV}O$(salen) catalysts for the asymmetric cyanation of aldehydes (Scheme 7.5). The authors reported enantioselectivities comparable to the homogeneous versions reported earlier by Bekolon[3] and the catalysts could be recovered up to four times without loss of performance.

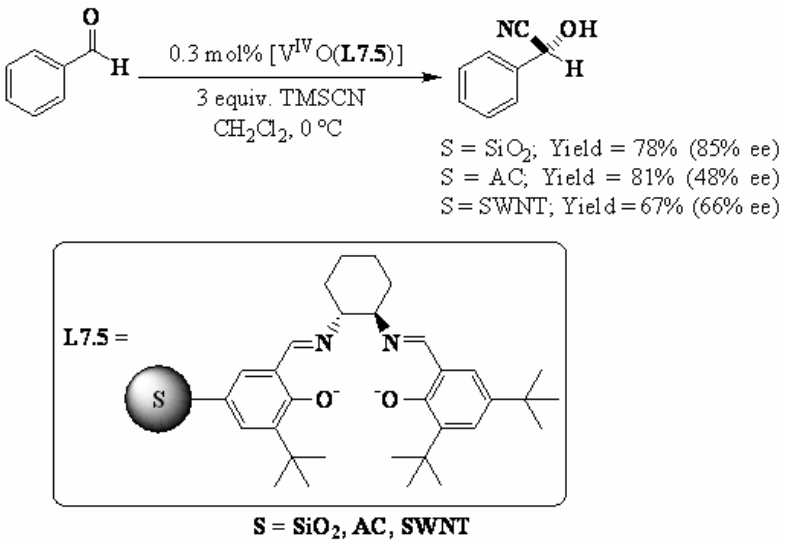

Scheme 7.5. Supported $V^{IV}O$(salen)-promoted asymmetric cyanation of aldehydes.

Other alternatives showcasing the potential of other immobilization techniques used in the preparation of heterogeneous early transition metal aminophenolate-class catalysts

include the zeolite-encapsulated $V^{IV}O$(salen) catalyst for the oxidation of styrene, cyclohexene and cyclohexane using hydrogen peroxide reported by Maurya and co-workers.[10] Scheme 7.6 shows the application of this system in the oxidation of styrene and the resulting products: styrene oxide (SO); phenylacetaldehyde (PHAA); benzaldehyde (BZA); benzoic acid (BZAC); 1-phenylethane-1,2-diol (PHED).

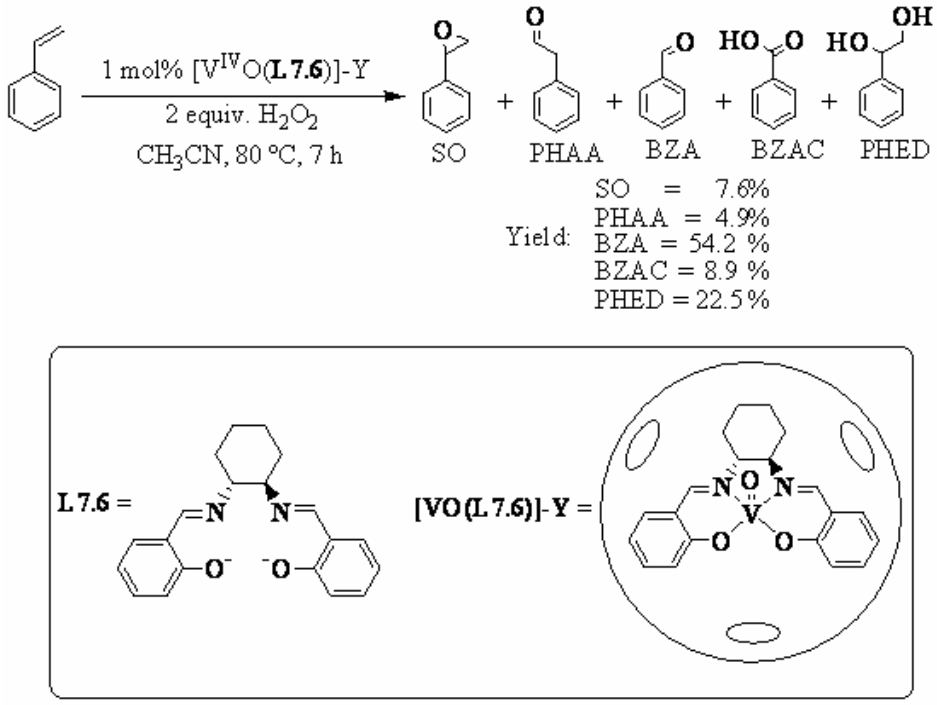

Scheme 7.6. Encapsulated $V^{IV}O$(salen)-promoted oxidation of styrene.

The major advantage of encapsulation is that the catalyst rarely requires structural modification, contrasting with the other immobilization techniques discussed earlier. Encapsulation imposes constraints only on the catalyst freedom of movement and on global mass transfer. While the authors did not monitor the catalyst for its selectivity or enantioselectivity but only for optimized styrene conversion, the system serves as an example of how the technique may be applied to other potentially enantioselective catalysts.

Another interesting immobilization technique is the use of room temperature ionic liquids (RTILs) as solvents. The rationale behind the use of ionic liquids is similar to the one behind catalyst encapsulation: the preservation of catalyst structure and

recoverability. Ionic liquids take this a step further by simplifying the entire immobilization process, which is made by simply dissolving the precatalyst or catalyst in the ionic liquid. The miscibility of ionic liquids with other solvents can be tuned, allowing the development of facile and properly adjusted catalyst and product separation procedures. One instance where ionic liquids were effectively used as solvents and catalyst immobilization supports was the 2002 report by Corma and co-workers[11] of a $V^{IV}O$(salen) catalyst for asymmetric cyanation of aldehydes in 1,3-dialkylimidazolium-type ionic liquids (Scheme 7.7).

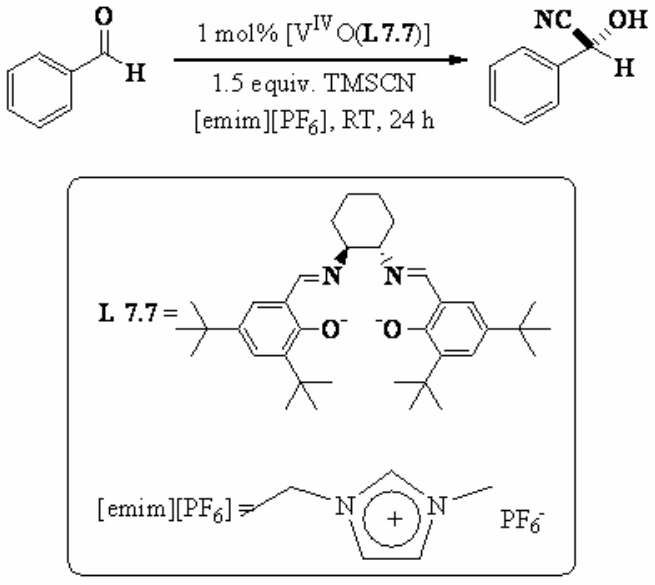

Scheme 7.7. RTIL-supported $V^{IV}O$(salen)-promoted asymmetric cyanation of aldehydes.

The authors observed that the ionic liquid not only managed to effectively immobilize the catalyst but also preserved catalyst performance. Indeed, the $V^{IV}O$(salen) catalyst was as effective in 1-ethyl-3-methylimidazolium hexafluorophosphate as it was in dichloromethane.

Despite the successful application of the heterogeneous aminophenolate-class catalytic system described, most address the recoverability issue partially: most can only be recovered a very limited number of times before the catalyst degrades extensively; most are derived from Schiff base ligands which are known to be susceptible to hydrolytic degradation. Conversely, reports on heterogeneous aminophenolate-class

catalysts derived from reduced Schiff base ligands are very limited, though their stability towards degradation makes them prime candidates for the development of resilient heterogeneous catalysts.

With these ideas in mind, this Chapter describes the preparation, study and application of heterogeneous versions of the Ti^{IV} and $V^{IV}O$ catalysts described in the previous Chapters.

7.2. Immobilized catalyst preparation and application

Two immobilization procedures were approached: covalent grafting onto the surface of an insoluble polystyrene resin and dissolution in a room temperature ionic liquid (RTIL) phase. The aminoacid-derived $V^{IV}O$ compounds bearing reduced Schiff base ligands described in Chapter 6 were more suited for covalent grafting due to the functionalized side-chains of L-cysteine and L-tyrosine. The covalent grafting of the Ti^{IV}(salan) and $V^{IV}O$(salan) proved much more laborious and as such dissolution in ionic liquids constituted the preferred immobilization method.

The heterogeneous catalysts will be discussed in separate sections according to metal center, ligand type and support type.

7.2.1. Polystyrene-supported Ti^{IV}(salan) catalysts

7.2.1.1. Resin modification and catalyst preparation

The preparation of the polystyrene-supported Ti^{IV}(salan) catalyst *R,R*-**57**, which is based on the prepared Ti^{IV}(salan) catalyst *R,R*-**31** described previously in Chapter 3, required prior modification of the chloromethylated polystyrene resin. This modification introduced a bifunctional spacer group, such as piperazine, capable of reacting with the chloromethyl groups present on the resin surface and the modified salicylaldehyde building blocks, thus enabling the stepwise preparation of the desired heterogeneous catalyst. Scheme 7.8 shows the entire preparation process of the heterogeneous Ti^{IV}(salan) catalyst *R,R*-**57**.

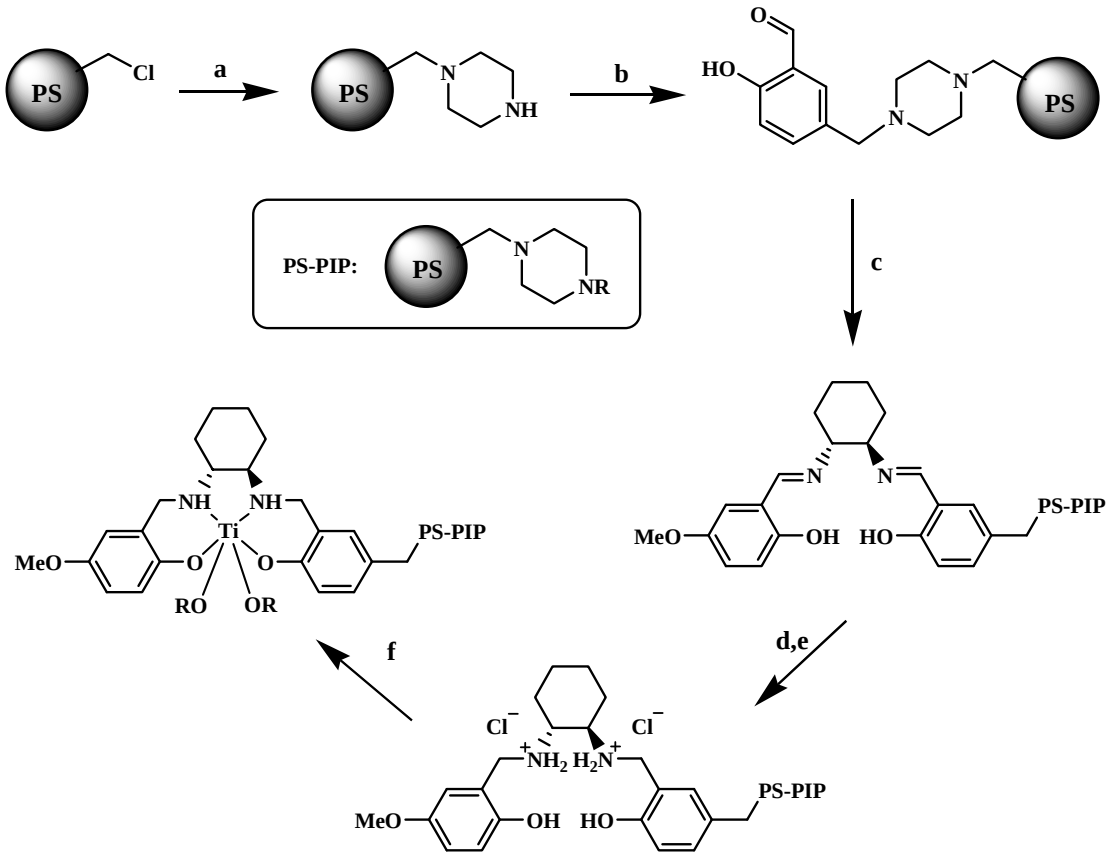

Scheme 7.8. Preparation of polystyrene-supported of the Ti^{IV}(salan) compound *R,R*-**57**. Reagents and conditions: a) piperazine, K_2CO_3, acetone, reflux, 72 h; b) 5-(chloromethyl)salicylaldehyde, K_2CO_3, THF, reflux, 72 h; c) (1*R*,2*R*)-cyclohexane-1,2-diamine, 5-methoxysalicylaldehyde, THF/MeOH (1:1); d) $NaBH_4$, THF/MeOH/H_2O; e) HCl (pH ≈ 2); f) $Ti^{IV}(O^iPr)_4$, H_2O.

Characterization of the obtained yellow solid was limited to IR spectroscopic analysis and thermogravimetric analysis. Elemental analysis of the final *R,R*-**57** compound was not carried out given that the usual CHNS analysis yields no useful information about metal loading and compound structure. EPR characterization of the resin using $V^{IV}O^{2+}$ cations as EPR probes was also made. Elemental analysis results allowed the approximate estimation of the resin nitrogen content, but as the ligand structure became bulkier with the inclusion of the necessary carbon-rich building blocks, the nitrogen content would gradually decrease and lead to erroneous chlorine substitution percentages. The estimation of the chlorine substitution by nitrogen was only meaningful for the first polystyrene-piperazine precursor, in which a 54% chlorine substitution was achieved. It is important to note that not all chloromethyl groups are accessible for

reaction. This applies especially for bulky nucleophiles. The estimation of the titanium loading was made by thermogravimetric analysis. A sample of *R,R*-**57** was submitted to a 10 ºC min^{-1} temperature ramp till 840 ºC to ensure the slow but complete combustion of the sample, leaving behind a white TiO_2 residue. A titanium loading of 1 mmol g^{-1} was obtained from the measurement of the TiO_2 residue mass. IR spectra were recorded from each precursor up to the final compound *R,R*-**57**. Table 7.1 list the relevant stretching modes and respective frequencies for *R,R*-**57** and its precursors: polystyrene-piperazine-salicylaldehyde (PS-PIP-SAL); polystyrene-piperazine-salan (PS-PIP-(5-MeOsal-*R,R*-chan)).

Table 7.1. IR stretching frequencies for *R,R*-**57** and its precursors.

Stretching mode	PS-PIP-SAL	PS-PIP-(5-MeO-sal-chan)	*R,R*-**57**
	Wavenumber (cm^{-1})		
ν(C=O)	1653		
ν(C-O)	1260	1267	1265
ν(Ti-O)			842

Characterization of *R,R*-**57** by solid-state NMR spectroscopy proved inadequate due to the interference caused by the aryl rings and methylene groups of the resin itself. In an attempt to probe the donor atoms present on the resin surface, the resin precursor to *R,R*-**57**, PS-PIP-(5-MeOsal-chan), was loaded with $V^{IV}O^{2+}$ cations using a DMF solution of $V^{IV}O(acac)_2$. After the resin was recovered, washed with THF and dried, it was analyzed by EPR spectroscopy. Figure 7.1 shows the EPR spectrum of the PS-PIP-(5-MeOsal-*R,R*-chan) precursor loaded with $V^{IV}O$ (VO-*R,R*-**57**) obtained at room temperature, without solvent, compared with the EPR spectrum of $V^{IV}O$(salan) compound *S,S*-**34** in DMSO, at 77 K.

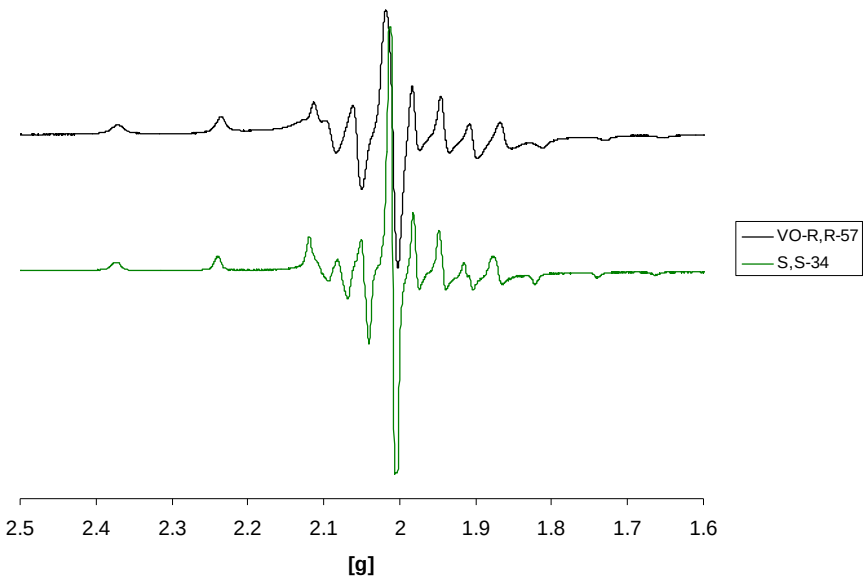

Figure 7.1. First derivative X-band EPR spectra taken from a solid sample of VO-*R*,*R*-**57**, at room temperature, and a DMSO sample of *S*,*S*-**34**, at 77 K..

The experimental $\mathbf{A_z}$ (161.0 $\times 10^{-4}$ cm^{-1}) and $\mathbf{g_z}$ (1.949) spin Hamiltonian parameters compare well with those obtained for the prepared $V^{IV}O$(salan) compounds described in Chapter 4. Indeed, the $\mathbf{A_z}$ of 161.0 $\times 10^{-4}$ cm^{-1} obtained for $V^{IV}O$-impregnated PS-PIP-(5-MeOsal-chan) is consistent with either a (N_{amine}, N_{amine}, O_{phenol}, O_{DMF}) donor group set ($\mathbf{A_z^{est}}$ = 162.7 $\times 10^{-4}$ cm^{-1}) or a a (N_{amine}, O_{phenol}, O_{phenol}, O_{DMF}) donor group set ($\mathbf{A_z^{est}}$ = 161.4 $\times 10^{-4}$ cm^{-1}), both probable given the characteristic flexibility of the salan-type ligands. These results serve as good indicators of the successful preparation of the resin precursor PS-PIP-(5-MeOsal-*R*,*R*-chan) and of *R*,*R*-**57** itself.

7.2.1.2. Catalytic application: asymmetric sulfoxidation of thioanisole

Polystyrene-supported catalyst *R*,*R*-**57** was tested in the asymmetric sulfoxidation of thioanisole with H_2O_2 under the conditions used for its homogeneous version *R*,*R*-**31**. The results obtained with *R*,*R*-**57**, including those obtained with *R*,*R*-**31** (See Chapter 3, section 3.3), are summarized in Table 7.2,.

Table 7.2. Sulfoxidation of thioanisole with the Ti^{IV}(salan) catalysts ***R,R*-31** and ***R,R*-57**.[a]

Entry	Catalyst	solvent	mol% catalyst	conv (%)	ee (%)	sulfone (%)
1[b]	***R,R*-57**	$(CH_3)_2CO$	6.6	62	0	24
2[b]	***R,R*-57**	AcOEt	3.3	60	0	23
3	***R,R*-31**	$(CH_3)_2CO$	1.0	63	38(R)	7
4	***R,R*-31**	AcOEt	1.0	88	47(R)	23

[a]Conditions: nS=1 mmol, nH_2O_2:nS=1.2, T = 0ºC, 4 mL of solvent and t=24 h. [b]Slow addition of oxidant.

The polystyrene-supported Ti^{IV}(salan) catalyst ***R,R*-57** exhibited inferior performance compared to its homogeneous version ***R,R*-31** in every aspect. Slow addition of oxidant was also necessary for ***R,R*-57** as deactivation occurred when the oxidant was added in a single portion. This marked difference in activities may be due to another important difference between the homogeneous and the heterogeneous versions. The homogeneous ***R,R*-31** is a polymeric μ-oxo Ti^{IV}(salan) compound and the important role of these μ-oxo bridges in catalyst performance was discussed in Chapter 3. The polystyrene resin used in the preparation of the heterogeneous ***R,R*-57** imposes movement constraints on the Ti^{IV}(salan) units. As the Ti^{IV} centers are effectively kept apart, the ability to form μ-oxo brigdes upon treatment with water may be greatly reduced. Considering the high oxophilicity of the Ti^{IV} species, a likely consequence of this spatial restraining is the enabling of pathways that promote the formation of TiO_2, resulting in catalyst deactivation.

7.2.2. Catalytic application of Ti^{IV}(salan) catalysts in RTILs

The prepared Ti^{IV}(salan) compounds described in Chapter 3, ***R,R*-28**, ***R,R*-30**,and ***S,S*-32**, were tested for their catalytic activity for asymmetric sulfoxidation of thioanisole in a series of 1,3-dialkylimidazolium- and 1,3-dialkylpyrrolidinium-type at room temperature ionic liquids. Other oxidants than H_2O_2 were used such as *tert*-butyl hydroperoxide (TBHP) and cumyl hydroperoxide (CHP). Figure 7.2 shows the structural formula and nomenclature of the employed RTILs. Table 7.3 lists the results obtained from this study.

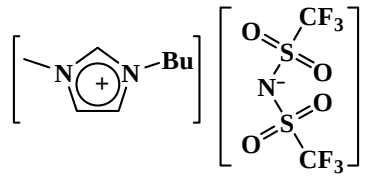

[bmim][NTf_2]

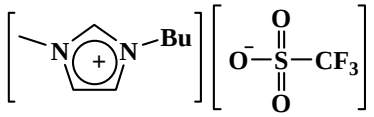

[bmim][OTf]

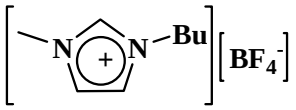

[bmim][BF_4]

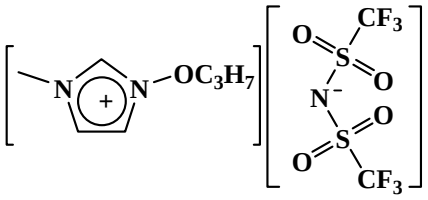

[C_3Omim][NTf_2]

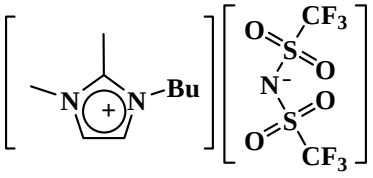

[bmmim][NTf_2]

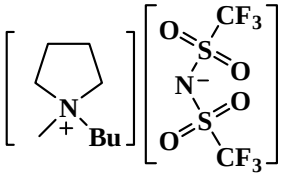

[bmpy][NTf_2]

Figure 7.2. Structural formulas of the employed room temperature ionic liquids (RTILs).

The control reactions carried out in the absence of Ti^{IV}(salan) catalyst showed that oxidation occurs, albeit slowly, at room temperature (entries 1 to 4). The ionic liquid [bmim][NTf_2] apparently facilitates the oxidation of thioanisole when H_2O_2 is used as oxidant. This result is interesting and worthy of future exploration, as it shows the potential of using ionic liquids as mediators of catalytic oxidations. When [bmim][BF_4] was used as solvent, high conversions but no enantiomeric excesses were obtained for *R,R*-**28**, *R,R*-**30**,and *S,S*-**32**, using H_2O_2 as oxidant (entries 5, 17 and 21). The highest sulfone percentages were obtained in these instances as well. Conversely, [bmim][NTf_2] proved beneficial to reactions using TBHP as oxidant. For instance, 19% enantiomeric excess was obtained with *R,R*-**28** when CHP or TBHP were used as oxidants, though a near complete conversion was obtained only with TBHP after the same 24 hour period (entries 7 and 8). Increasing the temperature from 10 ºC to 25 ºC did not have any significant impact on the enantioselectivity of *R,R*-**28** in [bmim][NTf_2] (entry 14).

Table 7.3. Sulfoxidation of thioanisole with the Ti^{IV}(salan) catalysts *R,R*-**28**, *R,R*-**30**,and *S,S*-**32** in RTILs.[a]

Entry	Catalyst	solvent	oxidant	T (ºC)	t (h)	n_{Ox}/n_S	conv. (%)	ee (%)	sulfone (%)
1		[bmim][NTf_2]	H_2O_2	25	22	1.2	45		2
2		[bmim][NTf_2]	TBHP	25	20	1.2	12		0
3		[bmim][NTf_2]	TBHP	25	22	0.5	8		0
4		[bmim][OTf]	H_2O_2	25	22	0.5	12		0
5	*R,R*-**28**	[bmim][BF_4]	H_2O_2	25	24	1.2	80	0	16
6	*R,R*-**28**	[bmim][NTf_2]	H_2O_2	10	24	2	25	4	1
7	*R,R*-**28**	[bmim][NTf_2]	CHP	10	24	2	45	19	10
8	*R,R*-**28**	[bmim][NTf_2]	TBHP	10	24	2	>99	19	10
9	*R,R*-**28**	[bmim][NTf_2]	H_2O_2	25	24	1.2	80	12	2
10	*R,R*-**28**	[C_3Omim][NTf_2]	H_2O_2	25	24	0.5	50	5	2
11	*R,R*-**28**	[bmmim][NTf_2]	H_2O_2	25	24	0.5	50	0	2
12	*R,R*-**28**	[bmim][OTf]	H_2O_2	25	24	1.2	>99	0	3
13	*R,R*-**28**	[bmpy][NTf_2]	H_2O_2	25	24	1.2	80	10	1
14	*R,R*-**28**	[bmpy][NTf_2]	TBHP	25	21	1.2	>99	18	2
15	*R,R*-**28**	[bmpy][NTf_2]	TBHP	0	20	0.5	14	7	0
16	*R,R*-**28**	[bmpy][NTf_2]	TBHP	-10	23	0.5	6	0	0
17	*R,R*-**30**	[bmim][BF_4]	H_2O_2	25	24	1.2	90	0	20
18	*R,R*-**30**	[bmim][NTf_2]	H_2O_2	10	24	2	20	0	0
19	*R,R*-**30**	[bmim][NTf_2]	CHP	10	24	2	35	0	6
20	*R,R*-**30**	[bmim][NTf_2]	TBHP	10	24	2	50	0	4
21	*S,S*-**32**	[bmim][BF_4]	H_2O_2	25	24	1.2	90	0	20
22	*S,S*-**32**	[bmim][NTf_2]	H_2O_2	0	24	1.2	70	0	10
23	*S,S*-**32**	[bmim][OTf]	H_2O_2	0	24	0.5	40	0	35
24	*S,S*-**32**	[bmim][NTf_2]	CHP	25	18	1.2	5	0	0
25	*S,S*-**32**	[bmim][NTf_2]	TBHP	25	18	1.2	30	0	16

[a]Conditions: nS=1 mmol, 1 mol% catalyst, 2 mL of solvent.

Moderate conversions and no enantiomeric excesses were observed with *R,R*-**30** in [bmim][NTf_2] (entries 18 to 20). Again, the best conversion in this ionic liquid was obtained when THBP was used as oxidant (entry 20). *S,S*-**32** gave high conversion, low sulfone percentage and no enantiomeric excess in [bmim][NTf_2] with H_2O_2 as oxidant (entry 22). Much lower conversions were obtained with the same catalyst when CHP or TBHP were used as oxidants (entries 24 and 35). When [bmim][OTf] was employed as solvent, a near complete conversion, low sulfone percentage and no enantiomeric excess

was obtained with *R,R*-**28** (entry 12). Using the same ionic liquid and 0.5 equivalents of H_2O_2, *S,S*-**32** gave a moderate conversion and an unexpectedly high sulfone percentage but no enantiomeric excess (entry 23). Moderate to low enantioselectivities were observed for *R,R*-**28** when [bmpy][NTf_2] is used as solvent, depending on the oxidant used. The use of TBHP resulted in approximately the double enantiomeric excess when comparing with the reaction with H_2O_2 (entries 13 and 14). Lower temperatures seem to have a significant detrimental effect on the reaction rate (entries 15 and 16). RTILs [C_3Omim][NTf_2] and [bmmim][NTf_2] served as examples of the effect exerted by the ionic liquid cation in catalyst enantioselectivity. Whereas moderate enantioselectivities were observed for *R,R*-**28** when [bmim][NTf_2] and [bmpy][NTf_2] were used as solvents (entries 7, 8, 13 and 14), no enantioselectivity was observed for the same catalyst when in [C_3Omim][NTf_2] and [bmmim][NTf_2] (entries 10 and 11). The influence of the ionic liquid anion manifested primarily in the conversions: hydrophilic anions such as BF_4^- and OTf^- favored high conversions when aqueous H_2O_2 was used while NTf_2^- favoured high conversions where TBHP was used. In general, while high conversions were obtained for *R,R*-**28**, *R,R*-**30**,and *S,S*-**32**, when using ionic liquids as solvents, the respective enantioselectivity was significantly lowered in these cases. This was particularly evident for *R,R*-**28**, which was the Ti^{IV}(salan) catalyst that exhibited the best enantioselectivity of those prepared and described in Chapter 3. Separation of the reaction products could be made by simple extraction with an apolar organic solvent, such as diethyl ether or *n*-hexane, leaving the catalyst in the ionic liquid phase.

7.2.3. Catalytic application of $V^{IV}O$(salan) catalysts in RTILs

The $V^{IV}O$(salan) compound *S,S*-**34** described in Chapter 4 was also tested for its catalytic activity towards the asymmetric sulfoxidation of thioanisole in a series of 1,3-dialkylimidazolium- and 1-alkylpyridinium-type room temperature ionic liquids. Figure 7.3 shows the structural formula and nomenclature of the employed RTILs in addition to the ones already mentioned in the previous section. Table 7.4 lists the results obtained from the catalytic runs made with these solvents and catalyst.

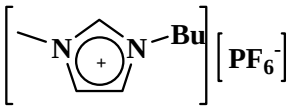

[bmim][PF_6]

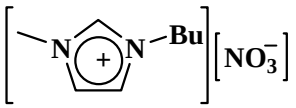

[bmim][NO_3]

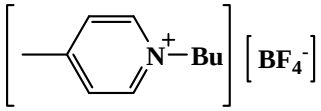

[bmpyr][BF_4]

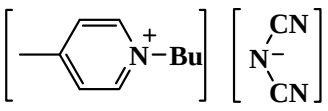

[bmpyr][$N(CN)_2$]

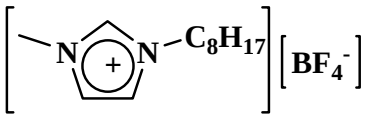

[omim][BF_4]

Figure 7.3. Structural formulas of the employed room temperature ionic liquids (RTILs).

Table 7.4. Sulfoxidation of thioanisole with the $V^{IV}O$(salan) catalyst *S,S*-**34** and H_2O_2 in RTILs.[a]

Entry	Catalyst	n_{Ox}/n_S	solvent	t (h)	conv. (%)	ee (%)	sulfone (%)
1		1.5	CH_2Cl_2	24	9	0	0
2		1.5	[bmpyr][BF_4]	24	77	0	12
3	*S,S*-**34**	1.5	[bmim][NO_3]	3	49	1	5
4	*S,S*-**34**	1.0	[bmim][NO_3]	4	55	2	0
5[b]	*S,S*-**34**	1.5	[bmim][NO_3]	3	90	4	32
6	*S,S*-**34**	1.5	[bmim][NTf_2]	4	93	0	20
7[b]	*S,S*-**34**	1.0	[bmim][NTf_2]	4	72	5	0
8	*S,S*-**34**	1.0	[bmim][NTf_2]	4	77	1	10
9[b]	*S,S*-**34**	1.0	[bmim][PF_6]	3	83	3	0
10[b]	*S,S*-**34**	1.0	[omim][BF_4]	4	82	4	32
11[b]	*S,S*-**34**	1.0	[bmpyr][BF_4]	4	99	6	8
12[b]	*S,S*-**34**	1.0	[bmpyr][BF_4]	4	99	0	6
13[b]	*S,S*-**34**	1.0	[bmpyr][$N(CN)_2$]	4	0	0	0
14[b]	*S,S*-**34**	1.0	[bmpyr][$N(CN)_2$]	4	5	0	0

[a]Conditions: nS=1 mmol, 2.5 mol% catalyst, room temperature, 2 mL of solvent. [b]Slow addition of oxidant.

Two control reactions were carried out with CH_2Cl_2 and [bmpyr][BF_4]. As expected, a very low conversion was obtained when using CH_2Cl_2 as solvent (entry 1). In contrast, an unusually high conversion was obtained after 24 hours with the 1-alkylpyridinium

RTIL [bmpyr][BF_4], at room temperature (entry 2). This may be due to metallic impurities present in the liquid or the liquid may indeed possess catalytic activity towards sulfoxidation. The reactions carried out in another 1-alkylpyridinium RTIL, [bmpyr][$N(CN)_2$], resulted in very low conversions, even when *S*,*S*-**34** was present (entries 13 and 14). This stands in contrast with the very high conversions obtained when [bmpyr][BF_4] was used as solvent, after the same reaction period of 4 hours (entries 11 and 12). Changing the RTIL anion from BF_4^- to $N(CN)_2^-$ proved detrimental to the point of nearly inhibiting the sulfoxidation reaction. The $N(CN)_2^-$ anion can inhibit the catalytic activity of *S*,*S*-**34** by either coordinating strongly to the $V^{IV}O$ metal centre or inducing the degradation of the oxidant. When 1,3-dialkylimidazolium-type ionic liquids were used, moderate to high conversions, but very low enantiomeric excesses, were obtained. The best result in terms of conversion, enantioselectivity and sulfone percentage was obtained when [bmim][PF_6] was used as solvent (entry 9). The lengthened alkyl chain in [omim][PF_6] only contributed to potentiate the formation of sulfone (entry 10). Changing from [bmim][PF_6] to [bmim][NTf_2] resulted in a lowered activity and a minor increase in enantioselectivity from 3 to 5% (entry 7). Addition of the oxidant in a single portion lowered enantioselectivity, maintained activity and increased sulfone formation (entry 8). Increasing the oxidant quantity resulted in increased conversions and a significant formation of sulfone (entries 6 and 7), though the slow addition of oxidant favored some enantioselectivity (entry 6). Changing from [bmim][NTf_2] to [bmim][NO_3] did not improved enantiomeric excesses and activities were lowered in two cases (entries 3 and 4). Slow addition of the oxidant favoured a very high conversion but also favored significant formation of sulfone (entry 5). These cases illustrate how high concentrations of oxidant can result in $V^{IV}O$(salan) catalyst deactivation, a phenomenon discussed previously in Chapter 4. Being [bmim][NO_3] particularly hydrophilic, the catalyst could have been subject to higher oxidant concentrations, resulting in deactivation by formation of inorganic diperoxovanadates. The remaining ionic liquids, [bmim][PF_6], [bmim][NTf_2], [omim][PF_6] and [bmpyr][BF_4], being more hydrophobic, behaved like apolar solvents by forming a biphasic system where mass transfer occurs only at the interface, which may have protected the catalyst from high oxidant concentrations.

In general, while the RTIL solvent phases increased the activity of *S,S*-**34** compared to reaction carried out in conventional solvents, enantioselectivity was noticeably lowered. As observed before, product separation could be made by simple extraction with apolar solvents, the catalyst remaining in the RTIL phase.

7.2.4. Polystyrene-supported aminoacid-derived $V^{IV}O$ catalysts

7.2.4.1. Resin modification and catalyst preparation

Several polystyrene-supported versions of the $V^{IV}O$ complexes bearing aminoacid-derived reduced Schiff base ligands (AARSB), described in Chapter 6, were prepared, characterized, and tested in the asymmetric sulfoxidation of thioanisole. L-aminoacids such as L-cysteine and L-tyrosine possess functionalized side-chains that allow direct anchoring of the aminoacid building block onto the polystyrene matrix. The preparation of the resin precursors could be made by following two synthetic routes: direct covalent anchoring of the L-tyrosine- and L-cysteine-derived ligands described in Chapter 2 (*S*-**17**, *S*-**18**, *R*-**19** and *R*-**20**) or direct covalent anchoring of the aminoacid precursor (S-alkyation or O-alkylation) followed by the on-site stepwise synthesis of the ligand. Due to the modular nature of this immobilization process, other L-aminoacids than L-tyrosine and L-cysteine were also used. The polystyrene-piperazine-salicylaldehyde (PS-PIP-SAL) described earlier is also employed. Scheme 7.9 shows the general preparation process of the heterogeneous $V^{IV}O$(AARSB) catalysts. Figures 7.4, 7.5 and 7.6 show the proposed structural formulas of the described heterogeneous $V^{IV}O$(AARSB) catalysts.

Both preparation procedures shown in Scheme 7.9 were attempted but the stepwise preparation method (A) was found preferable to the single step anchoring (B) of the AARSB ligand. Benzylation experiments with the ligand precursor compounds *S*-**17**, *S*-**18**, *R*-**19** and *R*-**20** have shown that the procedure (B) has chemoselectivity problems, given that the ligand precursor compound possess multiple nucleophilic atoms. This proved particularly important for the L-tyrosine-derived compounds. The sulfur atom in the L-cysteine-derived compounds allowed a greater chemoselectivity in the S-alkylation reactions. As such, compounds *S*-**58** and *S*-**59** were prepared according to procedure (A) while *R*-**60** and *R*-**61** could be prepared according to procedure (B). Compounds *S*-**62** to *S*-**65** were prepared adapting the procedure used for *R,R*-**57**, using the polystyrene-

piperazine (PS-PIP) resin precursor. Compounds *S*-**66** and *R*-**67** bearing tripodal ligands were prepared using the stepwise procedure (A), using a Mannich reaction instead of reductive amination.

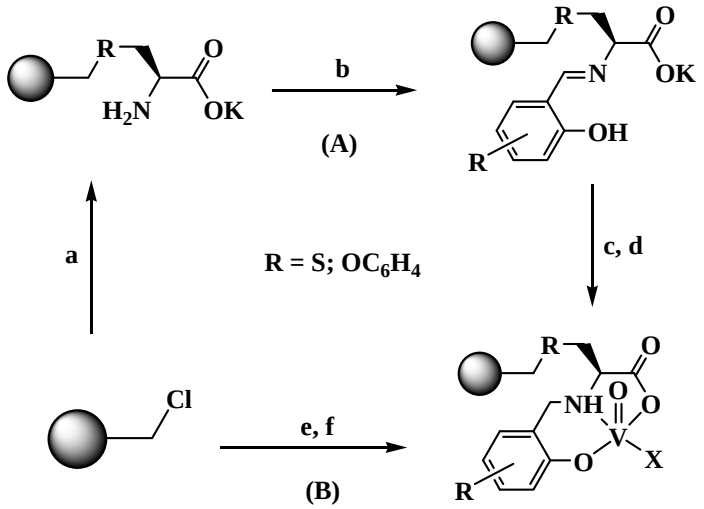

Scheme 7.9. Preparation of polystyrene-supported of an aminoacid-derived $V^{IV}O$(AARSB) compound. Reagents and conditions: a) L-tyrosine/L-cysteine, 2 equiv. KOH, 1:1 THF/MeOH, reflux, 72 h; b) salicylaldehyde/ 3-methoxysalicylaldehyde, 1:1 THF/MeOH, 72 h; c) $NaBH_4$, 1:1 THF/MeOH; d) $V^{IV}O(acac)_2$, 1:1:1 THF/MeOH/H_2O, 24 h; e) *S*-**17**/*S*-**18**/*R*-**19**/*R*-**20**, 2 equiv. KOH, 1:1 THF/MeOH, reflux, 72 h; f) $V^{IV}O(acac)_2$, 1:1:1 THF/MeOH/H_2O, 24 h. The letter X denotes a coordinated solvent molecule.

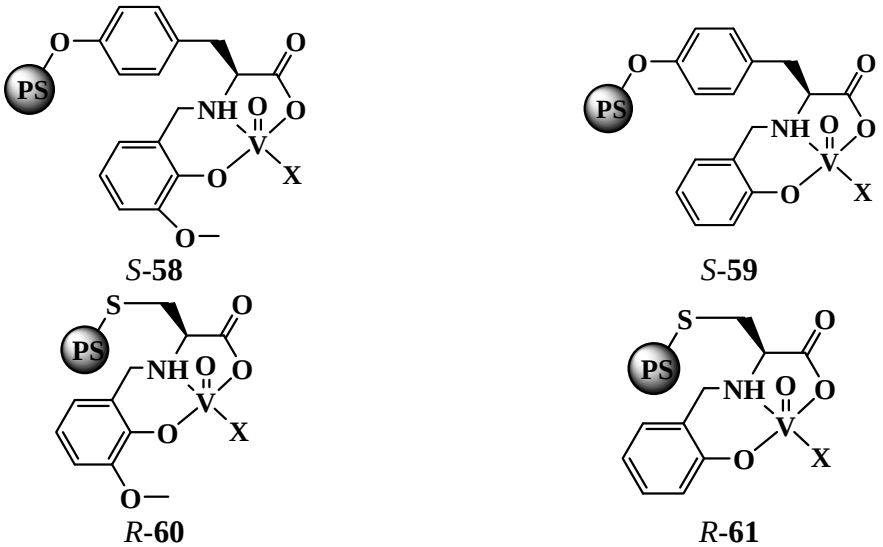

Figure 7.4. Structural formulas of the prepared aminoacid-derived compounds depicting their respective configuration. The letter X denotes a coordinated solvent molecule.

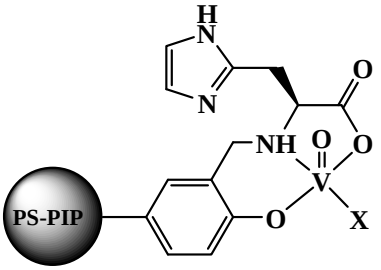

S-**62**

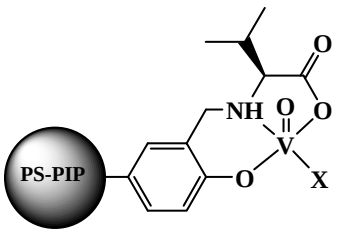

S-**63**

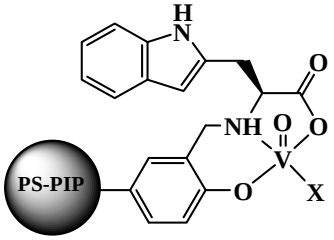

S-**64**

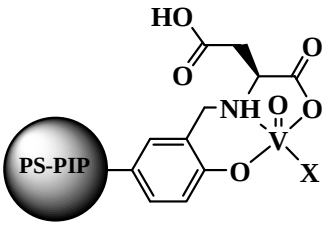

S-**65**

Figure 7.5. Structural formulas of the prepared aminoacid-derived compounds depicting their respective configuration. The letter X denotes a coordinated solvent molecule.

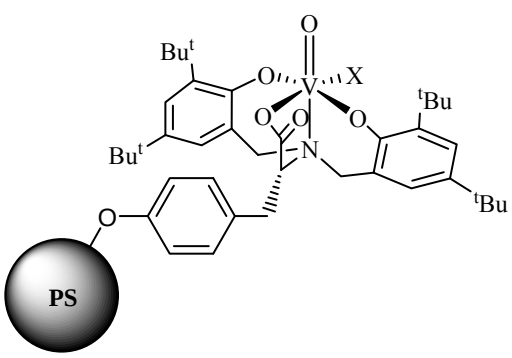

S-**66**

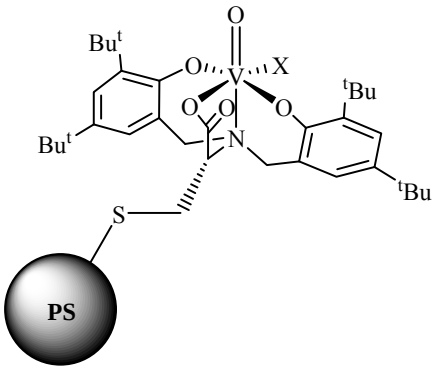

R-**67**

Figure 7.6. Proposed structural formulas of the prepared aminoacid-derived compounds depicting their respective configuration. The letter X denotes a coordinated solvent molecule.

Characterization was made primarily by EPR and IR spectroscopy, elemental analysis and thermogravimetric analysis whenever possible. Elemental analysis of the final $V^{IV}O$(AARSB) compounds was not carried out given that the usual CHNS analysis yields no relevant information about metal loading and compound structure. EPR proved particularly useful, as this technique provided direct information about the metal coordination sites, in turn providing information relative to the success of the preparation

of the resin precursors. In addition, the measurement of EPR spectra from the heterogeneous $V^{IV}O$(AARSB) catalysts often did not require the same sample preparation procedures necessary for the analysis of homogeneous $V^{IV}O$ compounds (use of solvent, sample freezing). Figures 7.7, 7.8 and 7.9 show the obtained EPR spectra for the prepared heterogeneous $V^{IV}O$(AARSB) compounds and Table 7.5 lists the calculated *z*-component spin Hamiltonian parameters. The *x*- and *y*-components parameters were calculated whenever possible, although these yield little information for the structural elucidation of these heterogeneous compounds.

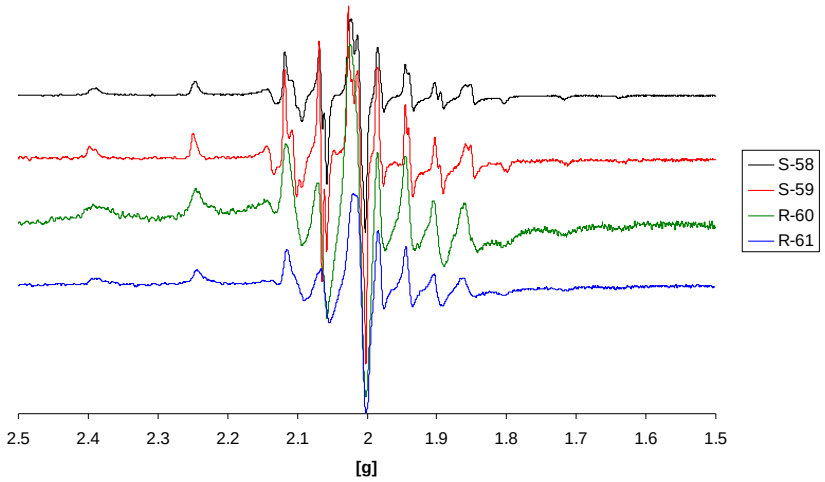

Figure 7.7. First derivative X-band EPR spectrum taken from solid samples of *S*-**58**, *S*-**59,** *R*-**60** and *R*-**61**, at room temperature.

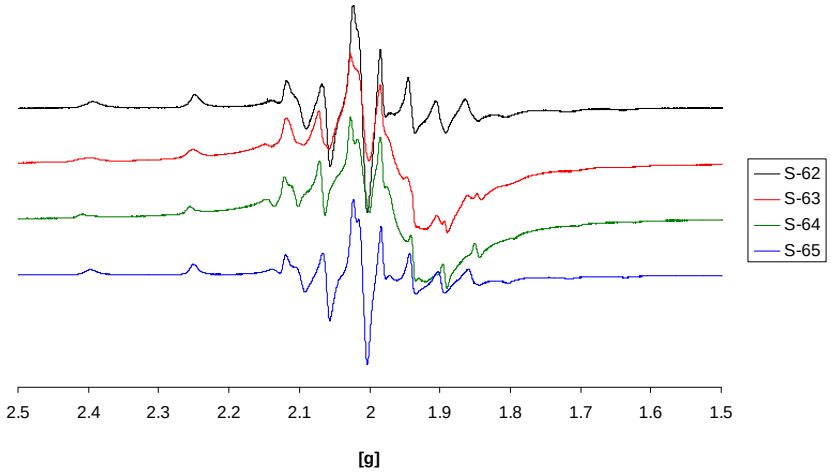

Figure 7.8. First derivative X-band EPR spectrum taken from DMF suspensions of *S*-**62**, *S*-**63,** *S*-**64** and *S*-**65**, at 77 K.

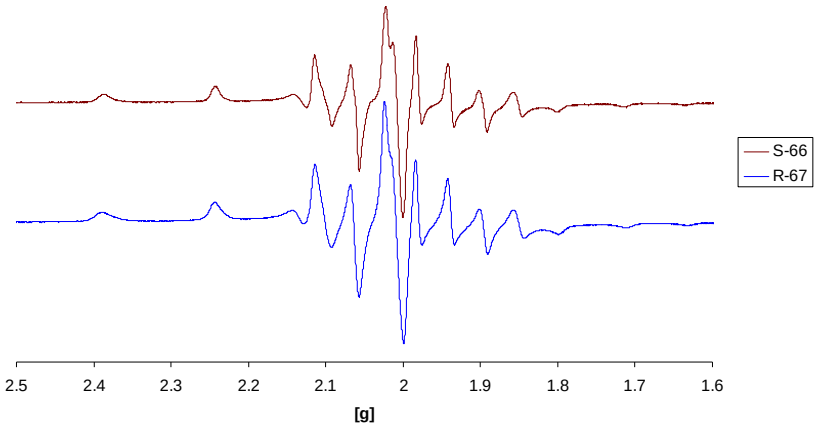

Figure 7.9. First derivative X-band EPR spectrum taken from solid samples of *S*-**66** and *R*-**67**, at room temperature.

Table 7.5. Experimental spin Hamiltonian parameters for the prepared heterogeneous $V^{IV}O$(AARSB) compounds obtained by EPR spectrum simulation.

Compound	g_x, g_y (or $g_{//}$)	A_x, A_y (or $A_{//}$) $\times 10^{-4}$ cm^{-1}	g_z (or $g_{//}$)	A_z (or $A_{//}$) $\times 10^{-4}$ cm^{-1}	Equatorial donor set
S-**58**[a]	1.983, 1.976	64, 62	1.947	168	O_{COO-}, N_{amine}, O_{ArO-}, O_{water}
S-**59**[a]	1.983, 1.978	66, 60	1.945	170	N_{amine}, O_{ArO-}, O_{water}, O_{water}
R-**60**[a]	1.982, 1.978	66, 57	1.944	168	O_{COO-}, N_{amine}, O_{ArO-}, O_{water}
R-**61**[a]	1.981, 1.977	65, 55	1.946	166	O_{COO-}, N_{amine}, O_{ArO-}, O_{water}
S-**62**[b]	1.979, 1.978	64, 56	1.945	168	O_{COO-}, N_{amine}, O_{ArO-}, O_{water}
S-**63**[b]			1.941	170	O_{COO-}, N_{amine}, O_{water}, O_{water} O_{ArO-}, N_{amine}, O_{water}, O_{water}
S-**64**[b]			1.939	175	O_{COO-}, N_{amine}, O_{water}, O_{water}
S-**65**[b]	1.979, 1.976	64, 58	1.944	169	O_{ArO-}, N_{amine}, O_{water}, O_{water} O_{COO-}, O_{ArO-}, O_{DMF}, O_{DMF}
S-**66**[a]	1.975, 1.980	63, 62	1.942	170	O_{ArO-}, N_{amine}, O_{water}, O_{water} O_{COO-}, O_{ArO-}, O_{DMF}, O_{DMF}
R-**67**[a]	1.977, 1.979	66, 58	1.940	171	O_{ArO-}, N_{amine}, O_{water}, O_{water} O_{COO-}, O_{ArO-}, O_{DMF}, O_{DMF}

[a] EPR spectrum measured with neat solid samples at room temperature. [b] EPR spectrum measured at 77 K with DMF as solvent.

Figure 7.10 shows the possible binding modes for the prepared heterogeneous $V^{IV}O$(AARSB) compounds, with the respective estimated $\mathbf{A_z}$ values. Compounds *S*-**58**, *R*-**60**, *R*-**61**, *S*-**65** and *S*-**66** exhibit experimental $\mathbf{A_z}$ values consistent with the expected binding mode **a**. Compounds *S*-**59**, *S*-**63**, and *S*-**64** have higher $\mathbf{A_z}$ values but binding mode **a** is assigned considering the simulation error resultant from line broadening. The

EPR spectra of compounds *S*-**63** and *S*-**64** show significant baseline distortion which may be due to spin-spin coupling between paramagnetic $V^{IV}O$ units, even in the presence of a resin swelling agent such as DMF. Nevertheless, the *z*-component spin Hamiltonian parameters were still calculated for both compounds. Binding modes **d**, **g** and **c**, which predict a N_{amine}, $O_{phenolate}$ or a $O_{carboxylate}$ *trans* to the V=O bond, can be considered for *S*-**59**, *S*-**63**, and *S*-**64**, respectively, although it is expected that these $V^{IV}O$ species bearing two solvent molecules in the equatorial plane readily undergo oxidation. The binding modes from **c** to **h** are included for comparative purposes.

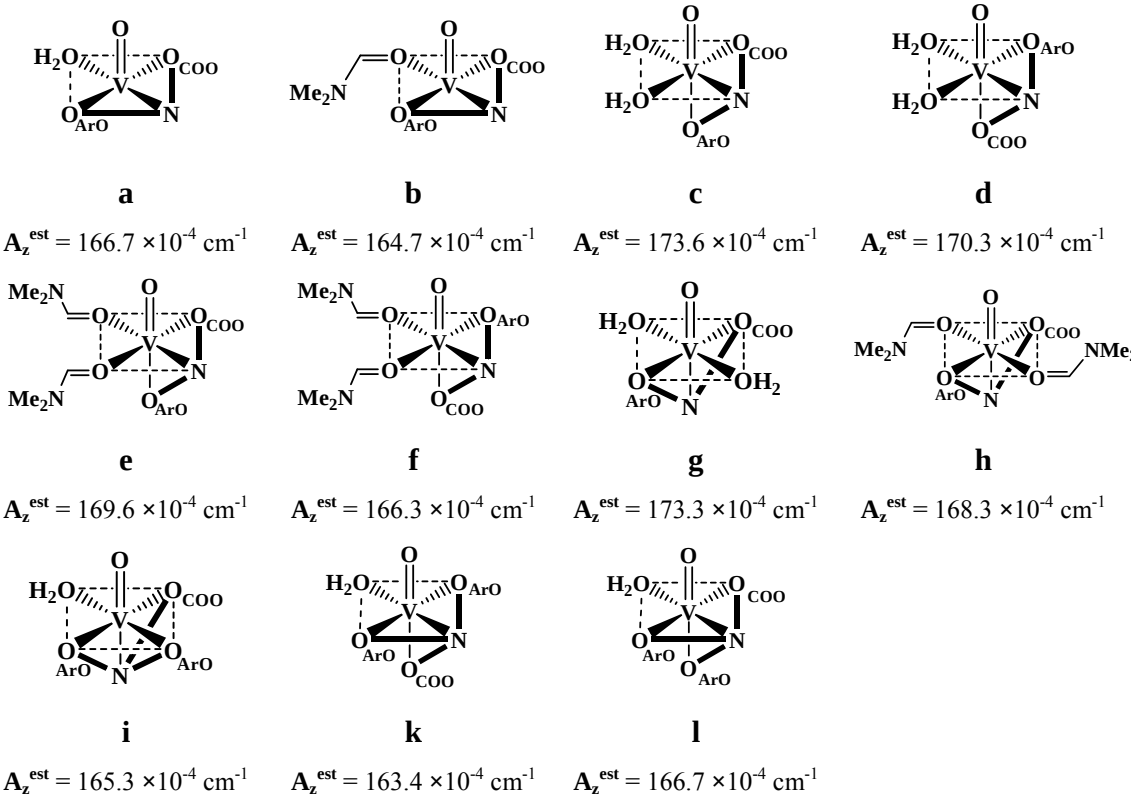

Figure 7.10. Possible geometries adopted by the $V^{IV}O$(AARSB) complexes immobilized in polystyrene.

The experimental $\mathbf{A_z}$ values obtained for all of aforementioned compounds compare well with those obtained for the homogeneous $V^{IV}O$(AARSB) compounds described in Chapter 6. This in itself is a good indication of the successful preparation of the respective heterogeneous versions described in this Chapter.

Compounds *S*-**66** and *R*-**67** with tripodal ligands exhibit experimental $\mathbf{A_z}$ values slightly higher than expected. Indeed, the experimental $\mathbf{A_z}$ values for both compounds are consistent with binding modes **c**, **d** and **g**, which predict two solvent molecules coordinated to the metal center in the equatorial plane. This in turn may indicate that only three out of four ligand donor atoms are coordinated if the coordination *trans* to the V=O bond is admitted. The $\mathbf{A_z^{est}}$ for binding modes **i**, **k** and **l** falls outside the accepted ± 3 × 10^{-4} cm^{-1} error range and therefore these binding modes were not considered. The obtained experimental $\mathbf{A_z}$ values for both compounds point to a unsuccessful preparation of the resin precursor bearing tripodal ligands.

The heterogeneous $V^{IV}O$(AARSB) compounds *S*-**58**, *S*-**59**, *R*-**60**, *R*-**61**, *S*-**66** and *R*-**67** were submitted to thermogravimetric analysis. Vanadium loading was calculated from the orange V_2O_5 residue left after complete combustion of the sample. The obtained vanadium loadings were the following: 1.1 mmolV g^{-1} for *S*-**58**; 0.9 mmolV g^{-1} for *S*-**59**; 0.5 mmolV g^{-1} for *R*-**60**; 0.4 mmolV g^{-1} for *R*-**61**; 0.8 mmolV g^{-1} for *S*-**66**; 0.8 mmolV g^{-1} for *R*-**67**.

Additional characterization of the heterogeneous compounds by IR spectroscopy was made. The relevant stretching modes and respective frequencies are listed in Table 7.6.

All compounds exhibit the expected $\nu(C=O)_{carboxyl}$ and ν(C-O) stretching bands. The ν(V=O) frequencies for *S*-**58**, *S*-**59**, *R*-**60**, *S*-**63** and *S*-**64** indicate the absence of axial V=O•••V=O interaction between $V^{IV}O$ centers. Conversely, the ν(V=O) band could not be identified in compounds *R*-**60**, *S*-**62**, *S*-**65**, *S*-**66** and *S*-**67**.

Table 7.6. Stretching modes and respective IR frequencies for the heterogeneous $V^{IV}O$(AARSB) compounds.

Stretching mode	*S*-**58**	*S*-**59**	*R*-**60**	*R*-**61**	*S*-**62**	*S*-**63**	*S*-**64**	*S*-**65**	*S*-**66**	*R*-**67**
	Frequency (cm^{-1})									
$\nu(C=O)_{carboxyl}$	1611	1704	1651	1634	1654	1612	1614	1633	1729	1617
ν(C-O)	1264	1265	1266	1242	1279	1269	1271	1268	1213	1297
ν(V=O)	993	955	965			967	933			

7.2.4.2. Catalytic application: asymmetric sulfoxidation of thioanisole

Polystyrene-supported catalysts *S*-**58**, *S*-**59**, *R*-**60**, *S*-**61**, *S*-**62**, *S*-**63**, *S*-**64**, *S*-**65**, *S*-**66** and *R*-**67** were tested in the asymmetric sulfoxidation of thioanisole with H_2O_2 under the same conditions used for the homogeneous $V^{IV}O$(AARSB) compounds described in Chapter 6. Recycling was attempted for all cases where very high conversions (>85%) were obtained. All the obtained results are presented in Tables 7.7, 7.8 and 7.9.

None of the tested heterogeneous $V^{IV}O$(AARSB) compounds exhibited enantioselectivity. Compound *S*-**58** gave high conversions coupled with relatively low sulfone percentages in ethyl acetate and could be recycled five times without loss of activity (entry 2, Table 7.7). Prior to catalyst recovery, the excess peroxide was decomposed with anhydrous sodium sulfite and the catalyst was regenerated in the process. Lowering the catalyst loading from 5.5 to 1.7 mol% resulted in lower conversions under the same conditions (entry 3, Table 7.7). Replacing ethyl acetate by acetone and lowering the catalyst loading from 5.5 to 3.3 mol% resulted in a high conversion and a slightly lower sulfone formation (entry 4, Table 7.7). Interestingly, the sulfoxidation reaction could be carried out in water, with *S*-**58** giving a conversion comparable to the one obtained in DCE, though the catalyst loading in water was higher (entries 1 and 5, Table 7.7). Compound *S*-**59** exhibited lower activity in ethyl acetate and acetone when compared to *S*-**58**, while performing comparably to the latter in DCE (entries 6, 7 and 8, Table 7.7). Compound *R*-**60** gave high conversions and low sulfone percentages when acetone was used as solvent (entries 9 and 10, Table 7.7).

Lowering the catalyst loading from 1.5 to 1 mol% resulted in a lower conversion (entry 10, Table 7.7). This catalyst also performed well in DCE, in terms of conversion and sulfone formation, and recycling was attempted (entry 11, Table 7.7). While the conversions were high throughout the five cycles, no safe information about the catalyst integrity can be taken from the slightly oscillating conversion values. Compound *R*-**61** also performed well in acetone, giving a high conversion and a very low sulfone percentage (entry 12, Table 7.7). This catalyst also exhibited high activity in DCE and recycling was successful (entry 13, Table 7.7). *R*-**61** gave high conversions and low sulfone percentages throughout the five cycles, but activity appeared to decrease slightly

by the fifth catalytic cycle. The same experiment was made at 25 ºC, but in this case noticeable catalyst degradation occurred (entry 14, Table 7.7). It should be noticed that the peroxide decomposition procedure was not applied in this case. The resulting lowering of activity may be due to the progressive leaching of the metal from resin. This also indicates that part of $V^{IV}O/V^{V}O$ centers may not remain bound to the resin sites during the reactions as a result of the diperoxovanadate formation, particularly if an excess of H_2O_2 is used as discussed in Chapter 4.

Table 7.7. Sulfoxidation of thioanisole with heterogeneous $V^{IV}O$(AARSB) catalysts *S*-**58**, *S*-**59**, *R*-**60** and *R*-**61**.[a]

Entry	Catalyst	solvent	mol% catalyst	T (ºC)	t (h/cyle)	cycle	conv (%)	ee (%)	sulfone (%)
1	*S*-**58**	H_2O	3.3	5	24	1	37	0	0
2	*S*-**58**	AcOEt	5.5	0	24	1	99	0	12
						2	99	0	13
						3	99	0	11
						4	99	0	10
3	*S*-**58**	AcOEt	1.7	0	24	1	59	0	8
4	*S*-**58**	$(CH_3)_2CO$	3.3	0	24	1	91	0	8
5	*S*-**58**	DCE	1.7	0	24	1	36	0	5
6	*S*-**59**	AcOEt	3.6	0	24	1	38	0	5
7	*S*-**59**	$(CH_3)_2CO$	1.4	0	24	1	0	0	0
8	*S*-**59**	DCE	1.4	0	24	1	37	0	5
9	*R*-**60**	$(CH_3)_2CO$	1.5	0	24	1	97	0	3
10	*R*-**60**	$(CH_3)_2CO$	1.0	0	24	1	81	0	5
11	*R*-**60**	DCE	2.5	0	24	1	90	0	6
						2	98	0	8
						3	89	0	9
						4	92	0	10
						5	85	0	8
12	*R*-**61**	$(CH_3)_2CO$	1.2	0	24	1	94	0	5
13	*R*-**61**	DCE	2	0	24	1	97	0	6
						2	99	0	9
						3	93	0	9
						4	97	0	10
						5	86	0	9
14	*R*-**61**	DCE	2	25	2	1	>99	0	8
						2	>99	0	6
						3	>99	0	4
						4	75	0	4
						5	12	0	0

[a]Conditions: nS=1 mmol, nH_2O_2:nS=1.2, 4 mL of solvent.

Table 7.8. Sulfoxidation of thioanisole with the heterogeneous $V^{IV}O$(AARSB) catalysts catalysts *S*-**62**, *S*-**63**, *S*-**64** and *S*-**65**.[a]

Entry	Catalyst	solvent	T (ºC)	t (h)	conv (%)	ee (%)	sulfone (%)
1	*S*-**62**	AcOEt	0	24	27	0	3
2[b]	*S*-**62**	AcOEt	0	24	79	0	3
3	*S*-**62**	AcOEt	25	72	32	0	2
4[c]	*S*-**62**	AcOEt	25	24	55	0	8
5	*S*-**63**	AcOEt	0	24	87	0	5
6[c]	*S*-**63**	AcOEt	25	24	>99	0	38
7[b]	*S*-**63**	$(CH_3)_2CO$	0	4	>99	0	5
8	*S*-**64**	AcOEt	0	24	15	0	0
9[b]	*S*-**64**	$(CH_3)_2CO$	0	24	82	0	1
10	*S*-**64**	DCE	25	24	31	0	5
11[b]	*S*-**65**	$(CH_3)_2CO$	0	24	70	0	1
12	*S*-**65**	$(CH_3)_2CO$	25	24	38	0	3

[a]Conditions: nS=1 mmol, nH_2O_2:nS=1.2, 50 mg of catalyst, 4 mL of solvent. [b]Slow addition of oxidant. [c]TBHP was used as oxidant.

Table 7.9. Sulfoxidation of thioanisole with the heterogeneous $V^{IV}O$(AARSB) catalysts *S*-**66** and *S*-**67**.[a]

Entry	Catalyst	solvent	mol% catalyst	T (ºC)	t (h)	conv (%)	ee (%)	sulfone (%)
1	*S*-**66**	$(CH_3)_2CO$	1.2	0	24	96	0	2
2	*S*-**66**	$(CH_3)_2CO$	2.4	25	4	93	0	4
3	*S*-**66**	DCE	1.2	0	24	7	0	0
4	*S*-**66**	DCE	2.4	0	24	60	0	15
5	*R*-**67**	$(CH_3)_2CO$	2.4	25	4	85	0	6
6	*R*-**67**	DCE	1.2	0	24	58	0	6
7	*R*-**67**	DCE	2.4	0	24	96	0	11

[a]Conditions: nS=1 mmol, nH_2O_2:nS=1.2, 50 mg of catalyst, 4 mL of solvent.

Compounds *S*-**62**, *S*-**63**, *S*-**64** and *S*-**65** were also tested in the asymmetric sulfoxidation, despite the undetermined vanadium loadings. The objective was to ascertain if the introduction of a piperazine spacer and the use of other L-aminoacid building blocks had any gain in enantioselectivity. Again no enantiomeric excesses were obtained for these compounds. Compound *S*-**62** showed a tendency towards deactivation in the presence of high peroxide concentrations, when using ethyl acetate as solvent. When the oxidant was added in a single portion, the obtained conversion was low (entry

1, Table 7.8). Slow addition of the oxidant resulted in a significant increase of activity without increasing sulfone formation (entry 2, Table 7.8). The same was observed at 25 ºC; single addition of oxidant resulted in deactivation (entry 3, Table 7.8). When TBHP was used instead of aqueous H_2O_2 and added in a single portion, a gain in conversion was obtained (entry 4, Table 7.8). Compound *S*-**63** did not share the same tendency to deactivate in the presence of high oxidant concentrations. High conversion was obtained in ethyl acetate at 0 ºC, with a single addition of aqueous H_2O_2 (entry 5, Table 7.8). Using TBHP instead of aqueous H_2O_2 and raising the temperature to 25 ºC resulted in near complete conversion and a significant sulfone formation (entry 6, Table 7.8). Near complete conversion and a very low sulfone percentage was also obtained in acetone, at 0 ºC, using aqueous H_2O_2 (entry 7, Table 7.8). Compound *S*-**64** gave low conversions in ethyl acetate and DCE, where in both cases the oxidant was added in a single portion, though the higher temperature used in the DCE run favored a higher conversion (entries 8 and 10, Table 7.8). Slow addition of oxidant in acetone significantly increased conversion while maintaining a very low sulfone formation (entry 9, Table 7.8). Compound *S*-**65** exhibited a similar behavior, where the slow addition of oxidant favored a high conversion and very low sulfone formation, in acetone (entry 11, Table 7.8). When the oxidant was added in a single portion, a reduction in conversion was obtained, even at 25 ºC (entry 12, Table 7.8).

Compounds *S*-**66** and *R*-**67**, which should bear tripodal ligand structures, were tested to observe if there was any difference in activity or enantioselectivity when an additional phenolate moiety was introduced to the structure. *S*-**66** exhibited high activity in acetone at 0 and 25 ºC, giving very high conversions and very low sulfone percentages (entries 1 and 2, Table 7.9). Changing the solvent to DCE resulted in lower activities (entries 3 and 4, Table 7.9). Lowering the catalyst loading resulted in a significantly lower conversion (entry 3, Table 7.9). *R*-**67** also exhibited high activity in acetone, giving high conversion and low sulfone percentage (entry 5, Table 7.9). This catalyst also performed better than *S*-**66** in DCE, under similar conditions, giving a significantly higher conversion (entry 6, Table 7.9). Doubling the catalyst loading resulted in almost the double of conversion under the same conditions (entry 7, Table 7.9). No enantiomeric excess was obtained with both *S*-**66** and *R*-**67** catalyst precursors.

7.3. Conclusions

Several immobilization techniques were applied in the development of heterogeneous Ti^{IV} and $V^{IV}O$ catalysts. Polystyrene-supported versions of the Ti^{IV}(salan) and $V^{IV}O$(AARSB) compounds described in Chapters 3 and 6 were prepared, characterized and tested in the asymmetric sulfoxidation of thioanisole. EPR spectroscopy was used to effectively probe the polystyrene resin precursor surface and obtain information about the metal binding sites. Metal loadings were determined by thermogravimetric analysis. In general, the polymer-supported catalysts exhibited high activities, favored low to very low sulfone formation but the final products were racemic in all cases. The L-histidine, L-tryptophane and L-aspartic acid-derived heterogeneous $V^{IV}O$(AARSB) catalysts showed a tendency towards deactivation in the presence of high oxidant concentrations. Catalyst recycling was possible with the L-tyrosine and L-cysteine heterogeneous $V^{IV}O$(AARSB) catalysts, provided that the proper oxidant quenching and catalyst regeneration procedure is carried out. Room temperature ionic liquids were used in place of conventional solvents as a mean to obtain immobilized Ti^{IV}(salan) and $V^{IV}O$(salan) catalysts without resorting to building block modification. In general, high conversions were obtained for the Ti^{IV}(salan) and $V^{IV}O$(salan) catalysts when RTILs were used as solvents, but enantioselectivities were significantly lower. The effect of the RTIL component ions manifested primarily in the catalyst activities, where the hydrophilic RTILs favored the use of aqueous H_2O_2 and the more hydrophobic RTILs favored the use of organic hydroperoxides. As expected, the final products were easily separated from the catalyst by simple extraction with an apolar solvent, leaving the catalyst in the ionic liquid phase.

Despite the low enantioselectivities exhibited by the tested heterogeneous catalysts, all show great potential as recyclable sulfoxidation catalysts.

7.4. Experimental section

7.4.1. General considerations

Unless stated otherwise, all preparations were made without using inert atmosphere techniques. All solvents, RTILs and reagents were purchased from commercial suppliers and used as received.

7.4.2. Characterization techniques

7.4.2.1. Infrared (FT-IR) Spectroscopy

FT-IR spectra were recorded in KBr using a *JASCO FT/IR-430* spectrometer.

7.4.2.2. Elemental Analysis (EA)

Elemental analyses were carried out at *Laboratório de Análises* of *Instituto Superior Técnico,* using EA110 CE automatic analyzer Instruments. The results presented are the average values obtained from two independent determinations.

7.4.2.3. High performance liquid chromatography (HPLC)

The analysis of the products obtained in catalytic sulfoxidation reactions was done by HPLC using a Jasco system equipped with a Daicel Chiralpak IA column, a 870-UV Intelligent UV-Vis detector, two 880-PU Intelligent HPLC Pumps, a 2-line degasser 880-51 and a Rheodyne 725i injector (5 μL). The system uses Borwin software for data acquisition and analysis.

7.4.2.4. Electron paramagnetic resonance spectroscopy (EPR)

The electron paramagnetic resonance (EPR) spectra were recorded at 77 K (on glasses made by freezing solutions in liquid nitrogen) and at room temperature (with neat samples) with a Bruker ESP 300E X-band spectrometer. The measured spectra were then simulated with the appropriate simulation software developed by Rockenbauer and Korecz.[12]

7.4.2.5. Thermogravimetric analysis

The thermogravimetric analyses were carried out with a Perkin-Elmer STA6000 thermal analyzer. Load temperature was 30 ºC and the final temperature was 840 ºC. The temperature ramp used for all samples was 10 ºC min^{-1}, with a hold time at 840 ºC of 20 minutes. For the Ti^{IV} compounds, metal loading was calculated by measuring the final mass of the white TiO_2 residue. For the $V^{IV}O$ compounds the metal loading was calculated similarly by measuring the final mass of the orange V_2O_5 residue.

7.4.3. General procedure for sulfoxidation of thioanisole

The catalytic experiments were carried out at atmospheric pressure, at a constant temperature, in a glass batch reactor, equipped with magnetic stirrer, thermometer and condenser. In a typical run the solid catalyst (0.25 to 10 mol%) and thioanisole (1 mmol) were dissolved in the appropriate solvent using 4 mL of conventional solvent or 2 mL of room temperature ionic liquid. Then 1.2 to 1.5 mmol of oxidant (H_2O_2, 30 wt% aqueous solution) or TBHP (5.5 M in decane) was added to the mixture. Control experiments were carried out in absence of catalyst. Samples of the reaction mixture were withdrawn periodically and analyzed on the Jasco HPLC system equipped with a Daicel Chiralpak IA column. The eluent used was hexane/ethyl acetate (60:40) with a flow of 1 mL/min. The calibration curves for each reagent and product, namely sulfide, sulfoxide and sulfone, were determined using similar HPLC procedures and these calibrations used for the quantitative analyses. Diphenylsulfone was used as an internal standard. Polystyrene-supported catalysts were recovered after excess peroxide was quenched with anhydrous sodium sulfite. Catalyst recovery consisted of simple filtration followed by washing with water, ethanol and acetone, in this order. Ionic liquid-supported catalysts remained in the ionic liquid phase after the reaction products were extracted with diethyl ether.

7.4.4. Polystyrene resin precursor preparation methods

Synthesis of polystyrene-piperazine, PS-PIP

Chloromethylated polystyrene (3.2 g, 1.4 mmolCl/g, 1% cross linked with divynilbenzene, 100–200 mesh) was swollen in acetone for 30 min. Piperazine (0.6 g, 6.9 mmol) and K_2CO_3 (0.89 g, 6.4 mmol) were added to the suspension. The mixture was stirred and heated at reflux for 3 days. The polymer beads were filtered and washed with water, acetone, and diethyl ether. The resin was dried under vacuum. Recovered mass: 3.35 g. Elemental analysis: expected nitrogen percentage for 100% substitution: 2.8 mmolN/g, N, 3.92%; found C 87.2, H 8.1, N 2.1 (ca. 1.5 mmolN/g, *ca*. 54% substitution of Cl).

Synthesis of polystyrene-piperazine-salicylaldehyde, PS-PIP-SAL

PS-PIP (2 g, 1.5 mmolN/g) was swollen in THF for 30 min. 5-(chloromethyl)salicylaldehyde (0.7g, 4.1 mmol) and K_2CO_3 (0.56 g, 4.1 mmol) were added to the polymer suspension. The mixture was stirred and heated at reflux for 3 days. The polymer beads were filtered, washed with water, acetone, and diethyl ether, and dried under vacuum. Recovered mass: 2.2 g. IR (cm^{-1}): 1653 ν(C=O), 1260 ν(C–O). Elemental analysis: found C 88.4, H 8.1, N 1.9.

Synthesis of polystyrene-piperazine-salicylaldehyde (5 mmolCl g-1, 5 % crosslinked with divinylbenzene), PS-PIP-SAL55

The preparation involved the same procedures used for PS-PIP-SAL and its respective precursors. Reagents: chloromethylated polystyrene (6 g, 5 mmolCl/g, 5% cross linked with divinylbenzene, 50–100 mesh), piperazine (2.6 g, 30 mmol), 5-(chloromethyl)salicylaldehyde (5.2 g, 30 mmol), K_2CO_3 (4.1 g, 30 mmol for piperazine alkylation; 4.1g , 30 mmol for alkylation with 5-(chloromethyl)salicylaldehyde). Recovered mass: 8.5 g. Elemental analysis: found C 65.0, H 6.8, N 4.7.

Synthesis of PS-PIP-(5-MeOsal-*R*,*R*-chan)

PS-PIP-SAL (1 g) was swollen in a mixture of THF:MeOH (1:1, 125 mL) for 30 min. The tartrate salt of (1*R*,2*R*)-cyclohexane-1,2-diamine (0.37 g, 1.4 mmol) and K_2CO_3 (0.19 g, 1.4 mmol) in water (25 mL) were added to the polymer suspension. The mixture was stirred for *ca.* 24 hours. Then 5-methoxysalicylaldehyde (0.21 g, 1.4 mmol, 0.17 mL) was added and the mixture was stirred for another 24 hours. The bright-yellow polymer beads were filtered and washed with water, acetone, and diethyl ether. The resin was again suspended in THF:MeOH:H_2O (1:1:0.2) and $NaBH_4$ was added in excess. The mixture was stirred until the bright-yellow color had disappeared completely. The pH was adjusted with concentrated aqueous HCl to *ca.* pH = 2. The polymer beads were filtered and washed with water, THF, and diethyl ether. The resin was dried under vacuum. Recovered mass: 1.2 g. IR (cm^{-1}): 1267 ν(C–O). Elemental analysis: found C 82.2, H 7.9, N 2.0 (ca. 1.4 mmolN/g, ca. 54% substitution).

Synthesis of PS-L-tyrosine

Chloromethylated polystyrene (4 g, 4.2 mmolCl/g, 2% cross linked with divinylbenzene, 200–400 mesh) was swollen in THF (75 mL) for 30 min. Separately, L-tyrosine (3 g, 16.8 mmol) was added to a methanolic (75 mL) solution of KOH (1.9, 33.6 mmol). The methanolic solution of L-tyrosine was added to the THF polymer suspension and the mixture was stirred and heated at reflux for 3 days. The polymer beads were filtered and washed with water, THF, and diethyl ether. The resin was dried under vacuum. Recovered mass: 4.1 g. Nitrogen anal. (for 100% substitution: 4.2 mmolN/g) N, 3.7%; found C 76.0, H 7.3, N 1.2 (ca. 0.9 mmolN/g, ca. 20% substitution of Cl).

Synthesis of PS-L-cysteine

Chloromethylated polystyrene (4 g, 4.2 mmolCl g^{-1}, 2% cross linked with divinylbenzene, 200–400 mesh) was swollen in THF (75 mL) for 30 min. Separately, L-cysteine (2 g, 16.8 mmol) was added to a methanolic (75 mL) solution of KOH (1.9, 33.6 mmol), under N_2 atmosphere. The methanolic solution of L-cysteine was added to the THF polymer suspension and mixture was stirred and heated at reflux for 3 days. The polymer beads were filtered and washed with water, THF, and diethyl ether. The resin

was dried under vacuum. Recovered mass: 5.35 g. Nitrogen and sulfur anal. (for 100% substitution: 4.2 mmolN/g; 4.2 mmolS/g) N, 3.9%, S, 8.8%; found C 64.8, H 6.1, N 3.1, S 7.24, (ca. 2.2 mmolN/g, 2.2 mmolS/g, ca. 52% substitution of Cl).

Synthesis of PS-*S*-17

PS-L-tyrosine (1 g) was suspended in a 1:1 mixture of THF and MeOH (50 mL) for 30 minutes. 3-methoxysalicylaldehyde (0.14 g, 0.9 mmol) was added to the suspension and the mixture was stirred for 24 hours. The resin acquired a bright orange coloration. The polymer beads were filtered and washed with methanol and THF. The orange resin was again suspended in a 1:1 mixture of THF and MeOH (50 mL) and $NaBH_4$ was added till the orange coloration shifted to an off-white coloration. The polymer beads were filtered and washed with water, methanol and THF. The resin was dried under vacuum. Recovered mass: 1.1 g. IR (cm^{-1}): 1701 ν(C=O), 1266 ν(C–O). Elemental analysis: found C 75.7, H 6.8, N 1.2.

Synthesis of PS-*S*-18

The procedure was similar to that of PS-*S*-**17**. Reagents: PS-L-tyrosine (1 g), salicylaldehyde (0.11 g, 0.9 mmol). Recovered mass: 1 g. IR (cm^{-1}): 1702 ν(C=O), 1213 ν(C–O). Elemental analysis: found C 71.8, H 6.3, N 1.1.

Synthesis of PS-*R*-19

Chloromethylated polystyrene (1 g, 3 mmolCl/g, 1% cross linked with divinylbenzene, 100–200 mesh) was suspended in THF (50 mL) for 30 min. *R*-**19** (0.8 g, 3 mmol) was separately added to a methanolic (50 mL) solution of KOH (0.5 g , 9 mmol). The methanolic solution of *R*-**20** was added to the THF polymer suspension and the mixture was stirred and heated at reflux for 3 days. The polymer beads were filtered and washed with water, THF, and diethyl ether. The resin was dried under vacuum. Recovered mass: 1 g. IR (cm^{-1}): 1731 ν(C=O), 1266 ν(C–O). Elemental analysis: found C 62.98, H 6.5, N 2.6, S 5.8.

Synthesis of PS-*R*-20

Chloromethylated polystyrene (1 g, 3 mmolCl/g, 1% cross linked with divinylbenzene, 100–200 mesh) was suspended in THF (50 mL) for 30 min. *R*-**20** (0.9 g, 3 mmol) was separately added to a methanolic (50 mL) solution of KOH (0.5 g , 9 mmol). The methanolic solution of *R*-**20** was added to the THF polymer suspension and the mixture was stirred and heated at reflux for 3 days. The polymer beads were filtered and washed with water, THF, and diethyl ether. The resin was dried under vacuum. Recovered mass: 1.3 g. IR (cm^{-1}): 1742 ν(C=O), 1242 ν(C–O). Elemental analysis: found C 70.0, H 6.5, N 1.5, S 3.8.

Synthesis of PS-PIP-SAL-L-histidine

PS-PIP-SAL55 (1.5 g) was suspended in THF (25 mL) for 30 min. L-histidine hydrochloride hydrate (1.5 g, 7.5 mmol) was separately added to a methanolic solution (25 mL) of KOH (0.8 g, 15 mmol). The L-histidine solution was then added to the polymer THF suspension and the mixture was stirred for 24 hours. The resin acquired a bright yellow coloration. The polymer beads were filtered and washed with methanol and THF. The resin was suspended again in a 1:1 mixture of THF and MeOH (50 mL) and $NaBH_4$ was added till the resin color shifted to off-white. The polymer, at this point a very fine powder, was filtered and washed with water, methanol and THF. The resin was dried under vacuum. Recovered mass: 1.3 g. IR (cm^{-1}): 1615 ν(C=O), 1270 ν(C–O). Elemental analysis: found C 62.28, H 7.5, N 5.9.

Synthesis of PS-PIP-SAL-L-valine

The procedure was similar to that of PS-PIP-SAL-L-histidine. Reagents: PS-PIP-SAL55 (1.5 g), L-valine (0.9 g, 7.7 mmol), KOH (0.5 g, 8 mmol). Recovered mass: 1.63 g. IR (cm^{-1}): 1615 ν(C=O), 1269 ν(C–O). Elemental analysis: found C 62.4, H 7.5, N 5.8.

Synthesis of PS-PIP-SAL-L-tryptophan

The procedure was similar to that of PS-PIP-SAL-L-histidine. Reagents: PS-PIP-SAL55 (1.5 g), L-tryptophan (1.5 g, 7.5 mmol), KOH (0.5 g, 8 mmol). Recovered mass: 1.7 g. IR (cm^{-1}): 1616 ν(C=O), 1266 ν(C–O). Elemental analysis: found C 71.8, H 7.7, N 7.0.

Synthesis of PS-PIP-SAL-L-aspartate

The procedure was similar to that of PS-PIP-SAL-L-histidine. Reagents: PS-PIP-SAL55 (1.5 g), L-aspartic acid (1.0 g, 7.5 mmol), KOH (0.8 g, 15 mmol). Recovered mass: 1 g. IR (cm^{-1}): 1614 ν(C=O), 1269 ν(C–O). Elemental analysis: found C 66.5, H 7.7, N 6.3.

Synthesis of the resin precursor to *S*-66, PS-tyr-(3,5-^{t}BuSAL)$_2$

PS-L-tyrosine (1 g) was suspended in a 1:1 mixture of THF and MeOH (100 mL) for 30 min. 2,4-di-*tert*-butyphenol (0.38 g, 1.8 mmol) was added to the suspension, along with formaldehyde (0.06 g, 2 mmol, 37 % aqueous solution). The mixture was heated to reflux for 3 days. The polymer beads were filtered and washed with water, methanol and THF. The resin was dried under vacuum. Recovered mass: 1.1 g. Elemental analysis: found C 76.3, H 7.3, N 1.2.

Synthesis of the resin precursor to *R*-67, PS-cyst-(3,5-^{t}BuSAL)$_2$

The procedure was similar to that of PS-tyr-(3,5-^{t}BuSAL)$_2$. Reagents: PS-L-cysteine (1 g), 2,4-di-*tert*-butyphenol (1.2 g, 6 mmol), formaldehyde (0.2 g, 7 mmol, 37 % aqueous solution). Recovered mass: 1.4 g. Elemental analysis: found C 66.8, H 6.6, N 2.9, S 6.7.

7.4.5. Polystyrene-supported Ti^{IV} compound preparation methods

Synthesis of PS-PIP-[Ti(5-MeOsal-*R*,*R*-chan)], *R*,*R*-57

PS-PIP-5-MeO-sal(*R*,*R*-chan)(0.62 g) was swollen in THF (100 mL) for 30 min. Ti^{IV}(O^{i}Pr)4 (0.35 g, 0.37 mL) was added to the polymer suspension. The mixture was stirred for 1 h. The polymer beads acquired a bright orange color. Water was added and a suspension of TiO_2 formed readily. At this point the resin changed to a yellow color. The polymer beads were filtered through a coarse filter and washed with copious amounts of water. The resin was suspended in water and was subjected to an ultrasound bath for 15 min and then filtered again through a coarse filter until all TiO_2 (small particles) had been removed. The resin was washed with THF and diethyl ether and dried under vacuum. Recovered mass: 0.74 g. IR (cm^{-1}): 1267 ν(C–O). Thermogravimetric analysis (TGA) indicates a titanium loading of 1 mmolTi g^{-1}.

7.4.6. Polystyrene-supported $V^{IV}O$ compound preparation methods

General preparation procedure

The appropriate resin precursor (0.5 g) was suspended in a 1:1 mixture of THF/MeOH (25 mL). $V^{IV}O(acac)_2$ (0.5 g, 2 mmol) was added to the suspension and the mixture was heated to 50 ºC for 24 hours. The resin was filtered and washed with methanol and THF. The washing procedure was repeated till all the excess $V^{IV}O(acac)_2$ was removed and the filtrate was colorless. Finally, the resin was washed in minimal amounts of water and methanol. The recovered resin was then dried under vacuum. This method was used for all the polystyrene-supported $V^{IV}O$(AARSB) compounds.

Synthesis of *S*-58

Reagents: $V^{IV}O(acac)_2$ (0.5 g, 1.9 mmol), **PS-*S*-17** (0.5 g). The compound was obtained as a grey solid. Recovered mass: 0.5 g. EPR: $\mathbf{A_z}$=167.6 $\times 10^{-4}$ cm^{-1}; $\mathbf{g_z}$=1.946. IR (cm^{-1}): 993 ν(V=O). TGA indicates a vanadium loading of 1.1 mmolV g^{-1}.

Synthesis of *S*-59

Reagents: $V^{IV}O(acac)_2$ (0.5 g, 1.9 mmol), **PS-*S*-18** (0.5 g). The compound was obtained as a grey solid. Recovered mass: 0.4 g. EPR: $\mathbf{A_z}$=161.7 $\times 10^{-4}$ cm^{-1}; $\mathbf{g_z}$=1.951. IR (cm^{-1}): 955 ν(V=O). TGA indicates a vanadium loading of 0.9 mmolV g^{-1}.

Synthesis of *R*-60

Reagents: $V^{IV}O(acac)_2$ (0.5 g, 1.9 mmol), **PS-*R*-19** (0.5 g). The compound was obtained as a grey solid. Recovered mass: 0.45 g. EPR: $\mathbf{A_z}$=166.4 $\times 10^{-4}$ cm^{-1}; $\mathbf{g_z}$=1.946. IR (cm^{-1}): 965 ν(V=O). TGA indicates a vanadium loading of 0.5 mmolV g^{-1}.

Synthesis of *R*-61

Reagents: $V^{IV}O(acac)_2$ (0.5 g, 1.9 mmol), **PS-*R*-20** (0.5 g). The compound was obtained as a grey solid. Recovered mass: 0.36 g. EPR: $\mathbf{A_z}$=167.5 $\times 10^{-4}$ cm^{-1}; $\mathbf{g_z}$=1.944. TGA indicates a vanadium loading of 0.4 mmolV g^{-1}.

Synthesis of *S*-62

Reagents: $V^{IV}O(acac)_2$ (0.5 g, 1.9 mmol), PS-PIP-SAL-L-histidine (0.5 g). The compound was obtained as a dark green solid. Recovered mass: 0.43 g. EPR: $\mathbf{A_z}$=167.8 $\times 10^{-4}$ cm^{-1}; $\mathbf{g_z}$=1.945.

Synthesis of *S*-63

Reagents: $V^{IV}O(acac)_2$ (0.5 g, 1.9 mmol), PS-PIP-SAL-L-valine (0.5 g). The compound was obtained as a green solid. Recovered mass: 0.51 g. EPR: $\mathbf{A_z}$=172.2 $\times 10^{-4}$ cm^{-1}; $\mathbf{g_z}$=1.941.

Synthesis of *S*-64

Reagents: $V^{IV}O(acac)_2$ (0.5 g, 1.9 mmol), PS-PIP-SAL-L-tryptophan (0.5 g). The compound was obtained as a light green solid. Recovered mass: 0.41 g. EPR: $\mathbf{A_z}$=174.5 $\times 10^{-4}$ cm^{-1}; $\mathbf{g_z}$=1.939. IR (cm^{-1}): 933 ν(V=O).

Synthesis of *S*-65

Reagents: $V^{IV}O(acac)_2$ (0.5 g, 1.9 mmol), PS-PIP-SAL-L-aspartate (0.5 g). The compound was obtained as a light brown solid. Recovered mass: 0.48 g. EPR: $\mathbf{A_z}$=169.1 $\times 10^{-4}$ cm^{-1}; $\mathbf{g_z}$=1.944. IR (cm^{-1}): 832 ν(V=O).

Synthesis of *S*-66

Reagents: $V^{IV}O(acac)_2$ (0.5 g, 1.9 mmol), PS-tyr-(3,5-^{t}BuSAL)$_2$ (0.5 g). The compound was obtained as a light green solid. Recovered mass: 0.4 g. EPR: $\mathbf{A_z}$=170.3 $\times 10^{-4}$ cm^{-1}; $\mathbf{g_z}$=1.942. TGA indicates a vanadium loading of 0.8 mmolV g^{-1}.

Synthesis of *R*-67

Reagents: $V^{IV}O(acac)_2$ (0.5 g, 1.9 mmol), PS-cyst-(3,5-^{t}BuSAL)$_2$ (0.5 g). The compound was obtained as a light green solid. Recovered mass: 0.42 g. EPR: $\mathbf{A_z}$=171.4 $\times 10^{-4}$ cm^{-1}; $\mathbf{g_z}$=1.940. TGA indicates a vanadium loading of 0.8 mmolV g^{-1}.

7.5. References

1 Fan, Q.; Li,Y.; Chan, A. S. C. *Chem. Rev.* **2002,** *102,* 3385-3466.

2 Shimada, Y.; Kondo, S.; Ohara, Y.; Matsumoto, K.; Katsuki, T. *Synlett* **2007**, *15*, 2445-2447.

3 (a) Belokon, Y. N.; Caveda-Cepas, S.; Green, B.; Ikonnikov, N. S.; Khrustalev, V. N.; Larichev, V. S.; Moscalenko, M. A.; North, M.; Orizu, C.; Tararov, V. I.; Tasinazzo, M.; Timofeeva, G. I.; Yashkina, L. V. *J. Am. Chem. Soc.* **1999**, *121,* 3968-3973. (b) Belokon, Y. N.; North, M.; Parsons, T. *Org. Lett.* **2000***, 2*, 1617-1619.

4 Drago, C.; Caggiano, L.; Jackson, R. F.W. *Angew. Chem*. **2005**, *117*, 7387-7389.

5 Green, S. D.; Monti, C.; Jackson, R. F. W.; Anson, M. S.; Macdonald, S. J. F. *Chem. Commun.* **2001**, 2594-2595.

6 Barbarini, A.; Maggi, R.; Muratori, M.; Sartori, G.; Sartorio. R. *Tetrahedron Asymm.* **2004**, *15,* 246-2473.

7 Ando, R.; Yagyu, T.; Maeda, M. *Inorg. Chim. Acta* **2004**, *357*, 2237-2244.

8 Anyanwu, U. K.; Venkataraman, D. *Green Chem.* **2005**, *7*, 424-425.

9 (a) Baleizão, C.; Gigante, B.; Garcia, H.; Corma, A. *J. Catal.* **2003**, *215*, 199-207. (b) Baleizão, C.; Gigante, B.; Garcia, H.; Corma, A. *Tetrahedron*, **2004**, *60*, 10461-10468.

10 Maurya, M. R.; Chandrakar, A. K.; Chand S. *J. Mol. Cat. A: Chemical* **2007**, 270, 225-235.

11 Baleizao, C.; Gigante, B.; Garcia H.; Corma, A. *Green Chem.* **2002**, *4*, 272-264.

12 Rockenbauer, A.; Korecz, L. *Appl. Magn. Reson.* **1996**, *10*, 29-43.

Chapter 8

Copper(II) Salan Complexes

8. Copper(II) Salan-type Complexes

8.1. Introduction

Copper is a relevant metal for diverse biological systems. It is an essential nutrient for humans, with the Cu^{I} and Cu^{II} oxidation forms having a role in several metabolic functions.[1] Because of its ubiquity in nature, notably in biological systems, its inclusion in mediators for chemical synthesis has received great attention: a biologically relevant and relatively cheap metal would prove beneficial environmentally and economically when considering the application of the derived catalysts in an industrial context. Given its late transition metal status, it is capable of mediating chemical processes that are typically mediated by its heavier, more expensive, late transition metal analogues, such as cross-couplings.[2] Additionally, copper compounds also mediate processes that are associated with early transition metals such as epoxidations, sulfoxidations and cyanohydrin synthesis.[3,4]

The chemistry of copper is dominated by the very stable paramagnetic Cu^{II} species, though the less stable Cu^{I} species were also amply studied, namely for cross-coupling reactions.[2b,5]

The combination of the apparent versatility of copper with the proven versatility of the aminophenolate-class of compounds, namely the salen-type, seemed inevitable. The intention behind this development was to combine a biologically relevant, relatively cheap and readily available metal capable of mediating reactions that are typically associated with either early or late transition metals with a ligand class known for its versatility and ease of preparation. Therefore, much effort has been put into studying Cu^{II}(salen) and Cu^{II}(Schiff base) compounds as catalysts for processes ranging from oxygen transfer to carbon-carbon and other carbon-heteroatom bond formation reactions. Notable examples include the aminoalcohol-derived Cu^{II}(Schiff base) catalyst for asymmetric Michael additions reported by Desimoni and co-workers[6] in 1995 (Scheme 8.1).

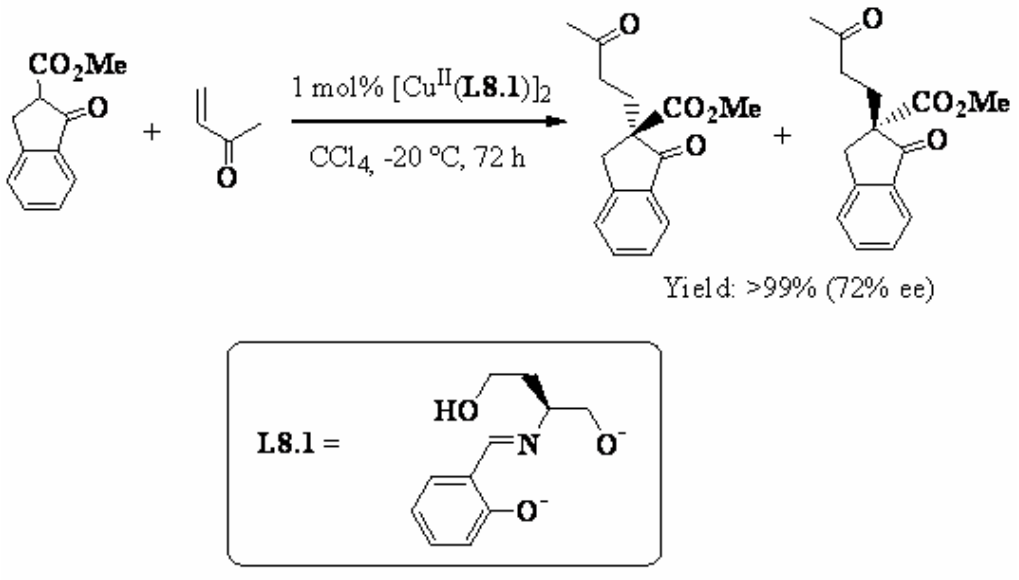

Scheme 8.1. Aminoalcohol-derived Cu^{II}(Schiff base)-promoted asymmetric Michael addition.

From 2000 to 2004, North and co-workers[7] developed an effective Cu^{II}(salen) catalytic system for the asymmetric synthesis of α,α-dialkylaminoacids (Scheme 8.2).

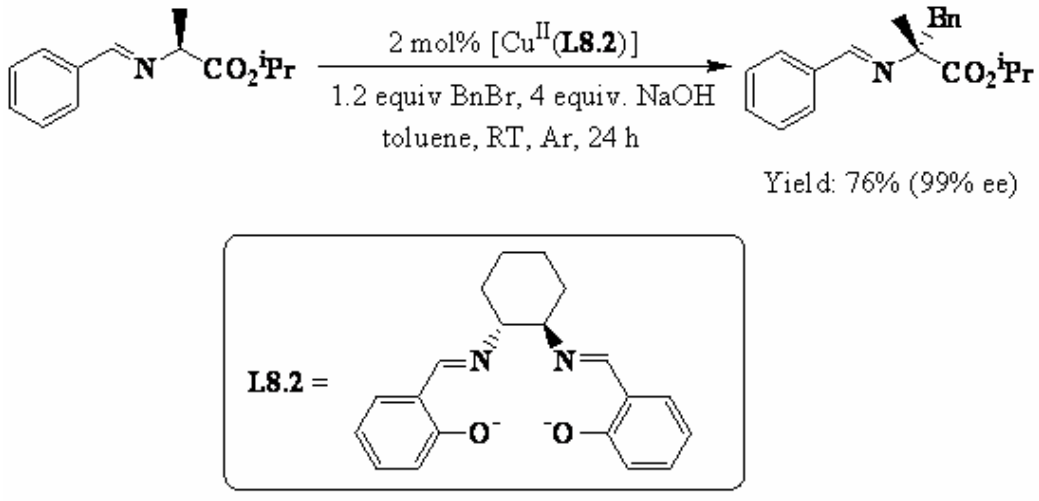

Scheme 8.2. Cu^{II}(salen)-promoted asymmetric alkylation of α-aminoacids.

In 2008, Wang and co-workers[8] reported an aminoalcohol-derived Cu^{II}(Schiff base) catalyst for the asymmetric nitroaldol reaction, also known as the Henry reaction, between aldehydes and nitromethane (Scheme 8.3). This system is notable due to its

ability to deliver very high yields and enantioselectivities while using very mild conditions and solvents with relatively low toxicity.

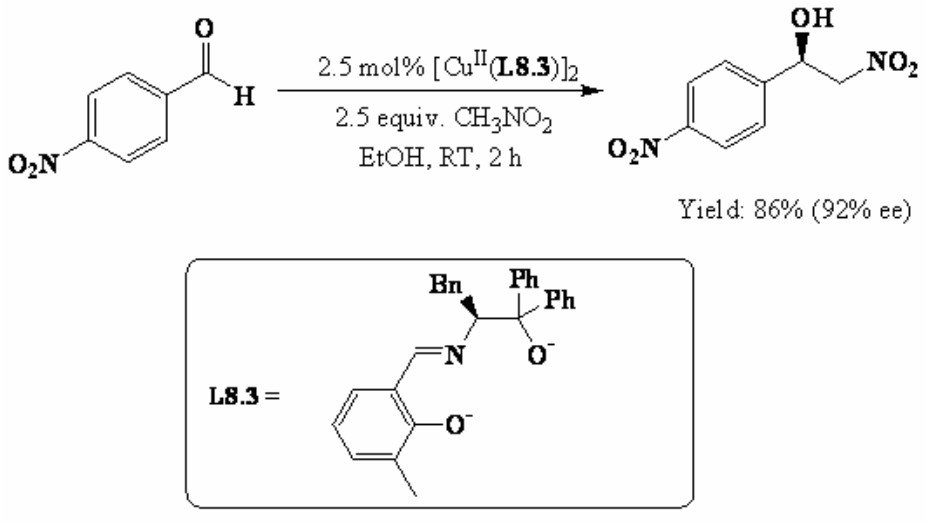

Scheme 8.3. Cu^{II}(salen)-promoted asymmetric nitroaldol reaction.

Other than carbon-carbon bond formation, the Cu^{II}(salen) class of catalysts has also been used successfully in Ulmann-type C-N cross-couplings. Recently, in 2010, Zhou and co-workers reported water soluble Cu^{II}(salen) catalysts that promoted the N-arylation of aliphatic amines in aqueous medium (Scheme 8.4).[9] While the system required high temperatures, the trade-off is that it replaced the traditional organic solvents used in this kind of reaction by water.

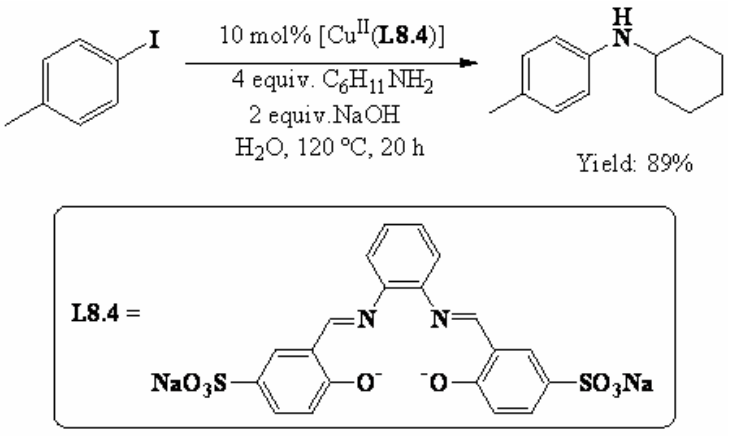

Scheme 8.4. Cu^{II}(salen)-promoted N-arylation.

Several authors used Cu^{II}(salen) compounds as catalysts for processes that are associated with catalysts that derive from early transition metals such as titanium and vanadium. In 1998, Cross and co-workers[10a] reported a Cu^{II}(salen) catalytic system for the asymmetric sulfoxidation of thioethers. While the yields were comparable to those obtained with the Ti^{IV}(salen) and $V^{IV}O$(salen) analogues reported by Fujita and co-workers, this system required greater catalyst loadings to give low enantioselectivities. Later in 2004, Zhu and co-workers[10b] attempted to improve on the Cu^{II}(salen) system by using a different amine, but the increase in enantioselectivity was minimal (Scheme 8.5).

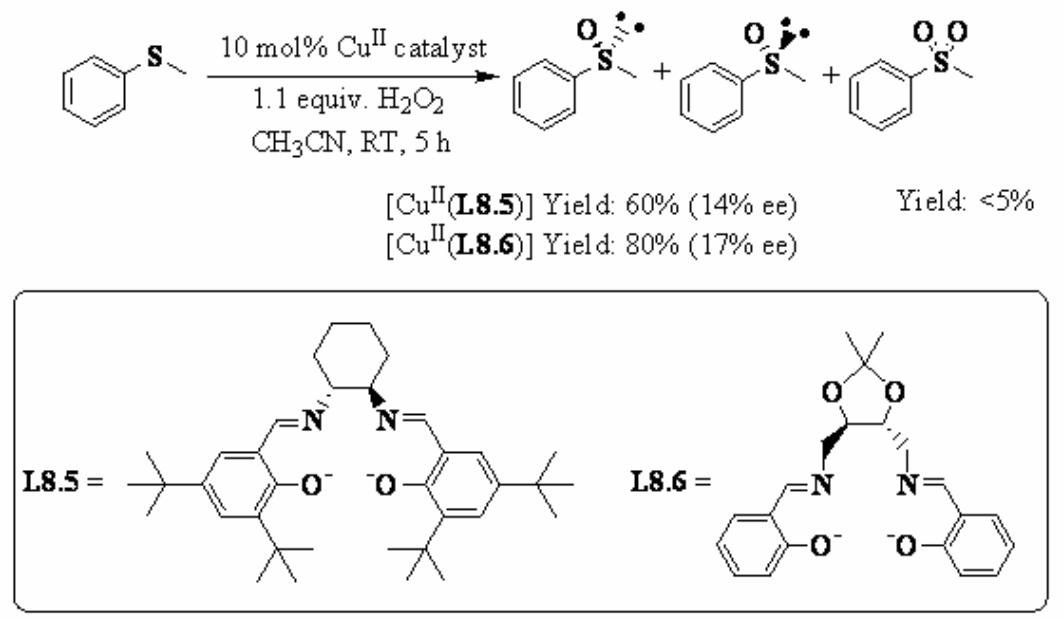

Scheme 8.5. Cu^{II}(salen)-promoted asymmetric sulfoxidation.

In 2010, Rayati and co-workers[11] reported a Cu^{II}(salen) catalytic system for the oxidation of styrene with TBHP (Scheme 8.6). The use of TBHP instead of H_2O_2 resulted in higher yields and lower formation of side-products, contrasting with what Maurya and co-workers[12] reported with a similar Cu^{II}(salen) system that used H_2O_2 as oxidant.

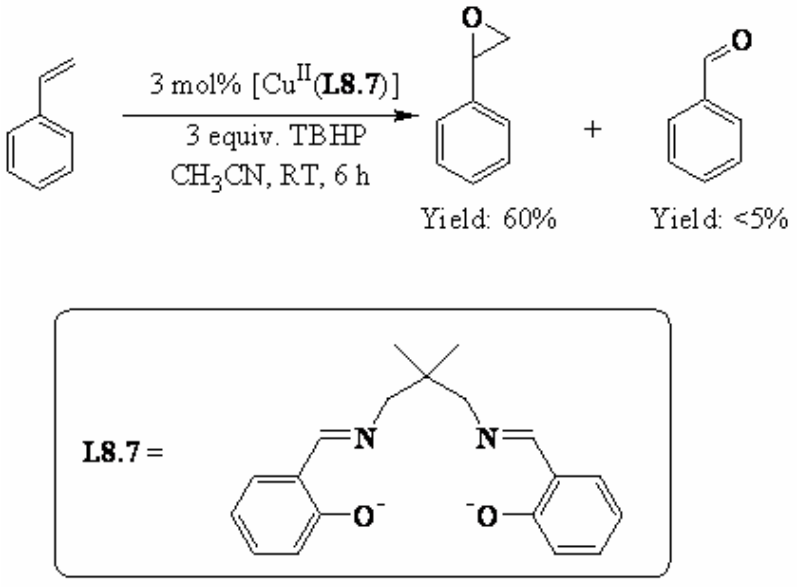

Scheme 8.6. Cu^{II}(salen)-promoted styrene oxidation.

In that same year, Rajagopal and co-workers reported a polymer-supported Cu^{II}(salen) catalytic system for asymmetric cyanohydrin synthesis which performed comparably to the homogeneous $V^{IV}O$(salen) analogues reported by North and co-workers (Scheme 8.7).[13,14]

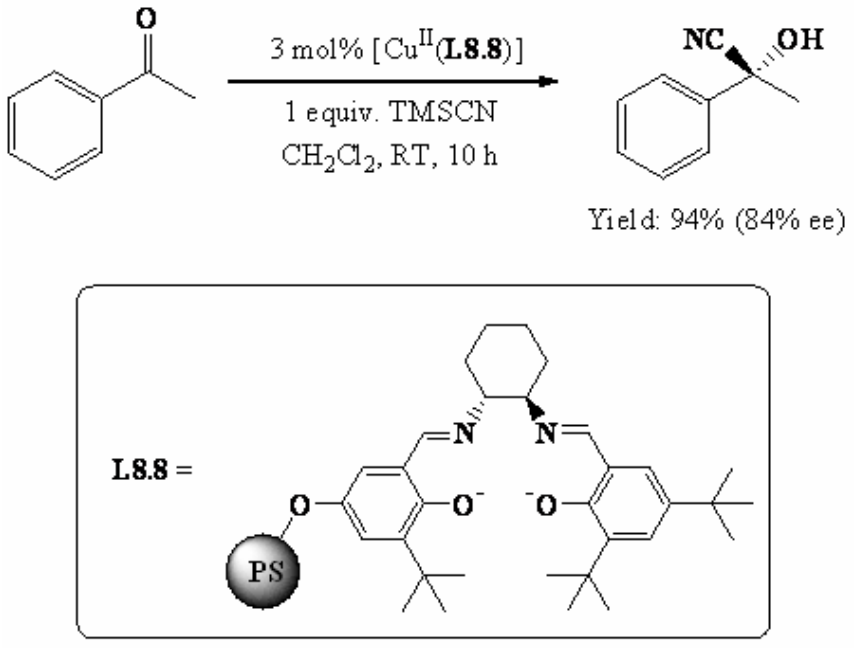

Scheme 8.7. Cu^{II}(salen)-promoted asymmetric cyanation of aldehydes.

The aforementioned instances attests the versatility of the aminophenolate-class Cu^{II}(salen) and Cu^{II}(Schiff base) catalysts. Another important aspect is the stability of catalysts bearing Schiff base ligands such as the salen. With the successful application of the Ti^{IV}(salan) and $V^{IV}O$(salan) catalytic systems, the corresponding Cu^{II}(salan) also saw an increased interest. Again, there are very few reports dealing with Cu^{II}(salan) compounds, particularly in respect to their application. Several authors have reported the preparation and characterization of Cu^{II}(salan) compounds, but few have reported on their catalytic activities and potential applications.[15,19d]

Following the same rationale behind the development of the Ti^{IV}(salan) and $V^{IV}O$(salan) catalysts, this Chapter describes the preparation and characterization of several Cu^{II}(salan) compounds, along with their application in the asymmetric sulfoxidation of thioethers.

8.2. Cu^{II}(salan) compound preparation: results and discussion

The preparation of the Cu^{II}(salan) compounds consisted on the adaptation of the procedure used for the preparation of the $V^{IV}O$(salan) compounds described in Chapter 4. These were readily prepared by reacting $Cu^{II}Cl_2$ with the appropriate salan-type ligand in alcoholic medium, without requiring inert atmosphere techniques. Similarly to the $V^{IV}O$(salan), the desired complex precipitates from the reaction mixture after the medium pH is adjusted to *ca*. 7-8 with aqueous potassium hydroxide, although excess base often promotes the formation of $Cu^{II}(OH)_2$ which would complicate the isolation of the desired complex. The solid compounds are air-stable, considering that Cu^{II} is the most stable oxidation state of copper. All Cu^{II}(salan) compounds were obtained as dark green solids after precipitation. Suitable crystals for single-crystal X-ray diffraction were obtained for compound *R,R*-**71**. Characterization was made mainly by EPR spectroscopy and elemental analysis, as both techniques provide enough information to confirm successful compound preparation. The results obtained by EPR and X-ray analysis will be discussed in separate sections. Figure 8.1 shows the structural formulas of the described Cu^{II}(salan) compounds *R,R*-**68**, *S,S*-**69**, *R,R*-**70** and *R,R*-**71**.

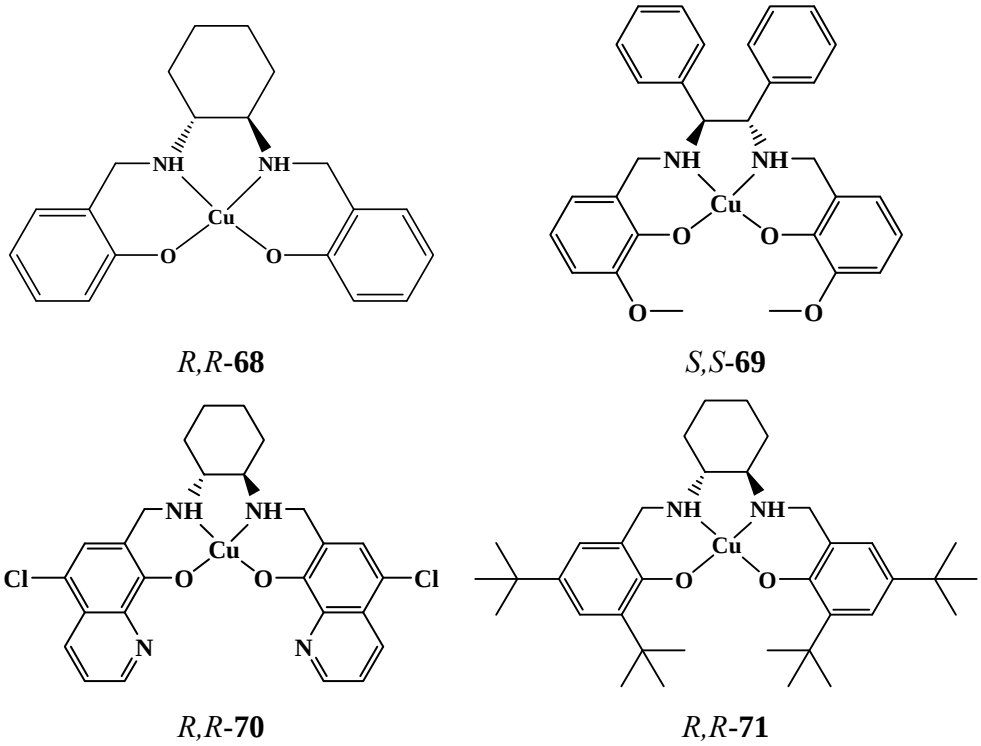

R,R-**68** *S,S*-**69**

R,R-**70** *R,R*-**71**

Figure 8.1. Structural formulas of the prepared Cu^{II}(salan) compounds depicting the *S* or *R* configuration at the stereogenic carbons. Upon coordination, the N_{amine} donor atoms also become stereogenic.

8.2.1. Characterization by EPR spectroscopy

Similarly to $V^{IV}O$, the magnetic properties of Cu^{II} can be described as a S=1/2 system. The two major isotopes of copper, ^{63}Cu and ^{65}Cu, possess a nuclear spin of 3/2. In addition, Cu^{II} is remarkably stable, more so than $V^{IV}O$. Cu^{II} has a $3d^9$ configuration and its complexes usually adopt square-planar, tetrahedral or highly distorted octahedral geometries. Being a $3d^9$ metal centre it is subject to the Jahn-Teller distortion and the axial bonds in octahedral complexes are normally severely elongated, while the equatorial bonds are shortened and stronger. The opposite can occur, but in the common cases the *d* orbital configuration shifts from octahedral to square-planar, due to splitting of the unevenly occupied e_g orbitals d_{z2} and d_{x2-y2}. In the octahedral and square-planar geometries the unpaired electron resides in the d_{x2-y2} orbital. It should be noted that this orbital, unlike d_{xy}, has its lobes pointing directly to the equatorial ligands, along the *x* and *y* axis of the octahedral or square-planar unit. As such, it participates heavily in bonding

and anti-bonding interactions and the unpaired electron occupying this orbital should be highly susceptible to donor atom influence. Owing to this, the unpaired electron will often couple with the nuclear spin of donor atoms such as ^{14}N.[17]

Indeed, the interaction with additional $I>0$ nuclei, also known as superhyperfine interaction, is one of the typical characteristics of Cu^{II} EPR. When a ^{14}N donor is coordinated to a Cu^{II} atom, an additional splitting of the hyperfine structure may be observed. The extent of this additional splitting will increase depending on the degree of covalent bonds formed and on the number of ^{14}N donors coordinated to the metal centre. This may be useful in assessing the number of nitrogen donors coordinated to the metal centre. While the same interactions can occur with $V^{IV}O$, the largely non-bonding nature of the d_{xy} orbital bearing the unpaired electron limits this sort of superhyperfine interactions and these are usually not seen in EPR spectra of $V^{IV}O$ compounds.

A typical anisotropic Cu^{II} EPR spectrum consists of 4 z-component hyperfine signals as a result of $I=3/2$ and a large $\mathbf{A_z}$. The hyperfine coupling constants $\mathbf{A_x}$ and $\mathbf{A_y}$ are comparatively small, so centre to high field signals often appear unresolved. Similarly to $V^{IV}O$ EPR, the $\mathbf{g_z}$ and $\mathbf{A_z}$ parameters are the ones used to characterize the Cu^{II} coordination sphere and geometry. The $\mathbf{g_x}$, $\mathbf{g_y}$ and $\mathbf{g_z}$ are also used to assess the electronic structure of the Cu^{II} centre by using the following equation:[16]

$$\mathbf{R = (g_y - g_z) / (g_x - g_y)} \qquad (8.1)$$

where **R** indicates which d orbitals, d_{z2} and d_{x2-y2}, contribute to the $S=1/2$ ground state. If $\mathbf{R}>1$, then the ground state comes from the d_{z2} orbital; conversely, if $\mathbf{R}<1$, the ground state comes primarily from d_{x2-y2}, as expected for octahedral and square-planar Cu^{II} complexes. Depending on the degree of anisotropy the spectra can be classified as “axial” or “rhombic” in the same way as in $V^{IV}O$ EPR. Because the majority of Cu^{II} complexes have symmetry lower than C_{4v} the respective EPR spectra are either “axial” or “rhombic” in most cases. Manually estimating the $\mathbf{g_z}$ and $\mathbf{A_z}$ parameters is relatively simple due to minimal overlapping of signals from the x and y components. However, manual estimation of parameters from the x and y components is not as straightforward and software simulation is usually required. Figure 8.2 depicts how this manual estimation may be carried out in a typical Cu^{II} EPR spectrum.

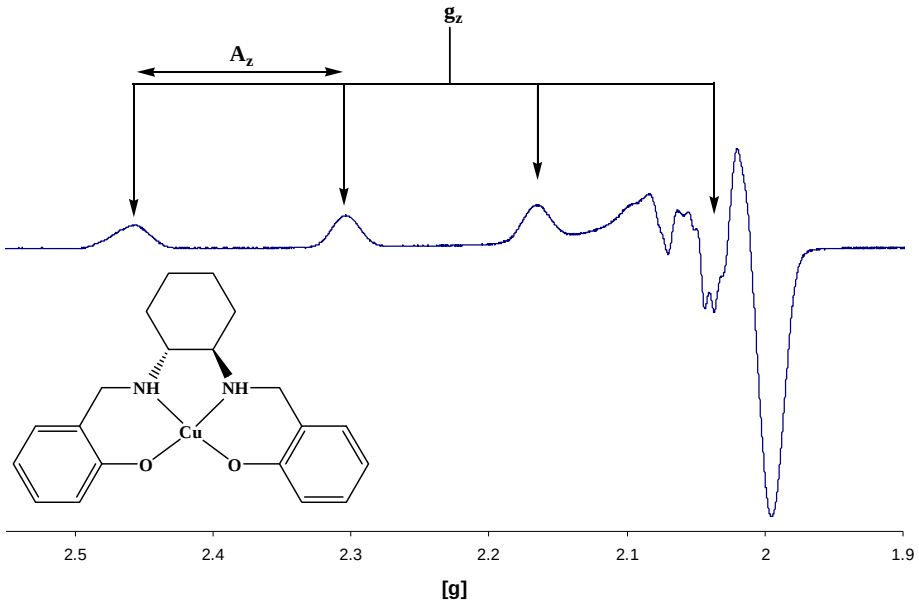

Figure 8.2. "Manual estimation" of $\mathbf{g_z}$ and $\mathbf{A_z}$ from the X-band EPR spectrum of *R,R*-**68** in DMF, recorded at 77K.

When the donor group set bound to the metal centre contains ^{14}N donor atoms, superhyperfine splittings may be observed. Each hyperfine signal should be expected to be further split into $2nI+1$ signals, each separated by a superhyperfine constant **a**. If the Cu^{II} is bound to a single ^{14}N donor, then each hyperfine signal should be split into a 1:1:1 triplet. If two ^{14}N are bound, then a 1:2:3:2:1 quintuplet should arise. When present, the superhyperfine structure is usually observable in the *xy* component signals, as the *z* component superhyperfine signals are undetectable due to line broadening.

Once the $\mathbf{g_z}$ and $\mathbf{A_z}$ are estimated, both values may be plotted in an experimental $\mathbf{g_z}/\mathbf{A_z}$ representation known as the Peisach-Blumberg plot.[17] In 1974, Peisach and Blumberg compiled experimental $\mathbf{g_z}$ and $\mathbf{A_z}$ values obtained from a wide range of model Cu^{II} compounds and constructed a $\mathbf{g_z}/\mathbf{A_z}$ plot. This representation allowed them to establish correlations between geometry, donor group set and experimental $\mathbf{g_z}$ and $\mathbf{A_z}$ data obtained from EPR spectra. The Peisach-Blumberg plot, akin to the additivity rule for $V^{IV}O$ EPR, allows the prediction of the donor group set and geometry of a Cu^{II} complex. Addison and co-workers[18] published an updated version of this plot in 1989 (See Figure 8.3), and introduced another empirical relation known as the tetrahedral distortion index, which is obtained by dividing $\mathbf{g_z}$ by $\mathbf{A_z}$ (in cm^{-1}). The larger this index is, the greater the

extent of the tetrahedral distortion. Values ranging from 100 to 135 cm indicate a square-planar geometry with minimal distortion.

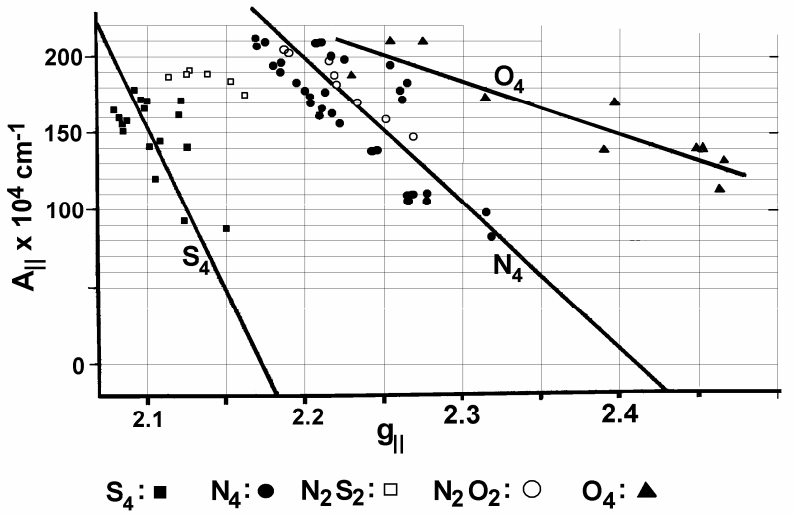

Figure 8.3. The Peisach-Blumberg plot as published by Addison and co-workers.[18] It depicts the correlation between $\mathbf{A}_{//}$ and $\mathbf{g}_{//}$ for a range of Cu^{II} complexes possessing the following donor atoms: S_4, N_4, O_4, N_2O_2, and N_2S_2.

The effect of tetrahedral distortion is responsible for the shift to higher $\mathbf{g}_z$ and lower $\mathbf{A}_z$ values, changing the $\mathbf{g}_z/\mathbf{A}_z$ ratio. Complexes with a distorted square-planar geometry are shifted to the lower right region of the plot.

The great disadvantage of this plot is its inability to reliably distinguish between square-planar N_4, N_2O_2 and O_4 donor groups. This distinction becomes clearer as tetrahedral distortion increases. The global charge of the complex also has an effect on $\mathbf{g}_z$ and $\mathbf{A}_z$. Change in charge from anionic to cationic will cause a shift in the $\mathbf{g}_z$ and $\mathbf{A}_z$ parameters in the same way as the tetrahedral distortion. The development of an additivity rule similar to the one developed for $V^{IV}O$ is hampered by the high uncertainty of the $\mathbf{g}_z$ and $\mathbf{A}_z$ parameters, resultant from tetrahedral distortion and overall charge. As such, it is not possible to identify each donor function coordinated to the Cu^{II} centre as for $V^{IV}O$. Nevertheless, the Peisach-Blumberg plot, when complemented with information obtained from other characterization techniques, still remains very useful for assessing the donor set and geometry of Cu^{II} complexes.

Figure 8.4 shows the obtained EPR spectra for compounds *R,R*-**68**, *S,S*-**69**, *R,R*-**70** and *R,R*-**71**. Table 8.1 lists the obtained spin Hamiltonian parameters. The

characterization of compounds *R,R*-**68**, *S,S*-**69**, *R,R*-**70** and *R,R*-**71** by EPR involved the use of the Peisach-Blumberg $\mathbf{g_z/A_z}$ plot as a means to ascertain the probable donor group set in each case and also to determine the extent of tetrahedral distortion. While it may be possible to distinguish a N_4 from a O_4 donor group set using this $\mathbf{g_z/A_z}$ plot, it is not possible to discern, in both cases, if all nitrogen donors are from amines or if all oxygen donors are from water molecules. Because of the inability to distinguish the bound ligands individually, unlike the "additivity rule" for $V^{IV}O$, the obtained $\mathbf{g_z}$ and $\mathbf{A_z}$ parameters were also compared with values obtained for Cu^{II}(salen) and Cu^{II}(salan) compounds reported by other authors, as a way to facilitate characterization.

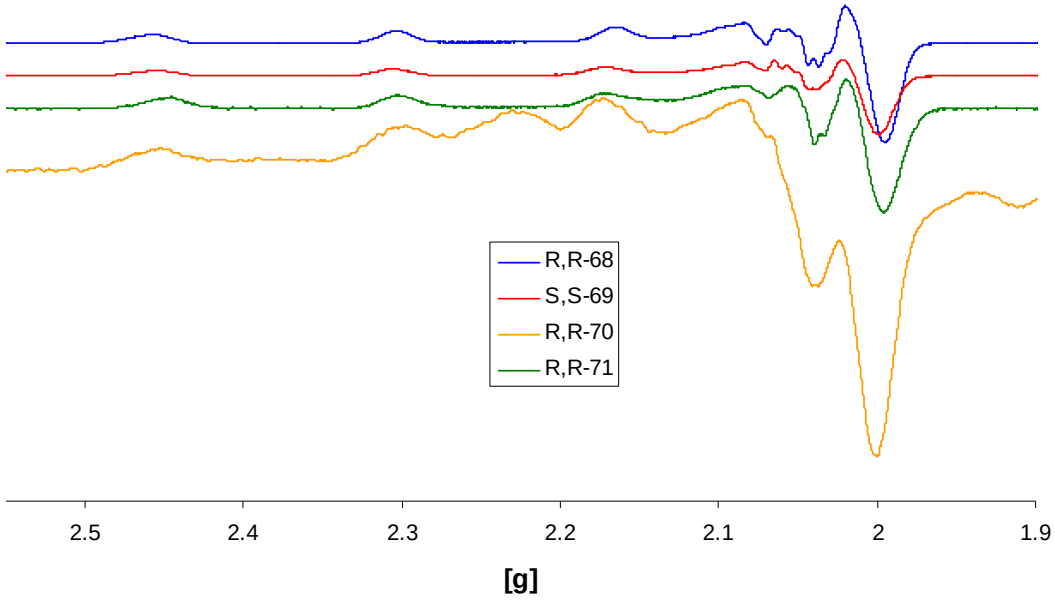

Figure 8.4. First derivative X-band EPR spectra of the prepared tetradentate Cu^{II} complexes. Spectra were recorded at 77 K from solutions of *R,R*-**68** and *S,S*-**69** in a 1:1 mixture of acetone/ethyleneglycol, with the exception of *R,R*-**70** which required a 4:1 mixture of DMSO/ethyleneglycol.

Table 8.1. Experimental spin Hamiltonian parameters for the prepared Cu^{II}(salan) compounds.[a]

Compound	$\mathbf{g_x, g_y}$ (or $\mathbf{g_\perp}$)	$\mathbf{A_x, A_y}$ (or $\mathbf{A_\perp}$) $\times 10^{-4}$ cm^{-1}	$\mathbf{g_z}$ (or $\mathbf{g_{//}}$)	$\mathbf{A_z}$ (or $\mathbf{A_{//}}$) $\times 10^{-4}$ cm^{-1}	$\mathbf{g_z/A_z}$ cm
R,R-**68**	2.038, 2.057	36.4, 10.6	2.235	189.3	118
S,S-**69**	2.037, 2.055	28.3, 22.5	2.239	184.9	121
R,R-**70**[b]	2.048	18	2.239	184.9	121
R,R-**71**	2.038, 2.056	36.1, 7.8	2.238	184.9	121

[a] EPR spectrum measured at 77 K with a 1:1 acetone:ethyleneglycol mixture as solvent. [b] EPR spectrum measured at 77 K with a 4:1 DMSO:ethyleneglycol mixture as solvent.

Figure 8.5 shows the updated Peisach-Blumerg plot containing the approximate location of the $\mathbf{g_z}$ and $\mathbf{A_z}$ values obtained for the prepared Cu^{II}(salan) compounds.

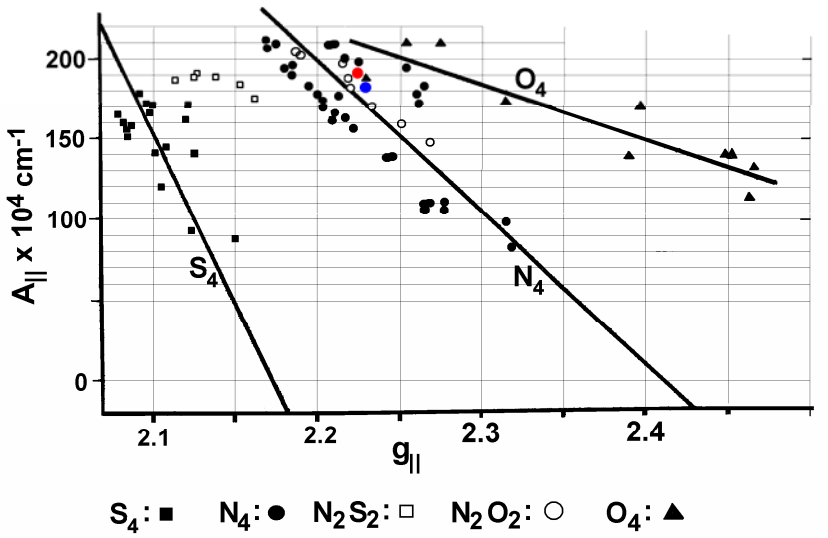

Figure 8.5. $\mathbf{A_{//}}$ and $\mathbf{g_{//}}$ correlation plot published by Addison and co-workers. It depicts the correlation between $\mathbf{A_{//}}$ and $\mathbf{g_{//}}$ for a range of Cu^{II} complexes possessing the following donor groups: S_4, N_4, O_4, N_2O_2, and N_2S_2. Compound *R,R*-**68** is identified as (•), *S,S*-**69**, *R,R*-**70** and *R,R*-**71** as (•).

As expected, compounds *R,R*-**68**, *S,S*-**69**, *R,R*-**70** and *R,R*-**71** are placed between the N_4/O_4 trend lines. However, no definitive conclusion as to whether the said complexes have indeed N_2O_2 donor set bound to the Cu^{II} can be made based on this $\mathbf{g_z}/\mathbf{A_z}$ representation alone. A closer examination of this plot will show that square-planar CuN_4, CuN_2O_2 and CuO_4 complexes have similar $\mathbf{g_z}/\mathbf{A_z}$ ratios, and that distinction occurs only between complexes with higher degrees of tetrahedral distortion. In addition, compounds *R,R*-**68**, *S,S*-**69**, *R,R*-**70** and *R,R*-**71** share very similar tetrahedral distortion indexes between 118 and 121 cm, which are within the expected range for square-planar Cu^{II} complexes with minimal tetrahedral distortion. A more definitive conclusion can be made about the probable donor set group bound present in the prepared Cu^{II}(salan) compounds after plotting the respective experimental $\mathbf{g_z}$ and $\mathbf{A_z}$ parameters with reference parameters for salen- and salan-type CuN_2O_2 complexes reported in the literature.[12,19] Figure 8.6 shows a $\mathbf{g_z}/\mathbf{A_z}$ representation where the $\mathbf{g_z}/\mathbf{A_z}$ ratios for the prepared Cu^{II}(salan) compounds are plotted along with literature $\mathbf{g_z}/\mathbf{A_z}$ ratios for salen- and salan-type CuN_2O_2 complexes.

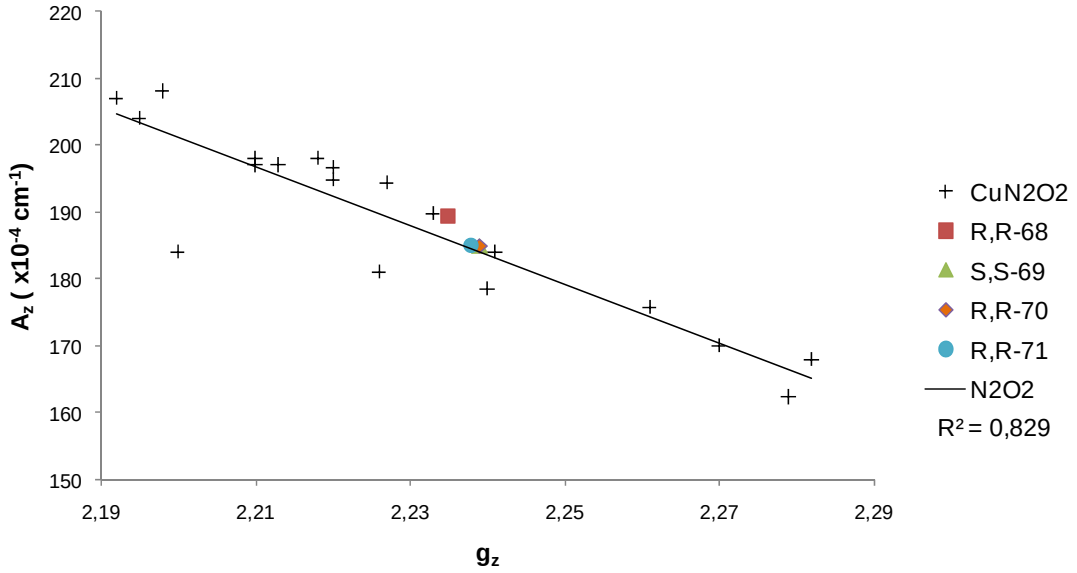

Figure 8.6. $\mathbf{A_z}$ and $\mathbf{g_z}$ correlation plot for a range of Cu^{II}(salen) and Cu^{II}(salan) complexes bearing a N_2O_2,(+) donor group set. The colored markers represent the prepared Cu^{II}(salan) compounds described in this Chapter.

By observing Figure 8.6 it is possible to conclude that compounds *R,R*-**68**, *S,S*-**69**, *R,R*-**70** and *R,R*-**71** most probably have a CuN_2O_2 core as these are placed along the best linear fit found for the surveyed literature $\mathbf{g_z}/\mathbf{A_z}$ ratios. It is also possible to observe the apparent diagonal relation between $\mathbf{g_z}$ and $\mathbf{A_z}$ values for the general N_2O_2 donor group set: increasing $\mathbf{g_z}$ is accompanied with a decrease in $\mathbf{A_z}$, indicative of tetrahedral distortion.

A noteworthy feature present in the EPR spectrum of *R,R*-**68** is the superhyperfine structure resultant from the additional coupling of the unpaired electron with the nuclear spin of two equivalent ^{14}N donor atoms. A resolved five-signal structure is present in the perpendicular region (high field) of the spectrum, as is depicted in Figure 8.7. The $\mathbf{a_\perp}^N$ superhyperfine coupling constant was calculated manually and the obtained value of 12×10^{-4} cm^{-1} is similar to those reported for other Cu^{II}(salan) compounds.[19d] The EPR spectrum of *S,S*-**69** shown in Figure 8.8 also presents a superhyperfine structure in the high field region. The less resolved signals do not allow calculation of the $\mathbf{a_\perp}^N$ value, but the structure is still indicative of coupling with two equivalent nitrogen donor atoms. Line broadening effects (spin-spin coupling, aggregation and movement restriction) in the spectra of *R,R*-**70** and *R,R*-**71** do not allow the observation of a superhyperfine structure.

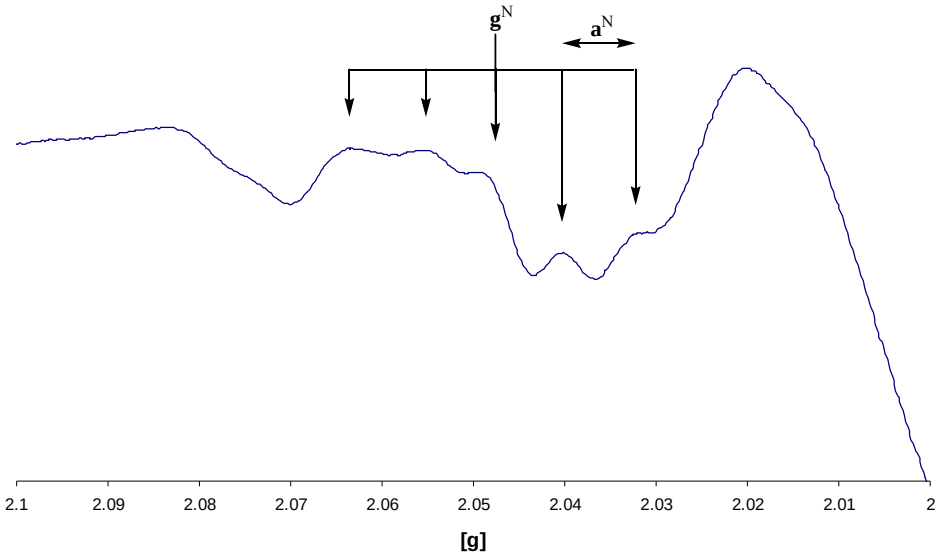

Figure 8.7. First derivative X-band EPR spectrum of *R,R*-**68** depicting the high field superhyperfine structure resultant from additional spin-coupling with two equivalent ^{14}N nuclei.

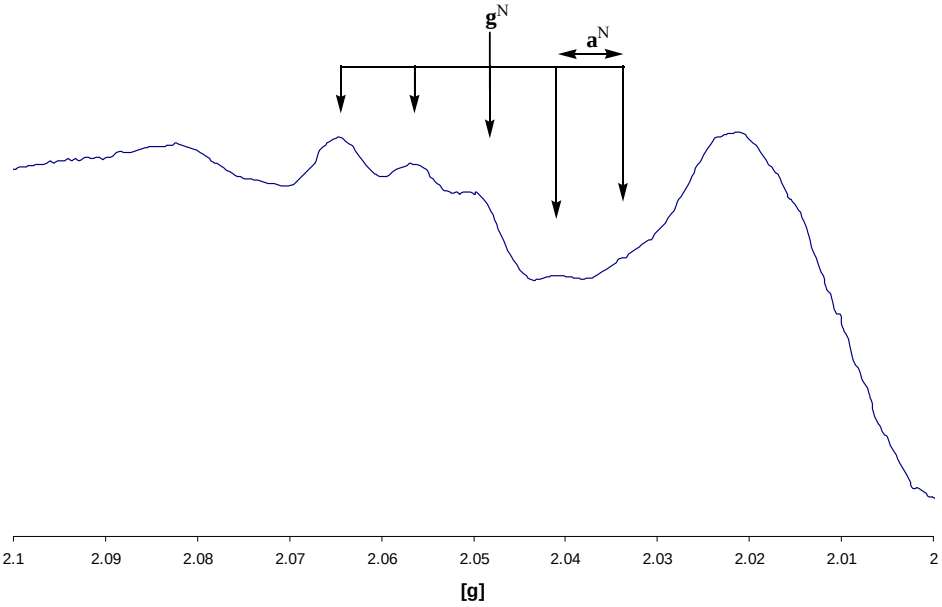

Figure 8.8. First derivative X-band EPR spectrum of *S,S*-**69** depicting the high field superhyperfine structure resultant from additional spin-coupling with two equivalent ^{14}N nuclei. The higher-field signals are severely broadened.

8.2.2. Characterization by X-Ray Diffraction

Important structural information was obtained by the X-ray diffraction of crystals *R,R*-**71**. The ORTEP diagram of *R,R*-**71** is presented in Figures 8.9 and the selected parameters are listed in Table 8.2.

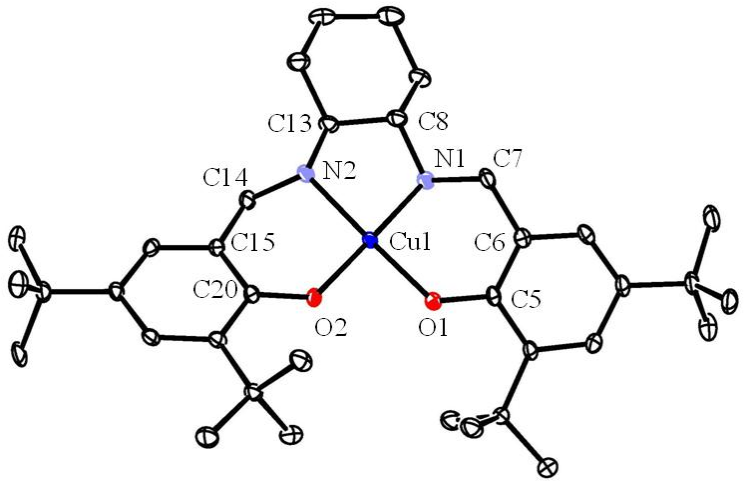

Figure 8.9. ORTEP-3 diagram of *R,R*-**71**, using 30 % probability level ellipsoids. The hydrogen atoms were omitted for clarity.

Table 8.2. Selected bond lengths and angles for *R,R*-**71**.

R,R-**71**			
Bond lengths (Å)		Bond angles (°)[a]	
Cu(1)-N(1)	1.9919(2)	O(1)-Cu(1)-O(2)	88.33(11)
Cu(1)-N(2)	1.9927(2)	O(1)-Cu(1)-N(1)	92.79(12)
Cu(1)-O(1)	1.8946(2)	O(2)-Cu(1)-N(2)	92.86(12)
Cu(1)-O(2)	1.8870(2)	N(1)-Cu(1)-N(2)	86.05(13)
C(7)-N(1)	1.4707(2)	C(7)-N(1)-Cu(1)	111.0(2)
C(14)-N(2)	1.4744(1)	C(14)-N(2)-Cu(1)	110.5(2)
		O(1)-Cu(1)-N(2)	177.84(12)
		O(2)-Cu(1)-N(1)	178.47(13)

The structure obtained for *R,R*-**71** exhibits a Cu^{II} center in a square-planar environment, which is consistent with what was predicted earlier by EPR. The asymmetric unit contains one molecule. *R,R*-**71** crystallizes in the triclinic system, space group *P*-1. Since the crystal structure has a centrosymmetric space group, a racemic mixture is present in the crystal. As such, 50% of the molecules present in the crystal

structure have *R* configuration at C(8) and C(13), with the nitrogen donors N(1) and N(2) exhibiting *S* configuration. The other 50% have opposite configurations at these atoms. The cyclohexane ring adopts the chair conformation. The Cu^{II}-donor atom bond distances do not differ significantly, with the Cu^{II}-$O_{phenolate}$ being *ca*. 0.1 Å shorter than the Cu^{II}-N_{amine} bonds. Additionally, the bond angles made between the *cis* Cu^{II}-$O_{phenolate}$ and the Cu^{II}-N_{amine} bonds are very approximate to 90º. Further attesting the square-planar geometry are the *trans* Cu^{II}-$O_{phenolate}$ and the Cu^{II}-N_{amine} bond angles with values very similar between each other and in turn very approximate to 180º. These bond lengths are very similar to the lengths reported in the literature for structurally related square-planar Cu^{II}(salan) compounds.[19d] Figure 8.10 illustrates the unequivocally square-planar geometry of the Cu^{II} center in this structure.

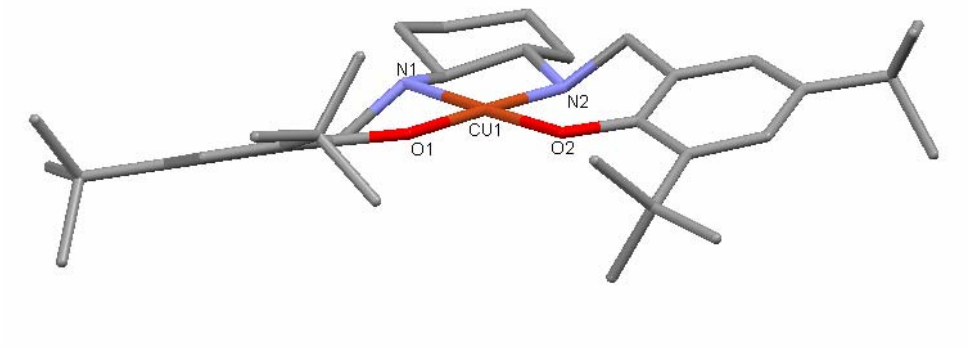

Figure 8.10. Wireframe diagram of *R,R*-**71** depicting the square-planar geometry of the Cu^{II} center.

Another expectation was that the flexible nature of the salan-type ligand would favor some degree of tetrahedral distortion of the Cu^{II} center, more so than related Cu^{II}(salen) compounds bearing more rigid salen-type ligands.[10a,20] Instead, the Cu^{II} center in *R,R*-**71** adopts a nearly strict square-planar geometry, contrasting with the clearly tetrahedrally-distorted structure of the Schiff base version of *R,R*-**71** reported earlier by Cross and co-workers in 1998.[10a] As a result of the rigid structure of *R,R*-**71**, the mean planes containing the 5- and 6-membered chelate rings do not deviate significantly from the mean plane containing the Cu^{II} center and the donor atoms. Indeed, the 5-membered

chelate ring Cu(1)-N(1)-C(8)-C(13)-N(3) forms an angle of about 4º with the plane defined by Cu(1)-O(1)-O(2)-N(1)-N(2). The 6-membered chelate rings Cu(1)-N(1)-C(7)-C(5)-C(6)-O(1) and Cu(1)-N(2)-C(14)-C(15)-C(20)-O(2) form angles of *ca*. 16º with the plane defined by Cu(1)-O(1)-O(2)-N(1)-N(2), respectively.

8.2.3. Elemental analysis

All the prepared Cu^{II}(salan) compounds, with the exception of *R,R*-**71**, gave elemental analysis results consistent with monomeric species having either water or alcohols as vestigial contaminants. Compound *R,R*-**71** failed to give acceptable elemental analysis results despite being possible to characterize it by X-ray diffraction.

8.3. Catalytic applications: asymmetric sulfoxidation of thioanisole

Similarly to what was done in the previous Chapters, the prepared Cu^{II}(salan) compounds were screened for their catalytic potential in the asymmetric sulfoxidation of thioanisole under a variety of conditions. The compounds were tested in DCE, ethyl acetate and acetone, at 0 ºC and room temperature. Contrary to what was initially expected, the tested compounds exhibited no catalytic activity, even at room temperature. Regarding sulfoxidation with aminophenolate-class Cu^{II}(Schiff base) catalysts, including the salen-type catalysts, the instances available in published literature consistently report moderate to high sulfoxide yields only at room temperature, with the *in situ tert*-leucinol-derived Cu^{II}(Schiff base) catalyst reported by Maguire and co-workers delivering high enantioselectivities of 79%.[21]

It is known that Cu^{I} and Cu^{II} species react with O_2 and H_2O_2 to form dinuclear and possibly interconvertible di-μ-oxo Cu^{III} and μ-η^1:η^1-peroxo or μ-η^2:η^2-peroxo Cu^{II} species which may exhibit different reactivities towards thioether oxidation (see Figure 8.11).[22] This reactivity also depends greatly on the supporting ligand structure.

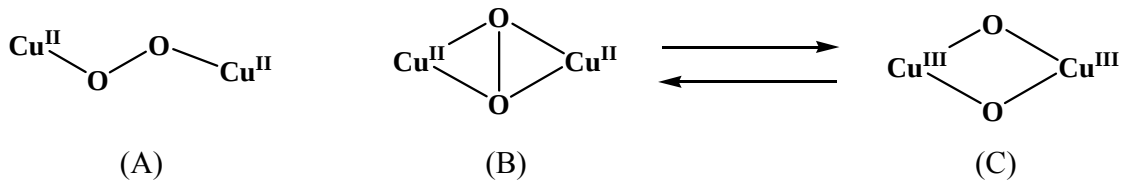

(A) (B) (C)

Figure 8.11. Possible copper-oxo and copper-peroxo species generated after reaction with active oxygen species: μ-η^1:η^1-peroxo Cu^{II} (A), μ-η^2:η^2-peroxo Cu^{II} (B) and di-μ-oxo Cu^{III} (C) species.

In fact, a report by Fukuzumi and co-workers showed that a dinuclear di-μ-oxo Cu^{III} species exhibited significantly better catalytic performance over a dinuclear μ-η^2:η^2 peroxo Cu^{II} species in thioether oxidation.[23] It has also been reported by Yoshizawa and co-workers that Cu^{II}-hydroperoxo species have weak oxidative power in organic substrate oxidation reactions.[24] While the mechanism of copper catalyzed thioether sufoxidation is not known presently and reactivity studies usually rely on complexes bearing ligands unrelated to the salen and salan class, the results reported by the groups of Fukuzumi and Yoshizawa give important clues regarding the reasons behind the apparent inactivity of the Cu^{II}(salan) compounds described in this Chapter. In the case of the tested Cu^{II}(salan) compounds, the possible pathways for the reaction with hydrogen peroxide were hypothesized and are presented below in Figure 8.12.

All of the species depicted in Figure 8.12 may be present simultaneously in the reaction medium. The non-activity of the tested Cu^{II}(salan) compounds may indicate that if these species are indeed present, then all are inactive, but due to different reasons. In the case of the hydroperoxo Cu^{II}(salan) species (A), it is known that Cu^{II}-hydroperoxo species typically do not exhibit accentuated catalytic activity in thioether sulfoxidation.[22,25] In the case of the remaining dinuclear species, non-activity may be due to impaired substrate access to the active oxygen sites as a result of the steric hindrance caused by the bulky Cu^{II}(salan) structures, as the reactivity of μ-η^1:η^1-peroxo, μ-η^2:η^2-peroxo Cu^{II} and di-μ-oxo Cu^{III} is intimately dependent of the ligand structure.[20c,21] Complementary spectroscopic studies and/or theoretical calculations are necessary to unveil relevant information regarding the behavior of Cu^{II}(salan) compounds in the presence of hydrogen peroxide and thioanisole.

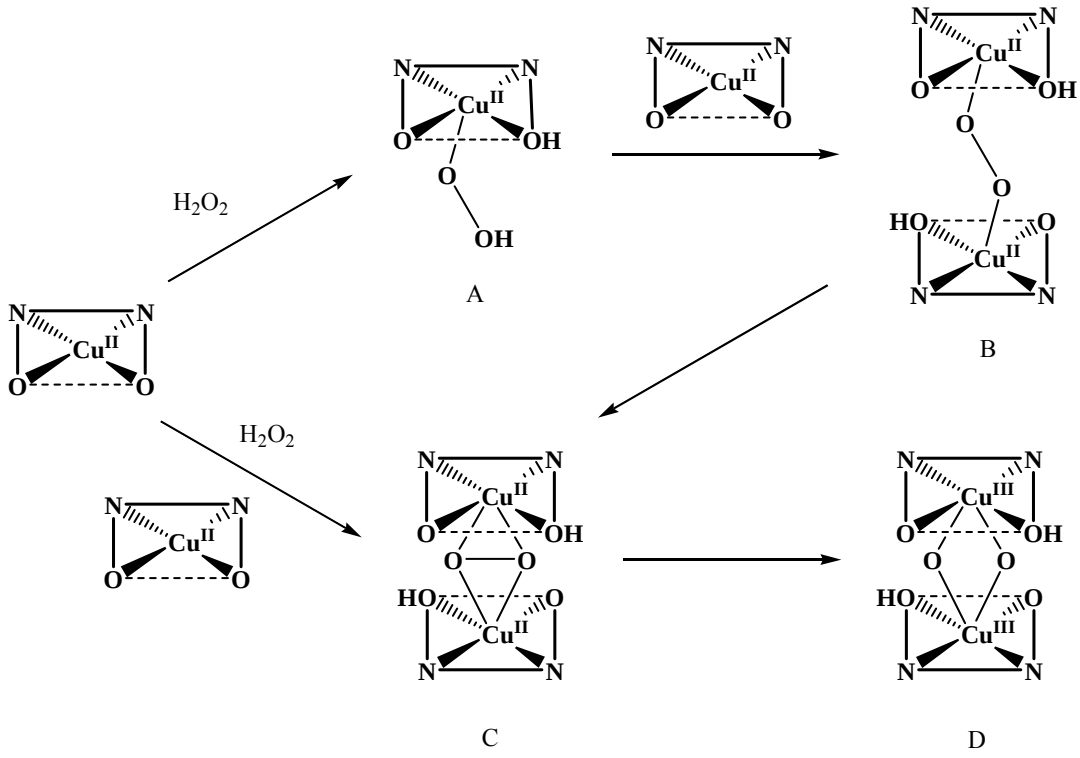

Figure 8.12. Possible pathways for the formation of hydroperoxo Cu^{II}(salan) (A), μ-η^1:η^1-peroxo (B), μ-η^2:η^2-peroxo Cu^{II}(salan) (C) and di-μ-oxo Cu^{III}(salan) (D) species after the reaction with H_2O_2.

8.4. Conclusions

Several Cu^{II}(salan) compounds were prepared and characterized by EPR spectroscopy and elemental analysis. EPR analysis results were consistent with square-planar Cu^{II} centers bound to a N_2O_2 donor group set for all cases. The X-ray structure obtained for *R,R*-**71** confirmed the square-planar geometry of the Cu^{II} center for this case. The prepared Cu^{II}(salan) compounds were employed as asymmetric sulfoxidation catalysts with hydrogen peroxide as the terminal oxidant. None of the tested compounds exhibited catalytic activity. The possible scenarios for this inactivity were hypothesized but complementary studies need to be carried out to verify the proposed reasons for catalyst non-activity.

8.5. Experimental section

8.5.1. General considerations

Unless stated otherwise all preparations were made without resorting to inert atmosphere techniques. All solvents and reagents were purchased from commercial suppliers and used as received.

8.5.2. Characterization techniques

8.5.2.1. Elemental analysis (EA)

Elemental analyses were carried out at *Laboratório de Análises* of *Instituto Superior Técnico,* using EA110 CE automatic analyzer Instruments. The results presented are the average values obtained from two independent determinations.

8.5.2.2. Electron paramagnetic resonance spectroscopy (EPR)

The electron paramagnetic resonance (EPR) spectra were recorded at 77 K (on glasses made by freezing solutions in liquid nitrogen) with a Bruker ESP 300E X-band spectrometer. The measured spectra were then simulated with the ROKI EPR simulation software developed by Rockenbauer and Korecz.[26]

8.5.2.3. X-Ray crystallography

Single crystals suitable for X-ray diffraction crystallography were obtained as described in the compound preparation methods. The data collection, structure solution and refinement for all the featured crystal structures in this Chapter were performed by Dr. Fernando Avecilla at the *Departamento de Química Fundamental* of *Universidade da Coruña*. X-ray data for *R,R*-**71** were collected on a Bruker Kappa X8 Apex CCD diffractometer at 100 K. Reflections were measured from a hemisphere of data collected of frames, each covering 0.3º in ω. The reflections measured were corrected for Lorentz

and polarization effects, and for absorption by semiempirical methods based on symmetry-equivalent and repeated reflections. Complex scattering factors were taken from the program package SHELXL.[27] The structures were solved by direct methods and refined by full-matrix least-squares methods on F^2. The non-hydrogen atoms were refined with anisotropic thermal parameters in all cases. The hydrogen atoms were left to refine freely.

Table 8.3. Crystal data, data collection and refinement data for compound *R,R*-**71**.

Compound	*R,R*-**71**	
Empirical formula	$C_{36}H_{56}N_2O_2Cu$	
Formula weight	612.37	
Temperature / K	100(2)	
Wavelength / Å	0.71073 Å	
Crystal system	Triclinic	
Space group	*P*-1	
Unit cell dimensions	a = 9.9147(11) Å	α= 117.610(2)°
	b = 13.8176(17) Å	β= 95.249(3)°.
	c = 14.8585(19) Å	γ = 103.768(2)°.
Volume / Å^3	1703.1(4)	
Z	2	
Density (calculated) / mg/m^3	1.194	
Absorption coefficient /mm^{-1}	0.673	
Crystal size / mm^3	0.24×0.07×0.07	
Reflections collected	13219	
Independent reflections	6365 [R(int) = 0.0444]	
Goodness-of-fit on F2	1.087	
Final R indices [I>2sigma(I)]	R1 = 0.0497, wR2 = 0.1297	
R indices (all data)	R1 = 0.0866, wR2 = 0.1657	

8.5.3. General procedure for sulfoxidation of thioanisole

The catalytic experiments were carried out at atmospheric pressure, at a constant temperature, in a glass batch reactor, equipped with a magnetic stirrer, thermometer and condenser. In a typical run, the solid catalyst (1 mol%) and thioanisole (1 mmol) were dissolved in the appropriate solvent (4 mL). Then the oxidant (1.2 to 1.5 mmol), hydrogen peroxide (30 wt%, aqueous solution) was added to the stirring mixture. Control experiments were carried out in absence of catalyst. Samples of the reaction mixture were

withdrawn periodically and analyzed on a Jasco HPLC system equipped with a Daicel Chiralpak IA column. The eluent used was hexane/ethyl acetate (60:40) with a flow of 1 mL/min. The calibration curves for each reagent and product, namely sulfide, sulfoxide and sulfone, were determined using similar HPLC procedures and these calibrations used for the quantitative analyses. Diphenylsulfone was used as an internal standard.

8.5.4. Cu^{II}(salan) compound preparation methods

General preparation procedure

Anhydrous $Cu^{II}Cl_2$ was added to a methanolic (25 mL) solution of the appropriate ligand. The pH was adjusted to *ca*. 7-8 with a 1 M aqueous solution of NaOH. The addition of water (25 mL) induced the complete precipitation of a Cu^{II} compound. The precipitate was filtered and washed with water, minimal amounts of methanol and diethyl ether. The recovered solid was then dried under vacuum. When necessary, the removal of $Cu^{II}(OH)_2$ impurities was made by dissolving the Cu^{II}(salan) compound in dichloromethane and filtering out the blue $Cu^{II}(OH)_2$ solid. The filtrate was then completely evaporated in a rotary evaporator and the Cu^{II}(salan) compound was recovered. This method was used for all the described Cu^{II} compounds.

Synthesis of [Cu^{II}(*R*,*R*-1)], *R*,*R*-68

Reagents: $Cu^{II}Cl_2$ (0.5 g, 3.7 mmol), *R*,*R*-**1** (1.5 g, 3.7 mmol). The compound was obtained as a dark green solid. Yield: 1.0 g, 86 %. EPR (acetone/ethyleneglycol, 1:1): $\mathbf{A_z}$=189.3 × 10^{-4} cm^{-1}; $\mathbf{g_z}$=2.235. Elemental analysis for $C_{20}H_{24}N_2O_2Cu \cdot 1CH_2Cl_2 \cdot 0.5H_2O$: calcd. C 52.34, H 5.65, N 5.81; found C 52.2, H 5.9, N 5.8.

Synthesis of [Cu^{II}(*S*,*S*-10)], *S*,*S*-69

Reagents: $Cu^{II}Cl_2$ (0.14 g, 1.0 mmol), *S*,*S*-**10** (0.58 g, 1.0 mmol). The compound was obtained as a dark green solid. Yield: 0.32 g, 59 %. EPR (acetone/ethyleneglycol, 1:1): $\mathbf{A_z}$=184.9 × 10^{-4} cm^{-1}; $\mathbf{g_z}$=2.239. Elemental analysis for $C_{30}H_{30}N_2O_4Cu \cdot 1.8H_2O$: calcd. C 62.28, H 5.85, N 4.84; found C 62.4, H 5.6, N 4.9.

Synthesis of [Cu^{II}(*R*,*R*-9)], *R*,*R*-70

Reagents: $Cu^{II}Cl_2$ (0.14 g, 1.0 mmol), *R*,*R*-**9** (0.64 g, 1.0 mmol). The compound was obtained as a dark green solid. Yield: 0.34 g, 61 %. EPR (DMSO/ethyleneglycol, 4:1): $\mathbf{A_z}$=184.9 × 10^{-4} cm^{-1}; $\mathbf{g_z}$=2.239. Elemental analysis for $C_{26}H_{24}N_4O_2Cl_2Cu{\cdot}1H_2O$: calcd. C 54.12, H 4.54, N 9.71; found C 54.0, H 4.6, N 10.0.

Synthesis of [Cu^{II}(*R*,*R*-8)], *R*,*R*-71

Reagents: $Cu^{II}Cl_2$ (0.14 g, 1.0 mmol), *R*,*R*-**8** (0.6 g, 1.0 mmol). The compound was obtained as a dark green solid. Yield: 0.4 g, 66 %. EPR (acetone/ethyleneglycol, 1:1): $\mathbf{A_z}$=184.9 × 10^{-4} cm^{-1}; $\mathbf{g_z}$=2.239. Crystals suitable for single crystal X-ray diffraction were grown from isopropanol solutions. 0.1g of *R*,*R*-**71** was dissolved in *ca*. 10 mL of isopropanol and the resulting solution was filtered and transferred to a clean lint-free 20 mL glass flask. Dark green crystals were obtained by slow evaporation of the solvent after four weeks.

8.6. References

1 Solomon, E. I.; Hemming, B. L.; Root, D. E., *Bioinorganic Chemistry of Copper*; Karlin K. D., Tyeklár Z. Eds.; Chapman & Hall: London **1993**.

2 (a) Beletskaya, I. P.; Cheprakov, A. V. *Coord. Chem. Rev.* **2004**, *248,* 2337-2364. (b) Do, H.; Daugulis, O. *Chem. Commun*. **2009**, 6433-6435. (c) Lin, C.; Wang, Y.; Fa, C. *Eur. J. Org. Chem.* **2010**, 4368-4371.

3 Punniyamurthy, T.; Rout, L. *Coord. Chem. Rev.* **2008**, *252*, 134-154.

4 Rajagopal, G.; Selvaraj, S.; Dhahagani, K. *Tetrahedron: Asymm.* **2010**, *21*, 2265-2270.

5 Lin, C.; Wang, Y.; Lee, C. *Eur. J. Org. Chem.* **2010**, 4368–4371.

6 Desimoni, G.; Dusi, G.; Faita, G.; Quadrelli, P.; Righetti, P. *Tetrahedron* **1995**, *51*, 4131-4144.

7 (a) Belokon, Y. N.; Davies, R. G.; North, M. *Tetrahedron Lett*. **2000**, *41*, 7245-7248. (b) Belokon, Y. N.; North, M.; Churkina, T. D.; Ikonnikova, N. S.; Maleev, V. I. *Tetrahedron*, **2001**, *57*, 2491-2498. (c) Belokon, Y. N.; Bhave, D.; D'Addario, D.; Groaz, E.; North, M.; Tagliazucca, V. *Tetrahedron* **2004**, *60*, 1849-1861. (d) Achard, T.; Belokon, Y. N.; Fuentes, J. A.; North, M.; Parsons, T. *Tetrahedron* **2004**, *60*, 5919-5930.

8 Gan, C.; Lai, G.; Zhang, Z.; Wang, Z.; Zhou, M. *Tetrahedron: Asymm.* **2006***,* 17, 725-728.

9 Wu, Z.; Zhou, L.; Jiang, Z.; Wu, D.; Li, Z.; Zhou, X. *Eur. J. Org. Chem.* **2010**, 4971-4975.

10 (a) Bunce. S.; Cross, R. J.; Farrugia, L. J.; Kunchandy, S.; Meason, L. L.; Muir, K. W.; O'Donnell, M.; Peacock, R. D.; Stirling, D.; Teat, S. J. *Polyhedron* **1998**, *17*, 4179-4187. (b) Zhu, H.; Dai, Z.; Huang, W.; Cui, K.; Gou, S.; Zhu, C. *Polyhedron* **2004**, *23*, 1131-1137.

11 Rayati, S.; Zakavi, S.; Koliaei, M.; Wojtczak, A.; Kozakiewicz, A. *Inorg. Chem. Comm.* **2010**, *13*, 203-207.

12 Maurya, M. R.; Singh, B.; Adão, P.; Avecilla, F.; Costa Pessoa, J. *Eur. J. Inorg. Chem.* **2007**, 5720-5734.

13 Rajagopal, G.; Selvaraj, S.; Dhahagani, K. *Tetrahedron. Asymm.* **2010**, *21*, 2265-2270.

14 Belokon, Y. N.; North, M., Parsons, T. *Org. Lett*. **2000**, *2*, 1617-1619.

15 Xiong, Y.; Wang, F.; Huang, X.; Wen, Y.; Feng, X. *Chem. Eur. J.* **2007**, *13*, 829-833.

16 Garriba, E.; Micera, G. *J. Chem. Ed.* **2006**, *83*, 1229-1232.

17 Peisach, J.; Blumberg, W. E. *Arch. Biochem. and Biophys.* **1974**, *165*, 691-708.

18 Sakaguchi, U.; Addison, A. W. *J. Chem. Soc. Dalton Trans.* **1979**, 600-608.

19 (a) Kasumov, V. T.; Köksal, F. *Spectrochim. Acta A* **2005**, *61*, 225-231. (b) Deshpande, S.; Srinivas, D.; Ratnasamy, P. *J. Cat.* **1999**, *188*, 261-269. (c) Valko, M.; Bofa, R.; Klement, R.; Koziek, J.; Mazfir, M.; Pelikan, P.; Morris, H.; Elias, H.; Moiler, L. *Polyhedron* **1997**, *16*, 903-908. (d) Klement, R.; Stock, F.; Elias, H.; Paulus, H.; Pelikan, P.; Valko, M.; Mazur, M. *Polyhedron* **1999**, *18*, 3617-3628. (e) Verquin, G.; Fontaine, G.; Abiaad, E.; Zhilinskaya, E.; Aboukaıs, A.; Bernier, J. *J. Photochem. Photobio. B*: *Bio*. **2007**, *86*, 272-278. (f) Sylvestre, I.; Wolowska, J.; Kilner, C. A.; McInnes, E. J. L.; Halcrow, M. A. *Dalton. Trans* **2005**, 3241-3249. (g) Ananth, K. M.; Kanthimathi, M.; Nair, B. U. *Trans. Met. Chem*. **2001**, *26*, 333-338. (h) Correia, I.; Dornyei, A.; Jakusch, T.; Avecilla, F.; Kiss, T.; Costa Pessoa, J. *Eur. J. Inorg. Chem.* **2006**, 2819-2830.

20 (a) Rusere, L. N.; Shalumova, T.; Tanski, J. M.; Tyler, L. A. *Polyhedron* **2009**, *28*, 3804-3810. (b) Plitt, P.; Pritzkow, H.; Oeser, T.; Kraemer, R. *J. Inorg. Biochem.* **2005**, *99*, 1230-1237.

21 Wojaczynska, E.; Wojaczynski, J. *Chem. Rev.* **2010**, *110,* 4303-4356.

22 (a) Lewis, E. A.; Tolman, W. B. *Chem. Rev.* **2004**, *104,* 1047-1067. (b) Mirica, L. M.; Ottenwaelder, X.; Stack, T. D. P. *Chem. Rev*. **2004**, *104*, 1013-1045. (c) Hatcher, L. Q.; Vance, M. A.; Narducci Sarjeant, A. A.; Solomon, E. I.; Karlin, K. D. *Inorg. Chem*. **2006**, *45*, 3004-3013.

23 Taki, M.; Itoh, S.; Fukuzumi, S. *J. Am. Chem. Soc.* **2002**, *124*, 998-1002.

24 Kamachi, T.; Lee, Y.; Nishimi, T.; Cho, J.; Yoshizawa, K.; Nam, W. *J. Phys. Chem. A* **2008,** *112,* 13102-13108.

25 Fujii, T.; Naito, A.; Yamaguchi, S.; Wada, A.; Funahashi, Y.; Jitsukawa, K.; Nagatomo, S.; Kitagawa, T.; Masuda, H. *Chem. Commun*. **2003**, 2700-2701.

26 Rockenbauer, A.; Korecz, L. *Appl. Magn. Reson.* **1996**, *10*, 29-43.

27 Sheldrick, G. M. *SHELXS-97*, revision 5.1; University of Göttingen: Göttingen, Germany, **1997**.